Wojciech Mazur · Marilyn J. Siegel
Tomasz Miszalski-Jamka · Robert Pelberg

# CT Atlas of Adult Congenital Heart Disease

Springer

# CT Atlas of Adult Congenital Heart Disease

Wojciech Mazur • Marilyn J. Siegel
Tomasz Miszalski-Jamka • Robert Pelberg

# CT Atlas of Adult Congenital Heart Disease

Springer

Wojciech Mazur
The Christ Hospital Heart and Vascular Center
of Greater Cincinnati
The Lindner Center for Research and Education
Cincinnati
OH
USA

Robert Pelberg
The Christ Hospital Heart and Vascular Center
of Greater Cincinnati
The Lindner Center for Research and Education
Cincinnati
OH
USA

Marilyn J. Siegel
Mallinckrodt Institute of Radiology
Washington University School of Medicine
St. Louis
Missouri
USA

Tomasz Miszalski-Jamka
Department of Clinical Radiology
and Imaging Diagnostics
4th Military Hospital
Wrocław
Poland

Center for Diagnosis
Prevention and Telemedicine
John Paul II Hospital
Kraków
Poland

Illustrations by: Michał Bratko, Kraków, Poland

ISBN 978-1-4471-5087-9 ISBN 978-1-4471-5088-6 (eBook)
DOI 10.1007/978-1-4471-5088-6
Springer London Heidelberg New York Dordrecht

Library of Congress Control Number: 2013941382



Printed on acid-free paper

Springer is part of Springer Science+Business Media (www.springer.com)

*To my wife, Eugenia, and my children, Andre and Jan Paul, for their love and support during the countless hours it took to create this text.*

*Wojciech Mazur*

*To my husband, Barry, my mentor, colleague, friend and loving spouse for his unwavering support and encouragement to make this project a reality.*

*Marilyn J. Siegel*

*To my marvelous parents, my beloved wife, Ania, and splendid daughters, Ania and Ewa for their tremendous love and constant support in my whole life.*

*I would like also to express my deepest and sincere gratitude to my mentors and tutors Professor Jacek Musiał, Professor Piotr Podolec, Professor Andrzej Szczeklik, and Professor Anetta Undas for their invaluable help and passion to medicine and science.*

*Tomasz Miszalski-Jamka*

*To my wonderful wife, Wendy, and my fantastic children, Josh, Adam and Noah for their never ending devotion and love and for their constant support without which projects like this would never come to fruition.*

*Robert Pelberg*

# In Appreciation

We extend a heart felt thank you to Lisa Ambach whose contributions to the editing and organization of this work were immense and without whom this book would not be possible. Thank you, also, to David Collins for his efforts in helping us complete this challenging project. Thank you to Chris Thomson and The Christ Hospital for their financial support of this work.

The authors would like to extend a sincere thank you to Mr Robert Banyś and Drs. Frandics Chan, Joao Carlos Costa, Kelly Han, Anthony Hlavacek, Eric Kimura-Hayama, Małgorzata Irzyk, Piotr Klimeczek, Maciej Krupiński, Bartosz Laskowicz, R. Rajesh Kannan, Vasco Silva, and Małgorzata Urbańczyk for their generous contributions in providing images for this work.

# Preface

Congenital heart disease (CHD) with a worldwide incidence of 0.8 % represents the most common class of inborn birth defects. Improvements in surgical techniques and medical management result in an increased life expectancy and lead to a greater number of children with CHD surviving into adulthood. It is now estimated that at least 85 % of children with CHD will survive to adulthood, and many of these patients will require follow-up medical care as an adult [1, 2].

Consequently, adult cardiologists will have the opportunity to care for increasing numbers of patients with congenital heart defects. In many instances, these patients have undergone palliative but not corrective procedures and may be at higher risk for the development of congestive heart failure, cardiac arrhythmia, and overall cardiovascular morbidity and mortality. Furthermore, as this adult congenital heart disease population ages, their risk of developing coronary artery disease is similar or in certain instances higher than the age- and risk-matched population.

The amount of time devoted to congenital heart disease during adult cardiovascular fellowships and radiology residencies is rather modest. Furthermore, most cardiologists and radiologists have limited experience in imaging adult patients with complex CHD. In addition, patient care is not infrequently transferred from pediatric to adult cardiologists who may not be adequately prepared to provide care for these patients. Moreover, the cardiologist or radiologist may encounter an adult patient presenting with unknown, corrected, or palliated CHD. Therefore, it is critical that they be familiar with the imaging appearances of corrected and uncorrected CHD classes and of their potential long-term complications.

Traditionally, invasive angiography was used to evaluate these patients. As imaging technology has advanced, noninvasive techniques such as echocardiography, magnetic resonance imaging (MRI), and multidetector computed tomographic angiography (CTA) are applicable. Despite its relatively low cost, portability, accessibility, and lack of radiation exposure, echocardiography is often limited in its ability to completely evaluate complex native and palliated CHD due to its operator dependency and potential lack of adequate acoustic windows. In addition, extracardiac structures such as the pulmonary arteries, pulmonary veins, and aortic arch are difficult to evaluate with echocardiography. For these reasons, MRI is superior to echocardiography but may be challenging due to prolonged imaging times and to the presence of image degrading metal implants (embolization coils and intravascular stents). Moreover, MRI is contraindicated in patients with pacemakers and defibrillators, which are frequently implanted in long-term survivors of CHD. Furthermore, the diagnostic capabilities of MRI are limited for the evaluation of the airways and lungs.

In the past several years, we have witnessed a rapid increase in the use of CTA, driven mainly by technical improvements that allow shorter imaging times and high spatial and temporal resolution. Thus, CTA combines widespread availability with the advantages of volumetric data acquisition, short acquisition times, and the possibility of simultaneous evaluation of myocardial and extracardiac structures, ventricular function, and coronary anatomy. The American College of Cardiology (ACC), the American Heart Association (AHA), and the Society of Cardiothoracic Computed Tomography (SCCT) have recognized CT as a reasonable and state-of-the-art imaging technique for the assessment of CHD, and this indication is listed as appropriate in the 2010 appropriateness criteria document [3].

This CT Atlas of Adult Congenital Heart Disease is intended to serve as a reference for pediatric and adult cardiologists and for radiologists. In addition to classic CHD, we have also included chapters on hereditary cardiomyopathies and aortopathies. This book includes comprehensive pathology descriptions and discussions of the utility of CTA in the diagnosis of adult CHD as well as details regarding the relevant techniques for designing CTA protocols required to evaluate CHD. There are a multitude of CTA images and drawings to help illustrate the pathologies and to serve as a reference.

Our goal is to give the cardiologist and radiologist a framework for recognizing patterns of CHD in adult patients. Although the primary focus of this Atlas is adult CHD, pediatric CHD cases prior to palliative or corrective procedures are also included to allow a better understanding of anatomy and pathophysiology. The Atlas is a result of the work of a select group of adult and pediatric cardiologists and radiologists, and every attempt has been made to present the most updated information. We expect you will find this book invaluable in the care of adults with CHD.

Cincinnati, OH, USA — Wojciech Mazur
St. Louis, MI, USA — Marilyn J. Siegel
Kraków and Wrocław, Poland — Tomasz Miszalski-Jamka
Cincinnati, OH, USA — Robert Pelberg

## References

1. Gatzoulis MA, Webb GD. Adults with congenital heart diseases: a growing population. In: Gatzoulis MA, Webb GD, Daubeney PEF, editors. Diagnosis and management of adult congenital heart disease. Edinburgh: Churchill Livingstone; 2003. p. 3–5.
2. Warnes CA, Liberthson R, Danielson GK, et al. Task force 1: the changing profile of congenital heart disease in adult life. J Am Coll Cardiol. 2001;37:1170–5.
3. Taylor AJ, Cerqueira M, Hodgson JM, Mark D, Min J, O'Gara P, Rubin GD; American College of Cardiology Foundation Appropriate Use Criteria Task Force; Society of Cardiovascular Computed Tomography; American College of Radiology, American Heart Association; American Society of Echocardiography; American Society of Nuclear Cardiology; North American Society for Cardiovascular Imaging; Society for Cardiovascular Angiography and Interventions; Society for Cardiovascular Magnetic Resonance. ACCF/SCCT/ACR/AHA/ASE/ASNC/NASCI/SCAI/SCMR 2010 Appropriate Use Criteria for Cardiac Computed Tomography. A Report of the American College of Cardiology Foundation Appropriate Use Criteria Task Force, the Society of Cardiovascular Computed Tomography, the American College of Radiology, the American Heart Association, the American Society of Echocardiography, the American Society of Nuclear Cardiology, the North American Society for Cardiovascular Imaging, the Society for Cardiovascular Angiography and Interventions, and the Society for Cardiovascular Magnetic Resonance. J Cardiovasc Comput Tomogr. 2010;4:407.e1–7.e33.

# Contents

# Part I

# Cardiac Embryology and the Normal Heart

# Cardiac Embryology

# 1

A minimum basic knowledge regarding cardiac embryogenesis is necessary to facilitate understanding congenital heart malformations. This chapter is meant as a basic overview to achieve this end and is not meant to fully encompass the totality of this complex subject.

The human embryo at the primitive streak stage (about 15 days after fertilization) is morphologically symmetrical [1]. The primordia of the cardiovascular system originate as clusters of paired, symmetrical mesenchymal cells in the coelomic mesoderm. These cells migrate and multiply and in some cases resorb to ultimately form the mature human heart. Errors in this process lead to congenital heart defects.

Initially located on the cephalad and dorsal aspect of the embryo, the mesenchymal cells migrate around the buccopharyngeal membrane of the forming foregut and join at the midline of the ventral aspect of the embryo. Subsequent infolding and fusion of primitive tissue along its long axis transforms a flat structure into a tubular shape. Initially, the cardiovascular primordia lie within the cephalad section of the undivided coelomic cavity. The right and left intracoelomic cavities approach the midline and join together, forming a midline thoracic cavity (the pericardium), which surrounds the primitive heart [1–3].

At first, the primitive heart is a straight median tube called the straight tube heart (Fig. 1.1a). The arterial and venous ends are relatively fixed in space requiring that the growth of the bulboventricular segments occur by bending of the cardiac tube. Soon, the primitive cardiac tube develops constrictions which define four future segments: atria, ventricle, bulbus cordis, conus, and truncus arteriosus (Fig. 1.1b) [2–4]. The cranial-most area is the bulbus conus, which connects cranially with the truncus arteriosus, which in turn connects to arterial structures (aortic arches and the dorsal aorta). Caudal to the bulbus cordis is the primitive ventricle. The caudal-most structure of the primitive heart is the primitive atrium, which connects to the sinus venosus, which in turn connects to the omphalomesenteric veins. At day 21–23, all structures are connected in series. There is no inner circulation, and the heart is simply a hollow, empty tube. The heart tube starts to beat on day 22, but circulation does not begin until days 27–29 [2–4].

The caudal-most areas, the primitive atrium and sinus venosus, are the primary determinants of atrial sidedness (situs). The atria are fixed in position early in development by the sinus venosus and its entering veins [5]. Errors in the early stage of heart tube development will result in abnormalities of atrial position (situs). Since atrial situs corresponds to visceral situs, abnormalities of atrial situs are often associated with abnormalities in the situs of other organs.

W. Mazur et al., *CT Atlas of Adult Congenital Heart Disease*,
DOI 10.1007/978-1-4471-5088-6_1, © Springer-Verlag London 2013

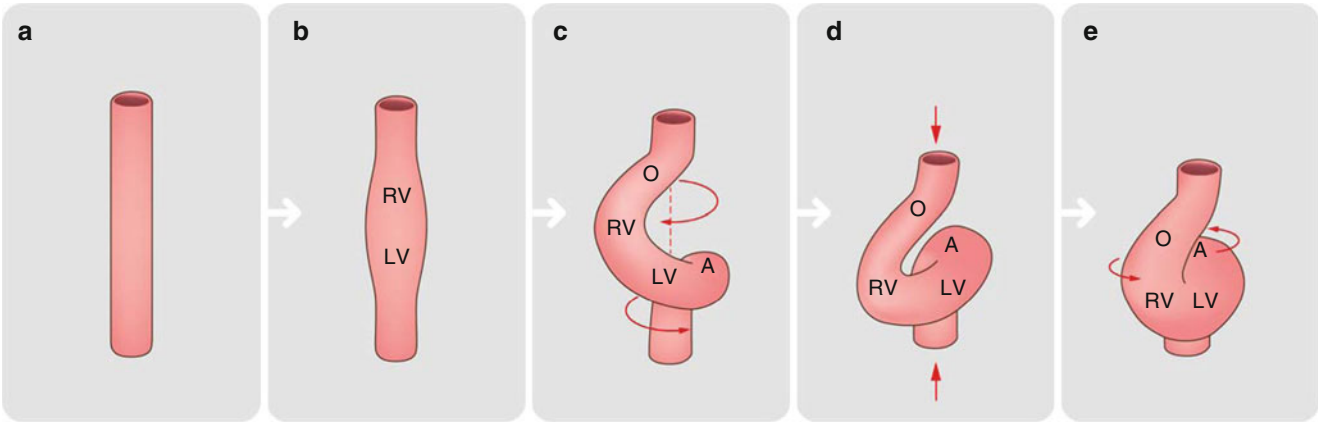


**Fig. 1.1** Looping of the primitive heart tube. Straight heart tube (**a**) curves ventrally (**b**) and twists around its craniocaudal axis to form a C-shaped loop (**c**). Subsequently, the distance between its cranial and caudal ends shortens (**d**) and the loop untwists with the ventral and leftward shift of the outflow tract, ventral shift of the primitive right ventricle and rightward shift of the atrioventricular canal (**e**). *RV* embryonic right ventricle, *LV* embryonic left ventricle, *O* common outflow tract, *A* common atrium

## 1.1 Ventricular Development and Cardiac Looping

The primitive heart tube continues to develop by continuous cellular migration and multiplication. On approximately day 23, the embryonic heart becomes morphologically asymmetric due to the right or left looping of the bulboventricular segments, forming either a rightward loop (dextra or D-loop) or a leftward loop (levo or L-loop), respectively (Fig. 1.1c) [6]. This process likely occurs due to differential migration and multiplication of primordial cardiac cells.

The bulbus cordis produces the morphologic right ventricle while the morphologic left ventricle is formed from the ventricle of the bulboventricular loop. Thus, the direction of the initial cardiac loop determines the eventual ventricular locations. During the looping process, the orientation of the heart changes from an anterior/posterior orientation to a left/right orientation and irreversibly establishes the relationship between the ventricles and the already-determined situs of the atria.

It should be noted that the bulboventricular looping (rightward or leftward) is independent of the process that determines the relative atrial positions (situs). While the atrial sidedness is determined by processes that determine visceral situs, the anatomical relationships between the ventricles and the aortic and pulmonary trunks are decided by the looping process. In D-looping, the bulbus cordis (future morphologic right ventricle) is to the right of midline and the bulboventricular segment (future morphologic left ventricle) is to the left. Conversely, in L-looping, the bulbus cordis (future right ventricle) is to the left of the bulboventricular segment (future left ventricle). D-loop is the normal (situs) cardiac loop and L-loop is a mirror image (inversus) loop.

As the heart tube loops, the bulboventricular segment acquires a U shape, causing the atrium and sinus venosus to become dorsal structures (Fig. 1.1d) [2].

Additionally, the looping pattern of the bulboventricular segments determines the irreversible relationship between the fourth and the sixth aortic arches which ultimately form the distal aortic and pulmonary trunks. Thus, bulboventricular looping patterns permanently determine the anatomic relationship between the aortic and pulmonary trunks. In D-looping with normal development, the pulmonary artery is located anteriorly, superiorly, and to the left of the aorta. In L-looping, the pulmonary artery is located anteriorly, superiorly, and to right of the aorta.

Figure 1.2 depicts D-looping versus L-looping.

Alterations in looping patterns can lead to four basic morphologic combinations: situs solitus with D-looping, situs solitus with L-looping, situs inversus with D-looping, or situs inversus with L-looping. Situs solitus refers to the correct sidedness of the morphologic atria and inversus refers to incorrect morphologic atrial sidedness. D-looping refers to correct ventricular sidedness and L-looping refers to a reversal of the morphologic ventricular sidedness.

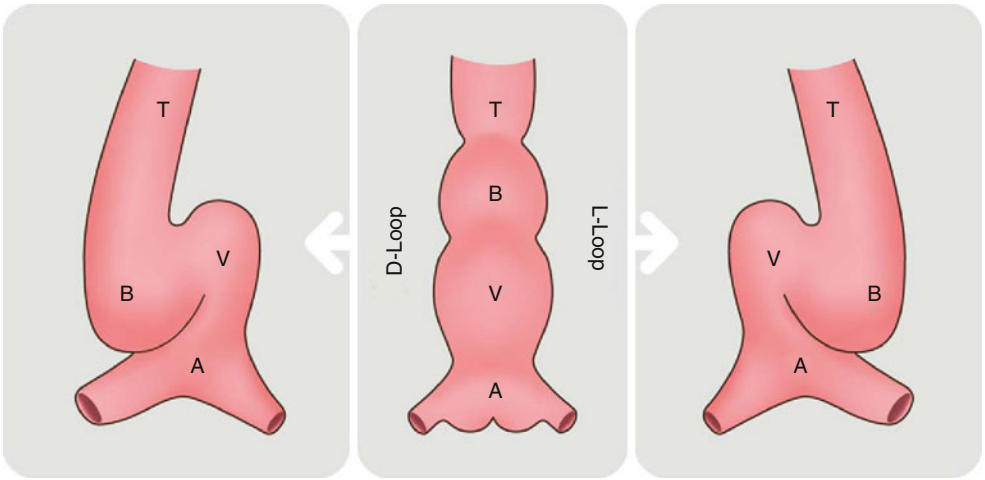


**Fig. 1.2** Diagram illustrates looping (bending) of the primitive cardiac tube. The cardiac tube is depicted from anterior view. The cardiac tube is comprised of the atrium (*A*), ventricle (*V*), bulbus cordis (*B*), and truncus arteriosus (*T*). The cardiac tube normally bends to right, forming a D-bulboventricular loop (D-loop). Rarely, the tube may bend leftward, forming L-bulboventricular loop (L-loop)

**Table 1.1** Depiction of the various situs and looping combinations

| Situs/loop type | Morphologic right ventricle | Morphologic right atrium | Morphologic left ventricle | Morphologic left atrium |
|---|---|---|---|---|
| Situs solitus/D-loop (normal) | Right sided<br>Connects with morphologic RA | Right sided<br>Connects to the morphologic RV | Left sided<br>Connects to the morphologic LA | Left sided<br>Connects to the morphologic LV |
| Situs solitus/L-loop | Left sided<br>Connects to the morphologic LA | Right sided<br>Connects to the morphologic LV | Right sided<br>Connects to the morphologic RA | Left sided<br>Connects to the Morphologic RV |
| Situs inversus/D-loop | Right sided<br>Connects to the morphologic LA | Left sided<br>Connects to the morphologic LV | Left sided<br>Connects to the morphologic RA | Right sided<br>Connects to the morphologic RV |
| Situs inversus/L-loop | Left sided<br>Connects to the morphologic LA | Left sided<br>Connects to morphologic RV | Right sided<br>Connects to the morphologic RA | Right sided<br>Connects to the morphologic LV |

Note that the looping pattern (D- versus L-) determines the ventricular relationships and the great artery relationships whereas the situs pattern (solitus versus inversus) determines the atrial sidedness

In the normal situation, situs solitus with D-looping, the morphologic atria are on their respectively correct sides (right atrium on the right, left atrium on the left) and the morphologic ventricles are also on the correct side such that the morphologic right ventricle connects with the right-sided atrium and the morphologic left ventricle connects with the left-sided atrium. In situs solitus with L-looping, the atria are again on their respectively correct sides but ventricles are reversed. The morphologic right ventricle (now anatomically left sided) connects to the left-sided atrium and the morphologic left ventricle (now right sided) connects to the right-sided atrium. In situs inversus with D-looping, the morphologic atria are reversed (right atrium on the left and left atrium on the right) but the ventricles are on their respectively correct sides. The morphologic right atrium (now anatomically left sided) connects to a morphologic left ventricle (left sided), and the morphologic left atrium (right sided) connects to a morphologic right ventricle (right sided). In situs inversus with L-looping, the atria are again reversed and the ventricles are also reversed. The morphologic left atrium (now right sided) empties into a morphologic left ventricle (right sided), and the morphologic right atrium (now left sided) empties into a morphologic right ventricle (left sided) [7].

Abnormalities in looping may also lead to ventricular and great artery transformations.

Table 1.1 depicts the various situs and looping combinations.

## 1.2 Left and Right Ventricular Outflow and Inflow Development

Subsequent to the development of the ventricles and the looping, the relationship between the truncoconal outlets and ventricular inflow structures is simultaneously but separately determined. The early looped cardiac tube has a single inlet (the common atrioventricular canal), which directs the venous blood to the primitive ventricle. The only outlet for this primitive ventricle is a primitive ventricular septal defect (VSD, also known as bulboventricular defect) through which blood is channeled into the bulbus cordis and from there into the common truncoconal tube. The atrioventricular canal eventually acquires a more right-sided position and a direct relationship to the bulbus cordis (Fig. 1.1e). This relationship leads to the maturation of the bulbus cordis into the definitive right ventricle. Simultaneously, the truncus arteriosus undergoes a shift to the left and differential growth that leads to the disappearance of the bulboventricular defect (VSD). Ultimately, the distal part of the bulbus cordis will form the outflow tract of both ventricles while the truncus arteriosus forms the roots of both great arteries.

Persistence of a primitive arrangement (atria to primitive ventricle to bulbus cordis to single truncoconal tube) will result in a double-inlet left ventricle (common AV canal entering the left ventricle only) or double-outlet right ventricle (persistent ventricular septal defect without atrioventricular valves or papillary muscles).

## 1.3 Formation of the Atrial Septum

Normal separation into two atrial cavities is a complex process involving formation of a septum primum and secundum, fusion of the septa with adjacent structures, and then resorption of septal tissue. At about day 35, atrial septation begins when the common atrium is indented by the bulbus cordis and truncus arteriosus, leading to formation of the septum primum, which arises on the posterosuperior aspect of the roof of the common primitive atrium medial to the entrance of the common venous sinus [8].

The septum primum grows caudally and anteriorly until it meets the growing endocardial cushions of the atrioventricular canal. Initially the septum primum has a defect connecting the two atria, called the ostium primum. This transient defect is closed when the anterior and the posterior medial endocardial cushions fuse. Before this fusion occurs, the septum secundum appears to the right of the septum primum. It also descends from the roof of the primitive atrium and it fuses with the septum primum except for an area in the posterosuperior part of the septum primum which continues to exist as the fossa ovalis. At about 42 days, the septum primum completely resorbs and the edge of the septum secundum then forms the rim of the fossa ovalis, which allows oxygenated blood from the inferior vena cava to cross into the left atrium in utero (Fig. 1.3) [9].

Defects in atrial division into two chambers produce the following atrial septal defects which occur in predictable locations:

1. Ostium primum ASD: caused by lack of fusion of the two endocardial cushions. The defect is in the caudal aspect of both the septum primum and secundum.
2. Secundum ASD: results from over resorption of the septum primum. The defect is located at the fossa ovalis.
3. Sinus venosus ASD: results from failure of formation (or resorption) of the septum secundum. This defect is located at the junction of the superior vena cava with the right atrium and is associated with anomalous drainage of the pulmonary veins.
4. Coronary sinus ASD: results from failure of development of the terminal section of the coronary sinus. It is located in the caudal posterior atrium, above the normal site of drainage of the coronary sinus.
5. Single atrium ASD: failure of complete formation of the atrial septum.

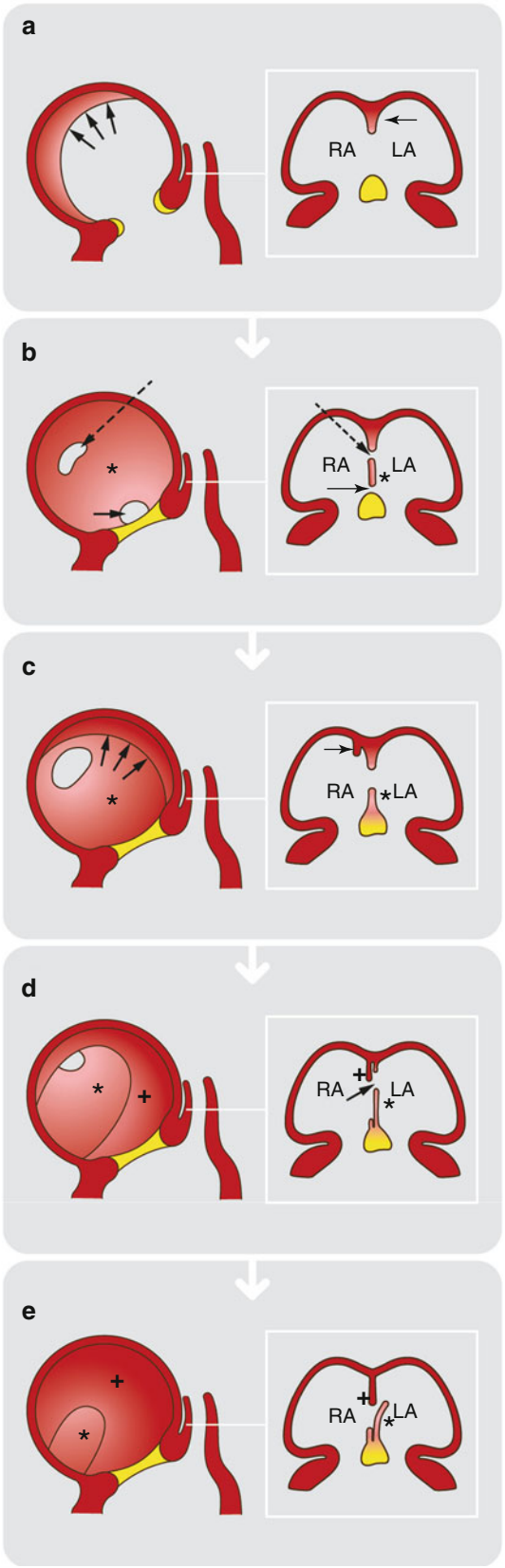


## 1.4 Formation of the Atrioventricular Canal and Interventricular Septum

Total closure of the ventricular septum (usually at 45 days of gestation) is a complex process involving convergence and fusion of the primitive ventricular septum with the posterior and anterior endocardial cushions and the conal ridges (dextro-dorsal and sinistro-ventral). The primitive interventricular septum appears shortly after the looping of the cardiac tube, starting as a muscular fold near the ventricular apex and growing toward the atrioventricular valves. The primary septum separates the primitive ventricle from the bulbus cordis. The upper edge of the primitive ventricular septum borders the bulboventricular defect or primitive VSD. In addition, trabeculations from the inlet region fuse to form a second septum called the inlet interventricular septum, which is in the same plane as that of the atrial septum [2]. The fusion of these two septa forms the bulk of the muscular interventricular septum. The septum then contacts the outflow septum.

The bulboventricular defect or primitive VSD closes by the end of week 7 by growth of the right and left bulbar ridges and the posterior endocardial cushion. The final section of the ventricular septum to close is composed of fibrous tissue (membranous septum), whereas the rest of the septum is composed of myocardial tissue. The normal site of the membranous ventricular septum is just caudal and posterior to the crista supraventricularis, overriding the septal implantation of the tricuspid valve when viewed from the right ventricular side. From the left ventricular side, the membranous septum is located below the aortic valve, between the right and the noncoronary cusps, in front of the bundle of His, and above its anterior subdivision.

Defects in formation of any component of the ventricular septum result in functional communications between both ventricles (ventricular septal defect, VSD) and exist in predictable locations:

**Fig. 1.3** Atrial septation. (**a**) Formation of primary atrial septum at the atrial roof (*arrows*). The atrioventricular cushions are marked in *yellow*. (**b**) The primary septum (*asterisk*) continuous to grow and separates the right and left atrium. The space between the leading edge of the primary septum and fusing atrioventricular cushions (*yellow*) is the primary atrial foramen (*solid arrows*). Before closure of the primary atrial foramen, a number of fenestrations develop at its dorsal portions to form the secondary atrial foramen (*dashed arrows*). (**c**) Formation of the true secondary atrial septum (*arrows*). (**d**) The primary septum forms the flap valve of the oval foramen (*arrow*). In this panel, the secondary septum is noted by the +. (**e**) When formed the secondary foramen in part has no rim, with a border formed by the atrial roof. Much later, subsequently due to separation of the right and left pulmonary veins and incorporations of their orifices to the left atrium, the deep infolding forms the so-called secondary septum. *LA* left atrium, *RA* right atrium, +: secondary septum

1. Perimembranous VSD: failure of complete formation of the membranous septum, resulting in a defect in the left ventricular outflow tract beneath the right and noncoronary cusp of the aortic valve.
2. Supracristal VSD: failure of formation of the infundibular (or conus) ventricular septum. The defect is just below the pulmonary valve in close proximity to the right coronary leaflet of the aortic valve.
3. Atrioventricular canal defect: failure of separation of the ventricular cavities associated with variable defects of the atrioventricular valves.
4. Muscular VSD: failure of formation of the muscular septum, resulting in one or multiple defects in the primitive ventricular septum.
5. Common ventricle: failure of formation of both the primitive ventricular septum and the endocardial cushion components, resulting in absence of the entire septum (occasionally the conal septum may be present).

## 1.5 Aortic and Pulmonary Trunk Formation

In the fifth week of embryogenesis, the bulbus cordis and the truncus arteriosus separate. The cephalad portion of the truncus arteriosus is relatively fixed in space by the branchial arches where the sixth arch (forms the pulmonary artery) is initially posterior to the fourth arch (forms the aorta). Continued growth of the conus (muscular region below the pulmonary valve) forces the root of the pulmonary artery anterior to become continuous with the right ventricular outflow tract. Conus growth also helps form the infundibulum (the separation of the right ventricular inflow and outflow tract).

Normal conus development causes the pulmonary trunk to twist around the ascending aorta. Truncal separation is formed by two truncal ridges, which grow caudally in a spiral fashion during normal development, forming the aorticopulmonary septum. At their caudal extreme, the truncal ridges swell and form outgrowths which are destined to become the semilunar valves (aortic and pulmonary valves) (Fig. 1.4). Thus, proper growth of the conus forces the proximal pulmonary artery anteriorly. The proximal pulmonary artery will then connect with the more posterior portion of the sixth arch (the normal more distal pulmonary artery lies behind the aorta). Contrarily, the aorta arises from the posterior, morphologic left ventricle and becomes continuous with the developing mitral valve proximally and ultimately connects to the more anterior portion of the fourth arch (since the more distal ascending aorta is anterior to the more distal pulmonary artery).

Abnormal conotruncal development leads to transposition of the great arteries (TGA) (discussed in a later chapter) which should be thought of as discordant ventriculoarterial connections without emphasis on the anteroposterior relationship between the aorta and pulmonary artery since this orientation is not mandatory for TGA. Here, the abnormally developing conus may result in the development of the infundibulum below the aortic valve moving it forward to form continuity with the morphologic right ventricle and resulting in the pulmonary artery and valve becoming continuous with the morphologic left ventricle. Most of the time when this abnormality occurs, the spiraling of the truncal ridges fails to occur and the aorta and pulmonary artery are then parallel to each other.

To summarize, when normal, D-bulboventricular looping occurs, the pulmonic valve is located in front of and cranial (anterior and superior) and to the left of the aortic valve. When abnormal, L-bulboventricular looping occurs, there is still a normal relationship between the great arteries but as a mirror image. The aorta, in this situation, arises from a right-sided morphologic left ventricle and the pulmonic valve is located above and cranial (anterior and superior) but to the right of the aortic valve. On the contrary, when transposition develops with a D-loop, the aorta remains to the right of the

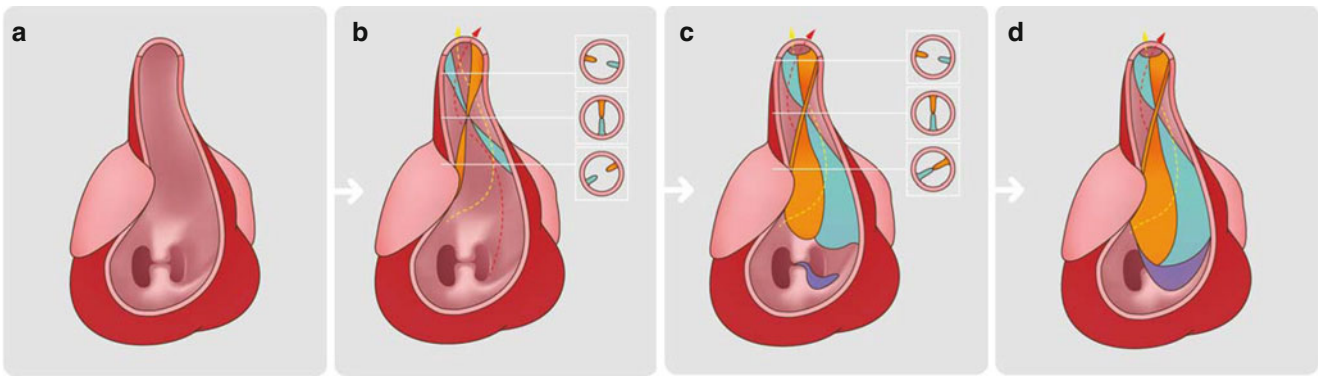


**Fig. 1.4** Conotruncal septation. The outflow tract denoted by the *arrow* in panel (**a**) is separated by the fusion of two longitudinal ridges (panel **b**), which form the spiral septum (panel **c**). The membranous part of interventricular septum is marked in *purple* (panel **d**)

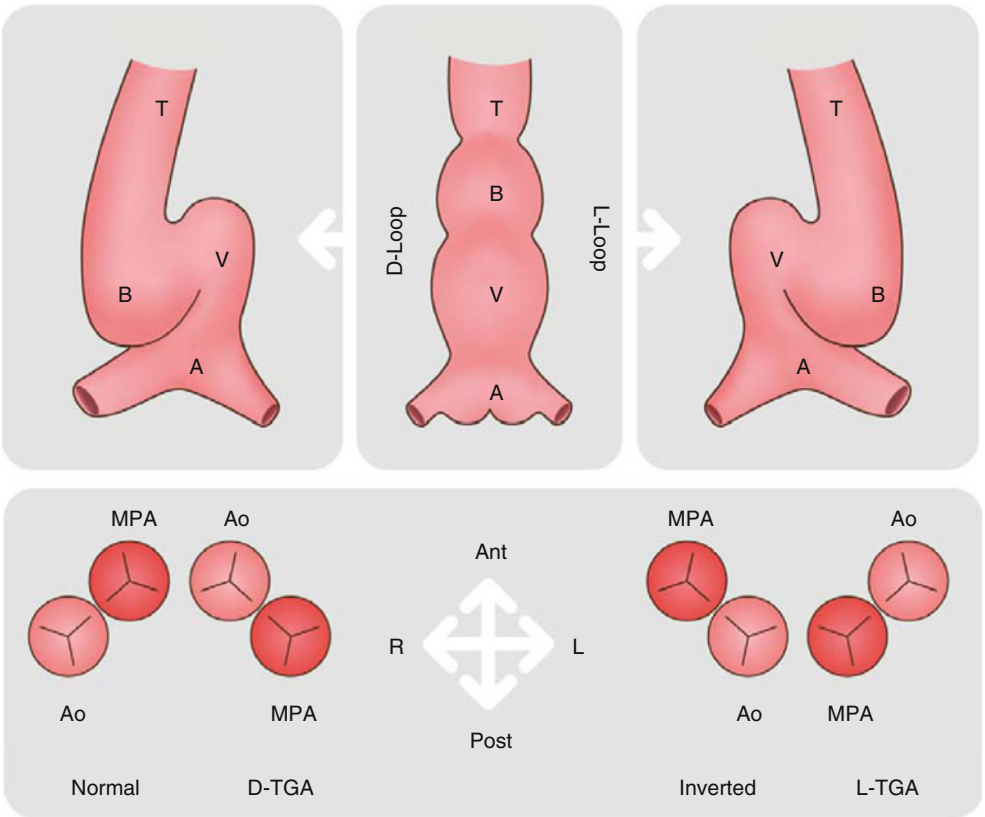


**Fig. 1.5** Artist's rendition of the possible orientation of the great arteries in relation to the various cardiac looping patterns. See text for explanation

transposed pulmonary valve but is now superior (D-TGA). In TGA with an L-loop the aorta remains left of the pulmonary artery and is again superior (L-TGA). See Fig. 1.5.

Other abnormalities of truncoconal formation result in pulmonary artery stenosis and atresia or tetralogy of Fallot. Failure of formation of the entire truncoconal septum produces persistent truncus arteriosus.

## 1.6 The Embryologic Development of Great Arteries

Normal aortic arch development results from the transformation of the branchial arteries. The involution of various branchial arteries and intersegmental arteries results in the adult configuration of the great arteries (Fig. 1.6) [10].

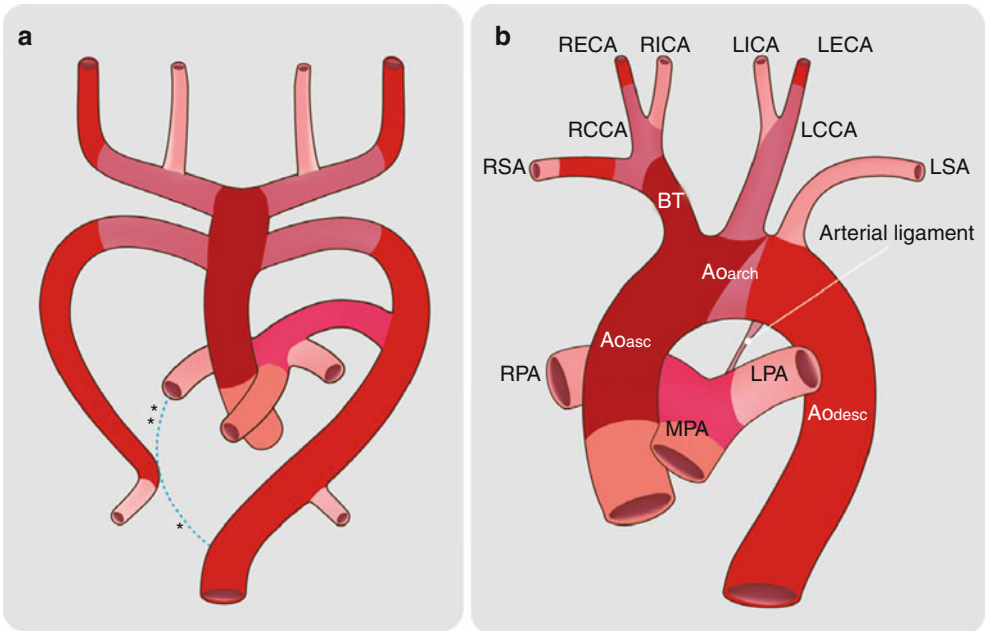


**Fig. 1.6** The embryologic development of the great arteries. Involution of the branchial arches and intersegmental arteries results in the formation of the usual configuration of the great arteries. Panel (**a**) depicts the involution of an intersegmental artery (*asterisks* and *dotted lines*). Panel (**b**) illustrates the usual great artery configuration. The colors of the various normal great artery configuration match the region of the branchial arch tree from which they arose. *Ao asc* ascending aorta, *Ao arch* aortic arch, *Ao desc* descending aorta, *BT* brachiocephalic trunk, *LCCA* left common carotid artery, *LECA* left external carotid artery, *LICA* left internal carotid artery, *LPA* left pulmonary artery, *LSA* left subclavian artery, *MPA* main pulmonary artery, *RCCA* right common carotid artery, *RECA* right external carotid artery, *RICA* right internal carotid artery, *RPA* right pulmonary artery, *RSA* right subclavian artery

## References


1. Angelini P. Embryology and congenital heart disease. Tex Heart Inst J. 1995;22:1–12.
2. Abdulla R, Blew GA, Holterman MJ. Cardiovascular embryology. Pediatr Cardiol. 2004;25:191–200. doi:10.1007/s00246-003-0585-1.
3. Pansky B. Review of medical embryology. New York: Macmillan; 1982. p. 291–355.
4. Van Mierop LHS. Morphological development of the heart. In: Berne RM, Sperelakis N, Geiger SR, editors. Handbook of physiology, section 2: the cardiovascular system. Bethesda: American Physiological Society; 1979. p. 1–28.
5. Vanpraagh R, Vanpraagh S, Vlad P, Keith JD. Anatomic types of congenital dextrocardia: diagnostic and embryologic implications. Am J Cardiol. 1964;13:510–31.
6. Kathiriya IS, Srivastava D. Left-right asymmetry and cardiac looping: implications for cardiac development and congenital heart disease. Am J Med Genet. 2000;97:271–9.
7. Shaher RM, Duckworth JW, Khoury GH, Moes CA. The significance of the atrial situs in the diagnosis of positional anomalies of the heart. I. anatomic and embryologic considerations. Am Heart J. 1967;73:32–40.
8. Steding G, Seidl W. Cardiac septation in normal development. In: Nora JJ, Talao A, editors. Congenital heart disease: causes and processes. New York: Futura; 1984. p. 481–500.
9. Wenink AC, Gittenberger-de Groot AC. The role of atrioventricular endocardial cushions in the septation of the heart. Int J Cardiol. 1985;8:25–44.
10. Pelberg R, Mazur W. Vascular CT angiography manual. London: Springer; 2011. p. 156–9.

# The Normal Heart

# 2

The heart lies in the middle mediastinum within the pericardial sac. The pericardial sac is formed by two layers: the outer layer known as the fibrous pericardium and the inner layer known as the serous pericardium. The serous pericardium contains two layers: visceral and parietal. The inner visceral layer covers the surface of heart and base of the great vessels. At the level of the great vessels, it reflects and becomes the parietal layer, which lines the thick fibrous pericardium. The fibrous pericardium fuses with the base of the great vessels and the diaphragm and it is attached to the sternum by the sternopericardial ligament.

The pericardial cavity is the potential space between the visceral and parietal serous layers. It contains a small amount of serous fluid, known as pericardial fluid. There are two recesses within this cavity: the transverse sinus and the oblique sinus. The transverse sinus is bounded anteriorly by the aorta and pulmonary artery and posteriorly by the roof of the left atrium and the right pulmonary artery. Laterally, the transverse sinus communicates with the rest of pericardial cavity. The oblique sinus is a blind-ending cavity behind the left atrium. Its borders are formed by reflections of serous pericardium. The upper border is formed by the pericardium between the superior pulmonary veins, the right border by the pericardium around the right pulmonary veins and inferior vena cava, and the left border by the pericardium around the left pulmonary veins (Fig. 2.1).

Figure 2.2: CT image demonstrating the transverse and oblique sinuses.

W. Mazur et al., *CT Atlas of Adult Congenital Heart Disease*,
DOI 10.1007/978-1-4471-5088-6_2, © Springer-Verlag London 2013

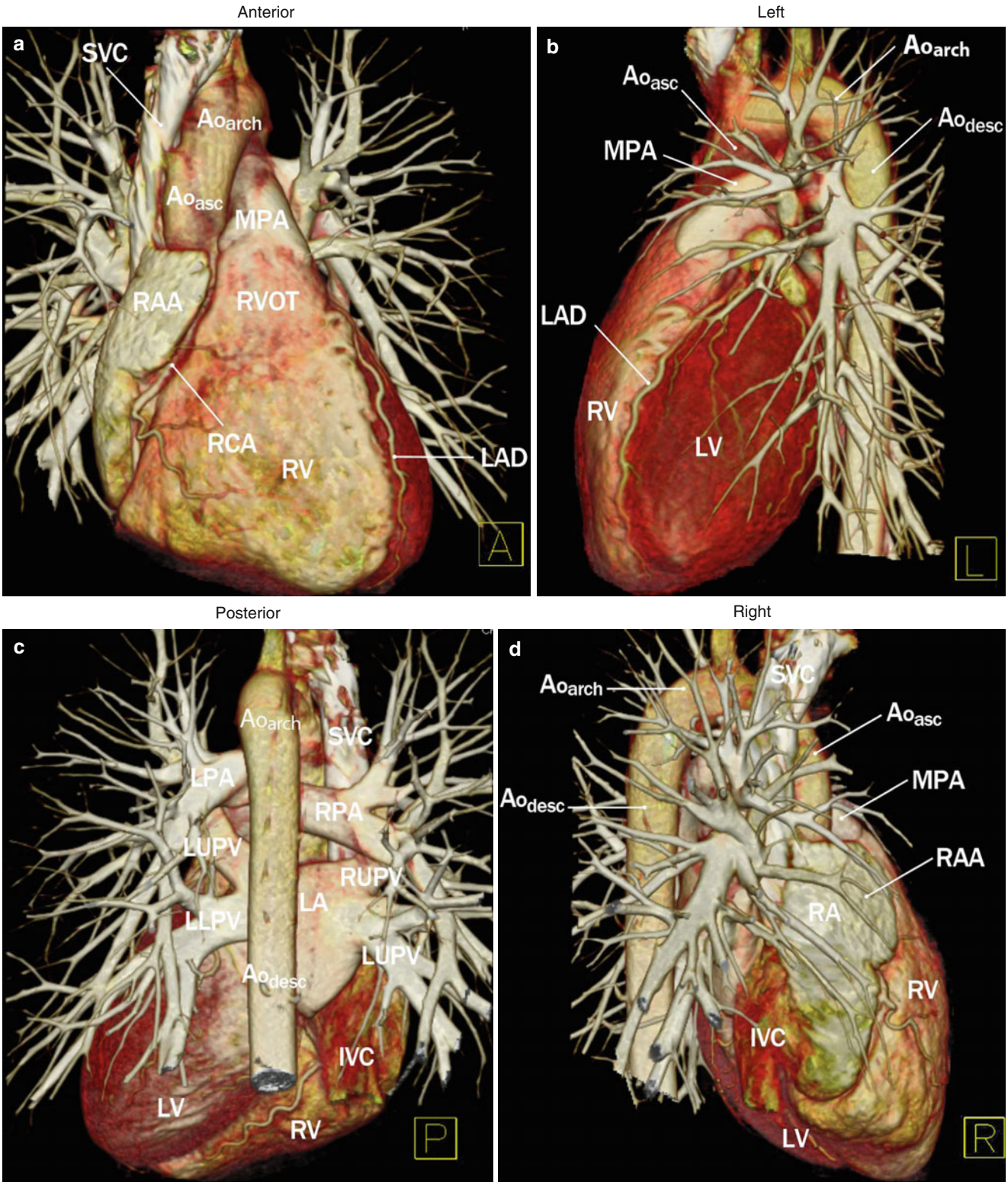


**Fig. 2.1** A 3D volume-rendered depiction of the normal heart. Panel (**a**) anterior view. Panel (**b**) left view. Panel (**c**) posterior view. Panel (**d**) right view. Panel (**e**) superior view. Panel (**f**) inferior view. $Ao_{arch}$ aortic arch, $Ao_{asc}$ ascending aorta, $Ao_{desc}$ descending aorta, *IVC* inferior vena cava, *MPA* main pulmonary artery, *LA* left atrium, *LAD* left anterior descending coronary artery, *LLPV* left lower pulmonary vein, *LPA* left pulmonary artery, *LUPV* left upper pulmonary vein, *LV* left ventricle, *PDA* posterior descending coronary artery, *RA* right atrium, *RCA* right coronary artery, *RPA* right pulmonary artery, *RLPV* right lower pulmonary vein, *RUPV* right upper pulmonary vein, *RV* right ventricle, *RVOT* right ventricular outflow tract, *SVC* superior vena cava, *RAA* right atrial appendage

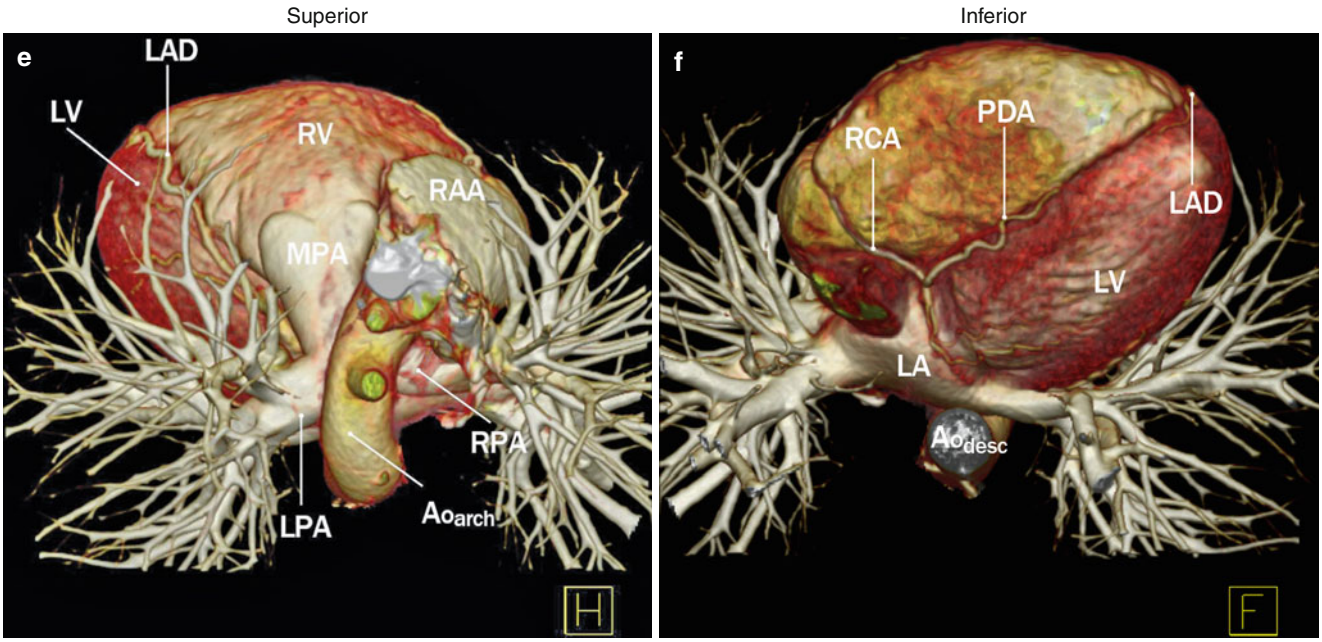


**Fig. 2.1** (continued)

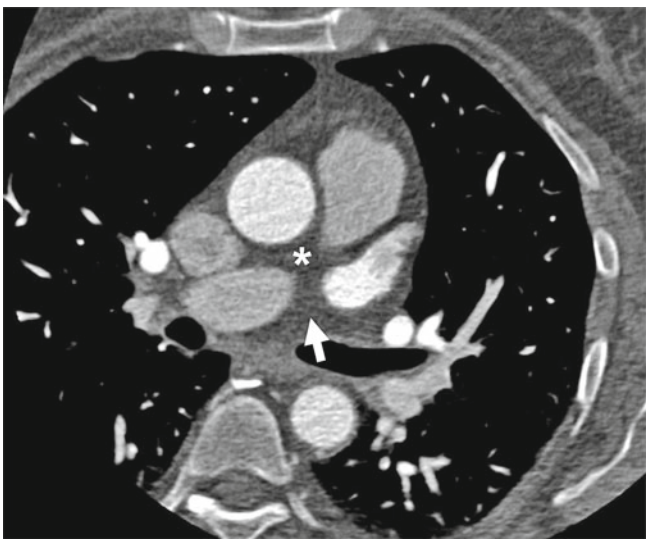

**Fig. 2.2** A CT image illustrating the transverse (*asterisk*) and oblique sinuses (*arrow*)

## 2.1 Right Atrium

The right atrium (RA) lies to the right and anterior to the left atrium (LA). It contains three basic components: the venous component, the appendage, and the vestibule of the tricuspid valve (Fig. 2.3).

The triangular-shaped right atrial appendage is separated externally from the superior and inferior vena cava by the terminal groove. Internally, the terminal groove corresponds to the location of the terminal crest which extends inferiorly from the left side of the superior vena cava (SVC) entrance to the right side of the inferior vena cava (IVC) opening where it ramifies into an isthmus between the IVC and tricuspid valve (cavotricuspid isthmus) [1, 2]. The most characteristic feature of the morphology of the right atrial appendage is the pectinate muscles that extend around the entire parietal margin of the atrioventricular junction. The sinus node is located within this chamber, usually lying to the right of the superior cavoatrial junction [3].

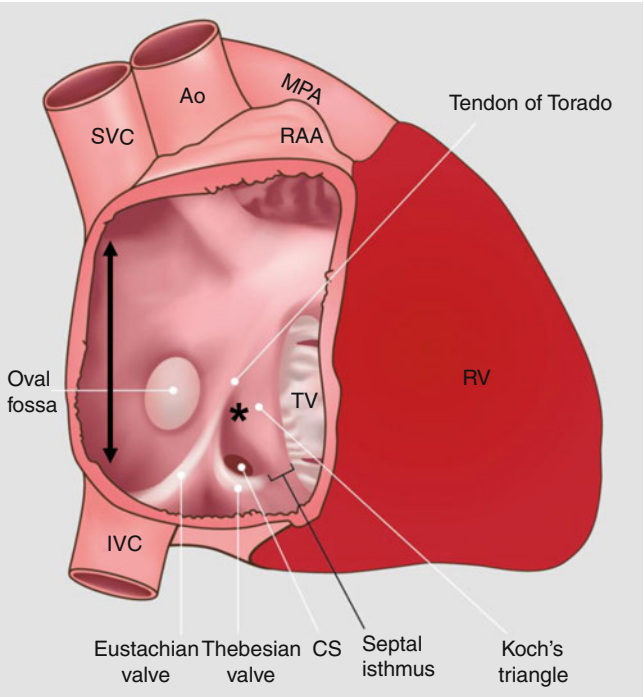


**Fig. 2.3** The anatomy of the right atrium contains three sections: the venous (*double arrow*), appendage (RAA), and the vestibule (*asterisk*). *Ao* aorta, *CS* coronary sinus, *IVC* inferior vena cava, *MPA* main pulmonary artery, *RAA* right atrial appendage, *RV* right ventricle, *SVC* superior vena cava, *TV* tricuspid valve

The venous portion of the right atrium is positioned in the right side of the right atrium. There is no well-defined border between the appendage and the venous component of the right atrium [4]. Superiorly and inferiorly the venous component connects with the SVC and IVC, respectively. The posterior atrial wall between the orifices of the cavae forms the intercaval area [2]. The opening of the SVC has no valve. The IVC orifice is guarded by the Eustachian valve, which extends anteriorly and to the left from the lateral margin of the IVC to the sinus septum (Eustachian ridge) [2, 5]. The coronary sinus enters the RA close to the right side of the IVC ostium. The Thebesian valve, a small crescent-shaped, sometimes fenestrated flap [2], accompanies the coronary sinus orifice.

The posterior aspect of the RA contains the atrial secundum, which is virtually confined to the fossa ovalis. The superior rim of the fossa ovalis is an extensive infolding between the venous component of the right atrium and the right pulmonary veins, while the posterior inferior rim is directly continuous with the sinus septum that separates the orifices of the IVC and the coronary sinus. The anteroinferior margin is adjacent to the triangle of Koch (see description below) [5–7]. The floor of the fossa ovalis is formed by a fibromuscular flap valve that fuses with the rim of the fossa ovalis, resulting in closure of the fossa. In 25–30 % of individuals, the anatomical fusion is incomplete (usually at the anterosuperior margin), leading to interatrial shunting in some individuals [2].

The vestibular component is positioned in the left side of the right atrium and forms the outlet of the RA. It contains the triangle of Koch, which is an anatomical landmark for the atrioventricular node (AV node). The triangle of Koch is demarcated by (a) the tendon of Torado, a fibrous structure formed by the junction of the Eustachian valve (valve of the IVC) and the Thebesian valve (valve of the coronary sinus); (b) the ostium of the coronary sinus posteriorly; and (c) the septal leaflet of the tricuspid valve [5, 8]. Of note, the septal isthmus is not truly septal but rather the inferior part of the anteromedial RA wall [2].

## 2.2 Left Atrium

The left atrium (LA) is located to the left and posterior to the RA. Like the RA, the LA has three basic components: (1) the left atrial appendage, (2) the venous component, and (3) the vestibule of the mitral valve. Unlike the RA, the venous component is considerably larger than the appendage.

The left atrial appendage is positioned at the left atrial margin. In contrast to the RA appendage, it is a smaller, fingerlike structure. It has a discrete junction with the LA venous component, which, unlike the RAA junction, is not marked by a terminal crest or terminal groove. Internally it contains a complex network of muscular ridges (pectinate muscles) and membranes with a comb-like appearance [5].

The venous component is located in the posterior LA and contains the orifices of the pulmonary veins. Typically, four distinct pulmonary venous ostia are present, although anatomical variability frequently occurs [9]. The right and middle lobe veins usually unite, so two trunks from each lung are formed (bilateral superior and inferior veins). The pulmonary veins perforate the fibrous layer of the pericardium and open separately into the upper and back part of the LA. Not infrequently, the two left pulmonary veins have a common opening and the three veins on the right side have separate openings into the left atrium. Occasionally, there is a left middle pulmonary vein. Therefore, the number of pulmonary veins opening into the left atrium can vary between three and five in the healthy population [10, 11].

Internally, ridge-like structures separate the ostia of the superior and inferior pulmonary veins [11]. The left pulmonary vein ostia are positioned more superiorly than the right pulmonary vein ostia. The left pulmonary veins are situated between the LA appendage and the descending aorta. The right pulmonary veins project behind the SVC or the RA. The atrial wall infolding between the entrances of the right pulmonary veins and the SVC forms the superior rim of the fossa ovalis.

The vestibule of the mitral valve forms the outlet of the LA and is positioned to the left and anteriorly in the LA. It forms part of the mitral isthmus which is situated between the left inferior pulmonary vein and mitral valve annulus [12]. The coronary sinus runs externally along the inferior aspect of the vestibular component at a variable distance from the mitral valve annulus and enters the RA.

## 2.3 Cardiac Valves

The cardiac valves are in close proximity to each other. The leaflets of three of the valves are in fibrous continuity, while the pulmonary valve leaflets are exclusively supported by a free-standing muscular infundibulum. The fibrous continuation between the mitral and aortic valve is established by the continuity between the anterior leaflet of the mitral valve (called the aortic leaflet) and the noncoronary and right coronary leaflets of aortic valve (Fig. 2.4). Laterally the fibrous tissue is thickened and forms the right and left fibrous trigones. The right fibrous trigone joins the membranous septum, creating the central fibrous body. Superiorly the aorto-mitral continuity extends into the interleaflet triangles positioned at the level of the noncoronary leaflet of the aortic valve. The central fibrous body brings the aortic and mitral valves into fibrous continuity with the tricuspid valve. The septal leaflet of the tricuspid valve is attached to the right ventricular aspect of the membranous septum which divides the septum atrioventricular and interventricular components. The morphology of the individual cardiac valves is elucidated further in the following sections.

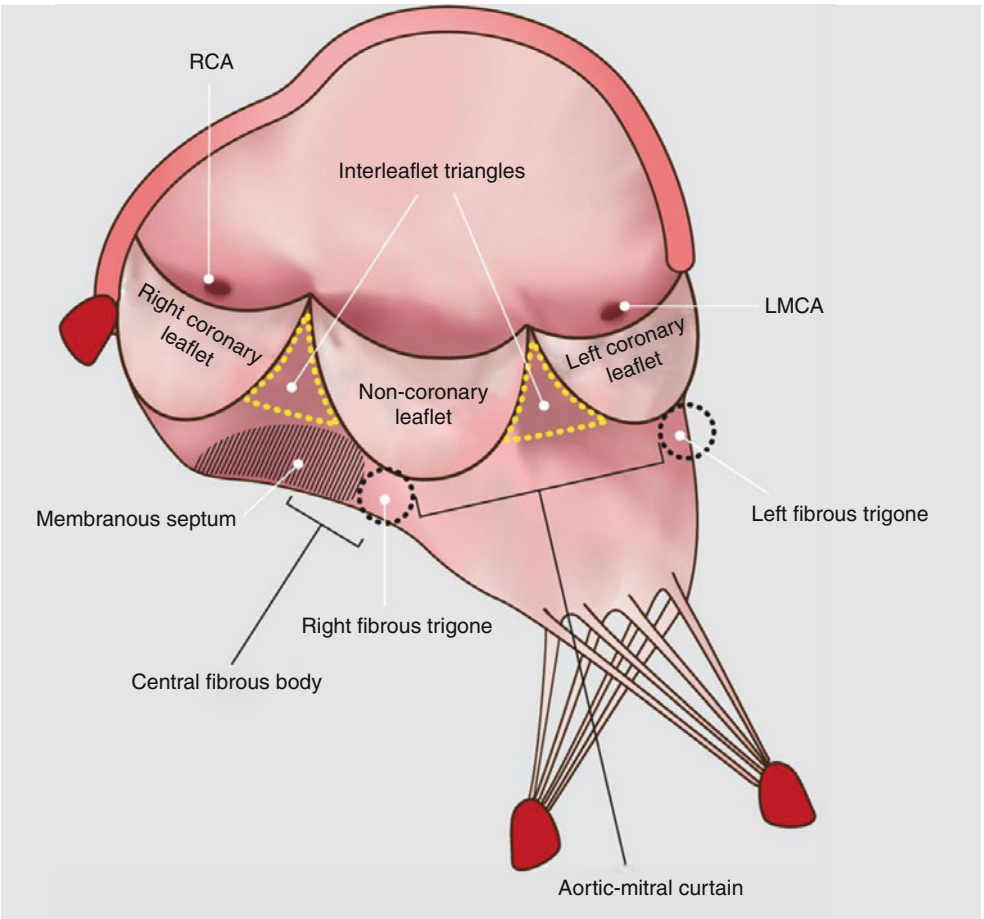


**Fig. 2.4** A rendition of the continuity between the mitral and aortic valves. The membranous septum is in continuation with the right fibrous trigone and the interleaflet triangle between the right and noncoronary aortic valve leaflets. The right fibrous trigone and the membranous septum form the central fibrous body of the heart. *RCA* right coronary artery, *LMCA* left main coronary artery

## 2.4 Right Ventricle and Tricuspid Valve

The right ventricle (RV) extends from the atrioventricular junction toward the left to the cardiac apex and cephalad to the ventriculoarterial junction. The tricuspid and pulmonary valves demarcate the RV from the right atrium and pulmonary trunk, respectively. The RV has three distinct components: (1) the inlet, (2) the apical, and (3) the outlet (Fig. 2.5) [13].

The inlet portion of the right ventricle surrounds the tricuspid valve, extending from its annulus to the insertions of the papillary muscles to the ventricular walls. The tricuspid valve annulus is positioned closer to the cardiac apex than the mitral valve annulus. It divides the membranous septum into atrioventricular (partition between the RV and LA) and interventricular sections (partition between the RV and LV). Generally, the tricuspid valve has three leaflets, although other configurations can be encountered. A distinguishing feature of the tricuspid valve is the direct attachment of its septal leaflet (tendinous cords attach directly to the interventricular septum). The septal leaflet is supported by an inferior papillary muscle (not always present) and a more constant medial papillary muscle. The anterosuperior leaflet is large and is usually supported by a prominent anterior papillary muscle arising from the apical portion of septomarginal trabeculations. The commissure between the septal and anterosuperior leaflets is supported by a medial papillary muscle. The inferior leaflet (also known as the mural or posterior leaflet) attaches to the diaphragmatic aspect of the RV via cords that insert either into small papillary muscles or into the ventricular wall itself.

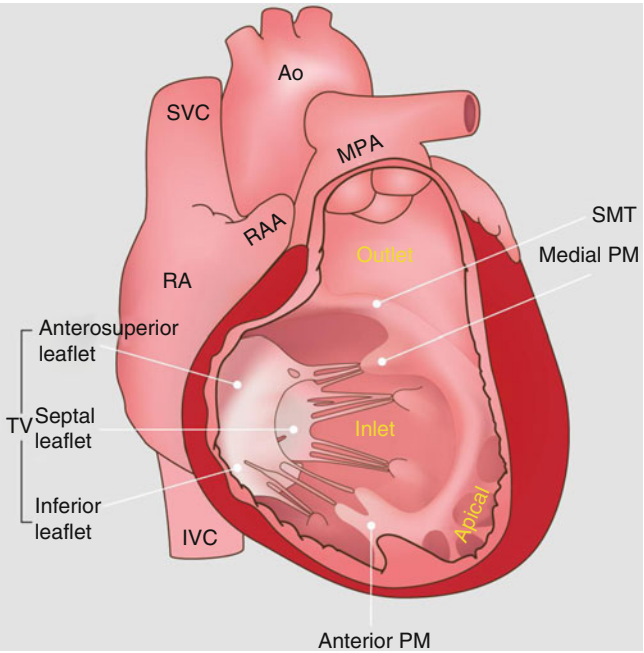


**Fig. 2.5** The anatomy of the right ventricle. Note the presence of the inlet, apical, and outlet components. *Ao* aorta, *IVC* inferior vena cava, *MPA* main pulmonary artery, *PM* papillary muscle, *PV* pulmonary valve, *RA* right atrium, *RAA* right atrial appendage, *SMT* septomarginal trabeculations, *SVC* superior vena cava, *TV* tricuspid valve

The apical trabecular part of the RV extends to the cardiac apex and contains coarse trabeculations.

The outlet portion of the RV consists of the infundibulum, a circumferential muscular structure that supports the leaflets of the pulmonary valve. The infundibulum is contiguous with the supraventricular crest, which comprises the ventriculo-infundibular fold and outlet septum (infundibular septum). The ventriculo-infundibular fold is part of the inner curve of the heart and it separates the tricuspid and pulmonary valves. The outlet septum (infundibular septum) separates the subpulmonary and subaortic outflow tract and also the aortic and pulmonary valve leaflets. The supraventricular crest inserts between the anterosuperior and posteroinferior limbs of septomarginal trabeculation (septal band), which is the muscular strap extending toward the RV apex reinforcing the septal aspect of the RV.

The anterosuperior limb of septomarginal trabeculation extends to the attachment of the pulmonary leaflet, overlying the outlet septum. The posteroinferior limb extends to the interventricular portion of the membranous septum, usually giving rise to the medial papillary muscle. The septomarginal trabeculation also gives rise to other muscular straps. Those trabeculations that extend from the anterior margin of the septomarginal trabeculation to the parietal RV wall form the septoparietal trabeculations. At the RV apex, the septomarginal trabeculation is divided into smaller straps. Some of these extend into the apical part of the RV and some of them support the tension apparatus of the tricuspid valve. One prominent trabeculation becomes the anterior papillary muscle, while another creates a moderator band, which attaches to the anterior papillary muscle and runs to the parietal wall of the RV.

Different segmental models of the RV have been proposed and are generally based on the division of the RV free wall into equal thirds (basal, mid-cavity, and apical) perpendicular to the long axis of the heart. Each level is also circumferentially divided into equal number of segments (i.e., three segments: anterior, lateral, and inferior) [14]. Several distinctive features help to distinguish the RV from the left ventricle. These features include (a) the closer proximity of the tricuspid valve to the apex, (b) the presence of uniformly coarse apical trabeculations, (c) trileaflet configuration of the atrioventricular valve with direct attachment of the septal leaflet to the interventricular septum, (d) presence of more than two papillary muscles, and (e) presence of the moderator band [14].

## 2.5 Left Ventricle and Mitral Valve

The left ventricle (LV) extends from the atrioventricular junction to the left and anterior to the heart apex and cephalad to the ventriculoarterial junction. The mitral and aortic valves separate the LV from the LA and aorta, respectively. Similar to the RV, the LV can be subdivided into three components: (1) inlet, (2) apical, and (3) outlet. The distinction between them, especially between the inlet and outlet portions, is less clear than in the RV.

The inlet component is composed of the mitral valve and its tension apparatus. The mitral valve has two leaflets: anterosuperior (anterior) and posteroinferior (posterior), which are supported by two prominent papillary muscles (anterosuperior and posteroinferior) with tendinous cords. The leaflets of the mitral valve have no direct septal attachments because the deep posterior diverticulum of the left ventricular outflow tract displaces the aortic leaflet away from the interventricular septum. The anterior leaflet is larger, more trapezoidal-like and is attached to approximately one-third of the circumference of the valvular orifice. This leaflet is in fibrous continuity with the aortic valve and, because of this, is often referred to as the aortic leaflet.

The posterior leaflet is smaller, more rectangular-like and is attached to approximately two-thirds of the circumference of the mitral valve annulus. It is divided into several segments that abut the aortic leaflet when the valve is closed. Although generally there are three segments, there may be as many as five or six segments of the posterior leaflet.

An alphanumeric nomenclature has been proposed by Carpentier that divides the leaflets into regions. Three regions are defined on the posterior leaflet as P1–P3 with opposing regions on the anterior leaflet called A1–A3 (Fig. 2.6) [15].

The apical component of the left ventricle extends beyond the papillary muscles to the apex of the heart and has finer trabeculations compared to those of the RV. This characteristic is useful for defining ventricular morphology on diagnostic imaging studies.

The outlet component of the LV supports the aortic valve and consists of both muscular and fibrous portions which is in contrast to the infundibulum of the right ventricle, which is comprised entirely of muscle. The fibrous tissue of the LV outlet forms the posterolateral aspect of the LV outlet and supports the aortic valve leaflets in the area of aorto-mitral continuity and the part of the membranous septum that is continuous with the right fibrous trigone and the interleaflet triangle between the right and noncoronary aortic leaflets. The lateral quadrant of the LV outflow tract is muscular and consists of the lateral margin of the inner curvature of the heart, which is delineated externally by the transverse sinus.

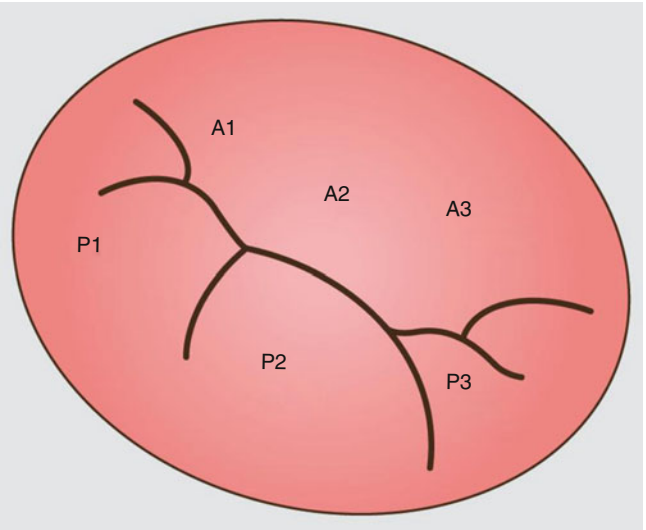


**Fig. 2.6** The segmentation of the anterior (*A*) and posterior (*P*) mitral valve leaflets

The American Heart Association recommendations has standardized a 17 segment model for LV evaluation [16]. The heart is divided into equal thirds perpendicular to the long axis, described as basal, mid-cavity, and apical levels. The basal and mid-cavity level is divided into six equal segments: (1) anterior, (2) anterolateral, (3) inferolateral, (4) inferior, (5) inferoseptal, and (6) anteroseptal. The apical level is divided into four equal segments: (1) anterior, (2) lateral, (3) inferior, and (4) septal. In addition, there is an apical segment formed by the apical cap beyond the end of the apical cavity.

## 2.6 Ventriculoarterial Junctions and Great Arteries and Semilunar Valves

The ascending aorta and main pulmonary artery arise from the LV and RV outlet components, respectively. The aortic and pulmonary roots contain valves with three semilunar cusps (thus called the semilunar valves) arising from dilatations of the arterial wall, termed the bulbous or sinus portions. The aortic and pulmonary roots then course into their respective tubular components with the junctions between the root and tubular section termed the sinotubular junctions. As previously described, the pulmonary root is entirely supported by a muscular, sleeve-like RV infundibulum, while the aortic root is supported by LV muscle and the fibrous continuity between the aortic and mitral valve [17].

The leaflets of the aortic valve has a three-pronged coronet, with each leaflet having attachments to the aorta and the ventricle. The pulmonary valve is constructed similarly. The leaflet attachments, as they extend to the sinotubular junction, are separated by fibrous, interleaflet triangles. The base of the crown is at the level of the basal points of the leaflet hinges within the ventricle, while the top of the crown is adjacent to the anatomic ring of the sinotubular junction [18–21]. The leaflet hinges attach to the ventriculoarterial junction at six points. The section of the arterial wall between the leaflet hinges becomes a hemodynamic ventricular structure, while the region of the ventricle at the base of each sinus becomes a hemodynamic arterial structure. Figure 2.7 presents the spatial relationship of the rings and the semilunar leaflet attachments.

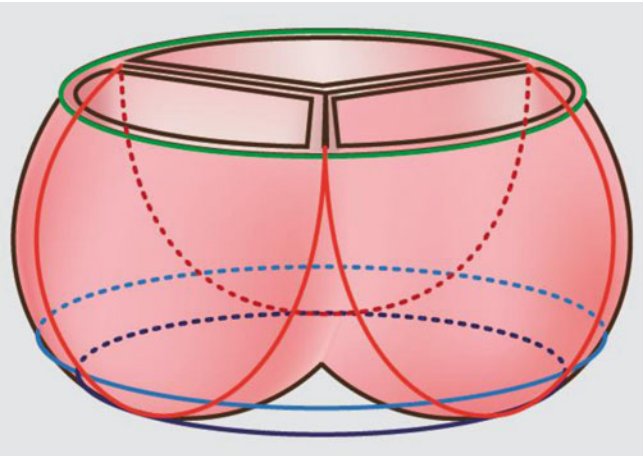

**Fig. 2.7** The aortic root and aortic valve. The leaflets of the aortic valve are attached within the arterial root in a semilunar fashion (*red lines*) and form the three-pronged coronet with leaflet hinges along the crown-like ring. The base of the crown is tangent to the virtual ring, which crosses the most base parts of the leaflet hinges (*navy blue ring*). The true anatomic ring of the ventriculoarterial junction (*blue ring*) crosses the attachment of the semilunar valves in six points. The leaflet attachments extend superiorly toward the sinotubular junction. The most upper portion is tangent to the virtual ring within the distal portion of the aortic root (*green line*)

The aortic root gives origin to the left and right coronary arteries, which arise from aortic sinuses. Two of the three aortic sinuses give rise to coronary arteries. The aortic sinuses and corresponding leaflets are designated according to coronary artery that arises from that particular sinus (left coronary sinus gives rise to the left main coronary artery and right coronary sinus gives rise to the right coronary artery). The left and right coronary leaflets face two leaflets of the pulmonary valve, also called left- and right-facing leaflet, respectively. The third pulmonary valve leaflet is described as nonfacing. The Leiden convention has been introduced to designate the sinuses in malformed hearts. According to this convention, in the normal heart, the right coronary artery arises from sinus #1, while the left coronary artery arises from sinus #2 [22].

The main pulmonary artery runs superiorly and posteriorly, while the ascending aorta passes upward and to the right. Both are covered with a rim of fibrous pericardium. As the main pulmonary artery emerges from the pericardium, it bifurcates into the right and left pulmonary arteries, which course into the hilum of each lung. The right pulmonary artery passes to the right under the aortic arch, posterior to the ascending aorta and SVC and it runs anterior to the esophagus and the right main stem bronchus. The left pulmonary artery travels to the left, anterior to the left main stem bronchus and descending aorta.

When the aorta exits the pericardium, it curves over the right pulmonary artery and travels to the left and posterior as the aortic arch. The aortic arch gives usually rise to (a) the brachiocephalic trunk, which bifurcates into the right common carotid artery and right subclavian artery; (b) the left common carotid artery; and (c) the left subclavian artery. Distal to the origin of the left subclavian artery, the aortic arch is connected with the pulmonary artery via the ligamentum arteriosum, which is the remnant of the ductus arteriosus. At this site, the aortic arch narrows slightly to form the aortic isthmus and continues in the posterior mediastinum as the descending aorta.

## 2.7 Coronary Arteries

The right and left coronary arteries originate from their respective aortic sinuses. The orifices are usually located in the upper third of the sinuses of Valsalva. The orifice of the left coronary artery is superior and posterior to that of the right coronary artery. The dominance of the coronary circulation (right vs. left) usually refers to the artery from which the posterior descending artery originates. Right dominance occurs in 85–90 % of individuals [23]. Left dominance occurs slightly more often in males than females [23].

### 2.7.1 Left Main Coronary Artery

The left coronary artery (LCA) originates from the left coronary sinus as the left main coronary artery (LMCA). The LMCA passes to the left and behind the right ventricular outflow tract and bifurcates into the left anterior descending (LAD) and circumflex (LCX) coronary arteries. In some cases, the LMCA trifurcates into the LAD, LCX, and ramus intermedius artery.

### 2.7.2 Ramus Intermedius Artery

The ramus intermedius (medianus) artery, if present, may run as a diagonal branch or obtuse marginal branch.

### 2.7.3 Left Anterior Descending Artery

From the bifurcation of the left main coronary artery, the LAD courses anteriorly and inferiorly in the anterior interventricular groove along the interventricular septum to the cardiac apex. In most cases, it courses over the apex and terminates at the diaphragmatic aspect of the heart. The LAD gives rise to septal perforator and diagonal branches. The septal perforator branches course perpendicularly into the anterior part of interventricular septum and interconnect with septal branches from the posterior descending artery. The diagonal branches course along the anterolateral wall of the left ventricle and supply the subadjacent myocardium.

### 2.7.4 Left Circumflex Artery

The LCX artery arises from the left main coronary artery and courses in the left atrioventricular groove. As it passes along this groove, it gives rise to obtuse marginal branches, which supply the lateral aspect of left ventricular myocardium as well as atrial branches which supply blood to the left atrium. In 85–95 % of individuals, the LCX terminates near the obtuse margin of the left ventricle [23]. In 10–15 % of individuals with LCA dominance, the LCX gives rise to a posterolateral branch, which continues as the posterior descending artery (PDA) in the posterior interventricular groove [23].

### 2.7.5 Right Coronary Artery

The right coronary artery (RCA) originates from the right sinus of Valsalva and enters the right atrioventricular groove. It curves posteriorly at the acute margin of the right ventricle and crosses the crux (the junction of the posterior interventricular groove with the left and right atrioventricular grooves). The conus (infundibular) artery is usually the first branch off the RCA. It runs superiorly and anteriorly and supplies the right ventricular outflow tract. However, it may also originate directly from the aorta or occasionally from the LCA. In approximately 50–60 % of individuals, the RCA gives rise to the sinoatrial node artery; in the remaining cases, the sinoatrial artery originates from the LCX artery [23].

At the level of the crux, the RCA also gives rise to the atrioventricular nodal artery, which runs upward to the atrioventricular (AV) node. Within the right atrioventricular groove, the RCA gives rise to several smaller marginal branches and a more prominent acute marginal branch which supplies the RV free wall. In the most common setting of RCA dominance, the RCA gives rise to posterolateral branches and continues as the posterior descending artery (PDA) along the posterior interventricular groove. As the PDA passes along the posterior interventricular groove, it gives rise to septal branches, which supply the posterior aspect of the interventricular septum.

## 2.8 Cardiac Veins

The cardiac venous system is generally divided into three systems: (1) coronary sinus and its tributaries, (2) anterior right ventricular veins, and (3) Thebesian veins [24]. The coronary sinus drains into the right atrium. The anterior cardiac veins drain directly into the right atrium. The small Thebesian veins drain directly into the four chambers of the heart.

### 2.8.1 Coronary Sinus

The coronary sinus drains most of the left heart and receives approximately 85 % of coronary venous blood. Its origin is usually defined at the junction of the great cardiac vein and the oblique vein of the left atrium. However, in some classifications, its origin is delineated as the site of the valve of Vieussens (prominent valve in the great cardiac vein where it turns around the obtuse margin to become the coronary sinus) [25]. The coronary sinus courses along the left atrioventricular junction and empties into the posteromedial aspect of the right atrium. The coronary sinus receives blood from the great, middle, oblique, and small cardiac veins. It also receives blood from the left inferior ventricular vein and left marginal vein [25].

### 2.8.2 Great Cardiac Vein

The great cardiac vein (also called anterior cardiac vein or anterior interventricular vein) passes superiorly from the cardiac

apex along the anterior interventricular groove and between the origin of the main pulmonary artery and left atrial appendage. It enters the left atrioventricular groove and terminates in the coronary sinus via the valve of Vieussens [26].

### 2.8.3 Middle Cardiac Vein

The middle cardiac vein (also called inferior interventricular vein or posterior interventricular vein) arises at the apex of the heart and runs superiorly along the posterior interventricular groove and terminates usually in the coronary sinus near its atrial orifice. Occasionally, it may directly enter the right atrium [26].

### 2.8.4 Oblique Cardiac Vein

The oblique cardiac vein (also termed vein of Marshall) descends along the lateral and inferior wall of the left atrium and joints the great cardiac vein to enter the coronary sinus [26, 27]. It is the remnant of the left superior vena cava.

### 2.8.5 Small Cardiac Vein

The small cardiac vein runs along the right coronary artery in the right atrioventricular groove, emptying into the coronary sinus or the right atrium.

### 2.8.6 Inferior Ventricular Vein

The inferior ventricular vein (also termed posterior vein) drains the lateral and diaphragmatic aspects of the LV, emptying into the coronary sinus [26]. However, it may also drain into the great cardiac vein.

### 2.8.7 Left Marginal Vein

The left marginal vein (also called obtuse marginal vein) courses over the left oblique marginal surface of the heart and terminates in the coronary sinus.

### 2.8.8 Anterior Right Ventricular Veins

The anterior right ventricular veins (also called anterior cardiac veins) comprise three or four vessels, which travel along the right ventricular surface in the right atrioventricular groove and open directly into the anterior wall of the right atrium. Unlike the cardiac veins, they do not enter the coronary sinus.

### 2.8.9 Thebesian Veins

The Thebesian veins are small venous tributaries that drain directly into the cardiac chambers. They are found primarily in the right atrium and right ventricle.

Figures 2.8, 2.9, 2.10, 2.11, 2.12, 2.13, 2.14, 2.15, and 2.16 are multiplanar reformats (MPR) computed tomographic (CT) views demonstrating the normal cardiac anatomy as depicted by CT.

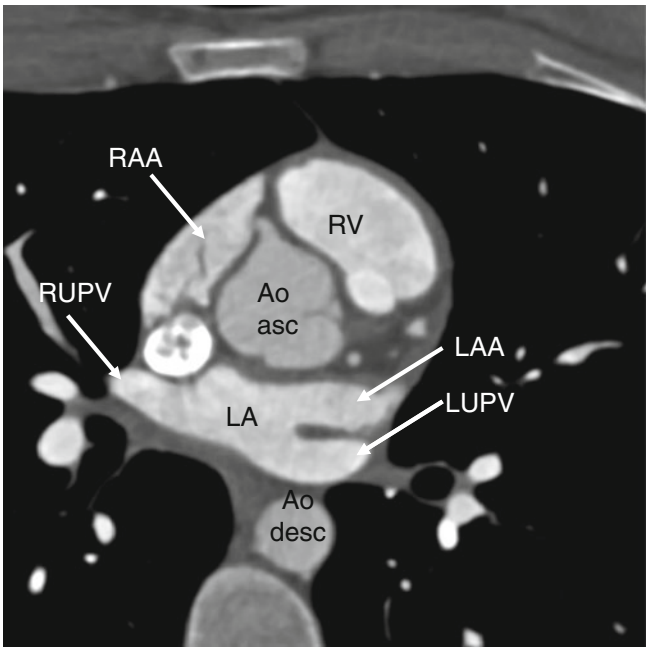


**Fig. 2.8** Normal cardiac anatomy. An axial multiplanar view in a plane just above the aortic valve at the level of the origin of the right coronary artery (RCA ostium). *RAA* right atrial appendage, *RUPV* right upper pulmonary vein, *SVC* superior vena cava, *RA* right atrium, *LA* left atrium, $Ao_{asc}$ ascending aorta $Ao_{desc}$ descending aorta, *LUPV* left upper pulmonary vein, *LAA* left atrial appendage, *RV* right ventricle

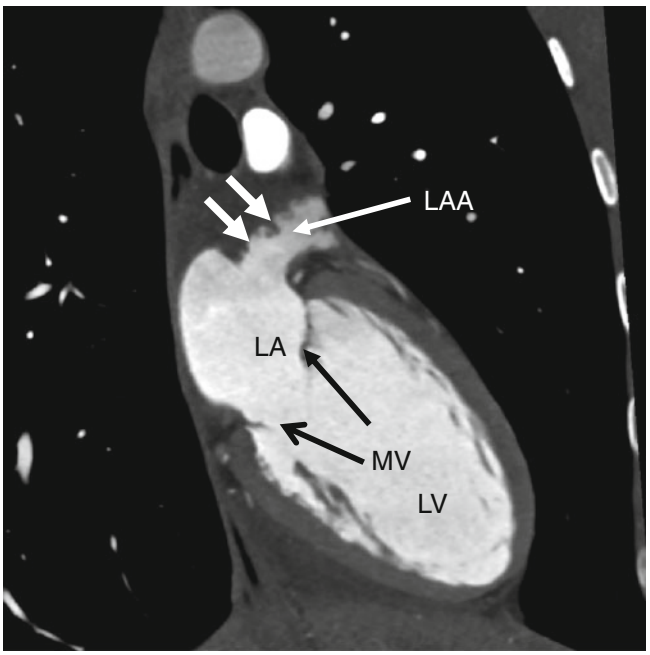


**Fig. 2.9** A transverse two-chamber multiplanar view depicting the normal appearance of the left atrial appendage. Note the discrete opening into the left atrium (LA). Also note the fingerlike pectinate muscles (*white arrows*). *LAA* left atrial appendage, *LV* left atrium, *MV* mitral valve

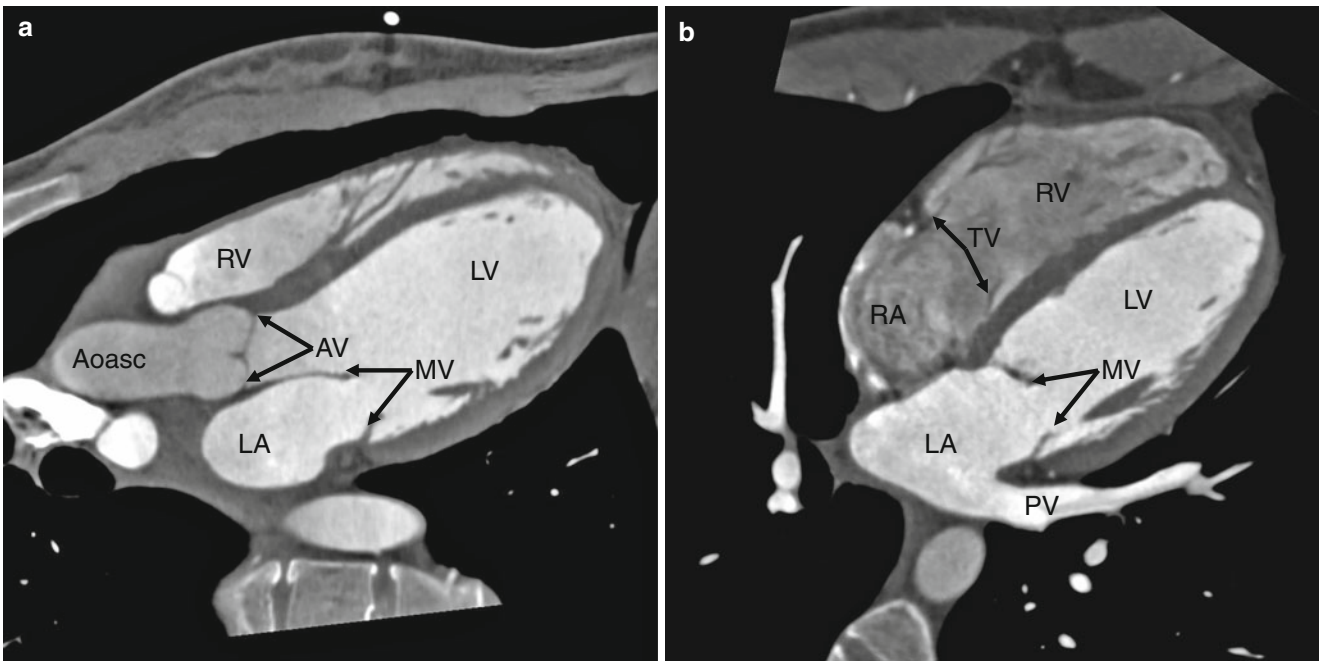


**Fig. 2.10** Panels (**a**) and (**b**) are oblique multiplanar views illustrating the heart in a computed tomographic five-chamber view and four-chamber views, respectively. $Ao_{asc}$ ascending aorta, *RA* right atrium, *RV* right ventricle, *LA* left atrium, *LV* left ventricle, *AV* aortic valve, *MV* mitral valve, *TV* tricuspid valve, *PV* pulmonary vein

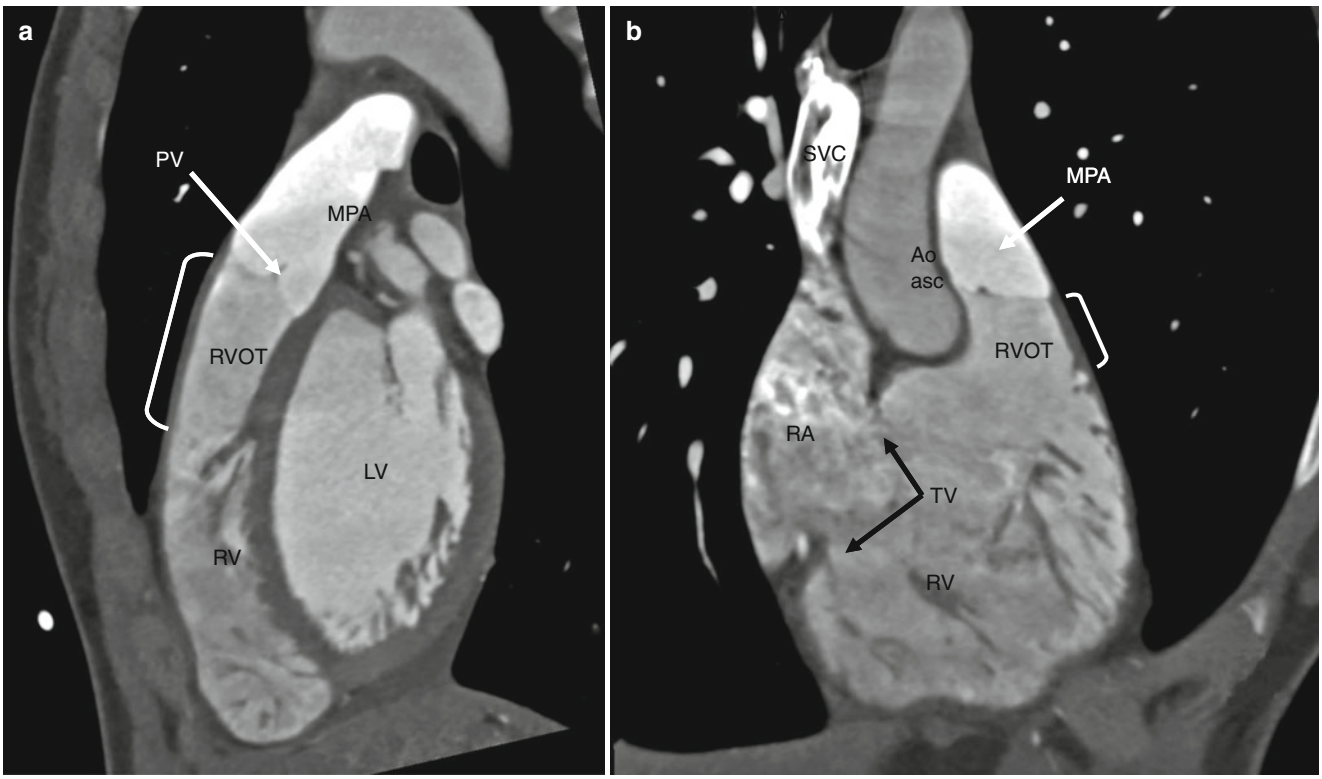


**Fig. 2.11** Normal appearance of the right ventricular outflow tract (*RVOT*). Panels (**a**) and (**b**) demonstrate multiplanar oblique views windowed to highlight the RVOT. Note the muscular infundibulum (*white brackets*). Also note the highly trabeculated appearance of the right ventricle (panel b). *MPA* main pulmonary artery, *PV* pulmonary valve, *RV* right ventricle, *RA* right atrium, *LV* left ventricle, *TV* tricuspid valve, $Ao_{asc}$ ascending aorta, *SVC* superior vena cava

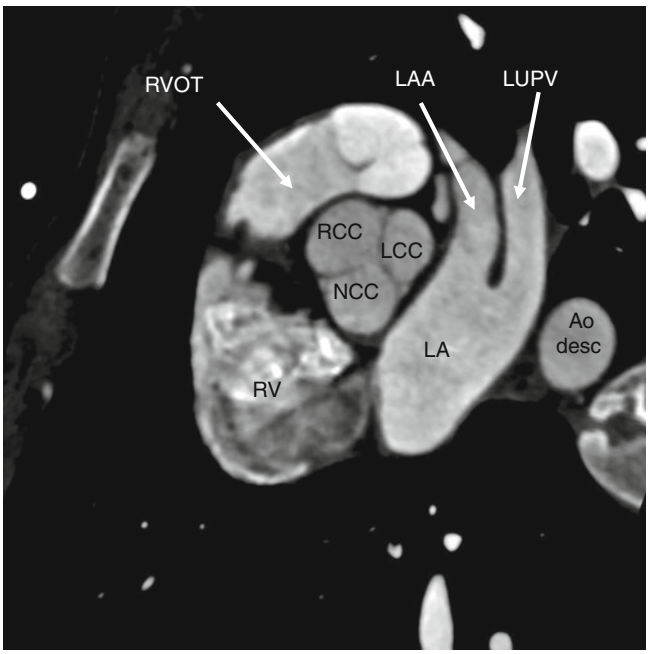


**Fig. 2.12** A multiplanar oblique view at the level of the aortic valve. This image depicts the normal appearing trileaflet aortic valve (*AV*). *LA* left atrium, *RV* right ventricle, *RVOT* right ventricular outflow tract, *PV* pulmonary valve, *LUPV* left upper pulmonary vein, *LAA* left atrial appendage, *Ao Desc* descending aorta, *LCC* left coronary cusp, *RCC* right coronary cusp, *NCC* noncoronary cusp

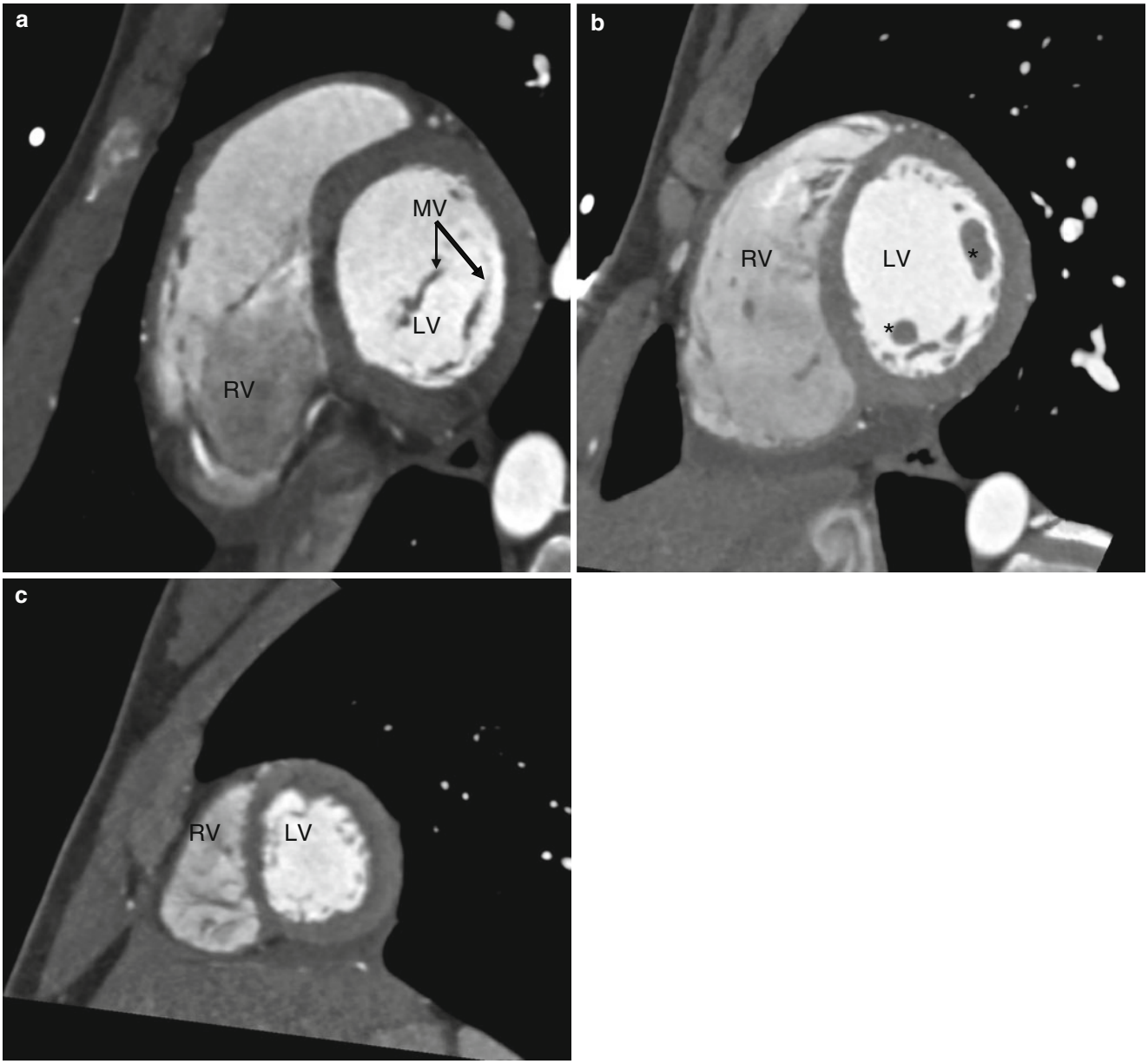


**Fig. 2.13** The normal heart in a multiplanar short-axis reformat at the basal level (panel **a**, level of the mitral valve), mid-level [panel **b**, level of the papillary muscles (*asterisks*)], and apical level (panel **c**). *RV* right ventricle, *LV* left ventricle, *MV* mitral valve

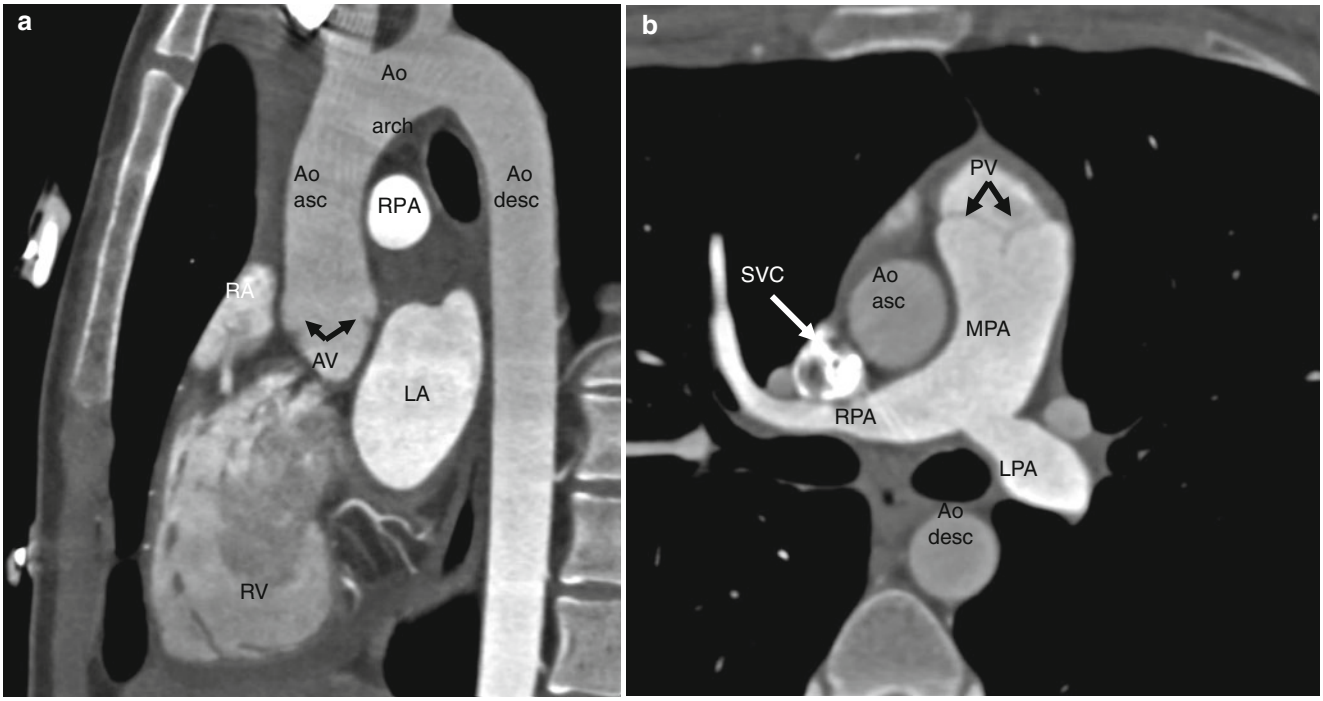


**Fig. 2.14** Panel (**a**) is a multiplanar sagittal view demonstrating the ascending aorta, aortic arch, and descending aorta. Panel (**b**) is an axial view at the level of the bifurcation of the pulmonary artery. Panel (b) is the view standardly used for measuring the size of the ascending aorta. *RA* right atrium, *LA* left atrium, *RV* right ventricle, *AV* aortic valve, $Ao_{asc}$ ascending aorta, $Ao_{arch}$ aortic arch, $Ao_{desc}$ descending aorta, *MPA* main pulmonary artery, *RPA* right pulmonary artery, *LPA* left pulmonary artery, *PV* pulmonary valve, *SVC* superior vena cava

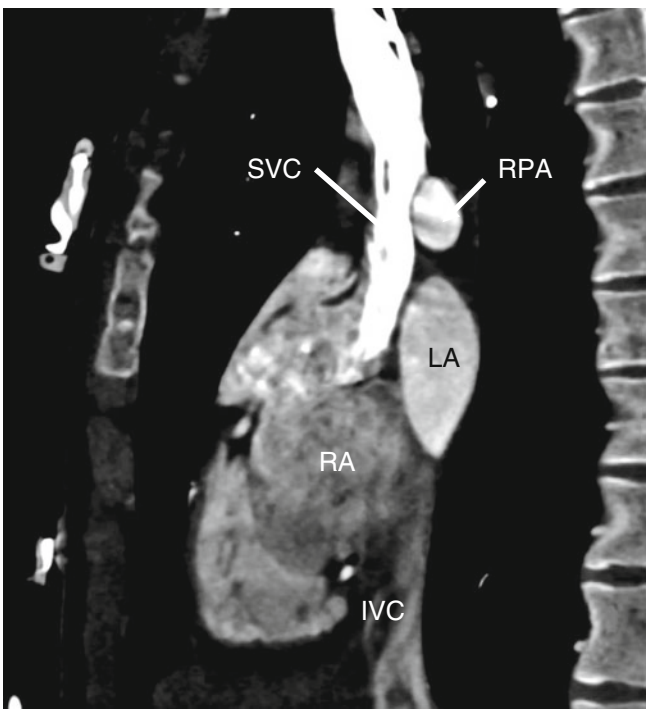


**Fig. 2.15** An oblique multiplanar cut demonstrating the normally appearing bicaval view. *SVC* superior vena cava, *IVC* inferior vena cava, *RA* right atrium, *RPA* right pulmonary artery, *LA* left atrium

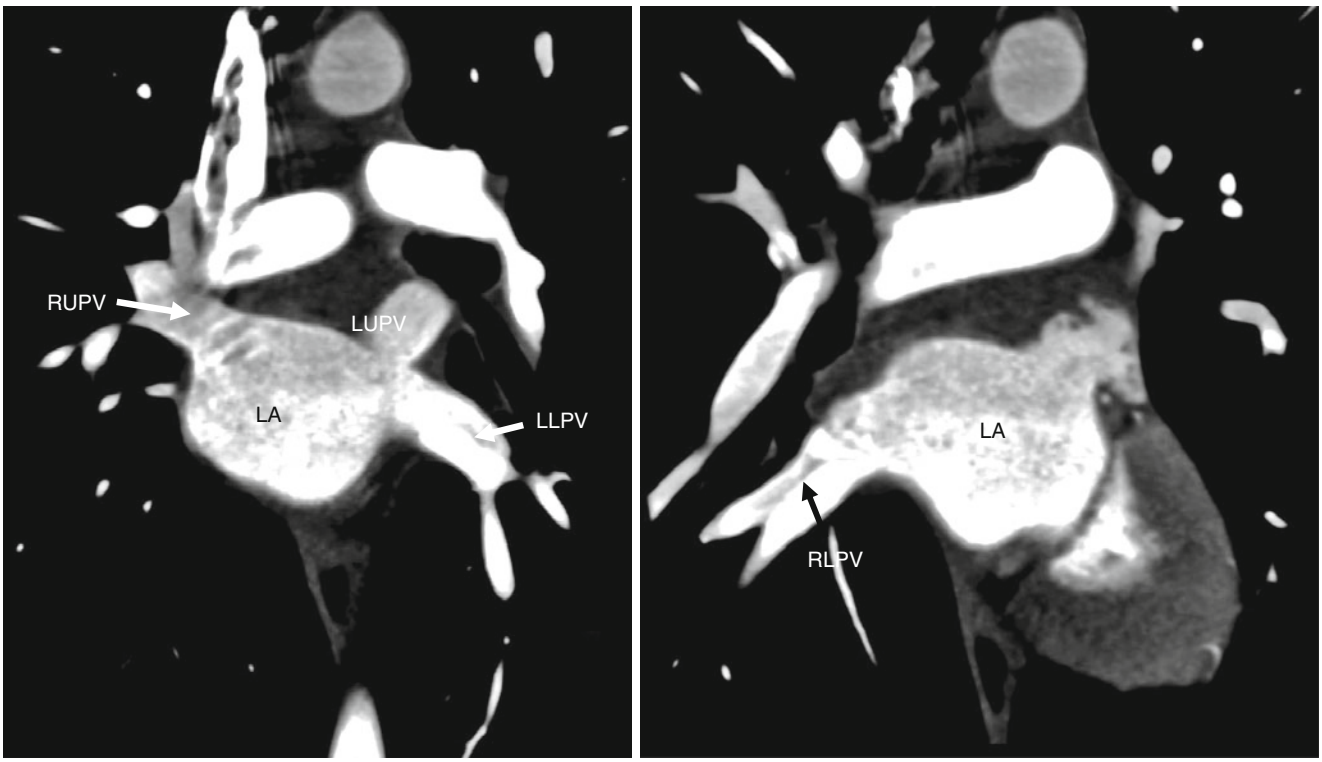


**Fig. 2.16** Oblique multiplanar cuts demonstrating the normal four pulmonary veins as they enter the left atrium. *RUPV* right upper pulmonary vein, *LUPV* left upper pulmonary vein, *RLPV* right lower pulmonary vein, *LLPV* left lower pulmonary vein, *LA* left atrium

## References


1. Sánchez-Quintana D, Anderson RH, Cabrera JA, Climent V, Martin R, Farré J, et al. The terminal crest: morphological features relevant to electrophysiology. Heart. 2002;88:406–11.
2. Ho SY, Sanchez-Quintana D. The importance of atrial structure and fibers. Clin Anat. 2009;22:52–63. doi:10.1002/ca.20634.
3. Truex RC, Smythe MQ, Taylor MJ. Reconstruction of the human sinoatrial node. Anat Rec. 1967;159:371–8. doi:10.1002/ar.1091590406.
4. Anderson RH, Cook AC. The structure and components of the atrial chambers. Europace. 2007;9 Suppl 6:vi 3–9. doi:10.1093/europace/eum200.
5. Corradi D, Maestri R, Macchi E, Callegari S. The atria: from morphology to function. J Cardiovasc Electrophysiol. 2011;22:223–35. doi:10.1111/j.1540-8167.2010.01887.x.
6. Anderson RH, Brown NA. The anatomy of the heart revisited. Anat Rec. 1996;246:1–7.
7. Anderson RH, Brown NA, Webb S. Development and structure of the atrial septum. Heart. 2002;88:104–10.
8. Ho SY, Sanchez-Quintana D, Cabrera JA, Anderson RH. Anatomy of the left atrium: implications for radiofrequency ablation of atrial fibrillation. J Cardiovasc Electrophysiol. 1999;10:1525–33.
9. Fynn SP, Kalman JM. Pulmonary veins: anatomy, electrophysiology, tachycardia, and fibrillation. Pacing Clin Electrophysiol. 2004;27:1547–59. doi:10.1111/j.1540-8159.2004.00675.x.
10. Kaseno K, Tada H, Koyama K, Jingu M, Hiramatsu S, Yokokawa M, et al. Prevalence and characterization of pulmonary vein variants in patients with atrial fibrillation determined using 3-dimensional computed tomography. Am J Cardiol. 2008;101:1638–42. doi:10.1016/j.amjcard.2008.01.053.
11. Kato R, Lickfett L, Meininger G, Dickfeld T, Wu R, Juang G, et al. Pulmonary vein anatomy in patients undergoing catheter ablation of atrial fibrillation: lessons learned by use of magnetic resonance imaging. Circulation. 2003;107:2004–10. doi:10.1161/01.CIR.0000061951.81767.4E.
12. Wittkampf FH, van Oosterhout MF, Loh P, Derksen R, Vonken EJ, Slootweg PJ, et al. Where to draw the mitral isthmus line in catheter ablation of atrial fibrillation: histological analysis. Eur Heart J. 2005;26:689–95. doi:10.1093/eurheartj/ehi095.
13. Goor DA, Lillehei CW. Congenital malformations of the heart: embryology, anatomy, and operative considerations. New York: Grune & Stratton; 1975. p. 1–37.
14. Haddad F, Hunt SA, Rosenthal DN, Murphy DJ. Right ventricular function in cardiovascular disease, part I: anatomy, physiology, aging, and functional assessment of the right ventricle. Circulation. 2008;117:1436–48.doi:10.1161/CIRCULATIONAHA.107.653576.
15. Carpentier A, Branchini B, Cour JC, Asfaou E, Villani M, Deloche A, et al. Congenital malformations of the mitral valve in children. Pathology and surgical treatment. J Thorac Cardiovasc Surg. 1976;72:854–66.
16. Cerqueira MD, Weissman NJ, Dilsizian V, Jacobs AK, Kaul S, Laskey WK, et al. American Heart Association Writing Group on myocardial segmentation and registration for cardiac imaging standardized myocardial segmentation and nomenclature for tomographic imaging of the heart: a statement for healthcare professionals from the Cardiac Imaging Committee of the Council on Clinical cardiology of the American Heart Association. Circulation. 2002;105:539–42.

17. Anderson RH, Freedom RM. Normal and abnormal structure of the ventriculo-arterial junctions. Cardiol Young. 2005;15 Suppl 1:3–16.
18. Piazza N, de Jaegere P, Schultz C, Becker AE, Serruys PW, Anderson RH. Anatomy of the aortic valvar complex and its implications for transcatheter implantation of the aortic valve.Circ Cardiovasc Interv. 2008;1:74–81. doi:10.1161/Circinterventions.108.780858.
19. Anderson RH. Clinical anatomy of the aortic root. Heart. 2000; 84:670–3.
20. Anderson RH, Devine WA, Ho SY, Smith A, McKay R. The myth of the aortic annulus: the anatomy of the subaortic outflow tract. Ann Thorac Surg. 1991;52:640–6.
21. Stamm C, Anderson RH, Ho SY. Clinical anatomy of the normal pulmonary root compared with that in isolated pulmonary valvular stenosis. J Am Coll Cardiol. 1998;31:1420–5.
22. Anderson RH. Transposition – introduction. Cardiol Young. 2005;15 Suppl 1:72–5.
23. Fuster V, Alexander RW, O'Rourke RA. Hurst's the heart. 10th ed. New York: McGraw-Hill; 2001. p. 53. ISBN 0-07-135694-0.
24. Singh JP, Houser S, Heist EK, Ruskin JN. The coronary venous anatomy: a segmental approach to aid cardiac resynchronization therapy. J Am Coll Cardiol. 2005;46:68–74. doi:10.1016/j.jacc.2005.04.017.
25. Loukas M, Bilinsky S, Bilinsky E, el-Sedfy A, Anderson RH. Cardiac veins: a review of the literature. Clin Anat. 2009;22: 129–45. doi:10.1002/ca.20745.
26. von Lüdinghausen M. The venous drainage of the human myocardium. Adv Anat Embryol Cell Biol. 2003;168:I–VIII, 1–104.
27. Ho SY, Sanchez-Quintana D, Becker AE. A review of the coronary venous system: a road less travelled. Heart Rhythm. 2004;1: 107–12. doi:10.1016/j.hrthm.2003.12.001.

# Normal Anatomic Variants and Imaging Artifacts Mimicking Pathology

# 3

There are many not uncommonly seen variants that may be mistaken as abnormal, and recognition of these normal variants will increase diagnostic imaging accuracy and reduce the incidence of false alarms.

## 3.1 Left Ventricular Diverticula

Congenital left ventricular (LV) diverticula (Figs. 3.1 and 3.2) are defined as any outpouching from the ventricle that is lined by ventricular myocardium. Its connection to the ventricle may be wide or narrow [1].

The incidence of congenital ventricular diverticula has been reported to be between 0.04 and 2.2 % in an autopsy series of patients dying of cardiac disease [1–3]. LV diverticula range in size from 0.5 to 9 cm in diameter and have been reported in nearly all LV locations. Most commonly, however, they are found in the left ventricular apex and along the inferior or inferoseptal wall left ventricular walls and at the right ventricular insertion point [4]. When multiple diverticula are present (40 % of the cases, Fig. 3.2), they tend to be in close proximity to each other [1].

The Cantrell syndrome is defined as the association of LV diverticula with congenital midline thoracoabdominal abnormalities, sternal and diaphragmatic defects, and partial absence of the inferoapical pericardium [5].

Congenital ventricular diverticula should be differentiated from acquired causes of ventricular aneurysms and pseudoaneurysms such as those that occur after myocardial infarction, myocardial inflammation, or cardiac trauma. These entities may be similar in appearance making differentiation by noninvasive imaging modalities challenging. Often, the correct diagnosis is made using associated clinical history and imaging abnormalities (h/o trauma or myocardial infarction with associated imaging abnormalities like ventricular thinning or calcification). In addition, acquired ventricular aneurysms consist of predominantly fibrous tissue and are associated with abnormal cardiac contour in diastole and myocardial bulging during systole.

Note that muscular ventricular septal defects that spontaneously close by overlapping ventricular trabeculations may also produce diverticular outpouching of the ventricle.

Ventricular noncompaction may have a similar appearance to that of a ventricular diverticulum. The diagnosis of ventricular noncompaction is confirmed by identifying more than three deep intertrabecular recesses and a systolic ratio of noncompacted to compacted layers of >2.2 [6, 7]. Ventricular noncompaction is discussed in detail in Part 4, Chap. 9.

W. Mazur et al., *CT Atlas of Adult Congenital Heart Disease*,
DOI 10.1007/978-1-4471-5088-6_3, © Springer-Verlag London 2013

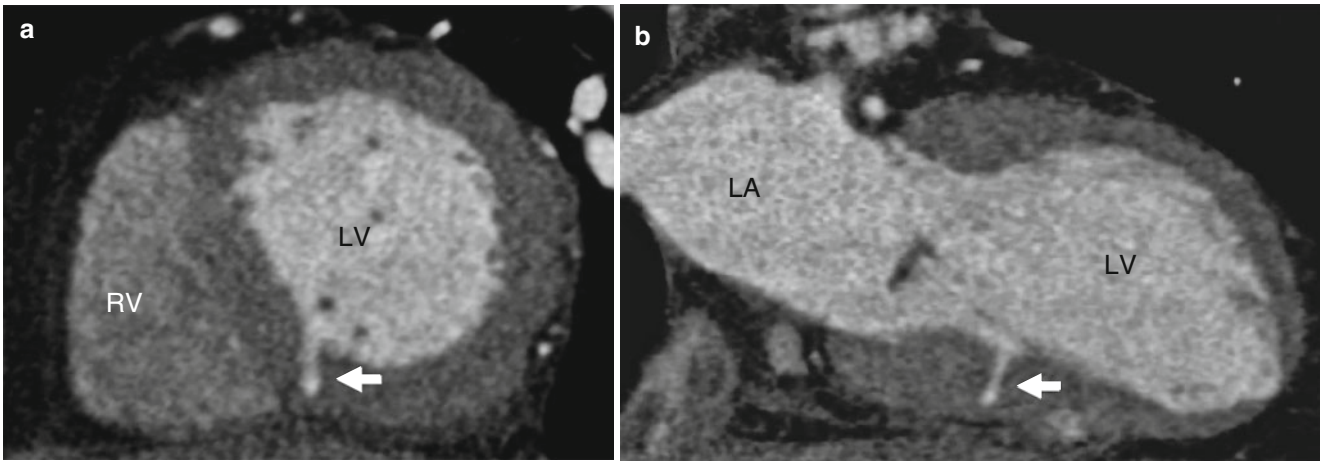


**Fig. 3.1** Left ventricular (*LV*) diverticulum. Panels (**a**) (short axis) and (**b**) (long axis) demonstrate a single diverticulum (*white arrows*) located at mid-ventricle level at the inferior right ventricular insertion site. *LV* left ventricle, *RV* right ventricle, *LA* left atrium (Image generously provided by Jill E. Jacobs, MD, FACR, Professor of Radiology, New York University Langone Medical Center)

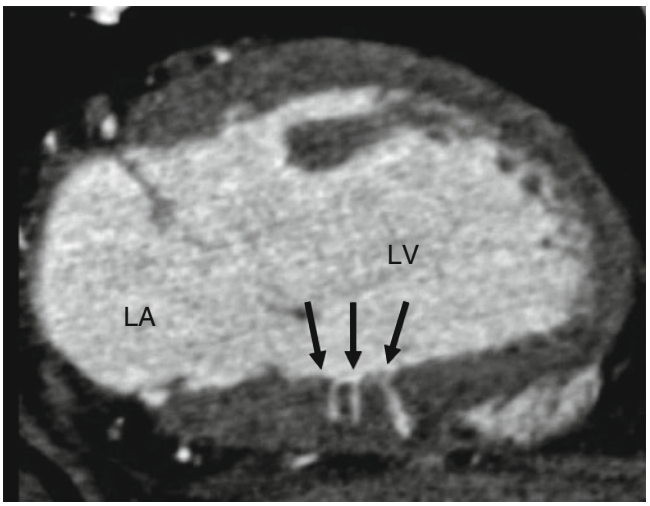


**Fig. 3.2** Multiple diverticula are seen in diastole (*arrows*). Diverticula must be differentiated from contained myocardial rupture which is a highly malignant finding. Contained rupture typically appears as a spiral dissection through necrotic tissue (not at acute angles) and is associated with a focal area of hypoperfusion, wall motion abnormality, and thrombotic occlusion of the associated coronary artery. *LV* left ventricle, *LA* left atrium (Image generously provided by Jill E. Jacobs, MD, FACR, Professor of Radiology, New York University Langone Medical Center)

## 3.2 Myocardial Bridging

Myocardial bridging (Fig. 3.3) is defined as the presence of an intramyocardial segment of a major coronary artery that normally has an epicardial course. The frequency of myocardial bridging observed by computed tomographic angiography (CTA) is nearly 60 % [8]. Myocardial bridging is typically a benign finding and the vast majority of myocardial bridges are asymptomatic. It is clinically significant only when associated with regional hemodynamic alterations. Hemodynamically significant findings typically occur only when myocardial bridging involves the left anterior descending artery. Even in adult patients with hypertrophic cardiomyopathy, myocardial bridging is not associated with increased risk of death, including sudden cardiac death.

Note that myocardial bridging is almost never seen in the right coronary artery since most of the course of the right coronary artery is not near the myocardium.

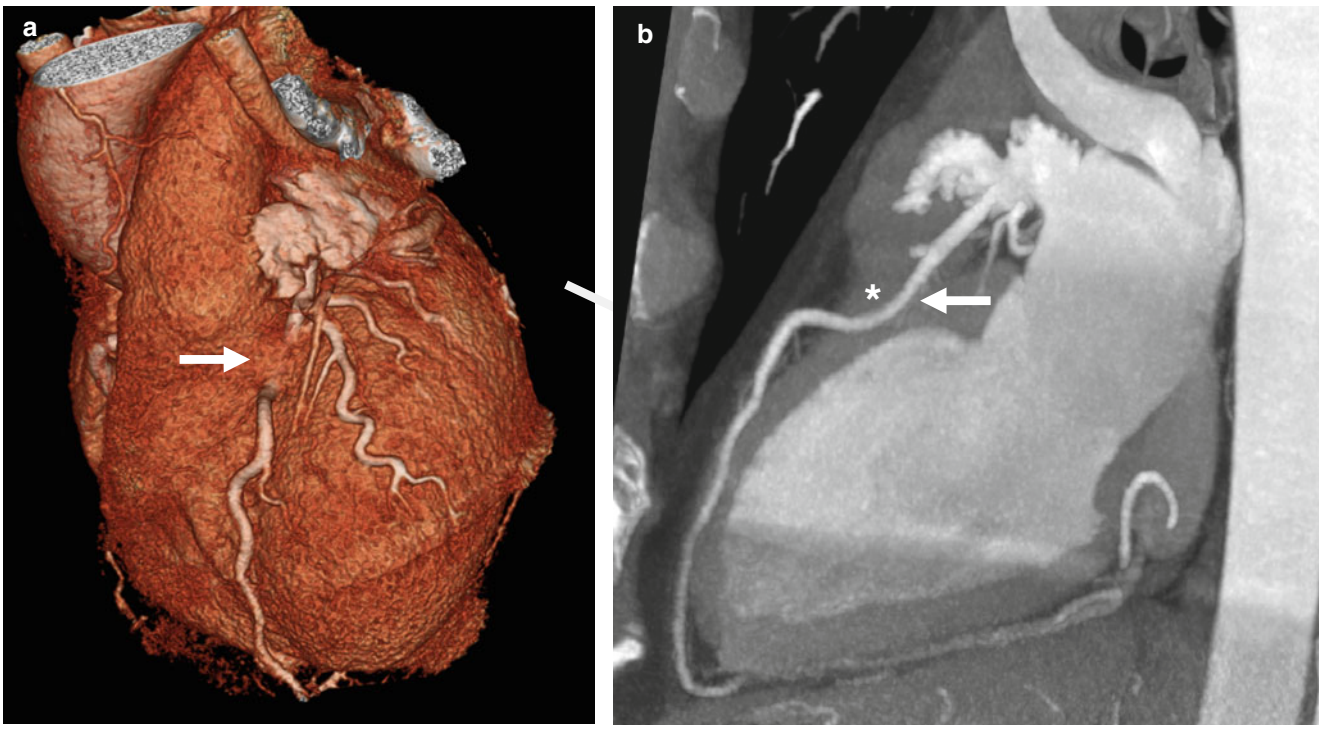


**Fig. 3.3** Myocardial bridging. Panel (**a**) (3D volume-rendered image) shows the "bridge" of myocardium overlying the proximal left anterior descending artery (*white arrow*). Panel (**b**) (maximum intensity projection in a transverse plane) illustrates the proximal left anterior descending artery coursing within the myocardium (*white arrow*) and the overlying "bridge of myocardium" (*white asterisk*)

## 3.3 Left Ventricular Trabeculations

Prominent left ventricular trabeculations (Fig. 3.4) have been reported in 323 of 474 autopsies (68 %) in normal human hearts and they occur equally in males and females (72 and 65 %, respectively) [9]. No variation is noted when age is considered [9]. Accordingly, prominent left ventricular trabeculations are considered to be common variants of the normal human heart, frequently visualized during CTA examinations, and these should not to be mistaken for isolated left ventricular noncompaction (described above).

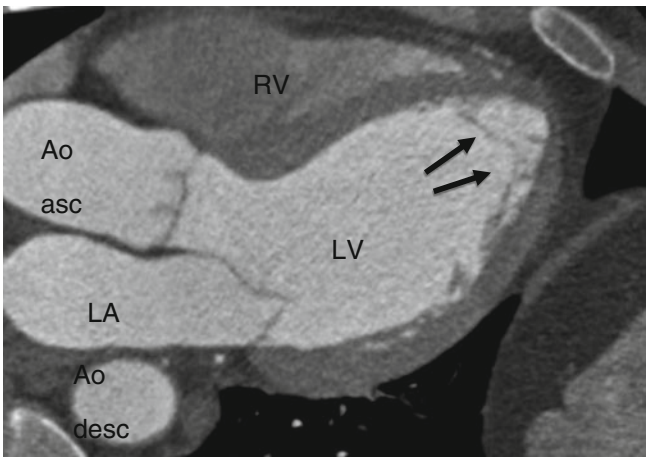


**Fig. 3.4** Normal left ventricular trabeculations (*arrows*) not associated with papillary muscles. These do not meet the criteria for isolated left ventricular noncompaction. *LV* left ventricle, *RV* right ventricle, *LA* left atrium, *Ao Asc* ascending aorta, *Ao Desc* descending aorta

## 3.4 Papillary Muscle Attachment to the Left Ventricular Free Wall

Traditionally, papillary muscles (PM) are depicted as arising directly from the solid portion of the ventricular walls. They are shown to have a broad base connecting them to the ventricular wall. The PM then taper to give rise to the origins of the chordae tendineae. More recently, state-of-the-art multidetector computed tomography (MDCT) has revealed that the base of the PM does not directly contact or join the solid portion of the ventricular heart walls but rather they contact the ventricular wall via a network of trabeculae carneae lining the ventricular cavities (Fig. 3.5) [10]. These trabeculae carneae lie above the actual surface of the solid portion of the heart walls. Both the left ventricular and right ventricular PM demonstrate this relationship [10]. This finding should not be mistaken for left ventricular noncompaction.

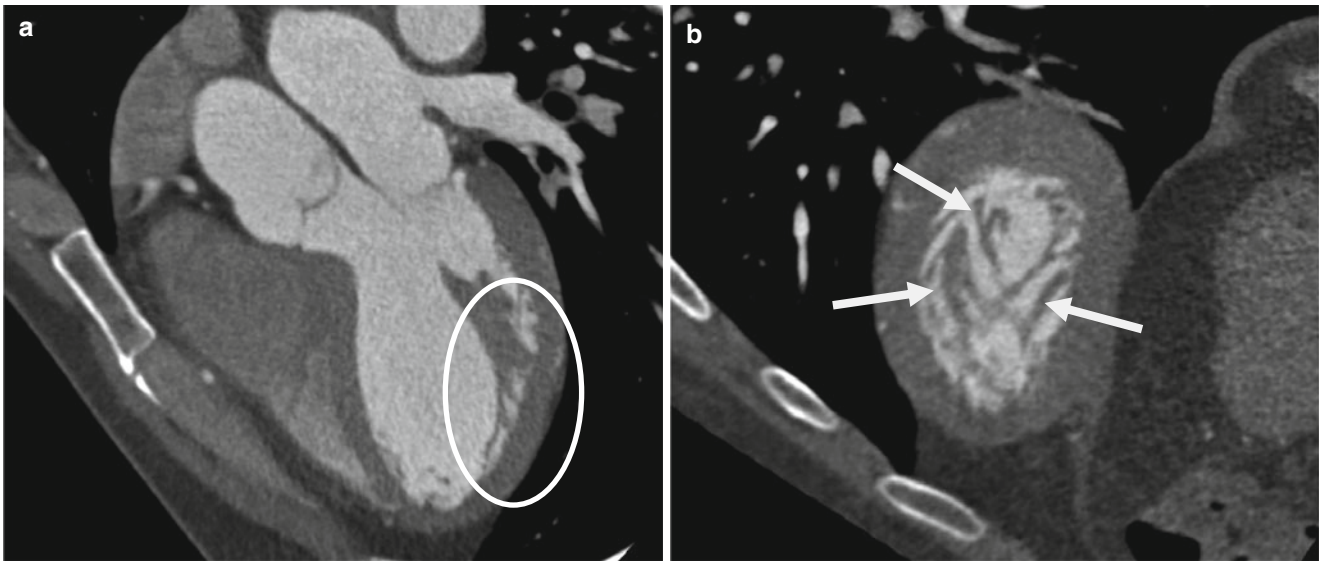


**Fig. 3.5** Panel (**a**) oblique maximum intensity reformat (MIP) demonstrating the multi-head attachment (*white oval*) of the left ventricular papillary muscle (*arrow*) into the free wall. Panel (**b**) oblique MIP image tangential to left ventricular cavity just beneath the base of the papillary muscles shows the multiple chordae tendineae (*arrows*), which are above the heart wall. In this view one can imagine potentially mislabeling this heart as noncompaction. *LV* left ventricle, *RV* right ventricle, *LA* left atrium, *Asc Ao* ascending aorta, *Desc Ao* descending aorta

## 3.5 Apical Thinning

Focal thinning of the left ventricular apex is a normal anatomic feature (Fig. 3.6). It is present in normal and hypertrophied ventricles. The mean myocardial thickness in normal apical areas of thinning is reported to be 1.2 mm, with the average diameter in the oblique coronal plane of 4.4 mm [11]. Segmental foci of thinning show normal wall motion during the cardiac cycle [11]. Normal apical thinning needs to be differentiated from apical infarction or scarring which are associated with a wall motion abnormality and may be calcified. Segmental infarction may also have a lower density relative to normally enhancing adjacent myocardium and may demonstrate fatty replacement or calcification. Other associated findings of chronic infarction include adjacent mural thrombus because of stasis of blood associated with decreased contractility and aneurysmal dilatation of the cardiac apex.

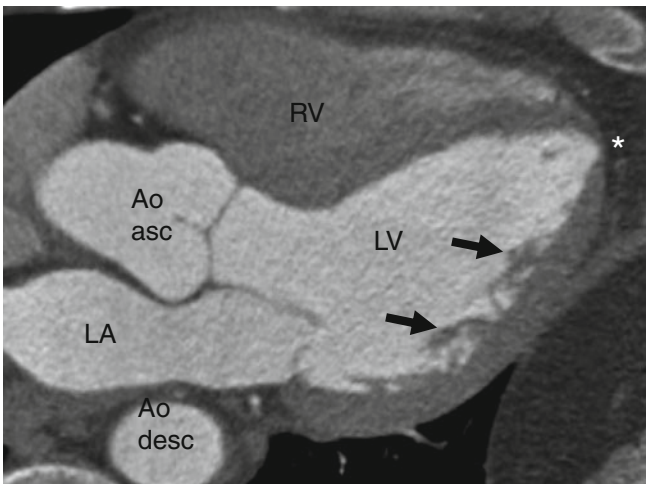


**Fig. 3.6** Apical thinning (*white asterisk*). Again noted normal papillary muscles (*black arrows*) giving rise to multiple chordae tendineae at their attachment site to the left ventricular wall. *LA* left atrium, *LV* left ventricle, *RV* right ventricle, *Ao Desc* descending aorta, *Ao Asc* ascending aorta

## 3.6 Left Atrial Pouch

The foramen ovale spontaneously closes soon after birth as a result of adhesions developing across the flap of the foramen ovale. If adhesions form only in part of the structure, a partial closure ensues and a pouch is formed (Fig. 3.7). In the majority of patients, left atrial pouches open into the left atrium. While it was initially felt that left atrial pouches are associated with thrombus formation and cryptogenic stroke [12], this belief has been refuted [13].

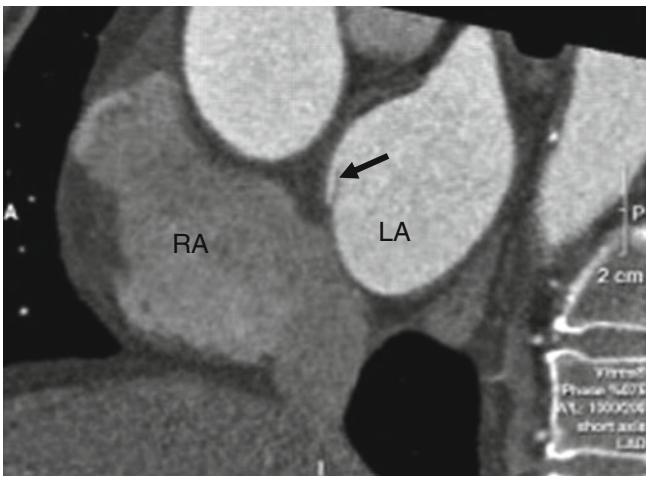


**Fig. 3.7** Left atrial pouch (*arrow*) on a CTA image. *RA* right atrium, *LA* left atrium (Reproduced with the kind permission of Elsevier Limited, Kidlington, Oxford, UK from Gurudevan et al. [16])

## 3.7 Contrast Reflux into the Inferior Vena Cava

Retrograde opacification of the inferior vena cava or hepatic veins on CTA is a specific but insensitive sign of right-sided heart disease at low contrast injection rates. However, the usefulness of this sign decreases with high contrast injection rates. During rapid contrast injection, a transient increase in right atrial pressure normally results in reflux of contrast into inferior vena cava and hepatic veins (Figs. 3.8 and 3.9) [14].

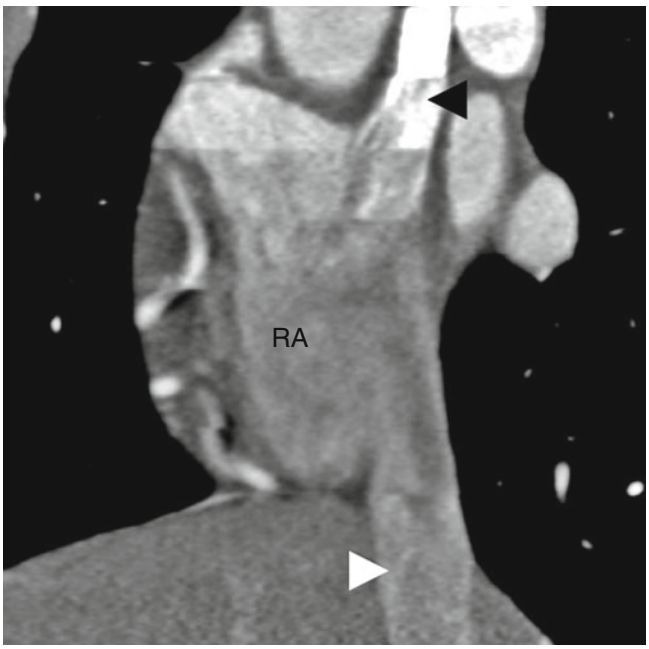


**Fig. 3.8** A computed tomographic angiogram in a healthy individual without heart disease showing a normal-size superior vena cava (SVC) (*black arrowhead*) and inferior vena cava (IVC) (*white arrowhead*) emptying into the right atrium (*RA*). Transient reflux of contrast is noted in the IVC and was caused by a rapid rate of contrast administration

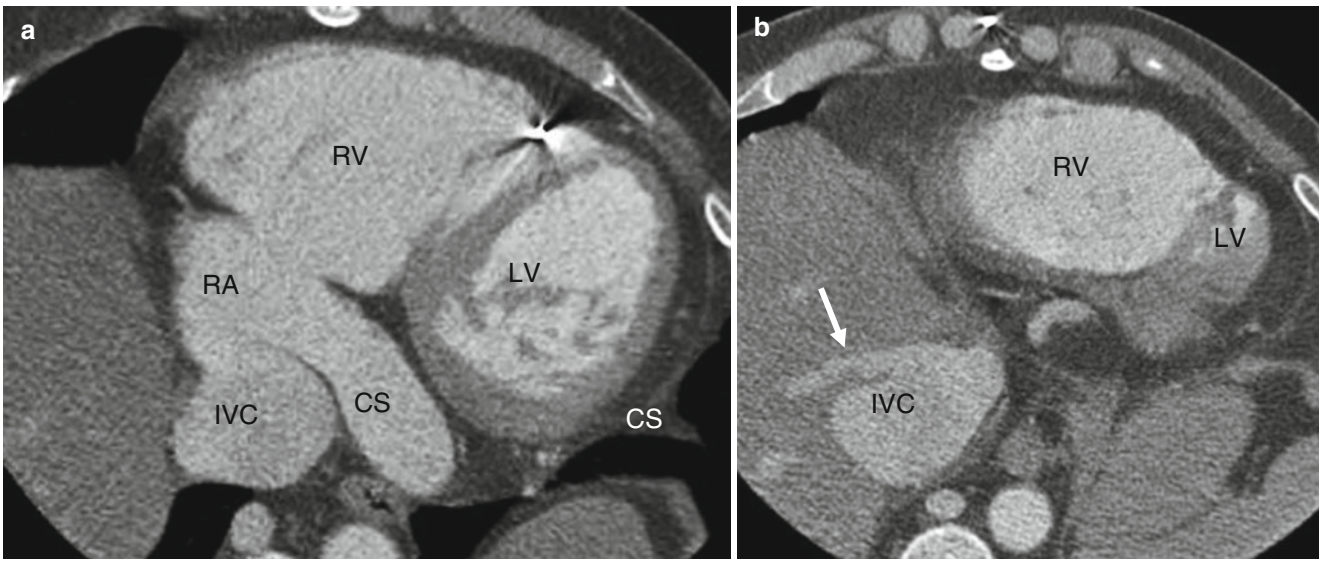


**Fig. 3.9** Panels (**a**) and (**b**) are CTA images in a patient with tricuspid atresia associated with severe right ventricle dysfunction and enlargement and tricuspid regurgitation. Note the markedly dilated inferior vena cava full with contrast as well as a dilated coronary sinus (*CS*) and hepatic vein (*white arrow*). *LV* left ventricle, *RV* right ventricle, *RA* right atrium, *CS* coronary sinus, *IVC* inferior vena cava

## 3.8 Contrast Mixing

A transient flow artifact can occur when contrast-rich blood enters venous blood without contrast (Figs. 3.10 a, b). Flow artifact from contrast mixing is particularly common in upper extremity injections and results from contrast-enhanced blood in the superior vena cava mixing with unenhanced blood from the inferior vena cava. Delayed scans are useful in separating contrast mixing artifacts from intracardiac masses since they allow time for homogenous enhancement of the right atrium and right ventricle. Care must be taken not to confuse the presence of unopacified blood with tumor or thrombus [15].

Incomplete opacification of venous blood is frequently seen in systemic venous baffles such as Fontan or Glenn circulations, where unopacified blood from the inferior vena cava and lower body mix with contrast-enhanced blood from the superior vena cava. Thus, delayed scans are required when evaluating this corrective anatomy.

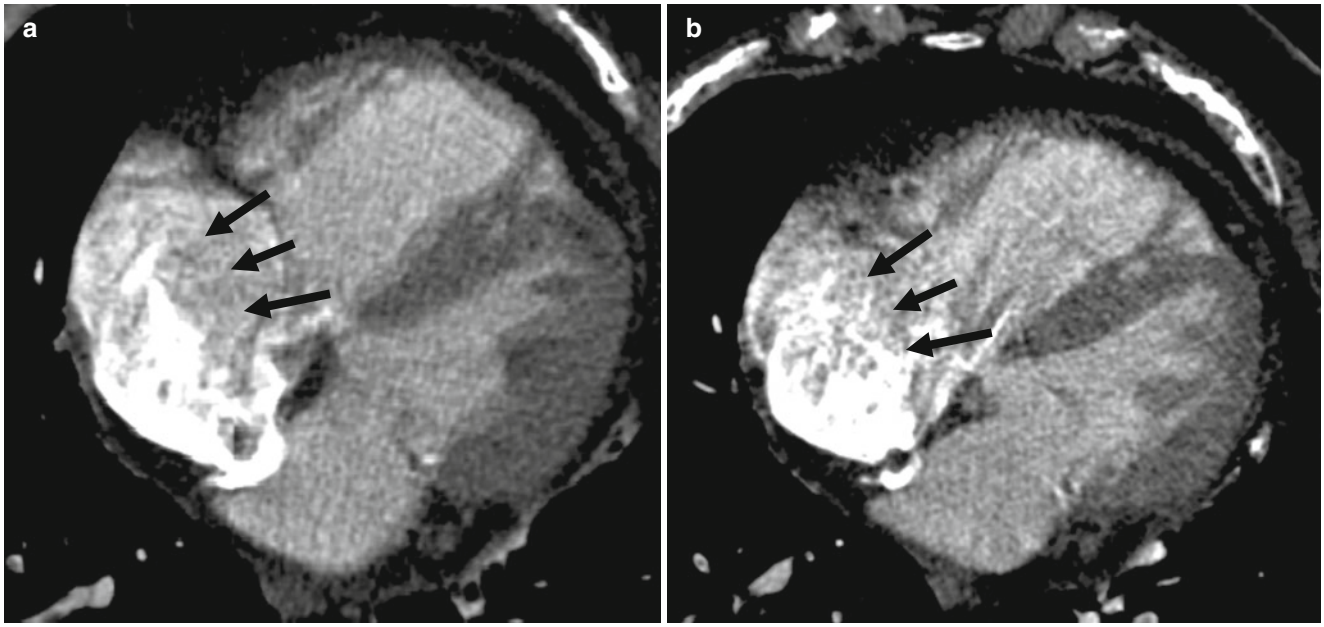


**Fig. 3.10** Panels (**a**) and (**b**) are from the same patient at different cardiac phases demonstrating incomplete contrast mixing mimicking a thrombus or mass (*arrows*) in the right atrium resulting from the inflow of high-density contrast from the superior vena cava mixing with the unopacified blood from the inferior vena cava. Examining multiple phases may help clarify the finding of incomplete contrast mixing by demonstrating changes in the opacification pattern among the various phases of the cardiac cycle

## References


1. Srichai MB, Hecht EM, Kim DC, Jacobs JE. Ventricular diverticula on cardiac CT: more common than previously thought. AJR Am J Roentgenol. 2007;189:204–8. doi:10.2214/AJR.06.1223.
2. Pressoir R, Downing JW. Congenital diverticula of the right ventricle of the heart: a case report. J Natl Med Assoc. 1980;72:262–4.
3. Mayer K, Candinas R, Radounislis C, Jenni R. Congenital left ventricular aneurysms and diverticula: clinical findings, diagnosis and course. Schweiz Med Wochenschr. 1999;129:1249–56.
4. Ohlow MA. Congenital left ventricular aneurysms and diverticula: definition, pathophysiology, clinical relevance and treatment. Cardiology. 2006;106:63–72. doi:10.1159/000092634.
5. Cantrell JR, Haller JA, Ravitch MM. A syndrome of congenital defects involving the abdominal wall, sternum, diaphragm, pericardium, and heart. Surg Gynecol Obstet. 1958;107:602–14.
6. Hamamichi Y, Ichida F, Hashimoto I, Uese KH, Miyawaki T, Tsukano S, et al. Isolated noncompaction of the ventricular myocardium: ultrafast computed tomography and magnetic resonance imaging. Int J Cardiovasc Imaging. 2001;17:305–14.
7. Stollberger C, Finsterer J, Blazek G. Left ventricular hypertrabeculation/noncompaction and association with additional cardiac abnormalities and neuromuscular disorders. Am J Cardiol. 2002; 90:899–902.
8. Kim PJ, Hur G, Kim SY, Namgung J, Hong SW, Kim YH, et al. Frequency of myocardial bridges and dynamic compression of epicardial coronary arteries: a comparison between computed tomography and invasive coronary angiography. Circulation. 2009; 119:1408–16. doi:10.1161/CIRCULATIONAHA.108.788901.
9. Boyd MT, Seward JB, Tajik AJ, Edwards WD. Frequency and location of prominent left ventricular trabeculations at autopsy in 474 normal human hearts: implications for evaluation of mural thrombi by two-dimensional echocardiography. J Am Coll Cardiol. 1987;9:323–6.
10. Axel L. Papillary muscles do not attach directly to the solid heart wall. Circulation.2004;109:3145–8.doi:10.1161/01.CIR.0000134276.06719.F3.
11. Johnson KM, Johnson HE, Dowe DA. Left ventricular apical thinning as normal anatomy. J Comput Assist Tomogr. 2009;33:334–7. doi:10.1097/RCT.0b013e3181870356.
12. Krishnan SC, Salazar M. Septal pouch in the left atrium: a new anatomical entity with potential for embolic complications. JACC Cardiovasc Interv. 2010;3:98–104. doi:10.1016/j.jcin.2009.07.017.
13. Tugcu A, Okajima K, Jin Z, Rundek T, Homma S, Sacco RL, et al. Septal pouch in the left atrium and risk of ischemic stroke. JACC Cardiovasc Imaging. 2010;3:1276–83. doi:10.1016/j.jcmg.2010.11.001.
14. Yeh BM, Kurzman P, Foster E, Qayyum A, Joe B, Coakley F. Clinical relevance of retrograde inferior vena cava or hepatic vein opacification during contrast-enhanced CT. AJR Am J Roentgenol. 2004;183:1227–32.
15. Katz DS, Loud PA, Hurewitz AN, Mueller R, Grossman ZD. CT venography in suspected pulmonary thromboembolism. Semin Ultrasound CT MR. 2004;25:67–80.
16. Gurudevan SV et al. Septal thrombus in the left atrium: Is the left atrial septal pouch the culprit? J Am Coll Cardiol Img. 2010;3:1284–6.

# Part II

# Basic Nomenclature and Approach to Evaluating Congenital Heart Disease Imaging

# Basic Nomenclature in Adult Congenital Heart Disease

4

The development of multidetector computed tomography has resulted in marked advancements in the diagnosis of congenital heart disease (CHD) which has renewed interest in the classifications and definitions used to describe the anatomy of the heart and great vessels. The sequential, segmental approach to analyzing CHD patient images was introduced nearly three decades ago and is used worldwide [1–5]. Thus, a thorough understanding of both the nomenclature and anatomy applied in this approach is essential to the proper and error-free interpretation of CHD CTA images [6]. The definitions described below are based on the segmental, sequential approach to classifying CHD which is described in Chap. 5.

## 4.1 Cardiac Orientation

Cardiac orientation or position refers to the relationship or axis of the base to the apex of the heart and may help to predict the presence of CHD. Early in fetal development, normal embryogenesis [situs solitus (normal atrial positions) and D-bulboventricular loop (normal ventricular positions)], results in the apex of the heart being situated in the right hemithorax. At the beginning of the second month, the apex of the heart migrates to the left hemithorax (normal adult position). In situs inversus with an L-loop (atria are reversed and ventricles are reversed), the opposite occurs (the apex of the heart migrates from the left hemithorax to the right hemithorax). Regardless of atrial situs, all D-loops should complete their development with the heart in the left chest (levocardia). On the contrary, all L-loops should end development with the heart in the right chest (dextrocardia). If the cardiac apex fails to shift, it may result in situs solitus with dextrocardia which is termed dextroversion or situs inversus with levocardia called levoversion. Thus, dextrocardia may occur from a D-loop that fails to shift leftward or an L-loop that completes its rightward shift. Mesocardia (midline heart) occurs when the ventricular apex does not complete its shift. Mesocardia may be associated with concordant (D-loop) or discordant (L-loop) ventricles as well as with heterotaxy syndromes.

Of note, positioning of the heart in the right chest with a left-sided cardiac apex can occur when the contents of the left chest force the heart to the right or when the volume of the right lung is reduced (for instance, due to pulmonary hypoplasia or collapse). This type of positioning is more appropriately termed dextroposition since the axis of the heart is usually normal.

To summarize, three different cardiac situs abnormalities are possible: levocardia, dextrocardia, and mesocardia (Fig. 4.1). Levocardia is defined as a normal cardiac position in the left chest with the cardiac base-to-apex axis pointing from upper right to lower left (normal cardiac base-to-apex axis points left to right). Dextrocardia refers to a heart located in the right chest with the base-to-apex axis pointing from the upper left to the lower right. Mesocardia refers to a heart that is usually in the midline with the base-to-apex axis directly from superior to inferior. Situs solitus with dextrocardia is termed dextroversion and situs inversus with levocardia is called levoversion.

W. Mazur et al., *CT Atlas of Adult Congenital Heart Disease*,
DOI 10.1007/978-1-4471-5088-6_4, © Springer-Verlag London 2013

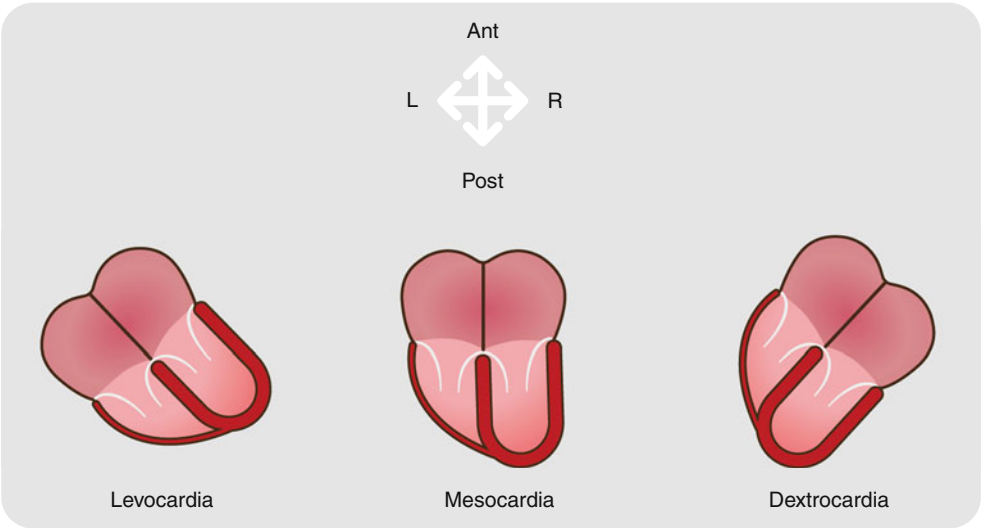


**Fig. 4.1** A depiction of the three possible cardiac situs abnormalities

## 4.2 Nomenclature for Thoracic and Visceral Situs

Situs or sidedness refers to the position or arrangement of structures or organs that are not bilaterally symmetric. There are three possible arrangements: normal also known as solitus, inversus (mirror image of normal), and ambiguous (not clearly solitus or inversus). In the ambiguous situation, features of situs solitus and situs inversus are present in the same person. Here the thoracic and abdominal organs cannot be lateralized and have neither the normal nor mirror image arrangement.

### 4.2.1 Situs Definitions

Thoracic Situs: The situs of the left and right lung is independent of the cardiac or abdominal situs but instead is identified by the anatomy of the respective bronchi, especially the relationship between the bronchi and pulmonary arteries [7]. The right main bronchus takes a more vertical course and branches at an earlier point than the more horizontally oriented left bronchus. See Fig. 4.2.

Abdominal Situs: Refers to the sidedness of the main visceral organs such as the liver, stomach, and spleen.

Atriovisceral Situs: Atrial situs is determined by the position of the morphologic right and left atria. Atrial development is simultaneous to venous return formation, and thus, the atrial locations are fixed early in development by the entering veins. The atrial situs is independently determined from and unaffected by the shape of the bulboventricular loop or the final locations of the ventricles. In turn, the atrial situs corresponds to the visceral and thoracic situs and abnormalities in atrial position usually correspond with parallel abnormalities in the visceral and thoracic situs.

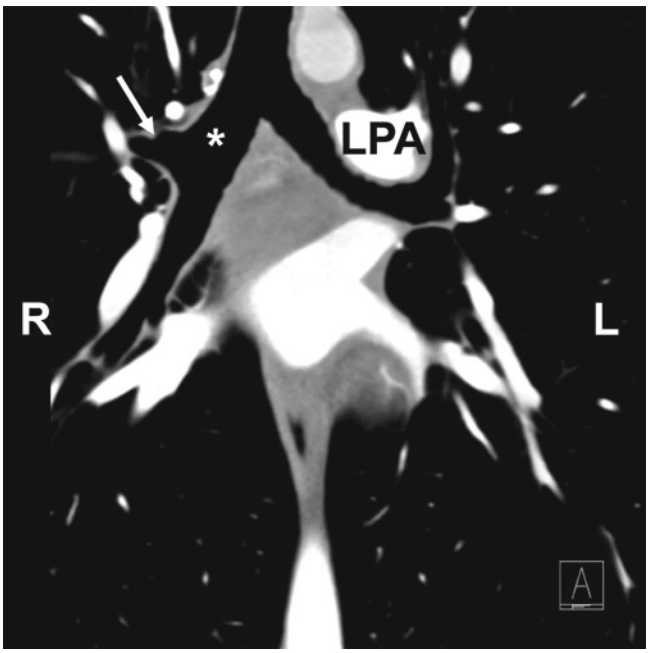


**Fig. 4.2** A coronal CT image demonstrating the normal central bronchial anatomy which can be used to help differentiate the morphologic right lung from the morphologic left lung. The right main stem bronchus (*asterisk*) is more vertically oriented with an early branch point (*white arrow*), *LPA* left pulmonary artery

Three designations are used in characterizing atrial situs: situs solitus, situs inversus, or situs ambiguous. Situs solitus (normal) and situs inversus are present when there is identifiable lateralization of the atrial chambers, meaning that atrial arrangement is congruent with thoracoabdominal organ arrangement [8, 9]. Situs solitus is present when the right atrium and liver are on the right side and the left atrium, stomach, and spleen are on the left side. The right lung is trilobed and the left lung is bilobed each with their usual

**Table 4.1** The characteristics of left and right isomerism

| Right isomerism | Left isomerism |
|---|---|
| Bilateral morphologic right atria | Bilateral morphologic left atria |
| Asplenia | Bilateral bilobed lungs |
| Bilateral trilobed lungs | Interrupted inferior vena cava |
| Symmetric liver | Partial anomalous pulmonary venous return |
| Total anomalous pulmonary venous return | |

bronchial pattern. The right pulmonary artery lies anterior to the right bronchus (eparterial position), and the left bronchus lies behind the left pulmonary artery (hyparterial position). Situs inversus is a mirror image of situs solitus.

It should be noted that atrial situs most often follows the thoracic and visceral situs. That is, atrial situs inversus is most often concomitant with thoracic and visceral situs inversus.

Ambiguous situs indicates that assignment or position of the right and left atria cannot be determined. Ambiguous situs may also be termed heterotaxy. Atrial situs ambiguity usually occurs concomitantly with visceral heterotaxia or situs ambiguity where the visceral organs are abnormally positioned across the left–right axis of the body. The term "isomerism" has been used to describe the combination of atrial situs ambiguity (heterotaxy) and visceral heterotaxy [8, 9]. Two forms of isomerism are recognized: right isomerism and left isomerism. Right isomerism is when there are bilateral morphologic right atria and is associated with asplenia and left isomerism (bilateral morphologic left atria) is associated with polysplenia. Right isomerism is also often associated with bilateral trilobed lungs (two right lungs, a symmetric liver across the midline, and total anomalous pulmonary venous return). Left isomerism is usually associated with bilateral bilobed lungs (two left lungs), interrupted inferior vena cava, and partial anomalous pulmonary venous return.

Note that the aorta and great veins generally have specific orientations depending on the situs and type of isomerism discussed in detail in Chap. 5. See Fig. 5.3.

See Table 4.1 for a characterization of isomerization.

Figure 4.3 illustrates the thoracic, atrial, and visceral situs seen with situs solitus, situs inversus, and situs ambiguous (right and left isomerism).

Atrial situs and ventricular looping are independent. Thus, any version of atrial situs may accompany a D-looped (correct ventricular sidedness) or L-looped (incorrect ventricular sidedness) heart. Figure 4.3 demonstrates this concept.

### 4.2.2 Definitions for the Atrial Chambers

Anatomically, atrial chamber differentiation is usually based on the distinctive features of the atrial appendages. Each appendage has intrinsic morphologic features. Typically, the right atrial appendage is a triangular, broad-based structure, while the left atrial appendage is smaller, thinner, and finger-like. The right atrium may be identified by locating the crista terminalis, a muscular band that runs from the entrance of the superior vena cava to that of the inferior vena cava. This structure separates the trabeculated right atrial appendage from the remainder of the right atrium. The left atrium lacks the crista terminalis. The thicker superior limbus of the atrial septum around the fossa ovalis is associated with the right atrium. The flap of the valve at the oval fossa is located in the left atrium. Additionally, the identification of inferior vena cava and the coronary sinus entering the right atrium is used as a criterion for identification.

The superior vena cava (SVC) is not an acceptable criterion to identify the morphologic right atrium since an anomalous SVC is not uncommon. Similarly, pulmonary vein anomalies are also commonly seen, and as such, identifying pulmonary venous connections is not a stern rule for identifying the morphologic left atrium.

Table 4.2 identifies the distinctive features differentiating the right from the left atrium.

### 4.2.3 Definitions for Cardiac Ventricles

The ventricular cardiac chambers are identified by their associated respective inlet valves. That is, the left ventricle is associated with the mitral (bileaflet) inlet valve (arises more superior than the tricuspid valve), and the right ventricle is associated with the tricuspid (trileaflet) inlet valve which arises below the membranous septum. Ventricles are composed of three parts: the inlet, outlet, and trabecular portions. The inlet contains the atrioventricular valves and the subvalvular apparatuses. The ventricular outlet portions are cephalad and lead to the great arteries. The trabecular portion extends from the papillary muscles to the ventricular apices.

There are several characteristics which are specific for the right ventricle and are useful in distinguishing the right from the left ventricle. These are the (a) infundibulum, (b) tricuspid valve apparatus, (c) apical trabeculations, and (d) moderator band. The infundibulum is a term that indicates the right ventricular outlet, which is a smooth muscular structure (also known as the conus or muscular conus). The left ventricular outlet is partially fibrous due to the aortic-mitral fibrous continuity.

The tricuspid valve apparatus has three leaflets and three papillary muscles; the papillary muscles are attached to both the interventricular septum and the free wall of the right ventricle. The mitral valve apparatus consists of an annulus and two leaflets, which connect to two papillary muscles via cord-like tendons called chordae tendineae. The papillary muscles insert only on the free lateral wall of the left ventricle

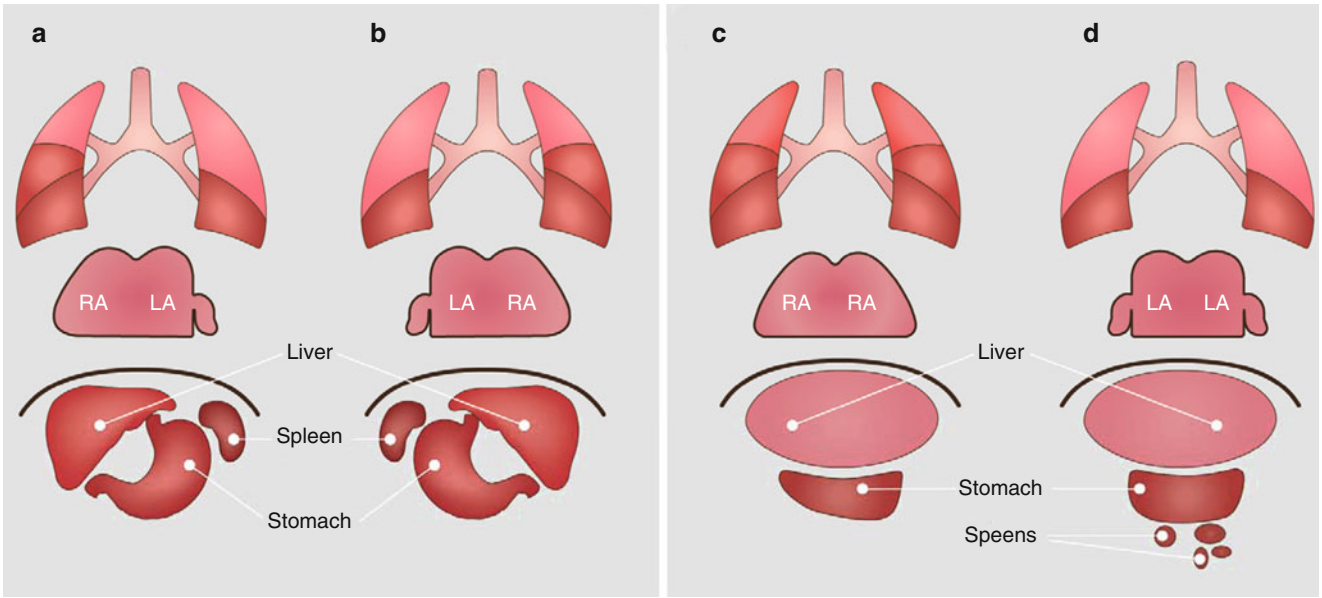


**Fig. 4.3** The correspondence of atrial, thoracic, and abdominal organs arrangement in situs solitus (**a**), situs inversus (**b**), right isomerism (**c**), and left isomerism (**d**). Note in panel (a) the trilobed right lung is rightward, the bilobed left lung is leftward, and the atria, liver, spleen, and stomach are on their correct sides. In panel (b) the lungs, atria, and visceral organs are reversed, mirror image. Panel (c) illustrates bilateral right lungs, bilateral morphologic right atria, and heterotaxy of the visceral organs. Panel (d) shows bilateral left lungs, bilateral morphologic left atria, and visceral heterotaxy with polysplenia

**Table 4.2** The characteristics that differentiate the right from the left atria

| Atrial differentiation | |
|---|---|
| Right atrium | Left atrium |
| Triangular broad appendage | Narrow based, thinner, and finger-like appendage |
| Contains crista terminalis | No crista terminalis |
| Thick superior limbus around fossa ovalis | Contains fossa ovalis flap |
| Inferior vena cava and coronary sinus connection | |

**Table 4.3** The characteristics that differentiate the right from the left ventricle

| Ventricular differentiation | |
|---|---|
| Right ventricle | Left ventricle |
| Presence of the infundibulum | Partially fibrous ventricular outlet |
| Associated with the tricuspid valve and tricuspid valve apparatus | Associated with the mitral valve and mitral valve apparatus |
| Course trabeculations | Fine trabeculations |
| Presence of the moderator band | Absence of moderator band |

(not on the septum). Again, the tricuspid valve is identified by its caudal location below the membranous septum.

The characteristics of the internal trabeculae of the ventricles also help to differentiate between the right and left ventricles. The right ventricular trabeculations are coarse; the left ventricular trabeculations are thinner, delicate structures. The moderator band is another distinguishing feature of the right ventricle. It extends from the septum to the free lateral wall of the right ventricle and contains part of the right bundle branch of the cardiac conduction system, which plays a role in the electrophysiologic conduction of the right ventricle's free wall.

Table 4.3 identifies the distinguishing characteristics of the right and left ventricles.

As discussed in Chap. 1, the ventricles may form according to a D-loop (normal) or L-loop (reversed) pattern. Because cardiac looping is independent of visceral situs development, both D-loop ventricles and L-loop ventricles may be concordant or discordant relative to visceroatrial situs. Concordant signifies a D-loop with situs solitus or L-loop with situs inversus. Discordant means D-loop with situs inversus or L-loop with situs solitus. In the case of ambiguous situs, concordance or discordance cannot be determined.

### 4.2.4 Definitions for Great Arteries

The great vessels are typically described by the terms solitus, inversus, dextro, and levo. Solitus refers to the normal anatomically relationship between the great vessels. Inversus refers to the mirror image anatomic relationship. Dextro describes great vessels on the right side of the body and levo indicates the great vessels are on the left.

The great arteries are most easily identified by their branches and not by their relationship to the ventriculoarterial valves. The left aortic arch (normal) typically gives rise to a brachiocephalic artery, left common carotid artery, and left subclavian artery. The pulmonary artery typically bifurcates into left and right pulmonary arteries. The coronary arteries predominantly arise from the sinuses of the aorta. The location of the conus can help to identify the pulmonary artery. Typically, the muscular conus is subpulmonic in location.

A common arterial trunk is defined as a vessel connected to the ventricle (or ventricles) via a common ventriculoarterial valve. The common trunk supplies the coronary, systemic, and pulmonary circulations directly. A solitary arterial trunk is defined as a vessel arising from ventricle or ventricles that does not give rise to intrapericardial pulmonary arteries. In this anomaly, the blood supply to the lung usually comes from collateral vessels originating from either the ascending or descending thoracic aorta.

## 4.3 Nomenclature to Describe Connecting Segments

A segment is the term used to describe a part or section of the cardiovascular system. A connection is the term that describes the junction between two cardiovascular segments. Again, note that atrial situs, great artery orientation, and ventricular looping do not specify atrioventricular connections. All of these variables are independent of each other.

### 4.3.1 Nomenclature for Atrioventricular Connections

There are five types of atrioventricular connection: concordant (normal), discordant, ambiguous, double-inlet, and absent connection. Concordant refers to a normal connection between segments. The right atrium connects to the morphologic right ventricle and the left atrium connects to the morphologic left ventricle. Discordant refers to the opposite of the normal connection. The right atrium connects to the morphologic left ventricle and the left atrium drains into the morphologic right ventricle. Ambiguous connection refers to connections in which half the atrioventricular junction is connected concordantly and the other half is discordantly connected. That is, there may be bilateral morphologic right or left atria. For example, one of the atria may correctly connect with its concordant ventricle and the opposite-sided morphologically identical atrium discordantly connects with the opposite ventricle. Concordant, discordant, and ambiguous connections occur in a biventricular heart. See Fig. 4.4.

In functionally univentricular hearts, there are three possible inlets: double inlet, single inlet, or common inlet. Double inlet refers to a functional univentricle connected to two separate atria with two separate atrioventicular valves. Single inlet refers to two separate atria with only one of the atria connected to the functional univentricle via one atrioventricular valve. The other atria connection is atretic. Single inlet may be either a right single inlet where the left-sided atrioventricular connection is atretic or left single inlet where the right-sided atrioventricular connection is atretic. A common inlet refers to when both atria are connected to a functional univentricle via one atrioventicular valve.

Figure 4.5 depicts an artist's rendition of the possible univentricular inlets.

### 4.3.2 Nomenclature for Atrioventricular Valvular Connections

Straddling is a feature of the chordae tendineae of an atrioventricular valve and describes chordae that cross a ventricular septal defect and have their attachments in the opposite ventricle. Overriding is a feature of the valve annulus which describes an annulus that crosses a ventricular septal defect and thus lies "over" more than one ventricle. Straddling and overriding often coexist. Figure 4.6 depicts the concepts of straddling and overriding.

### 4.3.3 Nomenclature for Ventriculoarterial Connections

There are four potential types of ventriculoarterial connection: concordant, discordant, double-outlet right ventricle, and double-outlet left ventricle. Similar to the atrioventricular connection, concordant refers to a normal connection between segments. The pulmonary artery arises from the right ventricle and the aorta from the left ventricle. Discordant refers to the opposite type of connection. The aorta arises from the right ventricle and the pulmonary artery arises from the left ventricle, which is seen in transposition of the great vessels. Double-outlet right ventricle means both great vessels originate from the right ventricle, and double-outlet left ventricle means the great vessels arise from the left ventricle. In both settings, only one valve, either the aortic or pulmonic valve, can be identified. Figure 4.7 depicts the possible ventriculoarterial connections.

Ventriculoarterial overriding refers to a situation when more than half of the area of the outlet overrides the ventricular septum. It is commonly seen in tetralogy of Fallot, where the aorta overrides the ventricular septum.

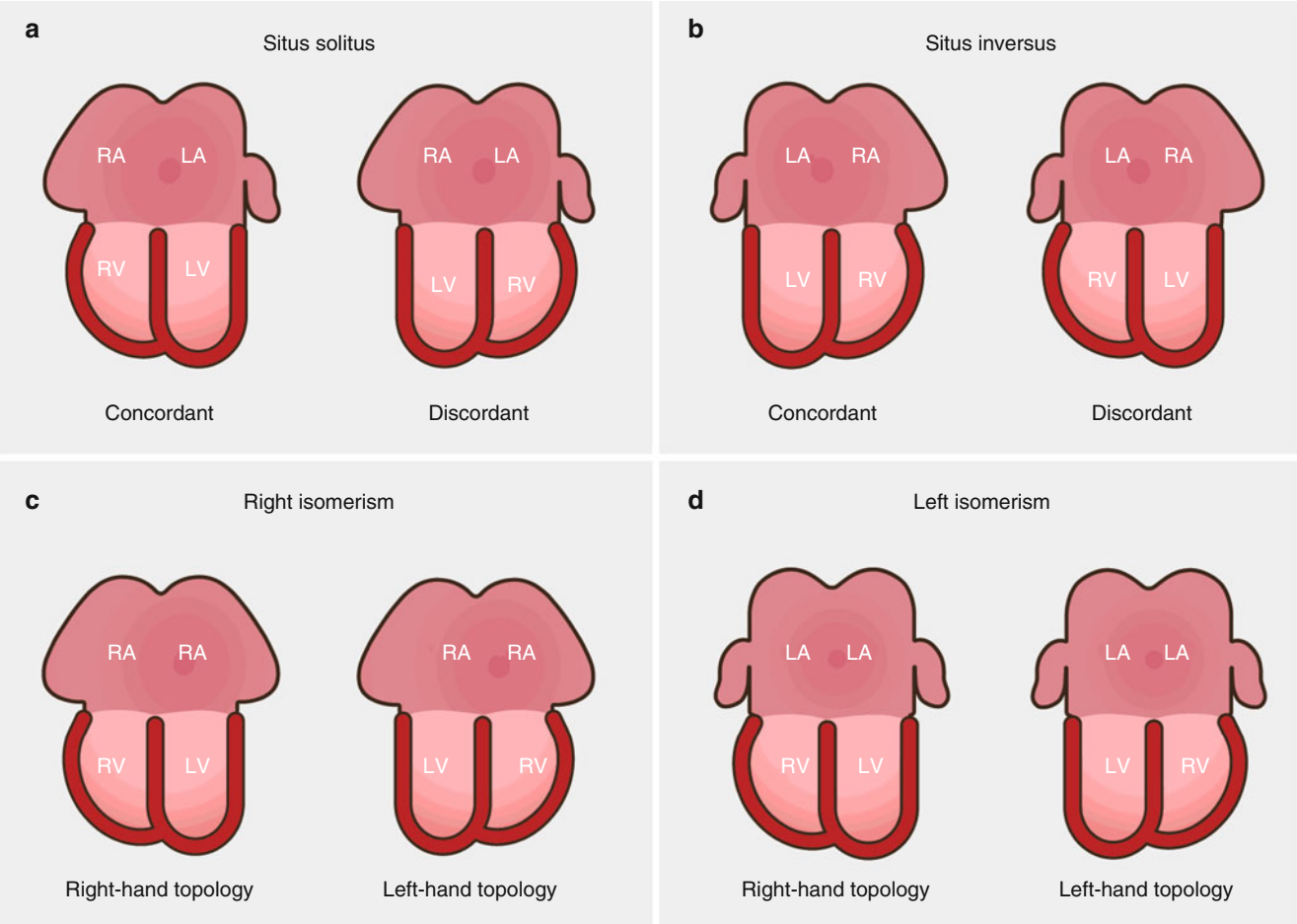


**Fig. 4.4** The variants of biventricular atrioventricular connections in situs solitus (**a**), situs inversus (**b**), right isomerism (**c**), and left isomerism (**d**) demonstrating the independence of situs and looping. In panels (a) and (b), concordant demonstrates normal ventricular sidedness (D-looping), while discordant demonstrates opposite ventricular sidedness (L-looping). In panels (c) and (d), right-handed topology refers to D-looping and left-handed topology refers to L-looping

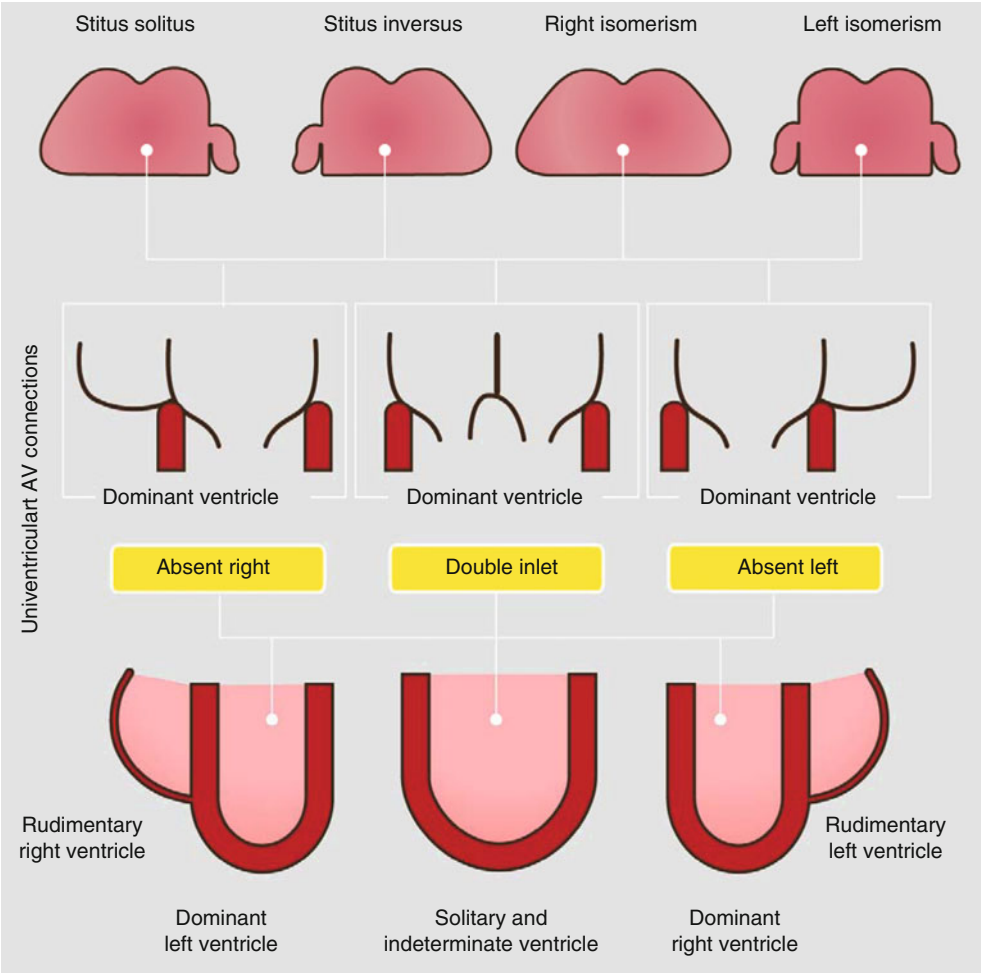


**Fig. 4.5** The variants of univentricular atrioventricular (*AV*) connections in situs solitus, situs inversus, and right and left isomerism

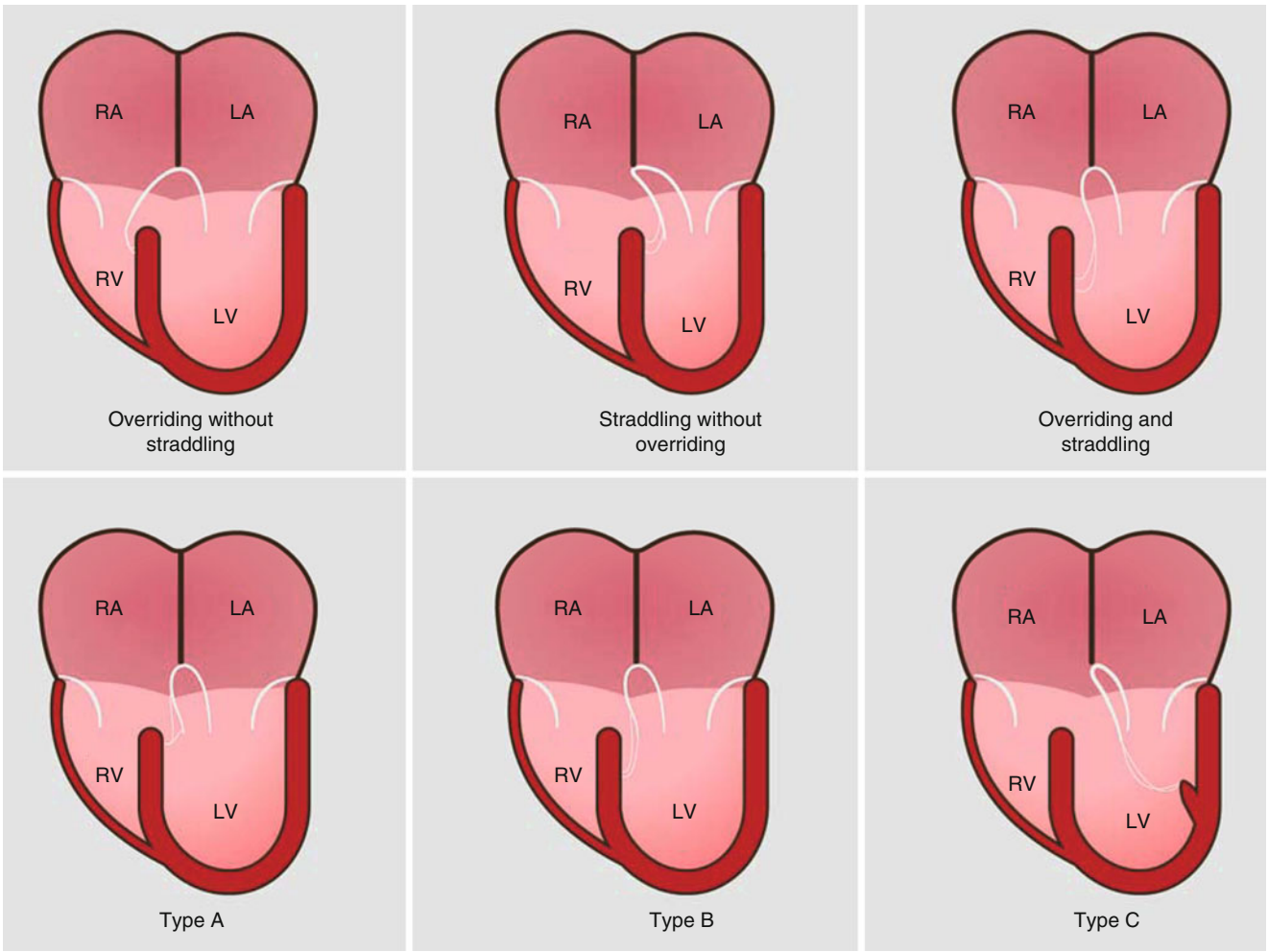


**Fig. 4.6** An artist's depiction of the concepts of straddling and overriding

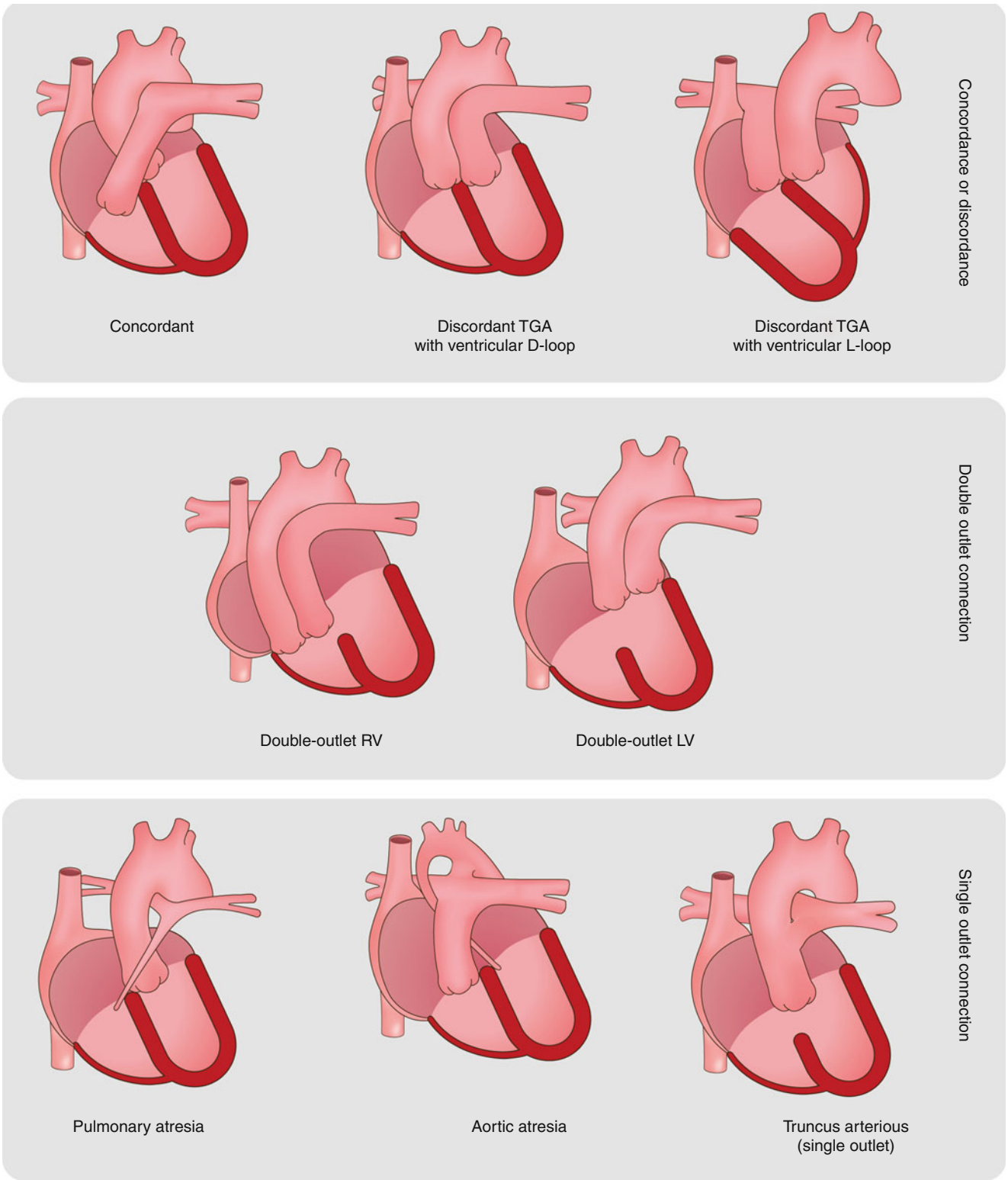


**Fig. 4.7** A depiction of the possible ventriculoarterial connections

## 4.4 Van Praagh Notation System

The nomenclature system used in the segmental, sequential approach developed by Van Praagh also includes a series of three letters, separated by commas, within parentheses which are used for conveying anatomic positioning. The first initial denotes the visceroarterial situs (S: solitus, I: inversus). The second initial marks the ventricular looping pattern (D: D-looping, L: L-looping). The third initial conveys the great artery positioning (S: solitus (normal)), I: inversus (with no transposition), D-TGA (D-transposition of the great arteries), L-TGA (L-transposition of the great arteries), D-MGA (D-malposition of the great arteries), L-MGA (L-malposition of the great arteries), A-TGA (ambiguous transposition of the great arteries), and finally A-MGA (ambiguous malposition of the great arteries) (Fig. 4.8). Thus, (S,D,S) would indicate the normal anatomy (solitus, D-looping, solitus), whereas (I, L, I) would indicate atrial situs inversus, ventricular L-looping, and inversus of the great vessels and (S,L,L-TGA) indicates atrial situs solitus, ventricular L-looping, and L-TGA.

Figure 4.9 depicts the various types of human hearts emphasizing the Van Praagh notation system [10].

Note that TGA is only one form of malposition. Malposition of the great arteries may also include double-outlet right ventricle, double-outlet left ventricle, and anatomically corrected malposition.

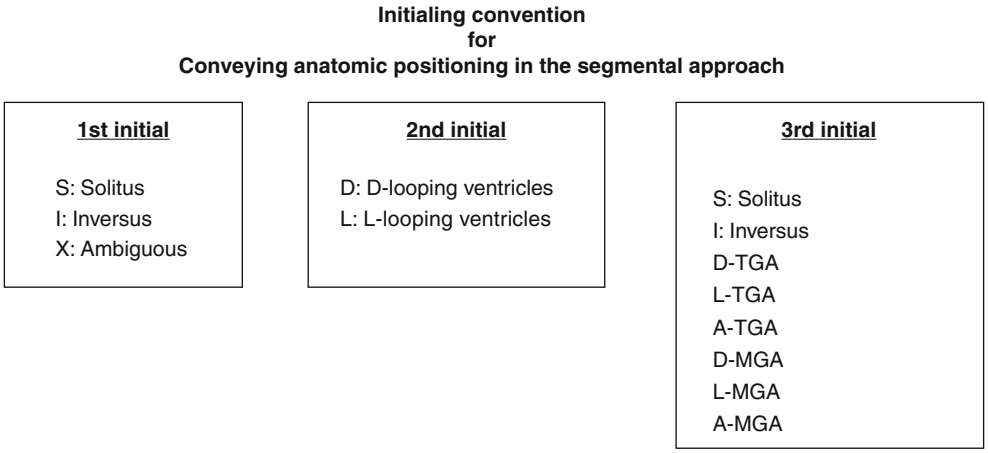


**Fig. 4.8** The initialing system used in the labeling of congenital heart disease patterns. The first initial is the atrial situs (*S* for solitus, *I* for inversus, *X* for ambiguous). The second initial involves the ventricular looping pattern (*D* for D-loop, *L* for L-loop) and the third letter is the spatial orientation of the great vessels (*S* for solitus, *I* for inversus, *D-TGA* for D-transposition of the great vessels, *L-TGA* for L-transposition of the great vessels, *A-TGA* for ambiguous transposition of the great vessels, *D-MGA* for D-malposition of the great vessels, *L-MGA* for L-malposition of the great vessels, *A-MGA* for ambiguous transposition of the great vessels)

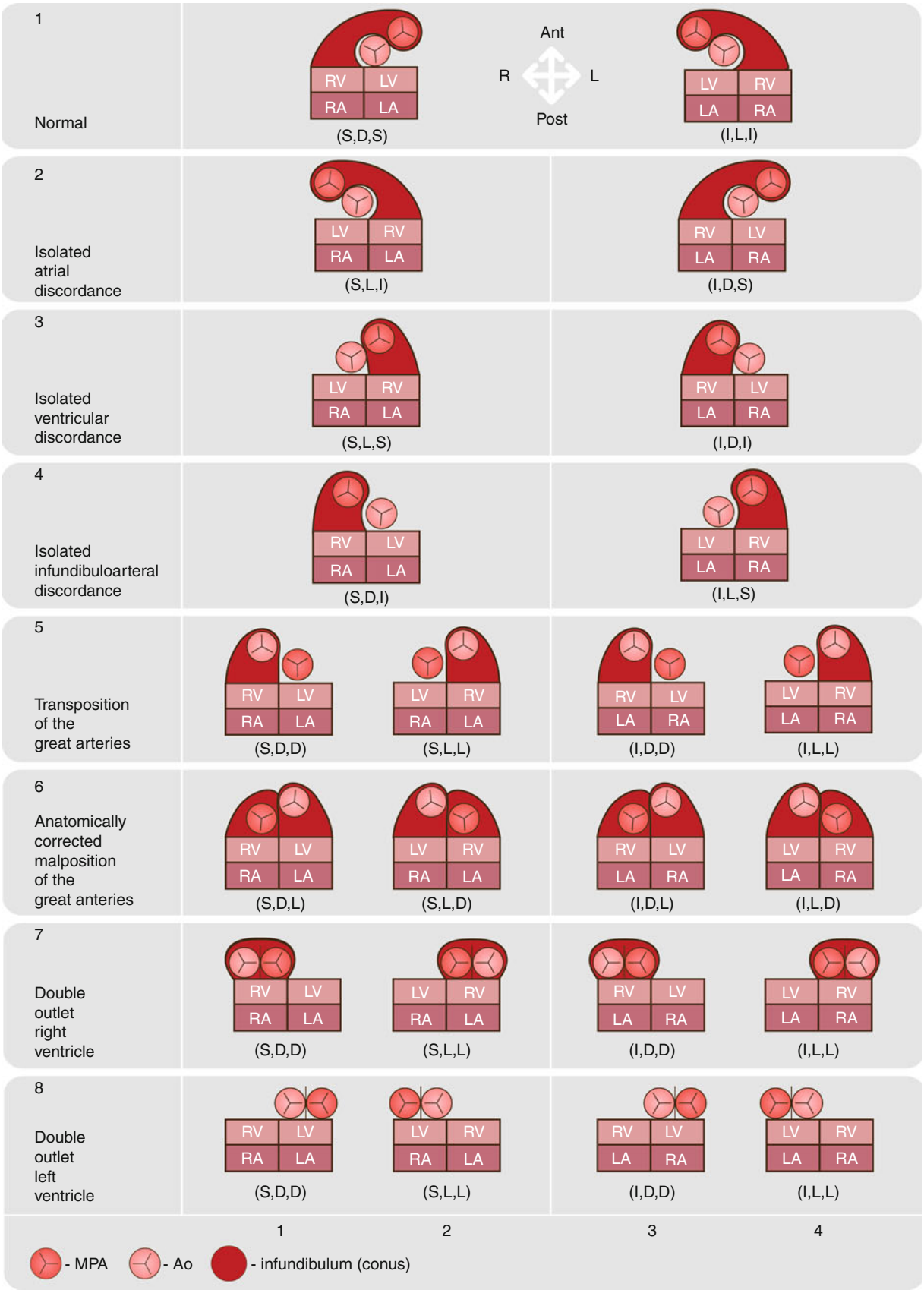


**Fig. 4.9** Depicts the various types of human hearts emphasizing the Van Praagh notation system (Reproduced with the kind permission of Ronald B. Foran, MD, Pediatric Cardiology Associates, Rockford Il)

## References


1. Anderson RH, Becker AE, Freedom RM, et al. Sequential segmental analysis of congenital heart disease. Pediatr Cardiol. 1984;5(4):281–7.
2. Van Praagh R. Terminology of congenital heart disease: glossary and commentary. Circulation. 1977;56(2):139–43.
3. Van Praagh R, Weinberg PM, Van Praagh S. Mal-position of the heart. In: Moss AJ, Adams FH, Emmanouilides GC, editors. Moss and Adams' heart disease in infants, children, and adolescents. 2nd ed. Baltimore: Williams & Wilkins; 1977. p. 394–417.
4. Van Praagh R. Diagnosis of complex congenital heart disease: morphologic-anatomic method and terminology. Cardiovasc Intervent Radiol. 1984;7(3–4):115–20.
5. Van Praagh R. The importance of segmental situs in the diagnosis of congenital heart disease. Semin Roentgenol. 1985;20(3):254–71.
6. Lapierre C, Dery J, Guerin R, Viremouneix L, Dubois J, Garel L. Segmental approach to imaging of congenital heart disease. Radiographics. 2010;30:397–411.
7. Van Mierop LH, Eisen S, Schiebler GL. The radiographic appearance of the tracheobronchial tree as an indicator of visceral situs. Am J Cardiol. 1970;26(4):432–5.
8. Jacobs JP, Anderson RH, Weinberg PM, et al. The nomenclature, definition and classification of cardiac structures in the setting of heterotaxy. Cardiol Young. 2007;17 suppl 2:1–28.
9. Moller JH, Nakib A, Anderson RC, Edwards JE. Congenital cardiac disease associated with polysplenia: a developmental complex of bilateral "left-sidedness". Circulation. 1967;36(5):789–99.
10. Praagh V. Normally and abnormally related great arteries. What have we learned. World J Pediatr Congenit Heart Surg. 2010;1(3):364–85.

# Segmental, Sequential Approach to CT Interpretation in Adult Congenital Heart Disease

5

The segmental, sequential, analytic approach was introduced by Van Praagh over 25 years ago [1–3]. This clinically useful approach is flexible and widely applicable to any imaging evaluation of congenital heart disease [4]. Using this logical approach, the morphologic features of the heart are determined sequentially by dividing the heart into three segments: visceroatrial situs or spatial arrangement (step 1), ventricular looping (step 2), and the spatial relationships of the great vessels (step 3). In step 4, the connections between the segments at the atrioventricular and ventriculoarterial levels are identified. Next, cardiac positioning is determined in step 5. Finally, step 6 involves the assessment for any associated malformation. See Fig. 5.1.

This chapter describes the sequential steps required for accurate and complete analysis of complex congenital heart disease during a review of any imaging study. By following these steps, the reader of cardiac computed tomographic angiography studies, for example, will more likely end with an accurate interpretation. Using the Van Praagh nomenclature and initialing system, a segmental, sequential, analytic approach to the cardiac anatomy is applied.

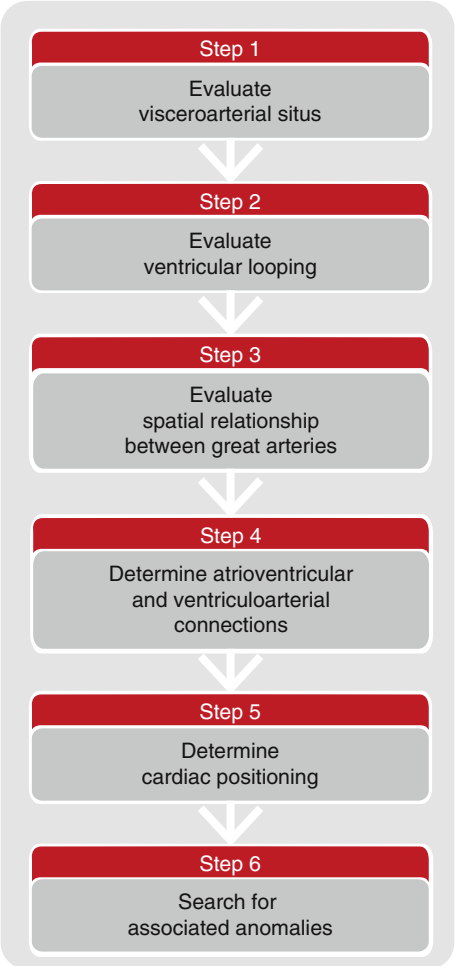


**Fig. 5.1** A depiction of the approach to the segmental, sequential analysis of congenital heart disease. Letters are used to convey anatomic positioning of the three cardiac segments. The first three steps in the analysis involve the determination of atrial situs (step 1) (solitus, *S*, or inversus, *I*, or ambiguous, *A*), the ventricular looping pattern (step 2) (D- or L-), and the great artery spatial orientation (step 3) (solitus, *S*; inversus, *I*; D-TGA; L-TGA; A-TGA; D-MGA; L-MGA; A-MGA). Step 4 identifies the atrioventricular and ventriculoarterial connections. Step 5 determines cardiac positioning. Step 6 identifies associated malformations

W. Mazur et al., *CT Atlas of Adult Congenital Heart Disease*,
DOI 10.1007/978-1-4471-5088-6_5, © Springer-Verlag London 2013

## 5.1 Assessment of Cardiac Anatomy

### 5.1.1 Step 1: Determination of the Visceroatrial Situs

There are three possible arrangements of the atria (termed situs): solitus (S, -, -,) (the normal arrangement), inversus (I, -, -,) (the mirror image arrangement), and ambiguous (also called heterotaxy) (A, -, -,). Heterotaxy includes right isomerism [bilateral morphologic right atria and bronchial tree anatomy (two morphologic right lungs)] and left isomerism [bilateral morphologic left atria and bronchial tree anatomy (two morphologic left lungs)] (Fig. 5.3, panel c and d).

On imaging studies, anatomic differentiation of the morphologic right from left atrial chambers is usually based on the different morphology of the atrial appendages. The right atrial appendage is blunt and has a broad base communicating with the rest of the atrium. The left atrial appendage is narrower and has a more restricted junction with the smooth-walled left atrium and is more trabeculated than the right atrial appendage (Fig. 5.2). In addition, the inferior vena cava is associated with the right atrium.

If the appendages are not adequately distinguishable, then determination of atrial situs can be made based on the thoracic and visceral situs. The atrial situs almost always follows the thoracic and visceral situs. That is, if the left lung (bilobed) can be identified as being on the left and the right lung (trilobed) can be identified as being on the right and, concomitantly, the spleen and stomach are on the right and the liver on the left, then atrial situs solitus is most likely.

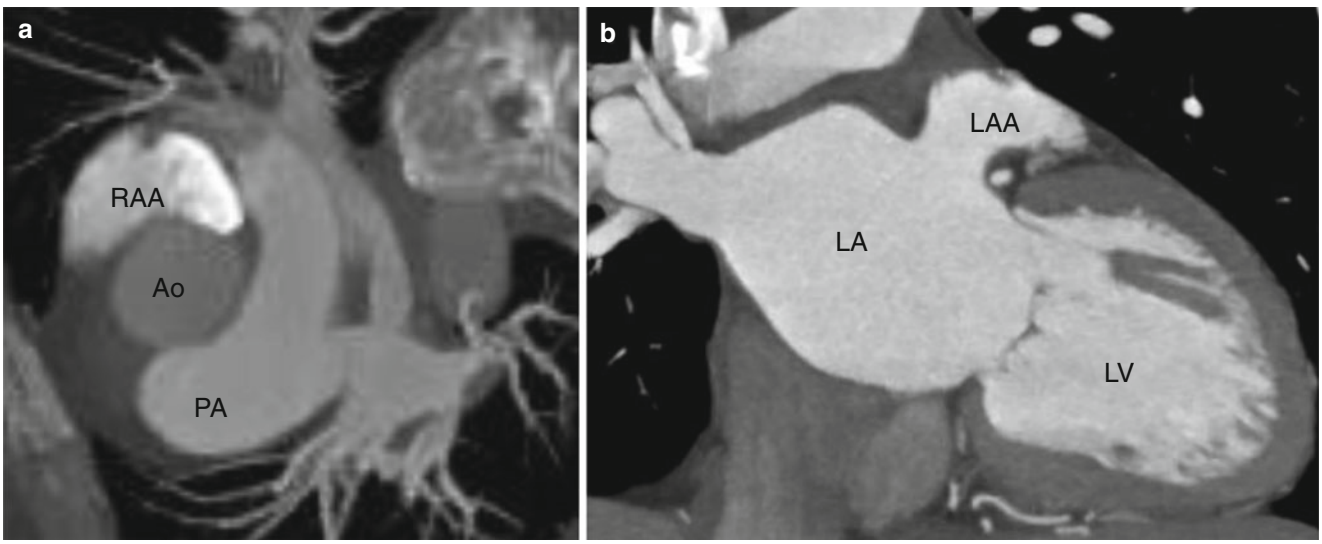


**Fig. 5.2** Computed tomographic (CT) examples of the right (panel **a**) and left (panel **b**) atrial appendages identifying the right and left atria, respectively. The right atrial appendage has a larger, broader connection to the right atrium, and the left atrial appendage has more trabeculations and a narrower connection with the left atrium. *RAA* right atrial appendage, *LAA* left atrial appendage, *RA* right atrium, *LA* left atrium, *RV* right ventricle, *LV* left ventricle, *PA* pulmonary artery

Inference can also be made from the spatial relationship among the abdominal great vessels and the spine (Fig. 5.3). The abdominal aorta usually descends slightly to the left of the spine with the inferior vena cava to the right of the spine and anterior to the aorta. Reversal of this pattern is seen with atrial situs inversus. Right isomerism is most commonly associated with the aorta and vena cava on the same side of the spine with the aorta being the more posterior of the two vessels. Left isomerism is usually associated with an interruption of the suprarenal portion of the inferior caval vein with azygous continuation to the right atrium.

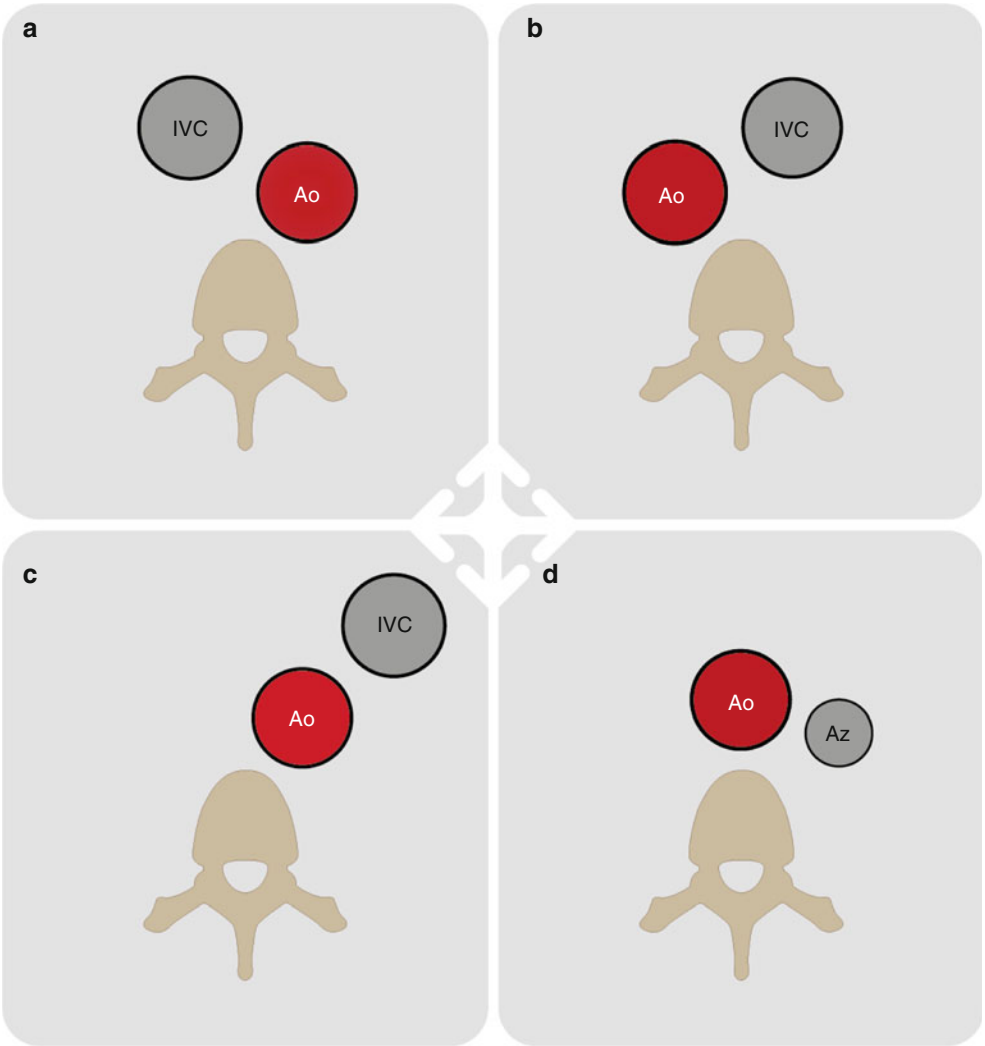


**Fig. 5.3** The spatial arrangement of aorta (*Ao*) and great veins in situs solitus (**a**), situs inversus (**b**), right isomerism (**c**), and left isomerism (**d**). *IVC* inferior vena cava, *Az* azygous vein. See text for description

### 5.1.2 Step 2: Determination of the Orientation of the Ventricular Loop

The second step is to assess the ventricular looping pattern. Two ventricular looping patterns are possible: D-loop (–, D, -) and L-loop (–, L, -). In early normal development, the heart is a linear tube containing primitive atria, the left ventricular segment, the bulbus cordis (which will develop into the right ventricle), and the truncus arteriosus (forms the great arteries). During subsequent development, the bulboventricular loop normally folds to the right, forming the D-loop morphology with subsequent positioning of the bulbus cordis (precursor to the right ventricle) to the right of the left ventricle. If the primitive heart tube loops toward the left, it forms the L-loop morphology with the right ventricle positioned to the left of the left ventricle (See Fig. 1.2). Figure 5.4, panel a, depicts a CT image of a D-loop (normal) heart and an L-loop heart, panel b, where the right and left ventricles are reversed.

The left and right ventricles are best differentiated by identifying the differences in morphology of the apical trabecular portion. The right ventricle has coarse apical trabeculations and a prominent moderator band crossing the ventricular chamber, whereas the left ventricle has finer trabeculations and no moderator band. The left ventricle has more prominent papillary muscles than the right ventricle (Fig. 5.5). In addition, the location of the atrioventricular and ventriculoarterial valves helps to differentiate between the right and left ventricles (see Chap. 4).

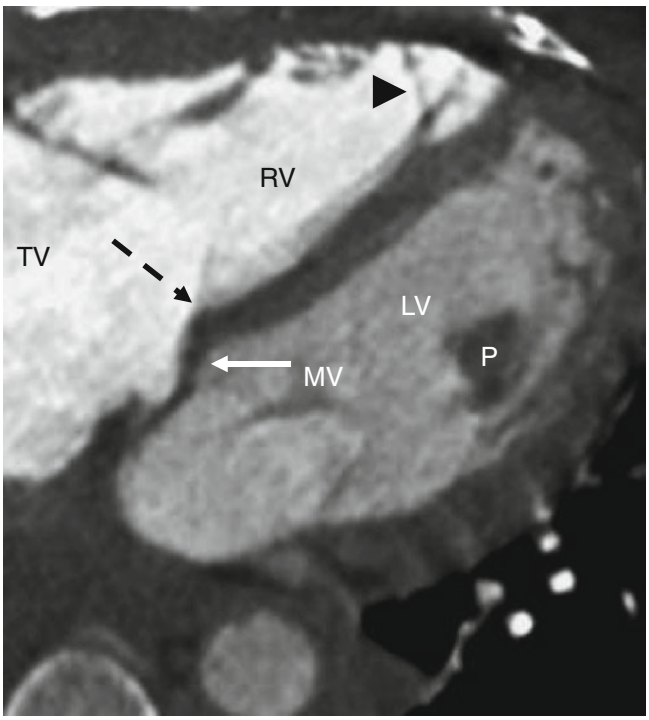


**Fig. 5.5** CT image illustrating the differing features of the right (*RV*) and left ventricles (*LV*). The RV has the moderator band (*black arrowhead*). The RV is associated with the tricuspid valve (*TV*) whose septal leaflet (*black dashed arrow*) inserts more apically than the anterior leaflet (*white arrow*) of the mitral valve (*MV*) which is associated with the LV. In addition, the LV papillary muscles (*P*) are more prominent than those in the RV

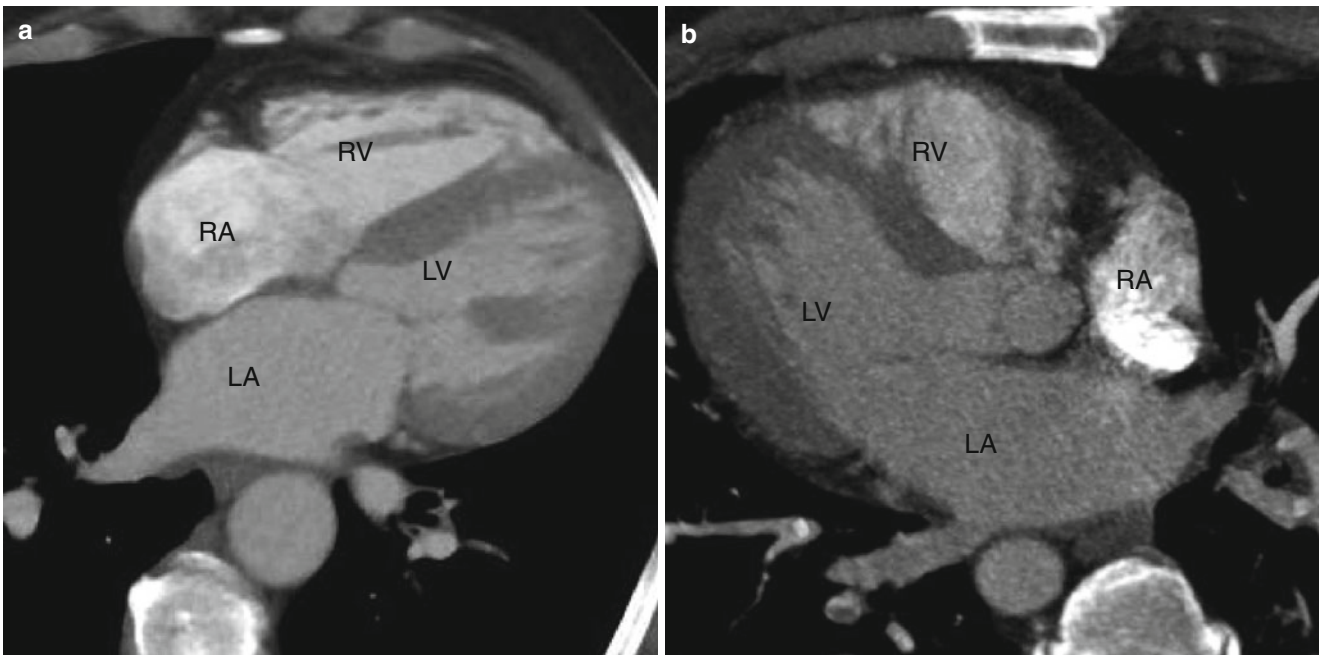


**Fig. 5.4** Panel (**a**) illustrates an example of a D-loop normal heart where the left ventricle (*LV*) is on the left and the right ventricle (*RV*) is on the right and anterior. Panel (**b**) depicts an L-loop where the RV is the leftward ventricle and the LV is the right-sided ventricle. The atria situs is normal (solitus) in both examples. *RA* right atrium, *LA* left atrium

### 5.1.3 Step 3: Determination of the Spatial Position of the Great Vessels

There are eight possible configurations of the great vessels: solitus or normal (–, -, S), inversus or mirror image (_, _, I), D-transposition of the great arteries (–, -, D-TGA), L-transposition of the great arteries, (–, -, L-TGA), A-transposition of the great arteries (–, -, A-TGA), D-malformation of the great vessels (–, -, D-MGA), L-malformation of the great vessels (–, -, L-MGA), and A-malformation of the great vessels (–, -, A-MGA). Remember, transposition is only one form of malposition. Figure 5.6 demonstrates 4 of these possibilities (solitus, inversus, D-TGA, and L-TGA).

The great vessels are identified by their branch vessels. The aorta gives rise to at least one coronary artery and most of the systemic circulation (Fig. 5.7). The main pulmonary trunk feeds at least one pulmonary artery (Fig. 5.8). In the normal arrangement, the aorta is posterior and to the right of the pulmonary artery (Fig. 5.9).

There are four possible types of conal (infundibular) anatomy that must be potentially identified: subpulmonary conus (normal), subaortic conus, bilateral conus, and bilaterally absent conus (Fig. 5.10). Subaortic conus is seen in cases of D- or L-transposition. Bilateral conus is found in cases of double-outlet right ventricle and bilaterally absent conus is noted in cases of double-outlet left ventricle.

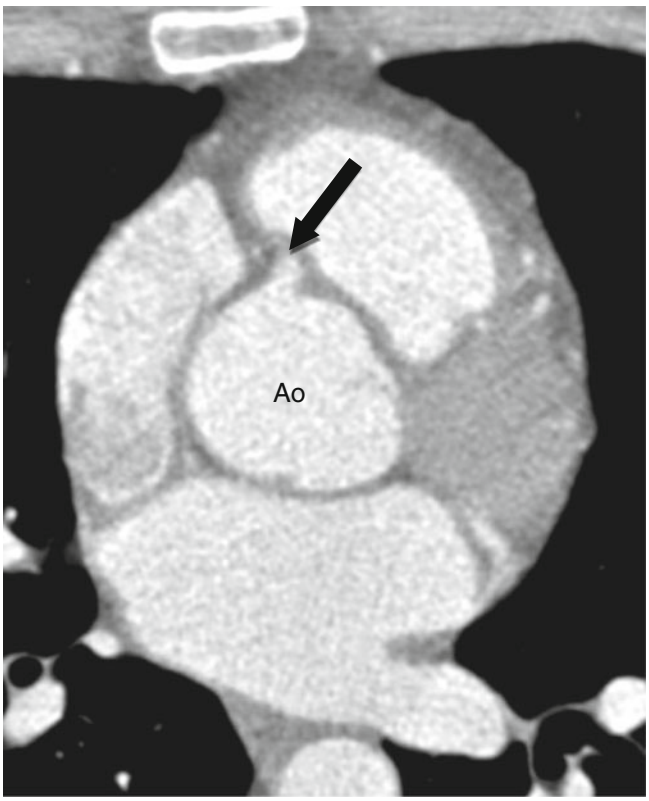


**Fig. 5.7** An axial CT image definitively identifying the aorta by its emanating coronary artery (*arrowhead*). In this instance, the right coronary artery. *Ao* aorta

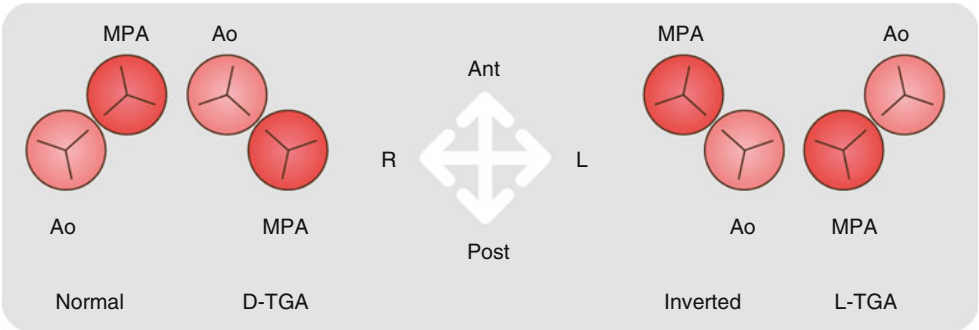


**Fig. 5.6** Spatial anatomy of the great vessels in four of the eight possible great vessel arrangements: normal, inverted (mirror image arrangement), dextro-transposition of the great arteries (D-TGA), and levo-transposition of the great arteries (L-TGA). Normal or D-TGA is seen in D-bulboventricular looping. In L-bulboventricular looping, the relationships are inverted. *Ao* aorta, *MPA* main pulmonary artery

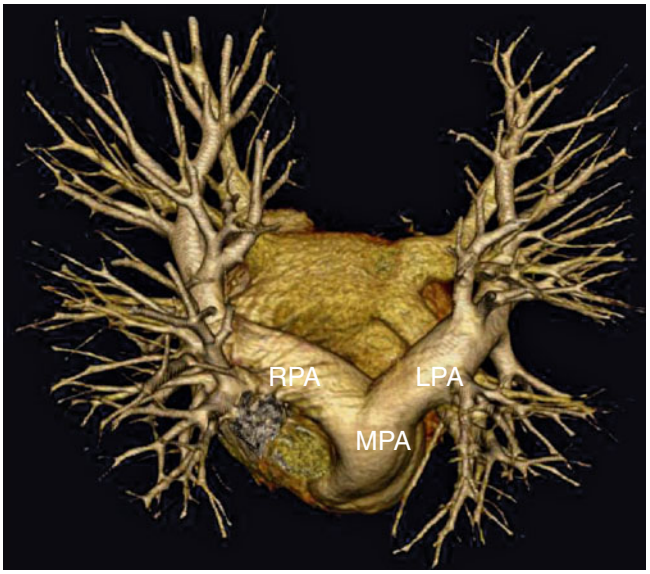


**Fig. 5.8** A volume-rendered posterior-oriented 3-D CT image identifying the main pulmonary artery by its associated branches. *MPA* main pulmonary artery, *RPA* right pulmonary artery, *LPA* left pulmonary artery. One or more pulmonary arteries arising from the main pulmonary artery is the signature of the pulmonary artery

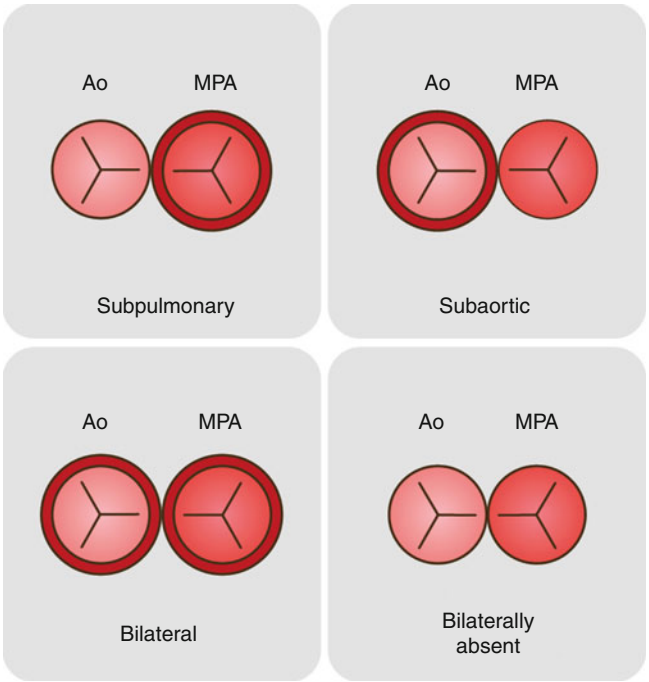


**Fig. 5.10** Normal conus anatomy: subpulmonary (normal), subaortic, bilateral, and bilaterally absent. Subaortic conus is common in transposition, whereas bilateral conus is seen in cases of double-outlet right ventricle and bilaterally absent conus is noted in double-outlet left ventricle. In this picture, the conus is represented by the *dark, red ring*

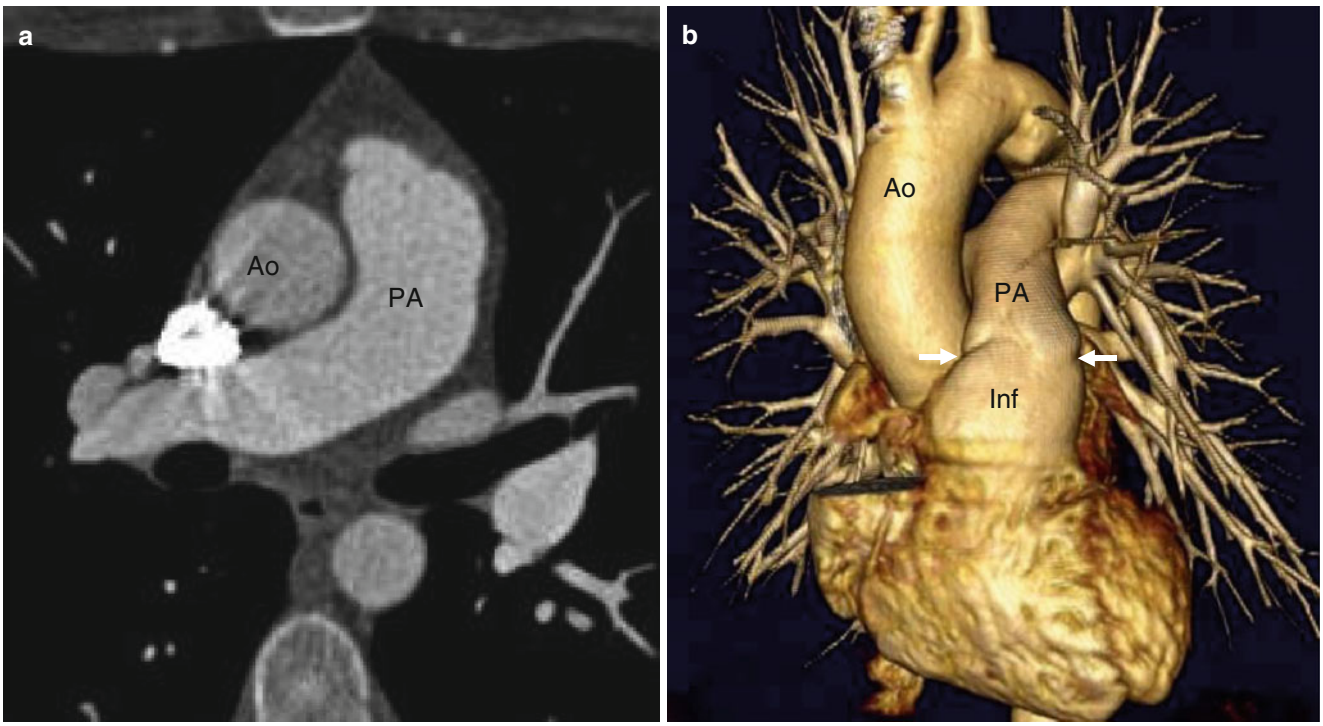


**Fig. 5.9** Panel (**a**) is an axial, maximum-intensity projection, CT image demonstrating the normal spatial orientation of the great vessels. The PA is to the left of the aorta. Panel (**b**) is a 3-dimensional volume-rendered CT image showing the aorta posterior and to the right of the pulmonary artery. *Ao* aorta, *PA* pulmonary artery, *white arrows* (pulmonary valve)

## 5.2 Assessment of Connecting Segments

Specification of atriovisceral situs, orientation of the ventricular loop, and spatial orientation of the great vessels do not specify the atrioventricular and ventriculoarterial connections. The atrioventricular and ventriculoarterial connections are independently determined embryologically and, thus, need to be separately evaluated in terms of biventricular versus univentricular connections (step 4).

### 5.2.1 Ventriculoarterial Connections

Step 4 begins with an assessment of the junction between the ventricles and great arteries. There are four types of ventriculoarterial connections: concordant (normal), discordant (mirror image/transposition of the great arteries), double outlet (double outlet right or left ventricle), and single outlet (common arterial trunk, aortic atresia, or pulmonary atresia). See Fig. 4.7.

### 5.2.2 Atrioventricular Connections

Following the ventriculoarterial connection analysis, step 4 also includes an evaluation of the atrioventricular connections. Biventricular atrioventricular connections refer to an arrangement where each atrium is connected to its own ventricle. Univentricular atrioventricular connections describe connections where only one ventricle is connected to the atrial mass. There are five types of atrioventricular connection: concordant (normal), discordant, ambiguous, double inlet, single inlet with absent right atrial connection, and single inlet with absent left atrial connection. Concordant, discordant, and ambiguous connections are associated with a biventricular heart. Double inlet and single inlet with an absent connection are used when there is a univentricular heart.

## 5.3 Cardiac Position

After specification of cardiac anatomy and assessment of connecting segments, the position of the heart in the chest cavity and the orientation of the apex need to be specified. For a complete discussion of cardiac position, see Chap. 4 and Fig. 4.1.

## 5.4 Assessment of Associated Malformations

Associated malformations need to be assessed in a segmental fashion at three levels: the heart, great vessels, and coronary arteries. At the level of the heart, the presence, size, and location of atrial and ventricular septal defects, the size of the cardiac chambers, and the presence and severity of ventricular outflow obstructions need to be documented. Great vessel anatomy needs to be reviewed for the presence of stenotic or hypoplastic segments as well as the presence of a patent ductus arteriosus. Next, an evaluation of systemic and pulmonary venous return should be performed. Coronary anatomy and the presence of coronary anomalies need to be noted as well, and coronary artery disease needs to be described according to published guidelines. Finally, the presence and any complications of palliative shunts, closure devices, and stents need to be reported.

## References

1. Van Praagh R. Terminology of congenital heart disease. Glossary and commentary. Circulation. 1977;56:139–43.
2. Van Praagh R. Diagnosis of complex congenital heart disease: morphologic-anatomic method and terminology. Cardiovasc Intervent Radiol. 1984;7:115–20.
3. Van Praagh R. The importance of segmental situs in the diagnosis of congenital heart disease. Semin Roentgenol. 1985;20:254–71.
4. Lapierre C, Dery J, Guerin R, Viremouneix L, Dubois J, Garel L. Segmental approach to imaging of congenital heart disease. Radiographics. 2010;30:397–411. doi:10.1148/rg.302095112.

# Part III

# CT Imaging Techniques in Adult Congenital Heart Disease

# Technical Principles of Computed Tomographic Angiography for Adult Congenital Heart Disease

6

The computed tomographic angiography (CTA) imaging protocol must be tailored to the suspected cardiac lesion and the type of prior surgical repair. The relevant parameters that need to be selected prior to imaging are contrast volume, contrast injection speed, the timing of the scan, slice collimation, scan length, tube voltage (kV), tube current (mA), and pitch. In addition, the imager must decide on the use of non-ECG-synchronized acquisition versus ECG synchronization (prospective or retrospective). In general, multidetector scanner with ≥64 rows is preferred for evaluation of congenital heart disease (CHD).

CTA protocols for assessing adult patients with known or suspected congenital heart disease are similar to standard coronary artery CTA imaging protocols with one major exception. For coronary artery imaging, scan timing is adjusted to avoid right ventricular contrast opacification since it may interfere with assessment of right coronary artery anatomy. In imaging CHD, adequate contrast opacification of both the right and left ventricles is necessary to adequately visualize the complex right- and left-sided anatomy. Not only must scan timing be altered to allow this, but at times, a delayed scan is necessary to allow adequate recirculation of contrast through complex anomalies and their potential corrections such that all the necessary anatomy is adequately opacified.

## 6.1 Contrast Agent Administration

Low-dose pre-contrast imaging is indicated in patients who have prior surgical repairs as it allows identification of calcified conduits and septal patches and minimizes the risk of confusing these expected changes with true postoperative complications, particularly vascular leaks. For contrast administration, a right-arm injection is preferred to avoid contrast artifacts often associated with injection into the left brachiocephalic vein. To reduce artifacts from undiluted contrast material, a saline bolus chaser should be used. We prefer the automated bolus tracking technique to determine the appropriate imaging delay. In adults, the region of interest is placed in the ascending aorta, and the attenuation threshold is set at 140 HU. An appropriate, fixed delay time (generally 15 s) may be used when the right heart, superior vena cava, or complicated shunts such as the Glenn shunt or the superior limb of a baffle are areas of interest.

To achieve both right and left ventricular opacification, a biphasic contrast injection protocol (contrast followed by a saline injection) is appropriate. Monophasic injections (contrast only) should be avoided since these cause excessive streak artifacts. If complex shunts such as Glenn or Fontan are present, additional delayed scanning should be performed 60 s after start of the contrast injection to opacify the venopulmonary circuit.

Imaging protocols for patients with CHD should closely mimic standard coronary artery imaging protocols since the detection of coronary artery disease remains pertinent since the prevalence of coronary artery disease is similar to that of the general population. In fact, recent studies support coronary angiography in patients with CHD older than 40 years before corrective surgery [1]. It is not unusual to perform corrective surgery in adults with congenital heart disease simultaneously with coronary artery bypass grafting [2]. In order to diagnose coronary artery images, aggressive heart rate reduction is required to prevent motion artifact. We prefer a resting heart rate of ≤60 beats per minute which not only helps to prevent motion artifact but also allows the use of radiation reduction protocols.

## 6.2 Slice Collimation (Slice Thickness)

Thicker detector collimation (2 mm) is preferable to reduce radiation dose and improve image quality, although visualization of small structures is diminished. In addition, the CTA acquisition time is lower when using thicker collimation, and consequently radiation dose and respiratory motion artifacts are reduced. However, if evaluation of small intracardiac structures or the coronary arteries is indicated, thinner collimation should be used.

W. Mazur et al., *CT Atlas of Adult Congenital Heart Disease*,
DOI 10.1007/978-1-4471-5088-6_6, © Springer-Verlag London 2013

Contrast volume is usually between 80 milliliters (ml) and 120 ml with higher volumes being used for more complex shunting anomalies to allow adequate mixing of contrast. The injection rate is generally between 5 and 7 ml/s.

## 6.3 Scan Length (Z-Axis Coverage)

Since the CTA radiation dose is directly proportional to the scan length, it is essential that the scan length be minimized to include only the area of interest. The typical scan length for adults is 12–13 centimeters (cm) and extends from just below the carina to slightly below the diaphragm. If great vessel anomalies are expected, a longer scan length extending superiorly may be required to allow visualization of the entire aortic arch area. A recent study has shown that for each 1 cm reduction in scan length, the retrospectively gated CTA radiation dose is reduced by 5 % [3].

## 6.4 ECG-Controlled Tube-Current Modulation

Modulating tube current during the R–R interval (ECG current modulation, ECG CM) has proven to be an effective dose reduction strategy in retrospective ECG-gated CTA [4]. Using ECG CM, the tube current outside the predetermined cardiac cycle is reduced relative to the current inside the pulsing window. In one series, tube current was maintained at its maximum during diastole and reduced to approximately 20 % of the maximum in systole. This approach has been shown to reduce radiation dose by as much as 40 % without loss of image quality [4]. The optimal ECG pulsing window for cardiac CTA depends on the patient's heart rate [5, 6].

## 6.5 Tube Voltage

Reducing the tube voltage from 120 to 100 kV can reduce radiation dose by up to 50 % [7]. Using a kV of 80 in appropriate patients may further reduce radiation exposure [7, 8]. In patients who weigh ≤85 kg or who have a body mass index (BMI) of ≤30 kg/meter $(m)^2$, a tube voltage of 100 kV is appropriate. Patients who weigh ≤60 kg or in those with a BMI ≤ 25 $kg/m^2$, a tube voltage of 80 kV may be used.

## 6.6 Pitch

Pitch is defined as the ratio of table travel (mm) per gantry rotation to scan length. The latest generation of dual-source CTA technology permits scanning at very high pitches. In single-source CTA, the maximum pitch is limited to approximately 1.5. In the high-pitch dual-source scanner, the second detector system is used to fill the imaging gaps created by high-pitch imaging [9]. By interweaving data from the two detectors, the pitch can be increased to as high as 3.4, thus reducing the acquisition time to image the entire chest to below 1 s [10]. The high-pitch mode has been demonstrated to provide artifact-free visualization of the coronary arteries at a radiation exposure less than 1 mSv [9].

## 6.7 Non-ECG-Gated Cardiac CTA

Since coronary artery anomalies are common in many types of congenital heart disease, ECG gating is often performed when CTA is used for the evaluation of CHD.

Non-ECG-synchronized CTA allows for fast acquisition of cardiac and extracardiac structures but limits the resolution of small cardiac and coronary structures because of cardiac motion artifacts. To improve image quality, detector collimation should be thicker in non-ECG-synchronized CTA. With current CTA systems, it has been shown that the origins and proximal segments of the coronary arteries are evaluable in 82 % of patients with CHD when non-ECG-synchronized CTA acquisition protocols are used [11].

## 6.8 ECG-Gated Cardiac CTA

Retrospective ECG-gated cardiac CTA uses oversampling of information across different phases of the cardiac cycle and across several consecutive heartbeats. Here, the data acquisition is obtained with continuous table motion and low-pitch scanning to allow overlap of slice data which results in higher radiation doses than when using non-ECG- synchronized CTA. However, synchronization to the ECG provides artifact-free visualization of cardiac and coronary structures even at elevated heart rates.

Although ECG synchronization allows for the assessment of left and right ventricular function, comparable information can be obtained by performing a non-ECG-synchronized scan to evaluate cardiac anatomy and morphology while utilizing echocardiography for functional information which cannot be obtained with non-ECG-gated scanning.

Prospective ECG-triggered CTA scanning is performed at user-selected predefined phases of the cardiac cycle. This acquisition mode uses the "step-and-shoot" approach, whereby radiation is delivered during a prospectively defined time window in mid-diastole. The table moves in a sequential manner and remains stationary while data are acquired. Because of the confinement of the radiation output to only a small part of cardiac cycle, prospectively triggered cardiac CTA may be performed with radiation doses as low as 1–5 millisieverts (mSv), compared to 12–15 mSv for a conventional retrospectively gated, helical scanning [12, 13].

Unlike retrospectively acquired scanning, prospective acquisition permits only static imaging of the heart since data are not acquired throughout every phase of the cardiac cycle. Thus, evaluation of cardiac function is not possible using prospective gating CTA techniques.

As a rule, gated studies are used as problem-solving techniques or when ventricular parameters are required. To date, prospective triggering has almost completely replaced retrospective triggering in patients with CHD if coronary artery evaluation is indicated. A retrospectively triggered scan should be used in patients with arrhythmia or in patients where artifact is expected so that reconstructions for a wider range of cardiac phases may be used to improve the diagnostic evaluation. If gating is to be performed in CHD patients with right heart failure, care must be exercised when using beta-blockers since their use can exacerbate the condition.

## 6.9 Padding

Radiation exposure from CTA can be minimized by shortening the time window during which images are acquired. Padding is the period of time during the cardiac cycle, beyond the minimum necessary, that the X-ray beam is activated for image acquisition. Padding is used to increase data collection and potentially improve the diagnostic value of the scan by increasing the number of possible phases that may be reconstructed and used for evaluation [14]. If all other scan parameters are kept constant, increased padding is associated with a greater radiation dose. Overall, the radiation dose increases by about 45 % for every 100 millisecond (ms) increase in the padding time ($p<0.001$) [14]. Without padding, the average radiation dose is 2.3 mSv in prospectively triggered scan. Conversely, when medium and long padding times are employed, radiation doses are 3.8 and 5.5 mSv, respectively [14].

## 6.10 Iterative Reconstruction

Traditionally, filtered back projection (FBP) is used to reconstruct the CTA scan data. Iterative reconstruction utilizes a computer model to reconstruct the CTA image. This more precise reconstruction method requires less signal to noise ratio (allowing reduced acquisition radiation doses) to accurately reconstruct a high-quality CTA image free of noise [15, 16]. The use of iterative reconstruction results in improved image quality with less noise than FBP while using lower radiation doses [16]. Iterative reconstruction is associated with a 27 % reduction in radiation dose compared with standard FBP methods ($p<0.001$) [15]. The median radiation doses are 2.3 mSv versus 4.1 mSv ($p<0.001$) for iterative reconstruction and FBP, respectively [15]. In addition, similar levels of image noise were achieved with 80 and 100 kV using iterative reconstruction compared to 120 kV with FBP, resulting in a 62 % reduction in effective dose [15, 16].

In summary, by combining several of the above-mentioned radiation-sparing methods, radiation doses in the 1 mSv range are now routinely possible, making CTA an attractive imaging technique for comprehensive evaluation of adults with CHD. Updated guidelines and comprehensive state-of-the-art review on radiation dose and dose-optimization strategies in CTA were published in 2011 [15].

## References


1. Yalonetsky S, Horlick EM, Osten MD, Benson LN, Oechslin EN, Silversides CK. Clinical characteristics of coronary artery disease in adults with congenital heart defects. Int J Cardiol. 2011. doi:10.1016/j.ijcard.2011.07.021.
2. Stulak JM, Dearani JA, Burkhart HM, Ammash NM, Phillips SD, Schaff HV. Coronary artery disease in adult congenital heart disease: outcome after coronary artery bypass grafting. Ann Thorac Surg. 2012;93:116–22. doi:10.1016/j.athoracsur.2011.09.013; discussion 122–3.
3. Hausleiter J, Meyer T, Hermann F, Hadamitzky M, Krebs M, Gerber TC, et al. Estimated radiation dose associated with cardiac CT angiography. JAMA. 2009;301:500–7. doi:10.1001/jama.2009.54.
4. Hausleiter J, Meyer T, Hadamitzky M, Huber E, Zankl M, Martinoff S, et al. Radiation dose estimates from cardiac multislice computed tomography in daily practice: impact of different scanning protocols on effective dose estimates. Circulation. 2006;113:1305–10. doi:10.1161/CIRCULATIONAHA.105.602490.
5. Leschka S, Scheffel H, Desbiolles L, Plass A, Gaemperli O, Valenta I, et al. Image quality and reconstruction intervals of dual-source CT coronary angiography: recommendations for ECG-pulsing windowing. Invest Radiol. 2007;42:543–9. doi:10.1097/RLI.0b013e31803b93cf.
6. Weustink AC, Mollet NR, Pugliese F, Meijboom WB, Nieman K, Heijenbrok-Kal MH, et al. Optimal electrocardiographic pulsing windows and heart rate: effect on image quality and radiation exposure at dual-source coronary CT angiography. Radiology. 2008;248:792–8. doi:10.1148/radiol.2483072098.
7. Bischoff B, Hein F, Meyer T, Hadamitzky M, Martinoff S, Schomig A, et al. Impact of a reduced tube voltage on CT angiography and radiation dose: results of the PROTECTION I study. JACC Cardiovasc Imaging. 2009;2:940–6. doi:10.1016/j.jcmg.2009.02.015.
8. Suess C, Chen X. Dose optimization in pediatric CT: current technology and future innovations. Pediatr Radiol. 2002;32:729–34. doi:10.1007/s00247-002-0800-x; discussion 751–4.
9. Achenbach S, Goroll T, Seltmann M, Pflederer T, Anders K, Ropers D, et al. Detection of coronary artery stenoses by low-dose, prospectively ECG-triggered, high-pitch spiral coronary CT angiography. JACC Cardiovasc Imaging. 2011;4:328–37.
10. Goetti R, Baumuller S, Feuchtner G, Stolzmann P, Karlo C, Alkadhi H, et al. High-pitch dual-source CT angiography of the thoracic and abdominal aorta: is simultaneous coronary artery assessment possible? AJR Am J Roentgenol. 2010;194:938–44. doi:10.2214/AJR.09.3482.
11. Goo HW, Yang DH. Coronary artery visibility in free-breathing young children with congenital heart disease on cardiac 64-slice CT: dual-source ECG-triggered sequential scan vs. single-source non-ECG-synchronized spiral scan. Pediatr Radiol. 2010;40:1670–80.
12. Halliburton SS, Abbara S, Chen MY, Gentry R, Mahesh M, Raff GL, et al. Society of Cardiovascular Computed Tomography. SCCT guidelines on radiation dose and dose-optimization strategies in cardiovascular CT. J Cardiovasc Comput Tomogr. 2011;5:198–224. doi:10.1016/j.jcct.2011.06.001.

13. Maruyama T, Takada M, Hasuike T, Yoshikawa A, Namimatsu E, Yoshizumi T. Radiation dose reduction and coronary assessability of prospective electrocardiogram-gated computed tomography coronary angiography: comparison with retrospective electrocardiogram-gated helical scan. J Am Coll Cardiol. 2008;52:1450–5. doi:10.1016/j.jacc.2008.07.048.
14. Labounty TM, Leipsic J, Min JK, Heilbron B, Mancini GB, Lin FY, et al. Effect of padding duration on radiation dose and image interpretation in prospectively ECG-triggered coronary CT angiography. AJR Am J Roentgenol. 2010;194:933–7. doi:10.2214/AJR.09.3371.
15. Leipsic J, Labounty TM, Heilbron B, Min JK, Mancini GB, Lin FY, et al. Estimated radiation dose reduction using adaptive statistical iterative reconstruction in coronary CT angiography: the ERASIR study. AJR Am J Roentgenol. 2010;195:655–60. doi:10.2214/AJR.10.4288.
16. Renker M, Ramachandra A, Schoepf UJ, Raupach R, Apfaltrer P, Rowe GW, et al. Iterative image reconstruction techniques: applications for cardiac CT. J Cardiovasc Comput Tomogr. 2011;5:225–30. doi:10.1016/j.jcct.2011.05.002.

# Part IV

# Congenital Dysplasias and Cardiomyopathies

# Arrhythmogenic Right Ventricular Dysplasia

7

Arrhythmogenic right ventricular dysplasia (ARVD) is a nonischemic, genetically determined, myocardial disease that involves primarily the right ventricle (RV) and is associated with life-threatening ventricular arrhythmias. Its prevalence has been estimated to vary from 1:2,500 to 1:5,000 and it is seen predominantly in males [1]. About 30–50 % of cases have a familial distribution [1]. ARVD is a major cause of sudden cardiac death in young athletes. Symptoms are usually exercise-related.

Pathologically, it is characterized by hypokinesia of the free wall of the right ventricle, fibrofatty replacement of the right ventricular myocardium, and right ventricular aneurysms. ARVD criteria were revised in 2010 [2]. The 2010 Task Force Criteria identify echocardiography, RV angiography, and magnetic resonance imaging (MRI) as appropriate imaging modalities in the diagnosis and assessment of ARVD [2]. While computed tomography (CT) is not listed as appropriate, more recent opinion favors CT as an appropriate imaging modality for this disease (second to MRI). Of note, myocardial fat in the RV detected by CT or MRI is not included in either the original or revised Task Force Criteria [2].

## 7.1 Imaging Features of ARVD

Characteristic CT findings include dilatation of the RV, extensive epicardial and myocardial fat, and a scalloped appearance of the RV free wall, corresponding to bulging, outpouching, or an aneurysm [3]. Fat can be seen in the RV interventricular septum and moderator band (Fig. 7.1). Fatty infiltration can also involve the left ventricle (LV) and appears as a wedge-shaped or band-like pattern in the subepicardium of the LV free wall. Of note, it may be difficult to differentiate fibrofatty replacement of the RV free wall from epicardial fat, as the RV free wall is usually thin (<4 mm). ARVD is a progressive disease that begins with segmental fatty infiltration of the RV and progresses to diffuse RV involvement.

Fatty tissue is identified by CT as low-attenuation tissue (negative Hounsfield units) that does not enhance with contrast. In addition, gated CT may identify global and segmental RV dysfunction that is characteristic of ARVD. The ARVD Task Force Criteria report specific MRI-derived values for RV end-diastolic volume index and for RV ejection fraction that may be applied to CT [2].

W. Mazur et al., *CT Atlas of Adult Congenital Heart Disease*,
DOI 10.1007/978-1-4471-5088-6_7, © Springer-Verlag London 2013

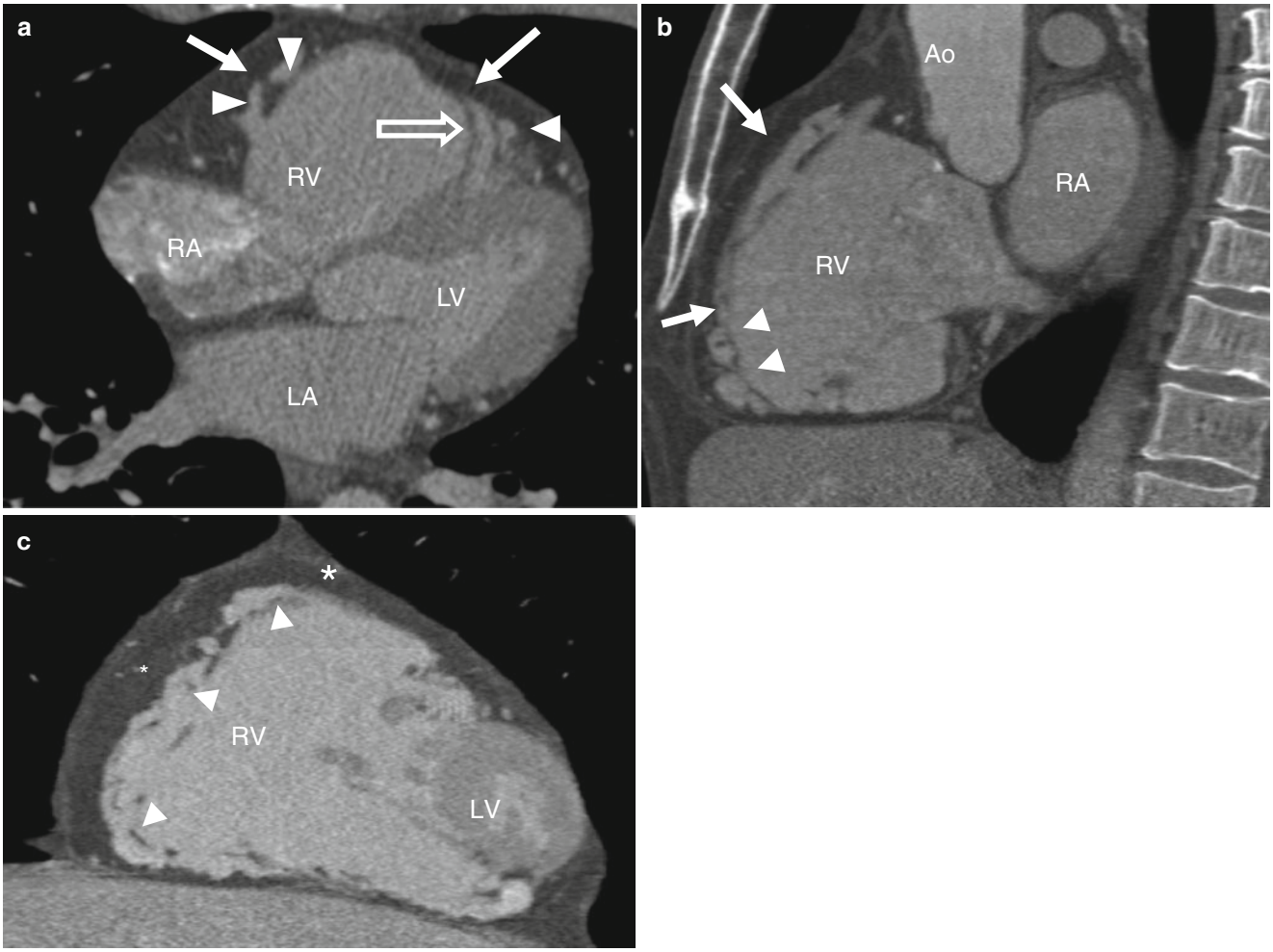


**Fig. 7.1** Panel (**a**): an axial computed tomographic (CT) image in an arrhythmogenic right ventricular dysplasia (ARVD) patient demonstrating profound right ventricle dilatation, extensive low-attenuation fatty tissue in the wall of the right ventricle (*white arrows*), and prominent trabeculae (*white arrowheads*). Fatty tissue is also seen in the moderator band (*open arrow*). Panels (**b**) and (**c**) are sagittal and coronal reformations, respectively, and show fat in the RV wall (*arrows*). Scallops are also noted along the RV wall (*white arrow heads*). The right ventricle is markedly dilated and the inferior wall is thinned. Also note abundant epicardial fat (*asterisks* in panel **c**). *RV* right ventricle, *LV* left ventricle, *RA* right atrium, *LA* left atrium, *Ao* aorta

## 7.2 Differential Diagnosis of Myocardial Fat

Myocardial fat is seen in adults with normal hearts and in steatosis associated with obesity, lipomatous atrial septal hypertrophy, old myocardial infarction (MI), cardiac lipoma, and other uncommon conditions such as tuberous sclerosis [4] and muscular dystrophies [5] (Table 7.1).

### 7.2.1 Right Ventricular Fat Infiltration in Asymptomatic Patients

Using a cutoff ≤30 Hounsfield units to define RV fat, Kim et al. [6] demonstrated RV fatty infiltration in 11–17 % of patients referred for coronary calcium scores. The most frequent location was the myocardium in the basal superior wall followed by middle superior wall and right ventricular outflow tract (RVOT). There was no association between body mass index and RV fatty infiltration in this study. The frequency and degree of myocardial fat did increase with increasing age [6, 7]. See Fig. 7.2.

**Table 7.1** Differential diagnosis of fatty infiltration of the myocardium

| Type of fat | Segmental location | Intramyocardial location | Myocardial thickness | Ventricle (size/function) |
|---|---|---|---|---|
| Physiologic | Anterolateral RV<br>Free wall<br>RVOT | Full thickness | Normal or increased | Normal/normal (RV) |
| Chronic infarct | Coronary artery territory<br>Typically LV | Subendocardial | Normal or decreased | Normal or dilated/normal or depressed (LV) |
| ARVD | RV and RVOT<br>Free wall<br>Trabeculae<br>Moderator band<br>RV side of ventricular septum<br>LV free wall | Subepicardial | Decreased | Dilated/depressed |

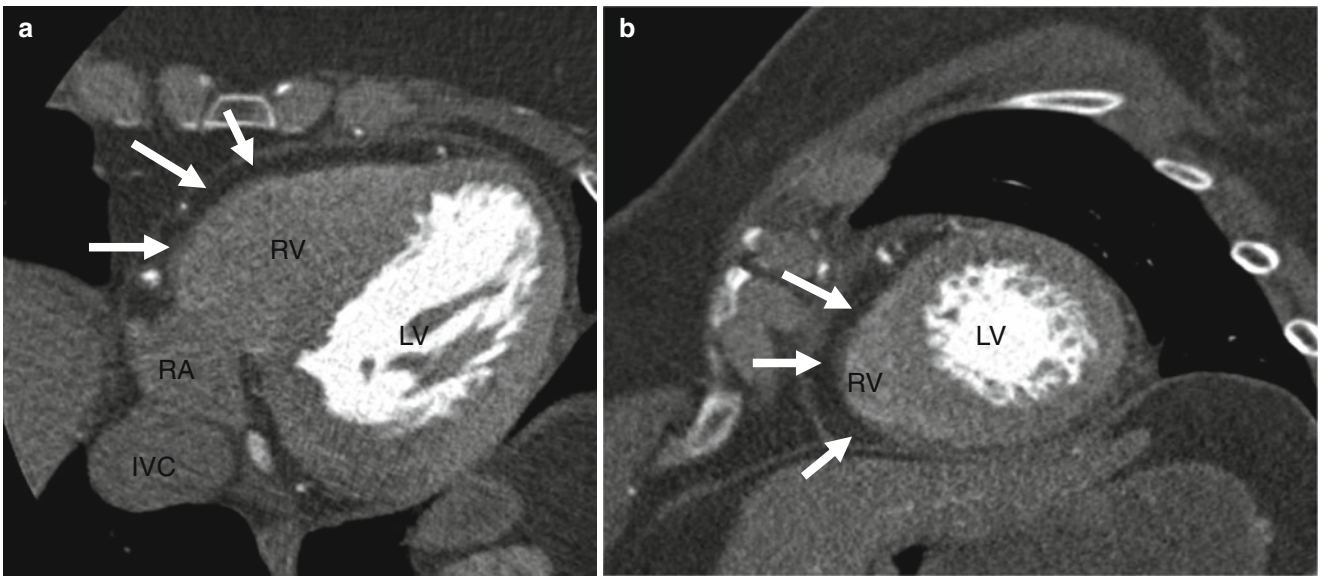


**Fig. 7.2** Physiologic myocardial fat in a 70-year-old woman with normal weight for age and without known cardiac disease. Panel **(a)** axial ontrastenhanced CT images showing fatty infiltration of the right ventricular (*RV*) free wall (*arrows*). Panel **(b)** short-axis CT image showing fat (*arrows*) in the anterior and lateral walls of the RV. RV myocardial fat must be distinguished from epicardial fat that lies between the *RV* wall and the pericardium.The myocardial fat is the thinner line of low-attenuation tissue within the RV wall. *LV* left ventricle, *IVC* inferior vena cava

### 7.2.2 Fatty Infiltration of an Old Myocardial Infarction

The prevalence of LV myocardial fat is 22–62 % among patients with an old myocardial infarction [8–10]. On CT, fat within a healed myocardial infarction is thin and linear or curvilinear in configuration and follows the distribution of the involved coronary artery. It is typically located in the subendocardial region. The transmural extent of myocardial fat is 75 % or less of the total myocardial thickness (Fig. 7.3).

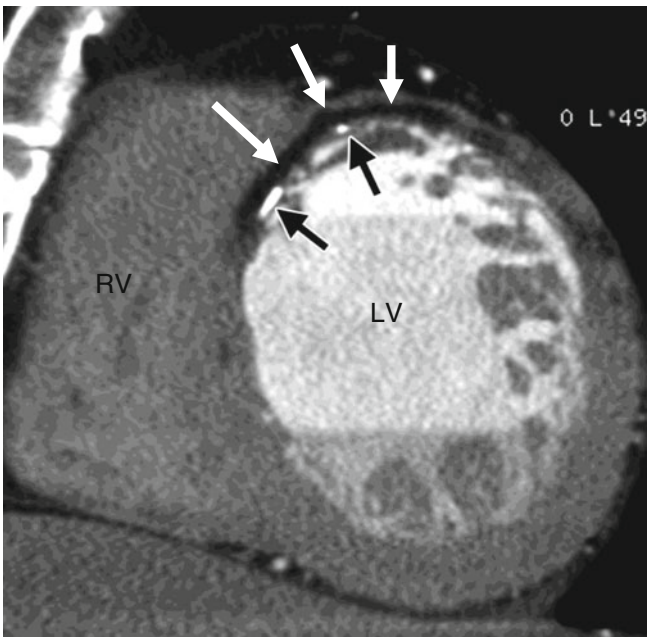


**Fig. 7.3** Fatty infiltration of a healed myocardial infarct in a 57-year-old man. This short-axis contrast-enhanced CT image shows subendocardial fat (*white arrows*) and small calcifications (*black arrows*) in the anterior wall of the left ventricle. *LV* left ventricle, *RV* right ventricle (Reproduced with kind permission of Radiological Society of North America, Oak Brook, IL from Kimura et al. [3])

### 7.2.3 Lipomatous Hypertrophy of the Interatrial Septum

Lipomatous hypertrophy of the intra-atrial septum is a benign condition in which unencapsulated fatty tissue accumulates within the interatrial septum. It is associated with increasing age and body mass as well as emphysema. Apart from a possible association with cardiac arrhythmias, it is usually an incidental finding. Its incidence in patients undergoing CT is reported to be 2.2 % [11, 12]. The CT characteristics are a dumbbell-shaped fat density mass in the interatrial septum, sparing the fossa ovalis (Fig. 7.4).

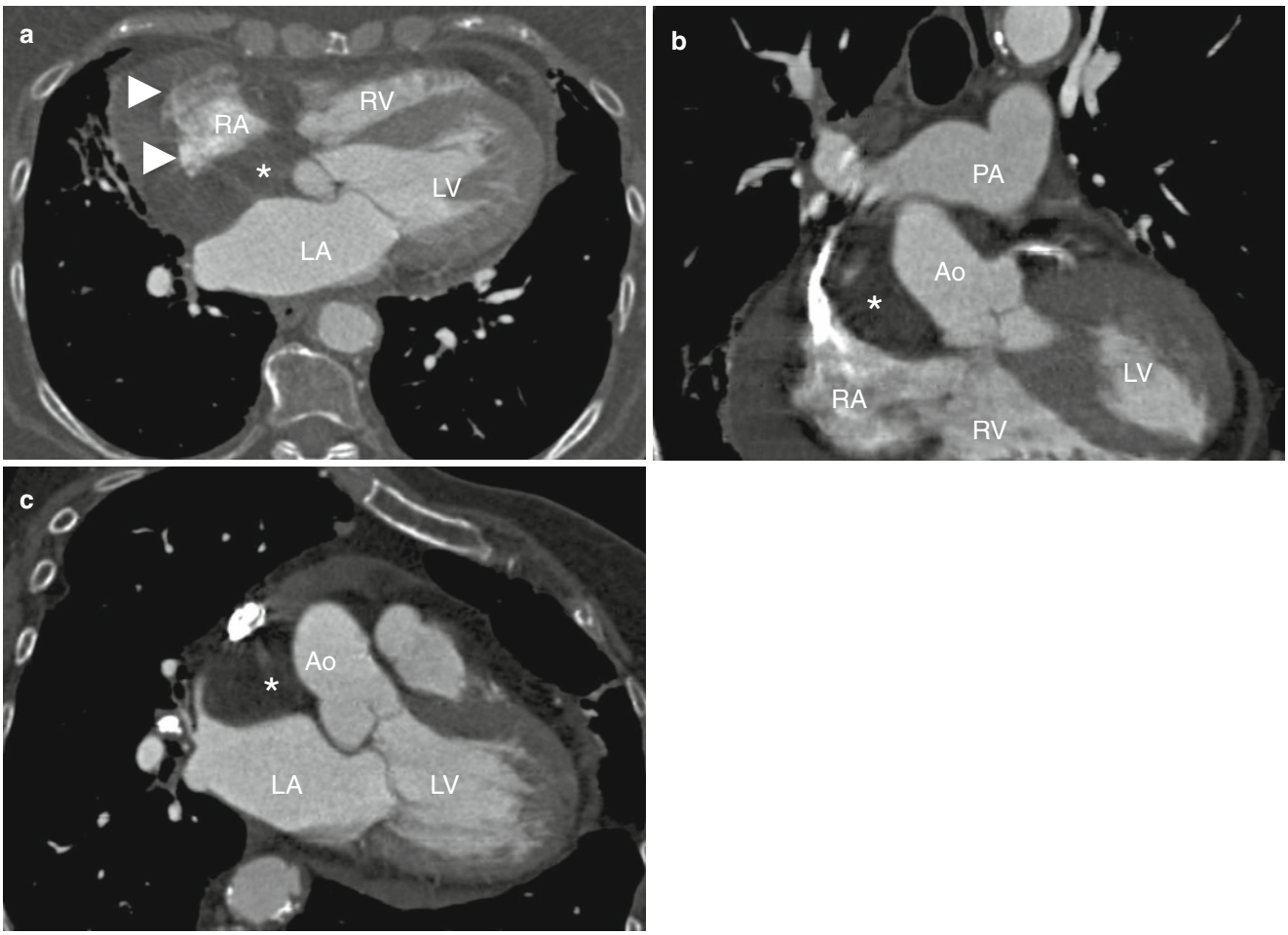


**Fig. 7.4** Lipomatous hypertrophy of the interatrial septum. Panel (**a**) is an axial image, panel (**b**) is a coronal orientation, and panel (**c**) is a three-chamber long-axis image. Each image shows a fatty mass (*asterisk*) in the interatrial septum. In panel (a), fatty tissue can be seen extending along the free wall of the right atrium as well (*arrow heads*). *LA* left atrium, *RA* right atrium, *RV* right ventricle, *Ao* aorta, *PA* pulmonary artery

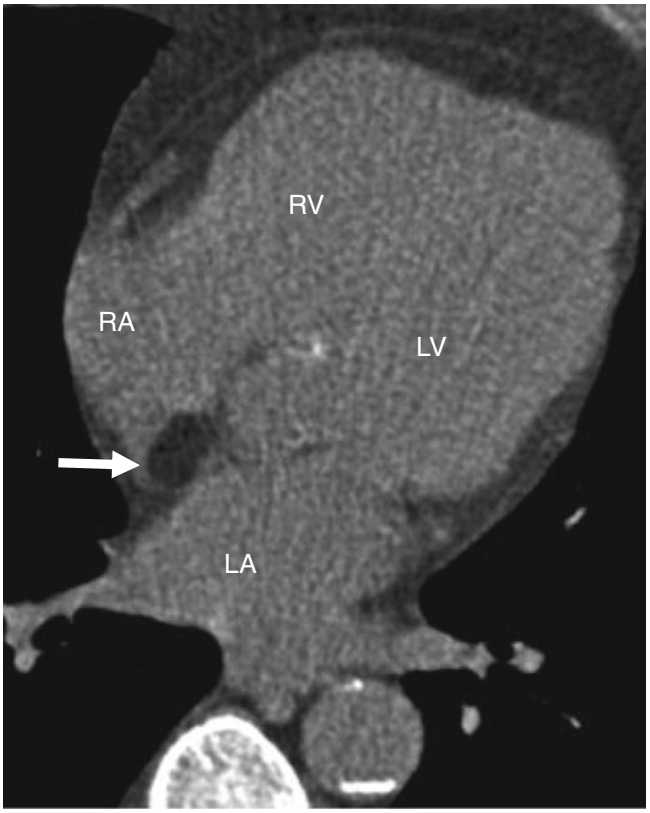


**Fig. 7.5** Cardiac Lipoma. A noncontrast axial CT scan demonstrating a well-defined focal fat-containing lesion (*arrow*) along the right atrial wall. *LA* left atrium, *RA* right atrium, *LV* left ventricle, *RV* right ventricle

### 7.2.4 Cardiac Lipomas

Cardiac lipomas are very rare, benign neoplasms composed of adipose tissue. They are much less frequent than lipomatous hypertrophy of the interatrial septum and are usually asymptomatic. However, large intracavitary lipomas may result in dyspnea due to blood flow obstruction. Additionally, involvement of the cardiac conduction system may result in arrhythmias. Cardiac lipomas are largely composed of mature adipocytes and they can originate from the subendocardium, subepicardium, or myocardium and may form in any cardiac location. Lipomas are most frequent, however, within the left atrium and left ventricle.

Unlike lipomatous hypertrophy, cardiac lipomas are encapsulated masses. Most are single lesions but multiple lipomas have been reported in patients with tuberous sclerosis. On CT, cardiac lipomas usually appear as well-marginated predominantly homogeneous masses, although they can contain soft tissue septation or strands (Fig. 7.5) [13]. The lesion shape may be spherical, polypoid, or sessile. Subpericardial lipomas may be very large, replace the pericardial sac, and may alter ventricular function.

## References

1. Peters S, Trummel M, Meyners W. Prevalence of right ventricular dysplasia-cardiomyopathy in a non-referral hospital. Int J Cardiol. 2004;97:499–501. doi:10.1016/j.ijcard.2003.10.037.
2. Marcus FI, McKenna WJ, Sherrill D, Basso C, Bauce B, Bluemke DA, et al. Diagnosis of arrhythmogenic right ventricular cardiomyopathy/dysplasia: proposed modification of the task force criteria. Circulation. 2010;121:1533–41. doi:10.1161/CIRCULATIONAHA.108.840827.
3. Kimura F, Matsuo Y, Nakajima T, Nishikawa T, Kawamura S, Sannohe S, et al. Myocardial fat at cardiac imaging: how can we differentiate pathologic from physiologic fatty infiltration? Radiographics. 2010;30:1587–602. doi:10.1148/rg.306105519.
4. Adriaensen ME, Schaefer-Prokop CM, Duyndam DA, Zonnenberg BA, Prokop M. Fatty foci in the myocardium in patients with tuberous sclerosis complex: common finding at CT. Radiology. 2009;253:359–63. doi:10.1148/radiol.2533082118.
5. Hunter S. The heart in muscular dystrophy. Br Med Bull. 1980;36:133–4.
6. Kim E, Choe YH, Han BK, Kim SM, Kim JS, Park SW, et al. Right ventricular fat infiltration in asymptomatic subjects: observations from ECG-gated 16-slice multidetector CT. J Comput Assist Tomogr. 2007;31:22–8.
7. Kirsch J, Williamson EE, Glockner JF. Focal macroscopic fat deposition within the right ventricular wall in asymptomatic patients undergoing screening EBCT coronary calcium scoring examinations. Int J Cardiovasc Imaging. 2008;24:223–7. doi:10.1007/s10554-007-9232-x.
8. Zafar HM, Litt HI, Torigian DA. CT imaging features and frequency of left ventricular myocardial fat in patients with CT findings of chronic left ventricular myocardial infarction. Clin Radiol. 2008;63:256–62. doi:10.1016/j.crad.2007.08.007.
9. Ahn SS, Kim YJ, Hur J, Lee HJ, Kim TH, Choe KO, et al. CT detection of subendocardial fat in myocardial infarction. AJR Am J Roentgenol. 2009;192:532–7. doi:10.2214/AJR.08.1608.
10. Ichikawa Y, Kitagawa K, Chino S, Ishida M, Matsuoka K, Tanigawa T, et al. Adipose tissue detected by multislice computed tomography in patients after myocardial infarction. JACC Cardiovasc Imaging. 2009;2:548–55. doi:10.1016/j.jcmg.2009.01.010.
11. Heyer CM, Kagel T, Lemburg SP, Bauer TT, Nicolas V. Lipomatous hypertrophy of the interatrial septum: a prospective study of incidence, imaging findings, and clinical symptoms. Chest. 2003;124:2068–73.
12. Stojanovska J, Attili AK. AJR teaching file: fat-containing mass in the interatrial septum. AJR Am J Roentgenol. 2010;195:S73–5. doi:10.2214/AJR.09.7173.
13. Salanitri JC, Pereles FS. Cardiac lipoma and lipomatous hypertrophy of the interatrial septum: cardiac magnetic resonance imaging findings. J Comput Assist Tomogr. 2004;28:852–6.

# Uhl Anomaly

# 8

Uhl anomaly is a very rare condition characterized by complete or partial absence of the right ventricular myocardium, which is replaced by fibroelastic tissue [1].

The true incidence of Uhl anomaly is unknown, but less than 100 confirmed cases have been described in the literature [2]. The cause is thought to be a high apoptotic activity, which begins during the perinatal period or early in infancy, leading to destruction of the right ventricular wall [2, 3]. Histologic examination reveals partial or total absence of the myocardium of the parietal wall of the right ventricle and direct apposition of the opposing endocardial and epicardial surfaces [4, 5]. This leads to thinning of the right ventricular free wall. Uhl anomaly usually presents in neonates or infants as right-sided heart failure. Patients rarely survive to adulthood. No effective treatment other than heart transplant has been shown to improve survival.

Computed tomography (CT) findings include an extremely thin-walled right ventricle with complete or partial absence of the right ventricular free-wall myocardium and a paucity of trabeculations (Figs. 8.1 and 8.2) [6, 7]. The tricuspid valve, interventricular septum, and left ventricular myocardium are normal.

Uhl anomaly needs to be distinguished from arrhythmogenic right ventricular dysplasia. Histologically, the latter disorder is characterized by patchy replacement of right ventricular myocardium with fibrofatty tissue, primarily occurring within the ventricular outflow tract and inlet or apical regions. Arrhythmogenic right ventricular dysplasia usually produces ventricular arrhythmias and manifests during adolescence, whereas Uhl anomaly presents in infancy with heart failure. CT shows fatty infiltration of the right ventricular free wall in arrhythmogenic right ventricular dysplasia which may help to differentiate it from Uhl anomaly, which has a paucity of myocardium and apical trabeculations as well as an absence of fatty infiltration.

W. Mazur et al., *CT Atlas of Adult Congenital Heart Disease*,
DOI 10.1007/978-1-4471-5088-6_8, © Springer-Verlag London 2013

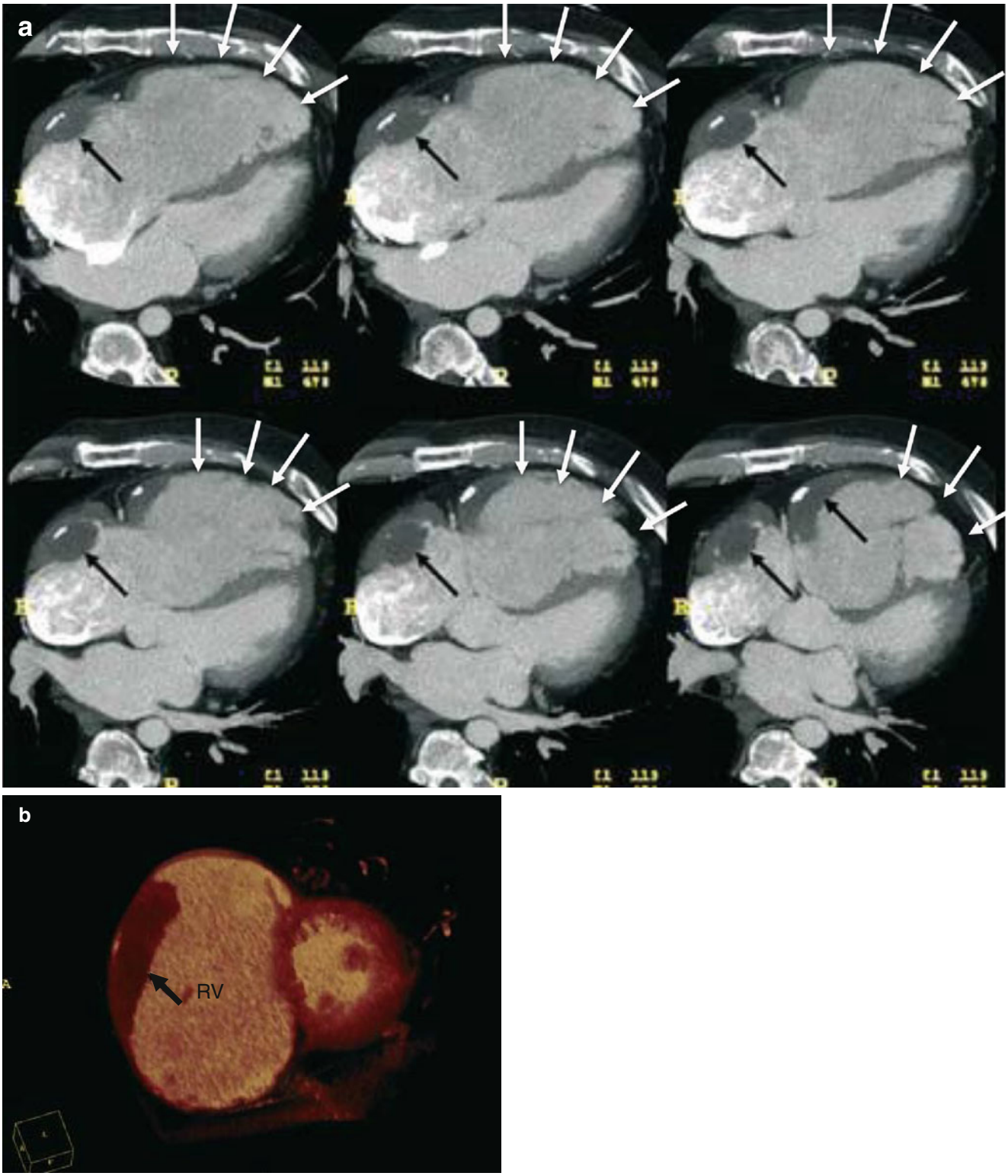


**Fig. 8.1** Partial Uhl anomaly in a 51-year-old man. Panel (**a**) is an axial image and panel (**b**) is a short-axis image. Both panels show partial absence of the right ventricular wall (*white arrows*). Note the massively dilated right ventricle (*RV*) and right atrium. Chronic mural thrombus with foci of calcifications is seen (*black arrows*). (Reproduced from Cheng et al. [7]. With kind permission of Springer-Verlag, Berlin Heidelberg, Germany)


**Fig. 8.2** Uhl anomaly. An axial scan obtained by a multisliced computed tomography scanner which dramatically illustrates an extremely dilated right ventricle (RV) with almost a complete absence of RV myocardium (*thin arrows*). The interventricular septal myocardium (*arrowheads*) is normal thickness (Reproduced from Ceviz et al. [6]. With kind permission from BMJ Publishing Group Ltd)

## References

1. Uhl HSM. A previously undescribed congenital malformation of the heart: almost total absence of the myocardium of the right ventricle. Bull Johns Hopkins Hosp. 1952;91:197–205.
2. Hebert J-L, Duthoit G, Hidden-Lucet F, et al. Fortuitous discovery of partial Uhl anomaly in a male adult. Circulation. 2010;121: e426–9. doi:10.1161/CIRCULATIONAHA.110.960773.
3. James T, Nicholas M, Sapire D, Patre P, Lopez S. Complete heart block and fatal right ventricular failure in an infant. Circulation. 1996;93:1588–600.
4. Gerlis L, Schmidt-Ott SC, Ho S, Ho SY, Anderson RH. Dysplastic conditions of the right ventricular myocardium: Uhl's anomaly vs arrhythmogenic right ventricular dysplasia. Br Heart J. 1993;69: 142–50.
5. Loire R, Tabib A. Arrhythmogenic right ventricular dysplasia and Uhl disease: anatomic study of 100 cases after sudden death. Ann Pathol. 1998;18:165–71.
6. Ceviz N, Kantarci M, Okur A. Electrocardiographic gated multislice computed tomography of Uhl's anomaly. Heart. 2004;90:886. doi:10.1136/hrt.2003.028837.
7. Cheng JF, Mohammed TL, Griffith BP, White CS. CT of Uhl's anomaly in an adult. Int J Cardiovasc Imaging. 2005;21:663–6.

# Left Ventricular Noncompaction (LVNC)

# 9

Left ventricular noncompaction (LVNC), also called spongiform cardiomyopathy, is a rare congenital cardiomyopathy that results from interrupted cardiac embryogenesis. Pathologically, it is characterized by prominent trabeculations and deep intertrabecular recesses, creating a "spongy" myocardium. The cause is thought to be an arrest in the gradual compaction of the loosely interwoven meshwork of myocardial fibers during endomyocardial morphogenesis at 5–8 weeks of fetal life. The condition predominately affects the left ventricle (LV).

Engberding and Bender first described LVNC as an isolated condition in 1984 [1]. Subsequently LVNC has been associated with other congenital anomalies such as obstruction of the right or left ventricular outflow tracts, complex cyanotic congenital heart disease, coronary artery anomalies, hypertrophic and restrictive cardiomyopathies, and recently with ARVD.

Originally reported to be present in only 0.05 % of adults [2], it is more frequently recognized primarily as result of high-resolution images of the left ventricular apex afforded by magnetic resonance imaging (MR) and computed tomography (CT) as compared to echocardiography. More recently, LVNC was reported in 2 % of patients undergoing MDCT for assessment of coronary artery disease [3]. LVNC may be associated with development of systolic and diastolic LV dysfunction, arrhythmias, congestive heart failure, and thromboembolic events. The age of onset and degree of clinical symptoms depend on the extent of the noncompacted cardiac segments [4].

Traditionally, echocardiography has been used to establish the diagnosis of myocardial noncompaction, although CT and MRI provide better visualization of the trabeculations. CT findings of LVNC are prominent trabeculations and deep recesses in the myocardium usually affecting the apical and basal surfaces of the left ventricle. The RV apex also may be involved [5, 6]. Based on MRI criteria, a noncompacted to compacted myocardium ratio (NC/C ratio) of 2:1 at end systole (or 2.3:1 in end diastole in the long axis) supports the diagnosis of LVNC. A recent, small CT study suggests that a ratio of noncompacted to normal myocardium of 2.2:1 in more than one myocardial segment suggests the diagnosis of LVNC [7]. Left ventricular systolic dysfunction and restrictive filling may be seen on cine imaging. CT examples of LVNC are presented in Figs. 9.1 and 9.2.

W. Mazur et al., *CT Atlas of Adult Congenital Heart Disease*,
DOI 10.1007/978-1-4471-5088-6_9, © Springer-Verlag London 2013

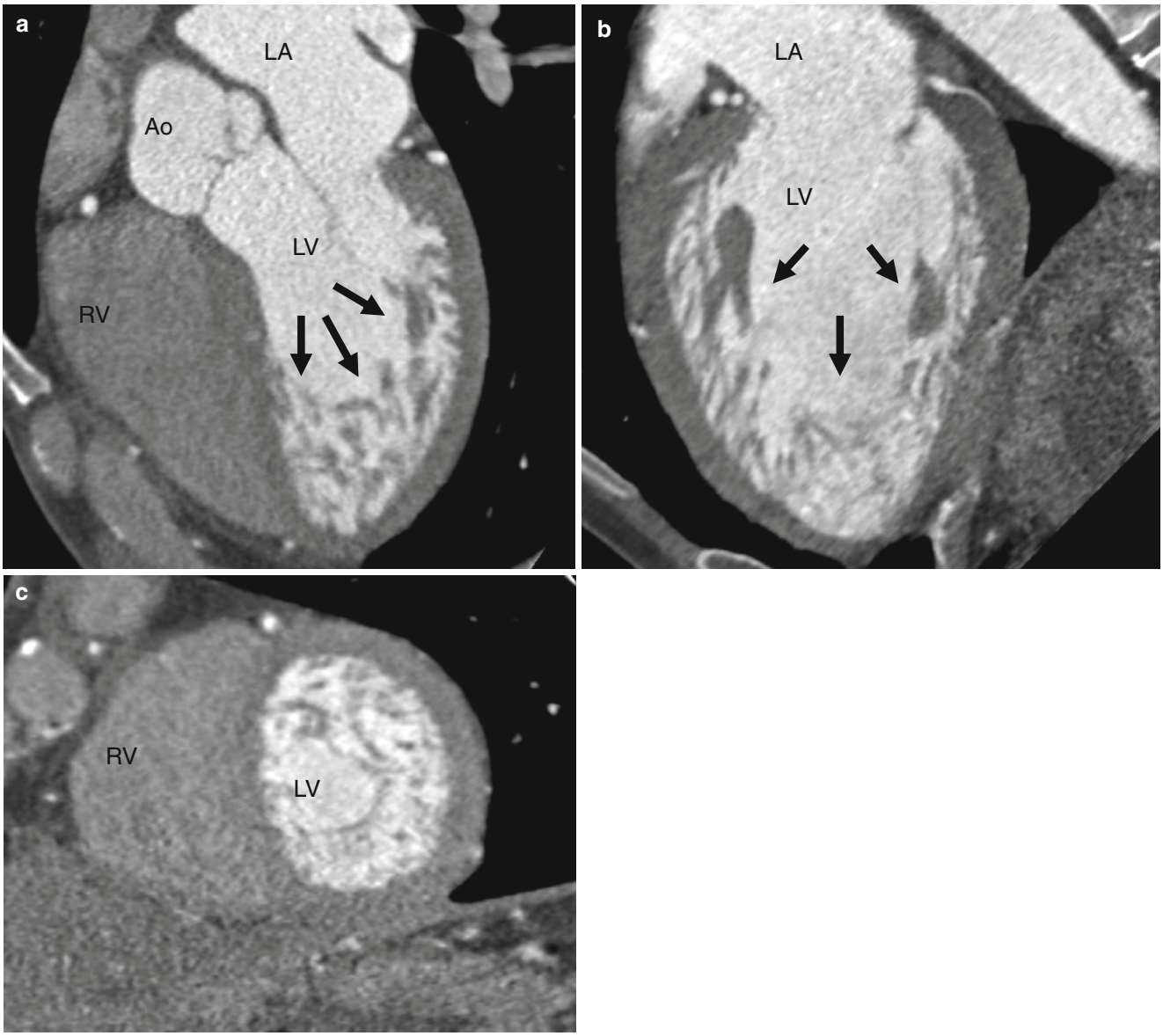


**Fig. 9.1** Left ventricular noncompaction (LVNC) in an asymptomatic marathon runner. Panel (**a**) is a five-chamber view, panel (**b**) is a two-chamber orientation, and panel (**c**) is a short-axis cut. Note the dilated left ventricle and the fine trabeculations with deep intertrabecular recesses (*arrows*) in the myocardium on the apical regions of the left ventricle. *LA* left atrium, *LV* left ventricle, *RA* right atrium, *RV* right ventricle, *Ao* aorta

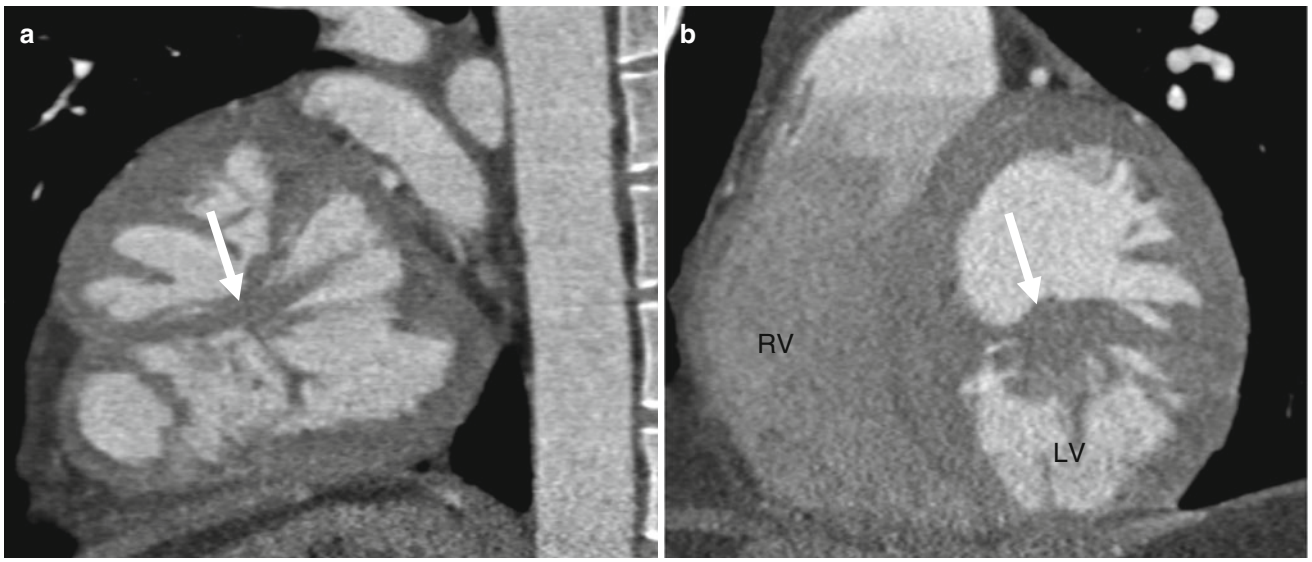


**Fig. 9.2** Left ventricular noncompaction (LVNC) in a 22-year-old patient presenting with a new-onset heart failure. Panel (**a**) a long-axis two-chamber computed tomographic (CT) view. Panel (**b**) a short-axis CT image. Note the thickening of the left ventricular wall with very prominent trabeculations and absence of distinct papillary muscles. The hypertrabeculation in the mid-left ventricle (*white arrow*) nearly separates the ventricle into two chambers. Ventricular septation is best appreciated in the short axis (*arrow*, panel b). *LV* left ventricle, *RV* right ventricle

## 9.1 Differential Diagnoses of LVNC

The differential diagnoses include prominent normal LV trabeculations (normal variant), hypertrophic cardiomyopathy (described in the following section), apical left ventricular thrombus, and endocardial fibroelastosis. However, using the above diagnostic criteria, LVNC is quite distinguishable if a high index of suspicion is maintained in the appropriate clinical presentation.

### 9.1.1 Normal Variant LV Trabeculations

Prominent LV trabeculations related to the attachment of the papillary muscles to the LV myocardium is a normal variant on CT (see Chap. 3). These trabeculations are few in number and rarely located in the apical region. The scarcity of apical involvement helps to differentiate between LVNC and normal trabeculation.

### 9.1.2 LV Thrombus

LV thrombus appears as a filling defect in the LV chamber. Left ventricular thrombi occur in regions of ventricular dyskinesia or aneurysm formation, both of which usually result from prior myocardial infarction. Thrombi have homogeneous attenuation on CT. The CT attenuation value is less than that of the myocardial wall and of normal ventricular trabeculations (Fig. 9.3). In addition, thrombi do not significantly enhance after contrast administration, whereas the LV wall shows modest contrast enhancement.

### 9.1.3 Endocardial Fibroelastosis

Endocardial fibroelastosis refers to a pronounced, diffuse thickening of the ventricular endocardium and presents as unexplained heart failure in infants and children less than or equal to 2 years of age. It is not a disease of adults.

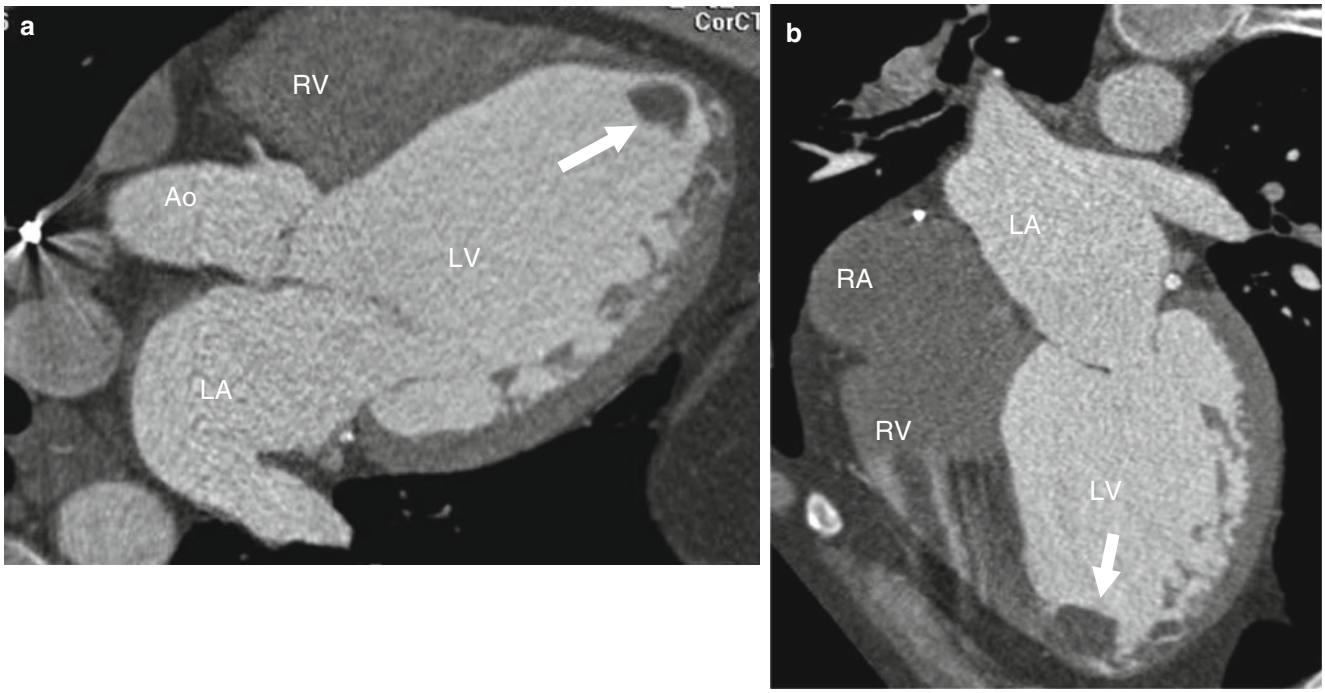


**Fig. 9.3** Left ventricular thrombus in a 50-year-old woman who suffered a recent myocardial infarction. Panels (**a**) and (**b**) are two long-axis contrast-enhanced CT scans showing a homogeneous soft tissue mass (*arrow*) in the apex of a dilated left ventricle (*LV*). The thrombus does not enhance and the attenuation of the thrombus is less than that of the left ventricular trabeculations and myocardial wall distinguishing it from normal myocardial tissue. *LA* lft atrium, *RA* right atrium, *RV* Right ventricle, *Ao* Aorta

## References


1. Chin TK, Perloff JK, Williams RG, Jue K, Mohrmann R. Isolated noncompaction of left ventricular myocardium. A study of eight cases. Circulation. 1990;82:507–13.
2. Ritter M, Oechslin E, Sutsch G, Attenhofer C, Schneider J, Jenni R. Isolated noncompaction of the myocardium in adults. Mayo Clin Proc. 1997;72:26–31. doi:10.1016/S0025-6196(11)64725-3.
3. Knickelbine T, Lesser JR, Haas TS, Brandenburg ER, Gleason-Han BK, Flygenring B, et al. Identification of unexpected nonatherosclerotic cardiovascular disease with coronary CT angiography. JACC Cardiovasc Imaging. 2009;2:1085–92. doi:10.1016/j.jcmg.2009.03.022.
4. Oechslin EN, Attenhofer Jost CH, Rojas JR, Kaufmann PA, Jenni R. Long-term follow-up of 34 adults with isolated left ventricular noncompaction: a distinct cardiomyopathy with poor prognosis. J Am Coll Cardiol. 2000;36:493–500.
5. Kirsch J, Williamson EE, Araoz PA. Non-compaction visualization using ECG-gated dual-source CT. Int J Cardiol. 2007;118:e46–7. doi:10.1016/j.ijcard.2006.12.056.
6. Lee H, Kim SY, Schoepf UJ. Isolated non-compaction of the left ventricle in a patient with new-onset heart failure: morphologic and functional evaluation with cardiac multidetector computed tomography. Korean J Radiol. 2012;13:244–8. doi:10.3348/kjr.2012.13.2.244.
7. Melendez-Ramirez G, Castillo-Castellon F, Espinola-Zavaleta N, et al. Left ventricular noncompaction: a proposal of new diagnostic criteria by multidetector computed tomography. J Cardiovasc Comput Tomogr. 2012;6(5):346–54.

# Hypertrophic Cardiomyopathy

# 10

Hypertrophic cardiomyopathy (HCM) is a genetic cardiac disease characterized by diffuse or segmental left ventricle (LV) hypertrophy associated with a nondilated ventricular chamber, in the absence of other cardiac or systemic disease that might be capable of producing the same degree of hypertrophy [1]. It is an important cause of sudden cardiac death in any age group. The prevalence of HCM is approximately 0.2–0.5 % of the general population.

Pathologic hallmarks of HCM are myocyte disarray and interstitial fibrosis [2]. HCM is inherited as an autosomal dominant trait and is caused by mutations in a sarcomeric gene which encodes protein components of the cardiac sarcomeres.

HCM can be seen as part of certain genetic and metabolic syndromes. These include Noonan syndrome (associated with pulmonary valve dysplasia and septal defects), mitochondrial myopathies, glycogen storage diseases (type II Pompe disease), as well as other rare conditions. In older patients, other systemic diseases associated with left ventricular hypertrophy (LVH) include hypertension, Friedrich ataxia, pheochromocytoma, neurofibromatosis, tuberous sclerosis, amyloidosis, lentiginosis (referring to the presence of lentigines or spotted areas on the skin due to sun exposure), and Fabry disease, a rare X-linked autosomal recessive metabolic storage disorder caused by a lack of lysosomal a-galactosidase [3].

Imaging plays a role in detecting HCM, characterizing its pattern (phenotype), classifying disease severity, and providing risk stratification criteria for sudden cardiac death. Echocardiography is the conventional imaging modality to screen for this condition, as it can characterize the pattern and distribution of increased LV wall thickness. However, it can underestimate the degree of LV hypertrophy, especially at the apical endocardial border.

Cardiac MRI using delayed gadolinium-enhancement technique provides information regarding the location and extent of fibrosis and is considered the examination of choice to establish the diagnosis of HCM when echocardiography is inconclusive. It allows multiplanar imaging which has the advantages of allowing complete coverage of the myocardium and better characterization of the pattern and distribution of LV hypertrophy.

Cardiac CT is not routinely used in patients with HCM since it is associated with radiation exposure. However, CT can be useful in those patients in whom detailed anatomy of the coronary arteries is needed and in patients with contraindications to MRI such as a pacemaker or aneurysm clips. The spatial resolution of CT is usually superior to MRI, allowing exquisite, noninvasive coronary artery angiography. Cardiac CT also provides comprehensive anatomical and functional information about the heart chambers and myocardium [4]. In retrospectively gated cardiac CT acquisition, systolic anterior motion (SAM) of the mitral valve can be easily assessed. In addition, delayed enhancement CT scanning provides information about myocardial scarring and fibrosis similar to that provided by MRI [5, 6]. CT has been reported to be useful in the assessment of patients undergoing septal alcohol ablation by enabling depiction of the exact extent and location of septal hypertrophy, systolic anterior motion of the mitral valve, and mitral valve leaflet–septal contact as well as septal perforator anatomy, which is of utmost importance in guiding septal ablation [7, 8]. See Table 10.1 for the utility of CT in the evaluation of HCM.

It should be noted that myocardial bridging is common in patients with apical hypertrophy and has been reported in the majority of patients presenting with typical or

**Table 10.1** The utility of CT in the evaluation of HCM

| |
|---|
| Distribution of hypertrophy |
| LV maximal wall thickness |
| LV outflow tract obstruction |
| Presence of fibrosis (delayed enhancement on CT) |
| Presence of systolic anterior motion of the mitral valve |
| Coronary anatomy |
| Evaluation of septal perforator arteries before alcohol septal ablation |

W. Mazur et al., *CT Atlas of Adult Congenital Heart Disease*,
DOI 10.1007/978-1-4471-5088-6_10, © Springer-Verlag London 2013

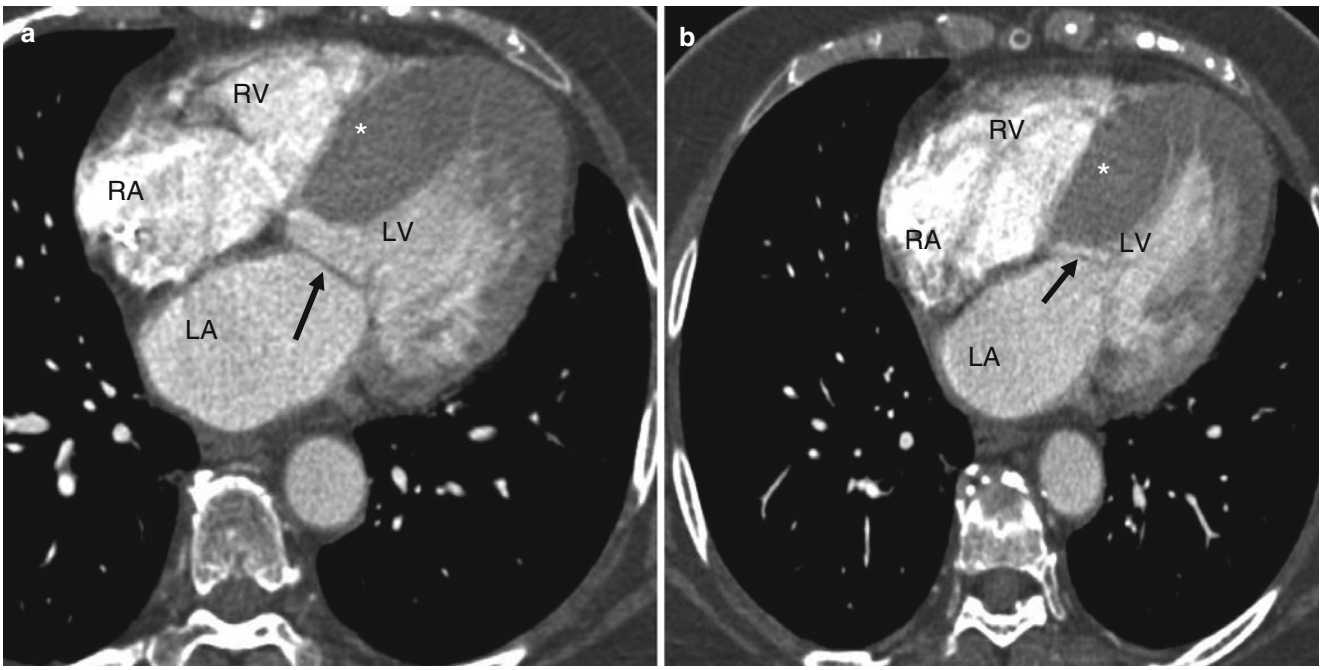


**Fig. 10.1** Representation of the asymmetric (septal) phenotype of HCM: panel (**a**) is an axial CT reconstructed in diastole. Panel (**b**) is an axial CT reconstructed in end systole in the same patient. In panel (a), note the markedly increased thickness (>30 mm) of the apical septal wall (*asterisk*) of the left ventricle (LV), with a thickened mitral leaflet (*black arrow*). This meets the diagnostic criterion of HCM, which is LV wall thickness greater than or equal to 15 mm in the end-diastolic phase. Panel (b) demonstrates the systolic anterior motion of the mitral leaflet (*black arrow* in panel b) which causes left ventricular outflow obstruction. *LA* left atrium, *RA* right atrium, *RV* right ventricle

atypical chest pain [9]. It can lead to myocardial ischemia by narrowing the intramyocardial segment of the affected coronary artery, which can be especially well seen on CT.

## 10.1 Phenotype Analysis

HCM is diagnosed when the LV wall thickness (typically the septum) is ≥15 mm in the end-diastolic phase [10]. It can be classified based on the distribution of the wall hypertrophy into the following phenotypes: asymmetric (Fig. 10.1) with and without dynamic LV outflow tract (LVOT) obstruction, apical (Fig. 10.2), midventricular (Fig. 10.3), and symmetric, mass-like, and noncontiguous [9] (Figs. 10.4a and 10.5) (see Table 10.2). HCM does not involve the basal or inferolateral segments of the LV, a helpful feature in differentiating HCM from other causes of LV hypertrophy [11]. Occasionally apical infarct can be identified by CT in the absence of coronary artery disease as a result of constriction of a distal LAD bridge (Fig. 10.6, black arrow). Recently, left ventricular myocardial crypts have been identified as a distinctive morphologic expression of HCM, occurring in patients with and without hypertrophy. Crypts may identify individual HCM family members before development of typical phenotype. Crypts are confined to the basal LV, most commonly in the ventricular septum or posterior LV free wall [12]. Example of LV crypt is presented in Fig. 10.6 (white arrow).

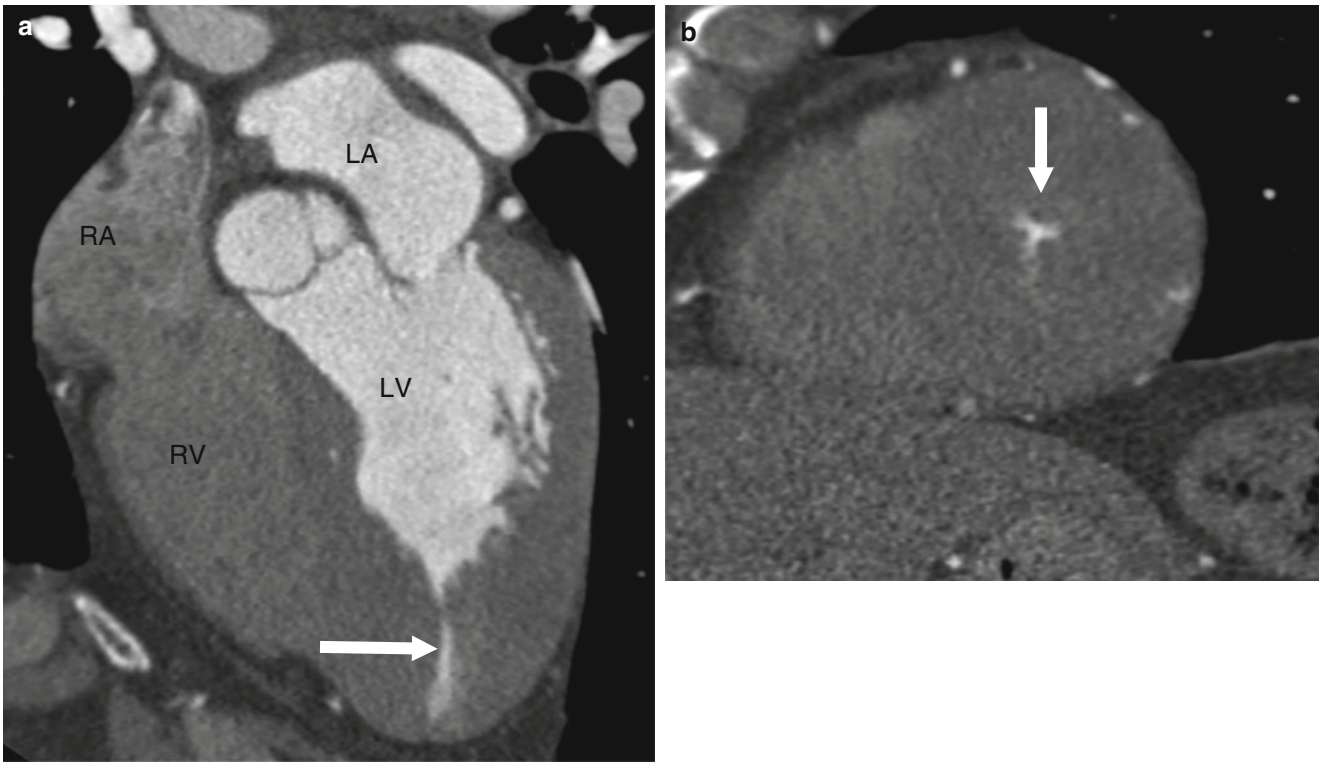


**Fig. 10.2** An apical variant of HCM. Panel (**a**) is an apical four-chamber view demonstrating the thickened apical myocardium and near cavity obliteration at end systole. Panel (**b**) is a short-axis cut at the level of the apex demonstrating the apical hypertrophy and almost complete obliteration of the left ventricle apical lumen (*arrow*) at end systole. *RA* right atrium, *RV* right ventricle, *LA* left atrium, *LV* left ventricle

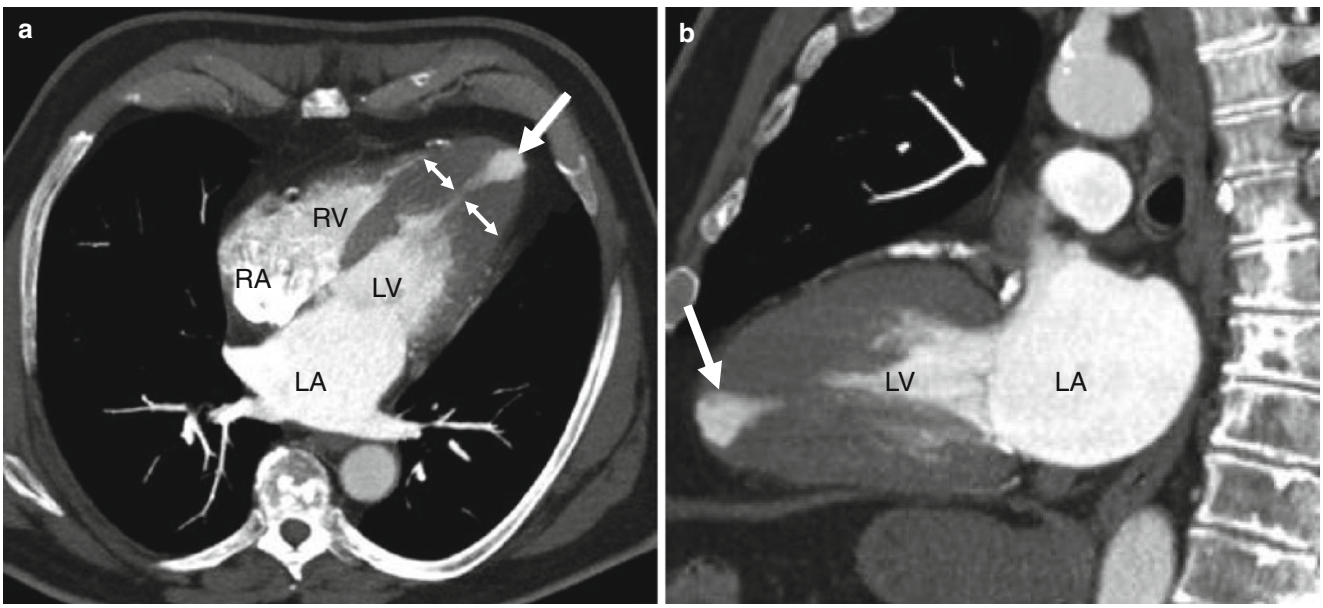


**Fig. 10.3** Midventricular HCM. Panel (**a**) is a four-chamber CT orientation, while panel (**b**) is a two-chamber CT view. Each shows concentrically thickened myocardium (2.5 cm maximum thickness, *double-headed arrows*) located in the middle third of the left ventricle (*LV*) walls. There is an acquired apical diverticulum (*white arrows*) caused by the abnormal physiology of the LV. *LA* left atrium, *RA* right atrium, *RV* right ventricle

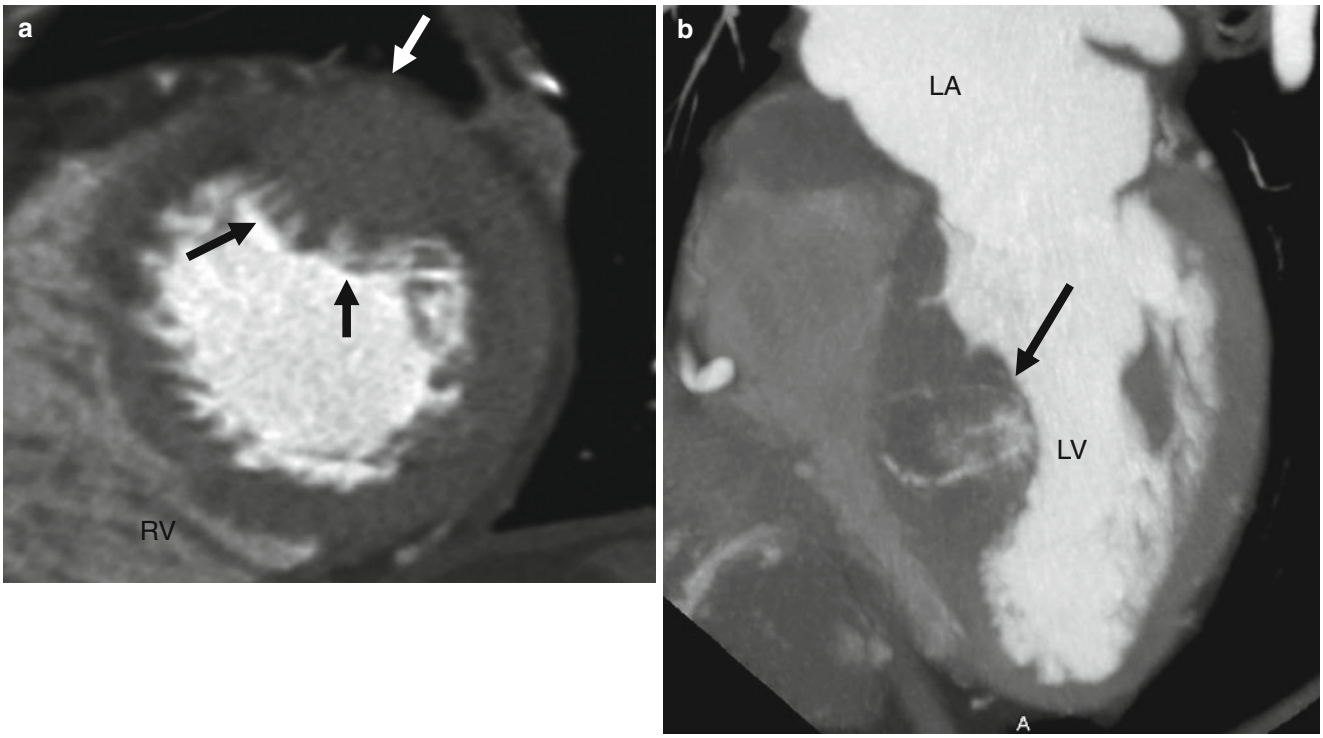


**Fig. 10.4** Mass-like HCM. Panel (**a**), a short-axis CT view, shows LV hypertrophy with mass-like bulging at the apical anterolateral wall (surrounded by *black* and *white arrows*). This form of HCM needs to be differentiated from a neoplastic mass. For comparison, panel (**b**) is a 4-chamber CT image of a patient with an intramyocardial metastasis (*black arrow*). Note the areas of patchy contrast enhancement of the metastatic mass which represents vascularization of the tumor. While mass-like HCM shows characteristics and enhancement similar to normal myocardium, tumors possess attenuation values different from the surrounding myocardium and also commonly demonstrate enhancement characteristics of increased vascularity such as that seen in panel (b). *LV* left ventricle, *RV* right ventricle (Panel **a** reproduced from Chun et al. [3]. With kind permission of Radiological Society of North America, Oak Brook, IL)

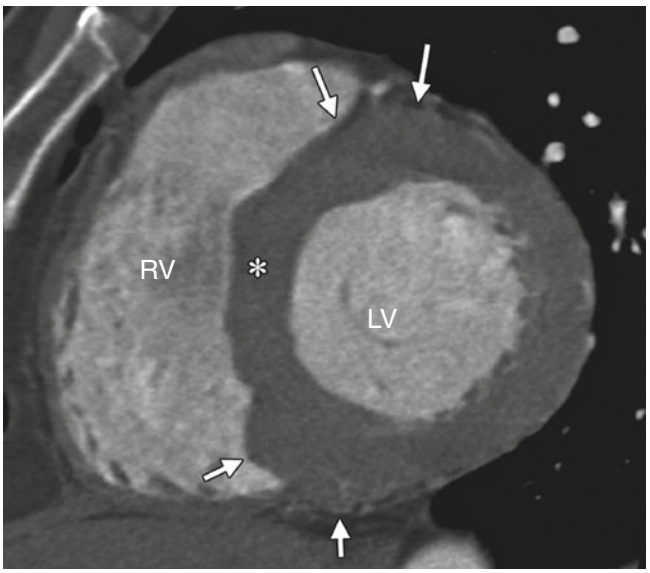


**Fig. 10.5** Noncontiguous HCM. A short-axis CT image demonstrating noncontiguous left ventricular hypertrophy of the anteroseptal and inferoseptal walls (*arrows*). The septal wall thickness is nearly normal (*asterisk*). *LV* left ventricle, *RV* right ventricle (Reproduced from Chun et al. [3]. With kind permission of Radiological Society of North America, Oak Brook, IL)

**Table 10.2** Phenotypic classifications of HCM

| *HCM phenotypes* |
|---|
| Asymmetric with or without LV outflow obstruction |
| Apical |
| Symmetric |
| Mass-like |
| Noncontiguous |

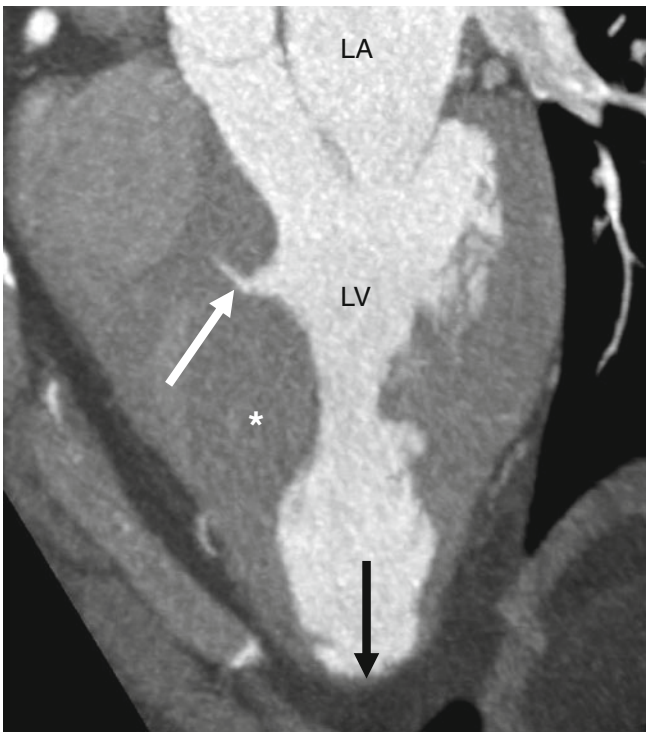


**Fig. 10.6** A four-chamber reconstruction in an HCM patient demonstrating wall thinning (*black arrow*) resulting from prior apical infarct. This patient has no coronary artery disease and the likely cause of infarct is a result of constriction of a distal left anterior descending myocardial bridge. Note the presence of a left ventricular (LV) crypt in the inferoseptal segment (*white arrow*). Reports suggest that an LV crypt precedes development of LV hypertrophy and as such it may identify mutation carriers before full phenotype development becomes apparent. The *asterisk* marks the markedly thickened septal myocardium. *LA* left atrium, *LV* left ventricle

## 10.2 Risk Stratification Criteria

Contrast-enhanced CT enables the diagnosis of HCM by enabling accurate measurements of the myocardial thickness and demonstration of the classic spade-shaped ventricular cavity during systole. In addition, it allows identification of risk stratification criteria associated with sudden cardiac death which include (*a*) LV maximal wall thickness 30 mm or more, (*b*) marked LV outflow tract obstruction (best assessed with echocardiography; CT can suggest the presence, but cannot confirm it or grade its severity), (*c*) decreased LV ejection fraction, (*d*) presence of fibrosis, and (*e*) presence of a perfusion defect indicating ischemia. Global LV functional volume analysis and ejection fraction are acquired using end-diastolic and end-systolic reformats of the CT data. Delayed myocardial enhancement can be used to characterize perfusion defects and fibrosis [11]. The presence of narrowing of the intramyocardial segment of a coronary artery, which can lead to myocardial ischemia, can also be identified on CT. In addition, CT can provide information on LV volume and the degree of mitral regurgitation [9].

## 10.3 Differential Diagnoses

The differential diagnoses of HCM include infiltrative diseases such as amyloidosis and sarcoidosis, which cause restrictive cardiomyopathy as well as LV hypertrophy due to aortic stenosis or hypertension.

In amyloidosis, amyloid protein is deposited in the myocardium, causing diffuse, symmetrical thickening of both ventricles and the septum and this thickening may involve the interatrial septum and atria.

Sarcoidosis, characterized by noncaseating granulomas, usually involves the interventricular septum (particularly the basal portion) and the lateral LV wall. Right ventricular infiltration with sarcoidosis is rare. In addition, cardiac sarcoidosis is an unusual finding in the absence of signs of other systemic involvement such as mediastinal lymphadenopathy or pulmonary parenchymal disease.

With aortic stenosis and systemic hypertension (compensatory LV hypertrophy), the LV wall undergoes compensatory hypertrophy caused by pressure overload and thus demonstrates a more concentric pattern of hypertrophy. Differentiation between HCM and compensatory hypertrophy can be difficult. In compensatory hypertrophy, systolic function is often normal and the LV wall rarely exceeds 15 mm in maximal thickness and rarely shows increased enhancement with contrast.

Occasionally, metastatic malignancy can present as focal hypertrophy (mimicking mass-like HCM) (Fig. 10.4b).

## References

1. Maron BJ, McKenna WJ, Danielson GK, Kappenberger LJ, Kuhn HJ, Seidman CE, et al. Task Force on Clinical Expert Consensus Documents. American College of Cardiology, Committee for Practice Guidelines. European Society of Cardiology American college of Cardiology/European society of cardiology clinical expert consensus document on hypertrophic cardiomyopathy. A report of the american college of cardiology foundation task force on clinical expert consensus documents and the european society of cardiology committee for practice guidelines. J Am Coll Cardiol. 2003;42:1687–713.
2. Soor GS, Luk A, Ahn E, Abraham JR, Woo A, Ralph-Edwards A, et al. Hypertrophic cardiomyopathy: current understanding and treatment objectives. J Clin Pathol. 2009;62:226–35. doi:10.1136/jcp.2008.061655.
3. Chun EJ, Choi SI, Jin KN, Kwag HJ, Kim YJ, Choi BW, et al. Hypertrophic cardiomyopathy: assessment with MR imaging and multidetector CT. Radiographics. 2010;30:1309–28. doi:10.1148/rg.305095074.
4. Ghersin E, Lessick J, Litmanovich D, Engel A, Reisner S. Comprehensive multidetector CT assessment of apical hypertrophic

cardiomyopathy. Br J Radiol. 2006;79:e200–4. doi:10.1259/bjr/53601277.
5. Saito H, Naito H, Takamiya M, Hamada S, Imakita S, Ohta M. Late enhancement of the left ventricular wall in hypertrophic cardiomyopathy by ultrafast computed tomography: a comparison with regional myocardial thickening. Br J Radiol. 1991;64:993–1000.
6. Shiozaki AA, Santos TS, Artega E, Rochitte CE. Images in cardiovascular medicine. myocardial delayed enhancement by computed tomography in hypertrophic cardiomyopathy. Circulation. 2007;115:e430–1.
7. Okayama S, Uemura S, Soeda T, Horii M, Saito Y. Role of cardiac computed tomography in planning and evaluating percutaneous transluminal septal myocardial ablation for hypertrophic obstructive cardiomyopathy. J Cardiovasc Comput Tomogr. 2010;4:62–5. doi:10.1016/j.jcct.2009.10.004.
8. Ghersin E, Soto V, Heldman AW. Multidetector computerized tomography can guide and document alcohol septal ablation in hypertrophic obstructive cardiomyopathy. Circulation. 2011;123:e5–7. doi:10.1161/CIRCULATIONAHA.110.975599.
9. Chen CC, Chen MT, Lei MH, Hsu YC, Chung SL, Sung YJ. Assessing myocardial bridging and left ventricular configuration by 64-slice computed tomography in patients with apical hypertrophic cardiomyopathy presenting with chest pain. J Comput Assist Tomogr. 2010;34:70–4.
10. Maron BJ. Hypertrophic cardiomyopathy: a systematic review. JAMA. 2002;287:1308–20.
11. Otto CM. Textbook of clinical echocardiography. Philadelphia: Saunders/Elsevier; 2009. p. 217–9.
12. Maron MS, Rowin EJ, Lin D, Appelbaum E, Chan RH, Gibson CM, et al. Prevalence and clinical profile of myocardial crypts in hypertrophic cardiomyopathy. Circ Cardiovasc Imaging. 2012;5(4):441–7. doi:10.1161/CIRCIMAGING. 112.972760.

# Part V

# Anomalies with Normal Chamber and Valve Sequence and Position

# Septal Defects

# 11

## 11.1 Atrial Septal Defects

Atrial septal defects (ASD) are seen in 1 per 1,500 live births and account for 30–40 % of all adult congenital heart disease [1]. There are five basic types of atrial septal defects (Fig. 11.1): (1) secundum ASD, (2) primum ASD, (3) sinus venosus ASD (superior and inferior types), (4) coronary sinus ASD, and (5) common atrium (simultaneous combination of two or more types of atrial septal defect) [2]. See Table 11.1.

As discussed in depth in Chap. 1, the normal septum develops via apposition of the septum primum, a thin membrane arising from the roof of the primitive atrium, and the septum secundum, a membrane arising from the ventrocranial wall of the primitive atrium. A defect in the central portion of the septum secundum, the foramen ovale, is normally closed by infolding of the atrial septa, forming an indentation referred to as the fossa ovalis. Defects within the area of the fossa ovale are known as secundum atrial septal defects. If there is an extensive deficiency of the atrial septum closure, the ASD can extend beyond the fossa ovale. Extension may occur superiorly or posteroinferiorly to the origin of the superior and inferior vena cava, respectively (sinus venosus ASD), inferiorly to the atrioventricular junction (primum ASD), or posteriorly to the coronary sinus (coronary sinus ASD).

### 11.1.1 Secundum (Fossa Ovale) ASD

This is the most common type of ASD in the general population and accounts for 70 % of ASDs and 6–10 % of all congenital heart disease [2]. The secundum ASD is usually an isolated lesion, but it can be seen in association with other forms of congenital heart disease. The two common associations are mitral stenosis (Lutembacher syndrome) and absent radius (Holt–Oram syndrome). Secundum ASD is also associated with mitral valve prolapse.

Figures 11.2, 11.3, 11.4, 11.5, and 11.6 are representative illustrations of the spectrum of secundum ASD.

### 11.1.2 Primum ASD

Primum atrial septal defects (Fig. 11.7), also called atrioventricular septal defects, account for 15–20 % of ASDs [2].

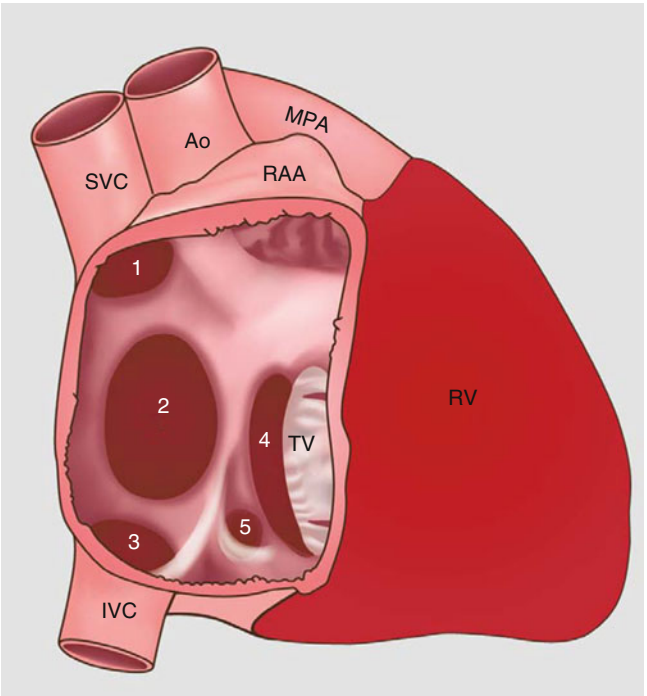


**Fig. 11.1** The variants of atrial septal defects: (*1*) superior sinus venosus defect, (*2*) secundum defect, (*3*) inferior sinus venosus defect, (*4*) primum defect, and (*5*) coronary sinus defect. *Ao* aorta, *MPA* main pulmonary artery, *IVC* inferior vena cava, *RAA* right atrial appendage, *RV* right ventricle, *SVC* superior vena cava, *TV* tricuspid valve

**Table 11.1** Types of ASD

| |
|---|
| Secundum |
| Primum |
| Sinus venosus (superior and inferior type) |
| Unroofed coronary sinus |
| Common atrium |

W. Mazur et al., *CT Atlas of Adult Congenital Heart Disease*,
DOI 10.1007/978-1-4471-5088-6_11, © Springer-Verlag London 2013

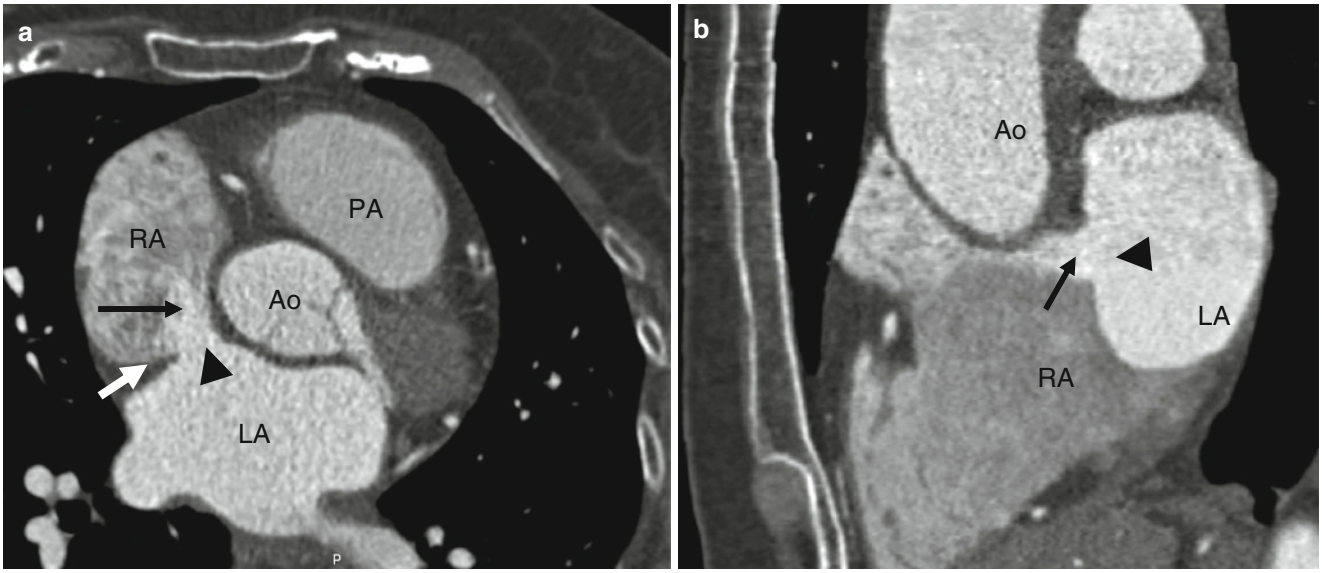


**Fig. 11.2** Panels (**a**) and (**b**) are small secundum atrial septal defects (ASD) (*black arrowheads*) limited entirely to the fossa ovale. The ASD in panel (a) demonstrates a good tissue rim thickness (*white arrow*). Note the jets of contrast (*black arrows*) entering the right atrium from the left atrium. The right atrial size is normal indicating the absence of volume overload. *RA* right atrium, *PA* pulmonary artery, *Ao* aorta, *LA* left atrium

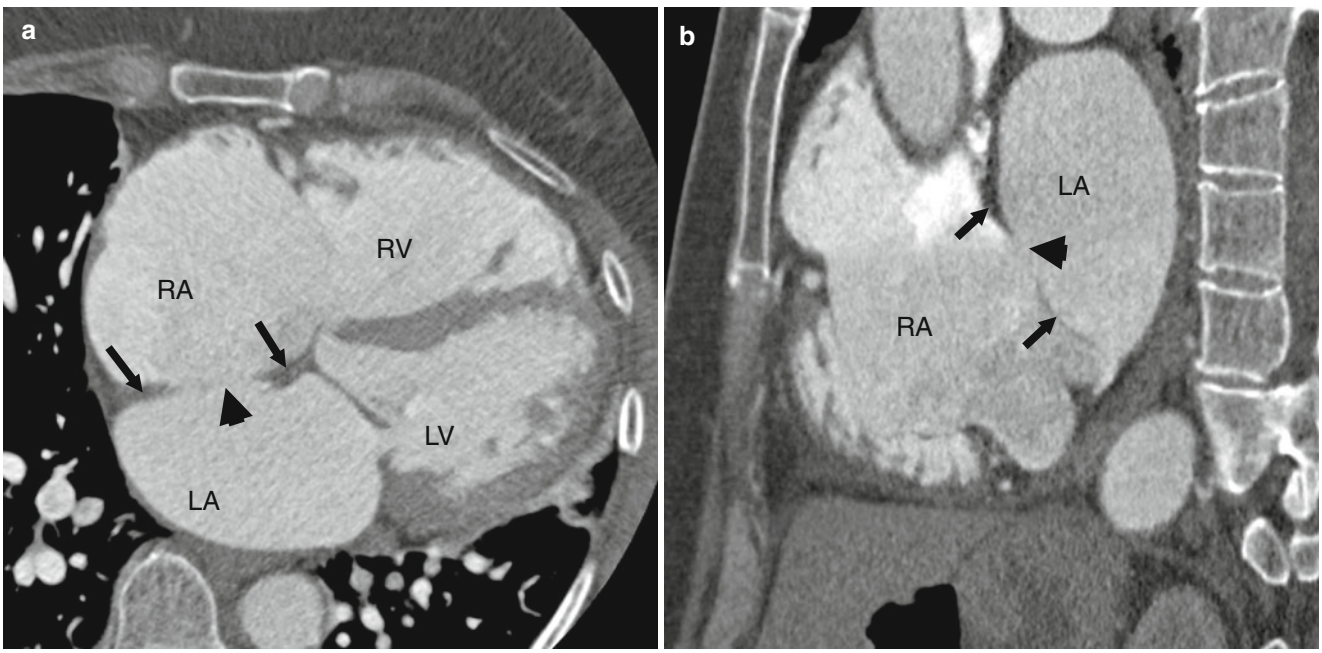


**Fig. 11.3** Panels (**a**) and (**b**) are large secundum atrial septal defects (ASD) (*black arrowheads*) associated with right atrial (panels a and b) and right ventricular enlargement (panel a), indicating volume overload. Note a good tissue rim, exceeding 3 mm in all directions (*black arrows*) in both panels. *LA* left atrium, *LV* left ventricle, *RA* right atrium, *RV* right ventricle

This ASD presumably results from failure of the endocardial cushion to close the ostium primum and occurs between the fossa ovalis and the level of the atrioventricular valves. Primum ASDs are often associated with atrioventricular valve abnormalities (cleft mitral valve) and with trisomy 21 and heterotaxy syndromes. Unrepaired primum ASDs are very rare in adults [3] since correction is usually necessary prior to adulthood.

### 11.1.3 Sinus Venosus ASD

A superior sinus venosus atrial septal defect occurs at the junction of the superior vena cava (SVC) and right atrium and accounts for 5–10 % of all ASDs [2]. It often coexists with partial anomalous pulmonary venous return, usually from the right upper lobe to the SVC near its junction with the right atrium. Sinus venosus ASDs are associated with an increased incidence of pulmonary hypertension due to increased flow to the lungs from the anomalous pulmonary venous return. An inferior sinus venosus ASD is much less common than a superior sinus defect and occurs at the junction of the inferior vena cava (IVC) and right atrium.

Treatment of sinus venosus ASDS is surgical closure and reimplantation of the anomalous pulmonary veins. Alternatively, a baffle may be created to correct return of the anomalous pulmonary venous flow back to the left atrium [2]. Rarely, the superior vena cava can enter the right atrium via an accessory vein.

Figures 11.8, 11.9, 11.10, 11.11, and 11.12 are examples of various types of sinus venosus ASD.

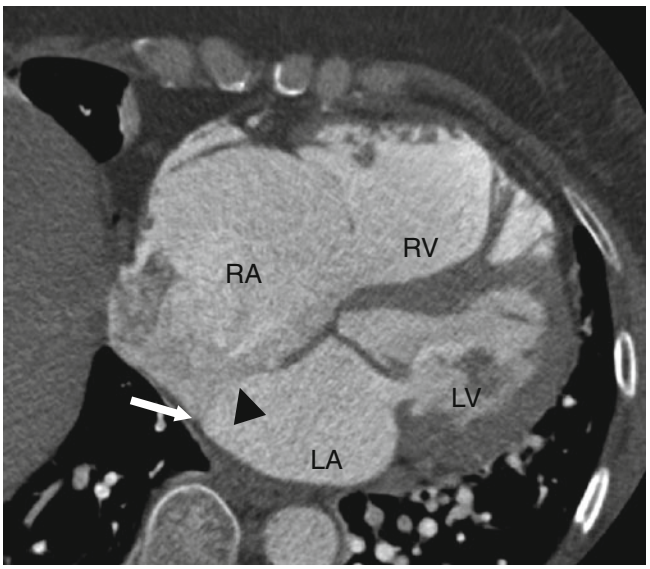


**Fig. 11.4** A large secundum atrial septal defect (ASD) (*black arrowhead*) with a posteroinferior rim deficiency (*white arrow*). *RA* right atrium, *RV* right ventricle, *LA* left atrium, *LV* left ventricle

### 11.1.4 Unroofed Coronary Sinus ASD

Unroofed coronary sinus ASD is rare, comprising less than 1 % of all atrial septal defects [2]. It is thought to result from a failure of separation of the superior wall of the coronary sinus with the left atrium, leading to a direct communication between the coronary sinus and the left atrium. It is usually associated with a persistent left superior vena cava (LSVC). Persistent LSVC occurs in 0.1–0.5 % of the general population and 8 % of anomalies drain into the left atrium [4]. An unroofed coronary sinus ASD is seen in 75 % of patients with persistent LSVC that drains into the left atrium [4]. Unroofed coronary sinus is classified into four groups. Type I is a completely unroofed coronary sinus with persistent LSVC. Type II is a completely unroofed coronary sinus without persistent LSVC. Type III is a partially unroofed

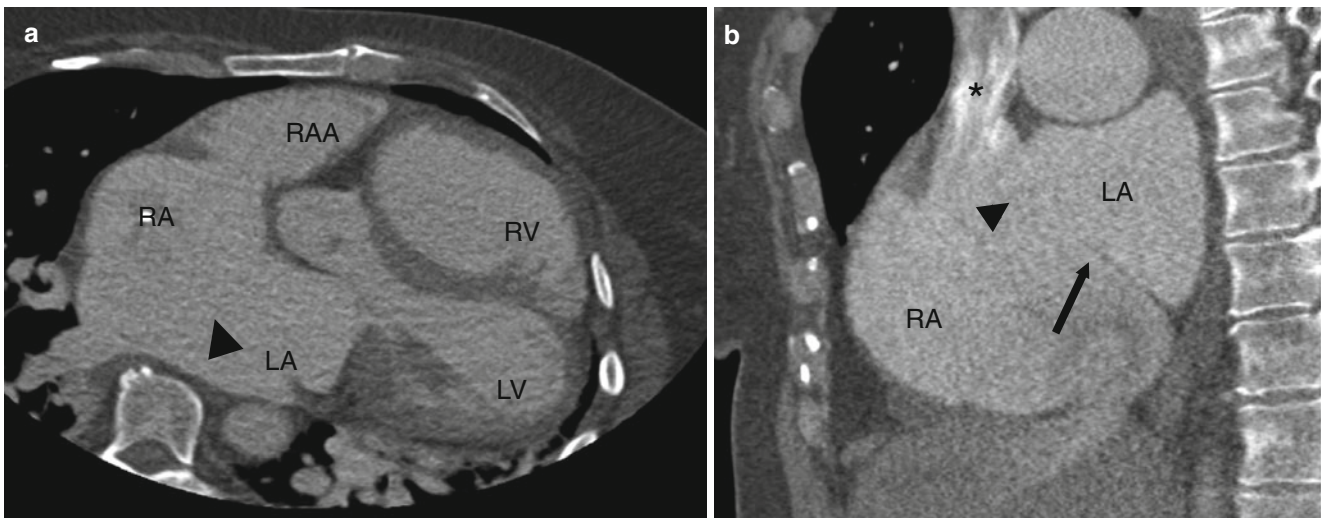


**Fig. 11.5** Panels (**a**) and (**b**) illustrate a CT image of a large secundum atrial septal defect (ASD) (*black arrowhead*). Panel (a) (axial plane) suggests that the ASD lacks both anterosuperior and posterosuperior rims and thus appears as one common atrium in this view. However, the sagittal view (panel b) demonstrates the presence of only a posteroinferior rim (*black arrow*). *RA* right atrium, *RV* right ventricle, *LA* left atrium, *LV* left ventricle, *Asterisk* superior vena cava, *RAA* right atrial appendage, *LAA* left atrial appendage

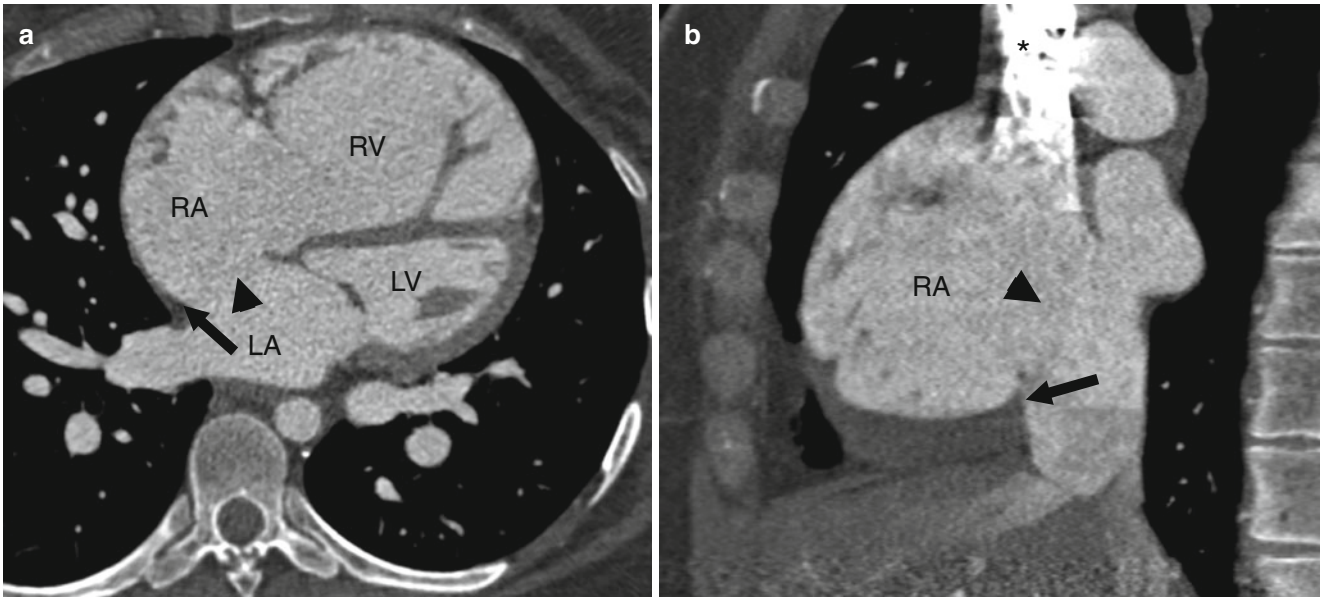


**Fig. 11.6** Panel (**a**) is a large secundum atrial septal defect (ASD) (*black arrowhead*) with the absence of an anterosuperior rim (*black arrow*). Panel (**b**) is a large secundum ASD (*black arrowhead*) lacking a posteroinferior rim (*black arrow*). *RA* right atrium, *RV* right ventricle, *LA* left atrium, *LV* left ventricle, *Asterisk* superior vena cava

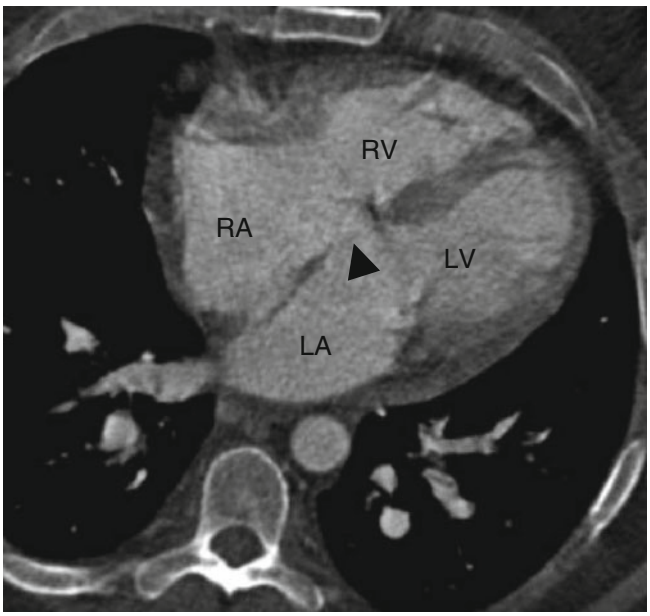


**Fig. 11.7** Primum atrial septal defect (ASD). An axial CT shows the ASD (*black arrowhead*) located between the level of the fossa ovalis and atrioventricular valves. This defect occurs in the lower part of the atrial septum close to the ventricular inlet valves. *RA* right atrium, *RV* right ventricle, *LA* left atrium, *LV* left ventricle

midportion coronary sinus defect. Type IV is a partially unroofed terminal portion coronary sinus defect. The fenestration from the coronary sinus into the left atrium typically occurs between the left atrial appendage and the left upper pulmonary vein [4].

Figure 11.13 is an example of an unroofed coronary sinus type ASD.

### 11.1.5 Common Atrium

Common atrium (confluence of two or more types of ASD defects) is characterized by complete absence of atrial septum and occurs in association with other complex defects, frequently heterotaxy syndrome. It is very rarely seen in the adult population [5].

Figure 11.14 depicts a common atrium.

### 11.1.6 Patent Foramen Ovale

Patent foramen ovale (PFO) is the most common form of interatrial communication. It is caused by a failure of fusion of the flap valve of the fossa ovalis. The prevalence of PFO declines progressively with age (34 % up to age 30 years, 25 % for age 30–80 years, and 20 % older than 80 years) [7]. Two types of PFO exist. The first is the incompetent valve type and results in right-to-left shunting only when right atrial pressure exceeds that of the left atrium such as during a Valsalva maneuver. The second type is called the stretched type and is due to high left atrial pressure (such as seen in left heart failure) which stretches the fossa ovalis flap valve to the point of incompetence, resulting in a left-to-right shunt. While a single defect is most common in PFO, multiple fenestrations may also be seen.

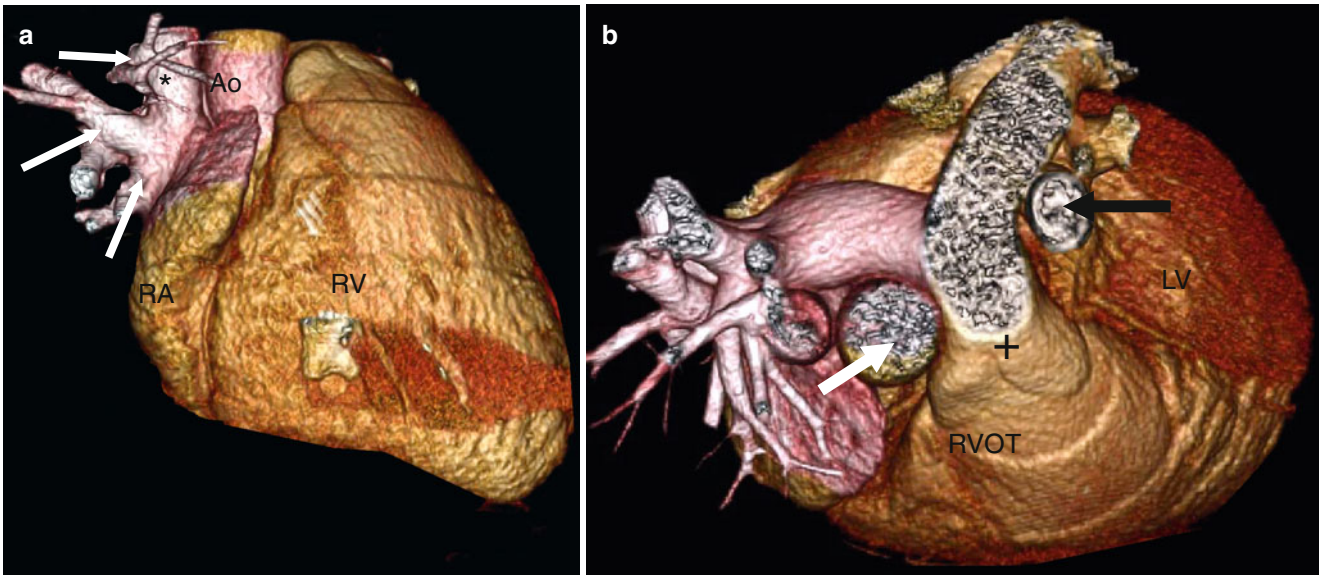


**Fig. 11.8** Panels (**a**) and (**b**) are 3D volume-rendered computed tomography images from a patient with a sinus venosus atrial septal defect. Panel (a) demonstrates partial anomalous pulmonary venous return (three right-sided pulmonary veins (*white arrows*) entering the superior vena cava, SVC). Panel (b) shows a left-sided SVC (*black arrow*). In this panel the normal SVC is depicted by the *white arrow*. *RVOT* right ventricular outflow tract. *Plus sign* (+): pulmonary artery. *RA* right atrium, *RV* right ventricle

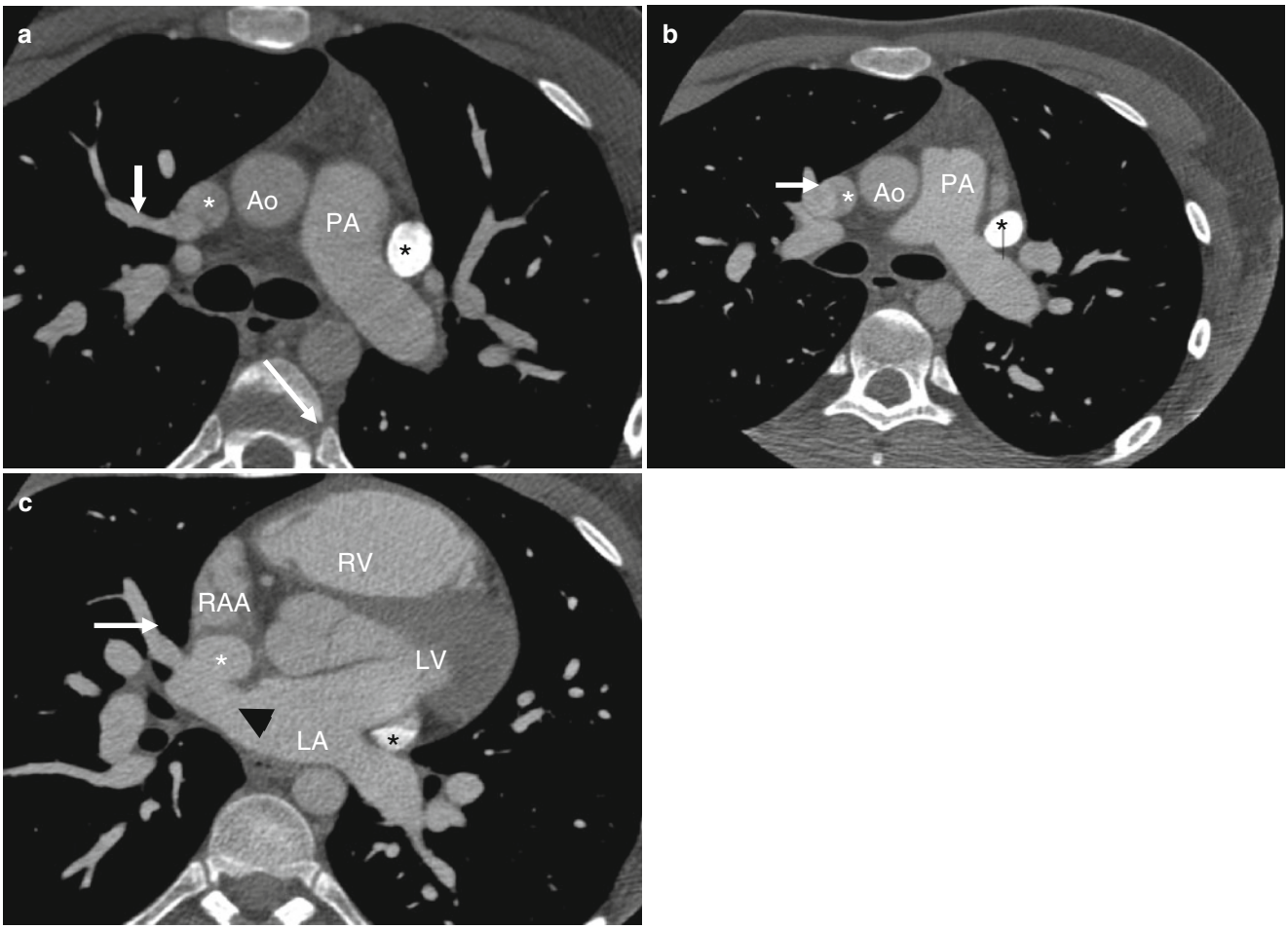


**Fig. 11.9** Maximum intensity projections of the sinus venosus atrial septal defect from the patient in Fig. 11.8. Here panels (**a**), (**b**), and (**c**) are axial views each showing 1 of the 3 anomalous pulmonary veins (*black arrows*, *white arrows*) entering the superior vena cava (*asterisk*). Panel (c) illustrates the SVC straddling both atria (*black arrowhead*). The persistent left-sided SVC is again noted by the *black asterisk*. *White asterisk* superior vena cava, *Ao* aorta, *PA* pulmonary artery, *RAA* right atrial appendage, *RV* right ventricle, *LA* left atrium, *LV* left ventricle

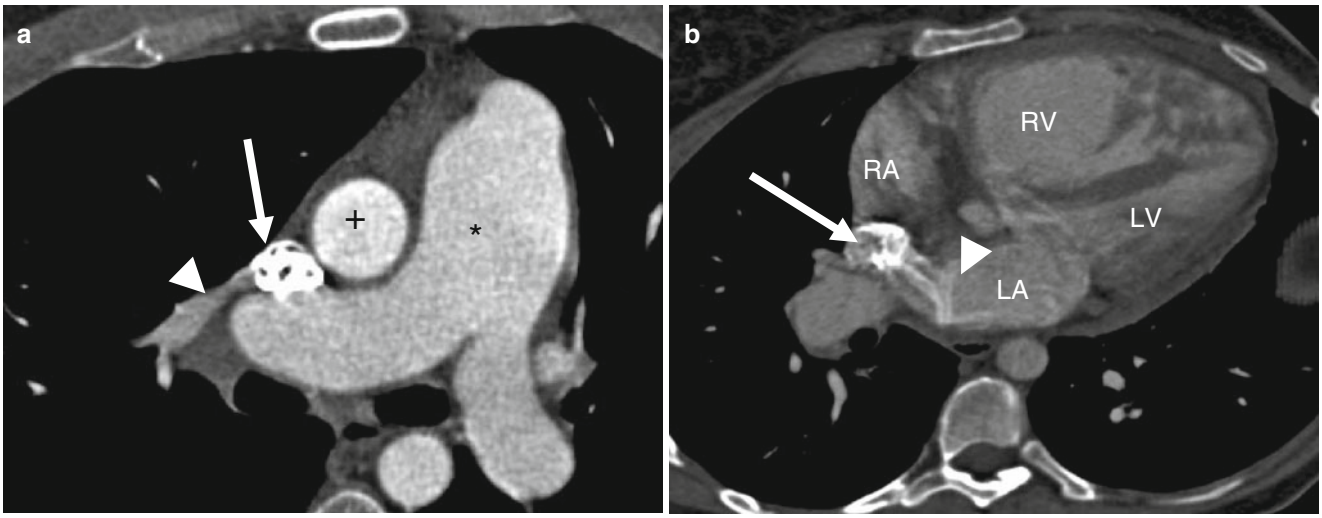


**Fig. 11.10** A superior sinus venosus atrial septal defect (ASD). Panel (**a**) is an axial scan demonstrating an anomalous vein (*white arrowhead*) from the right upper lobe entering the superior vena cava (SVC, *white arrow*). Note the enlarged pulmonary arteries resulting from pulmonary hypertension (*black asterisk*). Panel (**b**) is an axial view at a more inferior plane illustrating the actual ASD with a jet of contrast (*white arrowhead*) flowing from the SVC (*white arrow*) to the left atrium (*LA*). Typically the flow into the left atrium is along the lateral wall, as in this case. *RA* right atrium, *RV* right ventricle, *LA* left atrium, *LV* left ventricle, *Plus sign* (+) ascending aorta

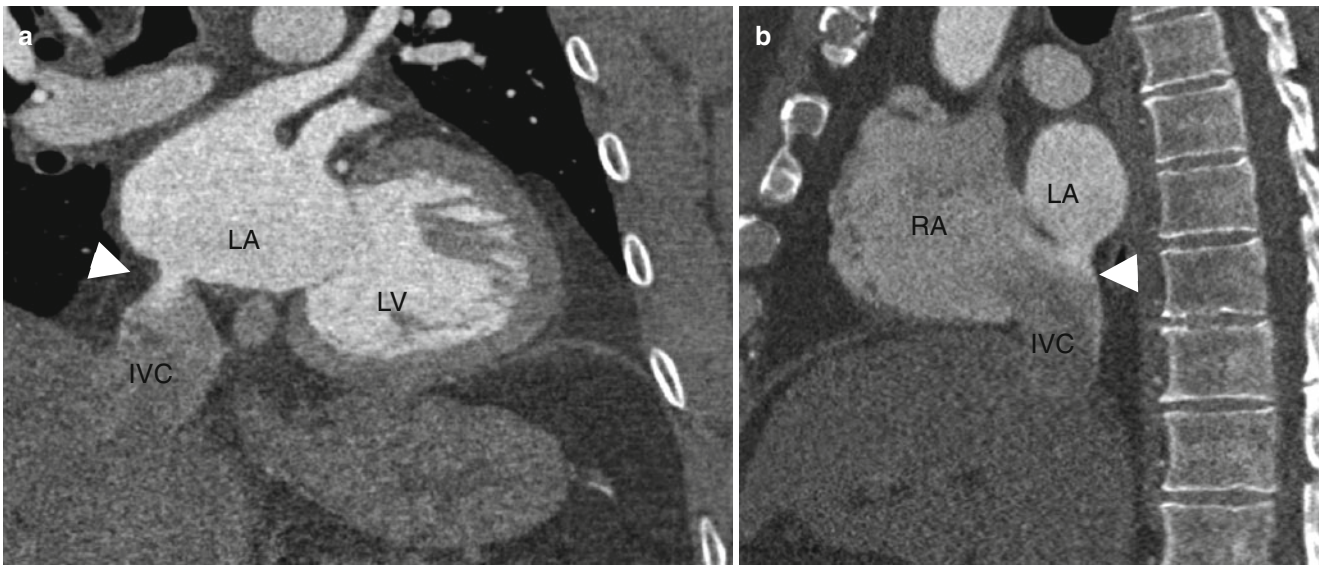


**Fig. 11.11** An example of an inferior sinus venosus ASD. Panels (**a**) and (**b**) are multiplanar reformatted images and depict a contrast-filled communication (panel a, *white arrowhead*) between the inferior vena cava (*IVC*) and left atrium (*LA*) with the IVC straddling both atria (panel b, *white arrowhead*). *LV* left ventricle, *RA* right atrium

Figure 11.15 is an example of a PFO seen on CT.

Atrial septal aneurysm (ASA) is associated with a PFO in 30 % of the cases [8]. ASA is defined as an abnormal bulging of the interatrial septum with an excursion of at least 10 mm and a base span of at least 15 mm [8]. This is thought to be due to redundancy of the valve of the fossa ovalis and/or excessive mobility of the atrial septum with ballooning into the right or left atrial chamber. ASA may be associated with mitral valve prolapse and atrial arrhythmias.

Figure 11.16 demonstrates an atrial septal aneurysm.

### 11.1.7 Clinical Findings of Atrial Septal Defects

Clinical findings of isolated atrial septal defects are usually related to left-to-right shunting. The degree of shunting is determined by the size of the defect and the relative compliance of the right and left ventricles. Secundum ASDs that have a sufficient rim of tissue around the septal defect can be closed percutaneously with septal occluder devices, most commonly the AMPLATZER septal occluder device. All other hemodynamically significant ASDs require surgical closure.


**Fig. 11.12** An unusual case of sinus venosus atrial septal defect (ASD). Panel (**a**) is an axial reformat, panel (**b**) is an oblique reformat, and panel (**c**) is a 3D volume-rendered image. All images show the superior vena cava (SVC, *white arrow*) entering the left atrium (*LA*) while an accessory vein (*white arrowheads*) enters the right atrium (*RA*). *LA* left atrium, *Ao* aorta, *RV* right ventricle

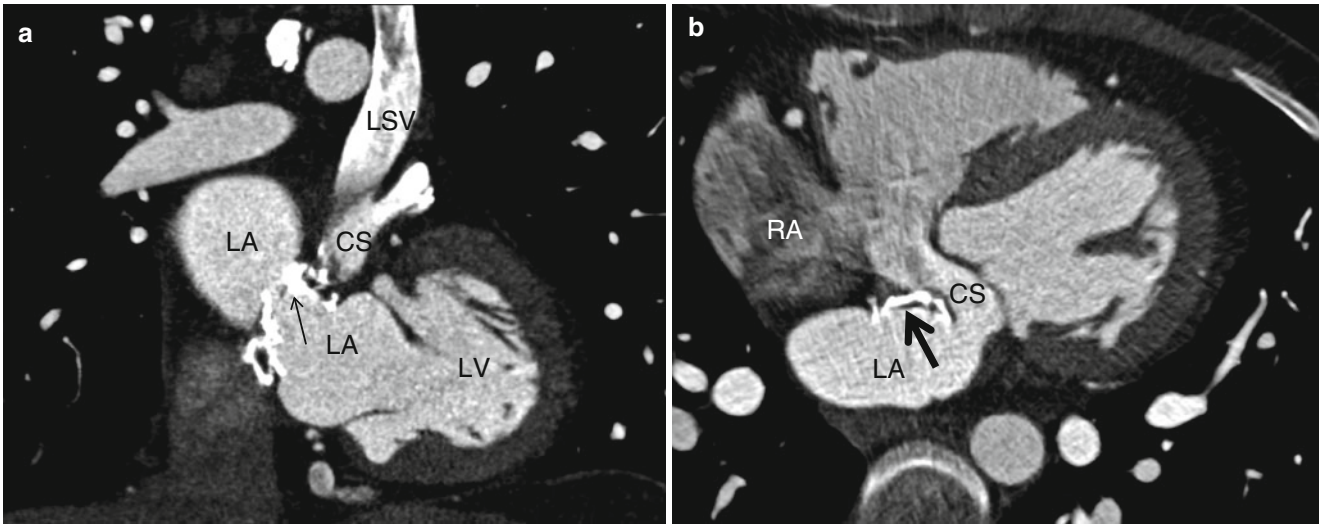


**Fig. 11.13** Represents an unroofed coronary sinus atrial septal defect in a 33 year old patient with repair in childhood who now presents with right sided heart failure and evidence of an intracardiac shunt. Panel (**a**) demonstrates a persistent left sided superior vena cava entering the coronary sinus. A calcified septal closure patch which does not cover the entire defect is also demonstrted (*arrow*). Panel (**b**) demonstrates an intra-atrial communication via the unroofed coronary sinus. *LA* left atrium, *RA* right atrium, *LSV* persistent left sided superior vena cava, *CS* coronary sinus, *LV* left ventricle

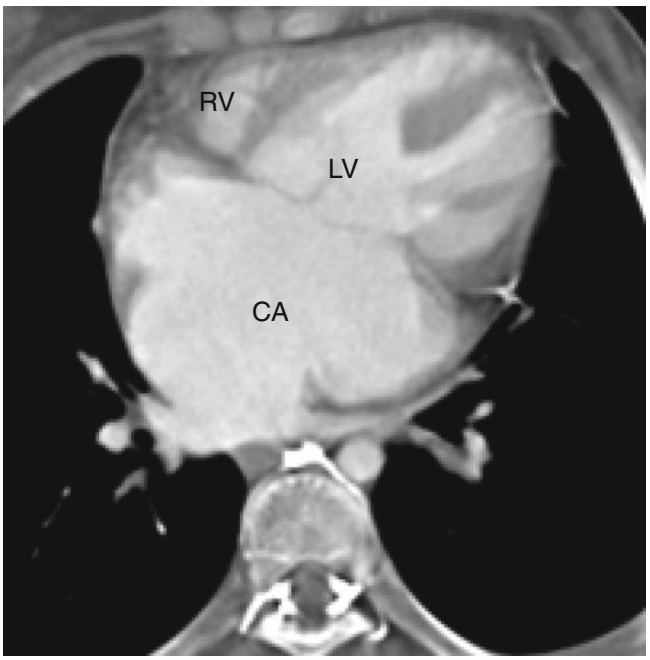


**Fig. 11.14** A depiction of a common atrium. This transverse view shows one common atrial chamber (*CA*) with complete absence of the atrial septum. *RV* right ventricle, *LV* left ventricle

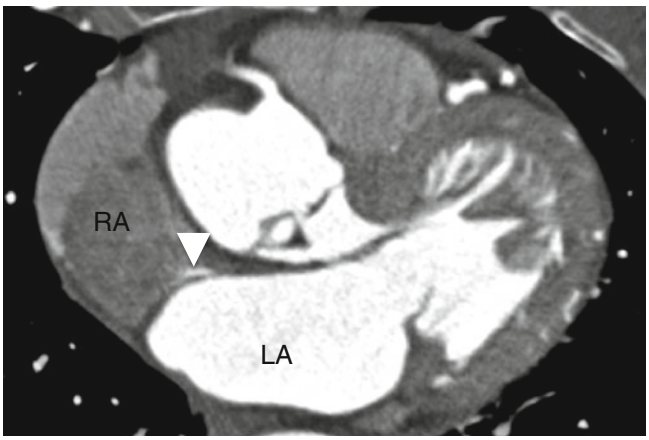


**Fig. 11.15** Patent foramen ovale. An axial scan shows a thin contrast jet (*white arrowhead*) that is directed parallel to the intra-atrial septum. Typically, the flow is along the anterior part of the atrium and parallels the atrial septum. *LA* left atrium, *RA* right atrium

### 11.1.8 Cardiac Computed Tomography (CT) in the evaluation of ASD

Echocardiography is the method of choice to diagnose ASD but CT can be used when echocardiography is indeterminate [8–12]. The CT diagnosis of ASD is based on identifying a defect in the septal tissue and/or the presence of increased contrast opacification in the right heart despite proper timing of the scan after contrast bolus administration. The typical appearance of an ASD on CT is that of a contrast jet from the left atrium to the right atrium. Other findings of a left-to- right shunt include right ventricular and right atrial enlargement. Secundum ASD can be differentiated from a patent foramen ovale by the appearance of the jet. A PFO has a very thin, channel-like appearance and the contrast jet is at a slight angle or parallel to the interatrial septum or atrial roof as it courses from the left atrium to the right atrium (Fig. 11.15) [13, 14]. The secundum and sinus venous defects are broader and the former flows into the central part of the left atrium, while the latter flows along the lateral wall (Figs. 11.2, 11.3, 11.4, 11.5, 11.6, 11.8, 11.9, 11.10, 11.11, and 11.12) [14, 15].

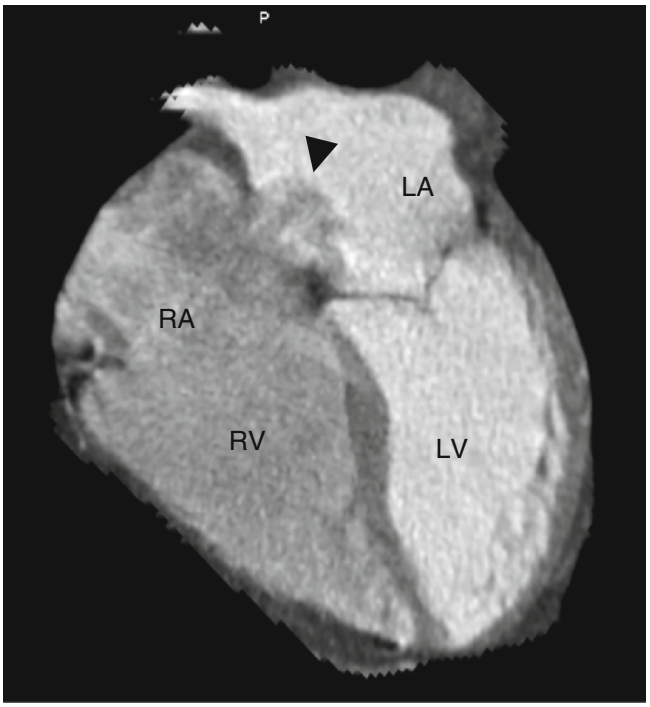


**Fig. 11.16** Atrial septal aneurysm (ASA, *black arrow*). This four-chamber view shows the bulging of the atrial septum with a base span >15 mm. The excursion is >10 mm. There is no contrast jet across the atrial septum in this aneurysm. Note the clear demarcation between the contrast-filled left atrium (*LA*) and the relatively contrast-poor right atrium (*RA*). ASA can mimic a left-to-right or bidirectional shunt due to excessive motion of very floppy interatrial septum. *RV* right ventricle, *LV* left ventricle

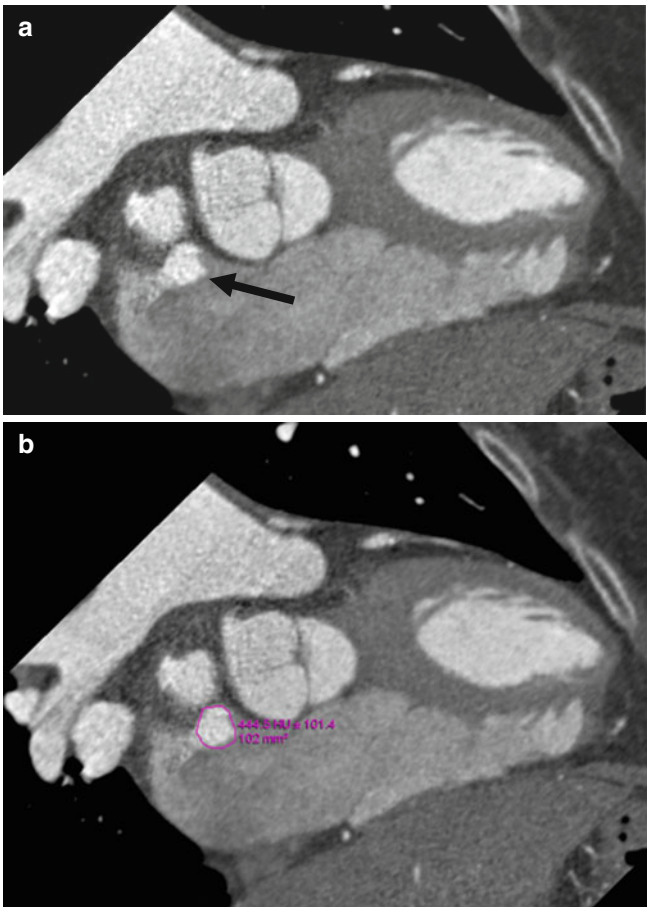


**Fig. 11.17** Measurement of the atrial septal defect (ASD) area. Oblique en face views allow measurement of defect dimension and area. CT images should be reconstructed so that the maximum size of the defect in long and short axis can be visualized and measured with electronic calipers at the workstation. Usually, an oblique reconstruction with en face view of the ASD suffices. Measurements are made at end systole to obtain the greatest size of the ASD. The area is automatically calculated by tracing the electronic calipers along the circumference of the ASD. *Circle* Traced area of the ASD, *black arrow* ASD

Associated findings of partial anomalous pulmonary venous return may be noted in sinus venosus-type ASDs (Figs. 11.8, 11.9, 11.10, 11.11, and 11.12). With primum ASDs, an associated cleft mitral valve or associated ventricular septal defects may be noted.

Morphological changes of pulmonary hypertension found in long-standing larger ASDs include pulmonary arterial and right heart chamber enlargement.

CT can provide accurate anatomic assessment prior to percutaneous closure of an ASD or PFO. The necessary measurements include an assessment of the long- and short-axis views of the defect and measurement of the area of the defect (Fig. 11.17) In addition, the thickness of the rim of surrounding tissue is important to note. Measurements are made in end systole.

Rim thickness is measured from the edge of ASD to the aortic valve (anterosuperior rim), tricuspid valve (anteroinferior rim), SVC (posterosuperior rim), and IVC (posteroinferior rim). Percutaneous closure is contraindicated with ASD >36 mm in size and rim thickness <3 mm. Anterosuperior rim deficiency is the most common contraindication to percutaneous closure and has been reported in up to 54 % patients referred for this procedure [16]. In patients with a large ASD, a posteroinferior rim thickness >10 mm is an important predictor of successful percutaneous closure.

While the information described above is obtainable by transesophageal echocardiography (TEE), the long axis of a large ASD can be underestimated with TEE compared to CT [16].

## 11.2 Ventricular Septal Defect

Ventricular septal defect (VSD) is the most common congenital heart disease and accounts for over 20 % of all congenital cardiac malformations [16]. It is a result of deficiency in interventricular septum continuity and it can be isolated or

**Table 11.2** Important information from CT assessment of ASD

| |
|---|
| Differentiate ASD from PFO |
| Measure defect size |
| Identify rim size |
| Identify right ventricular size and function (if retrospective gating) |
| Characterize pulmonary artery size |
| Identify associate defects (anomalous pulmonary veins, VSD, atrioventricular valve abnormalities, heterotaxy syndromes) |

it can occur in association with other congenital heart diseases.

### 11.2.1 Anatomic Types

The unified VSD nomenclature system [17, 18] recognizes four anatomic types of VSD (Fig. 11.18).

Type 1 (synonyms: subarterial, supracristal, conal, infundibular, subpulmonary) is located just beneath the semilunar valves and above the crista supraventricularis in the conal or outlet septum (Fig. 11.19). They are often associated with aortic regurgitation produced by prolapse of the anterior aortic valve leaflet. These defects can be bound by the fibrous annulus of the semilunar valves and/or muscular tissue. The VSD that is completely surrounded by muscle is termed a conal muscular VSD, while the subarterial VSD bound by fibrous continuity of the aortic and pulmonary valve leaflets is termed a juxta-arterial or doubly committed VSD. Type 1 VSD accounts for approximately 6 % of defects and spontaneous closure of this type of defect is uncommon [20].

Type 2 (synonyms: perimembranous, paramembranous, conoventricular) involves the membranous septum and is bordered by the atrioventricular septum (Fig. 11.20). Depending on the location, membranous VSDs are further classified as inlet, trabecular, outlet, and confluent. The latter involves multiple areas of the septum (i.e., the inlet, trabecular, and outlet portions). Type 2 is the most common VSD, accounting for approximately 80 % of defects [19].

Type 3 (synonyms: inlet, AV canal type, endocardial cushion) is located in the inlet of the right ventricular septum immediately inferior to the septal leaflet of the tricuspid valve (Fig. 11.21). Type 3 VSD may be associated with AV canal defect. This defect typically occurs in patients with trisomy 21 syndrome. Type 3 VSD accounts for 5–8 % of VSDs [19].

Type 4 (muscular) is entirely bordered by the muscular septum and has a rim totally composed of septal muscle (Fig. 11.22). Based on its location in the septum, it is classified as inlet, trabecular outlet, or confluent (involves multiple areas of the septum, including the inlet, trabecular, and outlet regions). Subclassifications of the inlet type include anterior, apical, and midventricular. Type 4 VSD

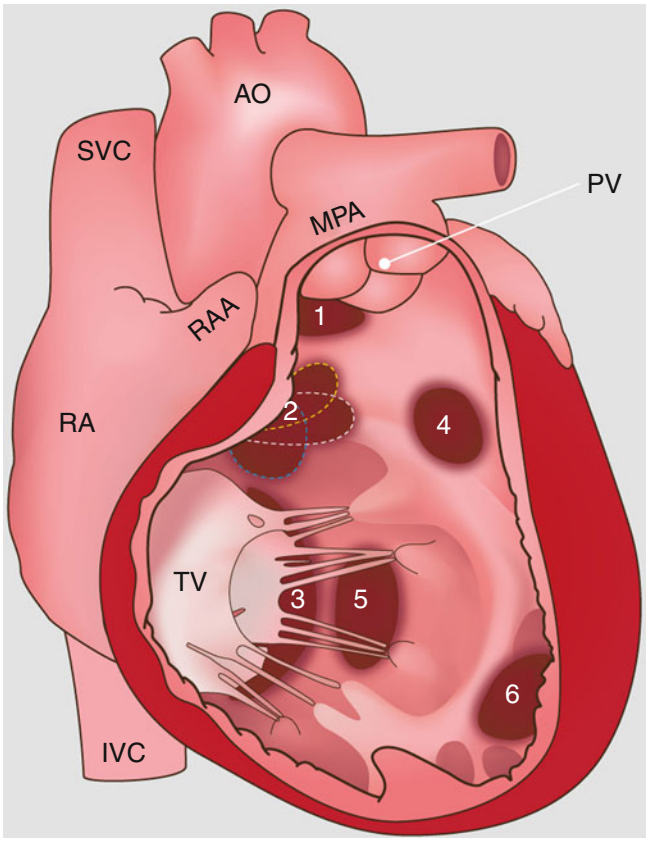


**Fig. 11.18** Types of ventricular septal defects: (*1*) subarterial defect, which lies in the left ventricular outflow tract just below the aortic valve; (*2*) perimembranous defect, which involves the membranous septum (*yellow*, *white*, and *blue* dashed circumference for outlet, trabecular and inlet subtype, respectively); (*3*) inlet or atrioventricular defect, which lies inferior to the septal leaflet of the tricuspid valve; and (*4*) outlet, (*5*) inlet and apical (*6*) muscular defects, which are entirely bounded by the muscular septum and are often multiple. *Ao* aorta, *IVC* inferior vena cava, *MPA* main pulmonary artery, *PV* pulmonary valve, *RA* right atrium, *RAA* right atrial appendage, *SVC* superior vena cava, *TV* tricuspid valve

accounts for 20 % of VSDs in infants and as spontaneous closure is common, the incidence is much lower in adults [19]. Muscular VSDs are frequently multiple. The term "Swiss-cheese" septum has been used to describe multiple muscular VSDs (Fig. 11.23).

Gerbode-type VSD (left ventricle to right atrium fistula) is characterized by a defect in the membranous septum separating the left ventricle and right atrium (Fig. 11.24). This type of VSD is extremely rare.

### 11.2.2 Clinical Findings of VSD

The physiologic consequences of VSD depend on the defect size and the ratio between systemic and pulmonary vascular resistance. Based on the ratio of VSD to aortic annulus

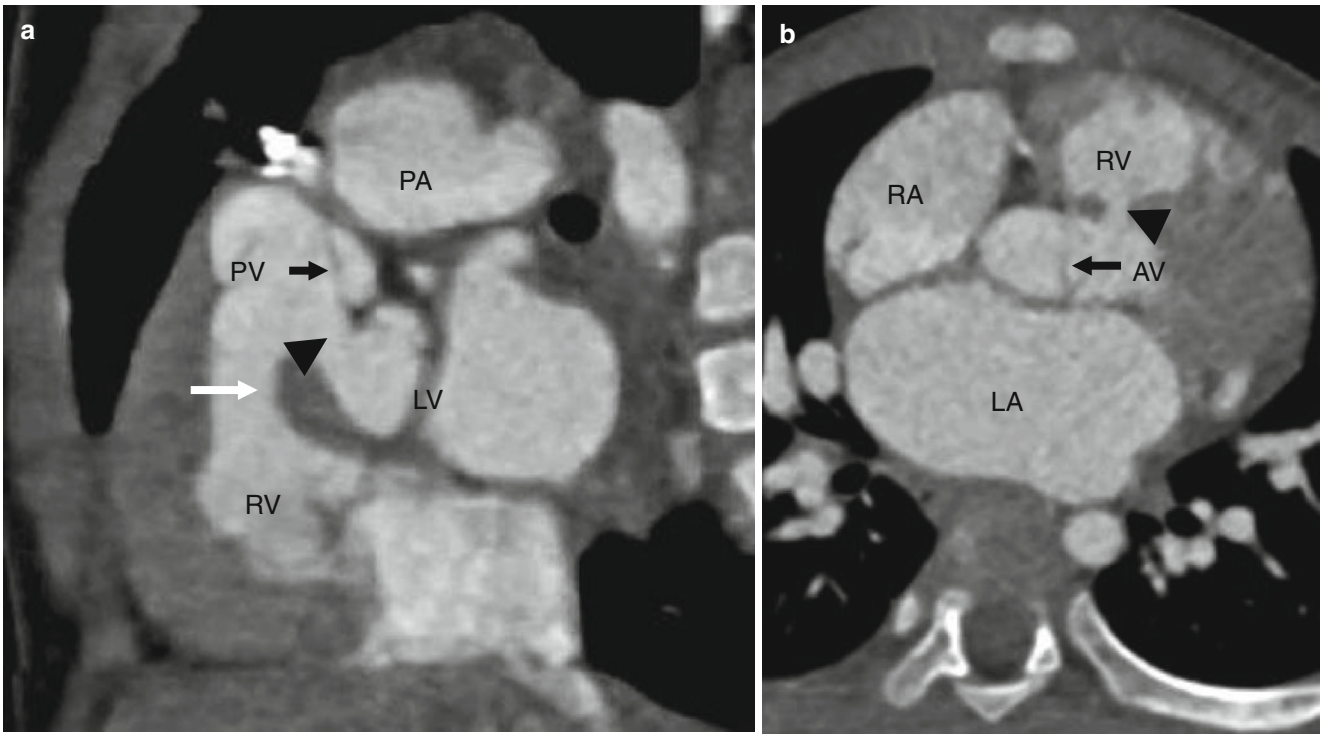


**Fig. 11.19** Computed tomography (CT) images of a type 1 ventricular septal defect (VSD) (synonyms: subarterial, supracristal, conal septal defect, infundibular, subpulmonary). Panel **a** is a sagittal picture and panel **b** is an axial slice. Panel **a** shows a communication (*black arrowhead*) that is localized underneath the pulmonary valve (*black arrow*) and above the supraventricular crest (*white arrow*). *LA* left atrium, *RA* right atrium, *LV* left ventricle, *RV* right ventricle, *PA* pulmonary artery, *PV* pulmonary valve, *AV* aortic valve (Images graciously provided by Motoo Nakagawa MD Department of Radiology, Nagoya City University Graduate School of Medical Sciences, Nagoya, Japan)

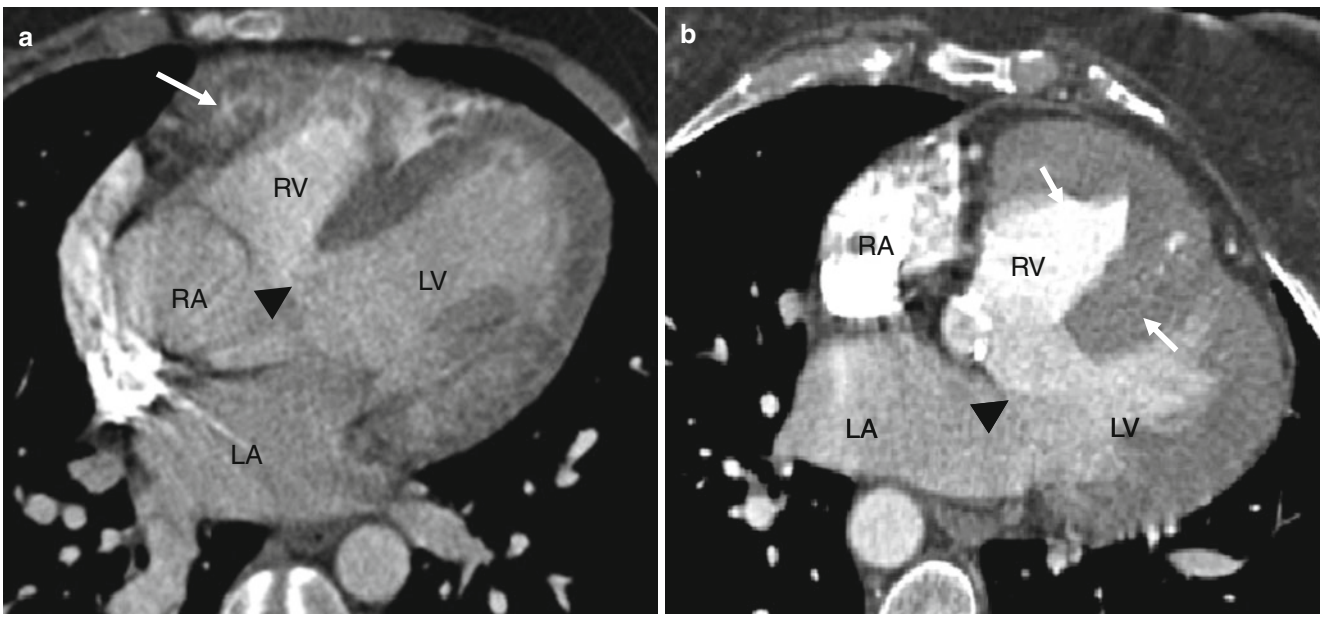


**Fig. 11.20** Type 2 ventricular septal defect (VSD). Panels (**a**) and (**b**) are axial computed tomography images from two separate patients with tetralogy of Fallot demonstrating perimembranous VSD (*black arrowhead*) and right ventricular hypertrophy (*white arrows*). *RA* right atrium, *RV* right ventricle, *LA* left atrium, *LV* left ventricle

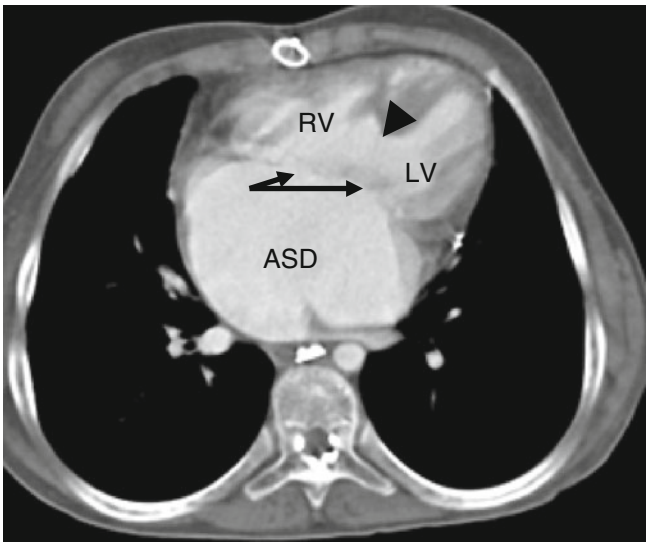


**Fig. 11.21** Type 3 VSD (synonyms: inlet, AV canal type, endocardial cushion defect). This axial computed tomography image shows the defect (*black arrowhead*) located in the inlet of the right ventricular septum. Also note the associated primum atrial septal defect (ASD) and single atrioventricular valve (atrioventricular canal morphology, *black arrows*) in this patient with trisomy 21 syndrome. *RV* right ventricle, *LV* left ventricle, *ASD* atrial septal defect

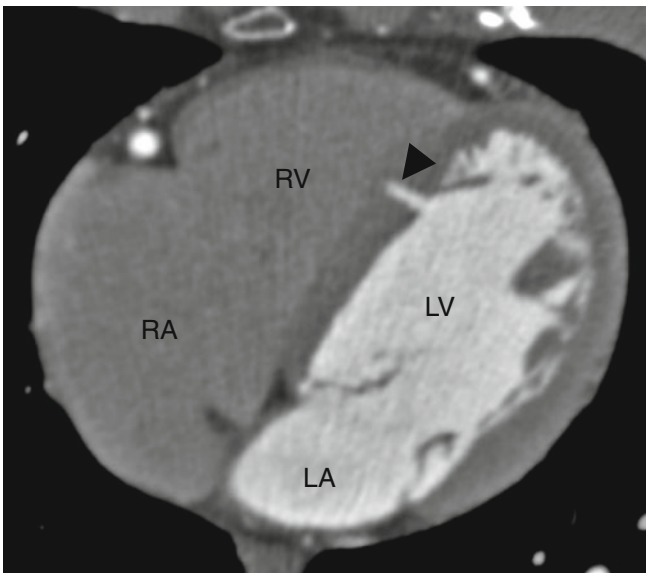


**Fig. 11.22** Type 4 (muscular) VSD. Transverse CT demonstrates contrast agent in the muscular interventricular septum (*black arrowhead*). Note the rim made up of septal muscle. *RA* right atrium, *RV* right ventricle, *LA* left atrium, *LV* left ventricle

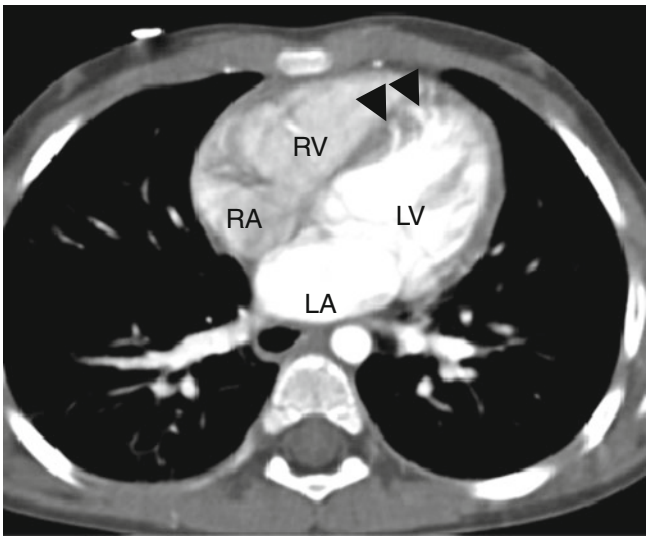


**Fig. 11.23** Type 4 VSD. Several contrast-filled defects (*black arrowheads*) are present in the interventricular septum (so-called Swiss-cheese septum). *RA* right atrium, *RV* right ventricle, *LA* left atrium, *LV* left ventricle

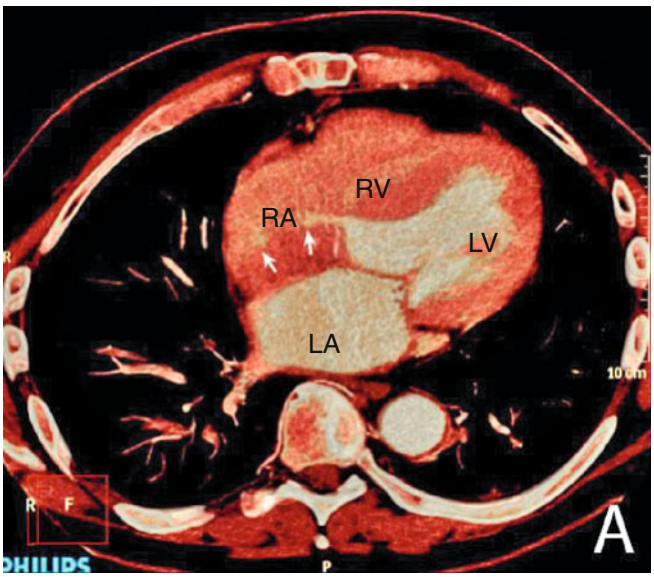


**Fig. 11.24** A color computed tomographic image demonstrating a Gerbode-type ventricular septal defect (VSD). Here, the defect resides in the membranous septum separating left ventricle and right atrium (atrioventricular septum) (Reproduced from Dragicevic et al. [35]. With permission of Leelakrishna Nallamshetty, MD, Department of Radiology, University of South Florida, Tampa General Hospital)

diameter, VSD defects are classified as small (≤0.25), moderate (0.25–0.75), and large (≥0.75) [18]. Physiologically, VSDs are classified as restrictive or nonrestrictive. Restrictive lesions are small and limit flow across the defect resulting in little or no functional disturbance. Nonrestrictive VSDs are larger lesions that allow significant hemodynamic shunting.

The magnitude of flow across a VSD depends on the systemic-to-pulmonary vascular resistance ratio. Initially, systemic vascular resistance is higher than pulmonary vascular resistance resulting in left-to-right shunting. This leads to

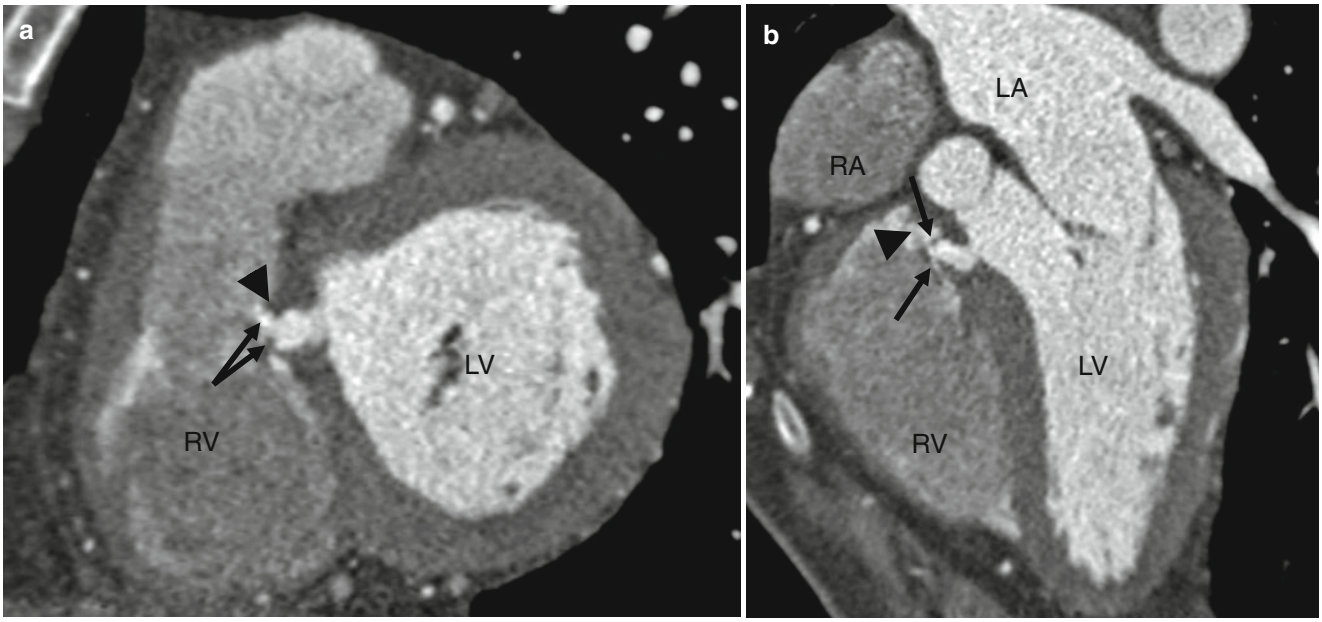


**Fig. 11.25** Closing type 2 VSD with tricuspid valve adherence. Panels (**a**, two-chamber view) and (**b**, four-chamber view) computed tomography scans showing a small ventricular septal defect (VSD) (*black arrowheads*) extending to the right side of the septum with the septal leaflet of the tricuspid valve (*black arrows*) adhering to the margins of the defect. A common mechanism of closure of perimembranous VSD is apposition of the septal leaflet of the tricuspid valve against the VSD. *RA* right atrium, *RV* right ventricle, *LA* left atrium, *LV* left ventricle

right ventricular volume overload and may manifest clinically as congestive heart failure in the first few weeks of life. If untreated, the pulmonary vascular resistance increases which then decreases left-to-right shunting. Finally, when pulmonary resistance exceeds systemic resistance, irreversible pulmonary hypertension (Eisenmenger syndrome) develops and the shunt is reversed to a predominant right-to- left shunt [20]. Identification of pulmonary hypertension is critical because if present, intervention to close the VSD is contraindicated since it could lead to acute right ventricular failure and shorter life expectancy than if the defect were left untreated [21].

With advancing age, complications of VSD may develop and include infective endocarditis, LV volume overload and heart failure, double-chambered right ventricle, relative subaortic stenosis, tachyarrhythmias and complete heart block, and progressive aortic regurgitation caused by aortic cusp prolapse into the right ventricle [22–24]. A rare complication of VSD which may be seen with supracristal and high perimembranous VSDs is significant aortic regurgitation. The high-velocity jet of blood created by flow across these VSDs residing below the aortic valve is potentially capable of pushing the adjacent cusp of the aortic valve into the right ventricle (Venturi effect) resulting in aortic regurgitation extending rightward under the septal leaflet of the tricuspid valve.

Approximately 25–40 % of perimembranous VSDs close spontaneously in the first 2 years of life and 90 % close within 10 years after birth [24]. Perimembranous defects occur beneath the aortic valve on the left side of the septum, extending to the right under the septal leaflet of the tricuspid valve. The most common mechanism of closure (85 %) of perimembranous VSD is either reduplication of leaflet tissue or apposition of the septal leaflet of the tricuspid valve against the VSD (Fig. 11.25).

Outpouching of a leaflet from the tricuspid valve may occur during perimembranous VSD closure creating the appearance of a ventricular septal aneurysm, the so-called windsock deformity. This is not a true aneurysm of the septum but rather it represents tricuspid valvular tissue that is pushed into the right ventricle as a result of the high-velocity blood flow created by the closing VSD (Figs. 11.26 and 11.27). It is the progressive development of this tissue along the right ventricular side of the septum that accounts for spontaneous closure of some perimembranous septal defects.

Small muscular VSDs have the greatest likelihood of spontaneous closure, with closure rates approaching 80–90 % by age 2 years [19]. Muscular defects decrease in size due to growth of the ventricular myocardium which ultimately may fill in the defect. VSDs that do not close spontaneously may be closed percutaneously with septal occluder devices. This approach is usually limited to muscular VSDs. Most other hemodynamically significant VSDs require surgical repair using a patch (Fig. 11.28).

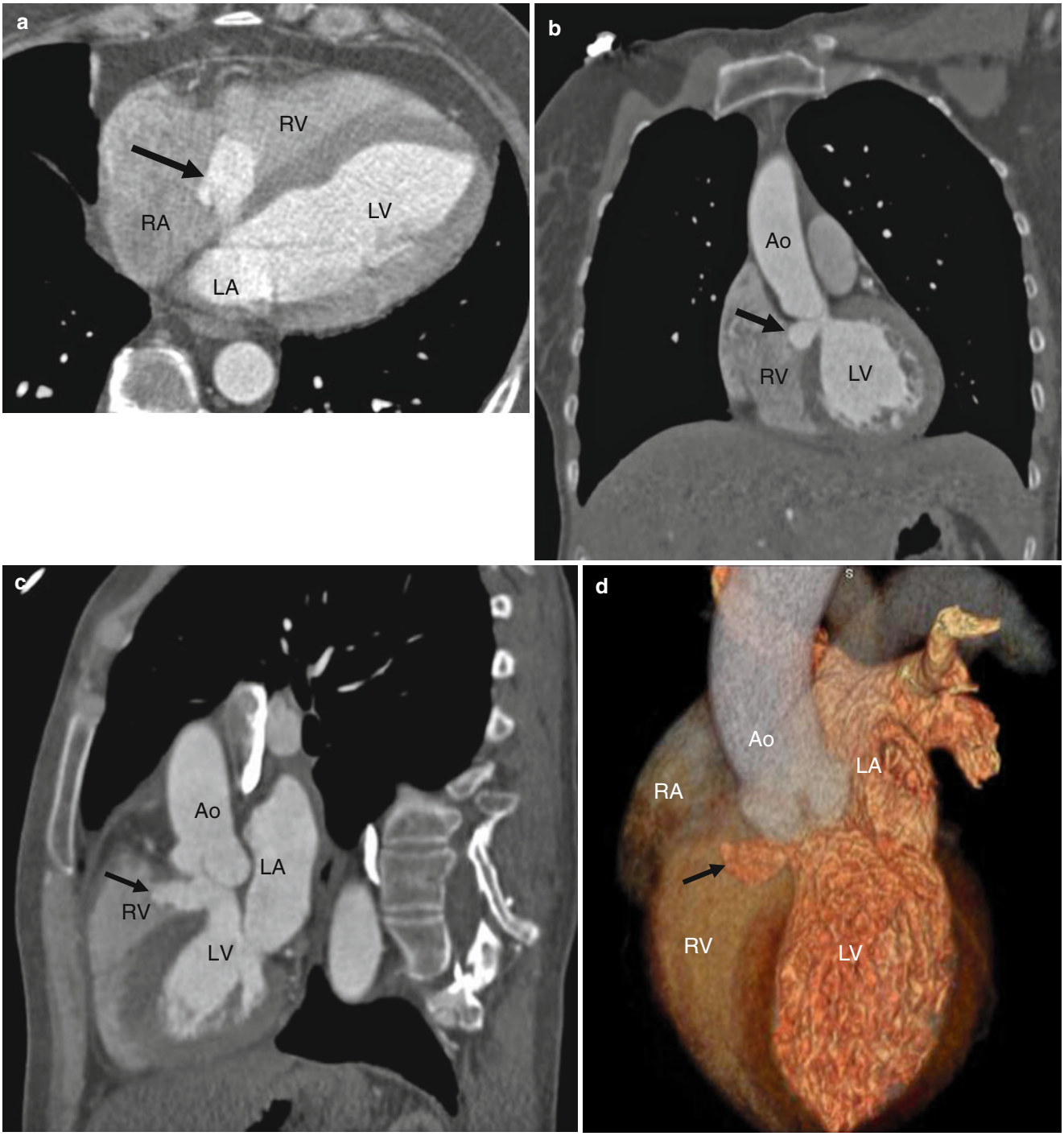


**Fig. 11.26** Closing type 2 VSD with windsock deformity. Panel (**a**, axial multiplanar reformat), panel (**b**, coronal multiplanar reformat), panel (**c**, sagittal multiplanar reformat), and panel (**d**, 3D volume-rendered reformat) showing an outpouching and protrusion of a septal tricuspid valve (*black arrows*) into the right ventricle (*RV*), creating the windsock deformity. This deformity has the appearance of a ventricular septal aneurysm. However, it is simply tricuspid valvular tissue being pushed into the right ventricle due to high-velocity blood flow across a small VSD. *Ao* aorta, *RA* right atrium, *RV* right ventricle, *LA* left atrium, *LV* left ventricle

### 11.2.3 Cardiac Computed Tomography (CT) in the Evaluation of VSD

Echocardiography remains the mainstay to detect shunting across the interventricular septum and to assess pulmonary artery pressure and biventricular function. ECG-gated CT can, however, provide anatomic and functional findings of VSD and may also demonstrate findings of secondary pulmonary hypertension when echocardiography is equivocal (Fig. 11.29) [9–12].

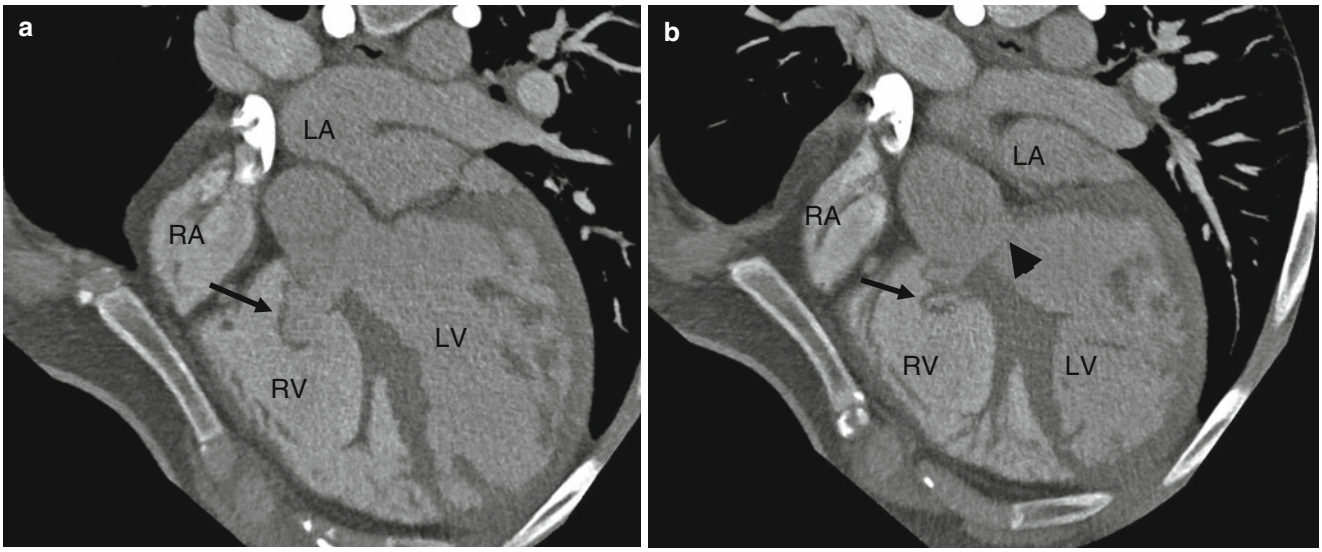


**Fig. 11.27** Example of a closing type 2 VSD associated with windsock deformity which did not result in complete closure. This abnormality likely resulted in the delayed onset of symptoms in this 28-year-old male. Panels (**a**) and (**b**) are oblique sagittal computed tomography scans showing prolapse of the tricuspid valve (*black arrow*) into the right ventricle (*RV*). Note also the presence of a subaortic membrane (*black arrowhead* in panel b) which is an acquired rather than congenital condition. *RA* right atrium, *RV* right ventricle, *LA* left atrium, *LV* left ventricle

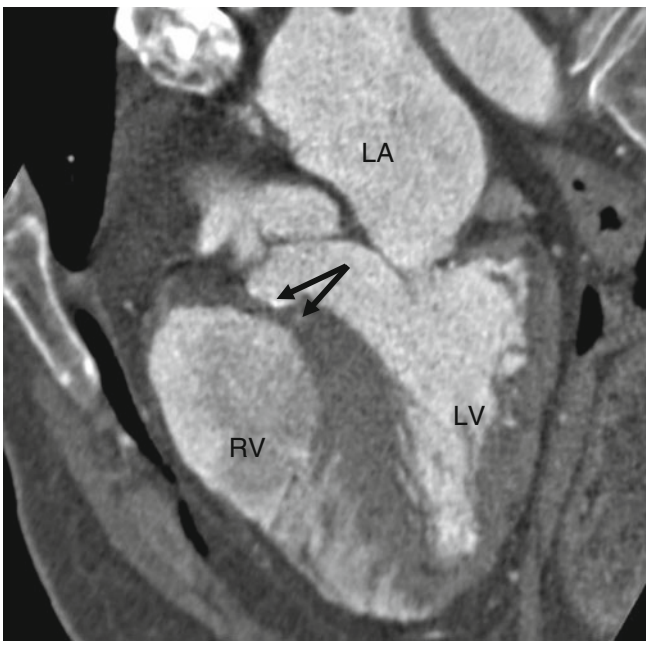


**Fig. 11.28** A surgically closed type 2 VSD. Note the calcified patch (*black arrows*) in the expected location of the membranous septum. *LA* left atrium, *RV* right ventricle, *LV* left ventricle

CT findings of VSD are the lack of continuity of the interventricular septum and a jet of contrast- or noncontrast-enhanced blood at the defect site. Small VSDs may only be seen in diastole as they can temporarily close in systole. At CT, the findings that need to be reported include (1) anatomic data regarding the type, number, location, and size of the VSD(s) measured at the end-diastolic phase as well as the chamber sizes; (2) functional data (if retrospective gating is used) including ventricular function and the presence or absence of aortic valve prolapse and aortic valve regurgitation, right or left ventricular outflow tract obstruction, and tricuspid valve regurgitation; and (3) findings of endocarditis and associated cardiac abnormalities (e.g., tetralogy of Fallot) should be noted as well [18].

In patients scheduled for VSD closure, the proximity of the VSD to the surrounding valves and the atrioventricular conduction axis should be determined to help surgical planning. After VSD closure, CT can be used to evaluate a residual shunt and the morphology of the VSD patch or closure device including calcifications [25]. Echocardiography will be needed to assess pulmonary artery pressure.

Table 11.3 outlines the important information that must be obtained from a CT examination of patient with a VSD.

## 11.3 Atrioventricular Septal Defect (AV Canal Defects)

Atrioventricular septal defect (AVSD) (synonyms: atrioventricular canal defect, endocardial cushion defect) is characterized by a common atrioventricular junction and a common atrioventricular valve [26]. AVSD accounts for 4–5 % of congenital heart diseases with an incidence of 0.19 in 1,000 live births [27].

### 11.3.1 Anatomy

AV canal defects arise from abnormal development of the endocardial cushions [28]. The inferior atrial septum, the

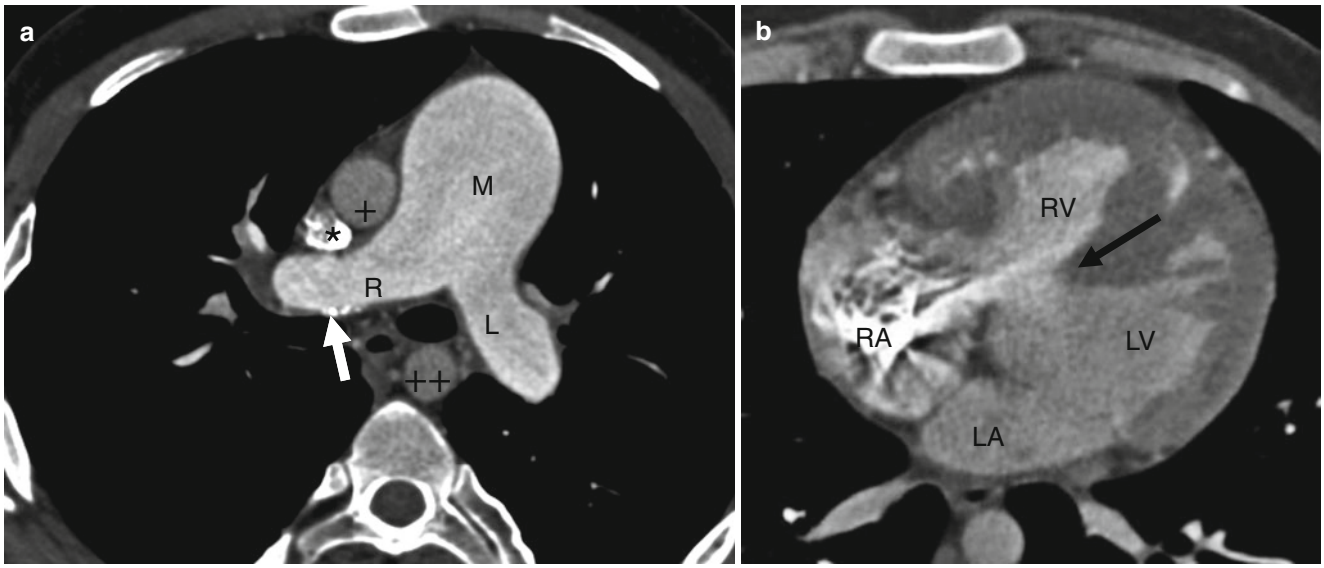


**Fig. 11.29** Pulmonary hypertension (Eisenmenger syndrome) due to unrepaired VSD. Panel (**a**) an axial computed tomogram showing a marked enlargement of the main (*M*) and proximal right (*R*) and left (*L*) pulmonary arteries indicating pulmonary arterial hypertension. Calcification is noted in the right pulmonary artery (*white arrow*). Panel (**b**) a computed tomogram slice reconstructed more caudally showing the perimembranous VSD (*black arrow*). Note the profound right ventricular hypertrophy. + ascending aorta, ++ descending aorta, *RA* right atrium, *RV* right ventricle, *LA* left atrium, *LV* left ventricle

**Table 11.3** An outline of the important information that should be obtained from a CT examination of patient with VSD

| |
|---|
| Type number, location, and size of ventricular septal defect |
| Morphology and size of the atria |
| Morphology, size, hypertrophy, geometry, and systolic function of the ventricles |
| Anatomy, size, and presence/magnitude of aortic and/or pulmonary outflow tract obstruction |
| Size function and morphology of valves including the presence/absence of aortic valve prolapse and aortic valve regurgitation |
| Anatomy, size, and spatial relationship of aorta and pulmonary artery |
| Presence of coexisting anomalies |

superior ventricular septum, the septal leaflet of the tricuspid valve, and the anterior leaflet of the mitral valve all develop from the endocardial cushion tissue. In AV canal defects, the superior and inferior cushions do not fuse completely, resulting in an atrial septal defect (ASD) at the inferior portion of the atrial septum and depending on the severity of the lesion, there may be an associated ventricular septal defect (VSD).

### 11.3.2 Morphology of Atrioventricular Septal Defects

The common atrioventricular valve consists of five leaflets: superior (anterior) and inferior (posterior) bridging leaflets, which override the interventricular septum; left mural leaflet; right inferior leaflet; and right anterosuperior leaflet. The space between the left ventricular components of the superior and inferior bridging leaflets is called the "cleft" [29].

A variety of different classifications have been used to categorize AVSDs, but the most common system divides the defects into three forms: (1) complete, (2) partial, and (3) transitional. The complete AVSD is characterized by both an ostium primum ASD immediately above or at the plane of the atrioventricular valve, a large VSD immediately below the plane of the atrioventricular valves, and a common atrioventricular valve (Figs. 11.30 and 11.31). The partial (incomplete) AVSD demonstrates an ostium primum-type ASD, but no VSD. A transitional or intermediate AVSD is similar to a complete AVSD, but the leaflets of the common atrioventricular valve are fixed to the ventricular septum, resulting in a small VSD.

Other rare variants include AVSD with interventricular communication, but no interatrial communication, which is functionally similar to inlet VSD with superior and inferior bridging leaflets fused to the atrial septum, and AVSD with no interventricular or interatrial communication and a common atrioventricular valve with superior and inferior leaflets fused both to the atrial and ventricular septa [30].

The Rastelli classification, which is not as commonly used as the above classification, divides AVSDs into three forms based on the morphology of the superior bridging leaflet, the degree of bridging, and the chordal attachments. Type A: The common bridging leaflet is attached to the inter-

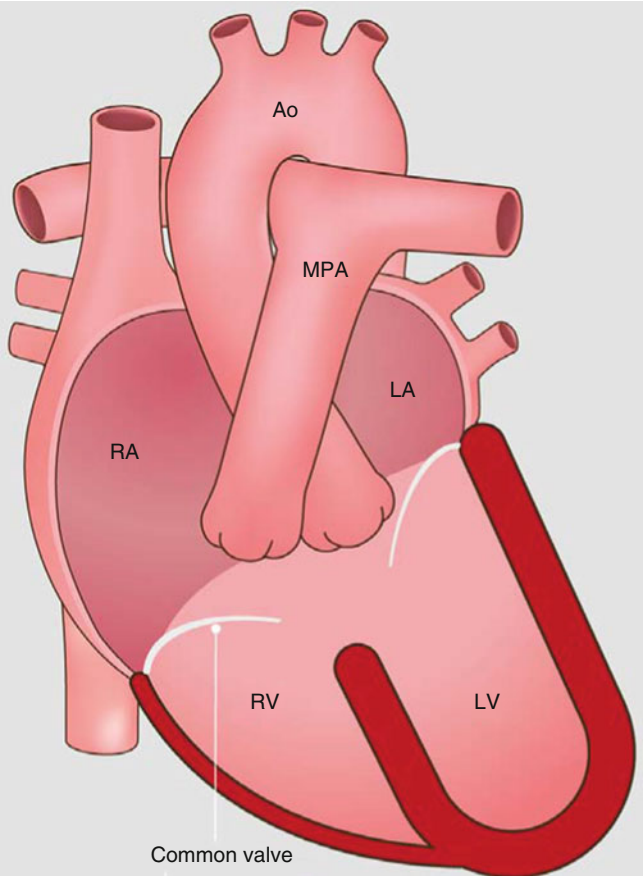


**Fig. 11.30** An artist's rendition of the anatomy of the complete form of an atrioventricular canal defect. Note the common atrioventricular valve straddling the atrial septal and ventricular septal defects. *RA* right atrium, *LA* left atrium, *RV* right ventricle, *LV* left ventricle, *Ao* Aorta, *MPA* main pulmonary artery

ventricular septum by multiple chordae tendineae, dividing the leaflet into both right and left components which are largely contained in the right and left ventricles, respectively. Type B: The common bridging leaflet is attached over the interventricular septum by an anomalous right ventricular papillary muscle which extends from the right ventricle to the left side of the common valve. Type C: The common bridging leaflet is not attached to the ventricular septum. Instead it is attached to an anterior papillary muscle in the right ventricle and floats freely over the septum.

### 11.3.3 Associations

AVSD may be isolated or associated with other congenital heart diseases, including tetralogy of Fallot and heterotaxy syndrome. In the asplenia syndrome, AVSD is virtually always present, while in polysplenia it occurs in 25 % of patients [30] (Fig. 11.32).

One-third of all children born with AVSDs also have trisomy 21 syndrome. Conversely, about 35–40 % of children

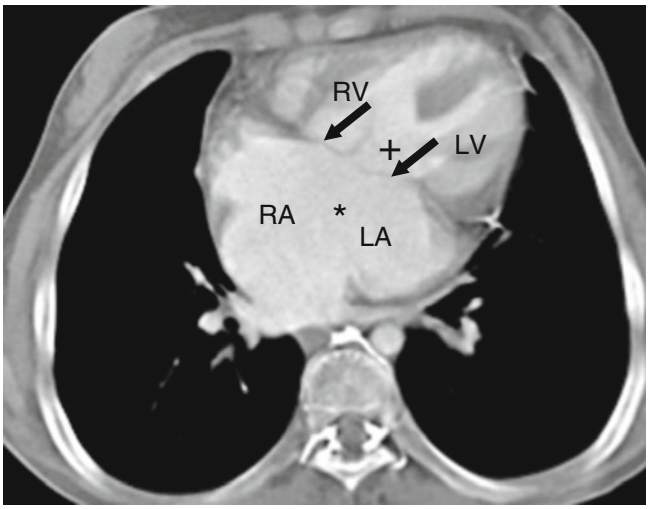


**Fig. 11.31** This computed tomographic (CT) image is from a 17-year-old woman with trisomy 21 syndrome who presented with dyspnea and was ultimately found to have a complete atrioventricular canal defect. This axial CT cut at the level of the inferior atrial septum demonstrates an ostium primum atrial septal defect, demonstrated by free flow between the right atrium (*RA*) and left atrium (*LA*) denoted by the *asterisk* and a large inlet ventricular septal defect demonstrated by free flow between the right ventricle (*RV*) and left ventricle (*LV*) and marked by the *plus sign*. There is also a common atrioventricular valve (*black arrows*)

with trisomy 21 have AVSDs [19, 32]. Complete AVSD most frequently occurs in patients with trisomy 21 syndrome (70–80 %), while partial AVSD is most common in individuals without trisomy 21 syndrome (>90 %) [18, 21].

### 11.3.4 Clinical Aspects

The physiology of the lesion depends on the degree of ventricular unbalance, the size of the atrioventricular septal defects, the atrioventricular valve competence, the degree of right-sided or left-sided outflow obstruction, and the pulmonary vascular resistance.

In most cases there is no ventricular dominance (balanced AVSD) and the common atrioventricular valve is shared to a similar extent by the left and right ventricles. The physiology is generally that of pulmonary overcirculation. Unbalanced AVSD occurs when the atrioventricular valve is dominantly committed to one ventricle. If more than 75 % of the common valve is committed to one ventricle, the atrioventricular connection becomes, by definition, a double inlet ventricle [30]. Both left and right ventricular dominance may occur. The dominance of one ventricle is associated with significant hypoplasia of the second one (single-ventricle physiology).

Patients with complete AVSD present in infancy with congestive heart failure and frequent pulmonary infections and most of them undergo early surgical repair. Half of

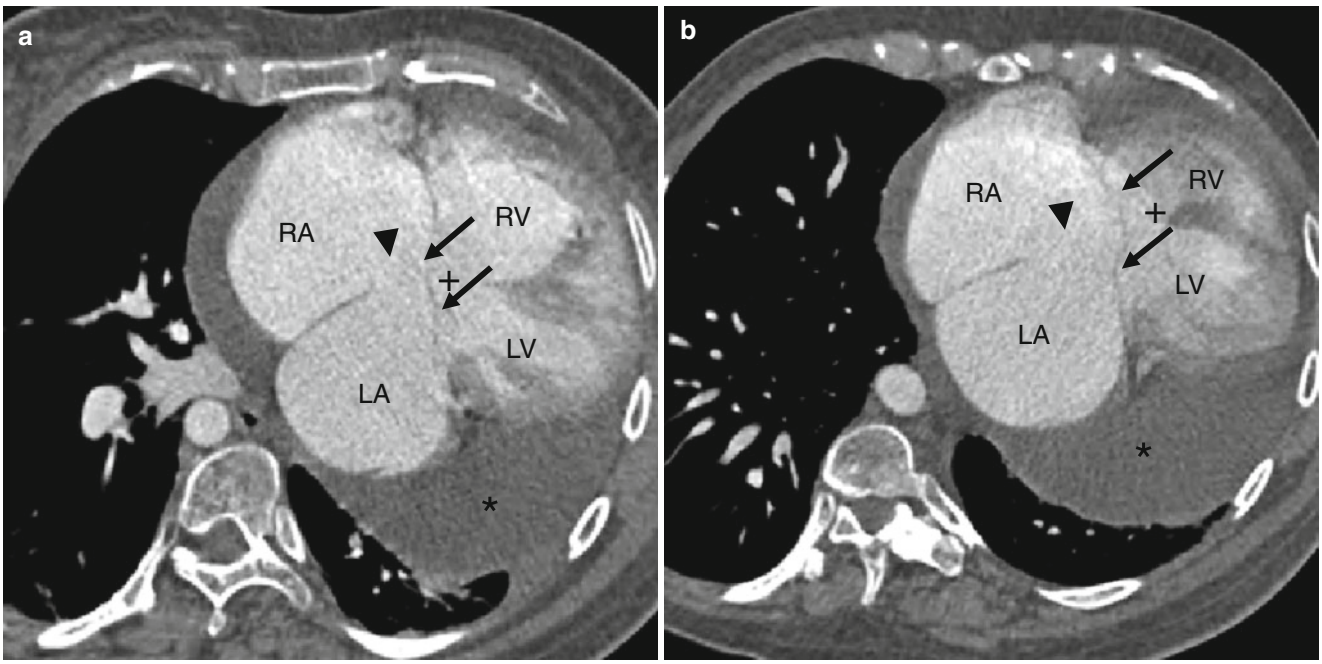


**Fig. 11.32** A case of a 31-year-old woman with asplenia, heterotaxy syndrome, and congenital heart disease who has not undergone any cardiac intervention. She demonstrates a complete atrioventricular canal defect. Panels (**a**) and (**b**) are two axial scans through the level of the inferior atrial septum showing communication between the right atrium (*RA*) and left atrium (*LA*) (an ostium primum septal defect, *black arrowhead*), a large connection between the right ventricle (*RV*) and left ventricle (*LV*) (ventricular septal defect, *plus sign*), and a single atrioventricular valve (*black arrows*). The combination of a primum ASD and an inlet VSD is consistent with a complete atrioventricular septal defect (canal defect). A large pericardial effusion is also present (*black asterisk*)

infants with untreated complete AVSD die in the first year of life from heart failure or pneumonia, and those who survive develop irreversible pulmonary hypertension [33]. Patients with partial AVSD are usually asymptomatic in infancy and early childhood and unrepaired partial AVSD may be seen in adults. Most adults become symptomatic before age 40 years. Treatment is surgical and involves closure of the atrial and ventricular septal defects and creation of a competent AV valve as best as possible.

### 11.3.5 Cardiac Computed Tomography (CT) in the Evaluation of AV Canal Defects

#### 11.3.5.1 Unrepaired AVSD

CT may provide useful information, especially when echocardiography is inconclusive. CT allows noninvasive assessment of cardiac chamber size and function (when retrospective gating is used) as well as a depiction of the atrial and ventricular septal defects, the common atrioventricular valve, and the presence of left and/or right ventricular outflow tract narrowing [8–12].

#### 11.3.5.2 Repaired AVSD

After repair, CT is performed for evaluation of residual shunting, which in patients with endocardial pacing has been shown to increase the risk of paradoxic emboli [11, 32]. It also can be used to assess atrioventricular valve regurgitation/stenosis and outflow tract obstruction [33, 34].

Tables 11.4 and 11.5 illustrate the important points regarding CT evaluation of patients with atrioventricular septal defects.

**Table 11.4** Important preoperative CT evaluation points with uncorrected atrioventricular septal defects

| |
|---|
| Morphology, size, type, and location of atrioventricular septal defect |
| Morphology and function of the common atrioventricular valve |
| Morphology, size, geometry, and systolic function of both ventricles |
| Morphology, extent, and location of left and/or right ventricular outflow tract obstruction |
| Morphology and size of atria |
| Presence of coexisting anomalies |

**Table 11.5** Important postoperative CT evaluation points with corrected atrioventricular septal defects

| |
|---|
| Abnormal residual intracardiac connections |
| Morphology and function of the common atrioventricular valve |
| Morphology, size, dilatation, and function of left and right ventricles |
| Morphology and size of left and/or right ventricular outflow tracts |

## References


1. Kaplan S. Congenital heart disease in adolescents and adults. natural and postoperative history across age groups. Cardiol Clin. 1993;11:543–56.
2. Webb G, Gatzoulis MA. Atrial septal defects in the adult: recent progress and overview. Circulation. 2006;114:1645–53. doi:10.1161/CIRCULATIONAHA.105.592055.
3. Rajiah P, Renapurkar R, Kanne J. Diagnosis of ostium primum defect at multidetector CT in an adult. J Thorac Imaging. 2009;24:234–6. doi:10.1097/RTI.0b013e3181a6d0d2.
4. Attenhofer Jost CH, Connolly HM, Danielson GK, Dearani JA, Warnes CA, Jamil Tajik A. Clinical features and surgical outcome in 25 patients with fenestrations of the coronary sinus. Cardiol Young. 2007;17:592–600. doi: 10.1017/S1047951107001412.
5. Hirai S, Hamanaka Y, Mitsui N, Isaka M, Mizukami T. Surgical repair of a common atrium in an adult. Ann Thorac Cardiovasc Surg. 2003;9:130–3.
6. Hart SA, Krasuski RA. Incidence of asymptomatic patent foramen ovale according to age. Ann Intern Med. 2009;150:431–2.
7. Corby JR. Patent foramen ovale, atrial septal aneurysm, and recurrent stroke. N Engl J Med. 2002;346:1331–13332.
8. Kerut EK, Norfleet WT, Plotnick GD, Giles TD. Patent foramen ovale: a review of associated conditions and the impact of physiological size. J Am Coll Cardiol. 2001;38:613–23.
9. Hughes Jr D, Siegel MJ. Computed tomography of adult congenital heart disease. Radiol Clin North Am. 2010;48:817–35. doi:10.1016/j.rcl.2010.04.005.
10. Leschka S, Oechslin E, Husmann L, Desbiolles L, Marincek B, Genoni M, et al. Pre- and postoperative evaluation of congenital heart disease in children and adults with 64-section CT. Radiographics. 2007;27:829–46. doi:10.1148/rg.273065713.
11. Siegel MJ. CT evaluation of congenital heart disease in adults. Appl Radiol. 2005;34:61–8.
12. Wiant A, Nyberg E, Gilkeson RC. CT evaluation of congenital heart disease in adults. AJR Am J Roentgenol. 2009;193:388–96. doi:10.2214/AJR.08.2192.
13. Funabashi N, Maeda F, Nakamura K, Suzuki K, Mita Y, Matsuo K, et al. Channel-like appearance of a patent foramen ovale with left to right shunt demonstrated by 64-slice computed tomography. Int J Cardiol. 2007;119:119–21. doi:10.1016/j.ijcard.2006.07.095.
14. Kim YJ, Hur J, Shim CY, Lee HJ, Ha JW, Choe KO, et al. Patent foramen ovale: diagnosis with multidetector CT–comparison with transesophageal echocardiography. Radiology. 2009;250:61–7. doi:10.1148/radiol.2501080559.
15. Ko SF, Liang CD, Yip HK, Huang CC, Ng SH, Huang CF, et al. Amplatzer septal occluder closure of atrial septal defect: evaluation of transthoracic echocardiography, cardiac CT, and transesophageal echocardiography. AJR Am J Roentgenol. 2009;193:1522–9. doi:10.2214/AJR.09.2854.
16. Hoffman JI, Kaplan S. The incidence of congenital heart disease. J Am Coll Cardiol. 2002;39:1890–900.
17. Jacobs JP, Burke RP, Quintessenza JA, Mavroudis C. Congenital heart surgery nomenclature and database project: ventricular septal defect. Ann Thorac Surg. 2000;69:S25–35.
18. Warnes CA, Williams RG, Bashore TM, Child JS, Connolly HM, Dearani JA, et al. ACC/AHA 2008 guidelines for the management of adults with congenital heart disease: a report of the American College of Cardiology/American Heart Association Task Force on Practice Guidelines (Writing Committee to Develop Guidelines on the Management of Adults with Congenital Heart Disease). Circulation. 2008;118:e714–833. doi:10.1161/CIRCULATIONAHA.108.190690.
19. Minette MS, Sahn DJ. Congenital heart disease for the adult cardiologist. Circulation. 2006;114:2190–7.
20. Brickner ME, Hillis LD, Lange RA. Congenital heart disease in adults. first of two parts. N Engl J Med. 2000;342:256–63. doi:10.1056/NEJM200001273420407.
21. Fuster V, Brandenburg RO, McGoon DC, Giuliani ER. Clinical approach and management of congenital heart disease in the adolescent and adult. Cardiovasc Clin. 1980;10:161–97.
22. Danchin N, Duval X, Leport C. Prophylaxis of infective endocarditis: French recommendations 2002. Heart. 2005;91:715–8. doi:10.1136/hrt.2003.033183.
23. Chiu SN, Wang JK, Lin MT, Chen CA, Chen HC, Chang CI, et al. Progression of aortic regurgitation after surgical repair of outlet-type ventricular septal defects. Am Heart J. 2007;153:336–42. doi:10.1016/j.ahj.2006.10.025.
24. Baumgartner H, Bonhoeffer P, De Groot NM, de Haan F, Deanfield JE, Galie N, et al. ESC guidelines for the management of grown-up congenital heart disease (new version 2010). Eur Heart J. 2010;31:2915–57. doi:10.1093/eurheartj/ehq249.
25. Hayabuchi Y, Mori K, Kitagawa T, Sakata M, Kagami S. Polytetrafluoroethylene graft calcification in patients with surgically repaired congenital heart disease: evaluation using multidetector-row computed tomography. Am Heart J. 2007;153:806.e1–8. doi:10.1016/j.ahj.2007.01.035.
26. Shinebourne EAHS, Ho S. Atrioventricular septal defect: complete and partial (ostium primum atrial septal defect). In: Gatzoulis MA, Webb GD, Daubeney PEF, editors. Diagnosis and management of adult congenital heart disease. 1st ed. Edinburgh: Churchill Livingstone; 2003. p. 179.
27. Samaánek M (1991) Prevalence at birth, "natural" risk and survival with atrioventricular septal defect. 1.
28. Jacobs JP, Burke RP, Quintessenza JA, Mavroudis C. Congenital heart surgery nomenclature and database project: atrioventricular canal defect. Ann Thorac Surg. 2000;69:S36–43.
29. Shuhaiber JH, Ho SY, Rigby M, Sethia B. Current options and outcomes for the management of atrioventricular septal defect. Eur J Cardiothorac Surg. 2009;35:891–900. doi:10.1016/j.ejcts.2009.01.009.
30. Loffredo CA, Hirata J, Wilson PD, Ferencz C, Lurie IW. Atrioventricular septal defects: possible etiologic differences between complete and partial defects. Teratology. 2001;63:87–93. doi:10.1002/1096-9926(200102)63:2<87::AID-TERA1014>3.0.CO;2-5.
31. Ebels T, Ho SY, Anderson RH, Meijboom EJ, Eijgelaar A. The surgical anatomy of the left ventricular outflow tract in atrioventricular septal defect. Ann Thorac Surg. 1986;41:483–8.
32. Santoro G, Marino B, Di Carlo D, Formigari R, Santoro G, Marcelletti C, et al. Patient selection for repair of complete atrioventricular canal guided by echocardiography. Eur J Cardiothorac Surg. 1996;10:439–42.
33. Birim O, van Gameren M, de Jong PL, Witsenburg M, van Osch-Gevers L, Bogers AJ. Outcome after reoperation for atrioventricular septal defect repair. Interact Cardiovasc Thorac Surg. 2009;9:83–7. doi:10.1510/icvts.2008.195180.
34. Stulak JM, Burkhart HM, Dearani JA, Cetta F, Barnes RD, Connolly HM, et al. Reoperations after repair of partial atrioventricular septal defect: a 45-year single-center experience. Ann Thorac Surg. 2010;89:1352–9.
35. Dragicevic N, Schmidlin E, Hazelton TR, Nallamshetty L. Gerbode ventricular septal defect diagnosed using cardiac CTA imaging. Radiology Case Rep. 2011;6:530. doi:10.2484/rcr.v6i3.530.

# Atrioventricular Valve Abnormalities

# 12

## 12.1 Ebstein Anomaly

Ebstein anomaly is a defect of the right ventricle that results in variable degrees of failure of delamination of the valve leaflets, leading to tricuspid valve regurgitation and right ventricular dysfunction. The classic pathology is apical (downward) displacement of the tricuspid valve leaflets (most frequently septal followed by posterior and anterior leaflets) with abnormal adherence of the leaflets to the underlying myocardium.

The major morphologic features are apical displacement of the septal leaflet ≥8 mm/m$^2$, dilatation of the "atrialized" portion of the right ventricle with variable degrees of thinning of the free wall of the right ventricle [1]. Dilatation of the right atrioventricular junction (true tricuspid annulus) is also seen [1]. See Fig. 12.1. Incompetence of the deformed tricuspid valve and the functional impairment of the right ventricle result in an impediment to forward flow of blood through the right side of the heart. Typically, there are other anatomic abnormalities including a large, redundant anterior leaflet with fenestration and varying degrees of tethering to the right ventricular wall. In most cases there is a patent foramen ovale or secundum atrial septal defect, resulting in a right-to-left shunt due to elevated right-sided pressures.

According to Carpentier's classification, Ebstein anomaly can be categorized as follows: type A: adequate RV volume; type B: large atrialized segment of the RV and mobile anterior leaflet; type C: restricted movement of anterior leaflet which may cause infundibular obstruction; type D: near-complete atrialization of the RV (Uhl's syndrome) [2].

### 12.1.1 Clinical Features

The downward displacement of the septal tricuspid valve leaflet is associated with discontinuity of the central fibrous body and septal atrioventricular ring, resulting in accessory atrioventricular connections and ventricular pre-excitation making the patient at risk of sudden death. Atrial arrhythmias are also common because of the enlargement of the atria.

Ebstein anomaly usually presents in neonates or infants with findings of congestive heart failure or profound cyanosis. Occasionally, however, the diagnosis is not made until late in life and presentations as late as the eighth decade have been reported [3]. Operative management of adult patients with Ebstein anomaly includes tricuspid valve repair or

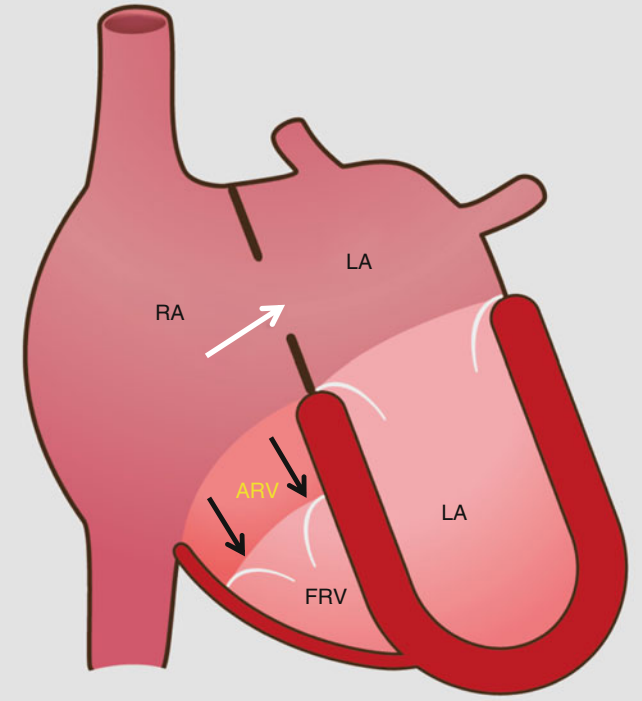


**Fig. 12.1** Schematic drawing of Ebstein anomaly. The tricuspid valve is displaced toward the apex of the right ventricle with subsequent "atrialization" of a portion of the morphologic right ventricle, which is contiguous with the enlarged right atrium. The functional right ventricle is small in size. Note the secundum atrial septal defect (*white arrow*) which is commonly associated with Ebstein anomaly. The *black arrows* point to the apically displaced tricuspid valve. *RA* right atrium, *ARV* atrialized right ventricle, *FRV* functional right ventricle, *LA* left atrium, *LV* left ventricle

W. Mazur et al., *CT Atlas of Adult Congenital Heart Disease*,
DOI 10.1007/978-1-4471-5088-6_12, © Springer-Verlag London 2013

replacement, closure of the atrial septal defect (if present), as well as bidirectional cavopulmonary shunt, which is useful in patients with severe right ventricular dilatation and/or dysfunction. Late complications in palliated as well as unoperated patients include right and left ventricular failure, atrial and ventricular arrhythmias, and sudden cardiac death.

### 12.1.2 Cardiac Computed Tomography (CT) in the Evaluation of Ebstein Anomaly

Ebstein anomaly is easily detected by CT [4–6]. Imaging findings include a large right atrium proper, a dilated atrialized right ventricle, a small true right ventricle along with apical displacement of the septal leaflet of the tricuspid valve, and a "sail-like" anterior tricuspid valve leaflet deformity (Fig. 12.2) [4–6]. The atrialized ventricular wall may be thinner than the distal functional right ventricle, and the heart may rotate posteriorly into the left hemithorax with bulging of the ventricles posteriorly. An atrial septal defect is an associated finding (Fig. 12.3). Cine CT can offer functional information in addition to anatomy when retrospective gating is employed.

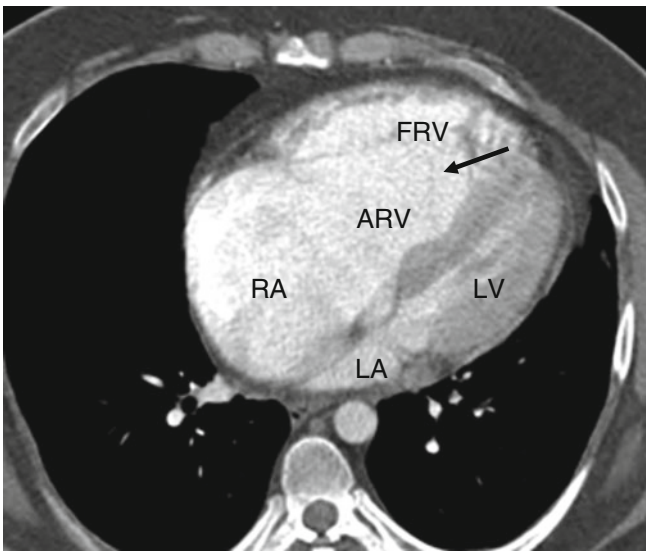


**Fig. 12.2** Ebstein anomaly. An axial computed tomographic scan showing a dilated right atrium (*RA*), atrialized right ventricle (*ARV*), and a small functional right ventricle (*FRV*). Note the apical displacement of the septal tricuspid leaflet (*black arrow*). *LA* left atrium, *LV* left ventricle

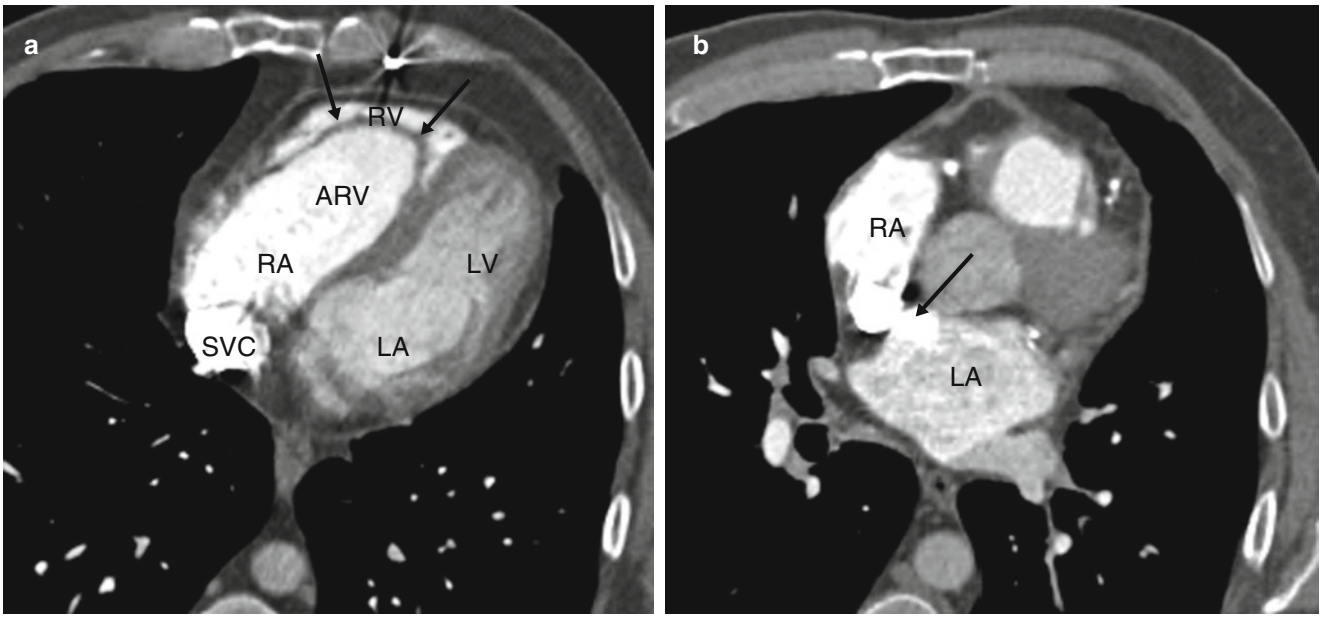


**Fig. 12.3** Ebstein anomaly. Panel (**a**) is an axial tomogram showing marked apical displacement of the septal tricuspid leaflet (*arrows*) resulting in atrialization of the right ventricle (*ARV*). Panel (**b**) is an axial cut at a more superior level demonstrating an atrial septal defect with contrast-enhanced blood (*arrow*) flowing into the left atrium (*LA*) from the right atrium (*RA*). *SVC* superior vena cava, *RV* right ventricle proper

## 12.2 Tricuspid Atresia

Tricuspid atresia is the third most common form of cyanotic congenital heart disease, with a prevalence of 0.3–3.7 % [7]. Tricuspid atresia is characterized by the absence of a tricuspid valve. There is no direct connection between the right atrium and right ventricle, resulting in a small or absent right ventricle that cannot adequately pump blood to the lungs (Fig. 12.4). Depending on the relationship with the great vessels, there are three types of tricuspid atresia. In type I, the great arteries are related normally. With type II, the great arteries are D-transposed, and in type III, the great arteries are L-transposed. These types are further subclassified according to the presence or absence of ventricular septal defects and pulmonary valve pathology [8, 9].

Associated defects coexist in 15–20 % of patients, most frequently transposition of the great vessels and persistent left-sided superior vena cava [7]. Atrial septal defect is obligatory in those patients. Extracardiac associations may include a right-sided aortic arch and an absent spleen.

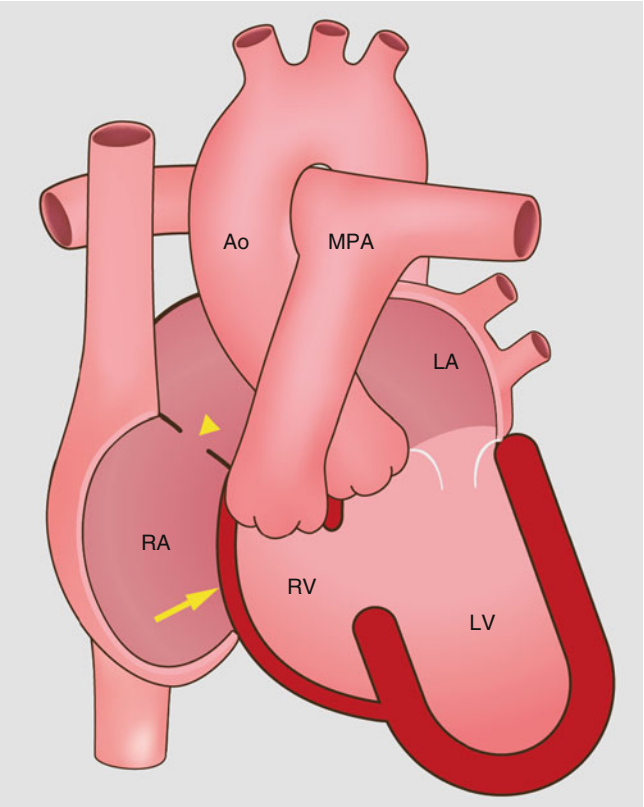


**Fig. 12.4** Schematic drawings of tricuspid atresia. The tricuspid valve is absent which prevents antegrade flow into the right ventricle. The right ventricle is hypoplastic. An atrial septal defect supplies blood flow to the left heart. *yellow arrow* absent tricuspid valve, *yellow arrowhead* atrial septal defect, *RA* right atrium, *RV* right ventricle, *LA* left atrium, *LV* left ventricle, *PA* pulmonary artery, *Ao* aorta

In patients with tricuspid atresia, venous blood returning to the right atrium can exit only through an interatrial communication. Because of the obligatory right-to-left shunt at the level of the atria, saturation of the left atrial blood is diminished. Additionally, intracardiac blood flow depends on coexisting pulmonary artery pathology. With coexistent pulmonary artery or pulmonary valve stenosis, pulmonary blood flow is reduced, resulting in worsening cyanosis. Pulmonary obstruction occurs most often in patients with tricuspid atresia and normal great artery anatomy. In the absence of pulmonary atresia or pulmonary stenosis, the volume of blood flowing to the lungs may be normal thus resulting in decreased cyanosis. Patients with D-transposed great arteries and tricuspid atresia typically have unobstructed pulmonary blood flow.

Tricuspid atresia patients ultimately develop left ventricular systolic dysfunction due to left ventricular volume overload related to the fact that venous blood must return to the left ventricle as well as to the presence of chronic hypoxemia. Left ventricular dysfunction may then lead to mitral annulus dilatation and mitral regurgitation, which further increases left ventricular volume overload.

### 12.2.1 Clinical Features

Tricuspid atresia is usually detected in infancy because of cyanosis, congestive heart failure, and growth retardation. Most patients with tricuspid atresia require some form of surgical treatment during the first year of life. Thus, most adults with tricuspid atresia have undergone surgical palliation. Since the primary lesion is not reparable, the basic features are still present in the palliated adult as are the findings of the palliative surgical procedure.

In neonates and infants, palliative or definitive surgery may be undertaken to connect the systemic circulation to the pulmonary circulation. Palliative surgery encompasses either a Blalock–Taussig shunt or a Glenn shunt (end-to-end anastomosis of the right pulmonary artery to the superior vena cava). Definitive surgery entails performing the total cavopulmonary Fontan procedure. The Fontan operation excludes the right ventricle through the formation of a right atrial-to- pulmonary artery connection or an extracardiac cavopulmonary anastomosis using a synthetic graft. Long-term complications of these palliative surgeries include right heart failure, mural thrombus, and dilatation of the cardiac/systemic veins that act as collateral vessels.

### 12.2.2 Cardiac Computed Tomography (CT) in the Evaluation of Tricuspic Atresia

CT has proven to be an excellent imaging modality to determine the anatomic features of tricuspid atresia [5, 6, 9, 10]. The classic finding is fatty tissue between the right atrium and the right ventricle in the expected location of the tricuspid valve and a small right ventricle (Fig. 12.5). The left ventricle is enlarged. Other features include atrial and/or ventricular septal defects (Fig. 12.6), transposition of the great arteries, and dilated inferior vena cava and hepatic veins due to passive congestion, mural thrombus, and collateral vessel formation. Postoperative CT can provide information on the patency of any shunts and on the size and morphology of the pulmonary arteries [11].

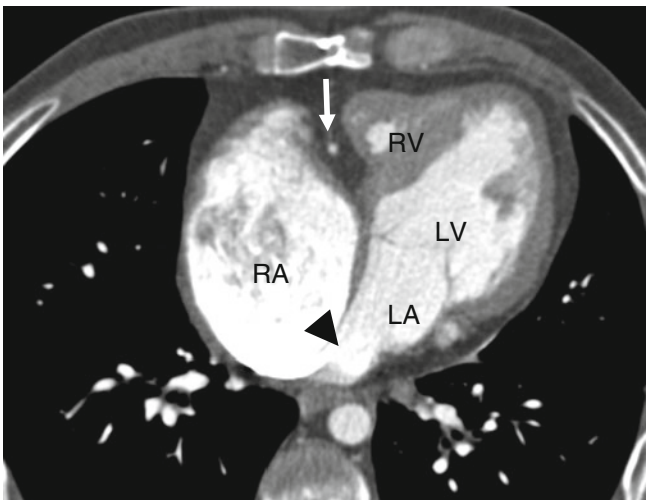


**Fig. 12.5** Tricuspid atresia. An axial computed tomogram showing fat in the atrioventricular groove (*arrow*). The right atrium (*RA*) is enlarged and the right ventricle (*RV*) is hypoplastic. The *black arrowhead* points out the obligatory atrial septal defect. *LV* left ventricle, *LA* left atrium

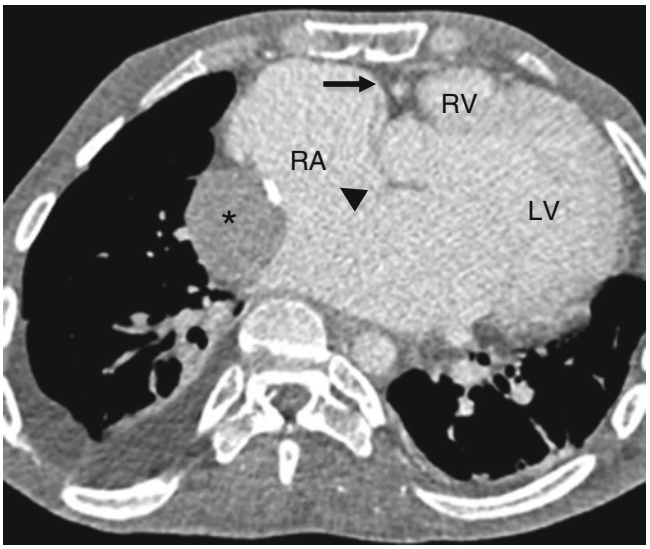


**Fig. 12.6** Tricuspid atresia with an atrial septal defect. This axial computed tomogram shows a fatty separation of the right atrium from the right ventricle (*arrow*), a hypoplastic right ventricle (*RV*), and enlarged right atrium (*RA*). A large atrial septal defect is noted (*black arrowhead*). *Asterisk*: extracardiac Fontan conduit. *LV* left ventricle

## 12.3 Congenital Mitral Inflow and Mitral Valve Abnormalities

### 12.3.1 Lesions Associated with Mitral Valve Obstruction

#### 12.3.1.1 Cor Triatriatum Sinister

Cor triatriatum accounts for 0.1–0.4 % of all congenital cardiac anomalies [12]. It is a result of embryologic failure of the common pulmonary vein to become incorporated into the left atrium during the fifth week of embryologic development [13]. As a result, the left atrium is divided by a fibromuscular membrane into two chambers. The superior chamber receives blood from the pulmonary veins, and the inferior chamber is connected to the left atrial appendage and mitral valve. The two chambers communicate with each other through openings in the membrane (Figs. 12.7 and 12.8). Associated anomalies occur in 50–80 % of cases and include a patent foramen ovale, patent ductus arteriosus, atrial and ventricular septal defects, and persistent left-sided superior vena cava [12].

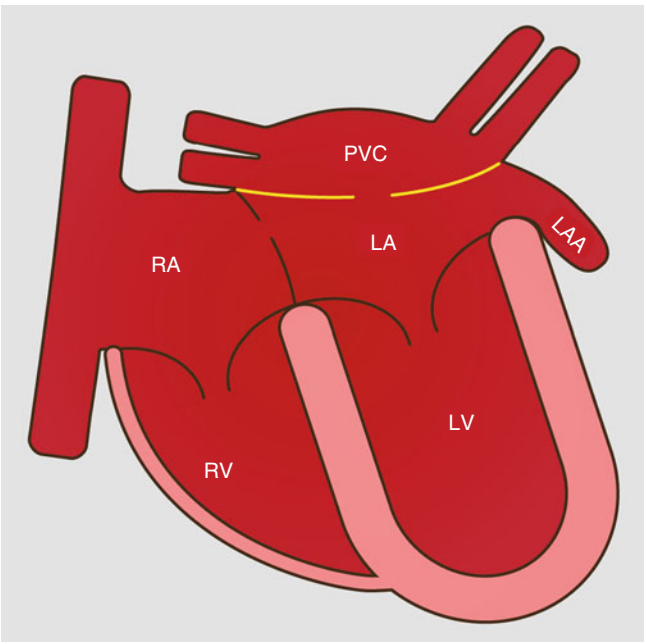


**Fig. 12.7** An artist's illustration of cor triatriatum. The interatrial membrane (*yellow*) separates the left atrium (*LA*) into a proximal portion containing the pulmonary venous confluence (*PVC*) and a distal portion with a left atrial appendage (*LAA*). *RA* right atrium, *RV* right ventricle, *LV* left ventricle

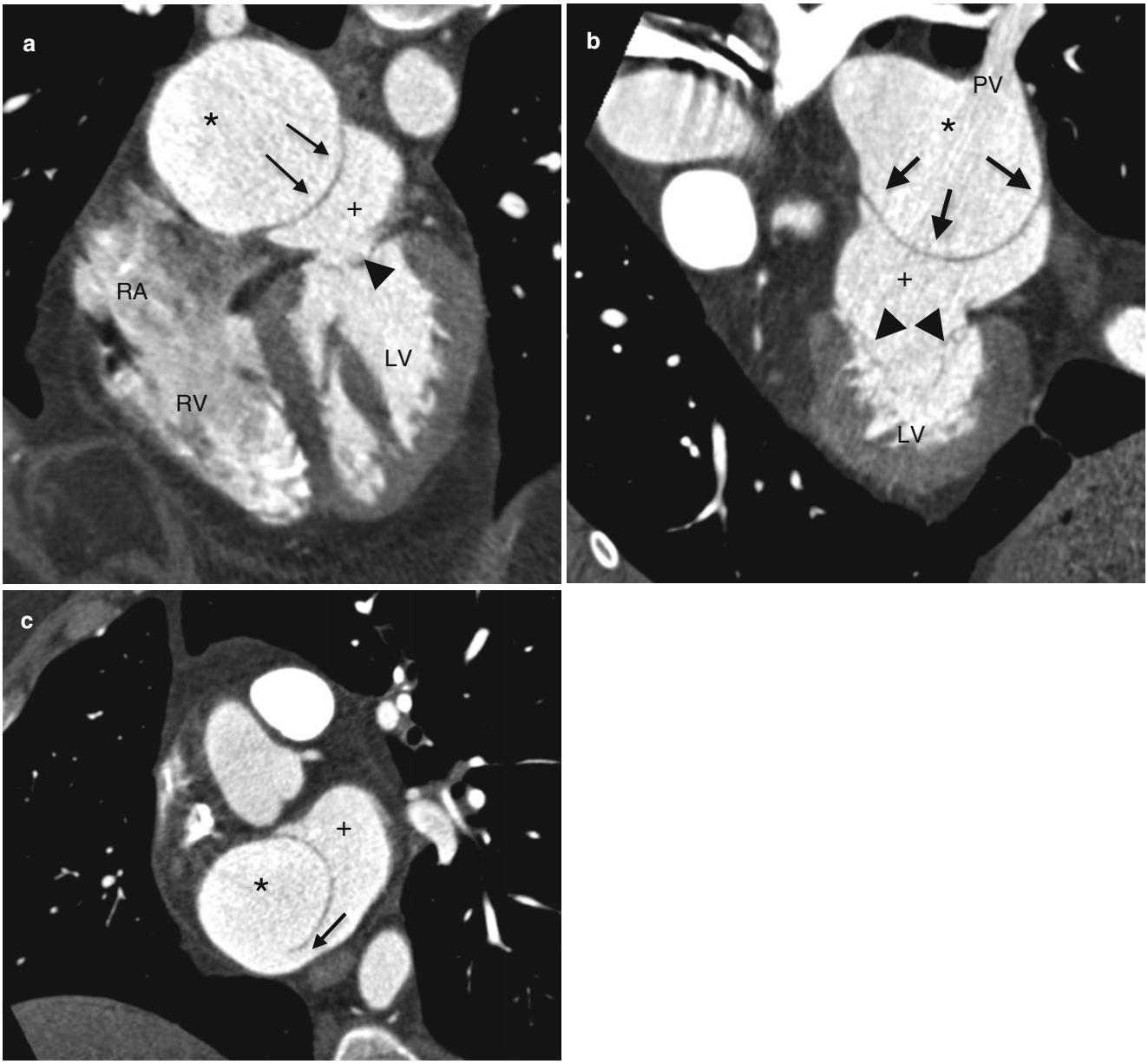


**Fig. 12.8** Cor triatriatum in a patient with shortness of breath treated for suspected exertional asthma. Panel (**a**) is a four-chamber computed tomographic (CT) view demonstrating the membrane separating the upper left atrial section (*asterisk*) which is dilated from the lower section (*plus sign*). The *black arrowhead* points to the mitral valve. Panel (**b**) is a two-chamber CT again showing the membrane (*black arrows*) separating the left atrium into two chambers, a proximal chamber receiving the pulmonary venous return (*asterisk*) and an inferior chamber connecting to the left atrial appendage (*plus sign*). Panel (**c**) is an oblique view showing the two atrial chambers (upper, *asterisk*, and lower, *plus sign*) communicating via a narrow orifice (*arrow*). *RA* right atrium, *RV* right ventricle, *LV* left ventricle

The size of the defect and the gradient across it determine the nature and severity of symptoms. The lesion is usually asymptomatic, but patients can present with findings of pulmonary hypertension, atrial fibrillation, and mitral regurgitation. Symptoms tend to mimic those of mitral stenosis. Surgical excision of the intra-atrial membrane is the treatment of choice for symptomatic patients. Percutaneous balloon dilatation is generally not effective in this condition.

#### 12.3.1.2 Supravalvular Mitral Ring

Supravalvular mitral ring is characterized by an abnormal rim of connective tissue on the atrial surface of the mitral valve. It is often circumferential and may at times adhere to the mitral valve leaflets causing a decrease in leaflet excursion and inflow obstruction. An isolated supravalvular mitral ring is rare. In the vast majority of cases, it is accompanied by other left-sided obstructive lesions. It often coexists with the Shone's complex (supravalvular mitral ring,

parachute mitral valve, subaortic stenosis, and coarctation of the aorta).

#### 12.3.1.3 Parachute Mitral Valve

Often part of the Shone's complex, the classic form of congenital parachute mitral valve, the chordae arise from a single centrally located papillary muscle. The leaflets and chordae are abnormally thick and short (Fig. 12.9). The mitral valve can be stenotic or regurgitant.

A variant of the classic form is the asymmetric parachute mitral valve. In contrast to the classic form, the asymmetric form has two separate papillary muscles, one being dominant. The dominant muscle is usually positioned higher in the left ventricle and attaches to the base and lateral wall of the ventricle (Fig. 12.10).

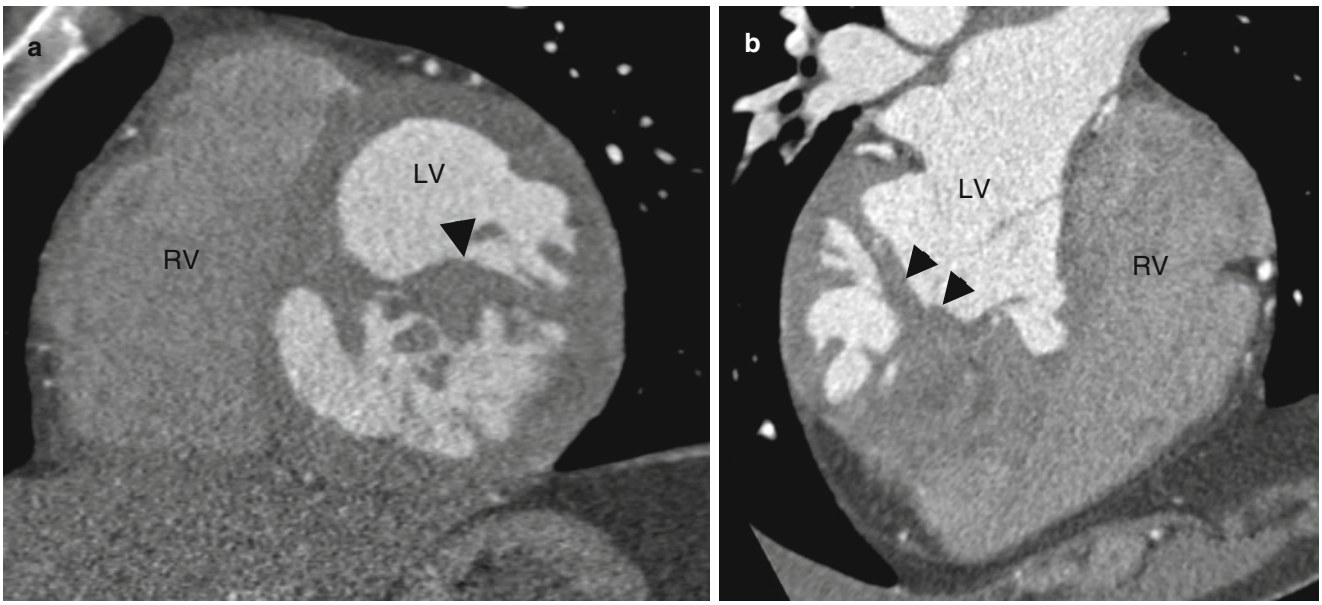


**Fig. 12.9** Parachute mitral valve. Panels (**a**, two-chamber computed tomogram) and (**b**, four-chamber view) show the chordae attached to a single thick papillary muscle or septation (*black arrowheads*) that divides the ventricle into two chambers. There are no distinct, clearly recognizable papillary muscles. *RV* right ventricle, *LV* left ventricle

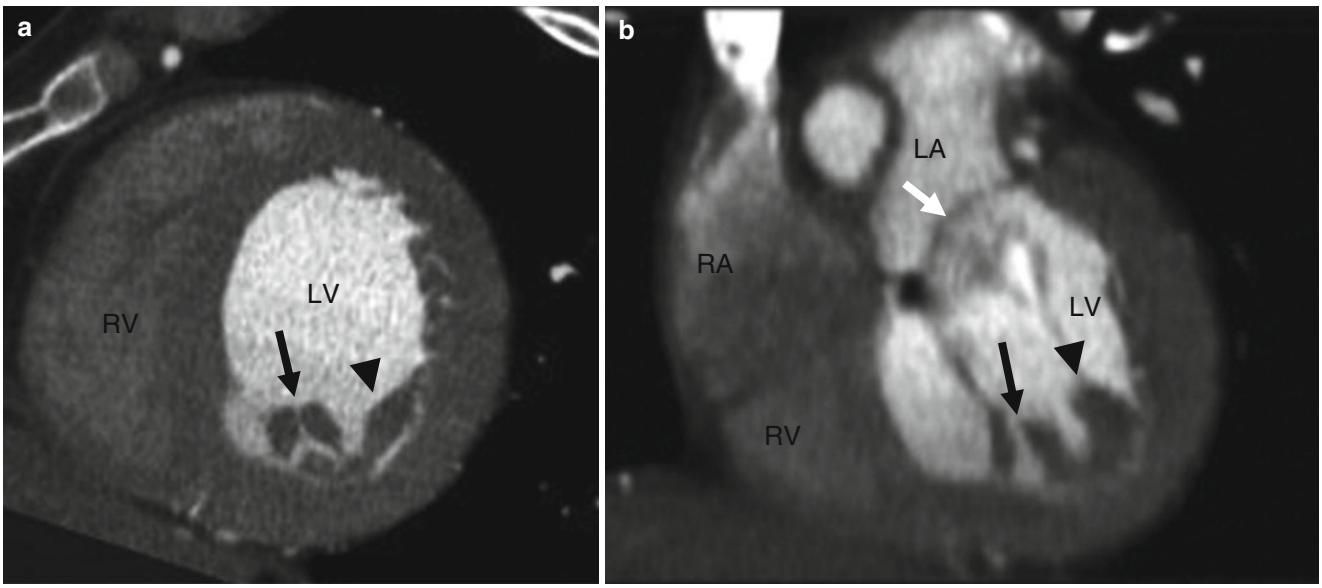


**Fig. 12.10** Asymmetric parachute mitral valve in a patient presenting with severe mitral regurgitation and mild mitral stenosis. Panel (**a**) is an oblique short axis cut and panel (**b**) is an oblique coronal view. Both demonstrate two abnormally close, thick, and short papillary muscles. The posteromedial papillary muscle (*black arrow*) has two heads and the anterolateral papillary muscle (*black arrowhead*) appears to be dominant. Note systolic prolapse of the anterior mitral leaflet (*white arrow* in panel b). *RA* right atrium, *RV* right ventricle, *LA* left atrium, *LV* left ventricle (Reproduced from Ucar et al. [14]. With kind permission from The British Institute of Radiology)

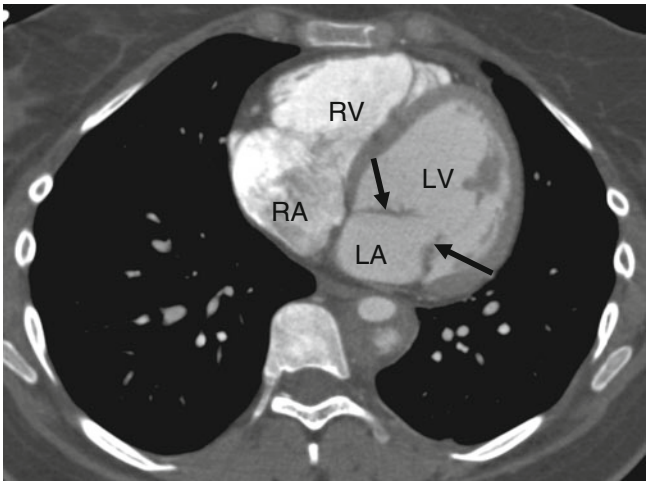


**Fig. 12.11** Congenital mitral stenosis. This computed tomographic angiogram shows thickened mitral valve leaflets (*black arrows*). There are a reduced number of chordae. *RA* right atrium, *RV* right ventricle, *LA* left atrium, *LV* left ventricle

#### 12.3.1.4 Congenital Mitral Valve Stenosis

Congenital mitral valve stenosis is characterized by thickened valve leaflets, thickened and shortened chordae, obliteration of the interchordal spaces, and reduction of the interpapillary distance [15] (Fig. 12.11). Severe stenosis of the mitral valve can result in a hypoplastic left ventricular cavity. Congenital mitral stenosis may be associated with supravalvular mitral ring and parachute mitral valve. Chronic elevation of left atrial pressure can cause atrial dilatation and pulmonary vascular hypertension. Prolonged pulmonary vascular hypertension may also lead to right ventricular dilatation and failure and tricuspid regurgitation.

### 12.3.2 Lesions Associated with Mitral Valve Insufficiency

#### 12.3.2.1 Double-Orifice Mitral Valve

This very rare anomaly characterized by an accessory bridge of leaflet tissue that divides the annulus into two orifices, both of which open into the left ventricle. Most commonly, the orifice is oriented toward the anterolateral commissure. When the orifice is oriented toward the posteromedial commissure, a coexisting atrioventricular canal defect is likely. Common associated anomalies are ventricular septal defect, aortic coarctation, and atrioventricular canal defects. Mitral insufficiency is seen in almost 50 % of patients, while mitral stenosis is seen in only 10–15 % of patients [16, 17].

#### 12.3.2.2 Mitral Arcade

Mitral arcade is characterized by the absence of chordae. In place of true chordae, there is a meshwork of tissue which attaches the leaflets to the papillary muscles (Fig. 12.12). Occasionally, the leaflets insert directly into the papillary muscles causing reduced valve mobility which causes malcoaptation and resulting mitral regurgitation. Functional mitral stenosis is uncommon [18, 19].

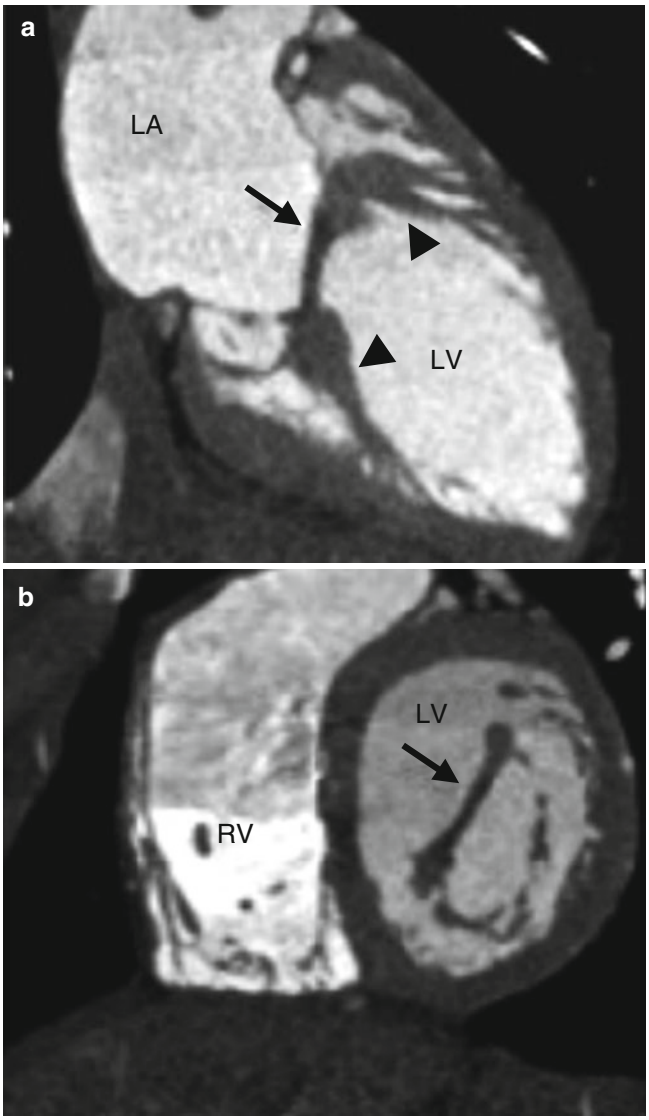


**Fig. 12.12** Congenital mitral valve arcade: Panel (**a**) is a long-axis cut and panel (**b**) a short-axis view demonstrating elongated papillary muscles (*arrowheads* in panel a) connected along the free edge of the anterior mitral leaflet by a bridge of abnormal tissue (*arrows* in panels a and b) resulting in restricted valve mobility (Reproduced from Morris et al. [19]. With kind permission of Elsevier Limited, Kidlington, Oxford, UK)

#### 12.3.2.3 Mitral Valve Prolapse (MVP)

MVP is the most common cause of mitral regurgitation and occurs when the valve leaflets "billow" backward into the atrium during systole. It is defined as systolic displacement of the mitral leaflets more than 2 mm beyond the annular plane into the left atrium. Pathologically, congenital prolapse

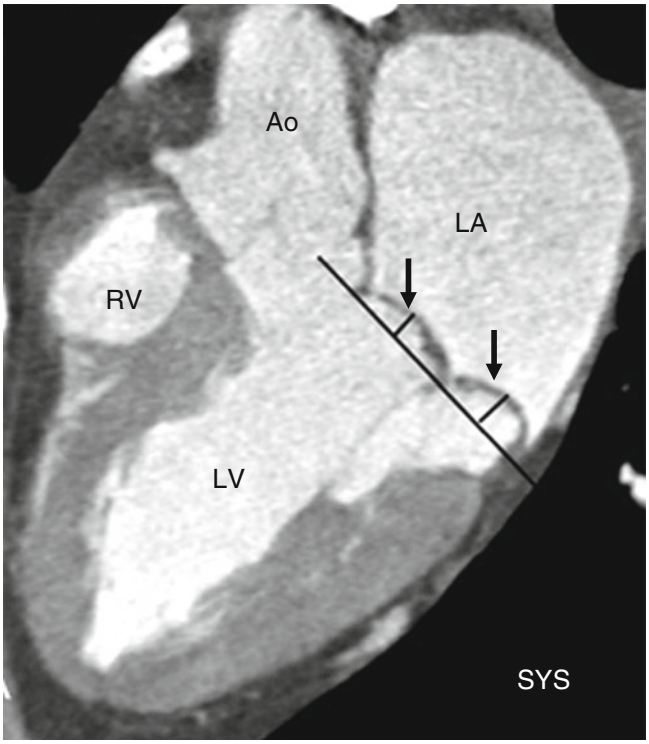


**Fig. 12.13** Mitral valve prolapse. This three-chamber computed tomogram demonstrates billowing (bowing of leaflet body) of both mitral valve leaflets (*arrows*) during systole. The leaflets are also thickened. The extent of billowing of the leaflet bodies below the mitral annulus plane is shown by the black lines. *RA* right atrium, *RV* right ventricle, *LA* left atrium, *LV* left ventricle (Reproduced from Feuchtner et al. [20]. With kind permission of Radiological Society of North America, Oak Brook IL)

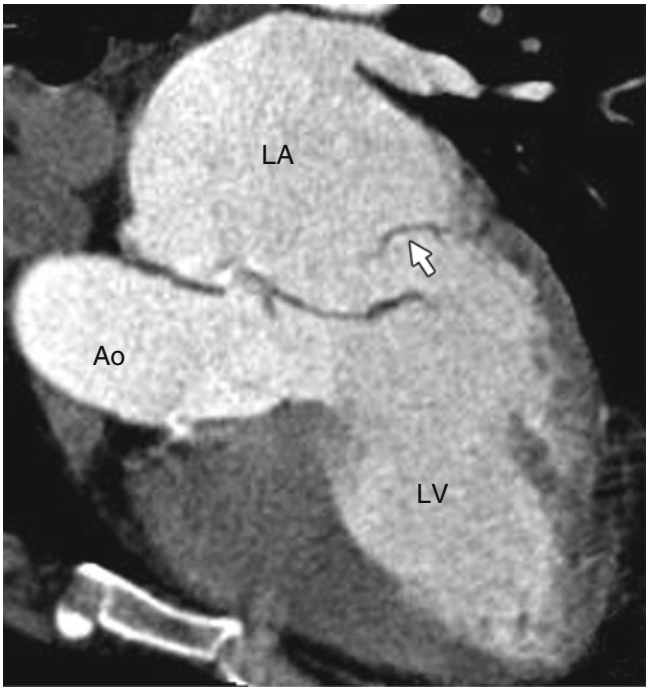


**Fig. 12.14** A computed tomographic example of a flail posterior leaflet (free-leaflet-edge prolapse, *arrow*). *LA* left atrium, *LV* left ventricle, *Ao* aorta (Reproduced from Feuchtner et al. [20]. With kind permission of Radiological Society of North America, Oak Brook IL)

is characterized by replacement of the dense fibrous collagen layer of the mitral valve apparatus by loose myxomatous tissue. This results in mitral annular dilatation, enlargement and thickening of the mitral valve leaflets, and chordal elongation. It can be subclassified into two types: billowing (bowing of the leaflet body) and flail leaflet (free-leaflet-edge prolapse). The middle scallop of the posterior leaflet (P2 segment) is the most often affected leaflet (Figs. 12.13 and 12.14).

#### 12.3.2.4 Mitral Valve Cleft

Congenital mitral valve cleft, also called isolated mitral cleft, is a rare cause of congenital mitral insufficiency. It is defined as a slit-like hole or defect in one of the leaflets. The anterior leaflet is involved more often than the posterior leaflet, and the affected leaflet is usually thickened and distorted (Fig. 12.15) [21, 22]. The extent of mitral regurgitation is dependent on the degree of extension of the cleft into the mitral annulus and the amount of coaptation between the leaflets. Although isolated clefts occur, more often the cleft is associated with other congenital heart defects, especially endocardial cushion defects. Isolated mitral cleft is directed toward the left ventricular outflow tract, whereas the cleft in the endocardial cushion defect is

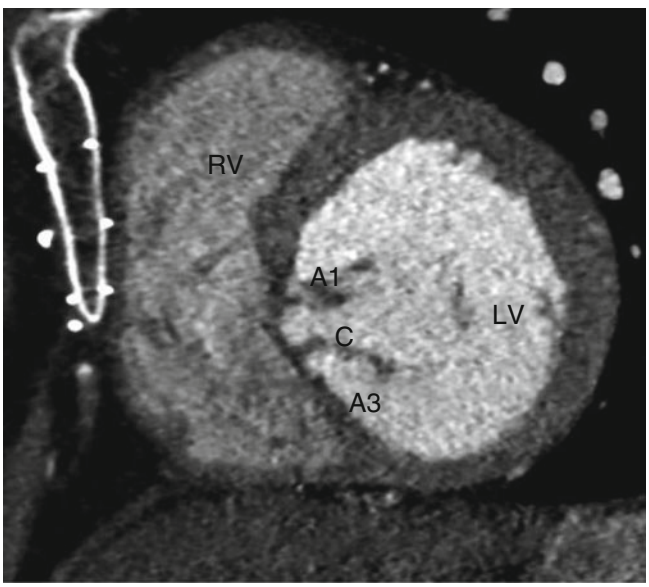


**Fig. 12.15** Cleft mitral valve. In this short-axis computed tomographic angiogram, the anterior leaflet contains a cleft such that the A2 segment is absent and the cleft is present in its place. *A1* A1 segment, *C* cleft, *A3* A3 segment (Image kindly provided by Anthony Hlavacek, MD, Medical University of South Carolina). *RV* right ventricle, *LV* left ventricle

pointed toward the inlet septum [23]. The isolated mitral cleft can be managed medically or surgically, depending on the degree of mitral regurgitation. Other associated heart diseases include tetralogy of Fallot, transposition of great

arteries, double-outlet right ventricle, tricuspid atresia, and double-inlet left ventricle.

#### 12.3.2.5 Computed Tomographic (CT) Imaging in Congenital Mitral Valve Anomalies

The diagnosis of mitral valve anomalies is best established by transesophageal echocardiography (TEE). CT is not the primary imaging tool for assessing cardiac valves but instead is used as a complementary imaging technique to echocardiography or MRI, especially in patients with poor quality echocardiography studies or patients with contraindication to MRI [24, 25]. Awareness of the CT appearances of the spectrum of abnormal mitral valves is important as these anomalies may be detected incidentally in patients undergoing CT for other clinical indications. CT protocols for valve evaluation are similar to those for coronary artery evaluation. Retrospectively gated data acquisition through the entire cycle is needed. Reconstructions are done at 10 % increments of the R–R interval. These can be combined sequentially to provide functional imaging data in a cine loop that allow evaluation of leaflet morphology and function.

The normal mitral valve is a bicuspid valve that consists of a semicircular anterior leaflet and a crescent-shaped posterior leaflet and is anchored to the mitral valve annulus [24]. The valve leaflets are supported by chordae tendineae, which attach to left ventricular papillary muscles. In healthy adults, the thickness of the chordae tendineae ranges from 0.4 to 1.2 mm. The normal circumference of the mitral valve annulus measures 10 cm and the mitral valve area measures 4–6 $cm^2$ [24].

The mitral valve area can be measured with CT during early diastole (usually 75 % of the R–R interval). Stenotic and regurgitant mitral valves can be identified by CT [24]. In addition, CT allows direct evaluation of the mitral leaflets, chordae tendineae, and papillary muscles including the presence of cleft, thickening, and calcification [24].

Typically, stenotic mitral valves have a funnel-shaped appearance and thickened leaflets [24, 25]. Secondary findings include compensatory left atrial dilatation, left ventricular dilatation (in mitral insufficiency), main pulmonary artery enlargement, and right ventricular hypertrophy (in mitral stenosis). Cine images may show restricted leaflet motion in stenosis and valve prolapse into the left atrium in insufficiency. The severity of mitral regurgitation can be quantified by calculating the regurgitant volume and fraction or by measuring the regurgitant orifice at end systole [25].

The reported sensitivity and specificity of CT in the diagnosis of mitral valve prolapse are 96 and 93 % (with transthoracic echocardiogram as the reference standard) [20]. Reformatted four-chamber views are most sensitive for establishing the diagnosis.

## References


1. Edwards WD. Embryology and pathologic features of Ebstein's anomaly. Prog Pediatr Cardiol. 1993;2:5–15.
2. Carpentier A, Chauvaud S, Mace L, Relland J, Mihaileanu S, Marino JP, et al. A new reconstructive operation for Ebstein's anomaly of the tricuspid valve. J Thorac Cardiovasc Surg. 1988;96:92–101.
3. Lincoln T, Stewart C, Shah P. An unusual first presentation of Ebstein's anomaly in a 72-year-old patient. Ann Thorac Surg. 2012;93:e19–20. doi:10.1016/j.athoracsur.2011.08.024.
4. Abbara S, Soni AV, Cury RC. Evaluation of cardiac function and valves by multidetector row computed tomography. Semin Roentgenol. 2008;43:145–53. doi:10.1053/j.ro.2008.01.009.
5. Goo HW, Park IS, Ko JK, Kim YH, Seo DM, Yun TJ, et al. CT of congenital heart disease: normal anatomy and typical pathologic conditions. Radiographics. 2003;23 Spec No:S147–65. doi:10.1148/rg.23si035501.
6. Hughes Jr D, Siegel MJ. Computed tomography of adult congenital heart disease. Radiol Clin North Am. 2010;48:817–35. doi:10.1016/j.rcl.2010.04.005.
7. Tandon R, Edwards JE. Tricuspid atresia. A re-evaluation and classification. J Thorac Cardiovasc Surg. 1974;67:530–42.
8. Weinberg PM. Anatomy of tricuspid atresia and its relevance to current forms of surgical therapy. Ann Thorac Surg. 1980;29:306–11.
9. Mochizuki T, Ohtani T, Higashino H, Sugawara Y, Tsuda T, Sekiya M, et al. Tricuspid atresia with atrial septal defect, ventricular septal defect, and right ventricular hypoplasia demonstrated by multidetector computed tomography. Circulation. 2000;102:E164–5.
10. Siegel MJ. CT evaluation of congenital heart disease in adults. Appl Radiol. 2005;34:61–8.
11. Siegel MJ, Bhalla S, Gutierrez FR, Billadello JB. MDCT of postoperative anatomy and complications in adults with cyanotic heart disease. AJR Am J Roentgenol. 2005;184:241–7.
12. Niwayama G. Cor triatriatum. Am Heart J. 1960;59:291–317.
13. Van Praagh R, Corsini I. Cor triatriatum: pathologic anatomy and a consideration of morphogenesis based on 13 postmortem cases and a study of normal development of the pulmonary vein and atrial septum in 83 human embryos. Am Heart J. 1969;78:379–405.
14. Ucar O, Vural M, Cicekcioglu H, Pasaoglu L, Aydogdu S, Koparal S. Case report: multidetector CT presentation of a parachute-like asymmetric mitral valve. Br J Radiol. 2008;81:e266–8. doi:10.1259/bjr/20218809.
15. Ruckman RN, Van Praagh R. Anatomic types of congenital mitral stenosis: report of 49 autopsy cases with consideration of diagnosis and surgical implications. Am J Cardiol. 1978;42:592–601.
16. Bano-Rodrigo A, Van Praagh S, Trowitzsch E, Van Praagh R. Double-orifice mitral valve: a study of 27 postmortem cases with developmental, diagnostic and surgical considerations. Am J Cardiol. 1988;61:152–60.
17. Zalzstein E, Hamilton R, Zucker N, Levitas A, Gross GJ. Presentation, natural history, and outcome in children and adolescents with double orifice mitral valve. Am J Cardiol. 2004;93:1067–9. doi:10.1016/j.amjcard.2004.01.015.
18. Collins 2nd RT, Ryan M, Gleason MM. Images in cardiovascular medicine. Mitral arcade: a rare cause of fatigue in an 18-year-old female. Circulation. 2010;121:e379–83. doi:10.1161/CIR.0b013e3181db1ee4.
19. Morris MF, Williamson EE, Topilsky Y, Espinosa RE, Cetta F, Burkhart HM, et al. Multi-imaging assessment of the congenital mitral arcade. J Am Coll Cardiol. 2011;57(18):1856. doi:10.1016/j.jacc.2010.06.069.
20. Feuchtner GM, Alkadhi H, Karlo C, Sarwar A, Meier A, Dichtl W, et al. Cardiac CT angiography for the diagnosis of mitral valve prolapse: comparison with echocardiography1. Radiology. 2010;254:374–83. doi:10.1148/radiol.2541090393.

21. Di Segni E, Kaplinsky E, Klein HO. Color Doppler echocardiography of isolated cleft mitral valve. Roles of the cleft and the accessory chordae. Chest. 1992;101:12–5.
22. McDonald RW, Ott GY, Pantely GA. Cleft in the anterior and posterior leaflet of the mitral valve: a rare anomaly. J Am Soc Echocardiogr. 1994;7:422–4.
23. Kohl T, Silverman NH. Comparison of cleft and papillary muscle position in cleft mitral valve and atrioventricular septal defect. Am J Cardiol. 1996;77:164–9.
24. Chen JJ, Manning MA, Frazier AA, Jeudy J, White CS. CT angiography of the cardiac valves: normal, diseased, and postoperative appearances. Radiographics. 2009;29:1393–412. doi:10.1148/rg.295095002.
25. Morris MF, Maleszewski JJ, Suri RM, Burkhart HM, Foley TA, Bonnichsen CR, et al. CT and MR imaging of the mitral valve: radiologic-pathologic correlation. Radiographics. 2010;30:1603–20. doi:10.1148/rg.306105518.

# Left Ventricular Outflow Tract Abnormalities

# 13

## 13.1 Aortic Valve Stenosis

Aortic valve stenosis refers to a narrowing of the lumen of the aortic valve. It is the most common cardiac valvular condition requiring valve replacement. Congenital stenosis is the most common cause of aortic valve stenosis. It is usually associated with anomalous valves, most commonly the bicuspid aortic valve. The congenitally stenotic aortic valve also may be unicuspid (acommissural or unicommissural) or, rarely, congenitally quadricuspid/quadricommissural. A dysplastic tricuspid aortic valve can also develop stenosis (Fig. 13.1).

### 13.1.1 Bicuspid Aortic Valve

Bicuspid aortic valve disease is the most common congenital heart defect, occurring in 0.5–2 % of the general population, with a 3:1 male predominance [1]. Morphologically, there is a single commissure at birth with two unequally sized leaflets. The incompletely separated leaflet has a central ridge (raphe). Typically, the bicuspid valve results from fusion of the right and left cusps. The noncoronary leaflet is most commonly normal. Rarely, the leaflets are symmetrical or there is no raphe ("pure" bicuspid valve). The most commonly associated anomalies are coarctation of the aorta and interrupted aortic arch, and conversely 50–75 % of patient with coarctation have a bicuspid valve [1, 2]. Other associated conditions include hypoplastic left heart syndrome, Shone syndrome, Williams syndrome, supravalvular stenosis, Turner syndrome, ventricular and atrial septal defects, patent ductus arteriosus, and single coronary artery or reversal of coronary dominance [2].

In the adult population, it is important to distinguish between a bicuspid valve and a tricuspid aortic valve prior to transcatheter aortic valve implantation as the bicuspid valve currently is considered a contraindication to this procedure in the U.S. Frequently, distinguishing a bicuspid aortic valve from a tricuspid, normal valve is difficult using echo due to heavy calcification of the aortic valve. CT can be helpful in this setting. CT is also useful to evaluate aortic valve size and valve opening area.

To diagnose a bicuspid valve, the valve must be visualized in systole, since in diastole the raphe may mimic a tricuspid valve. CT has been demonstrated to be highly sensitive and specific (94 and 100 %) for accurate differentiation between bicuspid and tricuspid valves [3]. Retrospective ECG-gated data acquisition through the entire cardiac cycle is necessary for this purpose.

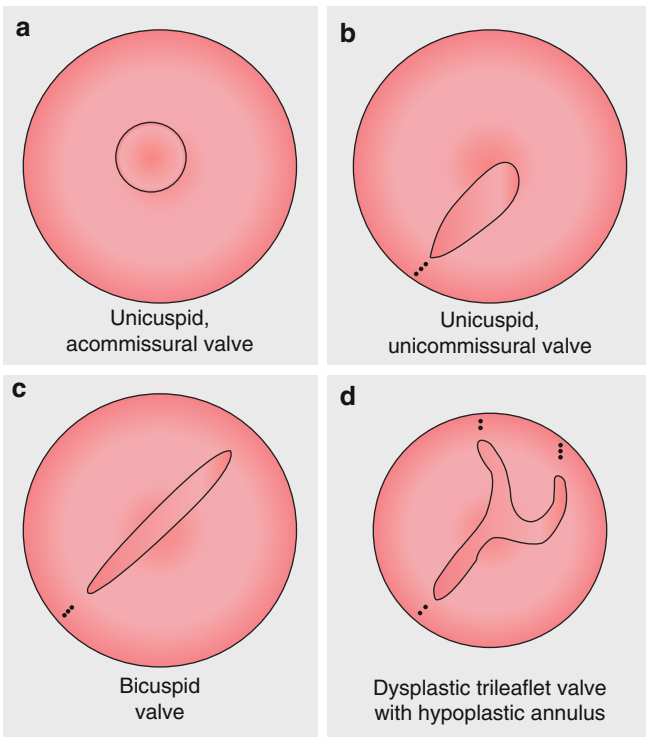


**Fig. 13.1** Morphologic variants of congenital aortic stenosis: Panel (**a**) unicuspid, acommissural valve. Panel (**b**) unicuspid, unicommissural valve. Panel (**c**) bicuspid valve. Panel (**d**) dysplastic, trileaflet valve with hypoplastic annulus

W. Mazur et al., *CT Atlas of Adult Congenital Heart Disease*,
DOI 10.1007/978-1-4471-5088-6_13, © Springer-Verlag London 2013

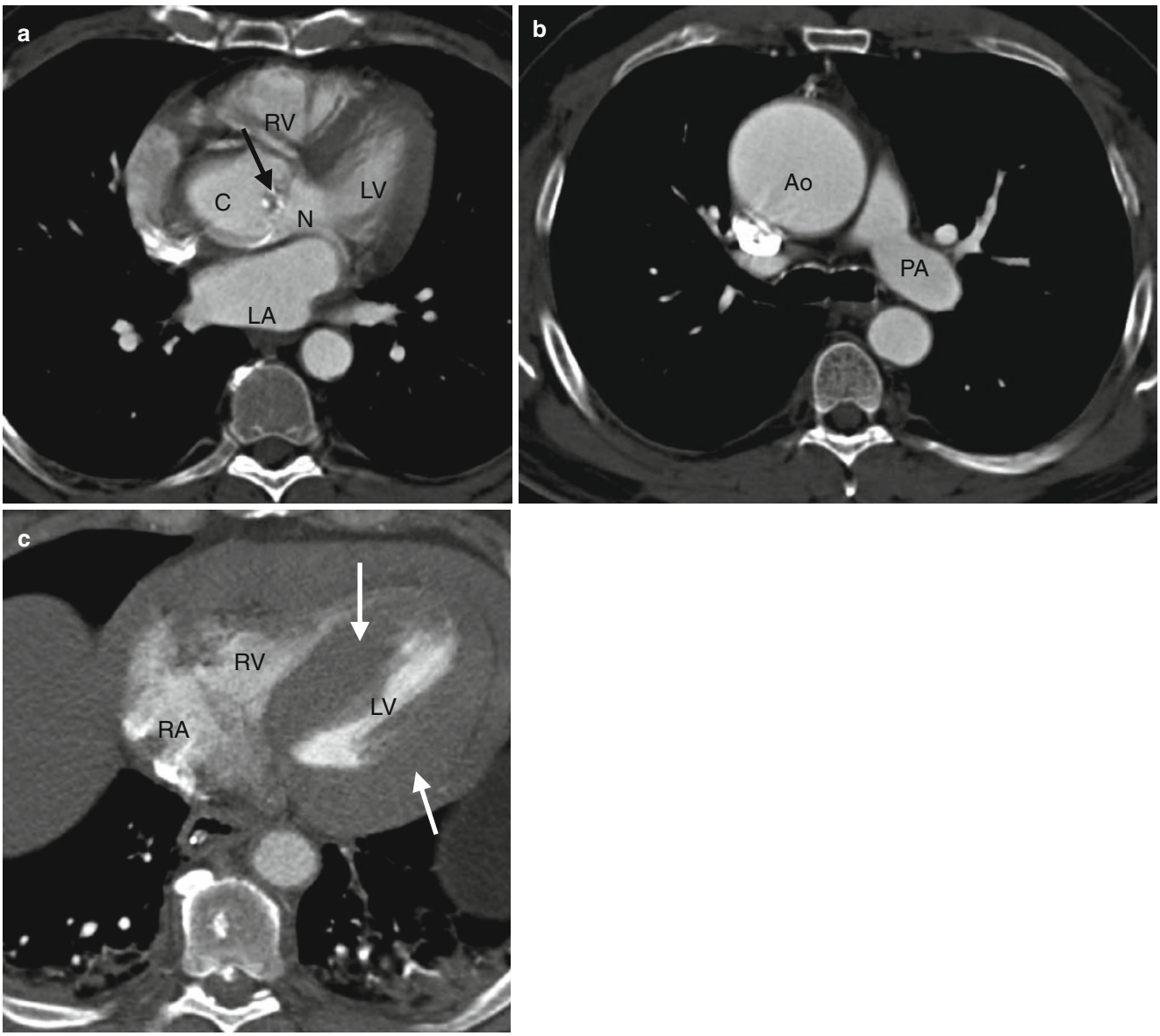


**Fig. 13.2** Bicuspid aortic valve in systole. Panel (**a**) is a short-axis computed tomogram in systole showing two asymmetric cusps and calcified raphe (*arrow*). The larger cusp (*C*) represents the fused right and left cusps. *N* noncoronary cusp. Panel (**b**) is an axial view reconstructed more superiorly and shows a dilated ascending aorta (*Ao*). Panel (**c**) is an axial cut at the level of the left ventricle. Note the profound left ventricular hypertrophy (*white arrows*). *RV* right ventricle, *LV* left ventricle, *LA* left atrium, *RA* right atrium, *PA* pulmonary artery

The classic CT finding of a bicuspid aortic valve is the presence of only two cusps [4]. In the axial plane, the orifice has a characteristic "fish-mouthed" appearance. In the long-axis view, the eccentric closure line and doming of the leaflets are observed. The two cusps are commonly asymmetric in size with one cusp being larger than the other. The cusps may be thickened and calcified, resulting in reduction of the aortic valve area (Figs. 13.2 and 13.3).

The presence of valvular calcifications can cause artifacts, but with CT these usually do not hinder the planimetric measurement of valve area. Studies have shown that planimetric CT measurements of the aortic valve area correlate significantly with transthoracic echocardiographic and transesophageal echocardiographic measurements [5, 6]. Aortic valve calcification can be quantified and is associated with the severity of aortic stenosis [7]. Cine images may show decreased excursion of the valve cusps.

Associated findings related to a bicuspid aortic valve include left ventricular hypertrophy and dilatation of the aortic root as well as ascending aorta and anomalies such as aortic coarctation and interrupted aortic arch. See Table 13.1.

The natural history of bicuspid aortic valve consists of gradual calcification and degeneration of the valve leaflets

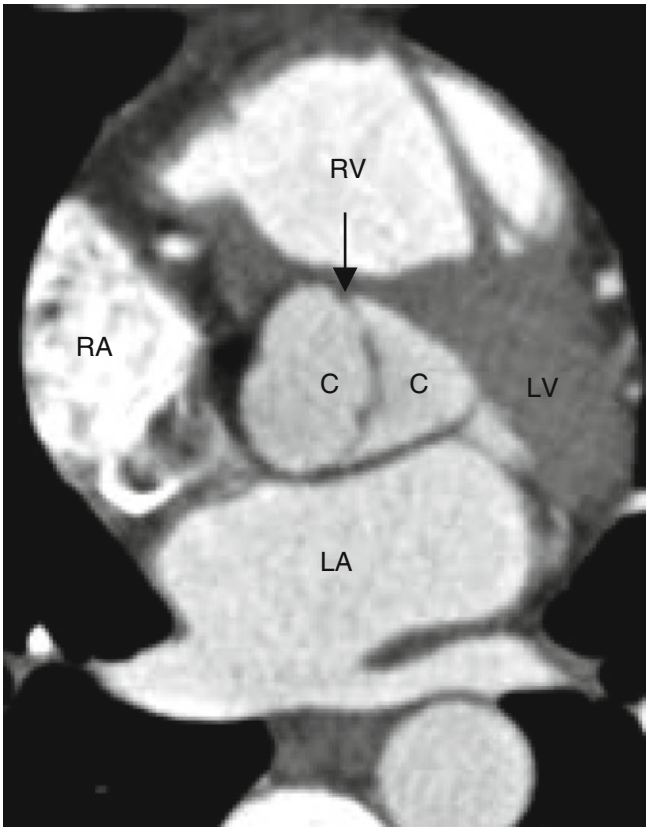


**Fig. 13.3** This short-axis scan demonstrates nearly symmetric bileaflet aortic valve cusps (*C*) and a thickened commissure (*black arrow*). Two symmetric-size cusps are less common than two asymmetric-size cusps: *RA* right atrium, *RV* right ventricle, *LA* left atrium, *LV* left ventricle

**Table 13.1** CT assessment of a bicuspid aortic valve

| |
|---|
| Retrospective ECG-gated data acquisition through entire cardiac cycle |
| Two valvular cusps with "fish-mouthed" orifice appearance, axial images |
| Doming of the valve, long-axis reconstructions |
| Dilated ascending aorta |
| Planimetry of aortic valve area with cine images to show valve excursion |
| Left ventricle hypertrophy, systolic function |
| Coronary artery anatomy |
| Associated lesions: commonly aortic coarctation and interrupted aortic arch |

resulting in aortic stenosis most commonly and sometimes aortic regurgitation. These findings occur most often in the fifth and sixth decades of life. Aortopathy consisting of dilatation of the aortic root and or ascending aorta can also develop In addition to valvular degeneration, aortic regurgitation may also occur secondary to ascending aorta and aortic root dilatation, which do commonly occur. In the Olmsted County study, up to 39 % of the population with bicuspid aortic valve demonstrated an ascending aorta diameter over 40 mm [8].

Surgical intervention is necessary in patients with bicuspid aortic valve and symptomatic aortic stenosis or aortic regurgitation. Approximately 3–6 % of patients will require surgical intervention for severe symptomatic regurgitation [8]. Surgical intervention usually consists of aortic valve replacement. For those aortic stenosis patients who are not surgical candidates and who do not have significant aortic regurgitation, balloon valvuloplasty may be performed. Balloon valvuloplasty is generally not indicated in the setting of heavy valvular calcification.

Surgical correction of symptomatic pediatric and young adolescent patients with a bicuspid aortic valve is sometimes performed using the Ross procedure (aortic valve replacement with an autologous pulmonary homograft and pulmonary valve replacement with a cadaveric allograft).

Surgery to correct the aortic root without valve replacement is performed in approximately 25 % of patients with bicuspid aortic valve [9]. In patients with a stenotic bicuspid aortic valve and ascending aortic or root aneurysm (maximum diameter>4.5 cm), concomitant aortic root replacement may be performed at the time of valve replacement. Because aortopathy is an associated characteristic of bicuspid aortic valves, the threshold for aortic aneurysm repair is reduced and smaller diameter aortas are replaced.

### 13.1.2 Dysplastic Tricuspid Aortic Valve

A dysplastic tricuspid aortic valve may develop concomitant thickening, stenosis, and calcification. The cusps of the valve may themselves be thickened, rolled, and redundant. Microscopic studies reveal that they consist of immature loose connective tissue. The valve orifice is obstructed by the dysplastic cusps. Dysplastic changes rather than commissural fusion are responsible for the functional aortic stenosis. These valves are generally not amenable to valvulotomy because obstruction is due to abnormal valve tissue.

### 13.1.3 Unicuspid Aortic Valve

Unicuspid aortic valve is an uncommon condition with an incidence of 0.02 % in the general population [10]. It is more common in men than women [10]. These valves form due to fusion of the cusps. Unicuspid valves are usually unicommissural with a posterior commissural attachment. Rarely, they are acommissural. This anomaly is commonly associated with aortic stenosis which is often asymptomatic. In asymptomatic patients, the diagnosis is most commonly made either at autopsy or by examination of surgically excised valves (60 % of cases) [11].

Unicuspid aortic valves share many of the features of bicuspid aortic valves (valvular dysfunction, aortopathy), but

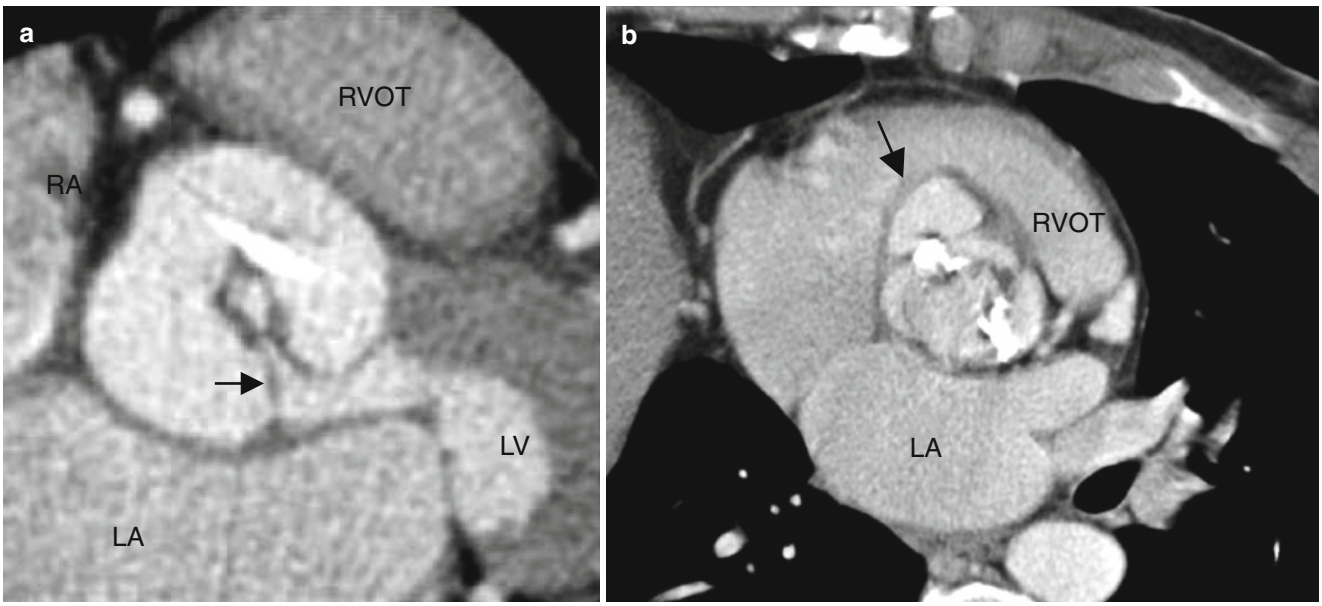


**Fig. 13.4** Panel (**a**) is an example of a unicuspid aortic valve resulting in symptomatic aortic stenosis in a middle-aged adult. This computed tomography angiogram shows a unicommissural (*arrow*) unicuspid valve. Note the circular, small valve opening in systole in the center of the image (Panel a was generously provided by Dr Jeffry M Schussler, Baylor University Medical Center). Panel (**b**) is an axial, oblique multiplanar reconstruction illustrating the fused leaflets typical for a unicuspid aortic valve. Panel (**b**) points to a coexisting sinus of Valsalva aneurysm (*black arrow*). *RVOT* right ventricular outflow tract, *RA* right atrium, *LA* left atrium, *LV* left ventricle (Panel (**b**) is reproduced from Dandes [35]. With kind permission of Springer-Verlag, Berlin Heidelberg)

complications occur earlier in life and progress at a faster pace. This anomaly should be suspected in patients presenting at a young age with clinically significant aortic stenosis. CT can confirm the valve morphology and demonstrate the absence of a commissure [10] (Fig. 13.4).

### 13.1.4 Quadricuspid Aortic Valve

Quadricuspid aortic valve is a rare congenital defect. It has no gender propensity. Typically, there are three equal-sized cusps with a fourth, smaller cusp. Aortic regurgitation commonly results (75 % of cases) and is caused by malcoaptation of the four valvular leaflets [12]. About 16 % of patients exhibit normal valve function [12]. Aortic stenosis, the most frequent complication of bicuspid valve, is less frequently seen with quadricuspid aortic valve. Quadricuspid aortic valves have been associated with patent ductus arteriosus, Ehlers–Danlos syndrome, hypertrophic obstructive cardiomyopathy, and subaortic stenosis. CT can depict the morphology of the valve and can also provide information about the presence of stenosis and regurgitation when viewed in cine mode [13]. See Fig. 13.5.

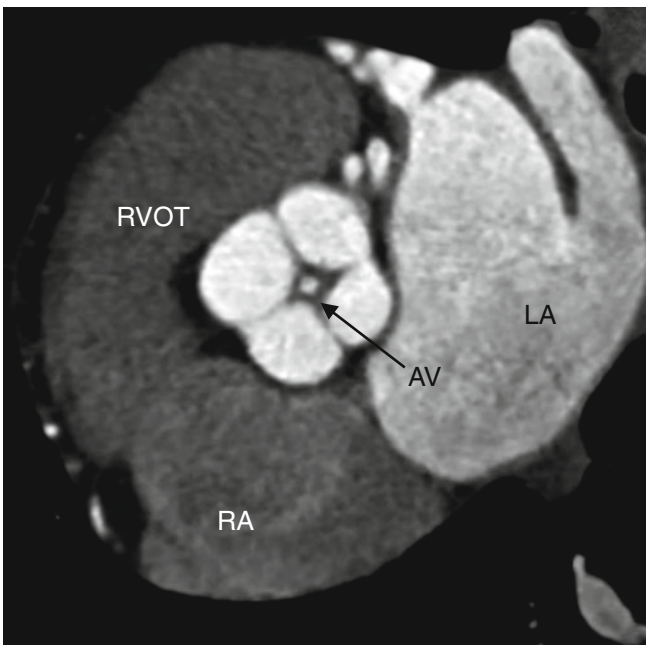


**Fig. 13.5** Quadricuspid aortic valve. An oblique axial slice in diastole shows four valve leaflets (two equal-sized large and two equal-sized smaller valve leaflets) with mild thickening and incomplete coaptation and central aortic insufficiency indicated by the circular contrast density centered in the valve orifice (labeled AV) during diastole. *LA* left atrium, *RA* right atrium, *RVOT* right ventricular outflow tract

### 13.1.5 Subaortic Stenosis in Adults

Subaortic stenosis is considered an acquired (rather than congenital) cardiac defect of postnatal development since it does not appear during embryologic development of the heart and occurs very infrequently in the neonatal period. The prevalence is approximately 6.5 % for all adults with

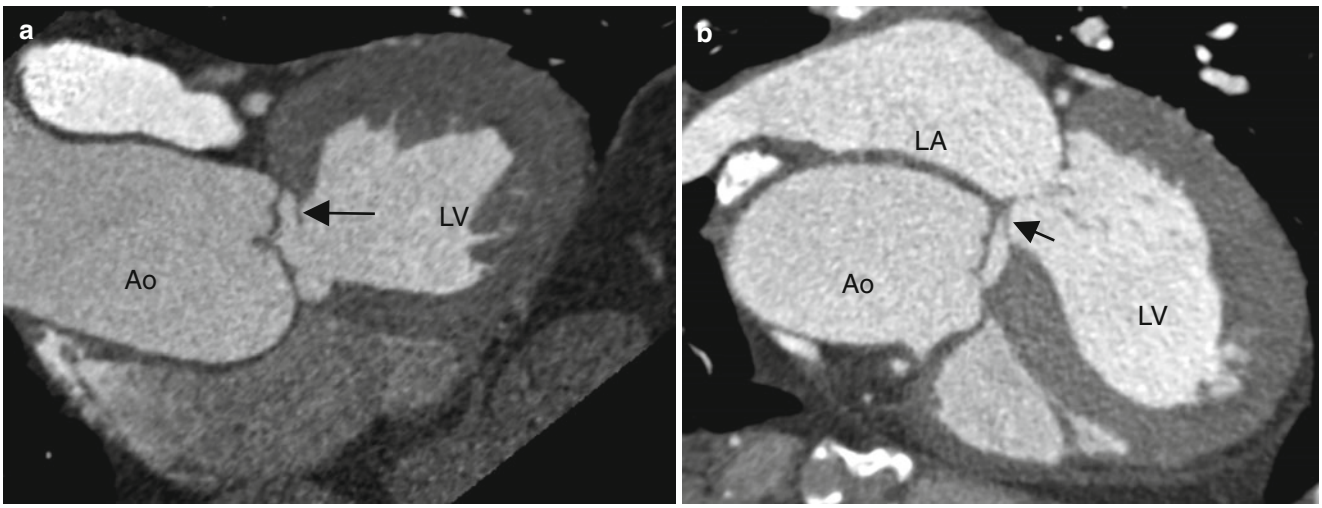


**Fig. 13.6** Short-segment subaortic stenosis in a 65-year-old male, who initially was diagnosed with hypertrophic cardiomyopathy with left ventricular outflow tract obstruction. Panels (**a**) and (**b**) are two reformatted CT scans showing a subaortic membrane (*arrow*) extending to the base of the anterior leaflet of the mitral valve (panel b). Note the dilation of the aorta and the left ventricular hypertrophy. *LV* left ventricle, *LA* left atrium, *Ao* aorta

congenital heart disease and 44 % have other associated congenital heart diseases [14]. It usually presents after the first year of life and causes severe left ventricular outflow tract obstruction (LVOT) and the development of heart failure during the first year of life.

The two most frequently associated defects are ventricular septal defect and aortic coarctation, but subaortic stenosis has also been identified in the presence of atrial septal defect, patent ductus arteriosus, bicuspid aortic valve, and double-outlet right ventricle. Of interest, the subaortic stenosis is often not initially recognized and, in many cases, is not diagnosed until years after surgical repair of the associated cardiac malformation.

Subaortic stenosis is classified into short-segment (more common) and long-segment obstruction [15]. Short-segment obstruction is defined as subaortic stenosis with a length of less than one-third of the aortic valve diameter, while by definition, long-segment obstruction has a stenosis length of more than one-third of the aortic valve diameter. Pathologically, this entity consists of a thin fibrous ridge or membrane in the LVOT. The resulting turbulent flow can damage the endothelium and result in fibrin deposition, which can lead to LVOT obstruction. The membrane often extends to the anterior leaflet of the mitral valve and occasionally to the right coronary cusp of the aortic valve.

Aortic regurgitation is the most common complication of subaortic stenosis, occurring in more than 50 % of patients [15]. Valvular damage due to the high-pressure subvalvular systolic jet originating at the level of stenosis appears to be the cause [16]. Severe left ventricular (often asymmetric) hypertrophy and dynamic LVOT obstruction can develop and may mask the existence of a subaortic membrane. These findings may result in a false diagnosis of hypertrophic cardiomyopathy.

Early surgical repair of subaortic stenosis has been advocated to prevent rapid progression of left outflow tract obstruction and development of significant aortic regurgitation. However, it can recur after adequate surgical resection. Reoperation rates vary between 4 and 35 % and the incidence of reoperation increases progressively with duration of follow-up [17, 18]. Computed tomography (CT) can show the subaortic membrane in the left ventricular outflow tract and the associated left ventricular hypertrophy and aortic root and ascending aorta dilatation [19].

See Fig. 13.6 for an example of subaortic stenosis.

### 13.1.6 Supravalvular Aortic Stenosis

Supravalvular aortic stenosis is a rare condition characterized by narrowing of the aorta close to its origin from the left ventricle. Branch pulmonary stenosis as well as ostial coronary stenosis can be associated findings. It typically occurs in association with Williams syndrome (mental retardation, dysmorphic faces, and transient hypercalcemia) [20, 21]. CT demonstrates the presence and extent of the stenosis. Associated findings such as left ventricular myocardial hypertrophy and bicuspid aortic valve may also be seen in association with this condition [22].

See Fig. 13.7 for an example of supravalvular aortic stenosis.

#### 13.1.6.1 Cardiac Computed Tomography (CT) in the Assessment of Left Ventricular Outflow Tract Abnormalities

CT can be a useful noninvasive modality for assessing aortic valvular, subaortic, and supravalvular stenosis when echocardiography and magnetic resonance do not provide

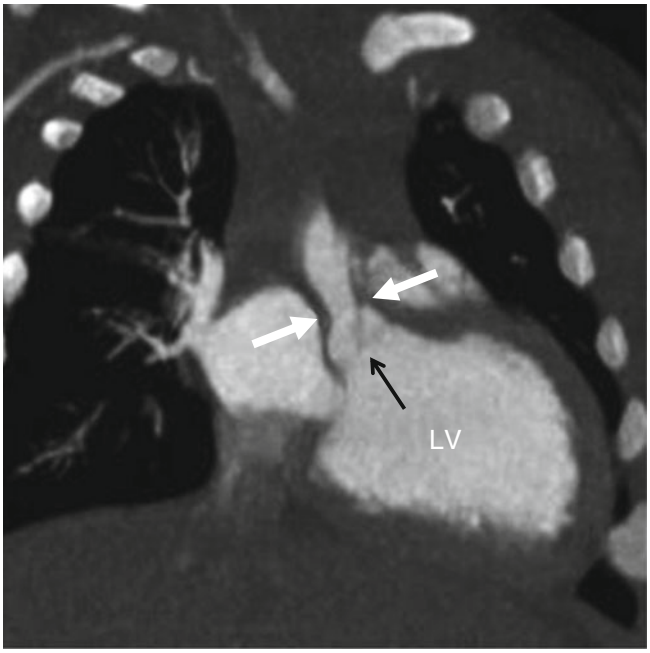


**Fig. 13.7** Williams syndrome with supra-aortic stenosis. Panel (**a**) is a coronal volumetric reconstruction demonstrating stricture (*white arrows*) of the ascending aorta. *Black arrow* aortic valve *LV* left ventricle (Reproduced from Dillman and Hernandez [36]. With kind permission of American Roentgen Ray Society, Leesburg, VA)

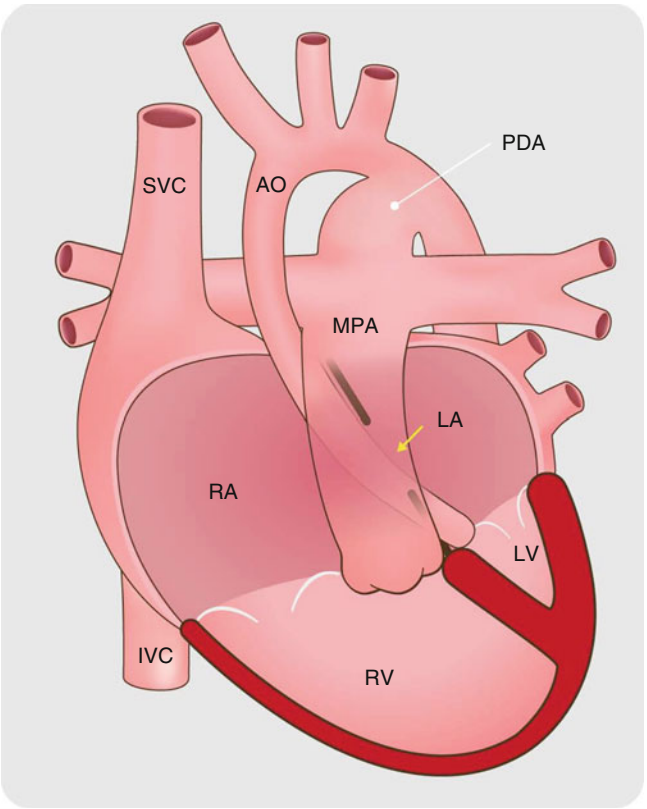


**Fig. 13.8** Schematic drawing of the hypoplastic left heart syndrome. The left ventricle is severely underdeveloped, and the aortic and mitral valves are hypoplastic or atretic and cannot allow sufficient blood flow. The aorta is also small and underdeveloped. Blood returns from the lungs to the left atrium and then flows through an atrial septal defect (*arrow*) to the right side of the heart. Blood enters the aorta via retrograde flow through a patent ductus arteriosus (*PDA*). *LV* hypoplastic left ventricle, *Ao* hypoplastic aorta, *RV* right ventricle

sufficient data. CT assessments should include evaluation of (a) the anatomy, size, and function of the aortic valve; (b) the presence, site, morphology, and size of subaortic and or supra-aortic obstruction; (c) the size of the aortic root and ascending aorta; (d) the size, wall thickness, and systolic function of the left ventricle; (e) the morphology and size of the left atrium; (f) the anatomy of the coronary arteries; and (g) coexisting anomalies. Following corrective interventions, cardiac CT can be used to exclude or confirm the recurrence of obstruction. The significant drawback of cardiac CT is its inability to measure pressure gradients across the stenotic lesions.

## 13.2 Hypoplastic Left Heart Syndrome

### 13.2.1 Definition

Hypoplastic left heart syndrome encompasses a spectrum of cardiac malformations characterized by hypoplasia of the left ventricle and ascending aorta and hypoplasia or atresia of the mitral and/or aortic valve [23]. The great vessels are normally aligned.

Hypoplastic left heart syndrome accounts for 2–3 % of all congenital heart diseases with an incidence of 2 in 10,000 live births [24]. It is twice as frequent in boys as in girls [24].

### 13.2.2 Morphology and Patterns of Blood Flow

In this syndrome, pulmonary venous blood enters the left atrium but cannot cross the atretic or stenotic mitral valve to enter the hypoplastic left ventricle (Fig. 13.8). The result is that left atrial blood is shunted across a defect in the atrial septum into the right atrium [24]. Most often the defect is highly restrictive (pinhole size), but it can be large and nonrestrictive. Restrictive flow in combination with obstruction at the mitral valve leads to venous pulmonary outflow obstruction and congestive heart failure. At the severe end of the spectrum encompassing aortic and mitral atresia, blood enters the aorta via retrograde flow through a patent ductus arteriosus (Fig. 13.10). At the milder end of the spectrum with aortic or mitral valve stenosis (not atresia), flow may enter the aorta through both the stenotic valve and a patent ductus arteriosus [23] (Fig. 13.9).

Associated anomalies include pre- and postductal coarctation of the aorta, transposition of the great arteries, patent

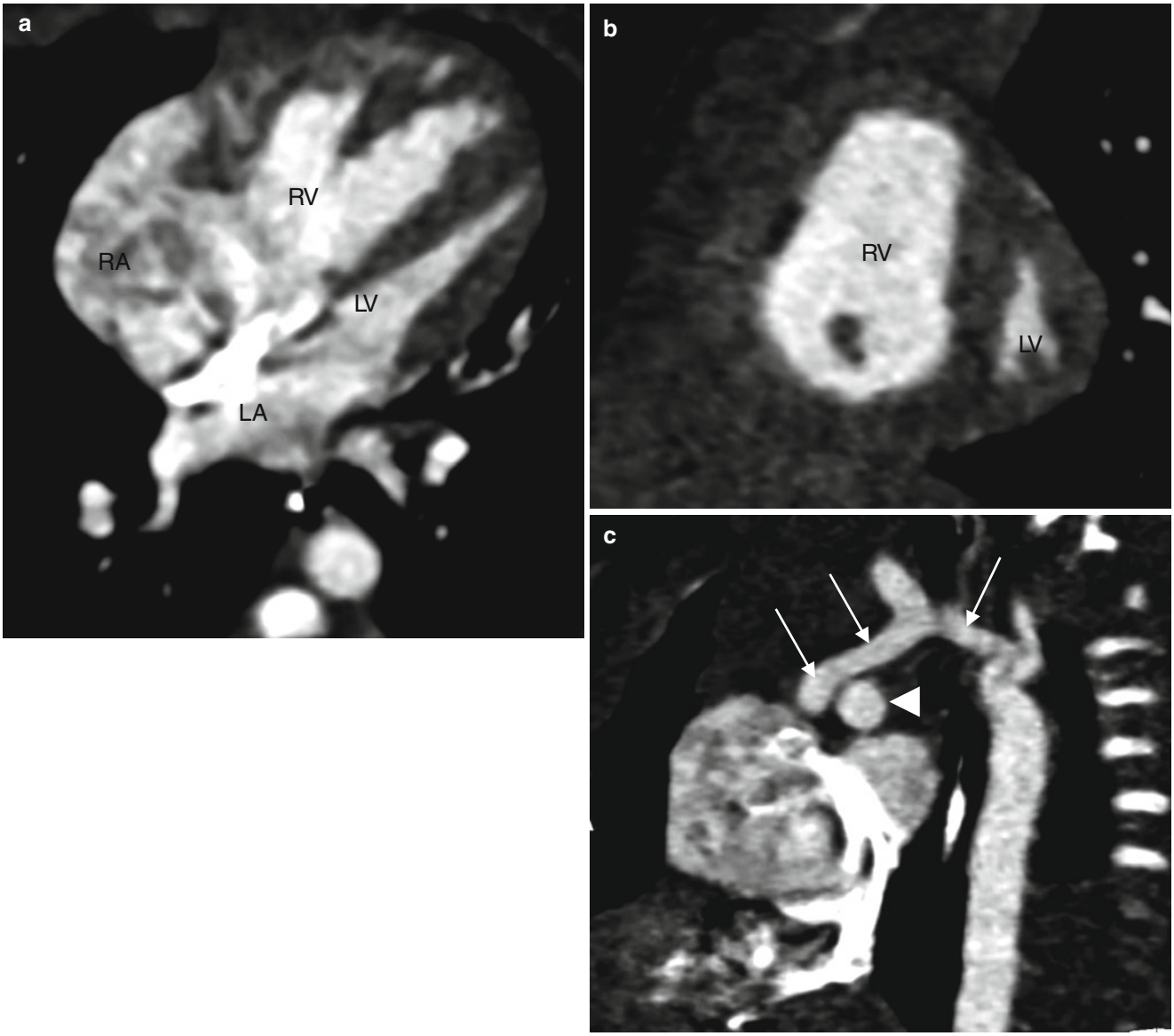


**Fig. 13.9** Hypoplastic left heart syndrome in a 2-day-old neonate with mitral and aortic stenosis, the milder end of spectrum. Panel (**a**), a four-chamber view, and panel (**b**), a two-chamber view, showing the small left ventricle (*LV*) and enlarged right atrium (*RA*) and right ventricle (*RV*). Panel (**c**) is an oblique sagittal reconstruction showing a very small ascending and transverse aorta (*arrows*). Note that the ascending aorta is smaller than the right pulmonary artery (*arrowhead*) next to it. *LA* left atrium (Images courtesy of Anthony M. Hlavacek, M.D., Medical University South Carolina)

ductus arteriosus, ventricular septal defect, atrial isomerism, and total anomalous pulmonary venous drainage [24, 25].

### 13.2.3 Prognosis

Hypoplastic left heart syndrome is virtually fatal if untreated. Despite improvements in surgical management, the medium survival time is 75, 70, and 65 % at 1, 5, and 10 years, respectively. However, there are an increasing number of subjects born with hypoplastic left heart syndrome who are entering adulthood [26].

### 13.2.4 Surgery

Therapeutic options include multistage reconstructive surgery based on a single-ventricle physiology, cardiac transplantation, and occasionally biventricular repair, which can be performed in subjects with less severe forms of hypoplastic left heart syndrome [27–29].

The multistage surgical approach consists of a series of three operations: the Norwood procedure (stage I), the hemi-Fontan or bidirectional Glenn procedure (stage II), and the Fontan procedure (stage III). These procedures are discussed in depth in Chap. 25. Orthotopic heart transplantation provides

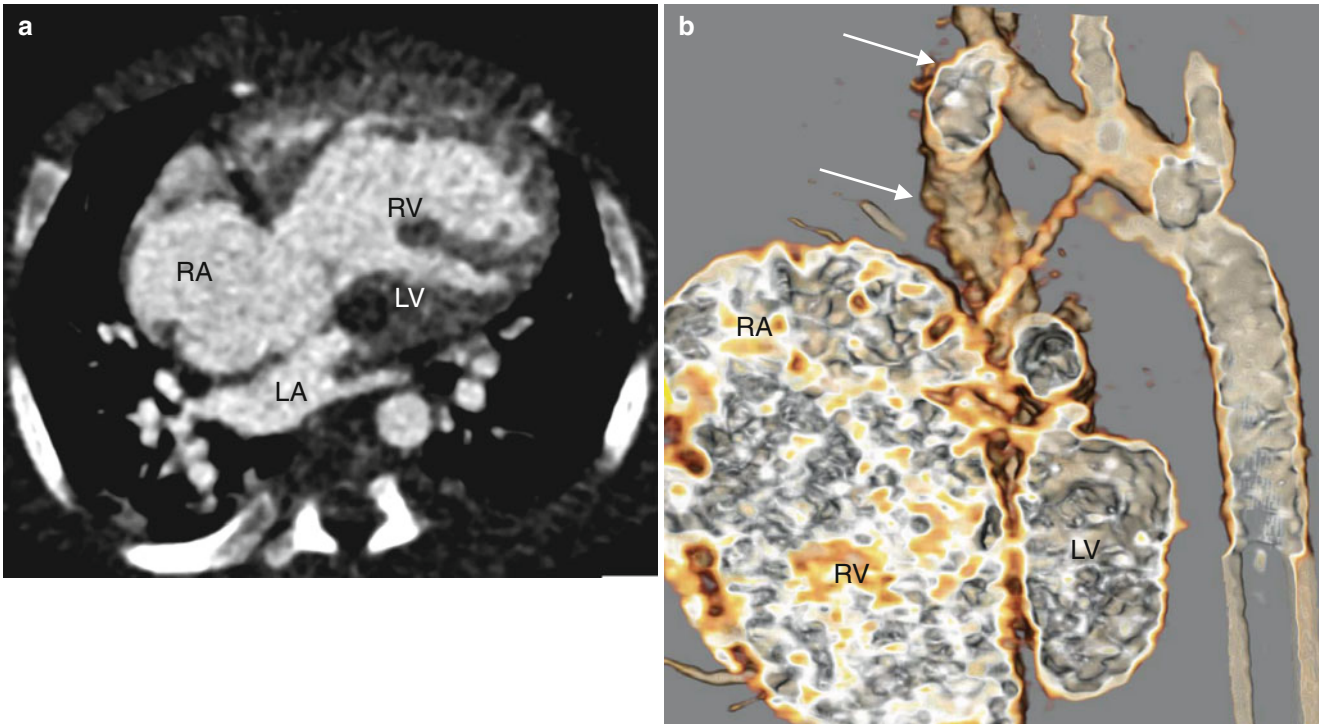


**Fig. 13.10** Hypoplastic left heart syndrome in a 3-day-old neonate with mitral and aortic atresia, the severe end of the spectrum. Panel (**a**) is a four-chamber computed tomogram (CT) showing the severely hypoplastic left ventricle (*LV*) and a large right atrium (*RA*) and right ventricle (*RV*). Panel (**b**) is a volume-rendered sagittal CT showing the extreme hypoplasia of the ascending aorta (*arrows*). *LA* left atrium (Images courtesy of Anthony M. Hlavacek, M.D., Medical University South Carolina)

an alternative therapy with results similar to those of the staged surgical palliation.

The goal of the three-stage surgical approach is to isolate the hypoplastic left ventricle from the circulation and to make the right ventricle the systemic pumping chamber (i.e., create a univentricular heart physiology) [26]. In stage I, performed in the neonate, the Norwood procedure traditionally consists of an atrial septectomy, Blalock–Taussig shunt, and an end-to-side anastomosis of the main pulmonary artery to the ascending aorta creating a "neoaorta" (Fig. 13.10) [27, 30, 31]. The second stage is a bidirectional cavopulmonary shunt (hemi-Fontan or bidirectional Glenn procedure) is usually performed at the age of 4–6 months when pulmonary arterial resistance has fallen to normal levels. The third stage consists of the creation of a Fontan circulation to direct blood from the inferior vena cava to the right pulmonary artery and is usually performed when the patient is 3–5 years of age [32, 33]. These surgical approaches are described in more detail in Part 7.

Complications of the corrective procedures include obstruction of the surgically constructed conduits, congestive heart failure, and arrhythmias.

#### 13.2.4.1 Cardiac Computed Tomography (CT) in the Evaluation of Hypoplastic Left Heart Syndrome

The long-term outcome in hypoplastic left heart syndrome remains to be determined. However, an increasing number of subjects will reach adolescence and adulthood after the Fontan procedure. CT is not performed for diagnosis of hypoplastic left heart syndrome. However, it is used for evaluation of postoperative complications [34]. In adults, CT is especially useful to assess complications associated with Fontan circulation, described in Part 7.

## References


1. Siu SC, Silversides CK. Bicuspid aortic valve disease. J Am Coll Cardiol. 2010;55:2789–800. doi:10.1016/j.jacc.2009.12.068.
2. Roos-Hesselink JW, Scholzel BE, Heijdra RJ, Spitaels SE, Meijboom FJ, Boersma E, et al. Aortic valve and aortic arch pathology after coarctation repair. Heart. 2003;89:1074–7.
3. Alkadhi H, Leschka S, Trindade PT, Feuchtner G, Stolzmann P, Plass A, et al. Cardiac CT for the differentiation of bicuspid and tricuspid aortic valves: comparison with echocardiography and surgery. AJR Am J Roentgenol. 2010;195:900–8. doi:10.2214/AJR.09.3813.
4. Hughes Jr D, Siegel MJ. Computed tomography of adult congenital heart disease. Radiol Clin North Am. 2010;48:817–35. doi:10.1016/j.rcl.2010.04.005.
5. Feuchtner GM, Muller S, Bonatti J, Schachner T, Velik-Salchner C, Pachinger O, et al. Sixty-four slice CT evaluation of aortic stenosis using planimetry of the aortic valve area. AJR Am J Roentgenol. 2007;189:197–203. doi:10.2214/AJR.07.2069.
6. LaBounty TM, Sundaram B, Agarwal P, Armstrong WA, Kazerooni EA, Yamada E. Aortic valve area on 64-MDCT correlates with transesophageal echocardiography in aortic stenosis. AJR Am J Roentgenol. 2008;191:1652–8. doi:10.2214/AJR.07.3703.
7. Koos R, Kuhl HP, Muhlenbruch G, Wildberger JE, Gunther RW, Mahnken AH. Prevalence and clinical importance of aortic valve calcification detected incidentally on CT scans: comparison with echocardiography. Radiology. 2006;241:76–82. doi:10.1148/radiol.2411051163.
8. Michelena HI, Desjardins VA, Avierinos JF, Russo A, Nkomo VT, Sundt TM, et al. Natural history of asymptomatic patients with normally functioning or minimally dysfunctional bicuspid aortic valve in the community. Circulation. 2008;117:2776–84. doi:10.1161/CIRCULATIONAHA.107.740878.
9. Michelena HI, Khanna AD, Mahoney D, Margaryan E, Topilsky Y, Suri RM, et al. Incidence of aortic complications in patients with bicuspid aortic valves. JAMA. 2011;306:1104–12. doi:10.1001/jama.2011.1286.
10. Gibbs WN, Hamman BL, Roberts WC, Schussler JM. Diagnosis of congenital unicuspid aortic valve by 64-slice cardiac computed tomography. Proc (Bayl Univ Med Cent). 2008;21:139.
11. Mookadam F, Thota VR, Garcia-Lopez AM, Emani UR, Alharthi MS, Zamorano J, et al. Unicuspid aortic valve in adults: a systematic review. J Heart Valve Dis. 2010;19:79–85.
12. Tutarel O. The quadricuspid aortic valve: a comprehensive review. J Heart Valve Dis. 2004;13:534–7.
13. Agarwal PP, Wells SA, Kolias TJ. AJR teaching file: aortic valve abnormality in a woman with progressive shortness of breath. AJR Am J Roentgenol. 2010;195:S70–2. doi:10.2214/AJR.09.7172.
14. Oliver JM, Gonzalez A, Gallego P, Sanchez-Recalde A, Benito F, Mesa JM. Discrete subaortic stenosis in adults: increased prevalence and slow rate of progression of the obstruction and aortic regurgitation. J Am Coll Cardiol. 2001;38(3):835–42. doi:org/10.1016/S0735-1097(01)01464-4.
15. Choi JY, Sullivan ID. Fixed subaortic stenosis: anatomical spectrum and nature of progression. Br Heart J. 1991;65:280–6.
16. Kitchiner D, Jackson M, Malaiya N, Walsh K, Peart I, Arnold R. Incidence and prognosis of obstruction of the left ventricular outflow tract in Liverpool (1960–91): a study of 313 patients. Br Heart J. 1994;71:588–95.
17. Coleman DM, Smallhorn JF, McCrindle BW, Williams WG, Freedom RM. Postoperative follow-up of fibromuscular subaortic stenosis. J Am Coll Cardiol. 1994;24:1558–64.
18. Brauner R, Laks H, Drinkwater Jr DC, Shvarts O, Eghbali K, Galindo A. Benefits of early surgical repair in fixed subaortic stenosis. J Am Coll Cardiol. 1997;30:1835–42.
19. Takx R, Schoepf UJ, Friedman B, Hlavacek AM, Henzler T. Recurrent subaortic membrane causing subvalvular aortic stenosis 13 years after primary surgical resection. J Cardiovasc Comput Tomogr. 2011;5:127–8. doi:10.1016/j.jcct.2011.01.004.
20. Martens MA, Wilson SJ, Reutens DC. Research review: Williams syndrome: a critical review of the cognitive, behavioral, and neuroanatomical phenotype. J Child Psychol Psychiatry. 2008;49:576–608. doi:10.1111/j.1469-7610.2008.01887.x.
21. Ozergin U, Sunam GS, Yeniterzi M, Yuksek T, Solak T, Solak H. Supravalvular aortic stenosis without Williams syndrome. Thorac Cardiovasc Surg. 1996;44:219–21. doi:10.1055/s-2007-1012022.
22. Kimura-Hayama ET, Melendez G, Mendizabal AL, Meave-Gonzalez A, Zambrana GF, Corona-Villalobos CP. Uncommon congenital and acquired aortic diseases: role of multidetector CT angiography. Radiographics. 2010;30:79–98. doi:10.1148/rg.301095061.
23. Tchervenkov CI, Jacobs JP, Weinberg PM, Aiello VD, Beland MJ, Colan SD, et al. The nomenclature, definition and classification of hypoplastic left heart syndrome. Cardiol Young. 2006;16:339–68. doi:10.1017/S1047951106000291.
24. Barron DJ, Kilby MD, Davies B, Wright JG, Jones TJ, Brawn WJ. Hypoplastic left heart syndrome. Lancet. 2009;374:551–64. doi:10.1016/S0140-6736(09)60563-8.
25. Rasiah SV, Ewer AK, Miller P, Wright JG, Barron DJ, Brawn WJ, et al. Antenatal perspective of hypoplastic left heart syndrome: 5 years on. Arch Dis Child Fetal Neonatal Ed. 2008;93:F192–7. doi:10.1136/adc.2006.112482.
26. Stumper O. Hypoplastic left heart syndrome. Heart. 2010;96:231–6. doi:10.1136/hrt.2008.159889.
27. Norwood WI, Lang P, Hansen DD. Physiologic repair of aortic atresia-hypoplastic left heart syndrome. N Engl J Med. 1983;308:23–6. doi:10.1056/NEJM198301063080106.
28. Bailey LL, Nehlsen-Cannarella SL, Doroshow RW, Jacobson JG, Martin RD, Allard MW, et al. Cardiac allotransplantation in newborns as therapy for hypoplastic left heart syndrome. N Engl J Med. 1986;315:949–51. doi:10.1056/NEJM198610093151507.
29. Tchervenkov CI, Tahta SA, Jutras LC, Beland MJ. Biventricular repair in neonates with hypoplastic left heart complex. Ann Thorac Surg. 1998;66:1350–7.
30. Sano S, Ishino K, Kawada M, Arai S, Kasahara S, Asai T, et al. Right ventricle-pulmonary artery shunt in first-stage palliation of hypoplastic left heart syndrome. J Thorac Cardiovasc Surg. 2003;126:504–9; discussion 509–10.
31. Akintuerk H, Michel-Behnke I, Valeske K, Mueller M, Thul J, Bauer J, et al. Stenting of the arterial duct and banding of the pulmonary arteries: basis for combined norwood stage I and II repair in hypoplastic left heart. Circulation. 2002;105:1099–103.
32. Giroud JM, Jacobs JP. Fontan's operation: evolution from a procedure to a process. Cardiol Young. 2006;16 Suppl 1:67–71. doi:10.1017/S1047951105002350.
33. Amodeo A, Galletti L, Marianeschi S, Picardo S, Giannico S, Di Renzi P, et al. Extracardiac fontan operation for complex cardiac anomalies: seven years' experience. J Thorac Cardiovasc Surg. 1997;114:1020–30; discussion 1030–1.
34. Gaca AM, Jaggers JJ, Dudley LT, Bisset 3rd GS. Repair of congenital heart disease: a primer-part 1. Radiology. 2008;247:617–31. doi:10.1148/radiol.2473061909.
35. Dandes E. Congenital rock and a hard place: unicuspid aortic valve with sinus of Valsalva aneurysm. Int J Cardiovasc Imaging. 2010;28(3):1–2.
36. Dillman JR, Hernandez RJ. Role of CT in the evaluation of congenital cardiovascular disease in children. AJR Am J Roentgenol. 2009;192:1219–31.

# Right Ventricular Outflow Tract Obstruction

# 14

## 14.1 Pulmonary Valve Abnormalities

Congenital pulmonary valve abnormalities encompass a spectrum of anomalies that result in right ventricular outflow tract (RVOT) obstruction. Based on the level of obstruction, there are three possible variants: (a) valvular, (b) subvalvular (infundibular stenosis), and (c) supravalvular.

### 14.1.1 Valvular Pulmonary Stenosis

Valvular pulmonary stenosis refers to a congenital narrowing at the level of the pulmonary valve. It is the most common cause of RVOT obstruction, accounting for 7–12 % of all congenital heart diseases [1].

Morphologic features of the stenotic pulmonary valve vary and include (a) the dome-shaped valve and (b) the dysplastic myxomatous valve. The most common morphology is the dome-shaped, tricuspid pulmonary valve with thickened, fused commissures, a narrow central opening (pinhole to several millimeters), preserved leaflet mobility, and poststenotic dilatation of the pulmonary artery. The valve annulus is usually abnormal and lacks fibrous support. The dome-like appearance results from protrusion of the fused valve leaflets into the pulmonary artery [2]. The main pulmonary artery is dilated in almost all cases, related to a high-velocity jet across the stenotic valve (Fig. 14.1). Relatively uncommon variants of valvular stenosis include unicommissural, bicuspid, and quadricuspid valves (Figs. 14.2 and 14.3).

Pulmonary valve dysplasia is characterized by thickened, redundant valvular leaflets, minimal or no commissural fusion, poor or absent leaflet mobility, and lack of poststenotic dilatation of the pulmonary artery. The obstruction is related to myxomatous replacement of the valve cusps and hypoplasia of the pulmonary valve ring.

The stenotic (dome-shaped or dysplastic) pulmonary valve may be an isolated lesion, although it is often associated with peripheral pulmonary stenosis, ventricular and atrial septal defects, tetralogy of Fallot, and Noonan syndrome (phenotypically Turner syndrome and genotypically XX or XY) [3]. Noonan patients with *PTPN11* mutations are more likely to have pulmonary valve stenosis than those without this mutation [3].

The hemodynamic consequence of pulmonic stenosis is proportional to the severity of the obstruction. Patients with moderate pulmonic stenosis are often detected in infancy and childhood, but they may be asymptomatic until adulthood. Eventually, the valvular obstruction induces changes in the right ventricle muscle, which hypertrophies, especially in the infundibular region, leading to ventricular dilatation, systolic dysfunction, and right-sided heart failure. Symptoms then include fatigue, dyspnea on exertion, cyanosis, and right heart failure. Progression of moderate pulmonary stenosis is not uncommon; mild pulmonary stenosis is rarely progressive [2].

Surgical intervention is necessary in symptomatic patients. Percutaneous balloon pulmonary valvotomy is widely used in the dome-shaped stenotic pulmonary valve. Recently, percutaneous valve replacement has been used in patients with dome-shaped stenotic valves [1]. Surgery is preferred in patients with dysplastic pulmonary valves and also in those with complications of pulmonary regurgitation, subvalvular stenosis, and severe tricuspid regurgitation [3]. The surgical approach includes a partial or total valvotomy, a transannular patch, and valve replacement. The latter is performed when there is significant valvular regurgitation. In addition, pulmonary homograft replacement may be needed. After interventions, patients should be followed for residual RVOT obstruction, pulmonary valve regurgitation, right ventricular dilatation and systolic dysfunction, and tricuspid valve regurgitation [2, 3].

### 14.1.2 Infundibular or Subvalvular Stenosis

Infundibular stenosis refers to obstruction at the level of the right ventricular infundibulum within the body of the

W. Mazur et al., *CT Atlas of Adult Congenital Heart Disease*,
DOI 10.1007/978-1-4471-5088-6_14, © Springer-Verlag London 2013

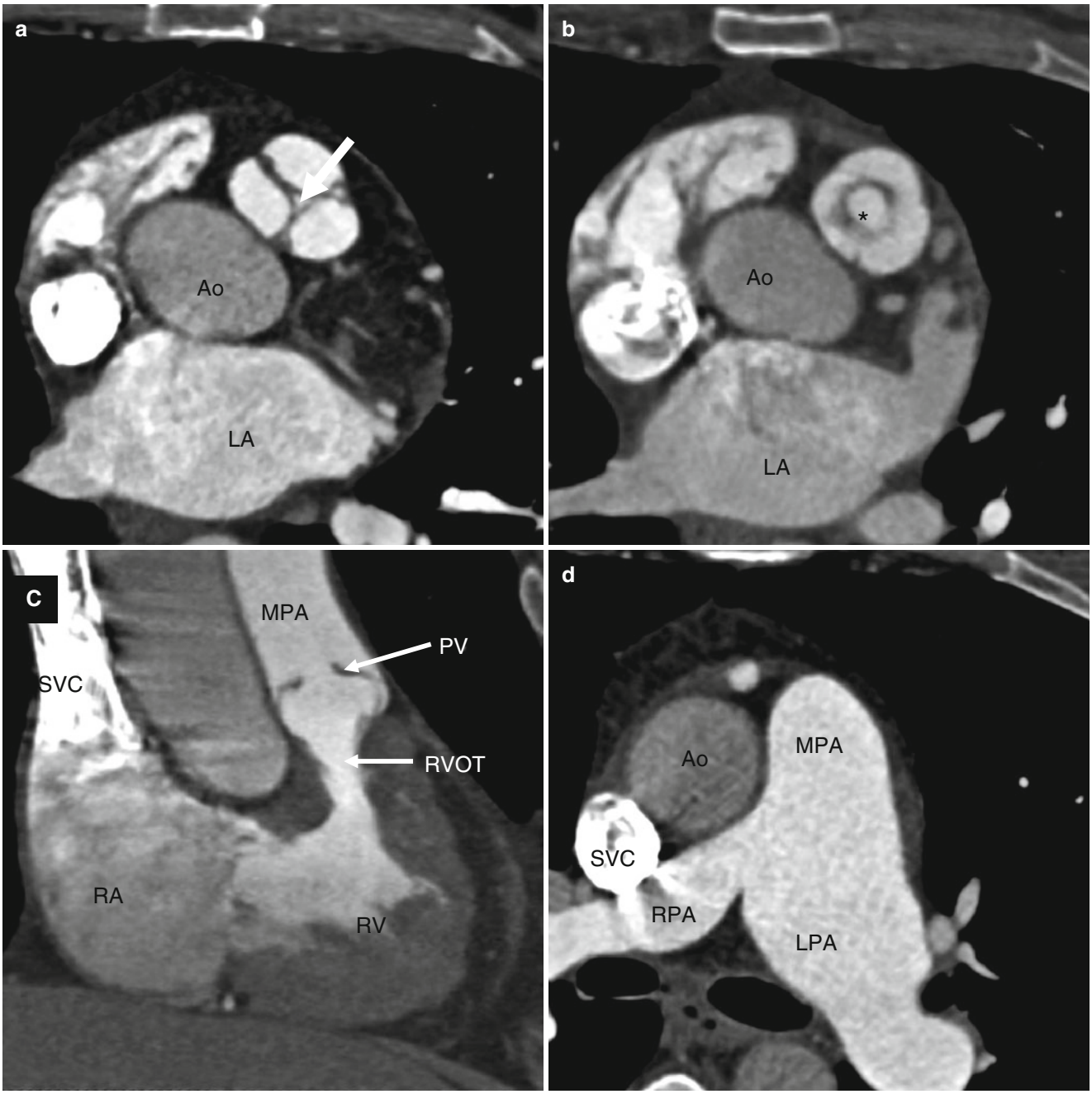


**Fig. 14.1** Valvular pulmonary stenosis. Panel (**a**) is an axial computed tomogram (CT) showing a trileaflet pulmonary valve with thickened commissures and a small central orifice (*arrow*). Panel (**b**) is a CT at a different anatomic level showing the stenotic pulmonary valve orifice (*asterisk*). Panel (**c**) depicts a coronal reformatted view showing the thickened and domed pulmonic valve (*PV*) and compensatory right ventricular (*RV*) hypertrophy with narrowing of the right ventricular outflow tract (*RVOT*). Panel (**d**) is an axial CT at a higher anatomic plane showing the dilated main (*MPA*) and left pulmonary (*LPA*) arteries. *RPA* right pulmonary artery, *SVC* superior vena cava, *Ao* aorta, *RA* right atrium

ventricle, as opposed to obstruction at the pulmonary valve, pulmonary artery, or its branches (Fig. 14.4). Primary infundibular stenosis is a rare cardiac malformation accounting for a small minority of RVOT obstruction.

There are two forms of infundibular stenosis. The first type is associated with a thickened muscular/fibrous infundibulum that narrows the right ventricular outlet. The narrowed area may be short or long and may be located immediately below the pulmonary valve or lower in the outflow tract. The second type is associated with stenosis of the infundibulum due to a fibrous or muscle band at the junction of the main cavity of the right ventricle and the infundibulum. The band divides the cavity into a high-pressure proximal and low-pressure distal chamber. This is referred to as a "double-chambered right ventricle" [3].

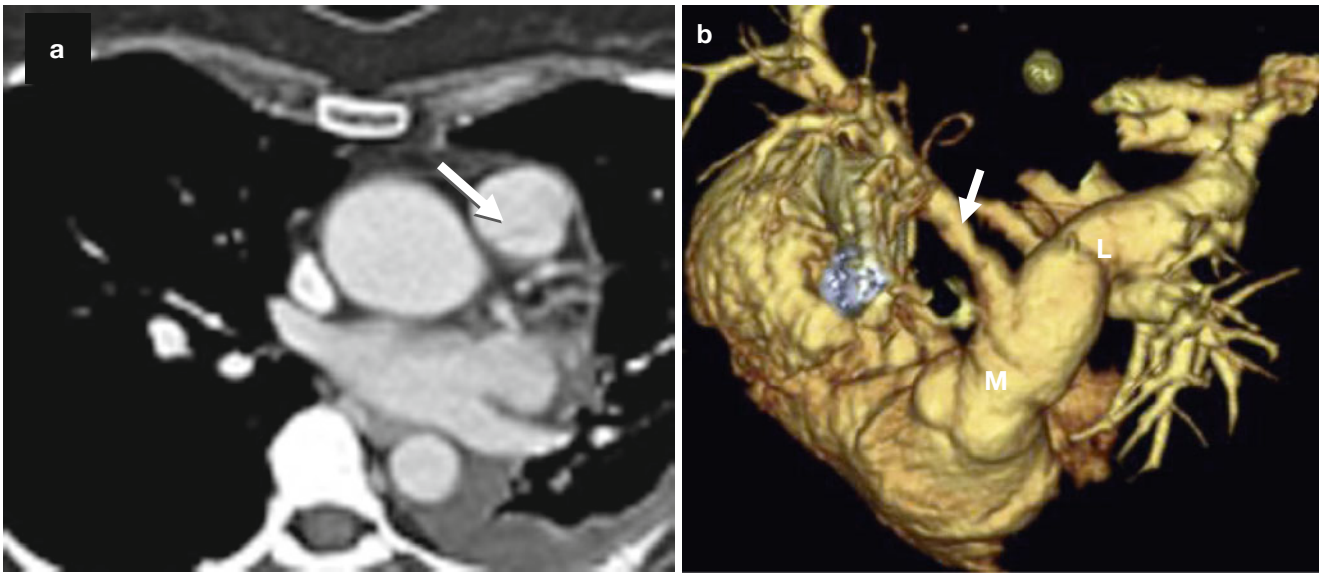


**Fig. 14.2** Bicuspid pulmonary valve. Panel (**a**) is an axial scan showing a pulmonic valve with two asymmetric cusps. The *arrow* points to the raphe between the two cusps. Panel (**b**) is a volume-rendered reconstruction showing the dilated main (*M*) and left (*L*) pulmonary arteries. For comparison, the right pulmonary artery (*arrow*) is of normal size

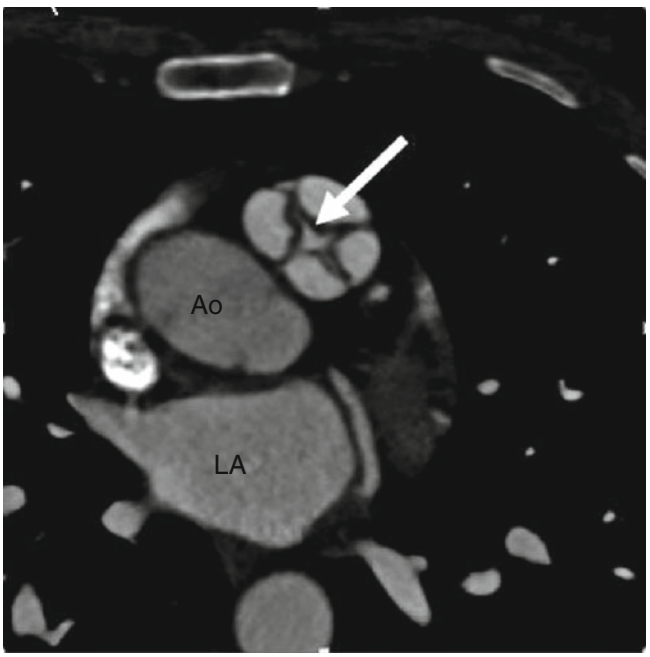


**Fig. 14.3** Quadricuspid pulmonic valve. An axial scan showing four pulmonary valve leaflets of equal size with commissural thickening and incomplete coaptation centrally (*arrow*). *Ao* aorta, *LA* left atrium

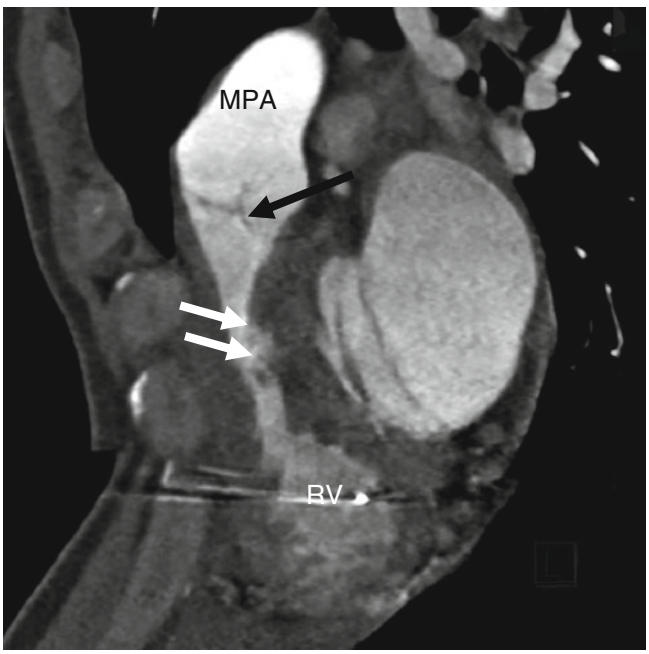


**Fig. 14.4** Subinfundibular pulmonary stenosis. Here is a reformatted image showing a narrowed infundibulum (*white arrows*). The pulmonic valve (*black arrow*) and main pulmonary artery (*MPA*) are normal. *RV* right ventricle

The anomalous muscle bundle may be an anomalous septoparietal band, anomalous apical shelf, or abnormal moderator band [1]. It typically extends between the interventricular septum (in the area of septomarginal trabeculation) and the anterior wall of the right ventricle and may take a diagonal or horizontal course through the ventricle [4]. Double-chambered right ventricles are rare, accounting for 1 % of congenital heart diseases [4]. Infundibular muscular obstruction is associated with ventricular septal defect, atrial septal defect, valvular pulmonary stenosis, tetralogy of Fallot, and double-outlet right ventricle [3].

The hemodynamic consequence of the obstruction is elevated pressure within the right ventricular cavity. This

high pressure is limited to the portion proximal or the infundibulum. Lower or even normal pressures are present beyond the obstruction site. RVOT obstruction usually progresses over time. Long-term complications include compensatory right ventricle hypertrophy with elevated end-diastolic pressures, elevated right atrial pressure and dilatation, and eventually right-sided heart failure. Complete or partial spontaneous closure of an associated ventricular septal defect may worsen the RVOT obstruction [3]. Most patients are diagnosed during childhood or adolescence and undergo surgical repair. However, unrepaired subinfundibular stenosis has been reported in adults [5–7].

Nonmuscular causes of infundibular obstruction are rare and include a prominent or displaced tricuspid valve, fibrous tags arising in the inferior vena cava or coronary sinus, sinus of Valsalva aneurysm, and aneurysm of the membranous portion of the interventricular septum [8–12].

Surgical intervention is considered in patients who are symptomatic or who have high-pressure gradients across the obstruction. Treatment of muscle bands involves resection of the muscle bundles and repair of associated lesions. Most patients do well after surgery and recurrence of obstruction is rare [13, 14]. Interventions for other subinfundibular obstructions include percutaneous balloon dilatation, stenting, and percutaneous alcohol ablation [15–17].

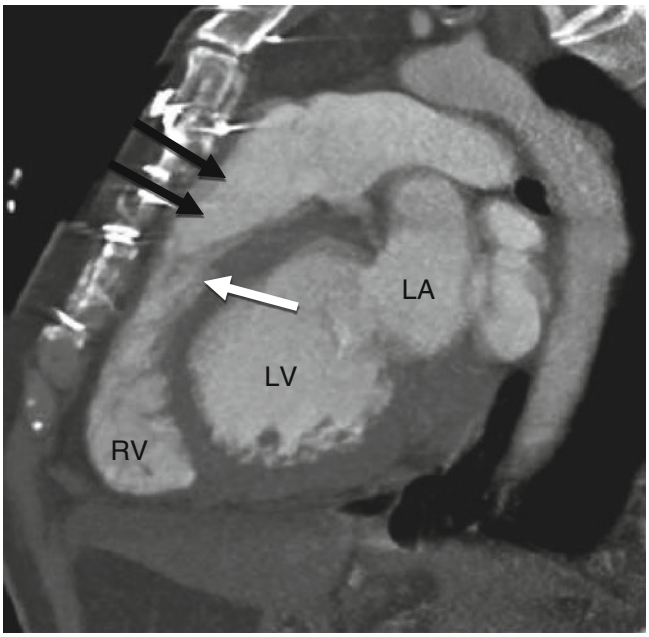


**Fig. 14.5** Supravalvular pulmonary stenosis in a patient with Williams syndrome. The patient had prior surgery for repair of a stenotic bicuspid aortic valve. This sagittal scan shows a narrowing of the main pulmonary artery (*black arrow*s) above the level of the pulmonic valve (*white arrow*). Left ventricular hypertrophy is related to recurrence of aortic valve stenosis

### 14.1.3 Supravalvular Stenosis

Supravalvular stenosis refers to obstruction at the level of the main, major, or peripheral pulmonary arteries [3]. Supravalvular stenosis is a rare abnormality that occurs in 2–3 % of patients with congenital heart disease (Fig. 14.5).

Supravalvular stenosis can involve the trunk, main, or peripheral pulmonary arteries. It can be isolated or involve multiple areas in one or both lungs [3, 18–20]. Based on the location, stenoses may be divided into four types. Type I is characterized by a single central stenosis (main, right, or left pulmonary artery). In type II, the stenosis is located at the bifurcation of the pulmonary arterial trunk, extending to the origins of the right and left pulmonary arteries. The type III stenoses are peripheral only. In type IV, there is combined central and peripheral stenoses [18]. Type I pulmonary supravalvular stenosis with central stenosis is most often associated with dilatation of the poststenotic portion of pulmonary. Poststenotic dilatation, if it occurs, is minimal in type II obstruction and is absent in type III stenosis. Most supravalvular stenoses are due to intimal or muscular proliferation but may be also produced by a pulmonary artery membrane or aneurysm [1].

A hemodynamically significant lesion is defined as ≥50 % diameter narrowing. In general, adults are asymptomatic unless they have high right ventricular pressures or associated cardiac disease. They may come to clinical attention because of a murmur, or they may be referred for computed tomographic angiography of a dilated main pulmonary artery found on a plain radiography [3]. Symptoms can mimic those of pulmonary thromboembolic disease and include fatigue and dyspnea.

Supravalvular stenosis is frequently associated with Noonan syndrome, Williams syndrome, tetralogy of Fallot, trisomy 21 syndrome, and Ehlers–Danlos syndrome and may be detected incidentally during evaluation of these conditions. These lesions, particularly peripheral stenoses, may be progressive.

Treatment of hemodynamically significant focal main, branch, or peripheral pulmonary artery stenoses is usually performed by balloon angioplasty. Patients with main or bifurcation stenoses who are not candidates for percutaneous intervention or who fail percutaneous angioplasty may require surgical dilatation or resection of the stenotic area to relieve right ventricular hypertension. Peripheral stenotic segments are usually not amenable to surgical intervention [3]. Recurrence of stenosis is not uncommon, particularly in peripherally stenotic lesions [3].

**Table 14.1** Evaluation of right ventricular outflow tract obstruction with computed tomography

| |
|---|
| Morphology, hypertrophy, size, and systolic function of right ventricle |
| Morphology and size of right atrium |
| Morphology, size, and function of pulmonic valve, including the systolic orifice area, and the presence of valvular regurgitation |
| Presence, size, morphology, and site of infundibular or subinfundibular obstruction |
| Presence, size, morphology, and site of pulmonary artery(ies) obstruction |
| Anatomy, size, and function of tricuspid valve |
| Coexisting anomalies |

### 14.1.4 Cardiac Computed Tomography (CT) in the Evaluation of Pulmonary Valve Abnormalities

CT can be a useful noninvasive modality when echocardiography and magnetic resonance do not provide sufficient data. It is especially useful for assessment of peripheral pulmonary artery stenosis [3, 21, 22]. CT findings of pulmonary valve obstruction include a narrowed or stenotic segment with or without poststenotic dilatation of the distal arterial segments, a jet of contrast material extending across a narrowed segment, and right ventricular hypertrophy. The elevated right ventricular pressure and volume may cause bowing of the interventricular septum to the left.

In valvular pulmonic stenosis, the main and left pulmonary arteries are dilated (see Figs. 14.1 panel d and 14.2 panel b). The turbulent jet across the valve extends preferentially into the main and left pulmonary arteries, sparing the right pulmonary artery. Poststenotic dilatation is less common with dysplastic valves than it is with the dome-shaped mobile pulmonic valves. Cine images may show decreased mobility of the valve leaflets.

CT assessments should include evaluation of (a) the morphology, wall thickness, size, and systolic function of right ventricle; (b) the morphology and size of the right atrium; (c) the morphology, size, and function of the pulmonary valve, including the systolic orifice area, and the presence of associated pulmonary valvular regurgitation; (d) the presence, site, morphology, and size of infundibular and subinfundibular obstruction; (e) the presence, size, morphology, and site of pulmonary artery obstruction; (f) the anatomy, size, and function of the tricuspid valve; and (g) coexisting anomalies. See Table 14.1. CT may also depict bronchial compression by the dilated pulmonary arteries, which cannot be demonstrated by echocardiography. In addition, rare complications such as compression of contiguous cardiac structures including compression of left main coronary artery may be detected with CT [3].

Following interventions, cardiac CT can be used to exclude or confirm recurrent obstruction. The major limitation of cardiac CT is its inability to measure pressure gradients across the stenotic lesions.

## 14.2 Pulmonary Atresia with Intact Ventricular Septum

### 14.2.1 Definition

Pulmonary atresia with intact ventricular septum is a rare congenital heart anomaly characterized by an atretic pulmonary valve, variable degrees of right ventricular and tricuspid valve hypoplasia, and coronary artery anomalies [23].

This anomaly accounts for 3 % of congenital heart defects with an incidence of 0.08 per 1,000 live births [24]. Despite the low prevalence, it is not an uncommon cause of cyanotic heart diseases in neonates.

### 14.2.2 Morphology

In this disorder, right ventricular morphology may vary. In its most mild form, there is a mildly hypoplastic chamber with a well-formed infundibulum and imperforate tricommissural pulmonary valve. As the severity progresses, a moderately hypoplastic chamber to a severely hypoplastic chamber with a narrowed or atretic infundibulum may be seen. Finally, a dysplastic pulmonary valve and ventriculocoronary artery connections may occur [25]. See Figs. 14.6 and 14.7. In addition, the tricuspid valve is dysplastic and demonstrates a spectrum of abnormalities, ranging from severe stenosis to severe regurgitation [26]

The diminutive, hypertrophic right ventricle often exhibits diffuse fibroelastosis [27, 28]. Ebstein anomaly coexists in 10 % of cases [26]. Furthermore, there is an obligatory right-to-left atrial shunt (via a patent foramen ovale or atrial septal defect). Pulmonary blood flow usually depends on a patent ductus arteriosus. Aortopulmonary collaterals originating from the thoracic aorta are rarely seen. The main, right, and left pulmonary arteries are usually small but rarely are atretic (Fig. 14.8).

The right atrium is usually enlarged. Left-sided volume overload from right-to-left atrial shunting can result in left atrial and left ventricular enlargement. Distortion of the interventricular septum and right ventricular hypertrophy may cause left ventricular outflow tract obstruction. Right ventricle-to-coronary artery fistulas (sinusoids), with or without stenosis, atresia, or ectasia, occur in nearly 50 % of patients at birth [25].

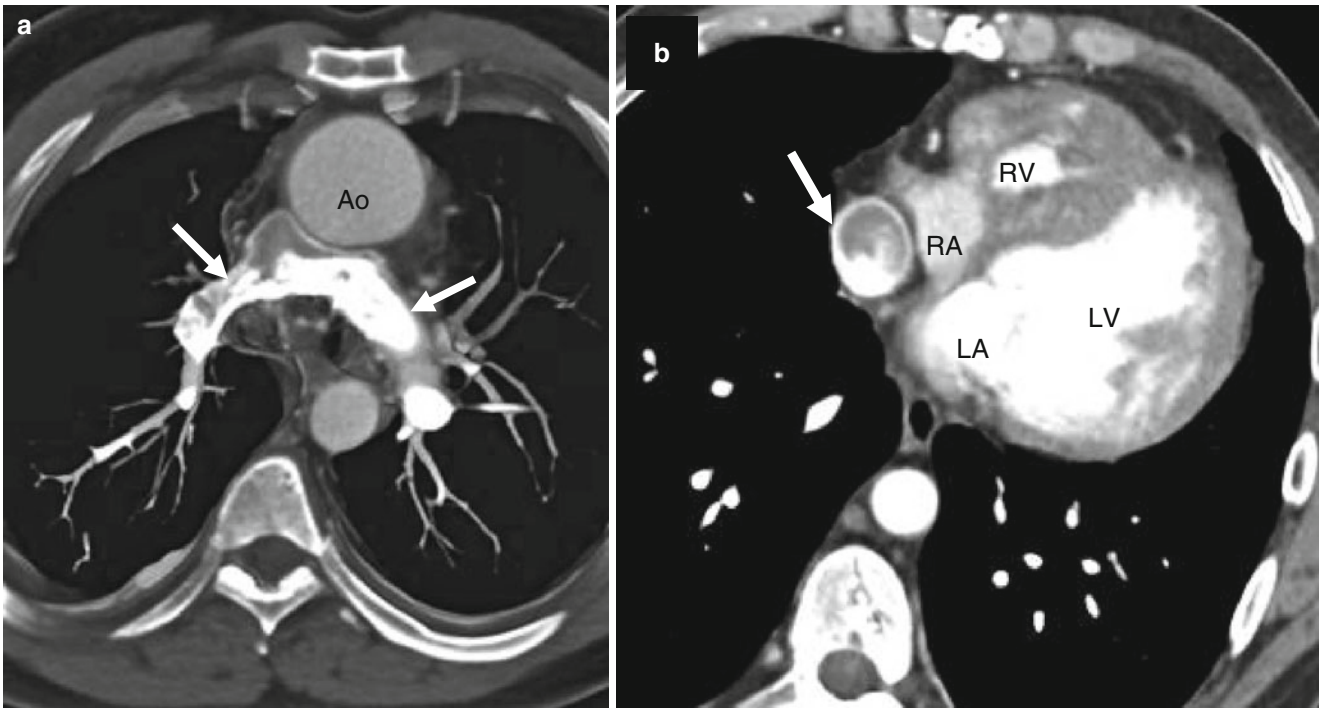


**Fig. 14.6** Pulmonary atresia with intact ventricular septum in a 32-year-old man with ventriculocoronary connections who underwent a Fontan procedure. Panel (**a**) is an axial computed tomogram (CT) showing the absence of the main pulmonary artery and slightly diminutive right and left pulmonary arteries (*arrows*). Panel (**b**) is an axial CT at a more caudal plane demonstrating a severely hypoplastic right ventricle (*RV*) and the Fontan conduit (*arrow*). For comparison, the left ventricle (*LV*) is normal in size. *Ao* aorta, *LA* left atrium, *RA* right atrium

### 14.2.3 Clinical Findings

Patients present in the neonatal period with cyanosis. Early survival depends on ductal patency until surgical repair can be performed to establish adequate pulmonary blood flow. Patients who have not undergone early surgical repair and have a patent ductus arteriosus may present as adults with dyspnea and mild central cyanosis [29, 30]. Surgically treated patients can present later in life with complications related to surgery [31, 32] and/or with sudden death, angina, and/or arrhythmias related to poor myocardial perfusion [26, 33].

### 14.2.4 Surgical Repairs

A palliative systemic-to-pulmonary artery shunt is done early in the neonatal period to establish an adequate source of pulmonary blood flow. The choice of subsequent definitive repair depends on the size and morphology of the right ventricle and tricuspid valve as well as the presence and extent of ventriculocoronary artery sinusoids (right-ventricular-dependent coronary circulation). The surgical options include biventricular, one-and-a-half-ventricle, and univentricular approaches [34]. Patients with the Ebstein-like variant may require tricuspid valve repair or conversion to tricuspid atresia physiology [35]. Patients with severe right ventricle-to-coronary artery sinusoids may need cardiac transplantation [36].

The biventricular repair approach is utilized if there is mild right ventricular and tricuspid valve hypoplasia without ventriculocoronary connections and without right ventricular outflow tract obstruction; a patch graft enlargement of the outflow tract and a surgical valvotomy (or, more recently, transcatheter perforation of the pulmonary valve) are performed. Controversy exists regarding the efficacy and safety of transcatheter valvotomy [36]. Procedure-related complications are not uncommon with this repair, with the mortality reaching 6 %. In addition, a substantial proportion of patients who undergo catheter valvotomy will need additional systemic-to-pulmonary shunts [37]. Pulmonary valvotomy is not performed in patients with right-ventricular-dependent coronary circulation since it can cause flow reversal in the ventriculocoronary sinusoids (coronary steal-like phenomenon), leading to myocardial ischemic injury.

The one-and-a-half-ventricle approach is applied when there is moderate to severe right ventricular and tricuspid

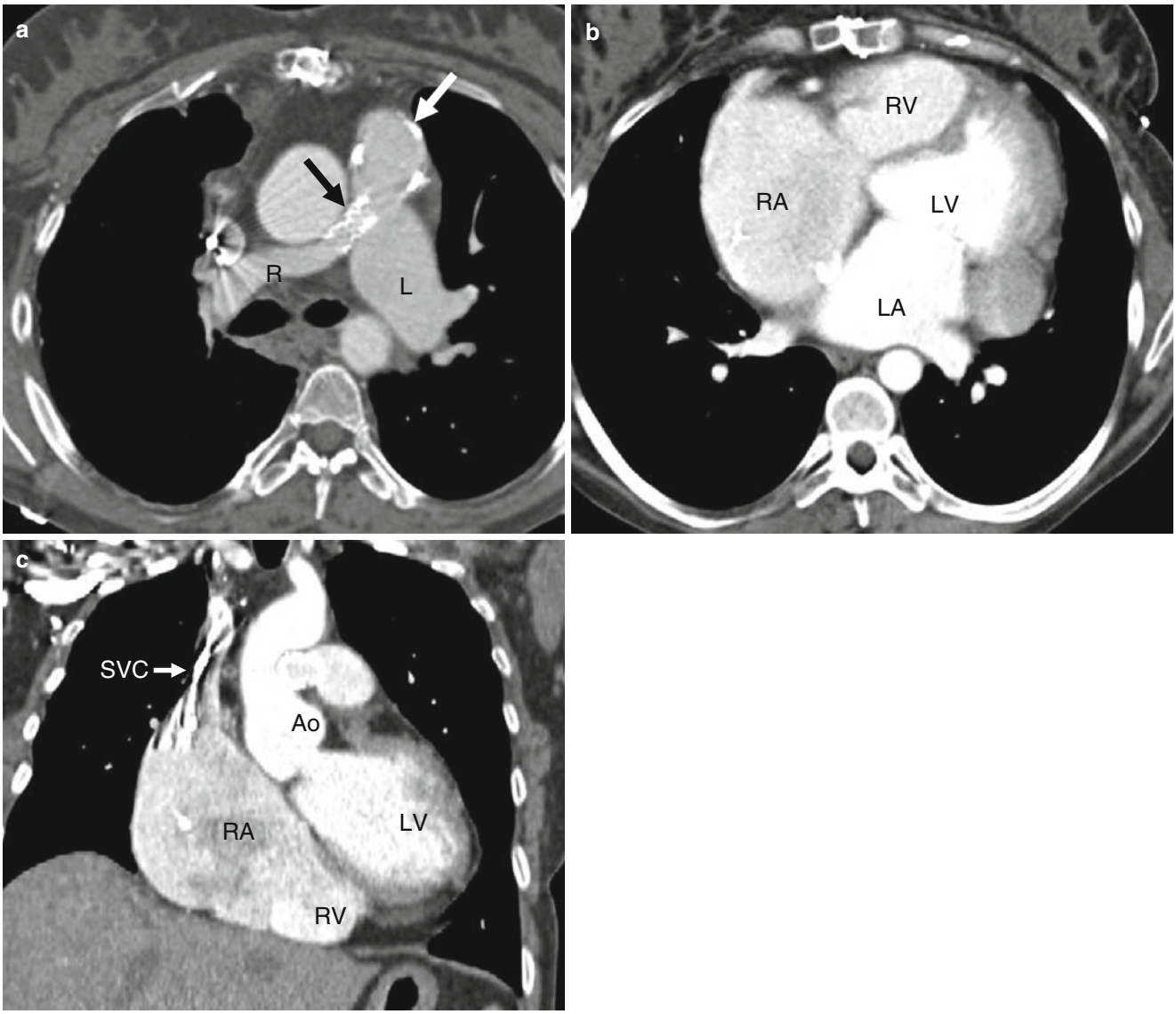


**Fig. 14.7** Pulmonary atresia with intact ventricular septum. This is an example of a 40-year-old woman who had undergone right ventricular outflow tract reconstruction, patch enlargement of the main pulmonary artery, and stenting of the right pulmonary artery as a child. Panel (**a**) an axial scan showing a calcified pulmonary artery patch graft (*white arrow*) and a stent (*black arrow*) in a small proximal right pulmonary artery (*R*). The left pulmonary artery (*L*) is normal size. Panels (**b**) (coronal section) and **c** (axial slice) show mild to moderate right ventricle (*RV*) hypoplasia, normal left ventricle (*LV*) size, and right atrial (*RA*) enlargement. The streaks in the superior vena cava (*SVC*) are flow artifacts. *LA* left atrium, *Ao* aorta

valve hypoplasia without ventriculocoronary connections; right ventricular outflow tract reconstruction and surgical or percutaneous valvotomy with bidirectional cavopulmonary anastomosis is performed [36]. An atrial septostomy may be needed to decompress the right atrium [38].

Finally, the univentricular approach is undertaken if the right ventricle and tricuspid valve are severely hypoplastic with ventriculocoronary connections and right-ventricular-dependent coronary circulation; a univentricular Fontan repair is needed to provide blood flow to the pulmonary arteries. Balloon arterial septostomy is usually performed as well [34].

### 14.2.5 Outcomes and Complications

If untreated, pulmonary atresia with intact ventricular septum is associated with poor outcomes. After biventricular and one-and-a-half-ventricle repair, patients may develop obstruction at the level of the pulmonic valve, right ventricular outflow tract, or pulmonary artery and/or pulmonary valve. In addition, tricuspid regurgitation may ensue. After the univentricular and one-and-a-half-ventricle repair, obstruction of systemic-to-pulmonary connections and restriction of the interatrial communication may result. Finally, myocardial ischemia may occur and may be related

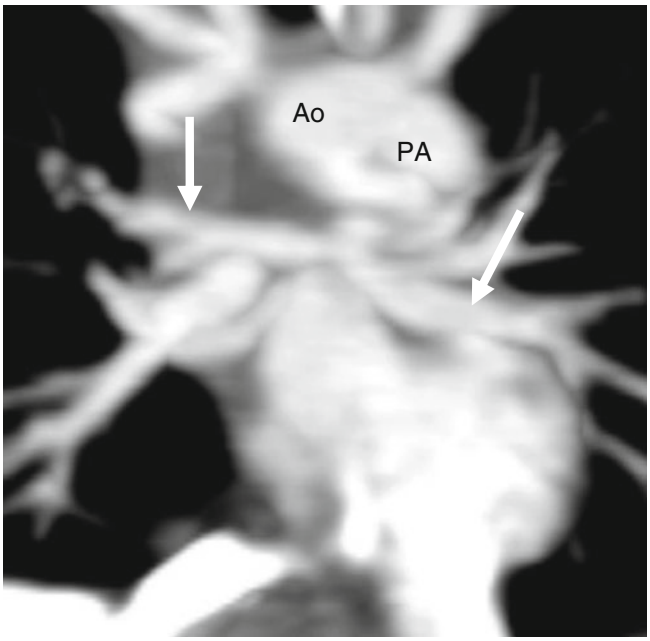


**Fig. 14.8** Pulmonary atresia with intact ventricular septum. This coronal reconstruction shows small main (*PA*) as well as small right and left pulmonary arteries (*arrows*). *Ao* aorta

**Table 14.2** Postoperative complications after corrective procedures for pulmonary atresia with intact ventricular septum

| |
|---|
| Left/right ventricular dilatation and systolic dysfunction |
| Obstruction at pulmonary valve, right ventricular outflow tract, and/or pulmonary artery(ies) |
| Pulmonary valve regurgitation |
| Tricuspid regurgitation |
| Obstruction of systemic-to-pulmonary connections |
| Coronary artery anomalies including coronary artery fistulas (especially to the right ventricle), stenoses, ectasia, and interruptions |
| Restriction of atrial connection, if present |
| Residual intracardiac connections |

to coronary artery anomalies [34]. Left, right, or biventricular dilatation and systolic dysfunction are also seen after these repairs. See Table 14.2.

### 14.2.6 Cardiac Computed Tomography (CT) in the Evaluation of Pulmonary Atresia with Intact Ventricular Septum

CT is a noninvasive modality for assessing patients with pulmonary atresia and intact ventricular septum when the echocardiographic and cardiac magnetic resonance evaluations are not diagnostic. CT assessment should include the evaluation of (a) the morphology, thickness, size, and systolic function of the ventricles; (b) the morphology and size of the atria and pulmonary arteries; (c) the presence and extent of residual pulmonary valve and right ventricular outflow tract obstruction especially after biventricular and one-and-a-half-ventricle repair; (d) the anatomy and function of the cardiac valves, especially the presence of pulmonary and tricuspid valve regurgitation after biventricular and one-and-a-half-ventricle repair; (e) the presence and patency of systemic-to-pulmonary connections; (f) the presence and magnitude of coronary artery anomalies including coronary artery fistulas, stenoses, ectasia, and interruptions; (g) the presence of residual intracardiac connections; and (h) coexisting anomalies. See Table 14.3.

**Table 14.3** The computed tomography assessment of pulmonary atresia with intact ventricular septum

| |
|---|
| Morphology, size, and systolic function of both ventricles |
| Morphology and size of atria |
| Presence and extent of residual pulmonary valve and right ventricular outflow tract obstruction |
| Anatomy and function of cardiac valves, including the size and presence of regurgitation of pulmonary and tricuspid valve |
| Presence and direction of interatrial shunts |
| Presence, patency, and direction of systemic-to-pulmonary connections |
| Presence and magnitude of coronary artery anomalies including coronary artery fistulas (especially to the right ventricle), stenosis, ectasia, and interruptions |
| Coexisting anomalies |

## 14.3 Pulmonary Atresia with Ventricular Septal Defect

### 14.3.1 Definition

Pulmonary atresia with ventricular septal defect (PA–VSD) is a heterogeneous malformation characterized by absence of luminal continuity between the right ventricle and pulmonary artery and a ventricular septal defect [39]. This anomaly has also been referred to as "pseudotruncus arteriosus" and "truncus arteriosus type 4." PA–VSD accounts for 2 % of congenital heart diseases with an incidence of 0.07 per 1,000 live births [40]. It is one of the common causes of cyanosis and hypoxemia in neonates [41, 42].

### 14.3.2 Morphology

In all cases of PA–VSD, there is absence of continuity between the right ventricle and pulmonary circulation. The central pulmonary arteries may be hypoplastic or absent, and the right and left pulmonary artery may communicate with each other (confluent pulmonary arteries) or may not

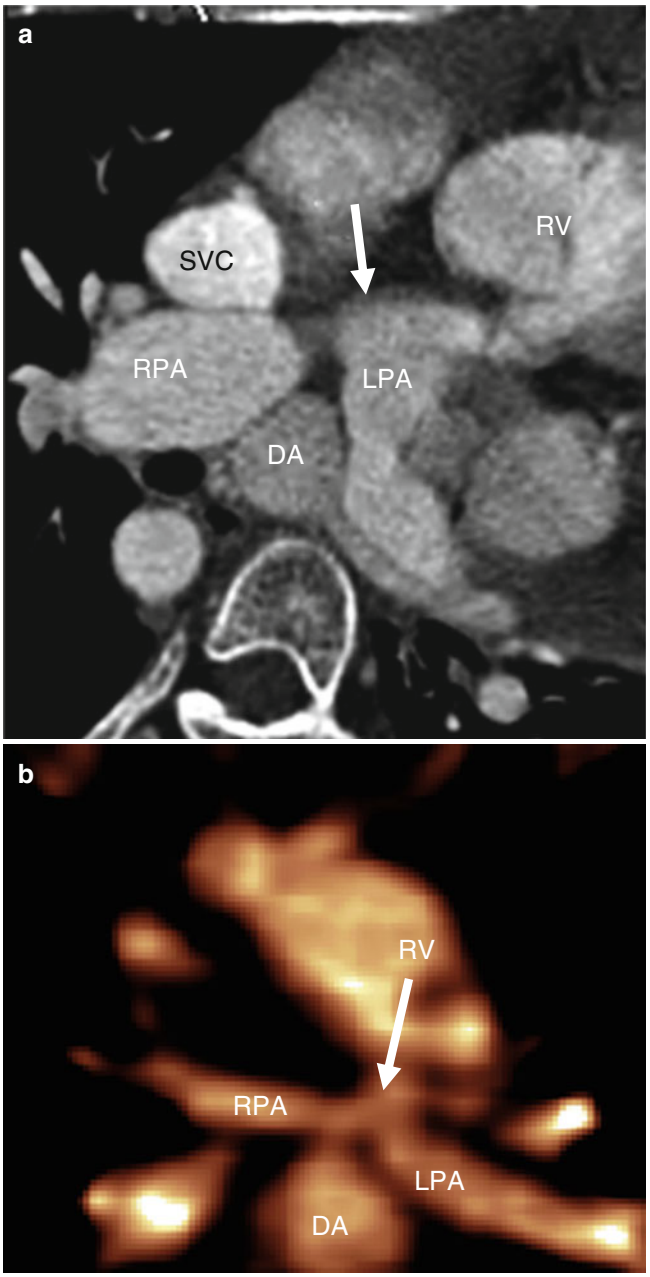


**Fig. 14.9** Pulmonary atresia with ventricular septal defect in two adults. Panel (**a**) is an axial reconstruction and panel (**b**) is a volume-rendered reformat. Each panel shows confluent pulmonary arteries (*arrow*). *RPA* right pulmonary artery, *LPA* left pulmonary artery, *DA* descending aorta, *RV* right ventricle

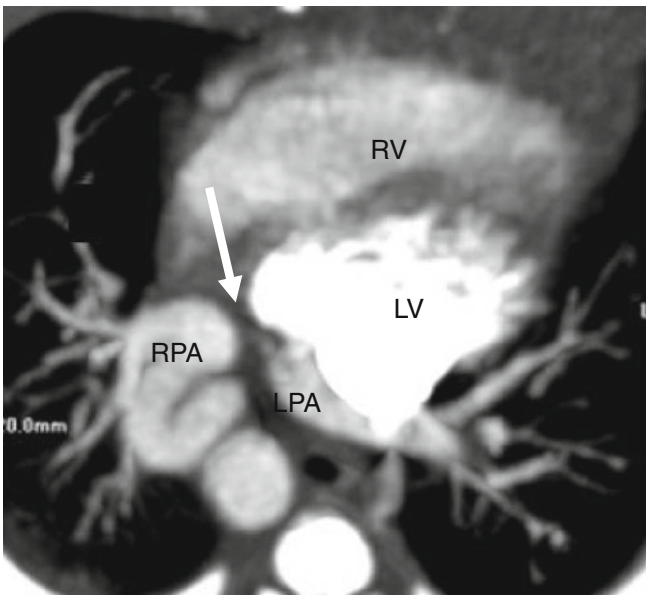


**Fig. 14.10** Pulmonary atresia with ventricular septal defect. This oblique, axial image shows nonconfluent right and left pulmonary arteries. The *arrow* points to the area of nonconfluence. *RPA* right pulmonary artery, *LPA* left pulmonary artery

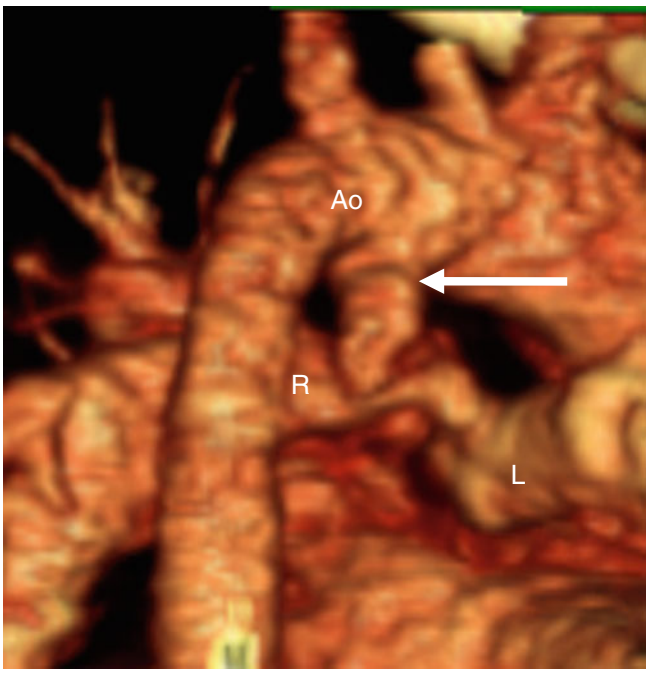


**Fig. 14.11** An example of type A pulmonary atresia with ventricular septal defect. Volume-rendered image shows confluent pulmonary arteries supplied by a patent ductus arteriosus (*arrow*) without major aortopulmonary collateral arteries. The pulmonary arteries are of adequate size. *R* right pulmonary artery, *L* left pulmonary artery

communicate (nonconfluent arteries) (Figs. 14.9 and 14.10) [39]. The blood supply to the lungs originates from a patent ductus arteriosus (PDA) and/or major aortopulmonary collateral arteries (MAPCAs).

Based on the morphology of the pulmonary circulation, PA–VSD is classified into three types. In type A, the native pulmonary arteries are present and are supplied by a patent ductus arteriosus (Fig. 14.11). There are no MAPCAs. In type B, the pulmonary blood flow is supplied by both native pulmonary arteries and MAPCAs (Fig. 14.12). In type C, the native pulmonary arteries are absent and the pulmonary circulation is only supplied by MAPCAs (Figs. 14.13 and 14.18) [43].

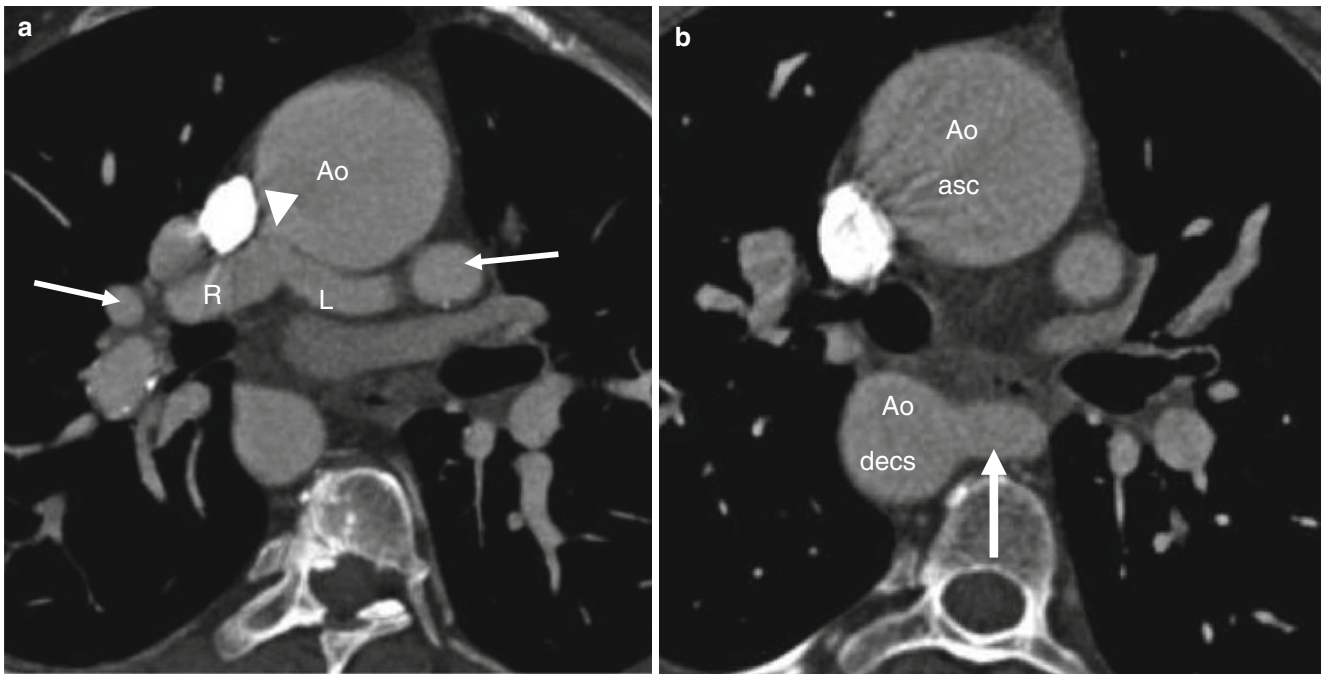


**Fig. 14.12** Type B pulmonary atresia with ventricular septal defect. A 40-year-old woman who underwent placement of a Waterston shunt at age 7 years and no additional surgical procedures. Panel (**a**) an axial computed tomography (CT) view shows separate branches of the left (*L*) and right (*R*) pulmonary arteries supplying the lungs. There are also hilar major aortopulmonary collateral vessels (MAPCAs) (*arrows*). Also note a right-sided aorta (*Ao*). The *arrowhead* denotes the Waterston shunt from the ascending aorta to the right pulmonary artery. Panel (**b**) an axial CT in a more superior plane shows a large left aortopulmonary collateral (MAPCA) (*arrow*) arising from a right-sided aorta (*Ao*)

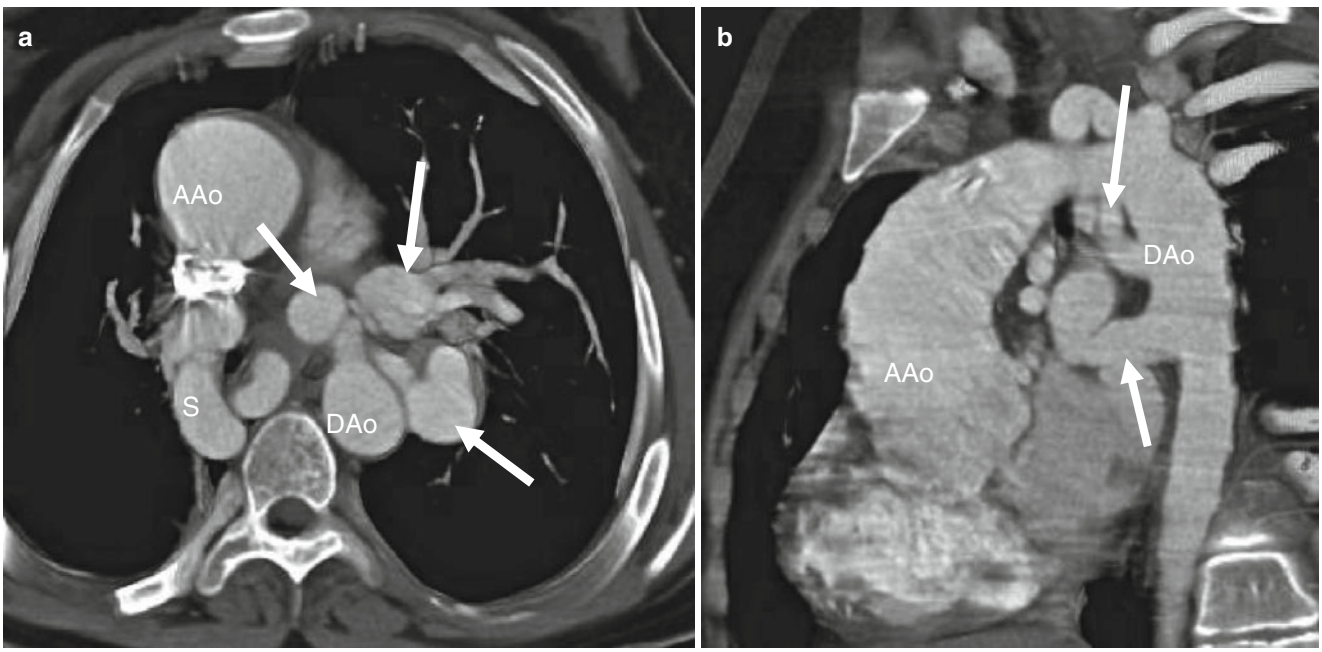


**Fig. 14.13** Type C pulmonary atresia with ventricular septal defect. An 18-year-old man who underwent a Blalock–Taussig shunt at age 3 years and no additional surgery. Panel (**a**) an axial CT shows multiple large aortopulmonary collaterals (MAPCAs) (*arrows*) and an enlarged ascending aorta (*AAo*). Panel (**b**) an oblique, sagittal view shows the entire pulmonary flow supplied by large major aortopulmonary collateral arteries (MAPCAs) (*arrows*) from the descending aorta (*Dao*). No native pulmonary arteries are seen. Again note the dilated ascending aorta (*Aao*). *S* superior vena cava

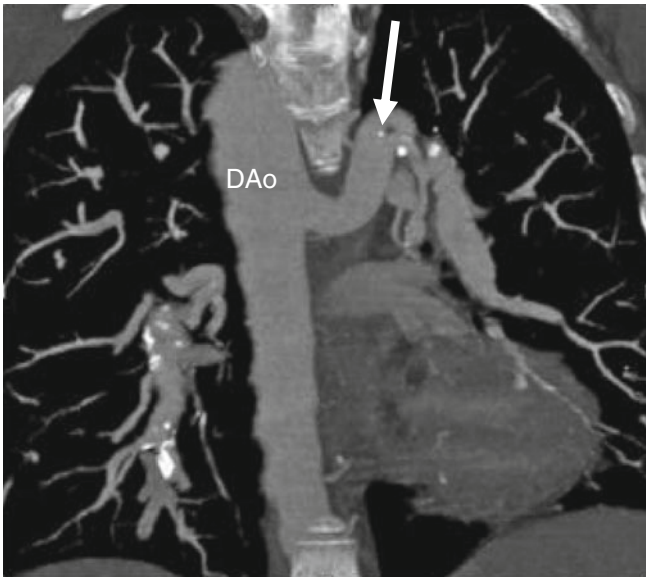


**Fig. 14.14** Major aortopulmonary collateral arteries (MAPCAs). A coronal view scan showing a large MAPCA (*arrow*) arising from the descending aorta (*Dao*) and connecting to the native pulmonary artery in the left hilum

MAPCAs represent fetal primitive intersegmental arteries that have failed to involute. They usually originate from the descending aorta and less often from the aortic arch, and they connect the systemic circulation to the native pulmonary arteries in the mediastinum or at the hilar, lobar, or segmental levels (Figs. 14.12, 14.13, and 14.14). Rarely, the bronchial, subclavian, internal mammary, intercostal, carotid, and/or coronary arteries will perfuse the pulmonary arteries. MAPCAs differ from bronchial arteries in several ways [44]. MAPCAs do not branch in the mediastinum, whereas bronchial arteries provide mediastinal branches. MAPCAs may follow the bronchi but do not supply branches to the bronchi. Unlike bronchial arteries, MAPCAs are not connected to intercostal arteries. Finally, MAPCAs have an elastic wall structure similar to that of the pulmonary artery or aorta and the bronchial arteries do not.

Stenosis is common in MAPCAs, particularly at the sites of aortic origin and pulmonary anastomoses. These stenoses may serve to protect the pulmonary circulation from pulmonary arterial hypertension. When MAPCAs are long standing, aneurysmal dilatation can occur (Fig. 14.15).

The patent ductus arteriosus (PDA) serves as a source of pulmonary blood flow. When the PDA connects with the central pulmonary artery confluence, the pulmonary arteries usually are of adequate size and there are no MAPCAs (see Fig. 14.11). When a PDA connects with only one pulmonary artery, there may be MAPCAs in the contralateral hemithorax.

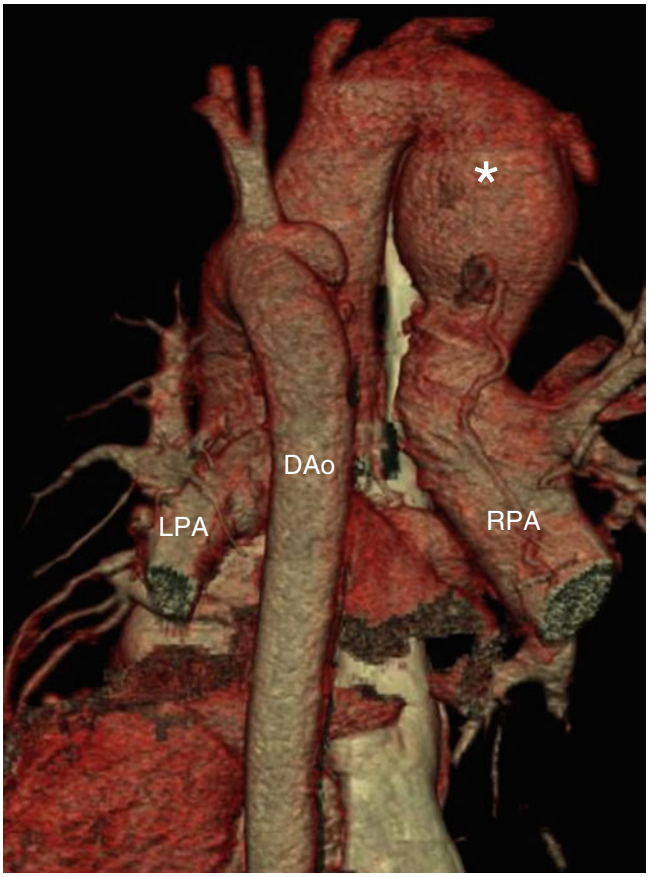


**Fig. 14.15** Aneurysmal dilatation of major aortopulmonary collateral artery (MAPCA) in 28-year-old man with pulmonary atresia with ventricular septal defect. An oblique lateral volume-rendered image demonstrates an aneurysmally dilated MAPCA (*asterisk*) that arises from the right brachiocephalic artery to supply the right pulmonary artery (*RPA*). *LPA* left pulmonary artery, *DAo* descending aorta (Images provided courtesy of Ramiah Rajeshkannan, Ponekara, India)

The VSD in PA–VSD is usually the membranous, nonrestrictive type (Fig. 14.16). The aorta can be entirely connected to the left ventricle or it may override the interventricular septum.

### 14.3.3 Associated Anomalies

Other anomalies associated with PA–VSD include heterotaxy, abnormalities of atrioventricular and ventriculoarterial connections (double-outlet right ventricle, double-outlet left ventricle, and transposition of great arteries), coronary artery anomalies (high takeoff of the coronary ostia), fistula(s) between coronary and pulmonary arteries, and aberrant origin of the right coronary artery from the left coronary sinus [44]. In addition, anomalies of the pulmonary and systemic venous systems (partial or total anomalous pulmonary

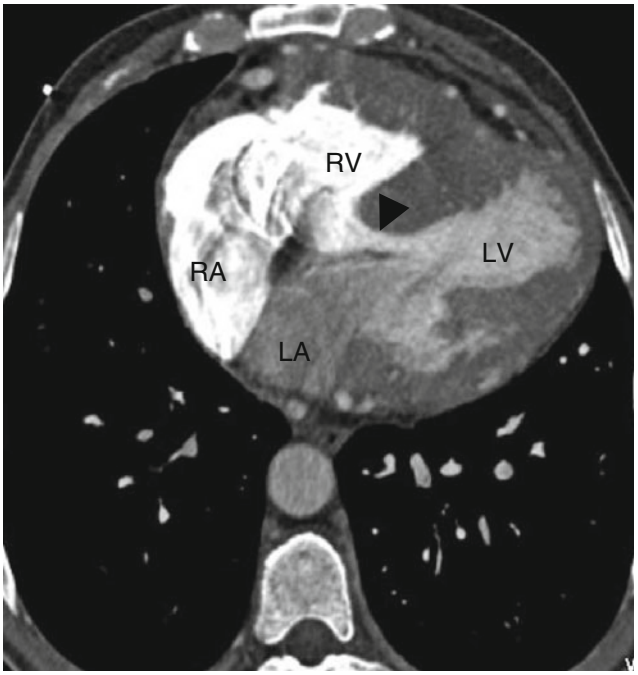


**Fig. 14.16** Ventricular septal defect (VSD) in a patient with pulmonary atresia and VSD. This axial CT shows a large subaortic (membranous) type VSD (*arrowhead*)

venous return, left-sided or bilateral superior venae cavae, and interrupted inferior vena cava) may accompany PA–VSD. Like tetralogy of Fallot with pulmonary stenosis, a right-sided aortic arch is frequently seen in PA–VSD (up to 25 % of cases) [45].

### 14.3.4 Clinical Features

Newborns with PA–VSD present with cyanosis and hypoxemia. Adults with palliated or unrepaired PA–VSD may present with central cyanosis, progressive dyspnea, and/or irreversible pulmonary hypertension due to overperfusion of the pulmonary circulation by MAPCAs.

### 14.3.5 Interventions

Surgical treatment is largely determined by the pulmonary artery morphology and the presence and extent of MAPCAs. If the native pulmonary arteries are well developed and there are no MAPCAs, palliative procedures (bidirectional Glenn shunt, Blalock–Taussig shunt, or Fontan procedure) can be performed in infants, and complete repair with a right ventricle-to-pulmonary artery conduit can be performed in older children. If there are multiple MAPCAs, a unifocalization procedure (connecting all MAPCAs to native pulmonary arteries) is needed before the complete repair [41]. Unifocalization is achieved by separating the MAPCAs from their systemic origin and joining them to a central pulmonary artery confluence via either a direct anastomosis or a prosthetic graft (Fig. 14.17).

### 14.3.6 Outcomes and Complications

Long-term survival of patients with PA–VSD is poor if palliation or repair is not performed [46]. Without surgical interventions, survival into adulthood is extremely rare and generally does not exceed three decades [47, 48]. The 5-, 10-, 15-, and 20-year long-term survival in palliated patients (those who only underwent systemic-to-pulmonary artery shunts, unifocalization, or right ventricular outflow tract repair without VSD closure) is 83, 73, 61, and 61 %, respectively [49]. In contrast, in repaired subjects the long-term survival is 92 % at 5 years, 86 % at 10 years, 83 % at 15 years, and 75 % at 20 years [48].

The late postoperative complications include (a) right and left ventricle failure and systolic dysfunction, (b) right ventricle-to-pulmonary artery conduit stenosis and/or regurgitation, (c) right ventricular outflow tract obstruction, (d) tricuspid valve regurgitation, (e) aortic root/annulus dilatation and aortic valve regurgitation, (f) residual MACPAs including stenosis/dilatation, (g) unifocalization and systemic-to-pulmonary shunt obstructions, and (h) residual intracardiac defects and endocarditis [43].

Table 14.4 lists the postoperative complications in the repair of PA–VSD.

### 14.3.7 Cardiac Computed Tomography (CT) in the Evaluation of Pulmonary Atresia with VSD

When echocardiography and magnetic resonance imaging cannot yield adequate diagnostic data, CT can be valuable to

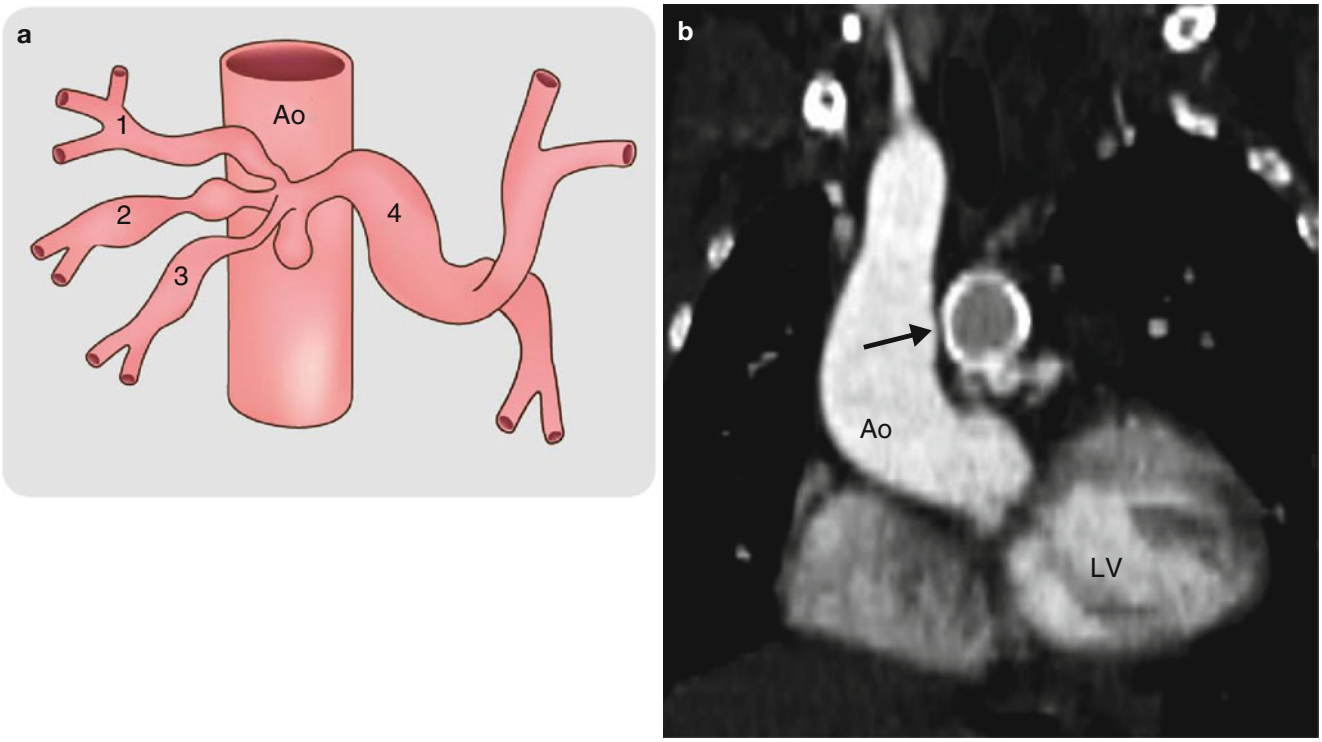


**Fig. 14.17** Unifocalization procedure. Panel (**a**) is a diagram showing the anastomosis of the bilateral major aortopulmonary collateral arteries (MAPCAs) (labeled *1*, *2*, and *3*) into a central conduit (*4*). This connects the aortopulmonary collateral vessels which have been ligated from the descending aorta to the pulmonary arterial confluence. Panel (**b**) is a coronal image showing a unifocalization conduit (*arrow*). *Ao* aorta, *LV* left ventricle

**Table 14.4** A list of the important potential postoperative complications after surgery to palliate pulmonary atresia with ventricular septal defect

| |
|---|
| Left/right ventricular dilatation and systolic dysfunction |
| Right ventricle-to-pulmonary artery conduit obstruction/regurgitation |
| Right ventricular outflow tract or pulmonary artery obstruction |
| Tricuspid regurgitation |
| Aortic root/annulus dilatation and aortic valve regurgitation |
| Residual MAPCAs, including presence of stenosis and/or dilatation |
| Systemic-to-pulmonary connection obstruction |
| Residual intracardiac connections |
| Intracardiac thrombi |
| Endocarditis |

depict the morphology of the pulmonary arteries and MAPCAs and postoperative complications [48, 50–53]. CT assessments should include delineation of (a) ventricular morphology, wall thickness, size, and systolic function, (b) atrial morphology and size, (c) right ventricular outflow tract size and patency, (d) right ventricle-to-pulmonary artery conduit obstruction or regurgitation, (e) pulmonary artery and MAPCA size and patency including unifocalization anatomy, (f) systemic-to-pulmonary connection patency, (g) tricuspid and aortic valve size and regurgitation, (h) aortic annulus and root size, (i) a residual ventricular septal defect, and (j) other anomalies.

Table 14.5 depicts the important aspects in the CT evaluation of PA–VSD before and after surgical palliation.

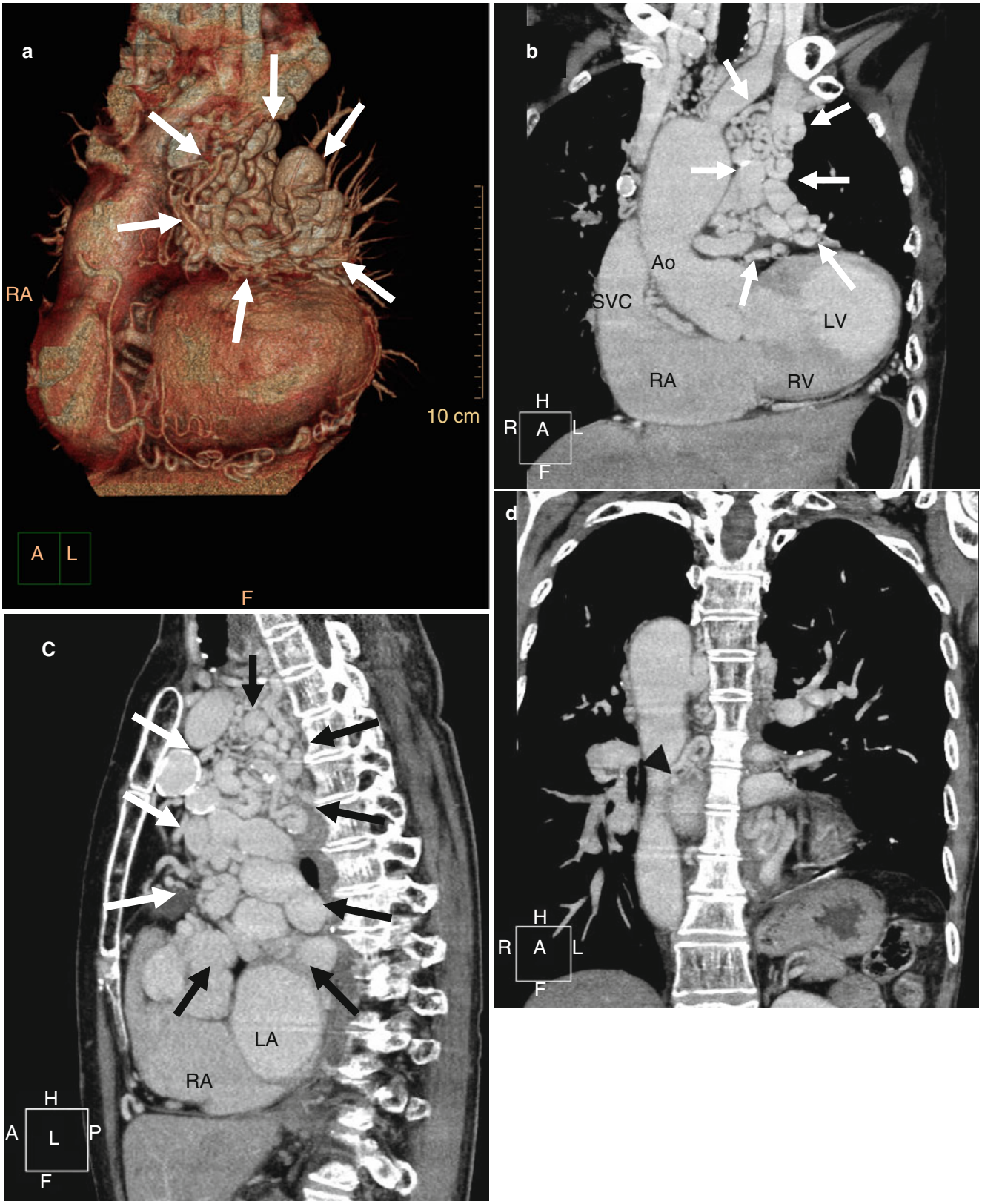


**Fig. 14.18** An example from a report of the longest surviving patient (59 year old) of pulmonary atresia with ventricular septal defect. Panel (**a**) is a 3D volume-rendered reconstruction showing the multiple well-developed major aortopulmonary collateral arteries (MAPCAS) (surrounded by *white arrows*). Panel (**b**) is a coronal maximum intensity projection illustrating the MAPCAS (surrounded by *white arrows*) which have a cavernous appearance. Panel (**c**) is a sagittal cut again demonstrating the extensive formation of MAPCAS (surrounded by the *white* and *black arrows*). Panel (**d**) is a coronal cut highlighting the posterior chest cavity and depicts the descending aorta giving rise to a MAPCA. The origin of this MAPCA is depicted by the *black arrowhead*. Panel (**e**) is an axial image also showing the origin of a MAPCA (*black arrow*) from the descending aorta. *Ao* aorta, *SVC* superior vena cava, *RA* right atrium, *RV* right ventricle, *LA* left atrium, *LV* left ventricle (Reproduced with the kind permission of Lippincott Williams & Wilkins from Fukui et al. [54])

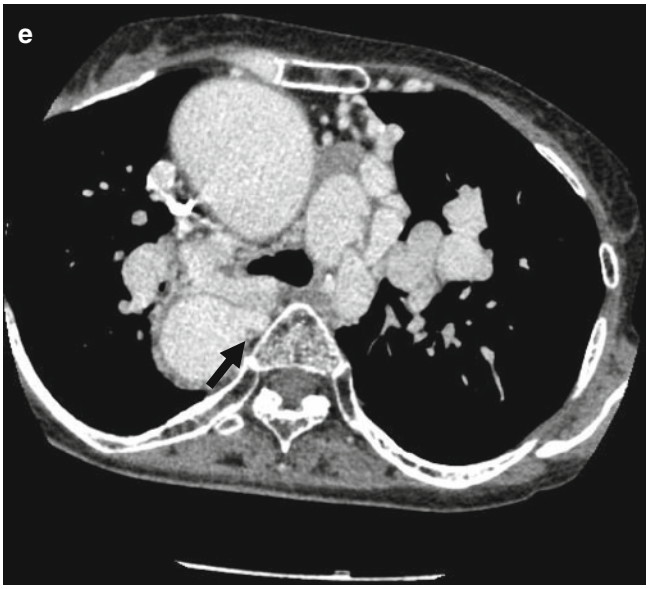


**Fig. 14.18** (continued)

**Table 14.5** A list of the important information to be obtained from a computed tomographic evaluation of pulmonary atresia with ventricular septal defect

| |
|---|
| Morphology, wall thickness, size, and systolic function of both ventricles |
| Morphology and size of atria |
| Morphology of right ventricular outflow tract, including size and patency |
| Morphology, obstruction, and regurgitation of right ventricle-to-pulmonary artery conduit |
| Anatomy of pulmonary circulation including pulmonary arteries and MAPCAs and stenosis and/or dilatation |
| Patency and direction of systemic-to-pulmonary connections |
| Anatomy and function of cardiac valves, including size and presence of tricuspid valve and aortic valve regurgitation |
| Size of aortic annulus and root |
| Presence of interventricular communication, including post-repair and residual leakage |
| Coexisting anomalies |

## References


1. Bashore TM. Adult congenital heart disease: right ventricular outflow tract lesions. Circulation. 2007;115:1933–47. doi:10.1161/CIRCULATIONAHA.105.592345.
2. Warnes CA, Williams RG, Bashore TM, Child JS, Connolly HM, Dearani JA, et al. ACC/AHA 2008 guidelines for the management of adults with congenital heart disease: a report of the American College of Cardiology/American Heart Association Task Force on Practice Guidelines (writing committee to develop guidelines on the management of adults with congenital heart disease). Circulation. 2008;118:e714–833. doi:10.1161/CIRCULATIONAHA.108.190690.
3. Dore A. Pulmonary stenosis. In: Gatzoulis MA, Webb GD, Daubeney PEF, editors. Diagnosis and management of adult congenital heart disease. 1st ed. Edinburgh: Churchill Livingstone; 2003. p. 299.
4. McElhinney DB, Goldmuntz E. Double-chambered right ventricle. In: Gatzoulis MA, Webb GD, Daubeney PEF, editors. Diagnosis and management of adult congenital heart disease. 1st ed. Edinburgh: Churchill Livingstone; 2003. p. 305.
5. McElhinney DB, Chatterjee KM, Reddy VM. Double-chambered right ventricle presenting in adulthood. Ann Thorac Surg. 2000;70:124–7.
6. Lascano ME, Schaad MS, Moodie DS, Murphy Jr D. Difficulty in diagnosing double-chambered right ventricle in adults. Am J Cardiol. 2001;88:816–9.
7. Wu MC, Ku PM, Chou MC, Huang TY. Usefulness of 64-slice computed tomography for evaluation of double-chambered right ventricle combined with atrial and ventricular septal defects. Tex Heart Inst J. 2009;36:74–5.
8. Chesler E, Korns ME, Edwards JE. Anomalies of the tricuspid valve, including pouches, resembling aneurysms of the membranous ventricular septum. Am J Cardiol. 1968;21:661–8.
9. Jones RN, Niles NR. Spinnaker formation of sinus venosus valve. case report of a fatal anomaly in a ten-year-old boy. Circulation. 1968;38:468–73.
10. Warnes CA, Maron BJ, Jones M, Roberts WC. Asymptomatic sinus of valsalva aneurysm causing right ventricular outflow obstruction before and after rupture. Am J Cardiol. 1984;54:1383–4.
11. Mohanakrishnan L, Vijayakumar K, Sukumaran P, Menon N, Prabu CR, Balaji S, et al. Unruptured sinus of valsalva aneurysm with right ventricular outflow obstruction. Asian Cardiovasc Thorac Ann. 2003;11:74–6.
12. Das SK, Jahnke EJ, Walker WJ. Aneurysm of the membranous septum with interventricular septal defect producing right ventricular outflow obstruction. Circulation. 1964;30:429–33.
13. Hachiro Y, Takagi N, Koyanagi T, Morikawa M, Abe T. Repair of double-chambered right ventricle: surgical results and long-term follow-up. Ann Thorac Surg. 2001;72:1520–2.
14. Moran AM, Hornberger LK, Jonas RA, Keane JF. Development of a double-chambered right ventricle after repair of tetralogy of fallot. J Am Coll Cardiol. 1998;31:1127–33.
15. Chandrashekhar YS, Anand IS, Wahi PL. Balloon dilatation of double-chamber right ventricle. Am Heart J. 1990;120:1234–6.
16. Gibbs JL, Uzun O, Blackburn ME, Parsons JM, Dickinson DF. Right ventricular outflow stent implantation: an alternative to palliative surgical relief of infundibular pulmonary stenosis. Heart. 1997;77:176–9.
17. Park SJ, Lee CW, Hong MK, Song JK, Park SW, Kim JJ. Transcoronary alcohol ablation of infundibular hypertrophy in patients with idiopathic infundibular pulmonic stenosis. Am J Cardiol. 1997;80:1514–6.
18. FRANCH RH, GAY Jr BB. Congenital stenosis of the pulmonary artery branches. a classification, with postmortem findings in two cases. Am J Med. 1963;35:512–29.
19. Kreutzer J, Landzberg MJ, Preminger TJ, Mandell VS, Treves ST, Reid LM, et al. Isolated peripheral pulmonary artery stenoses in the adult. Circulation. 1996;93:1417–23.
20. Prieto LR, Latson LA. Pulmonary stenosis. In: Moss AJ, Allen HD, editors. Moss and adams' heart disease in infants, children, and adolescents: including the fetus and young adult. 7th ed. Philadelphia: Wolters Kluwer/Lippincott Williams & Wilkins; 2008. p. 835.
21. Hughes Jr D, Siegel MJ. Computed tomography of adult congenital heart disease. Radiol Clin North Am. 2010;48:817–35. doi:10.1016/j.rcl.2010.04.005.
22. Siegel MJ. CT evaluation of congenital heart disease in adults. Appl Radiol. 2005;34:61–8.
23. Lacour-Gayet F. Congenital heart surgery nomenclature and database project: right ventricular outflow tract obstruction-intact ventricular septum. Ann Thorac Surg. 2000;69:S83–96.

24. Ferencz C, Rubin JD, McCarter RJ, Brenner JI, Neill CA, Perry LW, et al. Congenital heart disease: prevalence at live birth. The Baltimore-Washington Infant Study. Am J Epidemiol. 1985;121: 31–6.
25. Bichell D. Pulmonary atresia with intact ventricular septum. In: Nichols DG, editor. Critical heart disease in infants and children, vol. 2. Philadelphia: Mosby; 2006. p. 755.
26. Hanley FL, Sade RM, Blackstone EH, Kirklin JW, Freedom RM, Nanda NC. Outcomes in neonatal pulmonary atresia with intact ventricular septum. A multiinstitutional study. J Thorac Cardiovasc Surg. 1993;105:406–23, 424–7; discussion 423–4.
27. Bryan CS, Oppenheimer EH. Ventricular endocardial fibroelastosis. basis for its presence or absence in cases of pulmonic and aortic atresia. Arch Pathol. 1969;87:82–6.
28. Zuberbuhler JR, Anderson RH. Morphological variations in pulmonary atresia with intact ventricular septum. Br Heart J. 1979;41:281–8.
29. Robicsek F, Bostoen H, Sanger PW. Atresia of the pulmonary valve with normal pulmonary artery and intact ventricular septum in a 21-year-old woman. Angiology. 1966;17:896–901.
30. McArthur JD, Munsi SC, Sukumar IP, Cherian G. Pulmonary valve atresia with intact ventricular septum. Report of a case with long survival and pulmonary blood supply from an anomalous coronary artery. Circulation. 1971;44:740–5.
31. Bull C, Kostelka M, Sorensen K, de Leval M. Outcome measures for the neonatal management of pulmonary atresia with intact ventricular septum. J Thorac Cardiovasc Surg. 1994;107:359–66.
32. Jahangiri M, Zurakowski D, Bichell D, Mayer JE, del Nido PJ, Jonas RA. Improved results with selective management in pulmonary atresia with intact ventricular septum. J Thorac Cardiovasc Surg. 1999;118:1046–55.
33. O'Connor WN, Stahr BJ, Cottrill CM, Todd EP, Noonan JA. Ventriculocoronary connections in hypoplastic right heart syndrome: autopsy serial section study of six cases. J Am Coll Cardiol. 1988;11:1061–72.
34. Daubeney PEF. Pulmonary atresia with intact ventricular septum. In: Gatzoulis MA, Webb GD, Daubeney PEF, editors. Diagnosis and management of adult congenital heart disease. 1st ed. Edinburgh: Churchill Livingstone; 2003. p. 339.
35. Starnes VA, Pitlick PT, Bernstein D, Griffin ML, Choy M, Shumway NE. Ebstein's anomaly appearing in the neonate. A new surgical approach. J Thorac Cardiovasc Surg. 1991;101:1082–7.
36. Nykagen D. Pulmonary atresia and intact ventricular septum. In: Moss AJ, Allen HD, editors. Moss and adams' heart disease in infants, children, and adolescents: including the fetus and young adult. 7th ed. Philadelphia: Wolters Kluwer/Lippincott Williams & Wilkins; 2008. p. 859.
37. Ruiz CE, Zhang HP. Is balloon a challenge to scalpel in membranous pulmonary valve atresia or just a partner? Cathet Cardiovasc Diagn. 1997;40:414–5.
38. Van Arsdell GS, Williams WG, Maser CM, Streitenberger KS, Rebeyka IM, Coles JG, et al. Superior vena cava to pulmonary artery anastomosis: an adjunct to biventricular repair. J Thorac Cardiovasc Surg. 1996;112:1143–8; discussion 1148–9.
39. Tchervenkov CI, Roy N. Congenital heart surgery nomenclature and database project: pulmonary atresia–ventricular septal defect. Ann Thorac Surg. 2000;69:S97–105.
40. Samanek M, Voriskova M. Congenital heart disease among 815,569 children born between 1980 and 1990 and their 15-year survival: a prospective bohemia survival study. Pediatr Cardiol. 1999;20: 411–7.
41. O'Leary PW, Ewards WD, Julsrud PR, Puga FJ. Pulmonary atresia and ventricular septal defect. In: Moss AJ, Allen HD, editors. Moss and adams' heart disease in infants, children, and adolescents: including the fetus and young adult. 7th ed. Philadelphia: Wolters Kluwer/Lippincott Williams & Wilkins; 2008. p. 878.
42. Garne E, Nielsen G, Hansen OK, Emmertsen K. Tetralogy of fallot. A population-based study of epidemiology, associated malformations and survival in western Denmark 1984–1992. Scand Cardiovasc J. 1999;33:45–8.
43. Muhl IV, Sethia B. Pulmonary atresia with ventricular septal defect. In: Gatzoulis MA, Webb GD, Daubeney PEF, editors. Diagnosis and management of adult congenital heart disease. 1st ed. Edinburgh: Churchill Livingstone; 2003. p. 327.
44. Ellis K. The bronchial arteries and anomalous systemic arteries to the lungs in congenital heart and lung disease. In: Butler J, editor. The Bronchial circulation. New York: M. Dekker; 1992. p. 599–748.
45. Bharati S, Paul MH, Idriss FS, Potkin RT, Lev M. The surgical anatomy of pulmonary atresia with ventricular septal defect: pseudotruncus. J Thorac Cardiovasc Surg. 1975;69:713–21.
46. Bertranou EG, Blackstone EH, Hazelrig JB, Turner ME, Kirklin JW. Life expectancy without surgery in tetralogy of Fallot. Am J Cardiol. 1978;42:458–66.
47. Marelli AJ, Perloff JK, Child JS, Laks H. Pulmonary atresia with ventricular septal defect in adults. Circulation. 1994;89:243–51.
48. Greil GF, Schoebinger M, Kuettner A, Schaefer JF, Dammann F, Claussen CD, et al. Imaging of aortopulmonary collateral arteries with high-resolution multidetector CT. Pediatr Radiol. 2006;36:502–9.
49. Cho JM, Puga FJ, Danielson GK, Dearani JA, Mair DD, Hagler DJ, et al. Early and long-term results of the surgical treatment of tetralogy of fallot with pulmonary atresia, with or without major aortopulmonary collateral arteries. J Thorac Cardiovasc Surg. 2002;124:70–81.
50. Gaca AM, Jaggers KK, Dudley LT, Bisset GS. Repair of congenital heart disease: a primer–part 1. Radiology. 2008;247:617–31.
51. Maeda E, Akahane M, Kato N, Hayashi N, Koga H, Yamada H, et al. Assessment of major aortopulmonary collateral arteries with multidetector-row computed tomography. Radiat Med. 2006;24:378–83.
52. Murai S, Hamada S, Yamamoto S, Khankan AA, Sumikawa H, Inoue A, et al. Evaluation of major aortopulmonary collateral arteries (MAPCAs) using three-dimensional CT angiography: two case reports. Radiat Med. 2004;22:186–9.
53. Rajeshkannan R, Moorthy S, Sreekumar KP, Ramachandran PV, Kumar RK, Remadevi KS. Role of 64-MDCT in evaluation of pulmonary atresia with ventricular septal defect AJR. Am J Roentgenol. 2010;194:110–8.
54. Fukui D, Kai H, Takeuchi T, et al. Longest survivor of pulmonary atresia with ventricular septal defect. Well-developed major aortopulmonary collateral arteries demonstrated by multidetector computed tomography. Circulation. 2011;124:2155–7.

## 15.1 Patent Ductus Arteriosus

### 15.1.1 Definition

Patent ductus arteriosus (PDA) is the persistent communication between the descending aorta and main or proximal left pulmonary artery [1].

### 15.1.2 Epidemiology

Isolated PDA accounts for 5–10 % of congenital heart diseases with an incidence of 0.5 in 1,000 live term births [2].

### 15.1.3 Morphology

The patent ductus arteriosus is a vascular structure that connects the proximal descending aorta to the main or left pulmonary artery just distal to the left subclavian artery (Figs. 15.1, 15.2, and 15.3). During fetal life, the ductus arteriosus is a normal structure that allows most of the blood leaving the right ventricle to bypass the pulmonary circulation and enter the descending aorta effectively bypassing the developing lungs. Functional complete closure usually occurs within 24–48 h of birth in term neonates, although permanent closure does not occur until 2–3 weeks of life, and is related to fibrous band proliferation of the intimal lining of the duct. The resulting fibrous persists as the ligamentum arteriosum. Persistence of ductal patency in term infants after the neonatal period is considered abnormal [3]. Of note, failure of ductus arteriosus contraction in preterm neonates is not uncommon and is thought to be due to poor prostaglandin metabolism that stems from lung immaturity.

Most typically, a PDA is left-sided but it can be right-sided or bilateral. Although a left ductus arteriosus is a normal structure during normal fetal development, the presence of a right ductus arteriosus is usually associated with other congenital heart abnormalities most typically involving the aortic arch or conotruncal area.

### 15.1.4 Coexisting Abnormalities

In adults, a PDA is usually an isolated finding. Rarely, it is associated with other cardiac abnormalities. The most frequent association is an atrial septal defect or ventricular septal defect [1, 4]. Other associated cardiovascular anomalies include aortic coarctation, interrupted aortic arch, hypoplastic left heart and pulmonary atresia with ventricular septal defect (ductus-dependent lesions), tetralogy of Fallot, and discordant ventriculoarterial connections (non-ductus-dependent lesions).

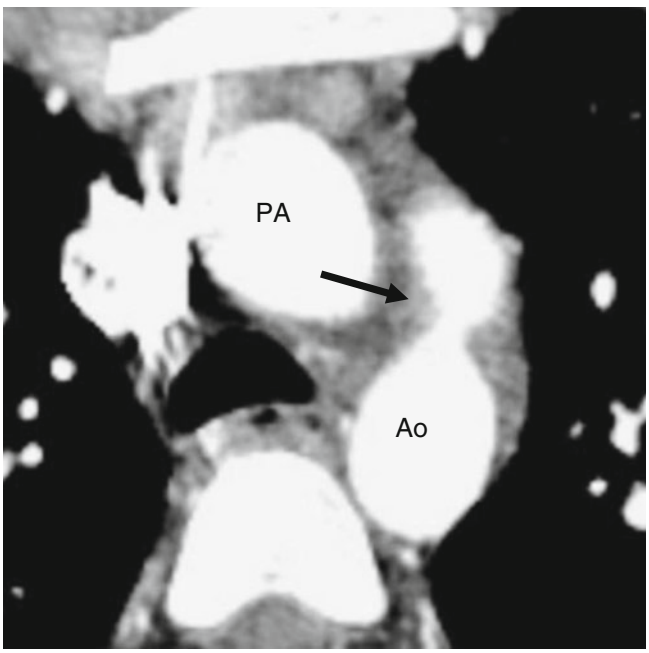


**Fig. 15.1** Patent ductus arteriosus. An axial contrast-enhanced computed tomogram illustrating a patent communication (*arrow*) between the pulmonary artery (*PA*) and proximal descending aorta (*Ao*)

W. Mazur et al., *CT Atlas of Adult Congenital Heart Disease*,
DOI 10.1007/978-1-4471-5088-6_15, © Springer-Verlag London 2013

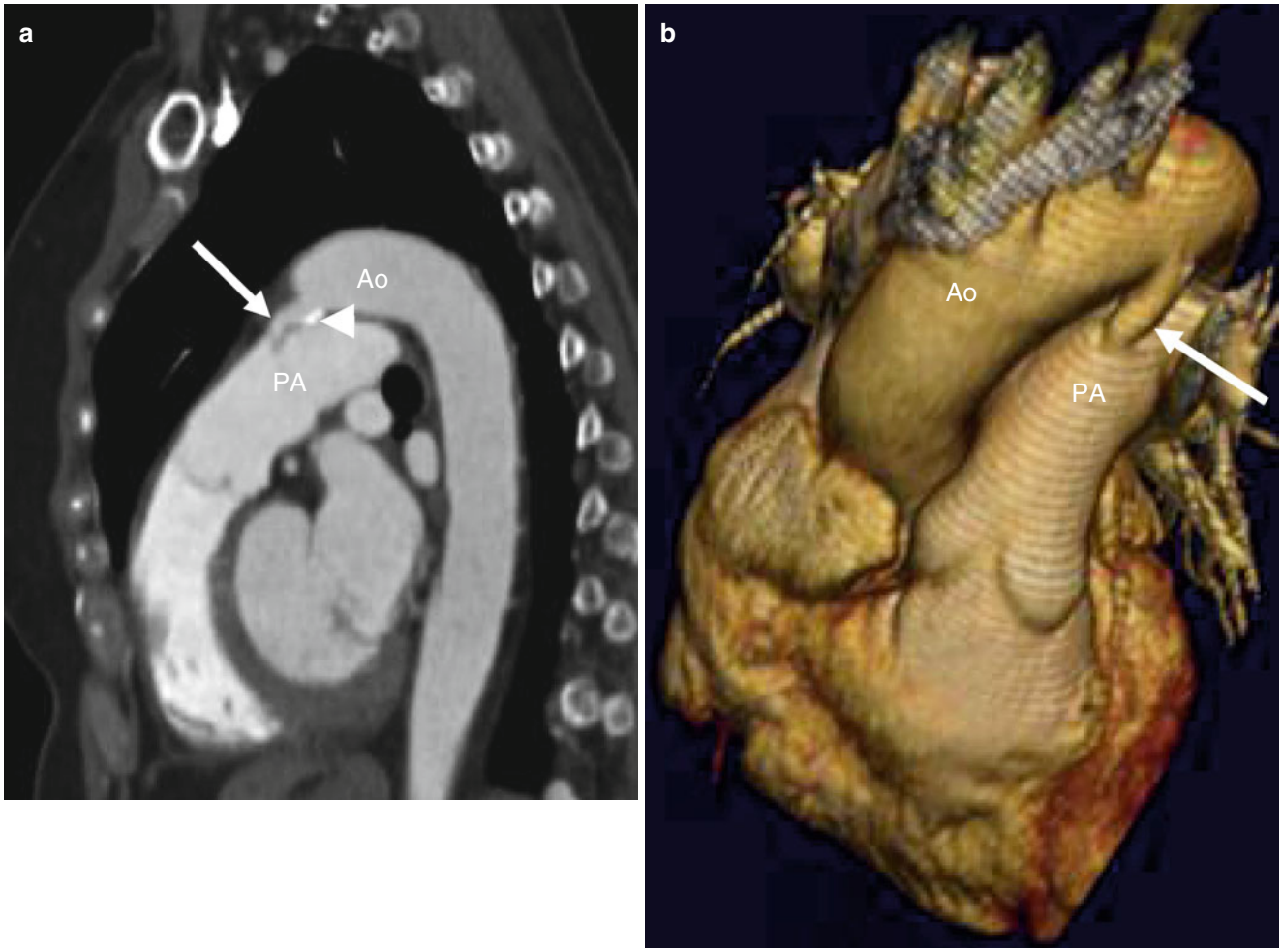


**Fig. 15.2** A 65-year-old female with a known patent ductus arteriosus presenting with chest pain. Panel (**a**) is a sagittal view and panel (**b**) is a 3D oblique coronal reconstruction. Each shows a communication (*arrow*) between the aorta (*Ao*) and main pulmonary artery (*PA*). The duct has a wide open aortic ampulla (13 mm diameter) and narrows at its junction with the pulmonary artery (3 mm diameter) (type A, Krichenko classification). Also note calcification at the ductal-aortic junction (*arrowhead* in panel **a**)

### 15.1.5 Clinical Features

The hemodynamic impact of a PDA in an otherwise normal cardiovascular system is determined by the magnitude of the shunt which depends on the ductal resistance and also on the pressure gradient between the aorta and the pulmonary artery. Small and restrictive PDAs usually cause little or no hemodynamic derangement and are asymptomatic. Rarely, bacterial endocarditis can occur. Moderate to large PDAs can result in pulmonary overcirculation and left heart volume overload. Chronic volume overload of the left heart can lead to onset of congestive heart failure in adulthood, usually starting in the third decade. In addition, long-standing left-to-right shunting and exposure of the pulmonary artery system to high pressures can lead to morphological changes in the pulmonary vasculature, resulting in increased pulmonary vascular resistance. When pulmonary vascular resistance exceeds systemic vascular resistance, ductal shunting reverses and becomes right to left (Eisenmenger physiology) [2].

### 15.1.6 Interventions

Ductus closure is usually indicated for patients who are symptomatic from significant left-to-right shunting through the PDA or who have left-to-right shunting resulting in left heart enlargement. The indications for closure of PDAs with small shunts, including those that are incidentally discovered, are less certain. Because endarteritis has been reported in patients with clinically silent PDAs, it has been advocated that any PDA should be routinely closed, especially given efficacy and safety of the percutaneous closure methods.

Transcatheter occlusion with coils or a duct occluder device has become the treatment of choice for most older children

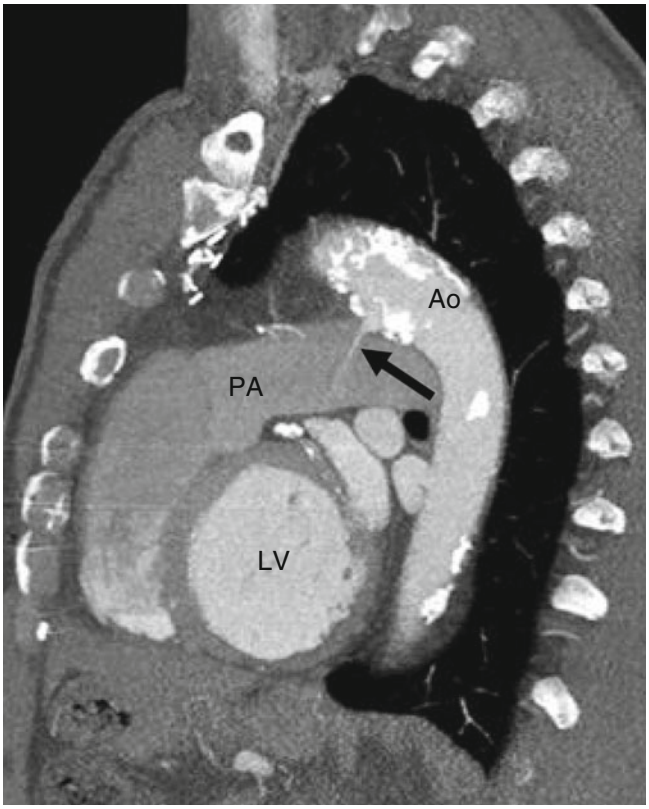


**Fig. 15.3** Patent ductus arteriosus. A 65-year-old man with history of a repaired patent ductus arteriosus as a teenager. Here, a sagittal reconstruction shows a jet of contrast-enhanced blood (*arrow*) flowing from the aorta (*Ao*) to the pulmonary artery (*PA*). The PDA is large and short (type B, Krichenko classification) *LV* left ventricle

**Fig. 15.4** Ductus diverticulum. The small diverticulum (*arrow*), which is a remnant of the patent ductus, does not connect with the pulmonary artery

and adults with PDAs. Complete closure rates usually exceed 90–95 %. In infants, PDA closure may be successful with indomethacin treatment. If indomethacin treatment is unsuccessful, PDAs are then usually closed with an external clip or surgical ligation or division.

### 15.1.7 Cardiac Computed Tomography (CT) in the Evaluation of PDA

CT enables excellent anatomic depiction of PDAs [5]. When other imaging techniques do not provide sufficient data, CT can be used as an additional tool for diagnosis. Although the channel between the aorta and pulmonary artery can be seen on axial images, it is best seen on sagittal or oblique multiplanar and/or 3D volume-rendered reconstructions (Figs. 15.2 and 15.3). Demonstration of a jet of blood from the aorta into the pulmonary artery via the PDA confirms the patency of the shunt [6, 7]. Of importance, a small diverticulum at the site of the ductus should not be confused with a patent ductus (Fig. 15.4). Unlike a PDA, the diverticulum will not demonstrate a patent connection with the pulmonary artery.

**Table 15.1** Krichenko classification of PDA [7]

| Type | Morphology |
|---|---|
| A (conical) | Well-defined aortic ampulla and constriction near the pulmonary artery |
| B (window) | Very large and very short |
| C (tubular) | Without constrictions |
| D (complex) | Multiple constrictions |
| E (elongated) | Constriction remote from the anterior edge of trachea |

Size and morphology of the ductus are important in planning closure procedures. The classification proposed by Krichenko et al. which divides PDA into five groups A–E (Table 15.1), related to the size of the PDA, presence or absence of constrictions, and, if present, the location of the constriction, has been useful to plan surgical or transcatheter closure procedure [8].

CT scans should be evaluated for the following: (a) location and size (length and width); (b) presence and extent of calcifications, constrictions, or aneurysms; (c) presence of vegetations; (d) size and morphology of the great arteries for the presence of pulmonary hypertension and dissection/rupture; (e) morphology, size, and function of the cardiac chambers, particularly the left atrium and left ventricle (which may be enlarged in patients with

**Table 15.2** CT assessment of PDA

| |
|---|
| Location, size, geometry, connections to great arteries, and relationship to neighboring structures |
| Presence of constrictions, aneurysms, and wall calcifications |
| Presence of vegetations suggestive of endocarditis |
| Size and morphology of the great arteries including the presence of aorta and pulmonary artery dissection and/or spontaneous rupture |
| Morphology, size, and function of the cardiac chambers |
| Presence of coexisting anomalies |

volume overload) and the right ventricle (which may be hypertrophied due to pulmonary hypertension and Eisenmenger syndrome); and (f) coexisting anomalies. See Table 15.2.

Ductal aneurysm, which may occur prior to or after repair, aortic and/or pulmonary artery dissection, and/or spontaneous rupture are associated with this anomaly [9–14]. After closure procedures, CT may help to assess residual shunting, thrombus formation, and protrusion of transcatheter occluder devices into the arterial lumen [2].

## 15.2 Aortopulmonary Window

### 15.2.1 Definition

Aortopulmonary window (AP window) is a communication between the main pulmonary artery and the ascending aorta in the presence of two separate semilunar valves [15]. It is caused by incomplete fusion of the two embryonic conotruncal ridges that normally give rise to the aorta and the pulmonary artery [16].

### 15.2.2 Epidemiology

AP window is a rare anomaly and accounts for 0.1–0.2 % of all congenital heart anomalies [17, 18].

### 15.2.3 Variants

Based on the Mori classification, there are three variants of the AP window defect:

(a) type I or proximal communication located near the semilunar valves, (b) type II or distal connection involves the pulmonary bifurcation at the level of the right pulmonary artery, and (c) type III or a connection characterized by total absence of the aortopulmonary septum. Occasionally there may be an intermediate form that has features of types I and II (Figs. 15.5 and 15.6) [19, 20].

### 15.2.4 Associated Anomalies

About 50 % of AP window defects are associated with other cardiac abnormalities. The most common associated lesions

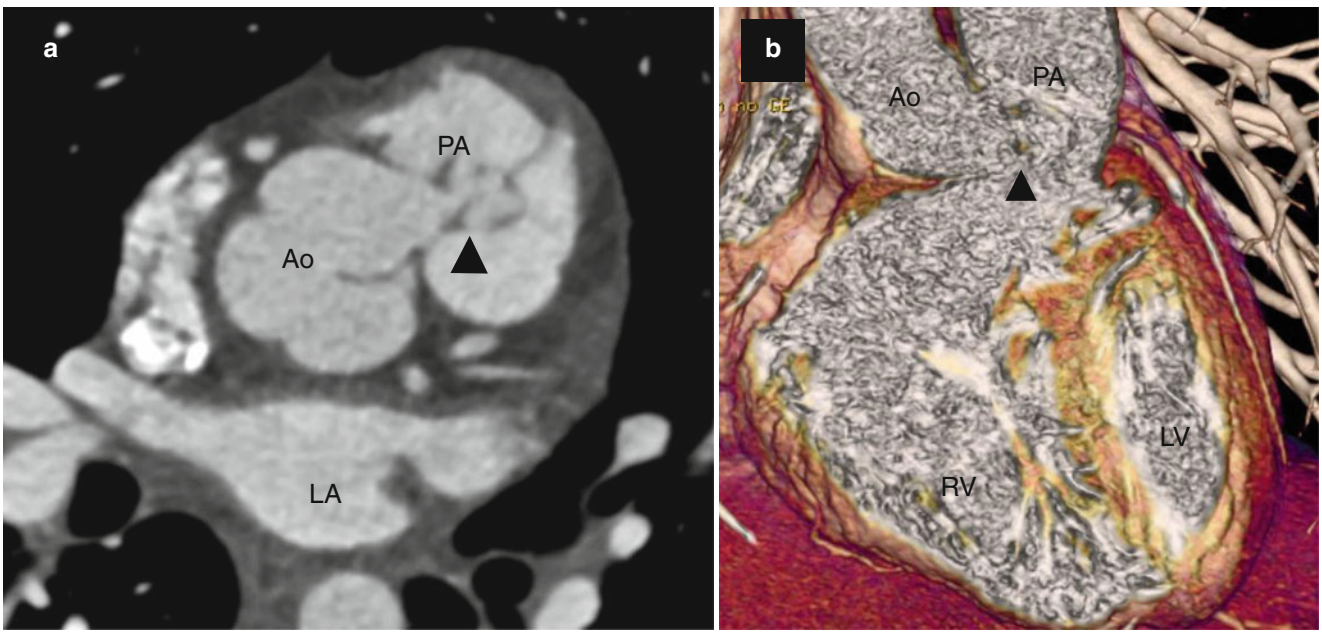


**Fig. 15.5** Type I aortopulmonary window in a 20-year-old woman without prior surgical repair. Panel (**a**) is an axial scan, while panel (**b**) is a volume-rendered view demonstrating a communication (*arrowheads*) between the aorta (*Ao*) and main pulmonary artery (*PA*) at the level of the semilunar valves. *LA* left atrium, *LV* left ventricle, *RV* right ventricle (Images provided courtesy of Eric T. Kimura-Hayama MD, Mexico City, Mexico)

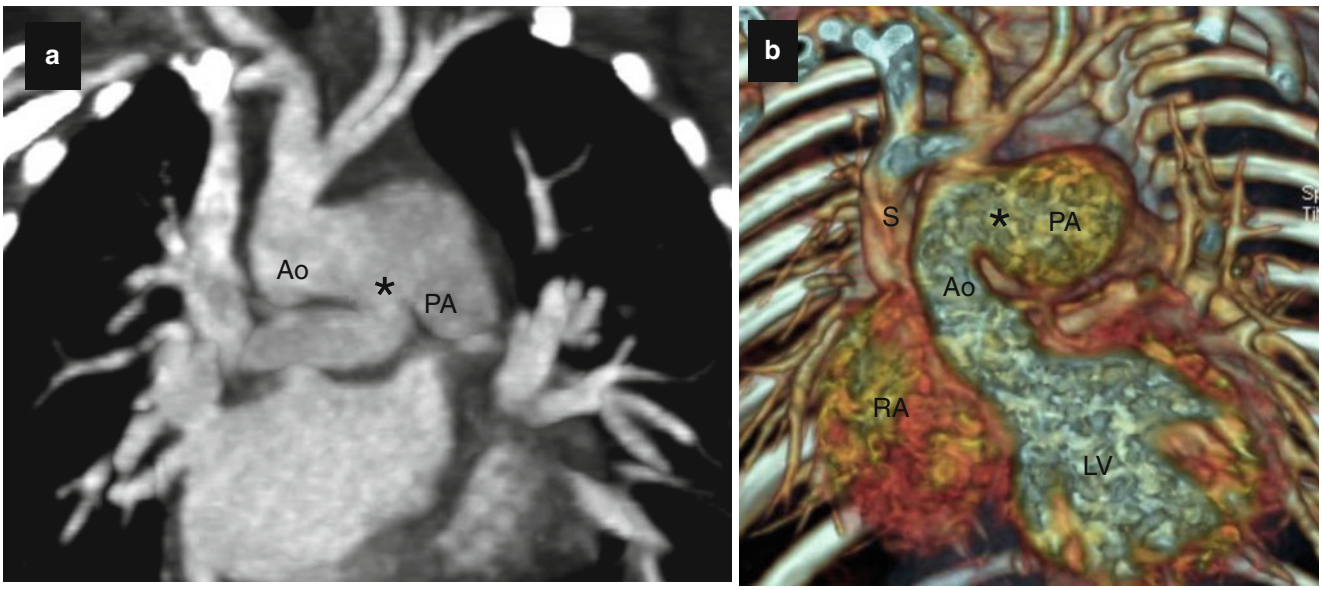


**Fig. 15.6** Type II aortopulmonary window in a 3-month-old infant. Panel (**a**) is a two-dimensional tomogram and panel (**b**) is a volume-rendered, coronal reconstruction. Each shows a communication (*asterisk*) between the aorta (*Ao*) and pulmonary artery (*PA*) just above the plane of the semilunar valves. *S* superior vena cava, *RA* right ventricle, *LV* left ventricle (Images provided courtesy of Eric T. Kimura-Hayama MD, Mexico City, Mexico)

**Table 15.3** Coexisting anomalies in aortopulmonary window

| |
|---|
| Coarctation of aorta or interrupted aortic arch |
| Abnormal origin of the right pulmonary artery from ascending aorta |
| Coronary artery anomalies |
| Ventricular septal defect |
| Tetralogy of Fallot |
| Transposition of great arteries |

are type A interruption of the aortic arch and aortic coarctation [15–17, 21, 22]. Other abnormalities include (a) anomalous origin of the right pulmonary artery from the right side of the ascending aorta, (b) anomalous origin of the coronary arteries, (c) ventricular septal defect, (d) tetralogy of Fallot, and (e) transposition of the great arteries (Table 15.3) [16].

The AP window needs to be distinguished from truncus arteriosus and hemitruncus, which also are characterized by communications between the aorta and pulmonary artery. In the AP window defect, there are separate aortic and pulmonary valves and the right and left pulmonary arteries arise from the main pulmonary artery. Truncus arteriosus has a single truncal valve. In hemitruncus, one pulmonary artery arises from the ascending aorta and the other from the right ventricle [23, 24].

### 15.2.5 Clinical Aspects of AP Window

Patients with AP window defects typically present in the neonatal period with heart failure and undergo cardiac surgery early in life [16]. The abnormality is rarely indentified later in adult life when dyspnea on exertion, cyanosis, and/or pulmonary hypertension develop. More often, adults present with postoperative complications, including residual or recurrent left-to-right shunt, obstruction of the ascending aorta or main or right pulmonary artery, or obstruction of a coronary artery. Surgical closure procedures include a pulmonary artery flap and pericardial patch. Small residual defects may be treated with a closure device implantation. Prognosis depends on the presence of coexisting anomalies. In general, survival is excellent in patients with isolated AP windows.

### 15.2.6 Cardiac Computed Tomography (CT) in the Assessment of AP Window

CT is a noninvasive tool to depict and characterize the AP window defect [25, 26]. In individuals with unrepaired AP windows, CT assessment should include (a) the presence, location, type, and size of the AP window; (b) size and morphology of the pulmonary artery and aorta, (c) size and function of the cardiac chambers; and (d) presence of coexisting cardiac abnormalities, including bronchial compression by dilated pulmonary arteries, which cannot be demonstrated by echocardiography (Table 15.4).

In patients who have undergone surgical repairs, the role of CT is to assess (a) the integrity of the patch or device closure and the presence of residual or recurrent shunting,

**Table 15.4** Computed tomography assessment in untreated patients with aortopulmonary window

| |
|---|
| Presence, location, type, and size of aortopulmonary window |
| Morphology, size, and course of great arteries |
| Morphology, size, geometry, and systolic function of both ventricles with outflow tracts |
| Morphology and size of atria |
| Presence of coexisting anomalies |

**Table 15.5** Computed tomography assessment in treated patients with aortopulmonary window

| |
|---|
| Integrity of aortopulmonary window closure patch/device (presence of residual or recurrent shunting) |
| Morphology, size, course, and obstruction of great arteries |
| Integrity of repair of coexisting anomalies |
| Morphology, size, and geometry of both ventricles with their outflow tracts, including systolic function of the ventricles |
| Morphology and size of atria |

(b) the course and size of the great vessels and pulmonary artery branches, and (c) the status of coexisting abnormalities (Table 15.5).

## 15.3 Aortic Coarctation and Interrupted Aortic Arch

### 15.3.1 Aortic Coarctation

Coarctation of the aorta is a congenital narrowing at the junction of the aortic arch and proximal descending aorta in the region of the ligamentum ductus arteriosus [1]. Demonstrating a male to female ratio as high as 2:1, it accounts for 5–8 % of all congenital heart defects with an incidence of 1 in 2,500 live births [27, 28].

Aortic coarctation is thought to be the result of a malformation of the aortic media, leading to a short-segment, shelflike posterior infolding of the aortic wall in the periductal region [28]. See Fig. 15.7. However, coarctation of the aorta may be a long segment and may also be associated with isthmus and arch hypoplasia [29–31]. Intrinsic aortic wall abnormalities, characterized by cystic changes in the aortic media associated with disruption of elastin and increased collagen deposition, predispose to dissection or rupture in the area of the coarctation as well as in the ascending or descending aorta [1].

Two major types of coarctation are recognized: (1) preductal (infantile) and (2) postductal (adult). In the preductal form of coarctation, the obstruction occurs immediately below the origin of the left subclavian artery at the insertion of the ductus arteriosus or ligamentum arteriosum (Fig. 15.8). This form of coarctation is associated with tubular hypoplasia of the transverse arch in addition to the focal constriction. The ductus arteriosus is usually patent and supplies blood to the descending aorta from the pulmonary artery.

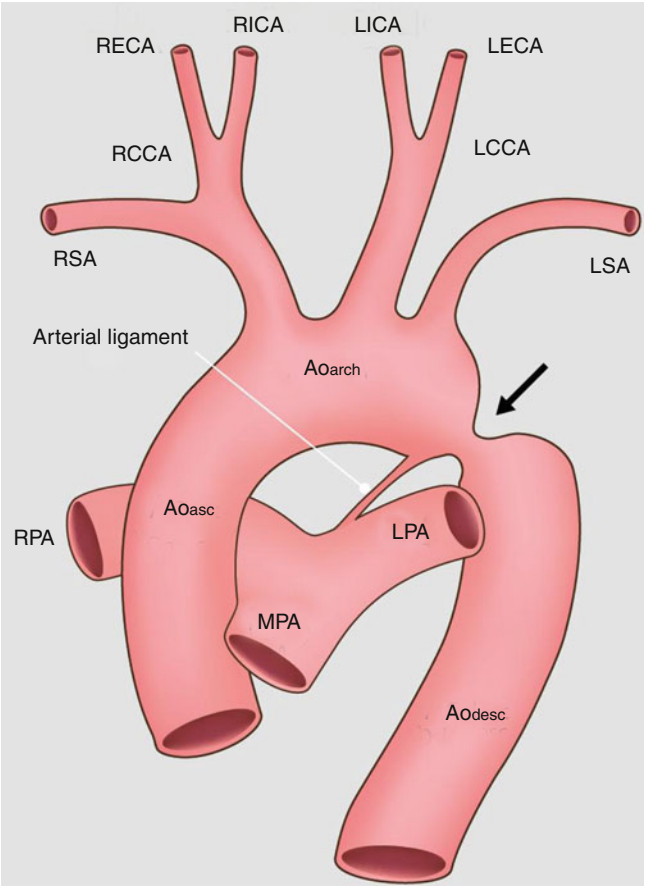


**Fig. 15.7** An artist's depiction of aortic coarctation. The coarctation (*black arrow*) is in the region of the embryologic ductus arteriosus at the junction of the transverse aortic arch and proximal descending aorta. *Ao asc* ascending aorta, *Ao arch* aortic arch, *Ao desc* descending aorta, *LCCA* left common carotid artery, *RCCA* right common carotid artery, *LSA* left subclavian artery, *RSA* right subclavian artery, *MPA* main pulmonary artery, *LPA* left pulmonary artery, *RPA* right pulmonary artery, *RECA* right external carotid artery, *RICA* right internal carotid artery, *LECA* left external carotid artery, *LICA* left internal carotid artery

In the postductal form, coarctation occurs below the level of the obliterated ductus arteriosus and produces a focal, shelflike indentation of the posterior aortic wall [1, 27–33]. See Fig. 15.9. The areas of the aorta proximal and distal to the coarctation may be dilated. The high pressure gradient across the area of obstruction leads to the formation of systemic collateral circulation to maintain blood flow to the lower pressure distal aorta. Collateral pathways include (1) internal thoracic (mammary) arteries, (2) intercostal arteries, (3) thoracoacromial and descending scapular arteries, and (4) vertebral arteries (Figs. 15.9 and 15.10). Inferior rib notching of the third to sixth ribs by dilated intercostal arteries is another characteristic imaging finding.

Preductal coarctation is associated with ventricular septal defects, patent ductus arteriosus, and hypoplastic left heart. Postductal coarctation is frequently associated with bicuspid

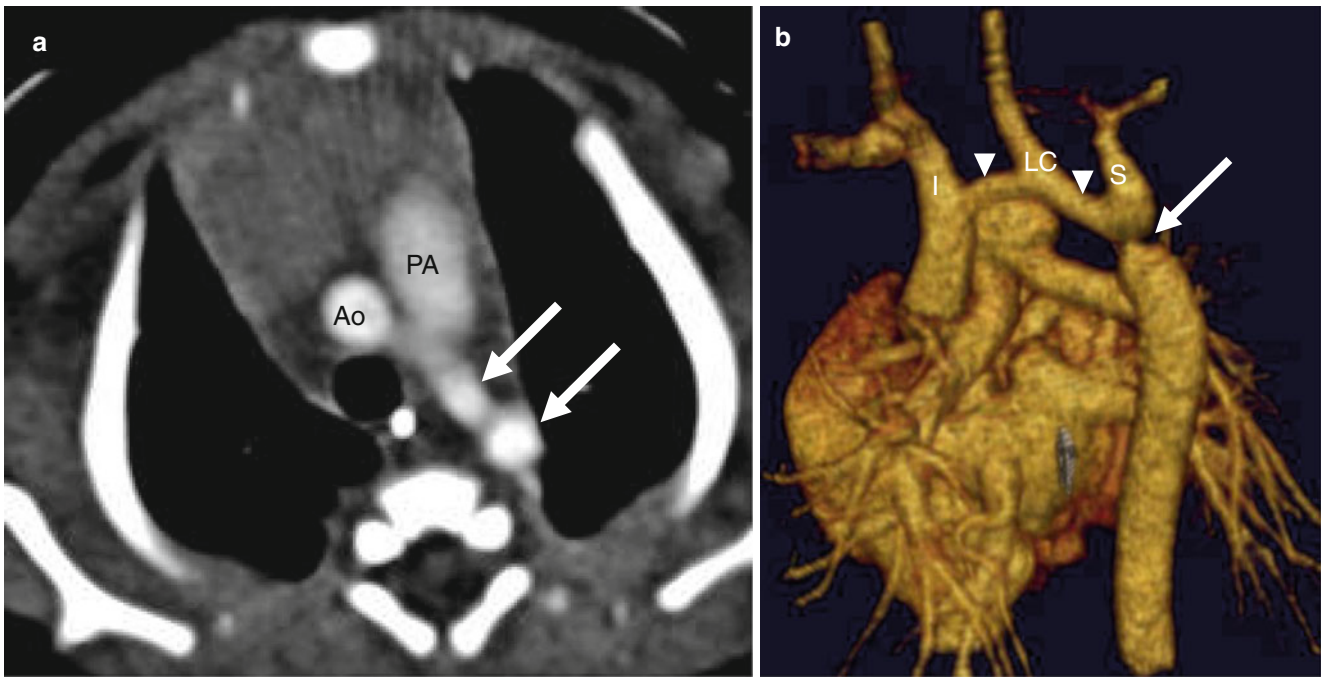


**Fig. 15.8** Preductal coarctation. Panel (**a**) is an axial image showing the decreased caliber of the descending aorta (*arrows*) compared with the transverse aortic arch (*Ao*). *PA* pulmonary artery. Panel (**b**) is a sagittal 3D volume-rendered image demonstrating a focal constriction (*arrow*) of the aortic lumen below the left subclavian artery (*S*) and long-segment hypoplasia of the transverse arch (*arrowheads*). *I* innominate artery, *LC* left carotid artery

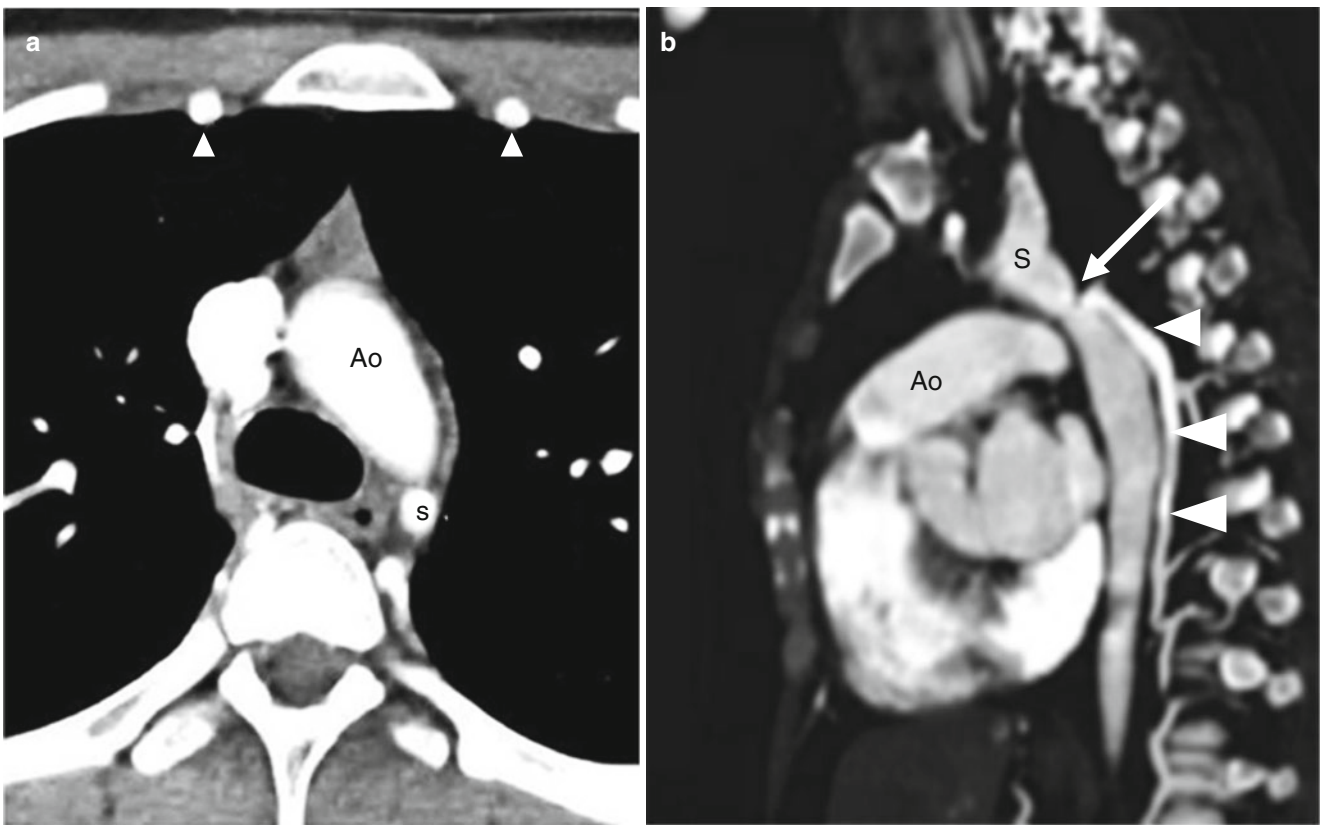


**Fig. 15.9** Postductal aortic coarctation. Panel (**a**) an axial scan showing narrowing of the descending aorta (*Ao*) distal to the origin of the left subclavian artery (*S*). Also note the enlarged internal mammary arteries (*arrowheads*). Panel (**b**) sagittal image demonstrating the characteristic narrowing (*arrow*) of the aortic lumen at the level of the ligamentum arteriosum. Also note the large posterior collateral vessel (*arrowheads*) and the mildly dilated ascending aorta (*Ao*). *S* subclavian artery

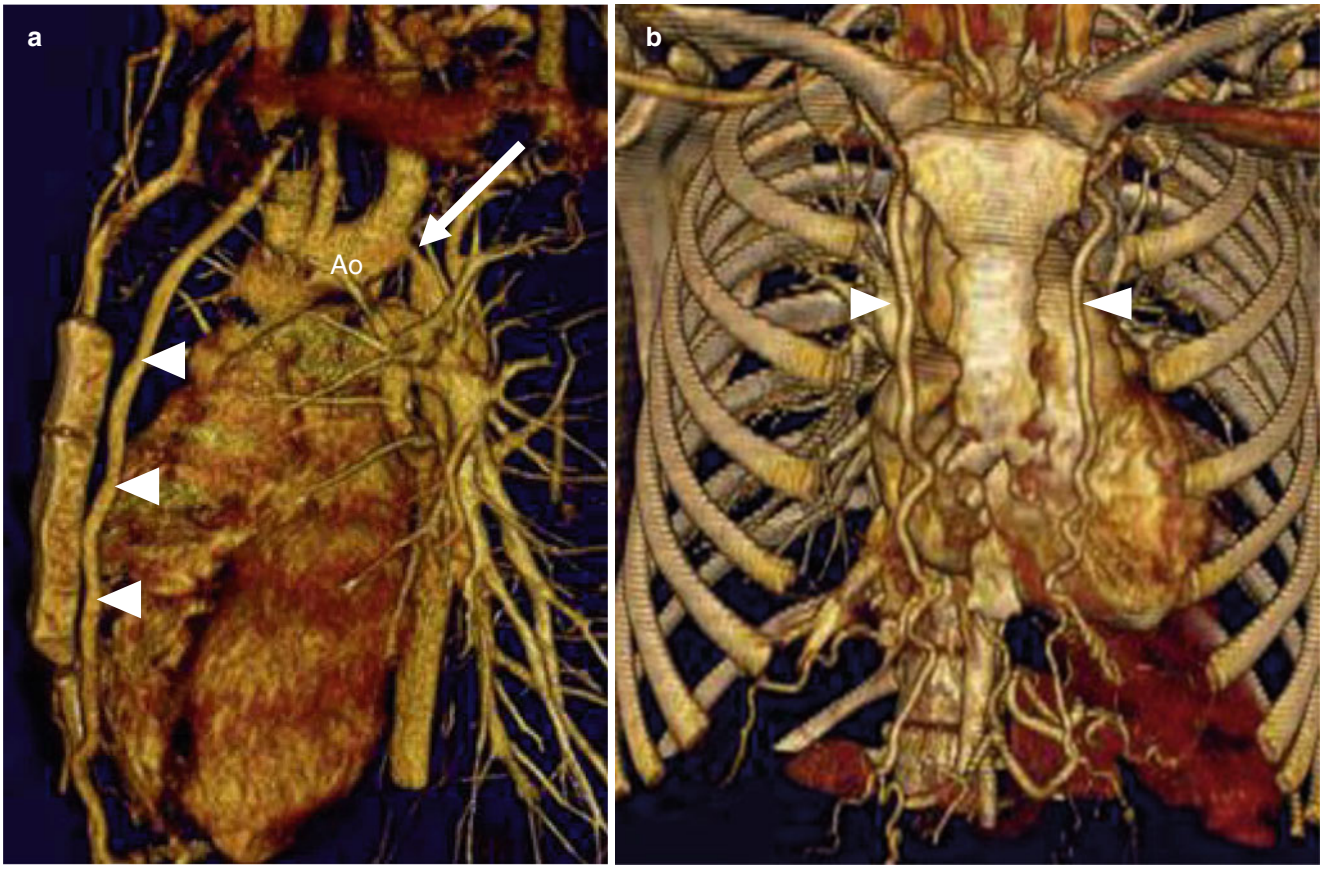


**Fig. 15.10** Aortic coarctation and collateral vessels. Panel (**a**) a sagittal scan shows the coarctation (*arrow*) and a large internal mammary artery (*arrowheads*). Panel (**b**) a coronal view confirms the enlarged internal mammary arteries (*arrowheads*). *Ao* aorta

aortic valve (22–85 % of cases), parachute mitral valve, hypoplastic mitral valve, aortic arch hypoplasia, and ventricular septal defects [1]. Bicuspid aortic valve may be complicated by aortic stenosis or regurgitation or both. Coarctation may also coexist with complex congenital heart diseases including transposition of the great arteries, double-inlet ventricle, double-outlet right ventricle, tricuspid atresia, and hypoplastic left heart syndrome [28].

Syndromes associated with aortic coarctation include Turner syndrome (15–20 % incidence of coarctation) and Shone's complex (left ventricular outflow tract obstruction and parachute mitral valve) [34].

Noncardiac associations include intracranial aneurysms (up to 10 % of coarctation cases) and spinal stenosis [1, 28, 32, 33, 35].

The clinical presentation and age at diagnosis of aortic coarctation are dependent on the severity of the obstruction and presence of other anomalies. The preductal form presents in infancy with congestive heart failure. Postductal coarctation can present in children or adults and may come to clinical attention because of a left sternal border systolic ejection murmur, systemic arterial hypertension in the upper extremities, and/or decreased lower extremity pulses [1, 27–31, 36]. Chronic hypertension and cerebrovascular accidents are late findings [36].

Untreated coarctation has a poor prognosis. Approximately 60 % of untreated infants with high-grade coarctation and 90 % with complicated coarctation die in the first year of life [28, 37]. In untreated patients, the mortality rate is reported to be 25, 50, 75, and 92 % at 20, 32, 46, and 60 years of age, respectively [38]. Surgery has substantially improved the long-term outcomes in infants with coarctation, although the survival rate in this group is still lower than that in an older population [38]. Coarctation in untreated adults may be asymptomatic due to the formation of systemic collateral vessels that reduce the gradient across the coarctation site masking the obstruction [1, 27, 28].

Treatment for coarctation consists of either open surgical repair or catheter interventions, including angioplasty and stent implantation. Resection and end-to-end anastomosis is the procedure of choice in neonates and infants with coarctation, although balloon angioplasty has been introduced as the bridge to surgery in critically ill subjects [39]. In adults, aortic coarctation can be treated percutaneously or with surgery [40, 41]. Surgical techniques include (a) resection and end-to-end anastomosis, (b) resection and extended end-to-end anastomosis, (c) prosthetic arch aortoplasty, (d) subclavian

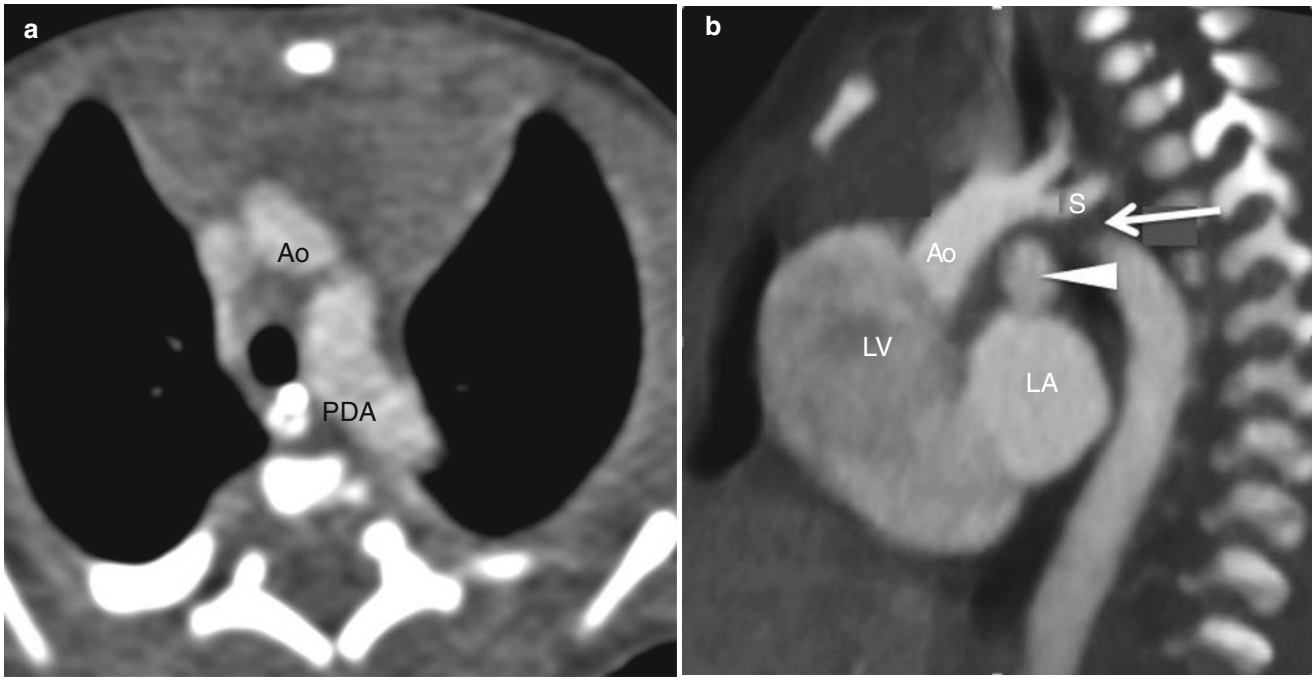


**Fig. 15.11** Interrupted aortic arch in a neonate. Panel (**a**) an axial section demonstrates a normal caliber transverse aortic arch (*Ao*). The vessel inferior to the arch is a large dilated patent ductus arteriosus (*PDA*), not to be confused with the descending aorta. Panel (**b**) a sagittal reconstruction shows interruption of the transverse arch (*arrow*) just below the origin of the left subclavian artery (*S*) and the large patent ductus arteriosus (*arrowhead*) which supplies the distal aorta. The ascending aorta is normal caliber. *Ao* ascending aorta, *LV* left ventricle, *LA* left atrium

flap aortoplasty, (e) interposition of a (tube) graft, and (f) bypass tube grafting [28, 29]. See Chap. 32 for a discussion of aortic coarctation surgical repairs.

### 15.3.2 Interrupted Aortic Arch

Interrupted aortic arch is a form of coarctation characterized by the lack of luminal continuity between ascending and descending aorta (Fig. 15.11). The condition is rare, accounting for 1 % to all 1.5 % of congenital heart disease [28, 42]. The Celoria–Patton classification identifies three types of interrupted arch based on the site of interruption. In type A, the interruption is distal to the left subclavian. Type B interruptions occur between the left carotid and left subclavian artery, and type C interruptions reside between the brachiocephalic trunk and left carotid artery [42]. In patients with an interrupted aortic arch, blood flow to the descending aorta is provided by an obligatory persistent arterial duct (Fig. 15.11).

This anomaly is commonly associated with ventricular septal defects, bicuspid aortic valves, left ventricular outflow tract obstruction, and aberrant right subclavian artery originating from the descending aorta. It also may be associated with complex heart lesions including common arterial trunk, aortopulmonary window, double-outlet right ventricle, and transposition of great arteries [42]. Type B interruption has been associated with the DiGeorge syndrome (hypocalcemia and T-cell defects due to thymic hypoplasia) [42]. Patients with interrupted aortic arch present in the neonatal period with respiratory distress, cyanosis, and congestive heart failure.

Surgical techniques for repair of the interrupted arch include (a) direct anastomosis after mobilization of both the ascending and descending aorta, (b) direct anastomosis with patch augmentation, and (c) interposition of a conduit. If necessary, the closure of ventricular septal defect and resection of the aortic stenosis is performed [43]. Mortality with these techniques ranges from 15 to 20 % [44]. The abnormality can be identified later in adult life if stenosis or significant collateral circulation develops [45].

### 15.3.3 Aortic Pseudocoarctation

Aortic pseudocoarctation is an unusual anomaly characterized by buckling or kinking of a tortuous aortic arch at the level of the ligamentum arteriosus (Fig. 15.12). It is thought to be the result of incomplete fusion of the third and seventh aortic dorsal segments. Although there may be some mild luminal narrowing and turbulence, the essential feature of pseudocoarctation is the absence of a hemodynamically significant pressure gradient. Therefore, there is no collateral

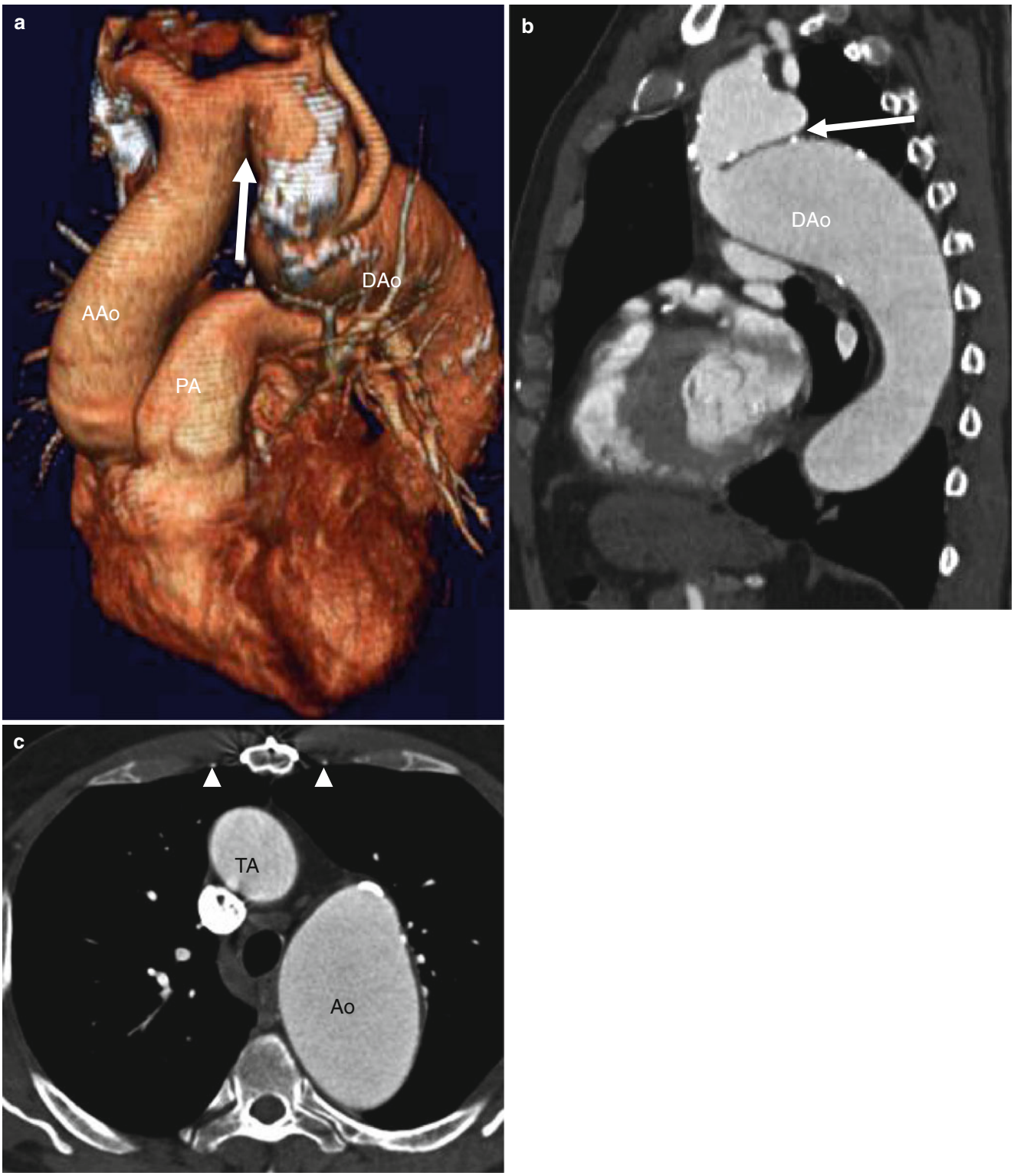


**Fig. 15.12** Pseudocoarctation. Panel (**a**) (3D sagittal) and panel (**b**) (oblique maximum intensity projection) reconstructions demonstrating the pronounced buckling of a tortuous aorta at the level of the ligamentum arteriosus (*arrows*). The "shelflike" fold is due to the buckling of the aorta. Note the absence of collateral vessel formation. Panel (**c**) an axial scan highlights that the internal mammary arteries (*arrowheads*) are normal caliber. *TA* transverse aortic arch, *AAo* ascending aorta, *Dao* descending aorta, *PA* pulmonary artery

vessel formation. This anomaly is usually asymptomatic and discovered incidentally on imaging studies and needs to be differentiated from a true aortic coarctation. Pseudocoarctation need not be treated.

### 15.3.4 Cardiac Computed Tomography (CT) in the Evaluation of Aortic Coarctation and Interrupted Aortic Arch

In the untreated coarctation and interrupted aortic arch, CT enables a detailed assessment of anatomy including the presence, site, morphology, and extent of luminal narrowing at the coarctation site as well as at the hypoplastic segment of the aortic arch and isthmus. Additionally, associated aortic dilatation, aneurysm formation, or aortic dissection may be identified. Luminal narrowing of the aortic arch and its branches can be seen. Collateral circulation may be identified. Finally, accompanying anomalies such as bicuspid aortic valve, mitral valve abnormalities, ventricular septal defects, and other congenital heart diseases should be identified [5, 46, 47]. However, CT cannot provide functional data such as the gradient across the coarctation.

In aortic coarctation, CT may identify collateral flow which is important in surgical planning. The aorta may be cross-clamped during surgical repair if collateral flow is sufficient for lower body perfusion. If collateral formation is inadequate, use of cardiopulmonary bypass for perfusion of the lower body may be indicated. Reconstructed images in sagittal and parasagittal planes best show the location and extent of coarctation. Coronal and sagittal reconstructions may help delineate rib notching and or collateral vessel formation.

In the post-intervention patient, the goals of CT imaging include evaluation of residual or recurrent stenosis(es), identification of potential endovascular stent-related complications (leaks, stent migration, stent fracture, in-stent thrombus, and aortic dissection), assessment of aortic dilatation, aneurysm formation and dissection, delineation of the aortic branch artery anatomy, assessment for collateral vessel formation, and characterization of any coexisting anomalies [48–50].

Since patients with aortic coarctation may experience accelerated atherosclerosis and premature coronary artery disease, evaluation of the coronary arteries is critical. Therefore, any CT evaluation should provide a noninvasive assessment of the presence, severity, and extent of coronary atherosclerosis in these patients. See Tables 15.6 and 15.7.

**Table 15.6** CT assessment in patients with coarctation of the aorta

| |
|---|
| Presence, site, morphology, and extent of luminal narrowing and or the hypoplastic segment |
| Presence, site, morphology, and extent of aortic dilatation and aneurysm formation of dissection |
| Presence, site, morphology, and extent of luminal narrowing of the aortic arch and branch vessels |
| Collateral circulation |
| Accompanying anomalies, especially bicuspid aortic valve and its complications |
| Other associated congenital heart disease |
| Presence, extent, and severity of associated coronary atherosclerosis |

**Table 15.7** CT assessment in postoperative patients with aortic coarctation

| |
|---|
| Presence, site, morphology, extent of residual luminal narrowing and/or recoarctation |
| Endovascular stent-related complications, including leak, migration, fracture, thrombosis presence, site morphology, and extent of aortic dilatation, aneurysm, or dissection |
| Anatomy and patency of aortic arch branch arteries |
| Presence and extent of collateral vessel formation |
| Coexisting anomalies including bicuspid aortic valve with its complications other associated congenital heart disease |
| Presence, extent, and severity of associated coronary atherosclerosis |

## 15.4 Aortic Arch Anomalies

Aortic arch anomalies represent a wide spectrum of symptomatic and asymptomatic congenital malformations that affect both the aortic arch and its branches.

Knowledge of the embryology of the great arteries is helpful in understanding the variations in the number, size, and position of the thoracic great vessels.

The normal left aortic arch and its branches develop from paired pharyngeal arches which form during the 4th and 5th weeks of development and undergo a process of orderly regression. There are six potential arches in the human embryo that are numbered craniocaudally as I, II, III, IV, V, and VI. Arch V may never form or incompletely forms and then regresses. Arches III, IV, and VI develop into the great arteries (Figs. 15.13 and 15.14). Arch III forms the common carotid arteries and the first part of the internal carotid arteries. Right arch IV forms the most proximal segment of the right subclavian artery, and left arch IV develops into the segment of the aortic arch between the left common carotid and the left subclavian arteries. Right arch VI creates the right pulmonary artery, and the left arch VI becomes the left pulmonary artery and the ductus arteriosus.

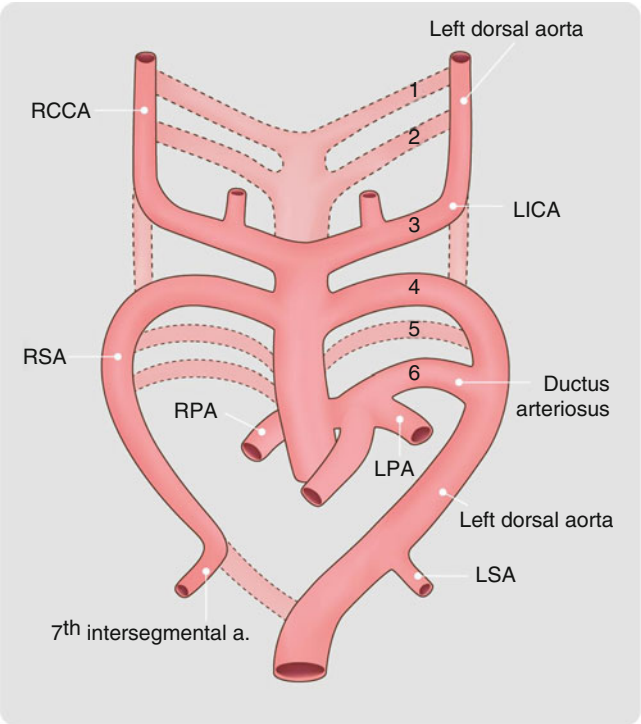


**Fig. 15.13** Normal embryologic development of the great arteries. At 6 weeks, the first and second pairs of branchial arches have virtually disappeared. The third arch forms the common carotid arteries. The right fourth arch becomes the proximal part of the right subclavian artery and the left fourth arch becomes part of the normal aortic arch. The distal parts of the subclavian arteries develop from the seventh intersegmental arteries. The fifth arch either never forms or involutes early. The sixth pair of arches forms the pulmonary arteries bilaterally. The left sixth arch also gives rise to the ductus arteriosus. Arches are numbered *1–6*. *RCCA* right common carotid artery, *LICA* left internal carotid artery, *RSA* right subclavian artery, *RPA* right pulmonary artery, *LSA* left subclavian artery, *LPA* left pulmonary artery

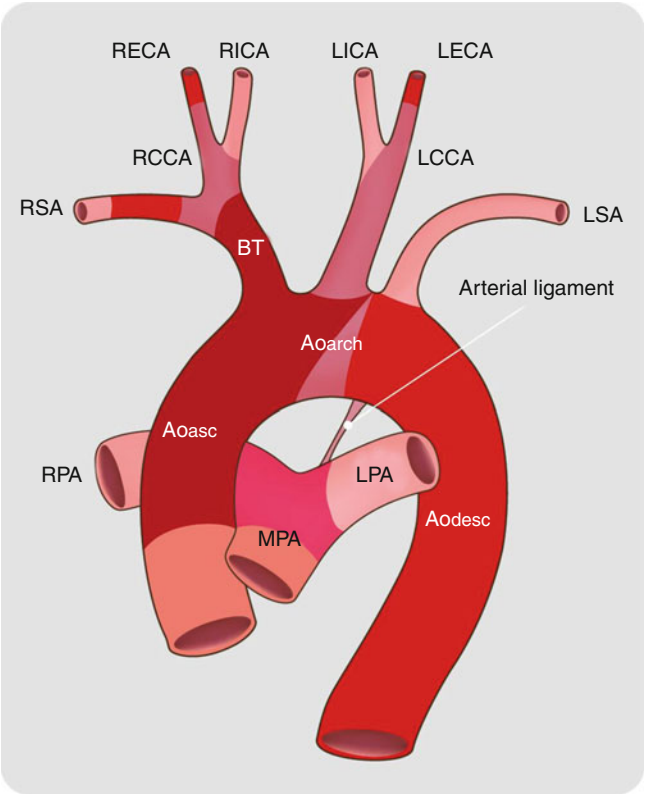


**Fig. 15.14** The normal adult aortic arch. The right subclavian and carotid arteries join to form the right brachiocephalic artery. The left subclavian and carotid arteries arise separately from the aorta. *Aoasc* ascending aorta, *Aoarch* aortic arch, *Aodesc* descending aorta, *MPA* main pulmonary artery, *RPA* right pulmonary artery, *LPA* left pulmonary artery, *BT* brachiocephalic trunk, *RSA* right subclavian artery, *RCCA* right common carotid artery, *RECA* right external carotid artery, *RICA* right internal carotid artery, *LCCA* left common carotid artery, *LICA* left internal carotid artery, *LECA* left external carotid artery, *LSA* left subclavian artery

In the 5th week, the two aortas fuse caudally below T4 to form a single aorta in the distal thorax and abdomen. Persistence of a segment of arch that should have regressed or regression of a segment of arch that should have persisted accounts for the development of most arch anomalies.

Arch anomalies can be subdivided into anomalies of position and arch branching and anomalies of number (i.e., supernumerary arches). The abnormalities of branching and position include left aortic arch with aberrant left subclavian artery, right aortic arch with mirror-image branching, right aortic arch with aberrant left subclavian artery, and cervical aortic arch. Supernumerary arches include double aortic arch and persistent fifth aortic arch.

Aortic arch anomalies may produce vascular rings that surround the thoracic anatomy (trachea and esophagus). The primary symptomatology associated with vascular rings relates to the structures that they encircle and may include dysphagia, odynophagia, wheezing, and shortness of breath with and without exertion. Arch anomalies that completely encircle the trachea and bronchi are referred to as "vascular rings." Vascular rings are more likely to be symptomatic than arch anomalies that only partially surround adjacent structures. The majority of symptomatic arch anomalies are diagnosed in infants; however, adults with vascular rings may be symptomatic.

### 15.4.1 Left Aortic Arch with Aberrant Right Subclavian Artery

The left aortic arch with an aberrant right subclavian artery is the most common congenital abnormality of the aortic arch vessels and occurs in about 0.5–2 % of the general population [51, 52].

Normally, the right subclavian artery is a continuation of the brachiocephalic artery which is the first major aortic arch branch vessel. In left aortic arch with aberrant right subclavian artery, the right subclavian artery is the last branch off the aortic arch. In this anomaly, the proximal to distal order of branching is as follows: right common carotid, left common carotid, left subclavian, and then the aberrant right subclavian (Figs. 15.15 and 15.16). The anomalous artery courses cephalad from left to right, crossing behind the

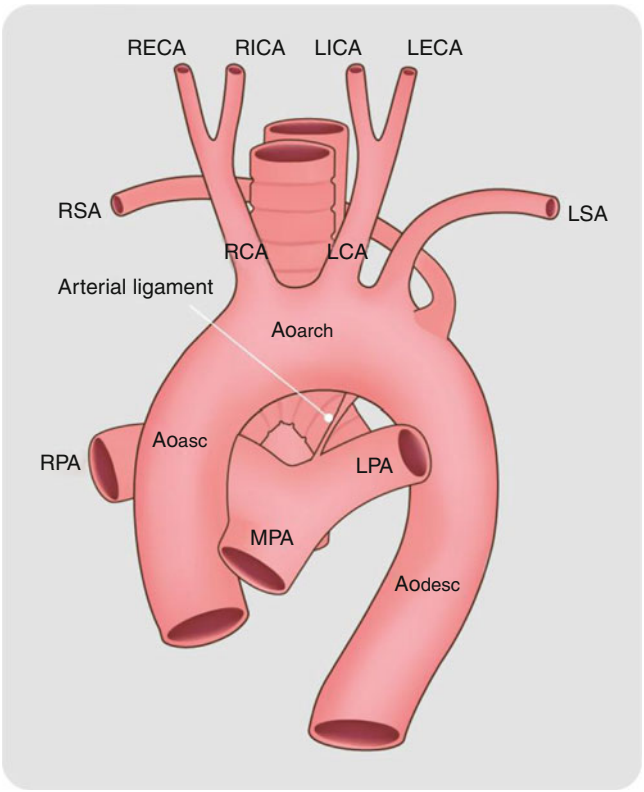


**Fig. 15.15** Left aortic arch with aberrant right subclavian artery. Note the right subclavian artery (*RSA*) is the last branch off the arch. *Ao asc* ascending aorta, *Ao arch* aortic arch, *Ao desc* descending aorta, *LPA* left pulmonary artery, *LSA* left subclavian artery, *LCA* left carotid artery, *MPA* main pulmonary artery, *RPA* right pulmonary artery, *RCA* right carotid artery, *Arrow* ligamentum ductus arteriosum, *RECA* right external carotid artery, *RICA* right internal carotid artery, *LICA* left internal carotid artery, *LECA* left external carotid artery

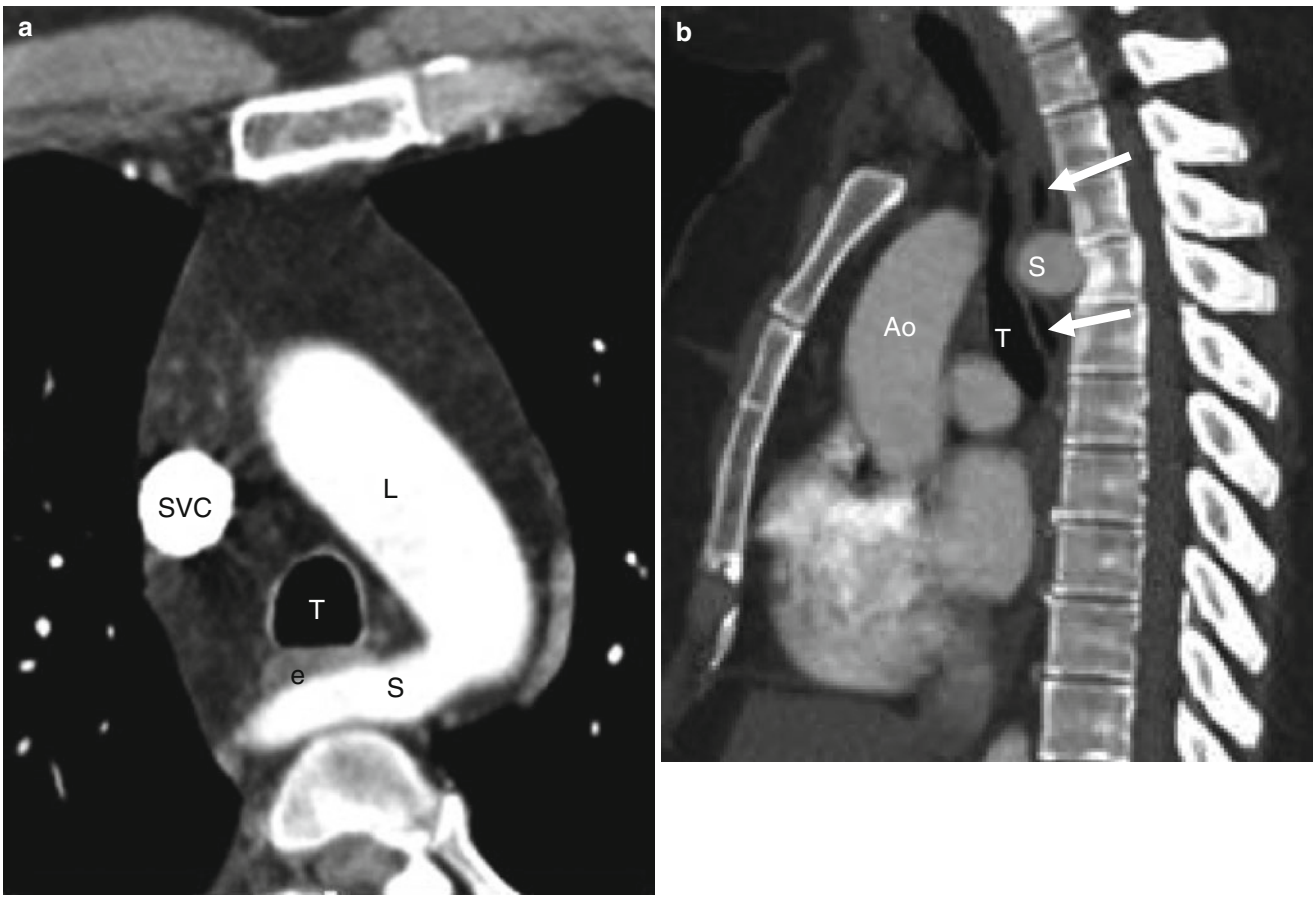


**Fig. 15.16** Left aortic arch with an aberrant right subclavian artery. Panel (**a**) is an axial image showing a left aortic arch (*L*) and an aberrant right subclavian artery (*S*) coursing posterior to the esophagus (*e*) and trachea (*T*). Panel (**b**) is a sagittal image demonstrating the right subclavian artery (*S*) coursing posteriorly and compressing both the esophagus (*arrows*) and trachea (*T*). *Ao* aorta, *SVC* superior vena cava

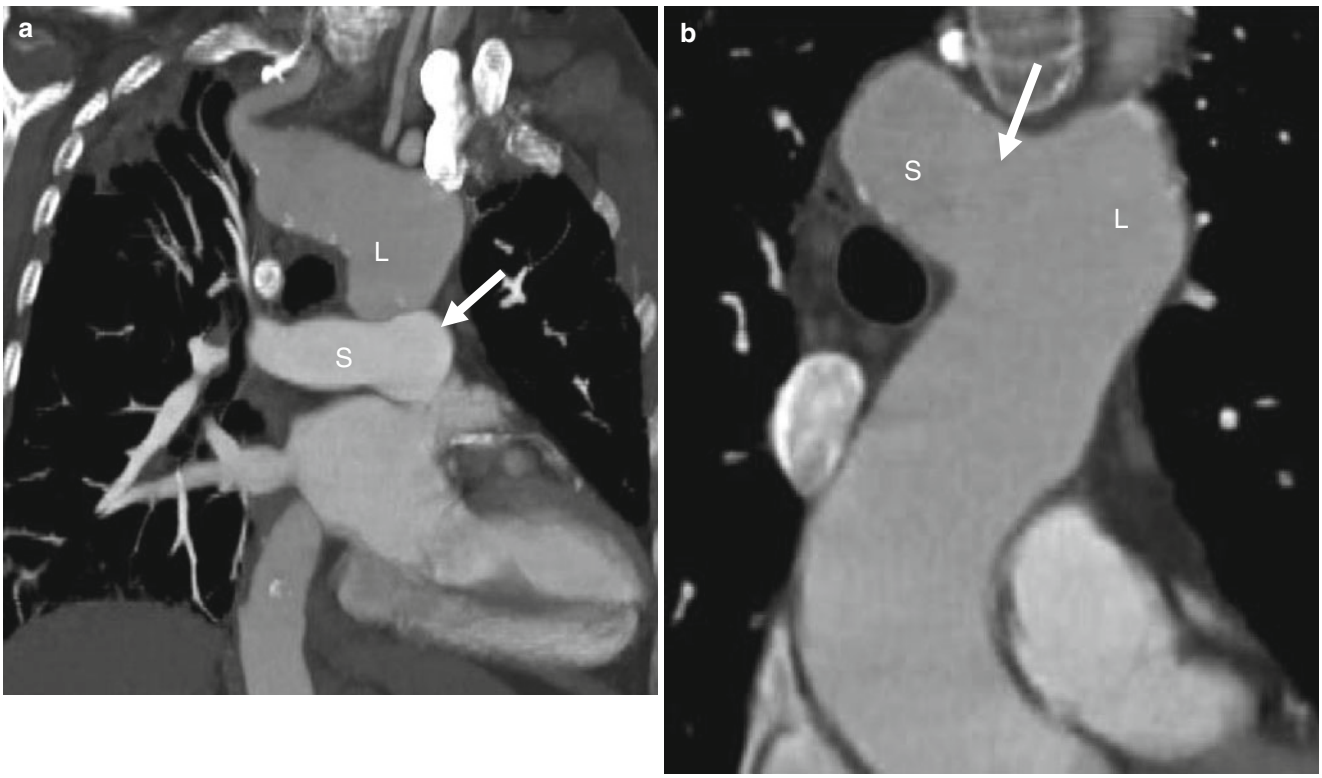


**Fig. 15.17** Left arch with aberrant right subclavian artery and diverticulum of Kommerell. Panels (**a**) and (**b**) are coronal views showing the left aortic arch (*L*) and an aberrant right subclavian artery (*S*), which is focally enlarged at its origin. This focal enlargement is termed a diverticulum of Kommerell (*arrow*)

trachea and esophagus to reach the right arm. Dilatation of the origin of the aberrant vessel, termed a diverticulum of Kommerell, is common (Fig. 15.17). The diverticulum of Kommerell itself may give rise to right subclavian artery. Atherosclerotic changes and intramural thrombus formation are known to occur within this diverticulum.

Left aortic arch with aberrant right subclavian artery is associated with a left ductus arteriosus (ductus arteriosum ligament) which completes the vascular ring. This malformation may be associated with other congenital heart diseases, most frequently tetralogy of Fallot and ventricular septal defects [50]. Its incidence is also increased in trisomy 21 syndrome [53].

This anomaly is usually asymptomatic and found incidentally on imaging examinations. However, if the aberrant subclavian artery is ectatic, it may compress the esophagus resulting in dysphagia (dysphagia lusoria). It may occasionally also result in airway compression which may result in wheezing and shortness of breath.

### 15.4.2 Rare Left Aortic Arch Anomalies

Left aortic arch with right descending aorta and a right arterial duct/ligament describes an arch anomaly in which the left-sided aortic arch takes a retroesophageal course and, from proximal to distal, gives rise first to the right carotid artery, followed by left carotid artery, left subclavian artery, and finally the right subclavian artery [51]. A vascular ring is completed by the right arterial duct/ligament.

Left aortic arch with isolation of the subclavian artery depicts an arch anomaly where the left subclavian artery originates exclusively from the pulmonary artery via an arterial duct or ligament. The subclavian artery is supplied by the pulmonary artery if the ductus arteriosus is patent. When arterial duct closes, the subclavian artery is supplied by retrograde flow from the vertebral artery.

### 15.4.3 Right Aortic Arch with Mirror-Image Branching

In the right aortic arch with mirror-image branching, the aortic arch branch arteries arise from the right arch in the following order from proximal to distal: left innominate artery, right carotid artery, and right subclavian artery (Figs. 15.18 and 15.19). The aorta usually descends on the right. The ductus ligamentum arteriosum is on the right, and thus, there is no vascular ring. A right aortic arch with mirror-image branching occurs in 2–3 % of population [54].

Most patients with this anomaly come to clinical attention because of associated heart disease, which is usually cyanotic. The common associated anomalies with a mirror-image

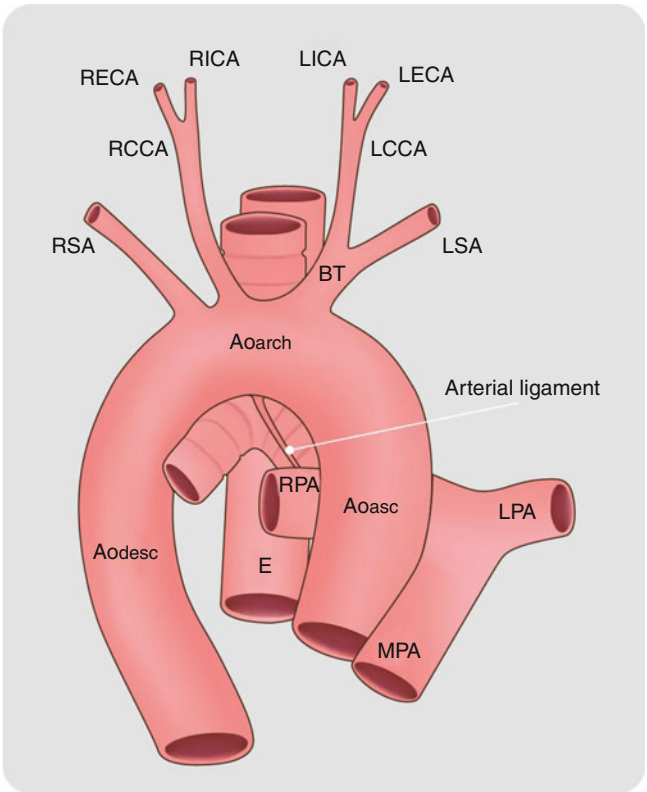


**Fig. 15.18** Right aortic arch with mirror-image branching. Branch arteries arise in the following proximal to distal order: left brachiocephalic trunk (*BT*)/innominate artery (*IA*), right carotid artery (*RCCA*), and right subclavian artery (*RSA*). *Ao asc* ascending aorta, *Ao arch* aortic arch, *Ao desc* descending aorta, *LCCA* left common carotid artery, *LPA* left pulmonary artery, *MPA* main pulmonary artery, *RPA* right pulmonary artery, *E* esophagus, *RECA* right external carotid artery, *RICA* right internal carotid artery, *LECA* left external carotid artery, *LICA* left internal carotid artery, *LSA* left subclavian artery

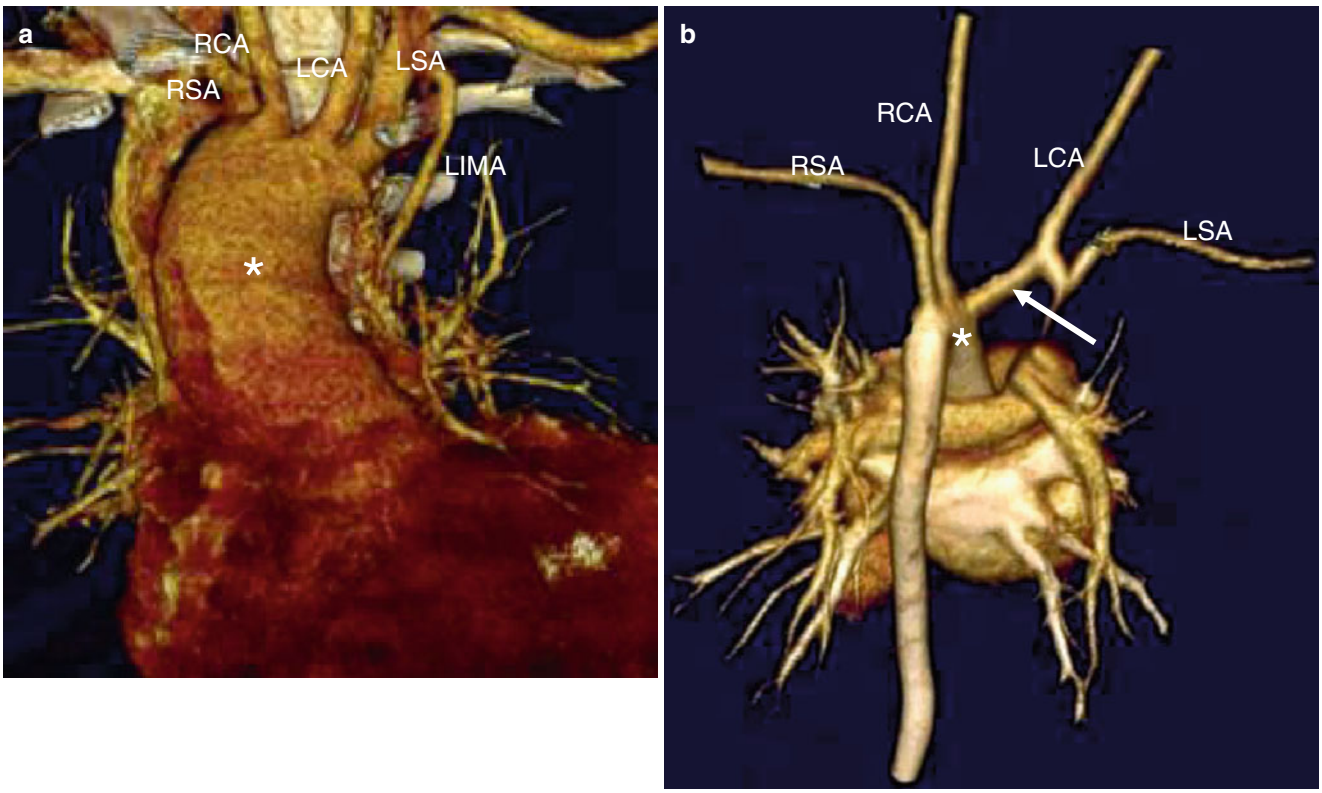


**Fig. 15.19** Right aortic arch with mirror-image branching. Panels (**a**) (anterior view) and (**b**) (posterior view) are coronal images in two different patients showing a right aortic arch (*asterisks*) with mirror-image branching. The great arteries originate from the arch in the following order: left common carotid artery (*LCA*), right common carotid artery (*RCA*), right subclavian artery (*RSA*), and left subclavian artery (*LSA*). *LIMA* left internal mammary artery. *Arrow* in panel (b) left innominate artery

right arch are tetralogy of Fallot, truncus arteriosus, pulmonary artery atresia with ventricular septal defect, tricuspid atresia, double-outlet right ventricle, and transposition of the great arteries [55]. Because of the concomitant heart disease, the right arch with mirror-image branching usually is discovered in infancy.

### 15.4.4 Right Aortic Arch with Aberrant Left Subclavian Artery

A right aortic arch anomaly with an aberrant left subclavian artery gives rise to the great arteries from proximal to distal in the following order: left common carotid artery, right common carotid artery, right subclavian artery, and left subclavian artery (Fig. 15.20). The aberrant left subclavian artery often arises from a diverticulum of Kommerell (Fig. 15.21). The descending aorta is commonly right-sided. A left-sided arterial duct (ductus ligament) is present and thus the malformation forms a vascular ring (formed by the right arch, left subclavian artery, and ligamentum arteriosum, which attaches to the left pulmonary artery) [51]. This anomaly accounts for 30–40 % of vascular rings [51].

### 15.4.5 Rare Right Aortic Arch Anomalies

Right aortic arch with left descending aorta and left arterial duct/ligament describes an arch anomaly in which the right-sided aortic arch takes a retroesophageal course and gives rise first to the innominate artery followed by the right carotid artery and finally the right subclavian artery, or it gives rise to the left carotid artery followed by the right carotid artery, right subclavian artery, and finally the left subclavian artery [51]. A vascular ring is formed by the right arch and the aberrant left subclavian artery and completed by the left arterial duct/ligament.

Right aortic arch with aberrant innominate artery represents an aortic arch anomaly where the right-sided aortic arch gives rise first to the right carotid artery, followed by the right subclavian artery, and finally to the left innominate artery [51]. The aberrant left innominate artery takes a retroesophageal course and bifurcates into left carotid artery and left subclavian artery.

Right aortic arch with isolation of the contralateral arch vessel is an arch anomaly in which an arch vessel originates exclusively from pulmonary artery via an arterial duct or ligament [51]. The left subclavian, left carotid, or left innominate artery may originate from the pulmonary artery. Isolated

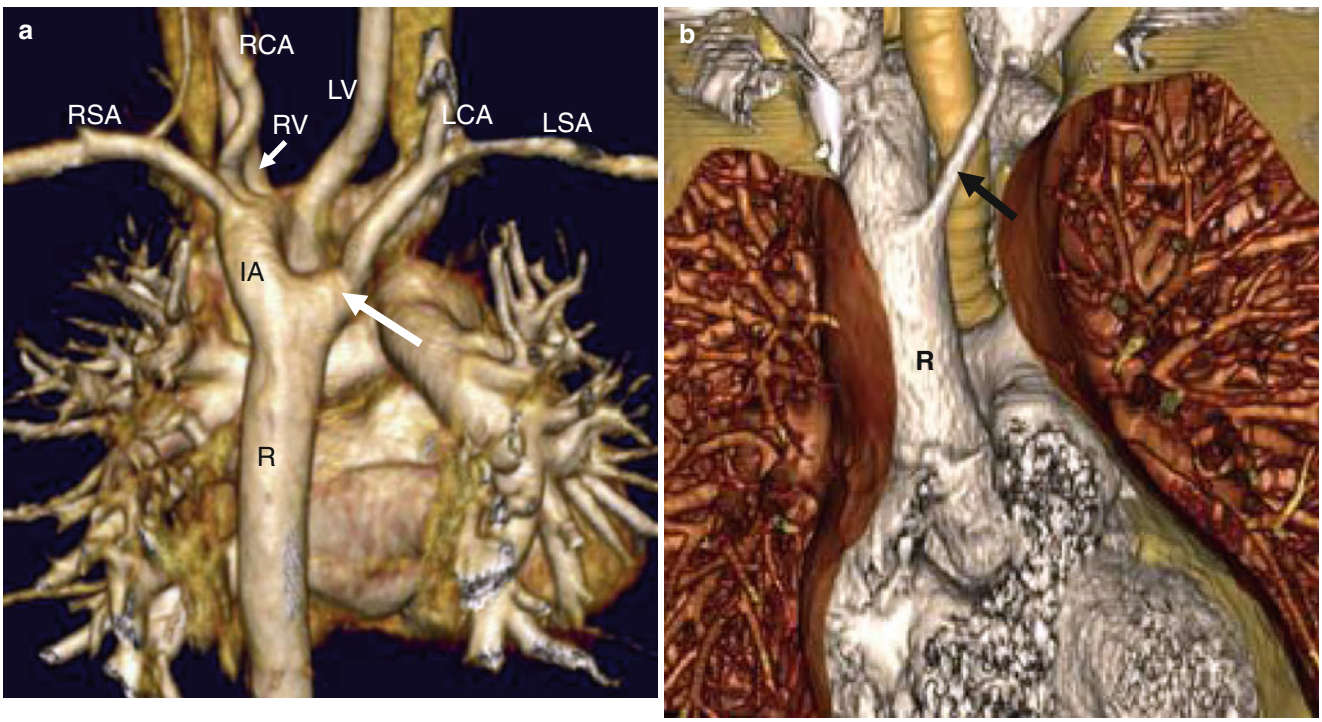


**Fig. 15.20** Right aortic arch with aberrant left subclavian artery. Panel (**a**) this coronal image viewed from the posterior perspective demonstrates a right aortic arch (*R*). An aberrant retroesophageal left subclavian artery (*LSA*) is the last artery to arise from the arch. The *arrow* indicates the site of origin of the LSA from a diverticulum of Kommerell. Panel (**b**) is a coronal image viewed anteriorly from a separate patient and demonstrates a right aortic arch (*R*) and the aberrant left subclavian artery (*arrow*) arising from the ascending aorta. *LCA* left common carotid artery, *RCA* right common carotid artery, *RSA* right subclavian artery, *IA* right innominate artery, *LV* left vertebral artery, *RV* right vertebral artery

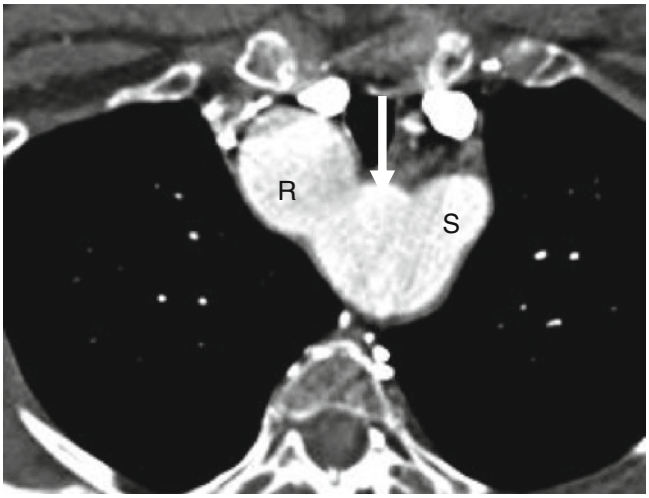


**Fig. 15.21** Right aortic arch with aberrant left subclavian artery. This axial view shows a right aortic arch (*R*) and aberrant right subclavian artery (*S*) arising from a large diverticulum of Kommerell (*arrow*)

left subclavian artery is the most common form of this anomaly. Isolated arch vessels are associated with congenital heart diseases, most frequently tetralogy of Fallot [56].

### 15.4.6 Cervical Aortic Arch

A cervical aortic arch is a rare anomaly characterized by a high-riding elongated aortic arch, which extends above the sternum into the neck before turning downward to descend in the thorax (Figs. 15.22 and 15.23). There is a retroesophageal course of the descending aorta with the retroesophageal aorta giving off the left subclavian artery. A right-sided cervical arch is more common than a left-sided cervical arch. The prevalence of cervical aortic arch is estimated at 0.01 % [57].

Cervical aortic arch is usually an isolated finding, but it may be accompanied by other cardiac abnormalities. The arch may be hypoplastic, tortuous, or obstructed and is frequently associated with aneurysm formation [57]. Other anomalies include absence of the innominate artery and origin of the contralateral subclavian artery from the descending proximal aorta. When the ligamentum arteriosum is on the side opposite of the arch, a vascular ring is formed.

Most patients are asymptomatic and the diagnosis is an incidental finding on imaging examinations. Clinical symptoms include dysphagia from the retroesophageal course of the aorta or from a vascular ring and a pulsatile neck mass.

### 15.4.7 Supernumerary Arches

#### 15.4.7.1 Double Aortic Arch

The double aortic arch is characterized by the presence of two aortic arches arising from a single ascending aorta

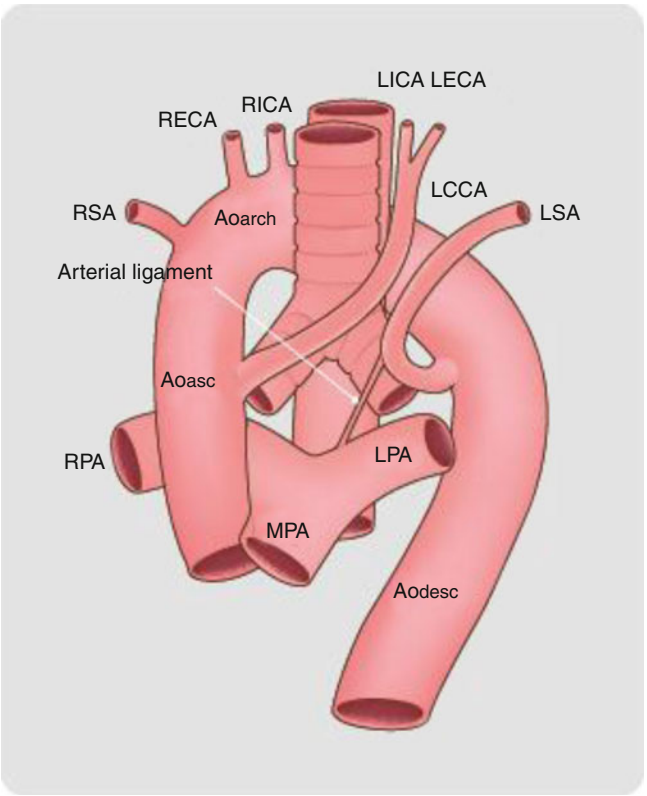


**Fig. 15.22** An artist's depiction of a cervical aortic arch. In this anomaly, the aortic arch extends above the sternum before descending in the thorax. *Ao asc* ascending aorta, *Ao arch* aortic arch, *Ao desc* descending aorta, *LPA* left pulmonary artery, *LSA* left subclavian artery, *MPA* main pulmonary artery, *RPA* right pulmonary artery, *RSA* right subclavian artery, *RECA* right external carotid artery, *RICA* right internal carotid artery, *LICA* left internal carotid artery, *LECA* left external carotid artery

(Figs. 15.24 and 15.25). Each arch gives rises to its own subclavian and carotid artery before uniting to form a single descending aorta, which is usually left sided. Both limbs of the double arch are usually patent and functioning. The right limb is typically larger and more cephalad than the left arch, but both arches may be the same size and occasionally, one arch, usually the left, may be hypoplastic or atretic with a fibrous band completing the vascular ring (Fig. 15.26). Double arches with hypoplastic or atretic components can still compress the esophagus and trachea and be symptomatic.

Double aortic arch is the most frequent vascular ring resulting in tracheoesophageal compression [50]. The left aortic arch usually takes a course similar to the normal left aortic arch, while the right aortic takes a course behind the esophagus to join the left aortic arch. Double arch is usually diagnosed in childhood, but it can be discovered incidentally in adults if the ring formed by the double arch is loose. Double aortic arch is usually an isolated finding but may be accompanied by cardiac malformations, most frequently tetralogy of Fallot and transposition of great arteries [58]. It

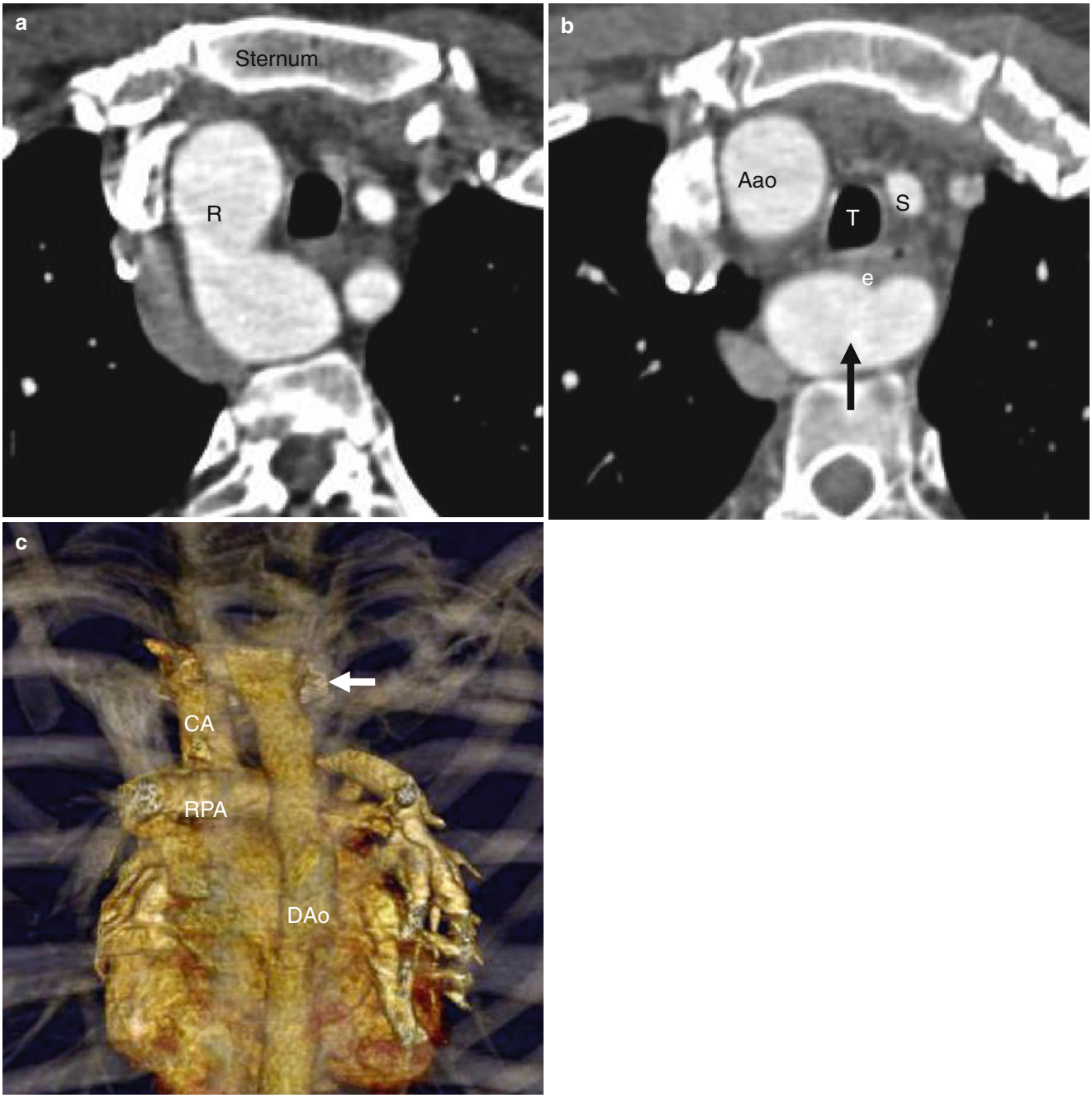


**Fig. 15.23** Cervical aortic arch. Panel (**a**) an axial image showing a right-sided aorta (*R*) extending to the sternum. Panel (**b**) this image shows that as the aorta descends; it crosses the mediastinum (*arrow*) posterior to the esophagus (*e*) and trachea (*T*). The left subclavian (*S*) artery arises from the retroesophageal aorta (origin is not visible in this view). *Aao* ascending aorta. Panel (**c**) an oblique 3D image viewed from the posterior showing the cervical arch (*CA*) ascending on the right above the sternum (*arrow*) before crossing the mediastinum to descend on the left. *Dao* descending aorta, *RPA* right pulmonary artery

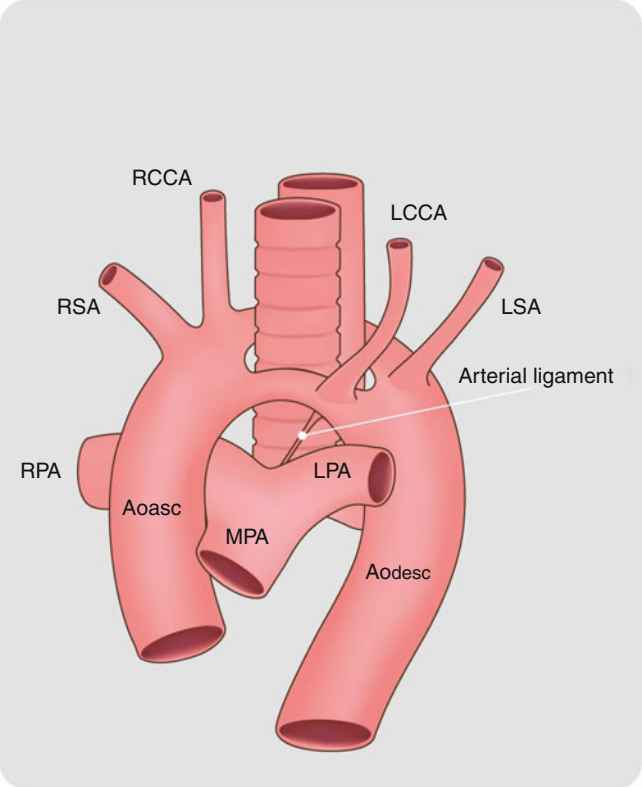


**Fig. 15.24** Double aortic arch. The persistence of both fourth arches results in the formation of a double aortic arch arrangement. Note that each arch gives rise to a separate carotid and subclavian artery. There is no innominate/brachiocephalic artery. *Ao asc* ascending aorta, *Ao desc* descending aorta, *LCCA* left common carotid artery, *LPA* left pulmonary artery, *LSA* left subclavian artery, *MPA* main pulmonary artery, *RCCA* right common carotid artery, *RPA* right pulmonary artery, *RSA* right subclavian artery

may be also associated with cervical aortic arch and coarctation of aorta.

### 15.4.8 Persistent Fifth Aortic Arch

Persistent fifth aortic arch is an anomaly in which both arches are present on the same side of the trachea. Two variants have been reported: (a) double aortic arch with both lumina patent and (b) double aortic arch with interrupted or atretic superior and patent inferior arch. In the more common second variant, the inferior arch extends from the innominate artery to the takeoff of the left subclavian artery levels [59]. Persistent fifth arch is usually accompanied by congenital heart malformations; however, it may be an isolated finding.

### 15.4.9 Cardiac Computed Tomography (CT) in the Evaluation of Aortic Arch Anomalies

CT enables detection and depiction of the morphology of aortic arch anomalies [5, 47, 56, 60]. The following parameters need to be assessed: (a) course and branching pattern of the aortic arch, (b) number of arches, (c) presence of a hypoplastic or atretic segment, (d) compression of the trachea or esophagus, and (e) accompanying anomalies and other congenital heart lesions.

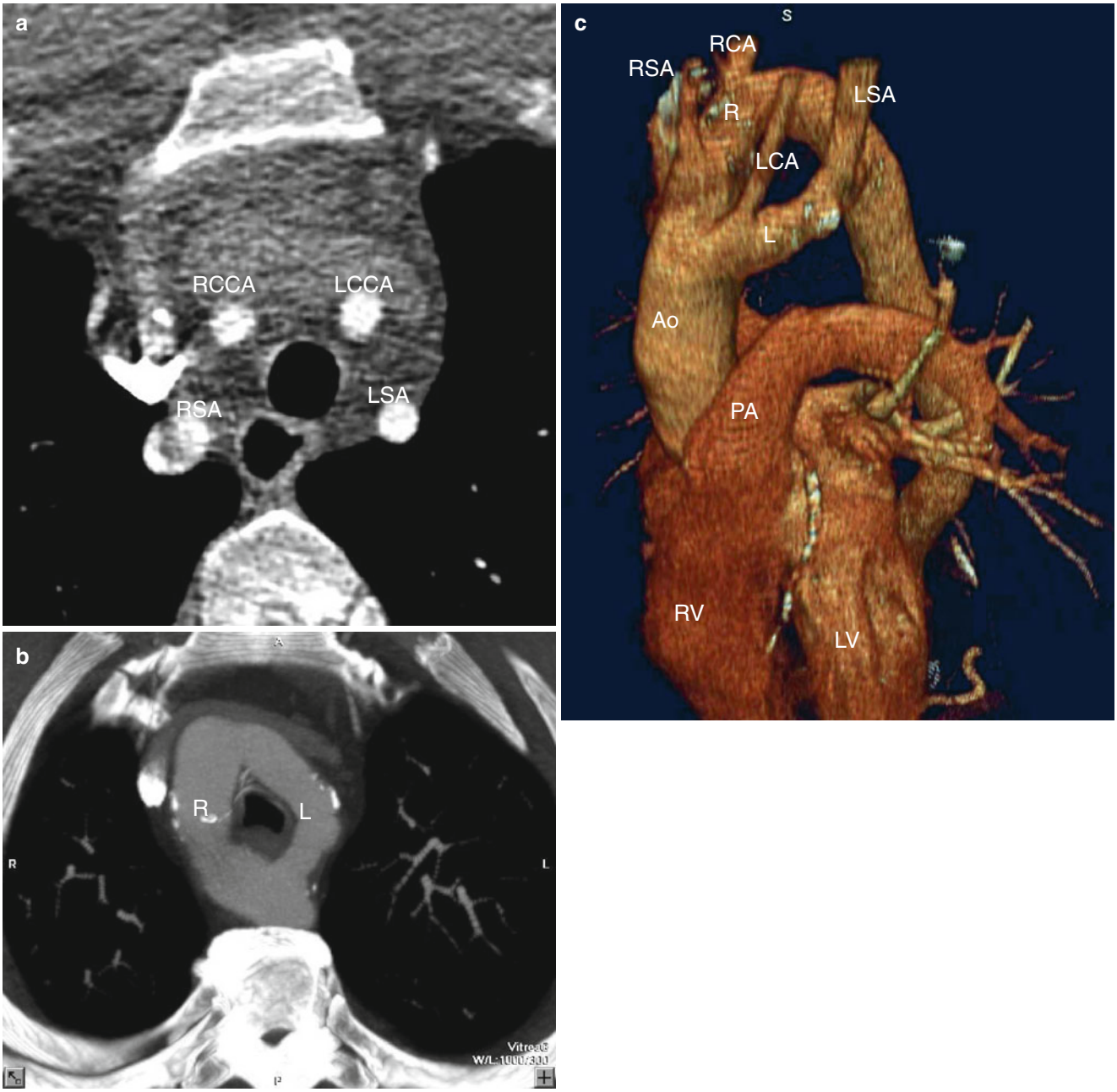


**Fig. 15.25** Double aortic arch. Panel (**a**) is an axial image showing four separate branch vessels. *RSA* right subclavian artery, *LSA* left subclavian artery, *RCCA* right common carotid artery, *LCCA* left common carotid artery. This anatomy is abnormal since in the normal anatomy there is right brachiocephalic artery and separate origins for the left carotid and subclavian arteries. Panel (**b**) is another axial CT section showing a complete ring around the esophagus and trachea formed by a double aortic arch (*R* right arch, *L* left arch). Panel (**c**) is a 3D volume-rendered sagittal view showing two arches that arise from the ascending aorta (*Ao*) and joining posteriorly. The right-sided arch (*R*) is of larger caliber and more superior than the left-sided arch (*L*). *RV* right ventricle, *LV* left ventricle, *PA* pulmonary artery, *LSA* left subclavian artery, *RSA* right subclavian artery, *RCA* right carotid artery, *LCA* left carotid artery

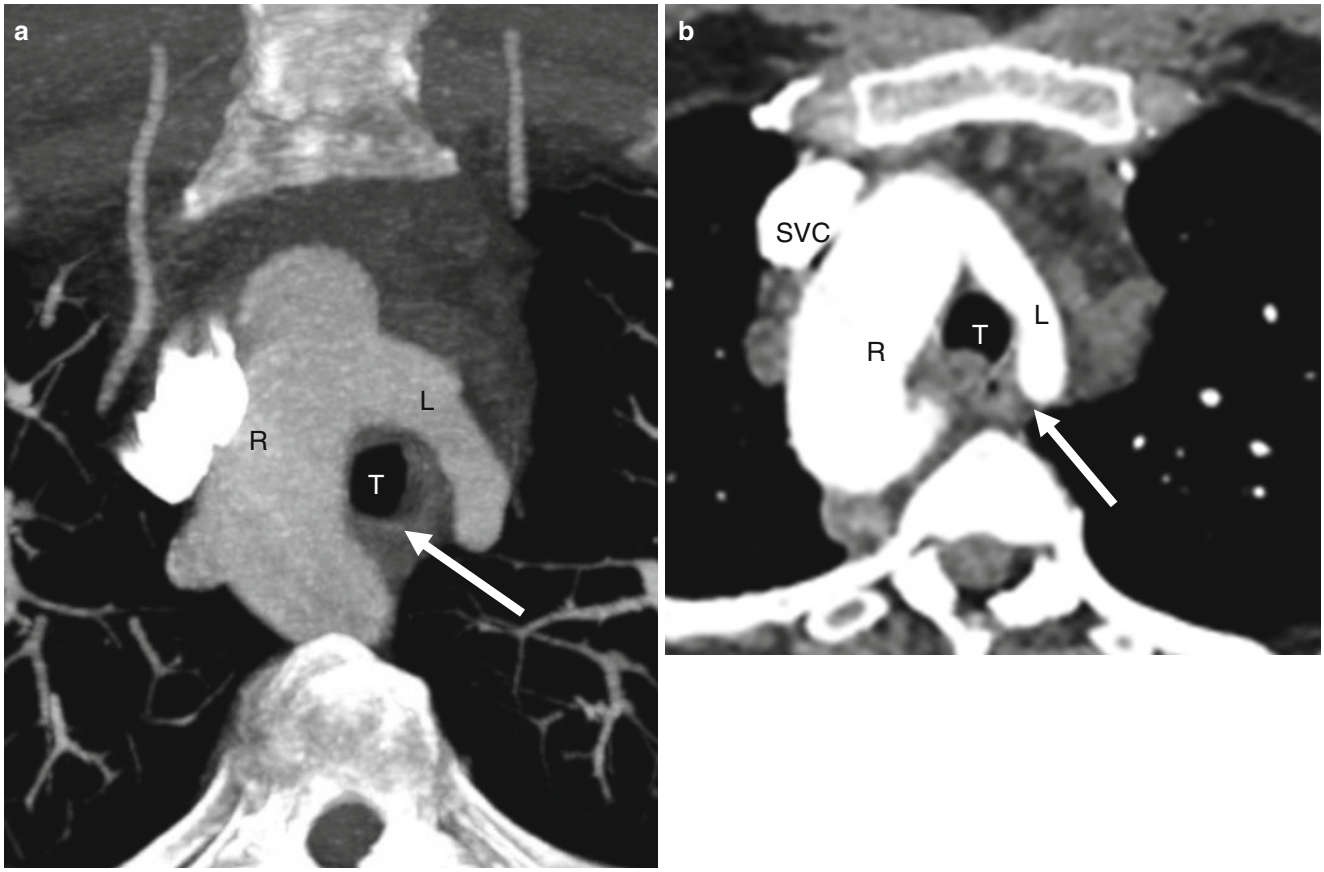


**Fig. 15.26** Double aortic arch with atretic left aortic arch. Panels (**a**) and (**b**) are axial scans in two patients showing both a right (*R*) and left (*L*) arches encircling the trachea (*T*). A fibrous band (*arrow*) joins the left aortic arch (*L*) to the larger descending right aortic arch (*R*). *SVC* superior vena cava

## 15.5 Sinus of Valsalva Aneurysm

The sinus of Valsalva aneurysm (SVA) is most often congenital and accounts for 0.1–3.5 % of all congenital heart diseases [61]. A 4:1 male predominance is reported [61]. The sinuses of Valsalva are normal dilatations of the aortic root wall that arise between the aortic valve annulus and the sinotubular ridge. These three sinuses are associated with a corresponding right, left, or noncoronary aortic valve cusps and are named as such (right sinus of Valsalva, left sinus of Valsalva, and noncoronary sinus of Valsalva).

SVA results from incomplete fusion of the distal bulbar septum that divides the truncus arteriosum into the aorta and the pulmonary artery, resulting in a localized weakness of the elastic lamina at the junction of the aortic media and the annulus fibrosus of the aortic valve [61]. As a result of exposure to high pressures, this area of localized weakness, which forms part of the sinuses of Valsalva, dilates and becomes aneurysmal.

The right coronary sinus is most commonly involved and accounts for 75–90 % of cases of SVA, followed by the noncoronary sinus and infrequently the left coronary sinus [61].

Common associated anomalies are ventricular septal defect, aortic insufficiency, bicuspid aortic valve, and less often coronary anomalies. Other associations are Marfan and Ehlers–Danlos syndromes.

### 15.5.1 Clinical Features

Aortic insufficiency is a common complication in both nonruptured and ruptured SVAs. Nonruptured SVAs typically remain clinically silent for many years and are often incidentally found at imaging performed for other clinical indications or for abnormal cardiac contours seen on chest radiography. Symptoms can develop if they cause mass effect on the conduction system resulting in complete heart block or extrinsically compress a coronary vessel leading to symptomatic ischemia [62]. Intracardiac rupture occurs most commonly in the third or fourth decade of life and results in sudden onset of chest pain and heart failure due to mass effect on adjacent cardiac structures. Rupture typically results in communication of the aortic sinus with the right ventricle or right atrium (especially if the aneurysm affects

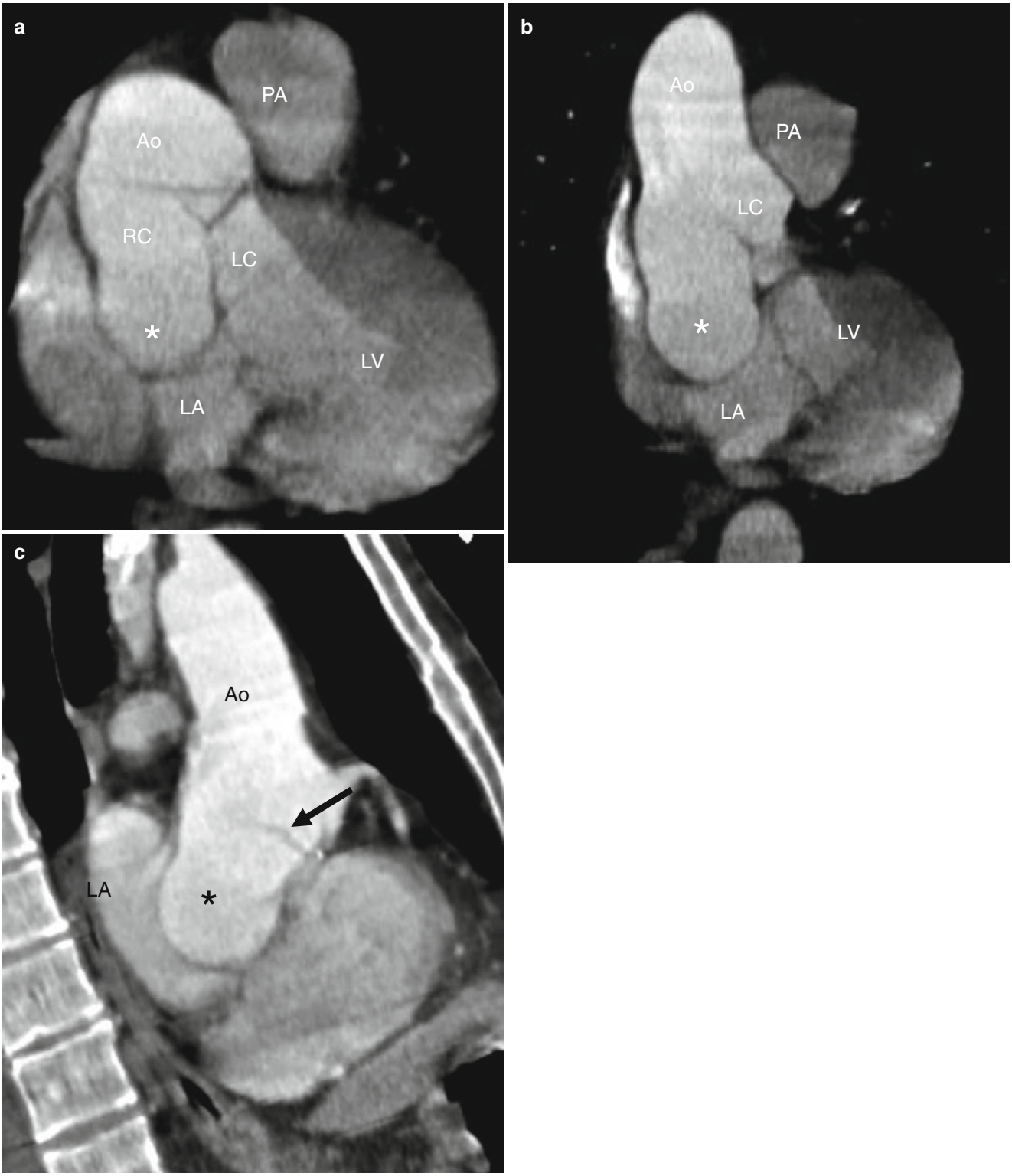


**Fig. 15.27** Nonruptured sinus of Valsalva aneurysm. Panel (**a**) an axial scan, panel (**b**) a coronal section, and panel (**c**) a sagittal view show aneurysmal dilatation of the noncoronary sinus of Valsalva. There is mild dilatation of the right and left coronary sinuses of Valsalva and mild ectasia of the proximal ascending aorta just distal to the cusps. The aneurysm compresses the left atrium. The *arrow* indicates the closed aortic valve. *Asterisk*: right coronary sinus of Valsalva aneurysm. *RC* right coronary cusp, *LC* left coronary cusp, *Ao* aorta, *LA* left atrium, *LV* left ventricle, *PA* pulmonary artery

the noncoronary cusp), which can lead to clinical signs of tricuspid atresia [63].

Management consists of operative resection of the aneurysmal wall and closure of the mouth with a patch with or without aortic valve surgery.

### 15.5.2 Cardiac Computed Tomography (CT) in the Evaluation of Sinus of Valsalva Aneurysm

CT is useful to confirm echocardiographic findings of SVAs and plan interventions and device selection in patients with SVA rupture [63–66]. Ruptured SVA is easily diagnosed with transthoracic echocardiography, but CT provides superior spatial resolution and coronary anatomy information prior to surgical procedures [65].

The CT criteria for diagnosis of a SVA are a saccular-shaped structure with an origin above the aortic annulus and normal dimensions of the adjacent aortic root and ascending aorta (Fig. 15.27) [63–66]. A giant SVA can protrude into the right ventricle or right atrium. SVA rupture on CT would manifest by the presence of a jet of contrast extending from the aneurysm into an adjacent cardiac chamber (Fig. 15.28). CT can also identify SVA compression of adjacent structures, including the coronary arteries.

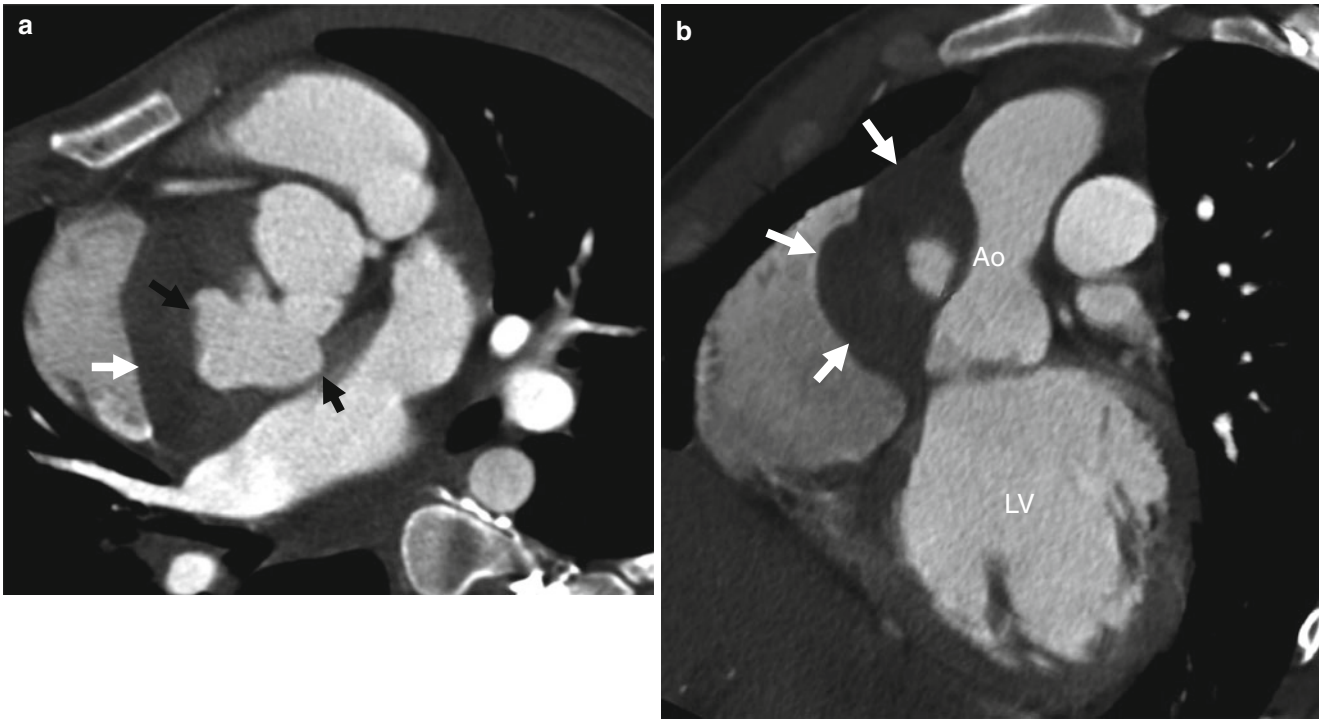


**Fig. 15.28** Rupture of the sinus of Valsalva in a 23-year-old man presenting with orthopnea. Panel (**a**) is an axial image showing a large, bizarre-shaped pseudoaneurysm (*black arrows*) with partial thrombi (*white arrow*) on the right side of the aortic root. Panel (**b**) is a coronal section showing a lobulated, low-attenuation lesion suggestive of a confined thrombus (*white arrows*) along the right side of the aortic root (Reproduced with kind permission of the Radiological Society of North America, Oak Brook, Il from Chae et al. [67]). *Ao* aorta, *LV* left ventricle

## 15.6 Genetic Aortopathies

There are several syndromic and nonsyndromic genetic conditions that are associated with the development of thoracic aortic aneurysms as well as aortic dissection, including Marfan syndrome, Loeys–Dietz syndrome, Ehlers–Danlos syndrome, Turner syndrome, as well as other genetic mutations (TGFBR1, TGFBR2, FBN1, ACTA2, COL3A1, MYH11) [68].

### 15.6.1 Marfan Syndrome

Marfan syndrome is an inherited multisystemic disorder of connective tissue with a prevalence of approximately 2–3 per 10,000 persons [69]. It is inherited in an autosomal dominant manner, although about 25–30 % of cases are sporadic [70]. Sporadic cases are caused by a mutation in the FBN1 gene that encodes fibrillin, a large glycoprotein that allows structural integrity of the vessel wall [70]. Defective microfibril production causes elastolysis of the connective tissue, which is associated with aneurysm formation and dissection. The classic characteristics of Marfan syndrome are abnormalities of the eyes (lens dislocation), skeleton (increased bone lengths, pectus excavatum, or pectus carinatum, scoliosis, joint laxity), and cardiovascular system (aneurysm and dissection).

Cardiovascular and valvular diseases occur in the majority of Marfan patients (>90 %) and are the cause of death in >90 % of the cases, with aortic rupture accounting for 80 % of the deaths. The average age of death in untreated patients is approximately 35 years versus 75 years in treated patients [71].

The most severe problems in Marfan syndrome include aortic root dilatation and dissection, which have historically been the causative factors in early patient demise. Annuloaortic ectasia, predominantly involving the aortic root, occurs in 60–80 % of adults with Marfan syndrome (Figs. 15.29 and 15.30) [71, 72]. It is characterized by dilatation of all three sinuses of Valsalva, with extension into the sinotubular junction and ultimately into the aortic annulus. Compared with atherosclerotic aortic aneurysms, aortic aneurysms in Marfan syndrome occur in younger patients, enlarge more rapidly, and rarely show intimal calcification or thrombosis [71, 72].

Aortic root dilatation is typically progressive and if untreated leads to aortic dissection or rupture (Fig. 15.31). Moreover, the outer wall of the false lumen of patients with Marfan syndrome is usually extremely thin, thus increasing the risk of rupture [73]. In addition, the dilatation of the aortic ring can cause aortic valve incompetence and regurgitation.

Dilatation of the main pulmonary artery is also common in Marfan syndrome and like dilatation of the ascending aorta, it occurs predominantly in the pulmonic root [73]. Mitral valve prolapse and mitral annular calcification before 40 years of age can occur as well [71].

### 15.6.2 Loeys–Dietz Syndrome

Loeys–Dietz syndrome (LDS) is an autosomal dominant genetic syndrome which has features similar to Marfan syndrome but which is caused by mutations in the genes encoding transforming growth factor beta receptor 1 (TGFBR1) or 2 (TGFBR2) [74–76]. The classic findings include vascular (cerebral, thoracic, and abdominal arterial aneurysms and/or dissections) and skeletal abnormalities (pectus excavatum or pectus carinatum, scoliosis, joint laxity, arachnodactyly, talipes equinovarus). Approximately 75 % of affected individuals have LDS type I with craniofacial manifestations (ocular hypertelorism, bifid uvula, cleft palate, craniosynostosis) and approximately 25 % have LDS type II with cutaneous manifestations (velvety and translucent skin, easy bruising, and wide atrophic scars). The natural cardiovascular history of LDS is development of arterial aneurysms, which have a high incidence of rupture. Median survival in Loeys–Dietz syndrome is 37 years, and the major cause of death is thoracic aortic dissection (67 %), followed by abdominal aortic dissection (22 %) and intracranial bleeding (7 %) [76].

Many of the cardiovascular findings in Loeys–Dietz syndrome are also found in Marfan syndrome patients, including increased risk of ascending aortic aneurysm and aortic dissection (Fig. 15.32). Dissection tends to occur at an earlier age than in Marfan syndrome and the diameter of the dissected aorta is usually less than that in Marfan syndrome. Pulmonary artery dilatation occurs in both LDS and Marfan syndrome. In contrast to Marfan syndrome, the majority (92 %) of patients with Loeys–Dietz syndrome have aneurysms of other vessels that are associated with a high risk of rupture. Similar to Marfan syndrome, CT is the study of choice to identify the vascular manifestations, which in turn helps in planning surgical intervention [77, 78].

### 15.6.3 Ehlers–Danlos Syndrome

Ehlers–Danlos syndrome (EDS) is an autosomal dominant disorder caused by heterozygous mutations in the COL3A1 gene encoding for type III procollagen. There are six major types and at least five minor types of Ehlers–Danlos syndrome. EDS type IV, also called vascular EDS, is characterized by arterial fragility and carries a poor prognosis because of the risk of life-threatening arterial dissection or rupture. The diagnosis of vascular EDS can be challenging as patients often have subtle phenotypic features (thin, translucent skin, hypermobility of small joints, tendon/muscle rupture, easy bruising). In fact, the diagnosis is often unexpected and made at the time of the first vascular complication [79]. Such complications are dramatic, presenting as sudden death, shock, stroke, and acute abdomen. Most patients have experienced a significant complication by age 20 years and more than 80 % by age 40 years. The median

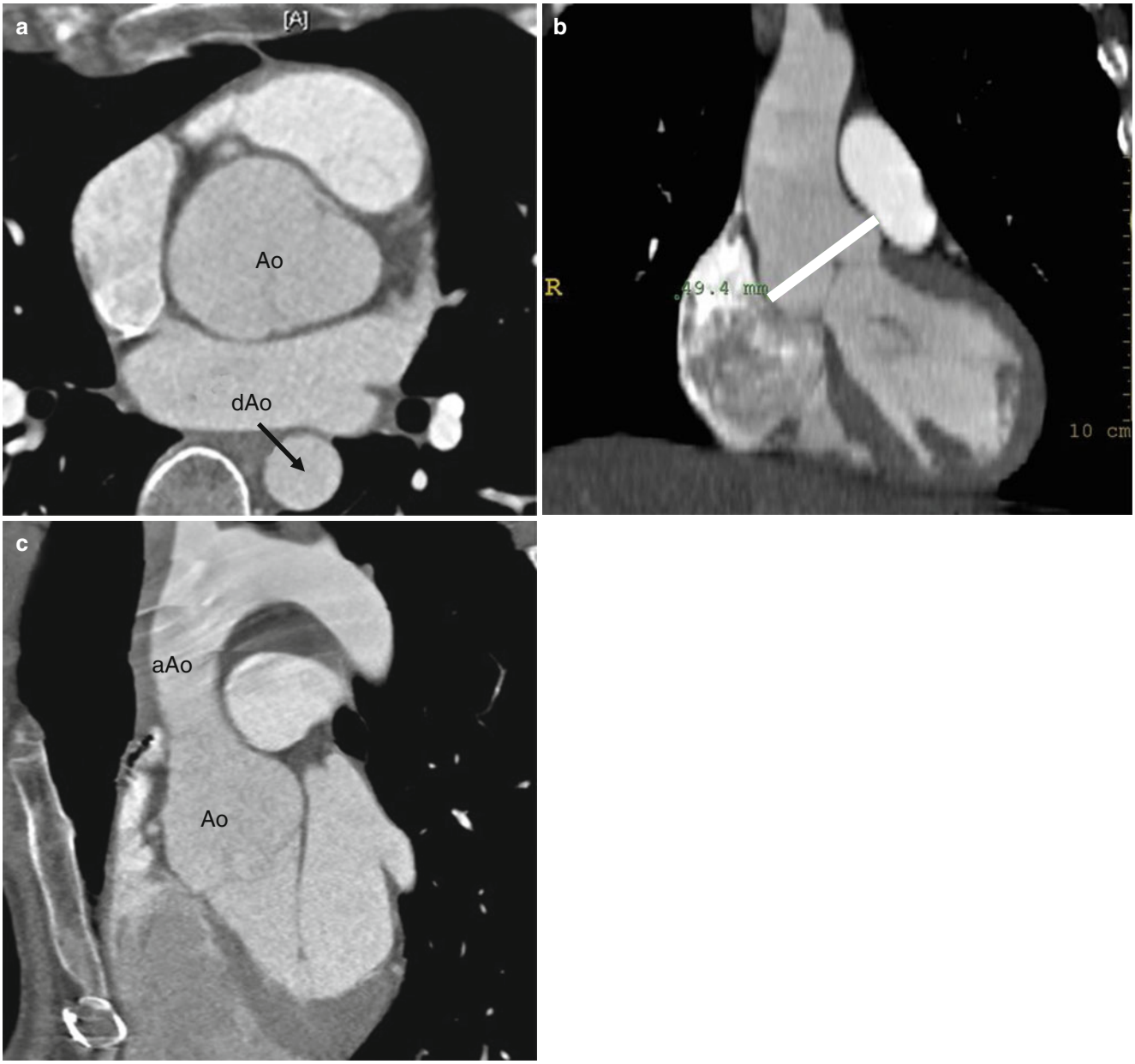


**Fig. 15.29** Annuloaortic ectasia in a patient with Marfan syndrome. Panel (**a**) is an axial scan, panel (**b**) a coronal image, and panel (**c**) a sagittal view. Each shows dilatation of the aortic root (*Ao*, panel a, line panel b). Note the normal size of the ascending aorta (*aAo*) and descending aorta (*dAo*). The aortic root maximum diameter is 4.9 cm. Also note the ectatic involvement of the sinuses of Valsalva

age of death is 48 years [79]. Aortic disruption accounts for many of the deaths in ED's type IV cases.

Similar to Marfan syndrome and LDS, patients with vascular-type EDS have multiple vascular complications, including aneurysm, dissection, and/or rupture of both major and minor arteries (Fig. 15.33). Arterial rupture may be preceded by aneurysm, arteriovenous fistulae, or dissection or may occur spontaneously. The common sites of arterial rupture are the thorax and abdomen followed by the head and neck and extremities. Vascular EDS and LDS share the complications of spontaneous rupture of the spleen, bowel, and uterus. In contradistinction to Marfan syndrome and LDS, vascular abnormalities are progressive in vascular EDS and patients with vascular EDS have a higher incidence of fatal complications from vascular surgery.

Similar to the other genetic aorthopathies, CT should be considered not only for diagnosis but also for surveillance of the disease [80]. Noninvasive imaging with CT or magnetic resonance imaging (MRI) is recommended as invasive catheterization increases the risk of vascular rupture and dissection.

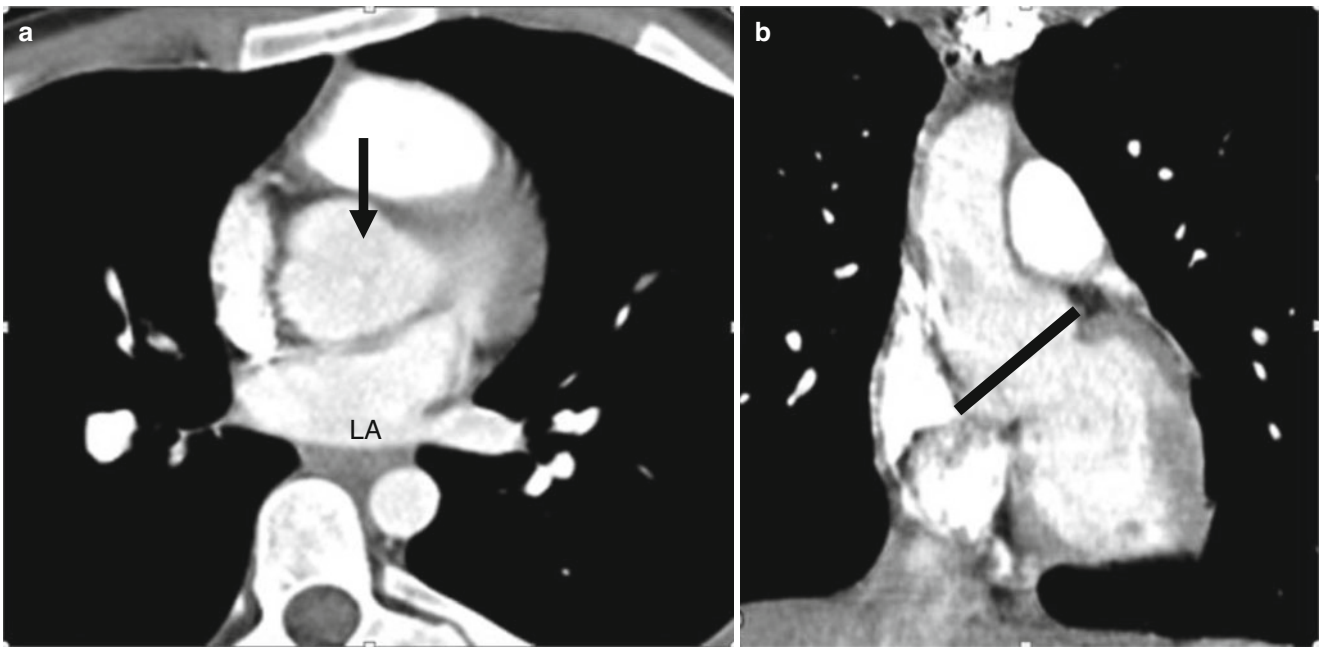


**Fig. 15.30** Annuloaortic ectasia in another patient with Marfan syndrome. Panel (**a**) an axial scan at the level of the left atrium (*LA*) shows dilatation of the aorta which involves the aortic valve annulus (*arrow*). Panel (**b**) a coronal view shows a maximum aortic root diameter of 4.1 cm (*black line*)

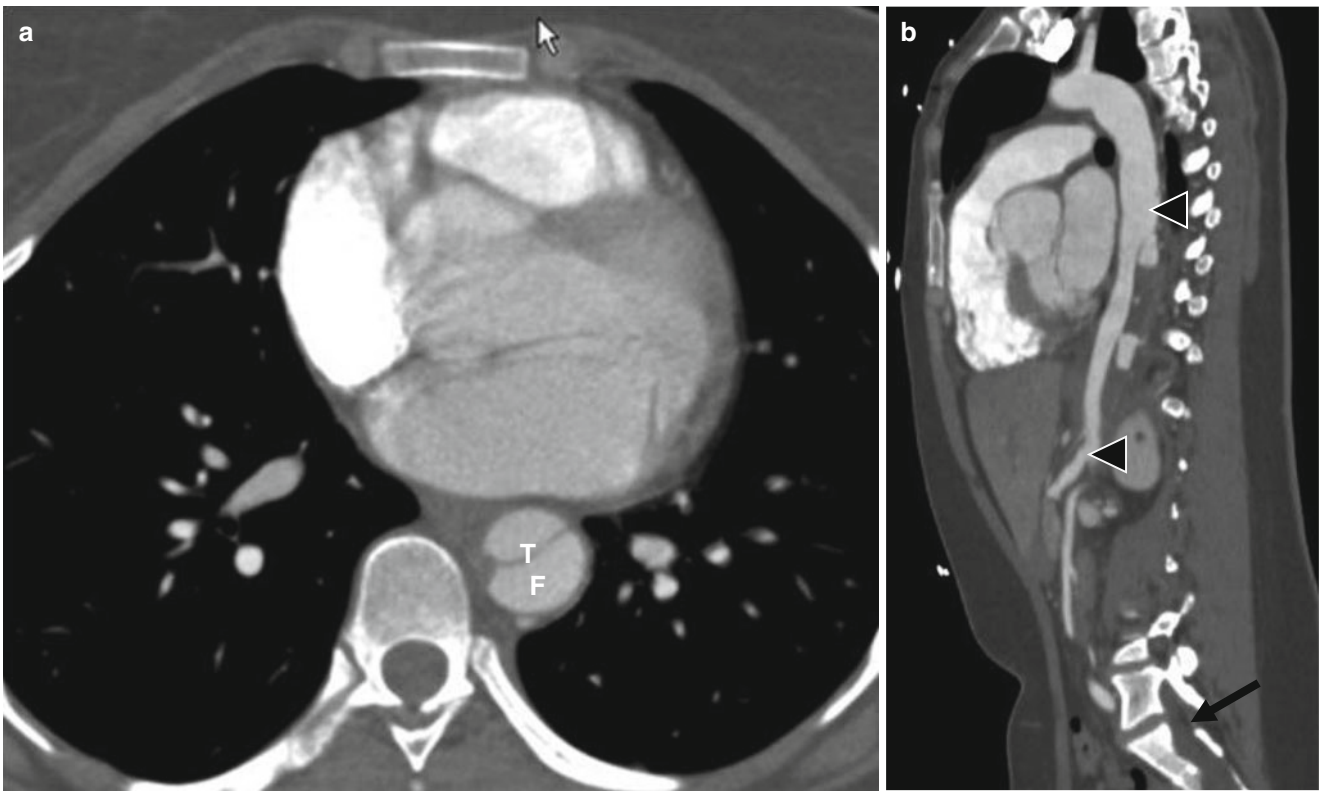


**Fig. 15.31** Aortic dissection in a patient with Marfan syndrome. This computed tomography scan demonstrates a type B aortic dissection (involving the descending thoracic aorta only). Panel (**a**) an axial view at the level of the left ventricle shows an intimal flap in the descending aorta separating the inner true (*T*) and outer false (*F*) lumens. Panel (**b**) a sagittal image of the aortic arch and the entire descending aorta demonstrates a dissection flap extending from the distal aortic arch into the abdominal aorta (*arrowheads*). The sagittal view also shows enlargement of the dural sac in the sacrum (*arrow*)

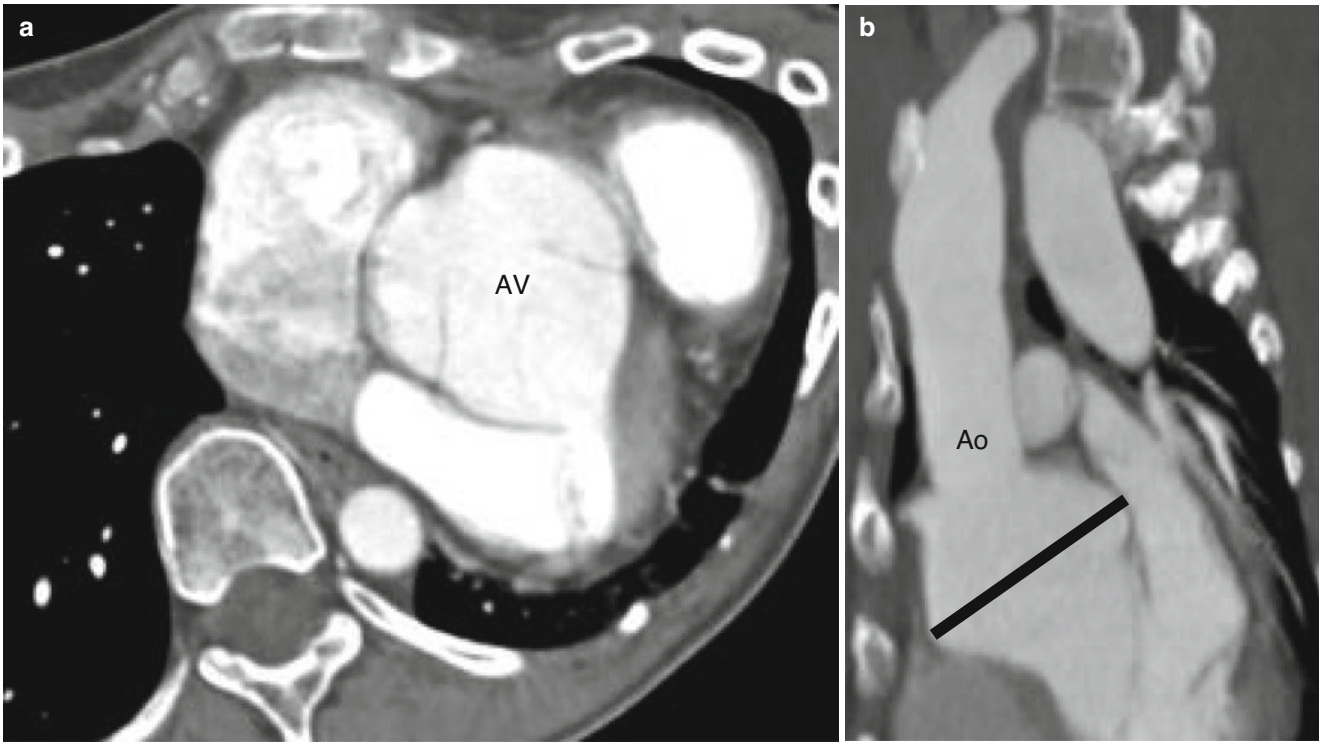


**Fig. 15.32** Aortic aneurysm in a patient with Loeys–Dietz syndrome. Panel (**a**) an axial view shows marked dilatation of the aorta at the level of the sinuses of Valsalva and involving the aortic valve (*AV*). Panel (**b**) a sagittal reformat shows dilatation of the aortic root (*black line*) and proximal ascending aorta. The aortic root maximum diameter is 5.8 cm. *Ao* aorta

### 15.6.4 Turner Syndrome

Turner syndrome or Ullrich–Turner syndrome (also known as "gonadal dysgenesis") is a 46XO chromosomal abnormality in which all or part of the second X chromosome is absent. Characteristic physical abnormalities are short stature, swelling, broad chest, low hairline, low-set ears, and webbed necks. Turner syndrome occurs in 1 in 2,500 to 1 in 3,000 live-born girls [81].

The prevalence of congenital heart disease among patients with Turner syndrome ranges from 17 to 45 % with no clear phenotype–genotype correlations [81]. Coarctation of the aorta and bicuspid aortic valve are the most common malformations associated with Turner syndrome. Other congenital cardiovascular malformations, such as partial anomalous venous drainage and aortic valve stenosis or aortic regurgitation, are also more common in Turner syndrome than in the general population.

The prevalence of aortic root dilatation ranges from 9 to 40 % and aortic dissection affects 1–2 % of patients with Turner syndrome [81, 82]. Coarctation of the aorta (unrepaired or repaired), bicuspid aortic valve, and/or hypertension are risk factors for aortic dissection. Routine surveillance is highly recommended in patients with aortic root dilatation [81, 82].

### 15.6.5 Indications and Surgical Repairs for Genetic Aortopathies

Elective replacement of the aortic root is suggested before critical enlargement or dissection occurs. Prophylactic cardiovascular surgery is performed for treatment of aortic aneurysm. Emergency surgery is indicated for aortic dissection. Surgical replacement of the aortic root may be indicated for survivors of acute proximal aortic dissection.

In patients with Marfan syndrome, elective aortic valve/graft surgery is usually considered when the aortic root diameter reaches 5.0 cm [68]. Earlier surgery is advocated if there is a family history of aortic dissection or a rapidly expanding aneurysm (>0.5 cm/year) or significant aortic regurgitation. In these cases, surgical intervention is suggested when the aortic root diameter reaches 4.0–4.5 cm. After operative repair of the aortic root, Marfan syndrome patients are at continuing risk for distal aortic aneurysm and dissection, but other arteries develop aneurysms infrequently [69]. See Fig. 15.34.

For patients with Loeys–Dietz Syndrome, surgical repair is recommended when the internal aortic diameter is equal to or greater than 4.2 cm by transesophageal echocardiography or the external diameter is equal to or greater than 4.4–4.6 cm by CT and/or MR imaging [68]. The vascular form of Ehlers–Danlos syndrome warrants a conservative approach to


**Fig. 15.33** Annuloaortic ectasia in a patient with Ehlers–Danlos syndrome. Panel (**a**) is a coronal reconstruction and panel (**b**) is a sagittal view. Each shows a dilated aortic root (*black line*). The aortic root maximum diameter is 4.8 cm. Panel (**c**) is an axial view of the neck showing a tortuous, dilated left carotid artery (*arrows*)

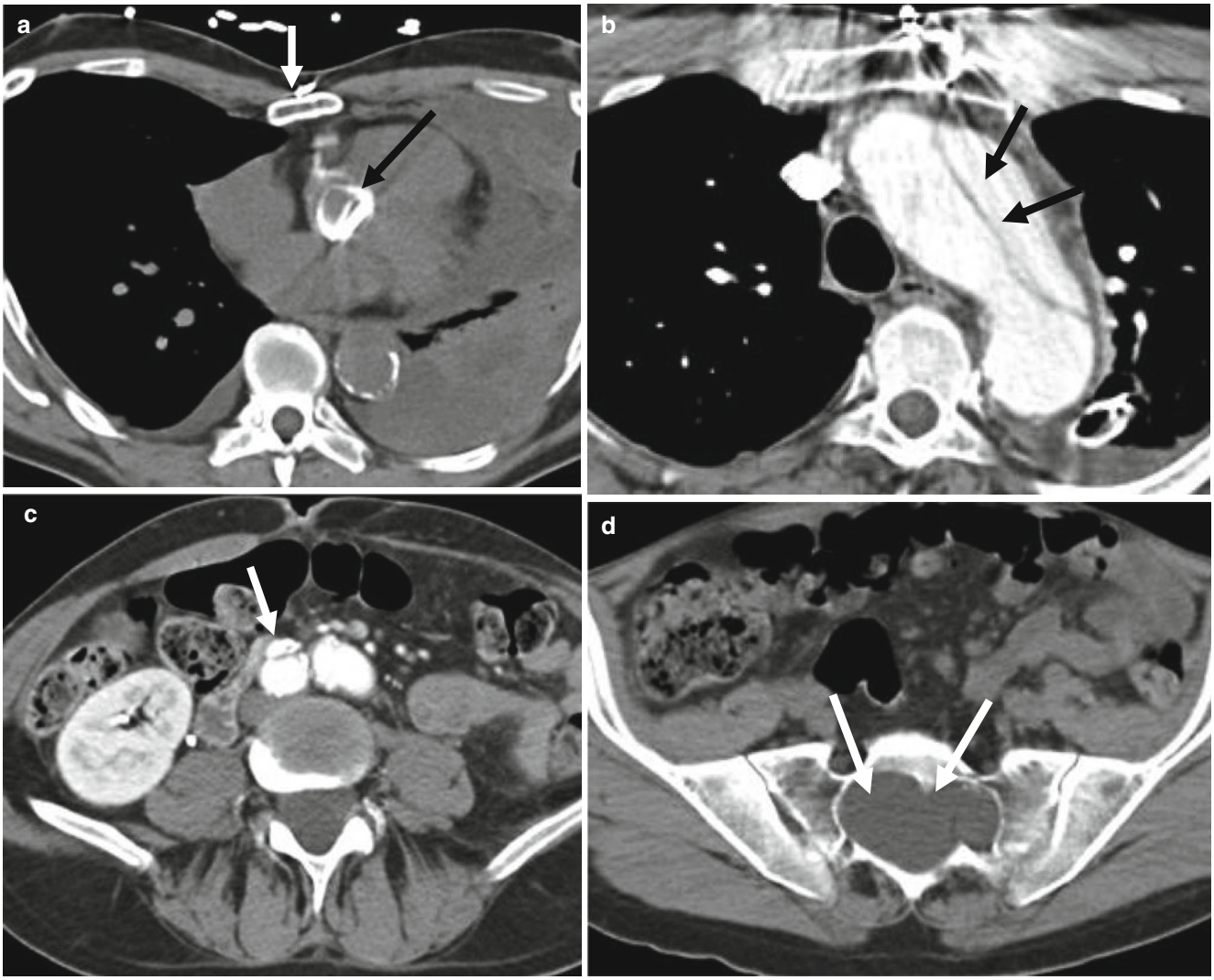


**Fig. 15.34** A 39-year-old man with Marfan syndrome who has undergone aortic root repair and aortic valve replacement after a type A dissection. Panels (**a**) and (**b**) are after the repair. Panel (a) is an axial scan showing the prosthetic aortic valve (*black arrow*). Also note the pectus excavatum deformity (*white arrow*). Panel (b), an axial view at a higher level, shows the residual type A dissection (involving the aortic arch) (*arrows*). Panel (**c**) is an image at the level of the pelvis and reveals the dissection flap extending into the right common iliac artery (*arrow*). Panel (**d**) is an axial reconstruction at the level of the mid-sacrum revealing ectasia of the dural sac at the S1 and S2 levels (*arrows*)

managing asymptomatic vascular abnormalities [68]. Surgical repair is complicated by friability of the vascular tissues, and some recommend surgery only when there is impending arterial rupture or life-threatening hemorrhage.

The preferred surgical repair for patients who have aortic root and sinuses of Valsalva dilatation but normal valve leaflets is excision of the native aortic sinuses and valve-sparing root resection (modified David reimplantation operation) [68]. The advantage of this strategy is that it preserves the aortic valve as well as the elastic properties of the native aortic root and it does not require postoperative anticoagulant administration which is especially important in this group of patients who are at high risk for aortic dissection. Composite valve–graft replacement, in which the dilated aortic segment is replaced by a prosthetic valve which is sewn into a tube graft with reimplantation of the coronary ostia (modified Bentall procedure), is an alternative surgery (Fig. 15.35). This surgery has low rates of morbidity and mortality and produces excellent long-term results. In patients who have associated aortic leaflet disease, a root replacement with a valve–graft conduit and reimplantation of the coronary artery ostia may be warranted (class I indication) [68].

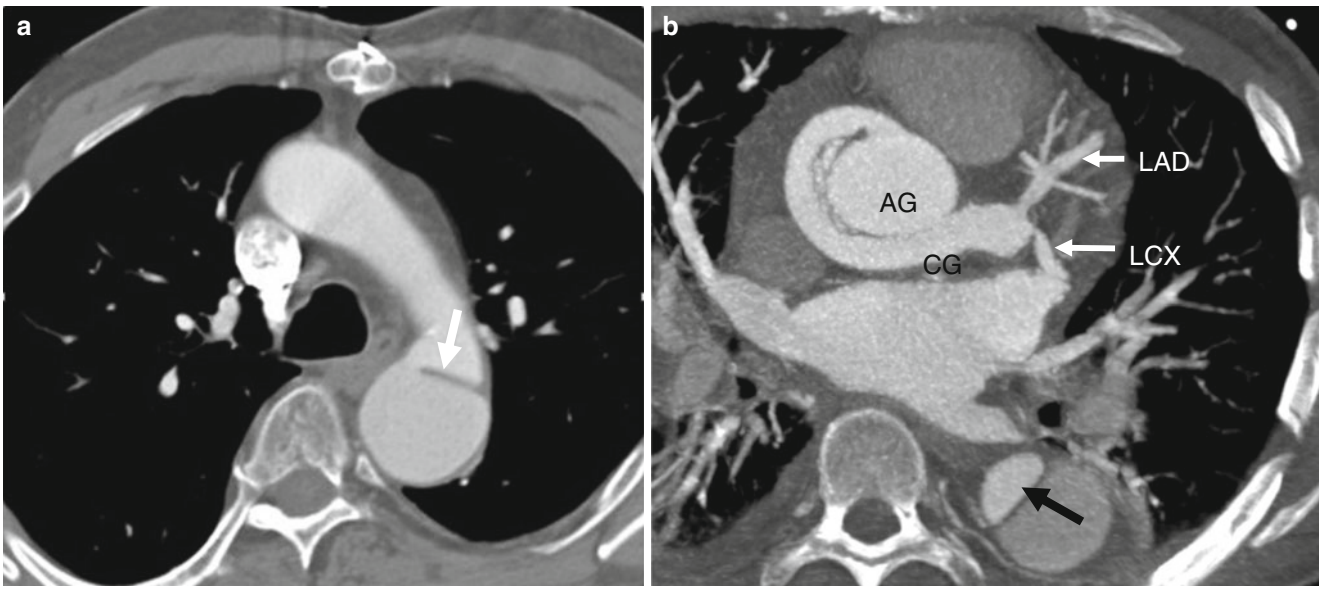


**Fig. 15.35** CT imaging of type A aortic dissection repair (Bentall procedure) in a Marfan patient. Panel (**a**) an axial image at the level of the proximal descending aorta showing the dissection flap (*arrow*). Panel (**b**) an axial image at the level of the aortic root again showing the dissection flap (*black arrow*) and the aortic root graft (*AG*) as well as the coronary graft (*CG*) from the ascending aortic graft to the proximal left anterior descending artery (*LAD*) and sequentially to the left circumflex artery (*LCX*)

### 15.6.6 Cardiac Computed Tomography (CT) in the Evaluation of Genetic Aortopathies

CT is a valuable imaging tool in patients with genetic or familial aortopathy. It can clearly demonstrate the diameters of the dilated aorta, sinotubular junction, and aortic root. ECG-gated images enable depiction of aortic valve function and eliminates motion artifact in the ascending aorta which may be mistaken for a dissection. On end-diastolic images, valvular regurgitation appears as a coaptation defect [71, 73].

CT is now established as the imaging modality of choice for suspected diagnosis of aortic dissection. It easily demonstrates the extent of dissection, the relationship of the true lumen and false lumen, as well as involvement of major aortic branch vessels. Classic CT findings of aortic dissection are an intimal flap and presence of a false lumen. Other findings include increased attenuation of the thrombosed false lumen on unenhanced CT scans representing acute hemorrhage, internal displacement of intimal calcification, and mediastinal and/or pericardial hematoma [73].

## 15.7 Pulmonary Artery Anomalies

The normal diameter of the main pulmonary artery is usually about two-thirds that of the ascending aorta and should not exceed 28 mm [83]. The main, left, and right pulmonary arteries lie entirely within the pericardium. The main pulmonary artery divides into the right and left pulmonary arteries behind and to the left of the ascending aorta. The right pulmonary artery has a longer course than the left, extends posteriorly and to the right from the main pulmonary artery, and divides into two lobar branches at the root of the right lung. The intrapericardial portion of the right pulmonary artery usually measures 12–15 mm in diameter. The left pulmonary artery courses over the left main bronchus and penetrates the root of the left lung, where it divides into two lobar branches. The left pulmonary artery measures 18–24 mm in diameter and has a shorter intrapericardial course than the right pulmonary artery [83]. Most congenital anomalies of the pulmonary arteries in adults are found incidentally on chest radiographs or computed tomography (CT)scans [84].

### 15.7.1 Proximal Interruption of Pulmonary Arteries

Proximal interruption of the right or left pulmonary artery is a rare developmental anomaly. The proximal pulmonary artery ends blindly at the hilum, usually within 1 cm of its origin from the main pulmonary artery, and blood supply to the lung is through systemic collateral vessels, mainly bronchial and transpleural collateral arteries [85, 86]. Interruption of the left pulmonary artery is usually associated with other congenital cardiovascular anomalies, including right aortic arch, septal defects, patent ductus arteriosum, and tetralogy of Fallot. Right-sided pulmonary artery interruption is more common than left-sided involvement and is usually an isolated finding [86].

Most affected patients come to clinical attention in the first year of life and present with dyspnea or recurrent

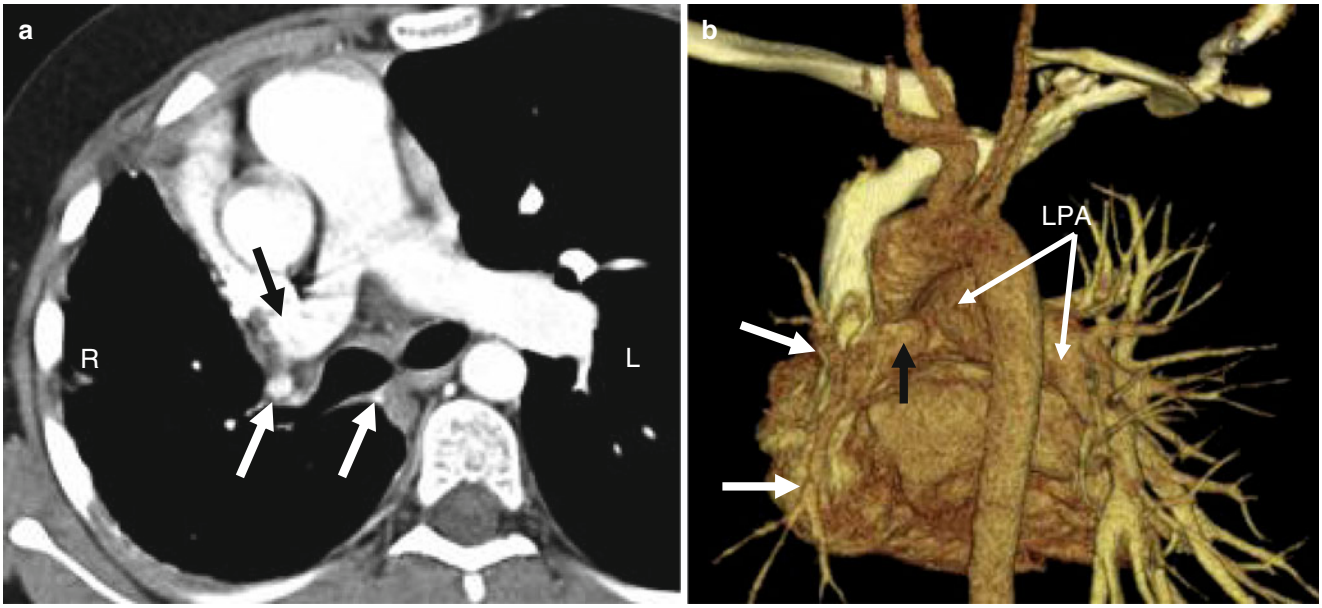


**Fig. 15.36** Proximal interruption of the right pulmonary artery. Panel (**a**) an axial tomogram showing proximal interruption of the right pulmonary artery (*black arrow*), mediastinal shift to the right side, and bronchial artery collateral vessels (*white arrows*). Panel (**b**), a 3D volume-rendered image, demonstrates the abrupt interruption of the right main pulmonary artery (*black arrow*) and multiple aortopulmonary collateral arteries supplying the right lung (*white arrows*). *R* right, *L* left, *LPA* left pulmonary artery

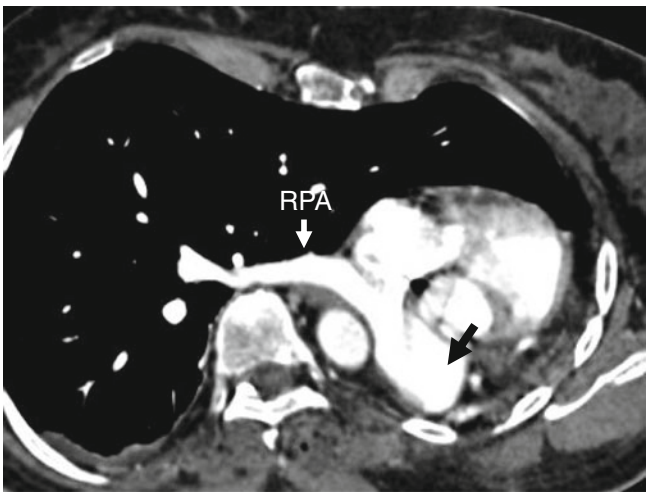


**Fig. 15.37** Proximal interruption of the left pulmonary artery. The diagnosis was made incidentally in an asymptomatic adult referred for scoliosis evaluation. This axial image shows a blind-ending left pulmonary artery (*arrow*) and mediastinal shift to the left side. *RPA* right pulmonary artery

pulmonary infections. However, patients can be asymptomatic and the diagnosis can be made as an incidental detection on chest radiographs or CT scans obtained for other clinical indications. Occasionally, adults with this disorder present with recurrent pulmonary infections or hemoptysis due to systemic-to-pulmonary arterial shunting.

Contrast-enhanced CT can clearly indentify the abnormal termination of the proximal pulmonary artery and the collateral arteries supplying the lung [84, 87–91]. Associated findings include decreased size of the affected lung, ipsilateral mediastinal shift, and diminished ipsilateral pulmonary vascularity (Figs. 15.36 and 15.37). The pulmonary venous drainage and bronchial branching pattern are normal. CT at lung windows may show serrated thickening of the pleura and subpleural parenchymal linear opacities or bands related to anastomoses of transpleural systemic collateral vessels with peripheral branches of the pulmonary artery. Systemic collateral vessels can originate from intercostal, mammary (internal thoracic), subclavian, and/or innominate arteries.

### 15.7.2 Pulmonary Artery Sling

With a pulmonary artery sling, the left pulmonary artery arises from the posterior aspect of the right pulmonary artery and crosses the mediastinum, passing between the trachea and esophagus to reach the left hilum. The left pulmonary artery thus forms a sling around the distal trachea and the proximal right main bronchus and may compress either structure [90–93].

This anomaly usually comes to clinical attention because of the compressive effect of the artery on the airway and/or associated tracheal or bronchial stenosis due to cartilaginous rings. It may also be asymptomatic and detected incidentally on imaging studies [93]. In the latter scenario, the posterior membranous component of the trachea is absent and the

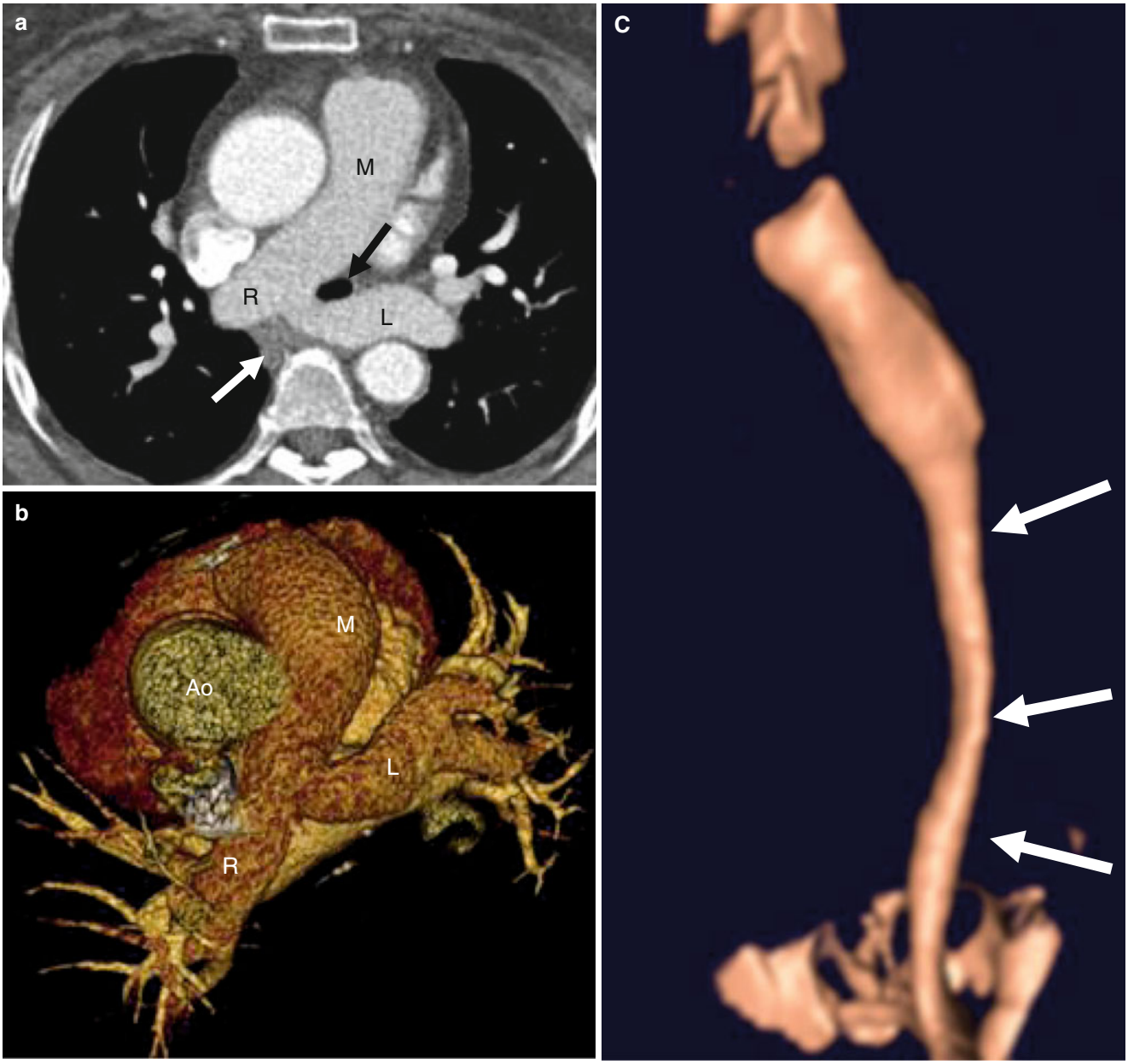


**Fig. 15.38** Pulmonary artery sling in a 58-year-old woman. Panel (**a**) an axial image showing the left pulmonary artery (*L*) arising from the posterior aspect of the right pulmonary artery (*R*) and crossing between the trachea (*black arrow*) and esophagus (*white arrow*) to reach the left hilum. Panel (**b**) a 3D volume-rendered reformat again showing the anomalous origin and course of the left pulmonary artery (*L*) and its relationship to the aorta (*Ao*). Panel (**c**) is a volume-rendered depiction of the airway showing a long-segment of distal tracheal narrowing (*arrows*). The diagnosis of complete tracheal rings was made during surgery. *M* main pulmonary artery

tracheal cartilages are O-shaped rather than U-shaped, resulting in either short- or long-segment tracheal stenoses.

The esophagus may be indented anteriorly but is rarely constricted enough to cause symptomatic obstruction. Congenital heart defects occur in approximately 50 % of patients with pulmonary artery sling, most commonly atrial septal defect, ventricular septal defect, and patent ductus arteriosus and less commonly, tetralogy of Fallot, tricuspid atresia, and double-outlet right ventricle. Bronchus suis ("pig" bronchus), characterized by separate high origin of the right upper lobe bronchus from the trachea, is also a common association.

Contrast-enhanced CT can simultaneously show the abnormal origin and course of the left pulmonary artery and the associated tracheobronchial narrowing including the presence of complete tracheal rings and the extent of tracheal stenosis (Fig. 15.38) [90–92]. In addition, dynamic CT during forced inspiration and expiration can show air trapping, further confirming the presence of bronchial obstruction.

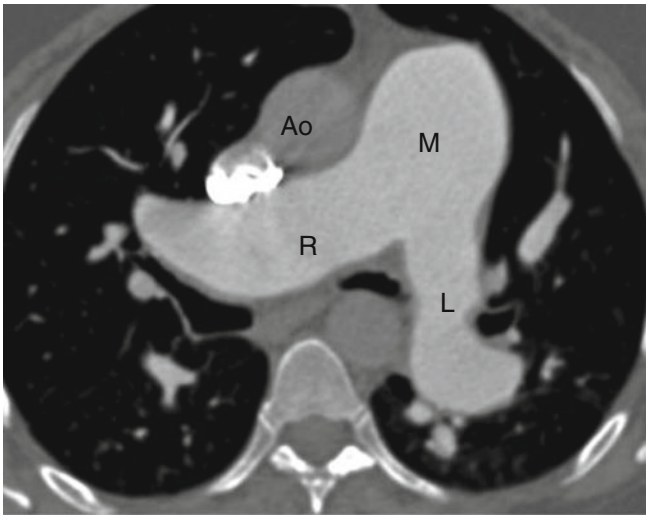


**Fig. 15.39** Idiopathic dilatation of the main pulmonary artery. This axial scan shows dilatation of the main pulmonary artery (*M*) extending into right (*R*) and left (*L*) pulmonary arteries. Pulmonic valve stenosis and pulmonary hypertension were excluded in this patient. *Ao* ascending aorta

In symptomatic patients, treatment is reimplantation of the anomalous left pulmonary artery and tracheal reconstruction in cases with congenital tracheal stenosis. Resection with end-to-end anastomosis is the preferred procedure for short-segment tracheal stenosis. Tracheoplasty is usually needed for repair of long-segment stenosis [94].

### 15.7.3 Idiopathic Dilatation of the Main Pulmonary Artery

Idiopathic dilatation of the pulmonary trunk refers to enlargement of the pulmonary outflow tract without pulmonary valvular stenosis. The right and left pulmonary arteries may or may not be dilated [95]. It is a diagnosis of exclusion and secondary causes such as pulmonic valvular stenosis and pulmonary hypertension need to be ruled out. This condition is benign, asymptomatic, and nonprogressive. It is usually incidentally detected on imaging studies (Fig. 15.39) [96].

## References

1. Warnes CA, Williams RG, Bashore TM, Child JS, Connolly HM, Dearani JA, et al. ACC/AHA 2008 Guidelines for the Management of Adults with Congenital Heart Disease: a report of the American College of Cardiology/American Heart Association Task Force on Practice Guidelines (writing committee to develop guidelines on the management of adults with congenital heart disease). Circulation. 2008;118:e714–833. doi:10.1161/CIRCULATIONAHA.108.190690.
2. Schneider DJ, Moore JW. Patent ductus arteriosus. Circulation. 2006;114:1873–82.doi:10.1161/CIRCULATIONAHA.105.592063.
3. Wilcox B, Cook A, Anderson R. Abnormalities of the great vessels. In: Wilcox BR, Cook AC, Anderson RH, editors. Surgical anatomy of the heart. 1st ed. Cambridge/New York: Cambridge University Press; 2004. p. 275.
4. Baumgartner H, Bonhoeffer P, De Groot NM, de Haan F, Deanfield JE, Galie N, Gatzoulis MA, Gohlke-Baerwolf C, Kaemmerer H, Kilner P, Meijboom F, Mulder BJ, Oechslin E, Oliver JM, Serraf A, Szatmari A, Thaulow E, Vouhe PR, Walma E, Task Force on the Management of Grown-up Congenital Heart Disease of the European Society of Cardiology (ESC), Association for European Paediatric Cardiology (AEPC). ESC guidelines for the management of grown-up congenital heart disease (new version 2010). Eur Heart J. 2010; 31:2915–57. doi:10.1093/eurheartj/ehq249.
5. Hughes D, Siegel MJ. Computed tomography of adult congenital heart disease. Radiol Clin N Am. 2010;48:817–35.
6. Goiten O, Fuhrman CR, Lacomis JM. Incidental finding on MDCT of patent ductus arteriosus: use of CT and MRI to assess clinical importance. Am J Roentgenol. 2005;184:1924–31.
7. Morgan-Hughes GJ, Marshall AJ, Roobottom C. Morphologic assessment of patent ductus arteriosus in adults using retrospectively EDG-gated multidetector CT. Am J Roentgenol. 2003;181:749–54.
8. Krichenko A, Benson LN, Burrows P, Moes CA, McLaughlin P, Freedom RM. Angiographic classification of the isolated, persistently patent ductus arteriosus and implications for percutaneous catheter occlusion. Am J Cardiol. 1989;63:877–80.
9. Cruickshank B, Marquis RM. Spontaneous aneurysm of the ductus arteriosus; a review and report of the tenth adult case. Am J Med. 1958;25:140–9.
10. Ross RS, Feder FP, Spencer FC. Aneurysms of the previously ligated patent ductus arteriosus. Circulation. 1961;23:350–7.
11. Marasini M, Rimini A, Zannini L, Pongiglione G. Giant aneurysm following coil occlusion of patent ductus arteriosus. Catheter Cardiovasc Interv. 2000;50:186–9.
12. Sardesai SH, Marshall RJ, Farrow R, Mourant AJ. Dissecting aneurysm of the pulmonary artery in a case of unoperated patent ductus arteriosus. Eur Heart J. 1990;11:670–3.
13. Cusick DA, Frederiksen JW, Mehlman DJ. Acute aortic dissection: association with patent ductus arteriosus. Am J Card Imaging. 1996;10:200–3.
14. Coard KC, Martin MP. Ruptured saccular pulmonary artery aneurysm associated with persistent ductus arteriosus. Arch Pathol Lab Med. 1992;116:159–61.
15. Jacobs JP, Quintessenza JA, Gaynor JW, Burke RP, Mavroudis C. Congenital heart surgery nomenclature and database project: aortopulmonary window. Ann Thorac Surg. 2000;69:S44–9.
16. Barnes ME, Mitchell ME, Tweddell JS. Aortopulmonary window. Semin Thorac Cardiovasc Surg Pediatr Card Surg Annu. 2011;14:67–74. doi:10.1053/j.pcsu.2011.01.017.
17. Samanek M, Voriskova M. Congenital heart disease among 815,569 children born between 1980 and 1990 and their 15-year survival: a prospective bohemia survival study. Pediatr Cardiol. 1999;20:411–7.
18. Kutsche L. Anatomy and pathogenesis of aorticopulmonary septal defect. Am J Cardiol. 1987;59:443–7. doi:10.1016/0002-9149(87)90953-2.
19. Mori K, Ando M, Takao A, Ishikawa S, Imai Y. Distal type of aortopulmonary window. Report of 4 cases. Br Heart J. 1978;40:681–9.
20. Ho SY, Gerlis LM, Anderson C, Devine WA, Smith A. The morphology of aortopulmonary windows with regard to their classification and morphogenesis. Cardiol Young. 1994;4:146–55.
21. Backer CL, Mavroudis C. Surgical management of aortopulmonary window: a 40-year experience. Eur J Cardiothorac Surg. 2002;21:773–9.
22. Bagtharia R, Trivedi KR, Burkhart HM, Williams WG, Freedom RM, Van Arsdell GS, et al. Outcomes for patients with an aortopulmonary window, and the impact of associated cardiovascular lesions. Cardiol Young. 2004;14:473–80. doi:10.1017/S1047951104005025.
23. Penkoske PA, Castaneda AR, Fyler DC, Van Praagh R. Origin of pulmonary artery branch from ascending aorta. Primary surgical repair in infancy. J Thorac Cardiovasc Surg. 1983;85:537–45.

24. Kutsche LM, Van Mierop LH. Anomalous origin of a pulmonary artery from the ascending aorta: associated anomalies and pathogenesis. Am J Cardiol. 1988;61:850–6.
25. Aggarwal HK, Gupta T, Jain D, Rohilla S. Aortopulmonary window-a rare presentation in post-partum female. Biomed Res. 2011;22:345–7.
26. Kimura-Hayama ET, Melendez G, Mendizabal AL, et al. Uncommon congenital and acquired aortic diseases: role of multidetector CT angiography. Radiographics. 2010;30:79–98.
27. Kenny D, Hijazi ZM. Coarctation of the aorta: from fetal life to adulthood. Cardiol J. 2011;18:487–95.
28. Kaemmerer H. Aortic coarctation and interrupted aortic arch. In: Gatzoulis MA, Webb GD, Daubeney PEF, editors. Diagnosis and management of adult congenital heart disease. Philadelphia: Elsevier/Saunders; 2011. p. 261.
29. Backer CL, Mavroudis C. Congenital heart surgery nomenclature and database project: patent ductus arteriosus, coarctation of the aorta, interrupted aortic arch. Ann Thorac Surg. 2000;69:S298–307.
30. Edwards JE, Christensen NA, Clagett OT, et al. Pathologic considerations in coarctation of the aorta. Mayo Clin Proc. 1948;23:324–32.
31. Zeltser H, Tabbutt S. Critical heart disease in the newborn. In: Vetter VL, editor. Pediatric Cardiology, the Requisites. Philadelphia: Elsevier Mosby; 2006. p. 31–50.
32. Elzenga NJ, Gittenberger-de Groot AC. Localised coarctation of the aorta. An age dependent spectrum. Br Heart J. 1983;49(4):317–23.
33. Reifenstein GH, Levine SA, Gross RE. Coarctation of the aorta; a review of 104 autopsied cases of the adult type, 2 years of age or older. Am Heart J. 1947;33:146–68.
34. Aboulhosn J, Child JS. Left ventricular outflow obstruction: subaortic stenosis, bicuspid aortic valve, supravalvar aortic stenosis, and coarctation of the aorta. Circulation. 2006;114:2412–22. doi:10.1161/CIRCULATIONAHA.105.592089.
35. Connolly HM, Huston 3rd J, Brown Jr RD, Warnes CA, Ammash NM, Tajik AJ. Intracranial aneurysms in patients with coarctation of the aorta: a prospective magnetic resonance angiographic study of 100 patients. Mayo Clin Proc. 2003;78:1491–9. doi:10.4065/78.12.1491.
36. Gersony WM, Rosenbaum MS. Congenital heart disease in the adult. New York: McGraw-Hill; 2002.
37. Campbell M. Natural history of coarctation of the aorta. Br Heart J. 1970;32:633–40.
38. Cohen M, Fuster V, Steele PM, Driscoll D, McGoon DC. Coarctation of the aorta. long-term follow-up and prediction of outcome after surgical correction. Circulation. 1989;80:840–5.
39. Bouzguenda I, Marini D, Ou P, Boudjemline Y, Bonnet D, Agnoletti G. Percutaneous treatment of neonatal aortic coarctation presenting with severe left ventricular dysfunction as a bridge to surgery. Cardiol Young. 2009;19:244–51. doi:10.1017/S1047951109003837.
40. Chessa M, Carrozza M, Butera G, Piazza L, Negura DG, Bussadori C, et al. Results and mid-long-term follow-up of stent implantation for native and recurrent coarctation of the aorta. Eur Heart J. 2005;26:2728–32. doi:10.1093/eurheartj/ehi491.
41. Shah L, Hijazi Z, Sandhu S, Joseph A, Cao QL. Use of endovascular stents for the treatment of coarctation of the aorta in children and adults: Immediate and midterm results. J Invasive Cardiol. 2005;17:614–8.
42. Celoria CG, Patton RB. Congenital absence of the aortic arch. Am Heart J. 1959;58:407–13.
43. Gaca AM, Jaggers JJ, Dudley LT, Bisset GS. Repair of Congenital Heart Disease: a Primer-Part 2. Radiology. 2008;248(1):44–60.
44. Sandhu SK, Pettitt TW. Interrupted aortic arch. Curr Treat Options Cardiovasc Med. 2002;4:337–40.
45. Brown JW, Ruzmetov M, Okada Y, et al. Outcomes in patients with interrupted aortic arch and associated anomalies: a 20-year experience. Eur J Cardiothorac Surg. 2006;29:666–73.
46. Cinar A, Haliloglu M, Karagoz T, et al. Interrupted aortic arch in a neonate: multidetector CT diagnosis. Pediatr Radiol. 2004;34:901–3.
47. Leschka S, Oechslin E, Husmann L, et al. Pre-and postoperative evaluation of congenital heart disease in children and adults with 64-section CT. Radiographics. 2007;27:829–46.
48. Kimura_Hayama ET, Melendez G, Mendizabal M, et al. Uncommon congenital and acquired aortic diseases: role of multidetector CT angiography. Radiographics. 2010;30:79–98.
49. Sebastia C, Quiroga S, Boye R, Perez-Lafuente M, Castella E, Alvarez-Castells A. Aortic stenosis: spectrum of diseases depicted at multisection CT. Radiographics. 2003;23:S79–91.
50. Siegel MJ. Coarctation of the aorta. In: Ho V, Reddy G, editors. Cardiovascular imaging: expert radiology series. Philadelphia: Elsevier; 2011. p. 535–41.
51. Weinberg PM. Aortic arch anomalies. In: Allen HD, editor. Moss and adams' heart disease in infants, children, and adolescents: including the fetus and young adult. 7th ed. Philadelphia: W. Kluwer/Lippincott Williams & Wilkins; 2008. p. 730.
52. Edwards JE. Malformations of the aortic arch system manifested as vascular rings. Lab Invest. 1953;2:56–75.
53. Goldstein WB. Aberrant right subclavian artery in mongolism. Am J Roentgenol Radium Ther Nucl Med. 1965;95:131–4.
54. Maiya S, Ho S. Vascular rings, pulmonary slings, and other vascular abnormalities. In: Gatzoulis MA, Webb GD, Daubeney PEF, editors. Diagnosis and management of adult congenital heart disease. 2nd ed. Philadelphia: Elsevier/Saunders; 2011. p. 277.
55. Knight L, Edwards JE. Right aortic arch. Types and associated cardiac anomalies. Circulation. 1974;50:1047–51.
56. Turkvatan A, Buyukbayraktar FG, Olcer T, Cumhur T. Congenital anomalies of the aortic arch: evaluation with the use of multidetector computed tomography. Korean J Radiol. 2009;10:176–84. doi:10.3348/kjr.2009.10.2.176.
57. Pearson GD, Kan JS, Neill CA, Midgley FM, Gardner TJ, Hougen TJ. Cervical aortic arch with aneurysm formation. Am J Cardiol. 1997;79:112–4.
58. Higashino SM, Ruttenberg HD. Double aortic arch associated with complete transposition of the great vessels. Br Heart J. 1968; 30:579–81.
59. Gerlis LM, Dickinson DF, Wilson N, Gibbs JL. Persistent fifth aortic arch. A report of two new cases and a review of the literature. Int J Cardiol. 1987;16:185–92.
60. Siegel MJ. Vascular rings and slings. In: Ho V, Reddy G, editors. Cardiovascular imaging: expert radiology series. Philadelphia: Elsevier; 2011. p. 542–8. Origin in adults: 64-MDCT appearance. AJR 188: W138–46.
61. Goldberg N, Krasnow N. Sinus of valsalva aneurysms. Clin Cardiol. 1990;13:831–6.
62. Walters MI, Ettles D, Guvendik L, Kaye GC. Interventricular septal expansion of a sinus of valsalva aneurysm: a rare cause of complete heart block. Heart. 1998;80:202–3.
63. Gunay R, Sensoz Y, Kayacioglu I. Giant unruptured non-coronary sinus of valsalva aneurysm presenting as tricuspid stenosis. Eur J Cardiothorac Surg. 2010;37:1471. doi:10.1016/j.ejcts.2009.12.034.
64. Mandel L, Gakhal M, Hopkins J. Percutaneous closure of recurrent non-coronary sinus of valsalva aneurysm rupture: utility of computed tomography in procedural planning. J Invasive Cardiol. 2010;22:336–8.
65. Utsunomiya D, Atsuchi N, Nishiharu T, Urata J, Awai K, Yamashita Y. Multi-slice CT demonstration of sinus of valsalva rupture. Int J Cardiovasc Imaging. 2006;22:561–4. doi:10.1007/s10554-005-9047-6.
66. Bricker AO, Avutu B, Mohammed TL, Williamson EE, Syed IS, Julsrud PR, et al. Valsalva sinus aneurysms: findings at CT and MR imaging. Radiographics. 2010;30:99–110. doi:10.1148/rg.301095719.
67. Chae EJ et al. Radiologic and clinical findings of Behçet disease: comprehensive review of multisystemic involvement. Radiographics. 2008;28:e31.
68. Hiratzka LF, Bakris GL, Beckman JA, Bersin RM, Carr VF, Casey DE, Jr, Eagle KA, Hermann LK, Isselbacher EM, Kazerooni EA,

Kouchoukos NT, Lytle BW, Milewicz DM, Reich DL, Sen S, Shinn JA, Svensson LG, Williams DM, American College of Cardiology Foundation/American Heart Association Task Force on Practice Guidelines, American Association for Thoracic Surgery, American College of Radiology, American Stroke Association, Society of Cardiovascular Anesthesiologists, Society for Cardiovascular Angiography and Interventions, Society of Interventional Radiology, Society of Thoracic Surgeons, Society for Vascular Medicine. 2010 ACCF/AHA/AATS/ACR/ASA/SCA/SCAI/SIR/STS/SVM guidelines for the diagnosis and management of patients with thoracic aortic disease. A report of the American College of Cardiology Foundation/American Heart Association Task Force on Practice Guidelines, American Association for Thoracic Surgery, American College of Radiology, American Stroke Association, Society of Cardiovascular Anesthesiologists, Society for Cardiovascular Angiography and Interventions, Society of Interventional Radiology, Society of Thoracic Surgeons, and Society for Vascular Medicine. J Am Coll Cardiol. 2010;55:e27–129. doi:10.1016/j.jacc.2010.02.015.

69. Pyeritz RE, McKusick VA. The MARFAN syndrome: diagnosis and management. N Engl J Med. 1979;300:772–7. doi:10.1056/NEJM197904053001406.
70. Dietz HC, Pyeritz RE. Mutations in the human gene for fibrillin-1 (FBN1) in the MARFAN syndrome and related disorders. Hum Mol Genet. 1995;4 Spec No:1799–809.
71. Kimura-Hayama ET, Melendez G, Mendizabal AL, Meave-Gonzalez A, Zambrana GF, Corona-Villalobos CP. Uncommon congenital and acquired aortic diseases: role of multidetector CT angiography. Radiographics. 2010;30:79–98. doi:10.1148/rg.301095061.
72. Kornbluth M, Schnittger I, Eyngorina I, Gasner C, Liang DH. Clinical outcome in the MARFAN syndrome with ascending aortic dilatation followed annually by echocardiography. Am J Cardiol. 1999;84:753–5, A9.
73. Ha HI, Seo JB, Lee SH, Kang JW, Goo HW, Lim TH, et al. Imaging of MARFAN syndrome: multisystemic manifestations. Radiographics. 2007;27:989–1004. doi:10.1148/rg.274065171.
74. Loeys BL, Dietz HC. Loeys-DIETZ syndrome. In: Pagon RA, Bird TD, Dolan CR, Stephens K, editors. GeneReviews. Seattle: University of Washington; 1993.
75. Loeys BL, Chen J, Neptune ER, Judge DP, Podowski M, Holm T, et al. A syndrome of altered cardiovascular, craniofacial, neurocognitive and skeletal development caused by mutations in TGFBR1 or TGFBR2. Nat Genet. 2005;37:275–81. doi:10.1038/ng1511.
76. Loeys BL, Schwarze U, Holm T, Callewaert BL, Thomas GH, Pannu H, et al. Aneurysm syndromes caused by mutations in the TGF-beta receptor. N Engl J Med. 2006;355:788–98. doi:10.1056/NEJMoa055695.
77. Kalra VB, Gilbert JW, Malhotra A. Loeys-DIETZ syndrome: cardiovascular, neuroradiological and musculoskeletal imaging findings. Pediatr Radiol. 2011;41:1495–504. doi:10.1007/s00247-011-2195-z; quiz 1616.
78. Johnson PT, Chen JK, Loeys BL, Dietz HC, Fishman EK. Loeys-DIETZ syndrome: MDCT angiography findings. AJR Am J Roentgenol. 2007;189:W29–35. doi:10.2214/AJR.06.1316.
79. Pepin M, Schwarze U, Superti-Furga A, Byers PH. Clinical and genetic features of EHLERS-DANLOS syndrome type IV, the vascular type. N Engl J Med. 2000;342:673–80. doi:10.1056/NEJM200003093421001.
80. Zilocchi M, Macedo TA, Oderich GS, Vrtiska TJ, Biondetti PR, Stanson AW. Vascular EHLERS-DANLOS syndrome: imaging findings. AJR Am J Roentgenol. 2007;189:712–9. doi:10.2214/AJR.07.2370.
81. Sybert VP, McCauley E. Turner's syndrome. N Engl J Med. 2004;351:1227–38. doi:10.1056/NEJMra030360.
82. Bondy CA. Congenital cardiovascular disease in TURNER syndrome. Congenit Heart Dis. 2008;3:2–15. doi:10.1111/j.1747-0803.2007.00163.x.
83. Molina P. Mediastinum: CT. In: Shirkhoda A, editor. Variants and pitfalls in body imaging. Philadelphia: Lippincott Williams & Wilkins; 2000. p. 3–35.
84. Castaner E, Gallardo X, Rimola J, Pallardo Y, Mata JM, Perendreu J, et al. Congenital and acquired pulmonary artery anomalies in the adult: radiologic overview. Radiographics. 2006;26:349–71. doi:10.1148/rg.262055092.
85. Kieffer SA, Amplatz K, Anderson RC, Lillehei CW. Proximal interruption of a pulmonary artery. Am J Roentgenol Radium Ther Nucl Med. 1965;95:592–7.
86. Sherrick DW, Kincaid OW, Dushane JW. Agenesis of a main branch of the pulmonary artery. Am J Roentgenol Radium Ther Nucl Med. 1962;87:917–28.
87. Davis SD. Case 28: proximal interruption of the right pulmonary artery. Radiology. 2000;217:437–40.
88. Mahnken AH, Wildberger JE, Spuntrup E, Hubner D. Unilateral absence of the left pulmonary artery associated with coronary-to-bronchial artery anastomosis. J Thorac Imaging. 2000;15:187–90.
89. Ryu DS, Spirn PW, Trotman-Dickenson B, Hunsaker A, Jung SM, Park MS, et al. HRCT findings of proximal interruption of the right pulmonary artery. J Thorac Imaging. 2004;19:171–5.
90. Siegel MJ, Earls JP, Chan F. Thoracic vascular anomalies. In: Rubin GD, Rofsky NM, editors. CT and MR angiography: comprehensive vascular assessment. Philadelphia: Wolters Kluwer Health/Lippincott Williams & Wilkins; 2009. p. 543–95.
91. Zylak CJ, Eyler WR, Spizarny DL, Stone CH. Developmental lung anomalies in the adult: radiologic-pathologic correlation. Radiographics. 2002;22 Spec No:S25–43.
92. Siegel MJ. Vascular rings and slings. In: Ho VB, Reddy GP, editors. Cardiovascular imaging. St. Louis: Saunders/Elsevier; 2011. p. 542–8.
93. Berdon WE, Baker DH, Wung JT, Chrispin A, Kozlowski K, de Silva M, et al. Complete cartilage-ring tracheal stenosis associated with anomalous left pulmonary artery: the ring-sling complex. Radiology. 1984;152:57–64.
94. Oshima Y, Yamaguchi M, Yoshimura N, Sato S, Muraji T, Nishijima E, et al. Management of pulmonary artery sling associated with tracheal stenosis. Ann Thorac Surg. 2008;86:1334–8. doi:10.1016/j.athoracsur.2008.04.020.
95. Deshmukh M, Guvenc S, Bentivoglio L, Goldberg H. Idiopathic dilatation of the pulmonary artery. Circulation. 1960;21:710–6.
96. van Rens MT, Westermann CJ, Postmus PE, Schramel FM. Untreated idiopathic aneurysm of the pulmonary artery; long-term follow-up. Respir Med. 2000;94:404–5. doi:10.1053/rmed.1999.0750.

# Coronary Artery Anomalies

# 16

Coronary artery anomalies represent a heterogeneous group of congenital disorders with different pathophysiology and clinical impact. By definition, they represent variants or deviations from the normal coronary artery anatomy [1].

## 16.1 Normal Anatomy of the Coronary Arteries

The aortic valve has three leaflets or cusps named the left, right, and noncoronary cusps. Just above the aortic valves there are three anatomic dilatations of the ascending aorta, known as the aortic sinuses of Valsalva. There are three sinuses of Valsalva which are named for the associated aortic valve cusp: left, right, and noncoronary. The left main coronary artery (LMCA) normally arises from the left sinus of Valsalva and the right coronary artery (RCA) arises from the right sinus of Valsalva. The noncoronary cusp is normally not associated with a coronary artery ostium.

The classic features of the normal coronary artery system include a right and left coronary circulation with separate ostia located at the aortic sinuses with 45–90° angles of origin from the aortic wall. The left coronary circulation has a common trunk called the LMCA that gives rise to all of the left coronary circulation branches. The proximal course of the LMCA coronary artery traverses the atrioventricular groove. There are branches to the ventricular myocardium and to the coronary arteries that terminate at the capillary bed. The coronary arteries are classified as "end circulation" since they represent the only source of blood supply to the myocardium [2].

### 16.1.1 Left Main Coronary Artery

The LMCA arises from the left aortic sinus of Valsalva. It bifurcates into the left anterior descending artery (LAD) (embedded in the anterior cardiac surface) and the left circumflex artery (LCx) (embedded in the posterior surface). Occasionally, the LMCA trifurcates into the LAD, the LCx, and a third vessel termed the ramus intermedius artery which arises between the takeoff of the LAD and LCx. The LAD and LCx arteries give off diagonal arteries and obtuse marginal arteries, respectively.

### 16.1.2 Right Coronary Artery

The right coronary artery (RCA) originates from the right aortic sinus of Valsalva and travels caudally through the right atrioventricular groove to reach the cardiac apex. The RCA gives off several branches, including the conus artery, sinus node artery, acute marginal artery, and posterior descending artery.

### 16.1.3 Epidemiology and Clinical Importance of Coronary Anomalies

The incidence of coronary artery anomalies is relatively rare and is estimated to affect approximately 1 % of the general population [1]. Yamanka and Hobs [3] reported a 1.3 % incidence of coronary anomalies in a series of 126,595 patients undergoing coronary angiography over a 28-year period. Although coronary artery anomalies are far less common than acquired coronary artery disease, they may have significant cardiovascular consequences, including myocardial ischemia, fatal arrhythmias, and sudden cardiac death [4]. Patients in whom the proximal segment of an aberrant vessel is compressed between the aorta and pulmonary artery have a high risk of exercise-related cardiac death [5].

Coronary artery anomalies are most often classified by their origin, course, termination, or aberrant intrinsic anatomy (Table 16.1). They can be both hemodynamically significant and insignificant. Hemodynamically significant anomalies are those that affect myocardial perfusion, leading to an increased risk of myocardial ischemia or sudden death. These anomalies potentially include (1) ectopic coronary

W. Mazur et al., *CT Atlas of Adult Congenital Heart Disease*,
DOI 10.1007/978-1-4471-5088-6_16, © Springer-Verlag London 2013

origin of the RCA or the left coronary artery (LCA) from the pulmonary artery, (2) ectopic coronary origin from the opposite aortic sinus, (3) single coronary artery, (4) coronary artery fistulae, and (5) myocardial bridging [5].

**Table 16.1** Coronary artery anomalies

| |
|---|
| *I. Anomalies of origination and course* |
| Absent left main trunk (split origination of left coronary artery) |
| Anomalous origin near aortic sinus of Valsalva |
| Anomalous origin from opposite of noncoronary sinus |
| Anomalous origin outside sinus of Valsalva |
| Anomalous pulmonary origin |
| Anomalous non-pulmonary origin |
| Single coronary artery |
| *II. Anomalies of intrinsic coronary arterial anatomy* |
| Congenital ostial stenosis/atresia |
| Coronary ectasia/aneurysm |
| Coronary hypoplasia |
| Absent coronary artery |
| Intramural course (myocardial bridging) |
| Coronary artery crossing |
| Doubled (duplicated) coronary artery |
| Anomalous origination of coronary artery branches |
| *III. Anomalies of termination* |
| Decreased number of arteriole/capillary ramifications |
| Coronary artery fistula |
| Extracardiac connections |

## 16.2 Anomalous Origin and Course of the Coronary Arteries

Excluding myocardial bridging, coronary artery anomalies of origin and course account for most coronary artery anomalies [5]. They represent up to 87 % of coronary anomalies diagnosed at invasive coronary angiography. These anomalies include (a) absent left main trunk, (b) anomalous origin near the sinus of Valsalva, (c) anomalous origin from the opposite or noncoronary cusp, (d) anomalous origin outside the sinus of Valsalva, and (e) single coronary artery.

### 16.2.1 Absent Left Main Trunk

In this anomaly, there are three or more coronary ostia. The left main artery is absent and there are separate ostia for the LAD and LCx arteries with otherwise normal LAD and LCx artery anatomy (Fig. 16.1) [7]. In other words, the LAD and LCx arteries have separate ostia emanating from the aorta. This anomaly may cause technical difficulties when performing conventional selective angiography.

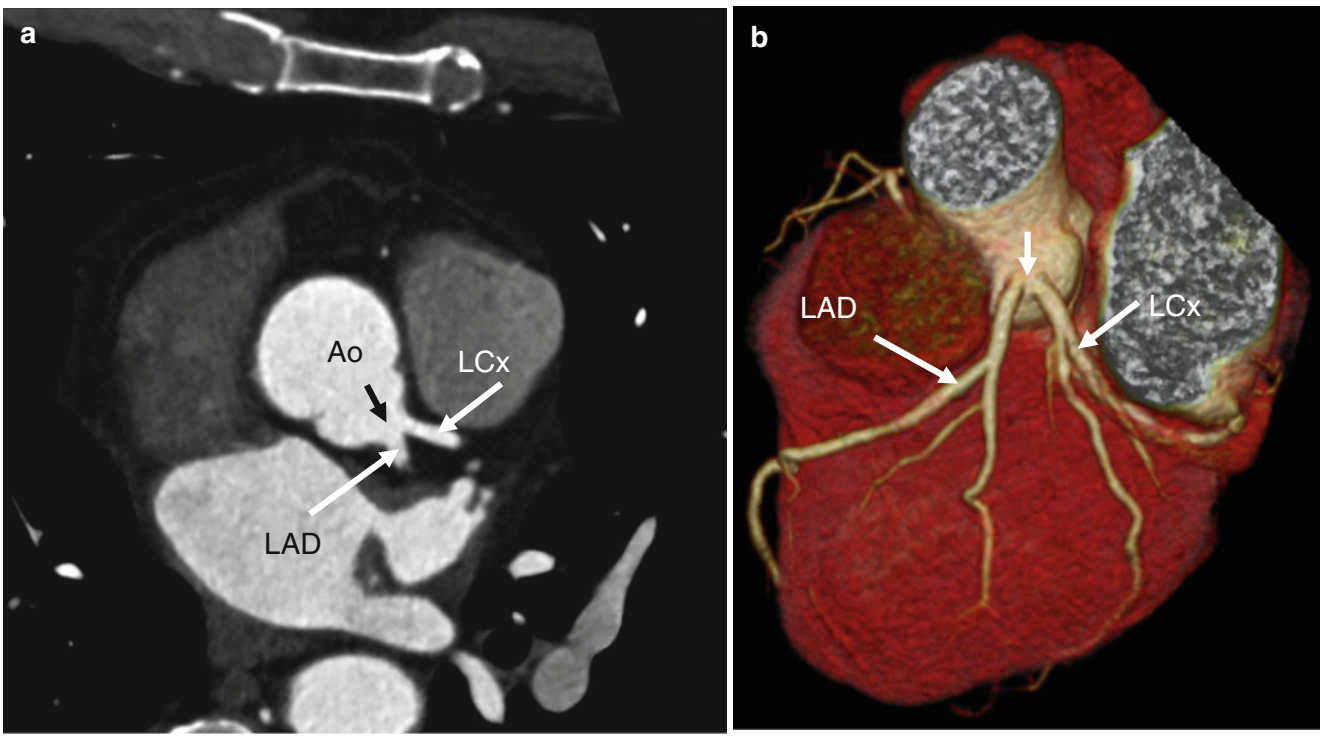


**Fig. 16.1** Absent left main trunk. The separate ostia (*black arrow* in panel **a** and *white arrow* in panel **b**) of the left anterior descending artery (*LAD*) and circumflex artery (*LCx*) in panel (**a**), a 2D multiplanar reformat and panel (**b**), a 3D volume-rendered reconstruction. *Ao* aorta

### 16.2.2 Anomalous Coronary Artery Origin near the Proper Sinus of Valsalva

This group of anomalies includes (a) a high ostium and (b) commissural ostium. High takeoff or high ostium refers to the origin of either coronary artery ostium above the sinotubular junction (i.e., between its sinus of Valsalva and the tubular part of the ascending aorta). See Figs. 16.2 and 16.3. This anomaly involves the RCA more frequently than the left and rarely has clinical significance unless interventional procedures are performed at which time it may add difficulty to the procedure. Awareness of the abnormal anatomy is important in order to avoid accidental ligation, transection, or cross-clamping at the time of surgery as well as to simplify the cannulation of the artery during surgery or arteriography. The coronary artery origin is usually located a few millimeters above the sinotubular junction, but an origin >5 cm above the junction has been reported [8].

Commissural coronary artery ostium is an extremely rare variant in which a coronary artery originates near or behind the commissure between two aortic valve cusps (Fig. 16.4). The combination of a slit-like coronary ostium and intimal proliferation of the aortic valve leaflet can contribute to lumen obstruction. This anomaly has been rarely associated with sudden cardiac death [9].

### 16.2.3 Anomalous Coronary Artery Origin from the Opposite or Noncoronary Sinus of Valsalva

Anomalous coronary artery origin from the opposite or noncoronary sinus of Valsalva represents the second most frequent reason for sudden cardiac death in the young (particularly during exercise) behind anomalous origin of the coronary artery near the sinus of Valsalva [10]. The diagnosis is challenging since patients have few prodromal symptoms and routine echocardiography is not sensitivity for detecting this abnormality [11–13]. This anomaly may be associated with sudden death, chest pain, arrhythmia, exercise-induced presyncope or syncope, left ventricular dysfunction, and findings of myocardial ischemia [14].

There are four anatomic patterns of anomalous origin of a coronary artery from the opposite or noncoronary sinus of Valsalva: (1) the LMCA arising from the right coronary sinus (Figs. 16.5 and 16.6), (2) the RCA arising from left coronary sinus (Fig. 16.7), (3) the LCx or the LAD arising from the right coronary sinus (Fig. 16.8), and (4) the LCA or the RCA arising from the noncoronary sinus (Fig. 16.9). There are also four different anatomical courses or distributions of the anomalous artery: (a) interarterial (between the aorta and pulmonary trunk, Fig. 16.7), (b) retroaortic (Figs. 16.5 and

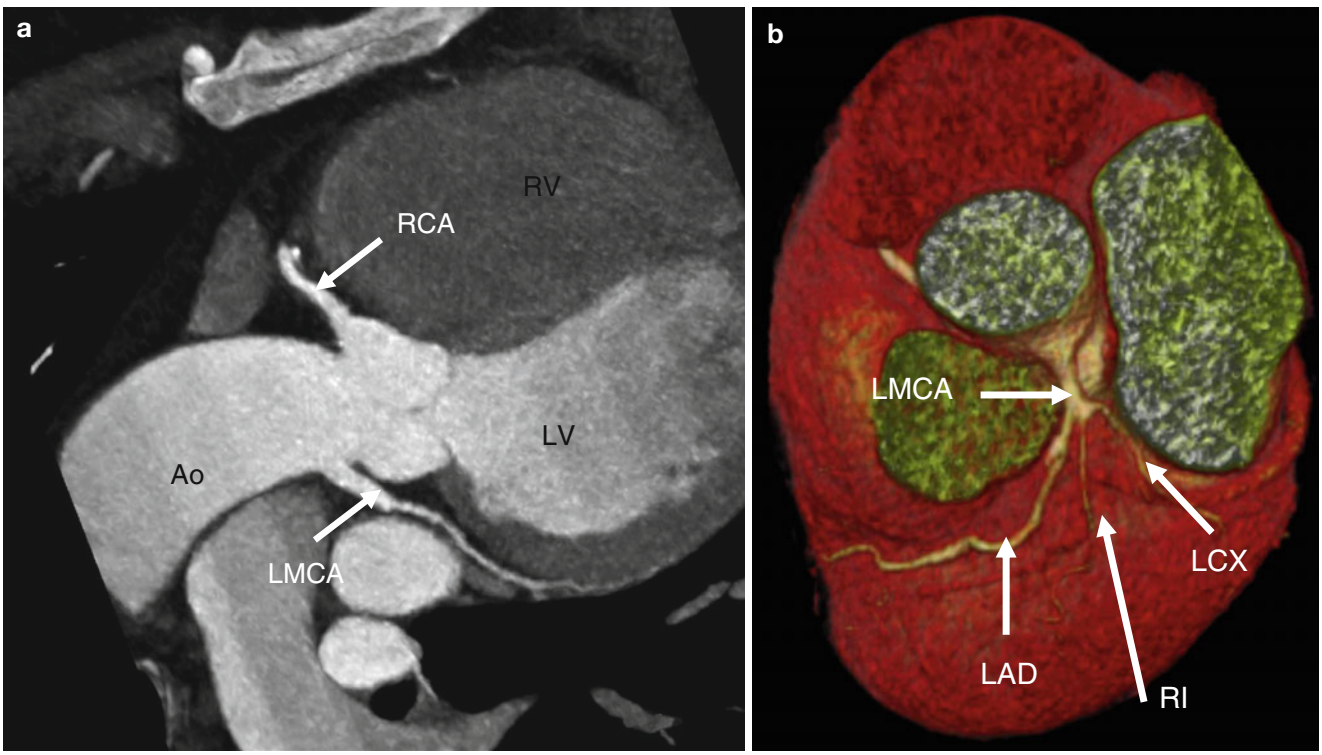


**Fig. 16.2** The high takeoff of the left main coronary artery (*LMCA*) in a 2D multiplanar reconstruction (panel **a**) as well as in a 3D volume-rendering reconstruction (panel **b**). The ostium of the left main coronary artery (*LMCA*) is located above the sinotubular junction of aorta. *LAD* left anterior descending artery, *LCx* left circumflex artery, *RCA* right coronary artery, *RI* ramus intermedius artery, *Ao* aorta, *LV* left ventricle, *RV* right ventricle

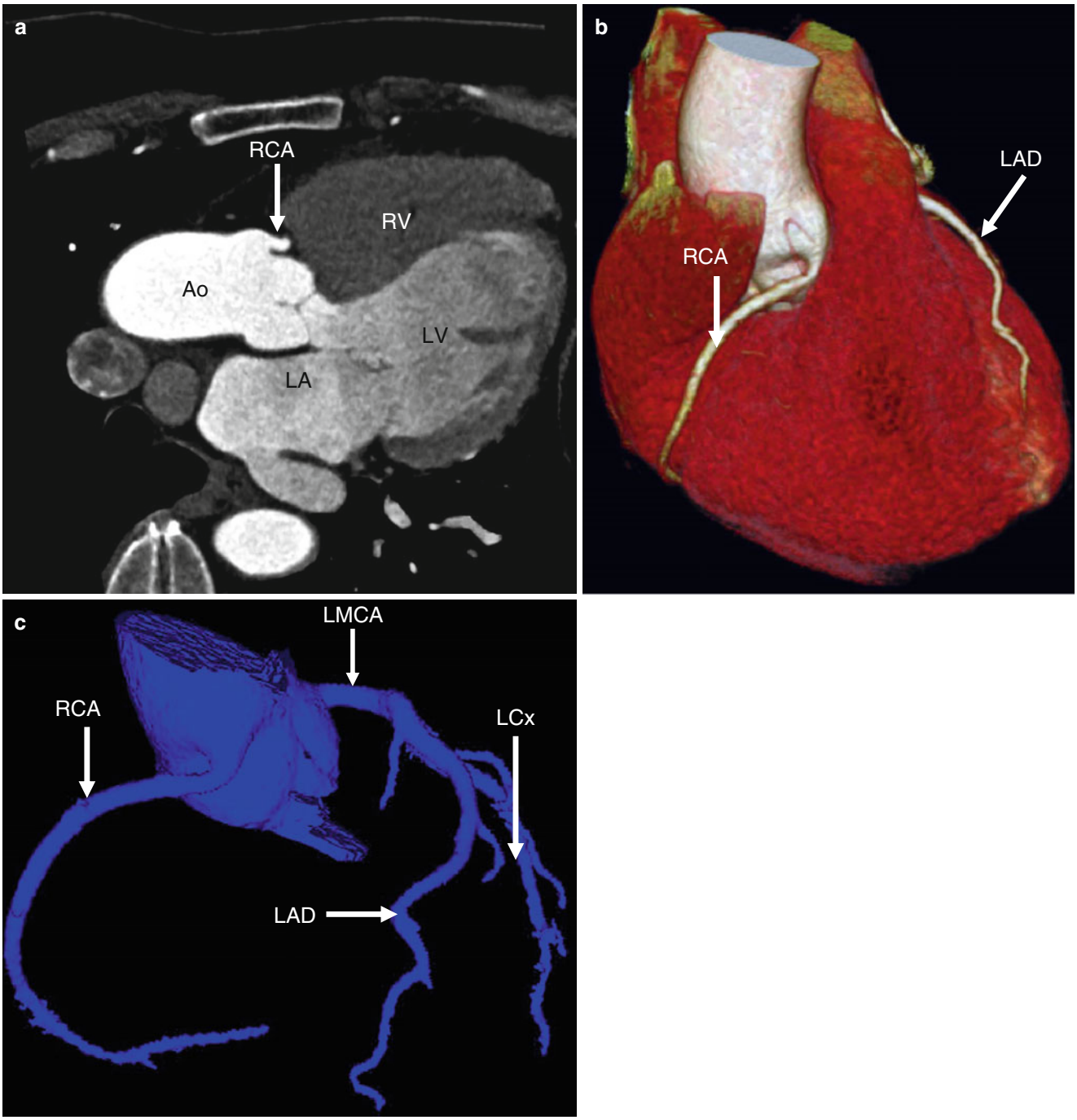


**Fig. 16.3** The high takeoff of the right coronary artery (*RCA*) in 2D multiplanar reconstruction (panel **a**) as well as in a 3D volume-rendering reconstruction (panel **b**) and a coronary artery tree format (panel **c**). The ostium of RCA is positioned above the sinotubular junction of aorta. *LAD* left anterior descending artery, *LCx* left circumflex artery, *LMCA* left main coronary artery

16.6), (c) prepulmonic, and (d) septal (also known as subpulmonic, Fig. 16.6). The precise path taken by the artery is of clinical importance. The interarterial course (previously called a malignant course) is associated with a high risk of sudden cardiac death, while the retroaortic, prepulmonic, and septal courses are considered low-risk anomalies.

High-risk anatomy (i.e., high risk for sudden cardiac death) can be associated with other abnormalities including a narrowed slit-like orifice of the coronary ostium, acute angle takeoff of the ostium, and an intramural course. An intramural course is characterized by a coronary artery whose origin travels diagonally through the wall of the aorta

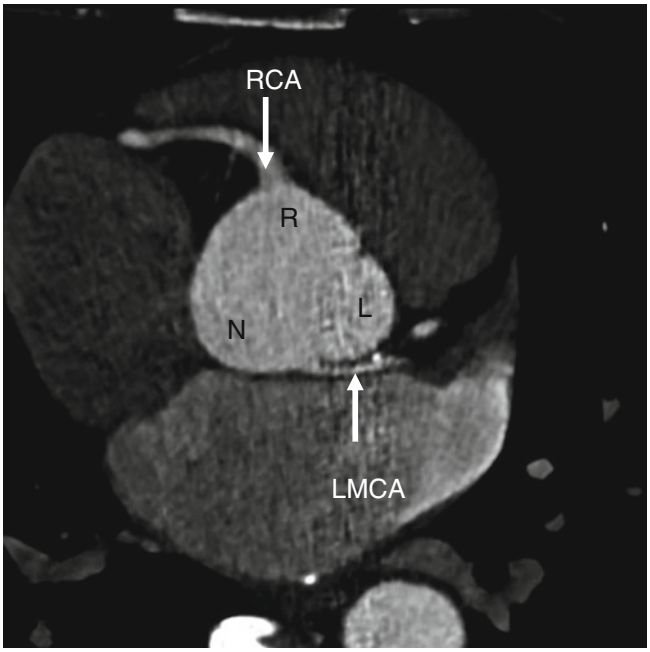


**Fig. 16.4** The commissural origin of left main coronary artery (*LMCA*). Note the presence of hypoplasia (*small caliber*) of the anomalous LMCA. The LMCA ostium is located at the commissure between left and noncoronary leaflets (*arrow*). *R* right coronary leaflet, *RCA* right coronary artery, *L* left coronary leaflet, *N* noncoronary leaflet

before exiting the aortic lumen as opposed to taking a perpendicular course directly through the aortic wall as it exits the aorta. This is identified by the acute angle takeoff, the slit-like origin, and the diagonal course between the great vessels [15]. To date, no single anatomical abnormality has been identified as the definitive cause of ischemia and sudden cardiac death [16].

The LMCA arising from the right coronary sinus of Valsalva is reported to occur in 0.017 % of patients undergoing coronary angiography (Figs. 16.5 and 16.6) [3]. It is associated with a high incidence of sudden cardiac death which is related to its frequently occurring interarterial course [17]. The interarterial course is associated with coronary arterial compression (worse in systole) which decreases coronary blood flow and may result in myocardial infarction. Anomalous coronary arterial flow can be further compromised during exercise due to aortic dilatation. A narrow slit-like orifice and an acute angle takeoff of the coronary ostium with a tangential proximal course of the ectopic coronary artery are also common pathologic findings and can contribute to sudden cardiac death. Surgical coronary revascularization is recommended in all patients with an anomalous, interarterial LMCA [14].

Less commonly, an anomalous LMCA may also take a retroaortic, prepulmonic, or septal (subpulmonic) course.

The RCA arising from the left coronary sinus Valsalva has been reported in approximately 0.2 % of patients scheduled for coronary angiography [3] (six times higher incidence than the LMCA arising from the right coronary sinus) (Fig. 16.7). It is associated with a lower risk of sudden cardiac death than LMCA arising from the right coronary sinus [12, 15, 18]. The most common course of an anomalous RCA arising from the left sinus of Valsalva is interarterial so this variant can be associated with sudden cardiac death [5].

Within the LCx or LAD arising from the right coronary sinus class of coronary anomalies, the LCx artery more frequently arises from the right coronary sinus than does the LAD artery (Fig. 16.8) [3, 19]. The vast majority of the time, the anomalous LCx artery passes behind the aortic root (i.e., retroaortic course) and has a good prognosis. It has not been associated with sudden death [20]. The LAD arising from the right coronary sinus is a very rare malformation. Rarely seen in patients with otherwise normal hearts, it has been associated with tetralogy of Fallot, double outlet right ventricle, and transposition of the great arteries. It may take either an interarterial or an intraseptal or prepulmonic course. The interarterial course portends a serious outcome, while the other intraseptal and prepulmonary routes are considered low-risk anomalies.

The LCA and the RCA arising from the noncoronary sinus are uncommon variants of coronary artery anomalies (Fig. 16.9) [19]. Both are usually benign and have no clinical relevance. Rarely they are associated with myocardial ischemia [21] and sudden cardiac death [22].

### 16.2.4 Anomalous Origin of the Coronary Artery Outside the Aortic Sinuses of Valsalva

Anomalous coronary arteries originating outside aortic sinuses of Valsalva may have a pulmonary origin or a nonpulmonary origin.

There are five anatomic patterns of anomalous pulmonary origin of coronary artery: (1) anomalous LMCA (LCA, left coronary artery) from the pulmonary artery (also known as ALCAPA or Bland–White–Garland syndrome), (2) anomalous RCA from the pulmonary artery, (3) anomalous LCx artery from the pulmonary artery, (4) anomalous LAD artery from the pulmonary artery, and (5) anomalous RCA and LCA from the pulmonary artery [6]. Of those anomalies, ALCAPA is most common, while the other variants are extremely rare.

ALCAPA (Bland–White–Garland syndrome, Fig. 16.10) has an incidence of 1 in 300,000 live births [14]. This anomaly results in a coronary steal phenomenon caused by the flow of blood from the higher pressure coronary arterial system to the lower pressure pulmonary arteries and results in impaired myocardial perfusion.

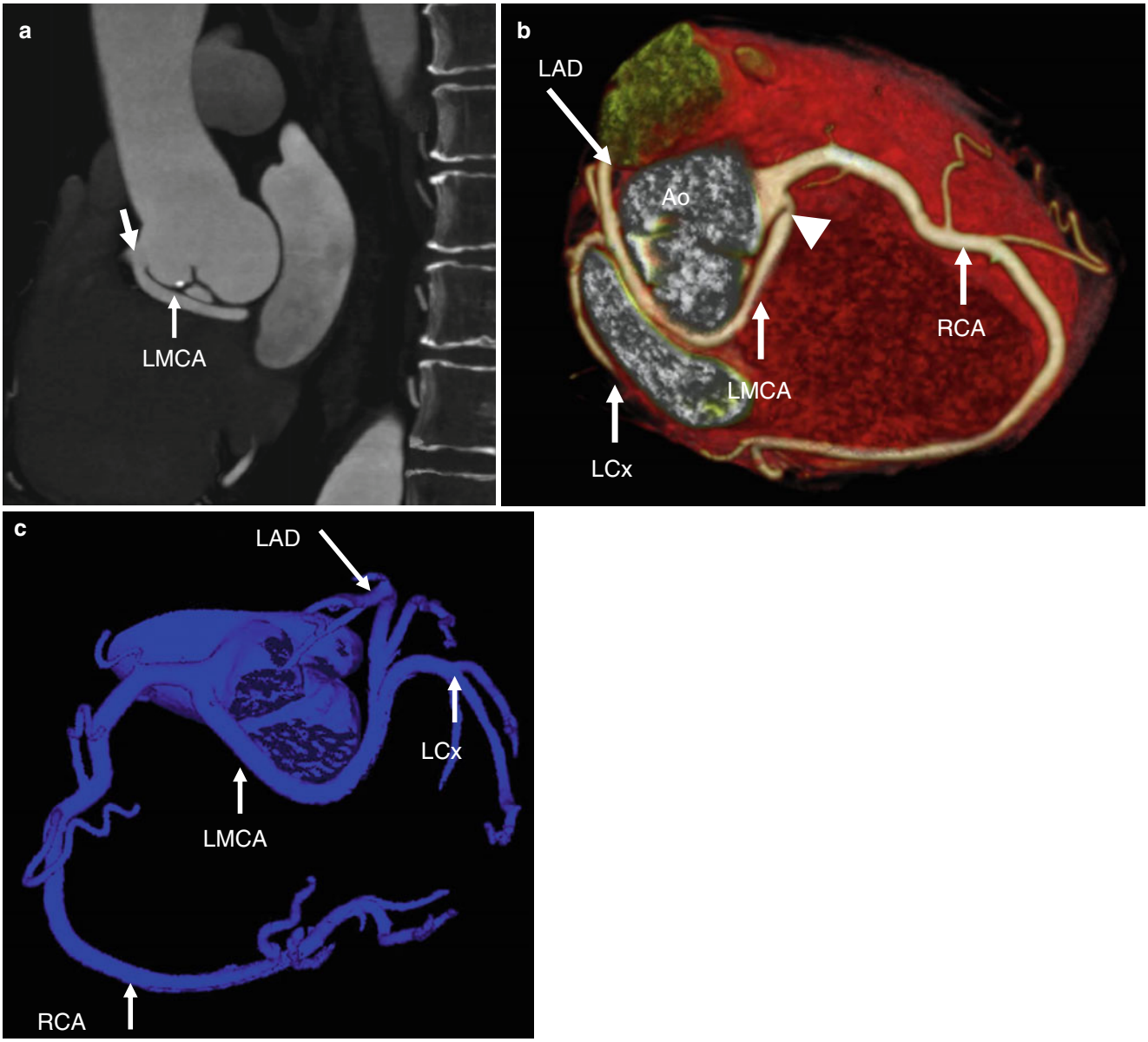


**Fig. 16.5** The abnormal origin of left main coronary artery (*LMCA*) from the right coronary sinus together with the right coronary artery (*RCA*) in a maximum intensity projection (panel **a**), a 3D volume-rendered image (panel **b**) and a coronary artery tree format (panel **c**). The LMCA follows the retroaortic course (seen best in panels a and b) and bifurcates subsequently into the left anterior descending artery (*LAD*) and circumflex artery (*LCx*). Note the normal width of LMCA ostium and the acute angle (*arrowhead*) just after its origin. The *arrow* in panel (a) points to the RCA ostium which is moving out of plane. *Ao* aorta

Based on age at presentation and survival patterns, ALCAPA has been classified as infantile types or adult types [23]. The infantile form presents days to weeks after birth with severe left ventricular dysfunction and mitral regurgitation due to an inadequate intercoronary collateral circulation. The prognosis is poor in the absence of early surgical intervention and approximately 90 % of untreated infants die in the first weeks to months of life. Very few patients survive to adulthood [24].

In the adult type, the development of extensive intercoronary collaterals, which feed the LCA territory, as well as a restrictive opening between the LCA and the pulmonary trunk, lead to near-normal left coronary perfusion and longer survival [25]. These patients may remain asymptomatic until adulthood despite silent, recurrent ischemia. In adults, clinical manifestations of ALCAPA include left ventricular dysfunction, mitral regurgitation, exercise-induced myocardial

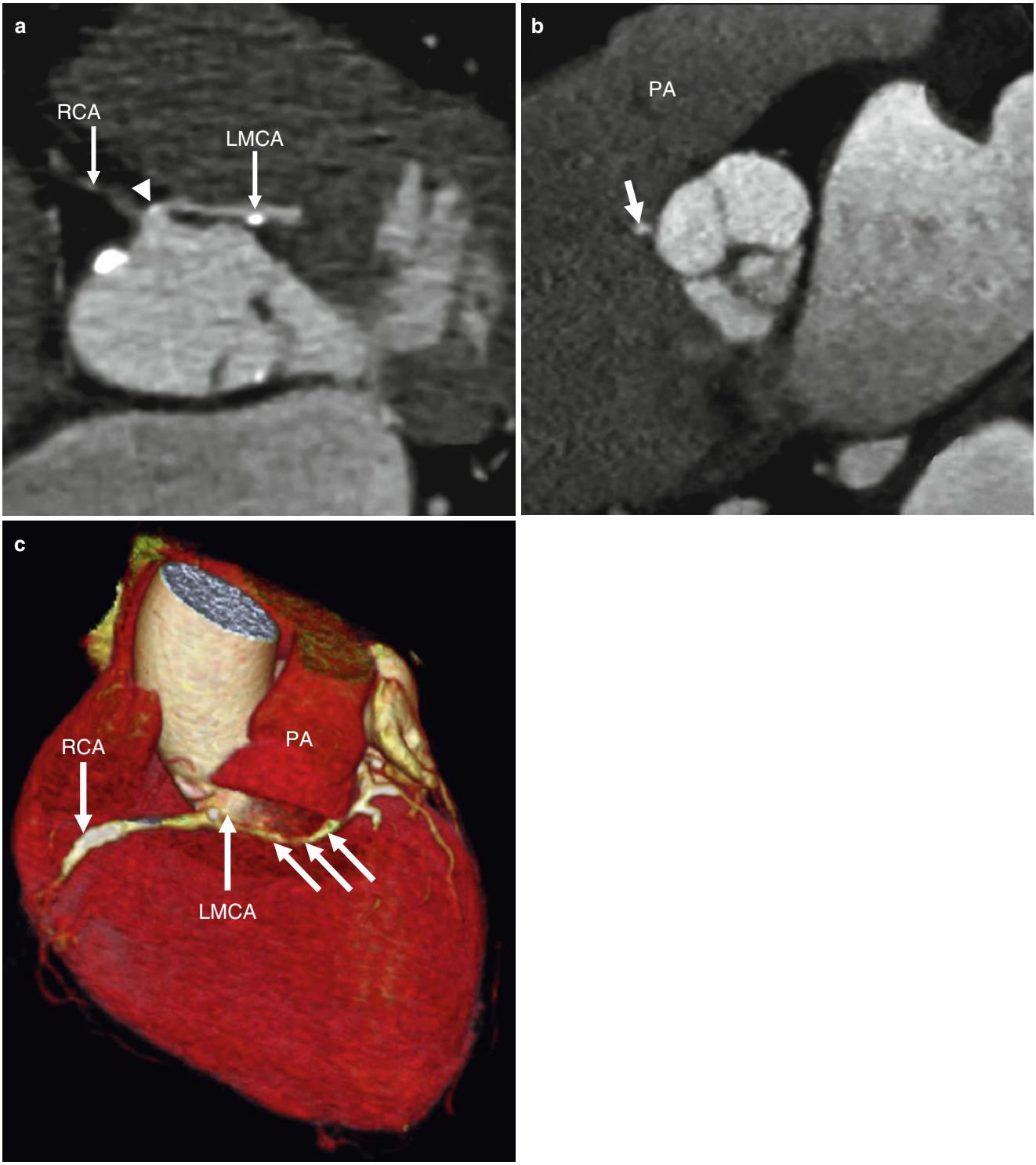


**Fig. 16.6** The abnormal origin of left main coronary artery (*LMCA*) from the right coronary sinus together with the right coronary artery (*RCA*) in 2D multiplanar reformat (panels **a** and **b**) and 3D volume-rendered reconstruction (panel **c**). The LMCA follows the subpulmonary course (*single arrow* in panel b and *multiple arrows* in panel c). Note the hypoplasia of the anomalous artery (*small caliber*) and acute angle (*arrowhead* in panel a) at its origin. *PA* pulmonary artery

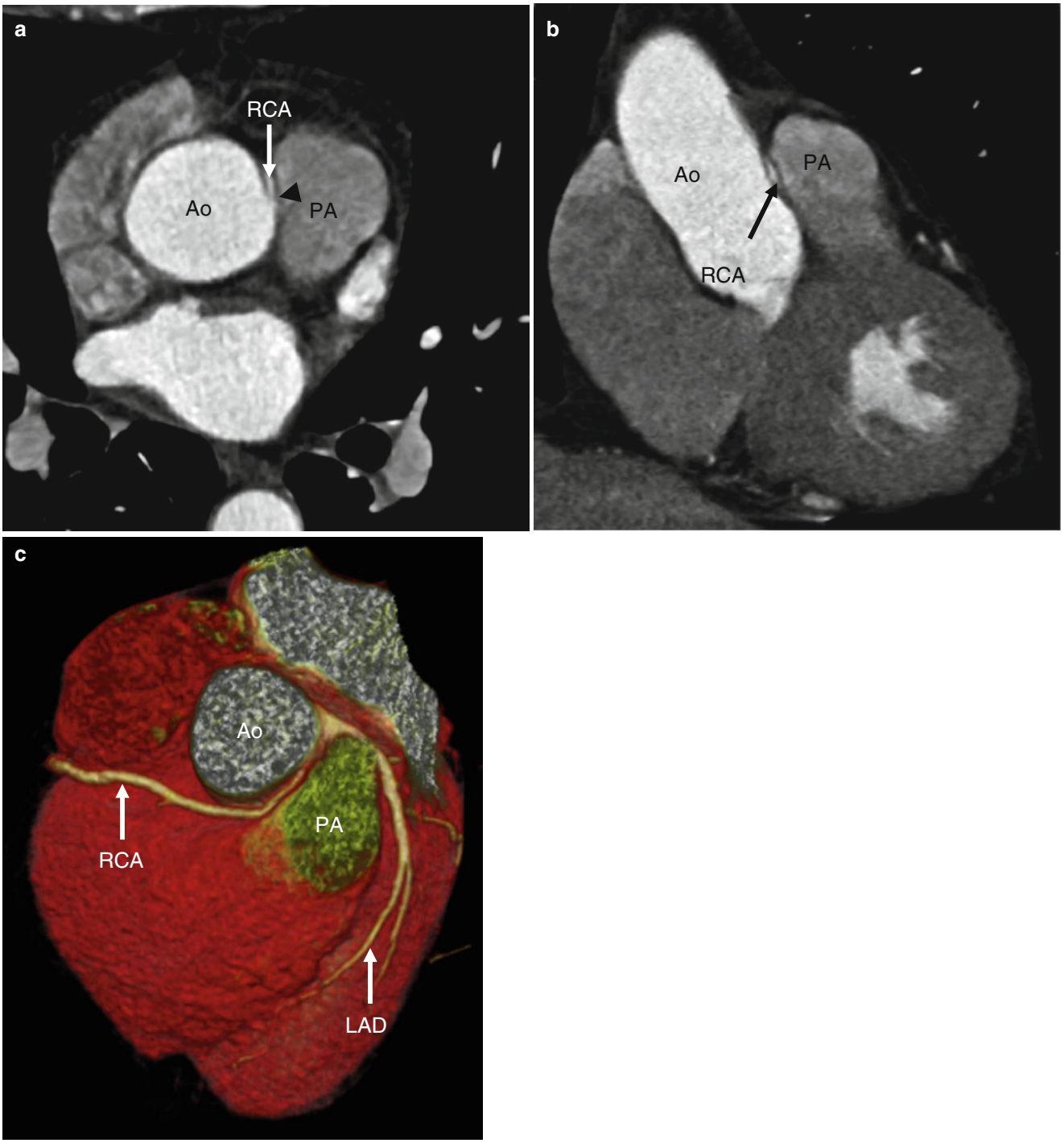


**Fig. 16.7** The abnormal origin of right coronary artery (*RCA*) from the left coronary sinus together with the left main coronary artery (*LMCA*) in 2D multiplanar reformat (panels **a** and **b**) and 3D volume-rendered reconstruction (panel **c**). The RCA follows the interarterial course (between the pulmonary artery and aorta). Note the hypoplasia (*small caliber*), acute angle takeoff, diagonal course between the great arteries and slit-like origin all of which define it as intramural (*arrowhead* in panel a). This anomaly takes intramural course as identified by the acute angle takeoff and the slit-like origin and diagonal course as it travels between the aorta and the pulmonary artery. *LAD* left anterior descending artery, *PA* pulmonary artery, *Ao* aorta

ischemia, myocardial infarction, heart failure, cardiac arrhythmia, and sudden cardiac death.

The anomalous LCA may arise from the pulmonary artery at or above the level of the pulmonary sinuses (high takeoff) or very close to a valvular commissure. At the pulmonary sinus level, the anomalous ostium most commonly originates from the left posterior pulmonary sinus (so-called right-handed sinus). Less commonly, it arises from the right posterior (left-handed) sinus or from the anterior (nonfacing) pulmonary sinus [26, 27].

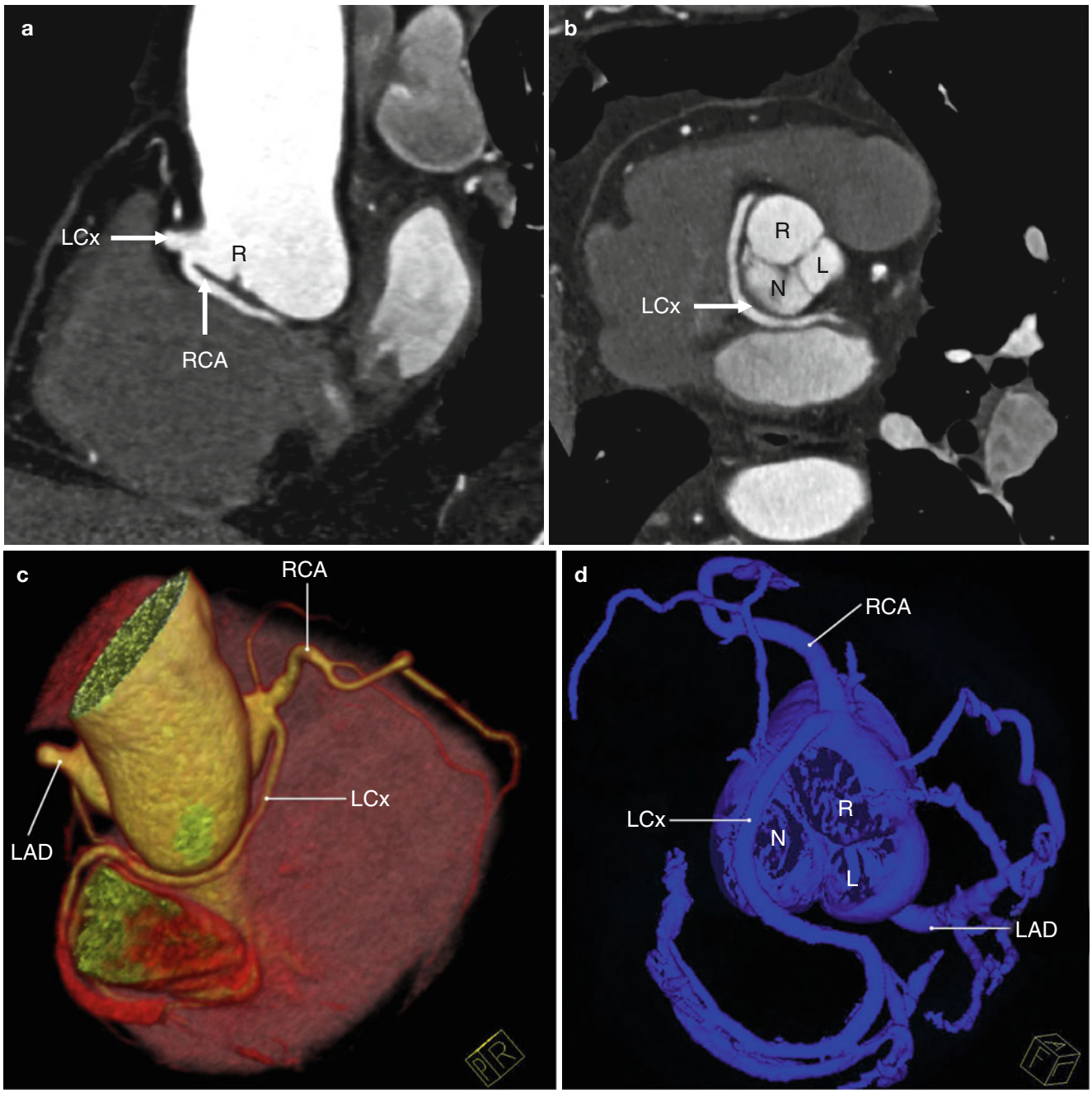


**Fig. 16.8** The abnormal origin of left circumflex artery (*LCx*) from the right coronary sinus together with the right coronary artery (*RCA*) in a multiplanar reformat (panels **a** and **b**) and 3D volume-rendered reconstruction (panel **c**) and a coronary tree format (panel **d**). The LCx follows the retroaortic course. Note the normal position of the left anterior descending artery (*LAD*). *R* right aortic sinus of Valsalva, *L* left aortic sinus of Valsalva, *N* noncoronary aortic sinus of Valsalva

Once the diagnosis of ALCAPA is established, prompt surgical reconstruction is indicated to restore a normal dual coronary artery, which usually results in near-total myocardial recovery [88]. In infantile-type ALCAPA, the surgical reconstruction strategies include direct reimplantation of the anomalous LCA into the aorta, creation of an intrapulmonary baffle from the left coronary ostia to the aorta (Takeuchi procedure, Fig. 16.11), or coronary bypass grafting (Fig. 16.12) [25]. Since in most cases the anomalous ostium arises from the left posterior sinus, aortic reimplantation is usually technically easy and allows full anatomical correction. In adult-type ALCAPA, ligation of the LCA from the pulmonary artery, combined with coronary artery bypass grafting utilizing the internal mammary artery or a saphenous

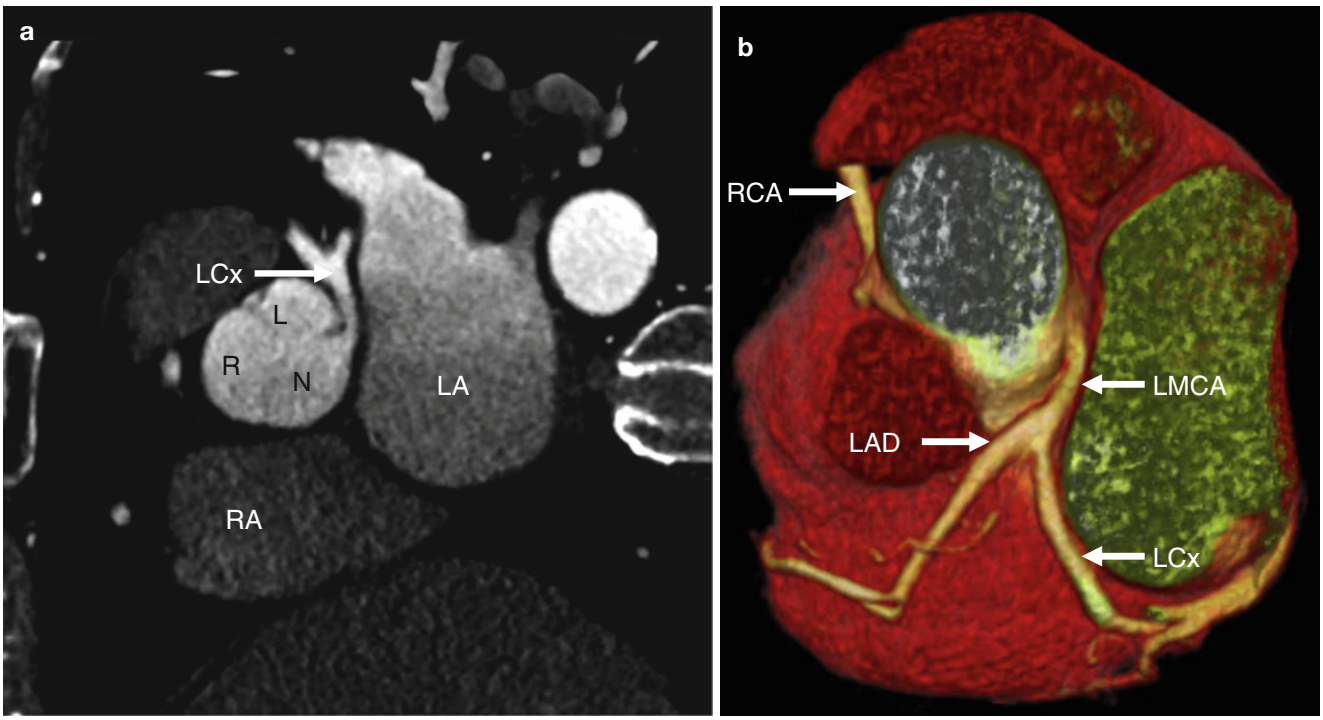


**Fig. 16.9** The abnormal origin of the left main coronary artery (*LMCA*) from the noncoronary sinus. Panel (**a**) is a multiplanar reformat and panel (**b**) is a 3D volume-rendered reconstruction. The right coronary artery (*RCA*) arises normally from the right coronary sinus. *LAD* left anterior descending artery, *LCx* left circumflex artery, *R* right coronary sinus, *N* noncoronary sinus, *L* left coronary sinus

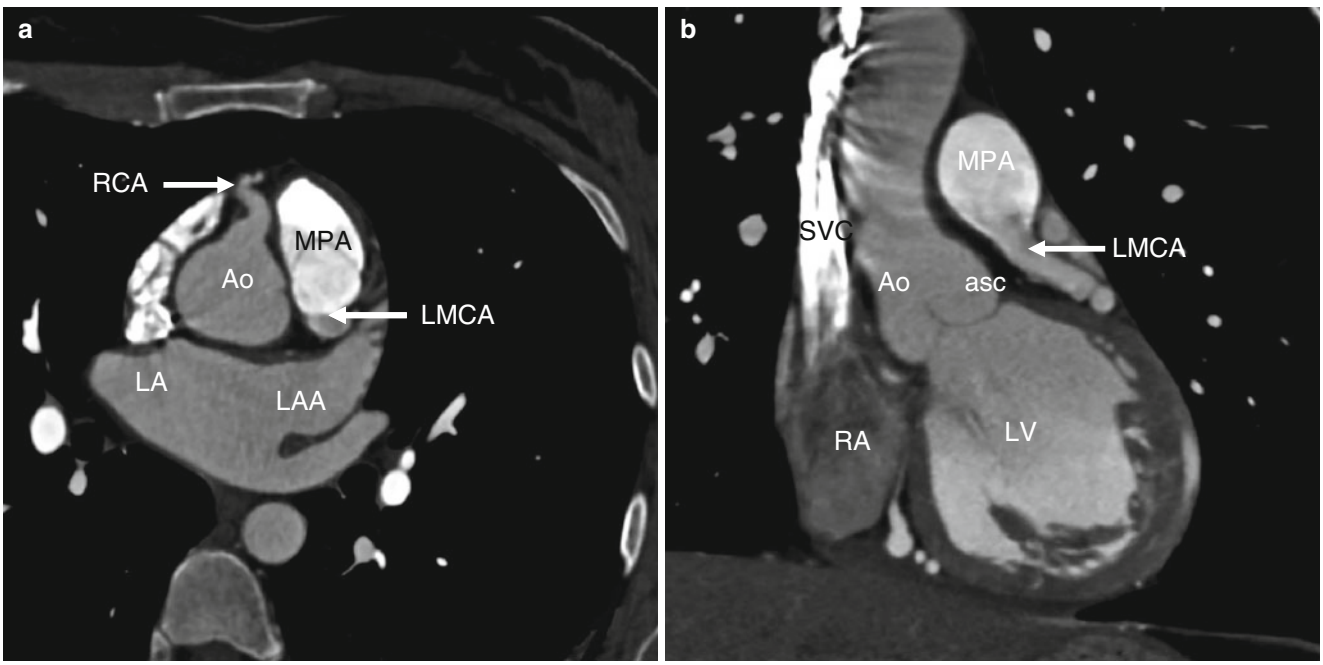


**Fig. 16.10** Anomalous pulmonary origin of left main coronary artery (*LMCA*) from the main pulmonary artery (*MPA*) also known as ALCAPA or Bland–White–Garland syndrome. Panels (**a**) and (**b**) are multiplanar reformats demonstrating the takeoff of the LMCA from the MPA. Panels (**c**) and (**d**) illustrate the very large and tortuous right coronary artery (*RCA*) which provides oxygenated myocardial blood supply for the whole myocardium via an extensive collateral circulation to the branches of the left coronary circulation and seen best in panel (c and d) and shown by the *arrows*. Note the flow of blood from the left coronary artery to the MPA. *Aoasc* ascending aorta, *LA* left atrium, *LAA* left atrial appendage, *LAD* left anterior descending artery, *LCx* left circumflex artery, *LV* left ventricle, *RA* right atrium, *RV* right ventricle, *SVC* superior vena cava

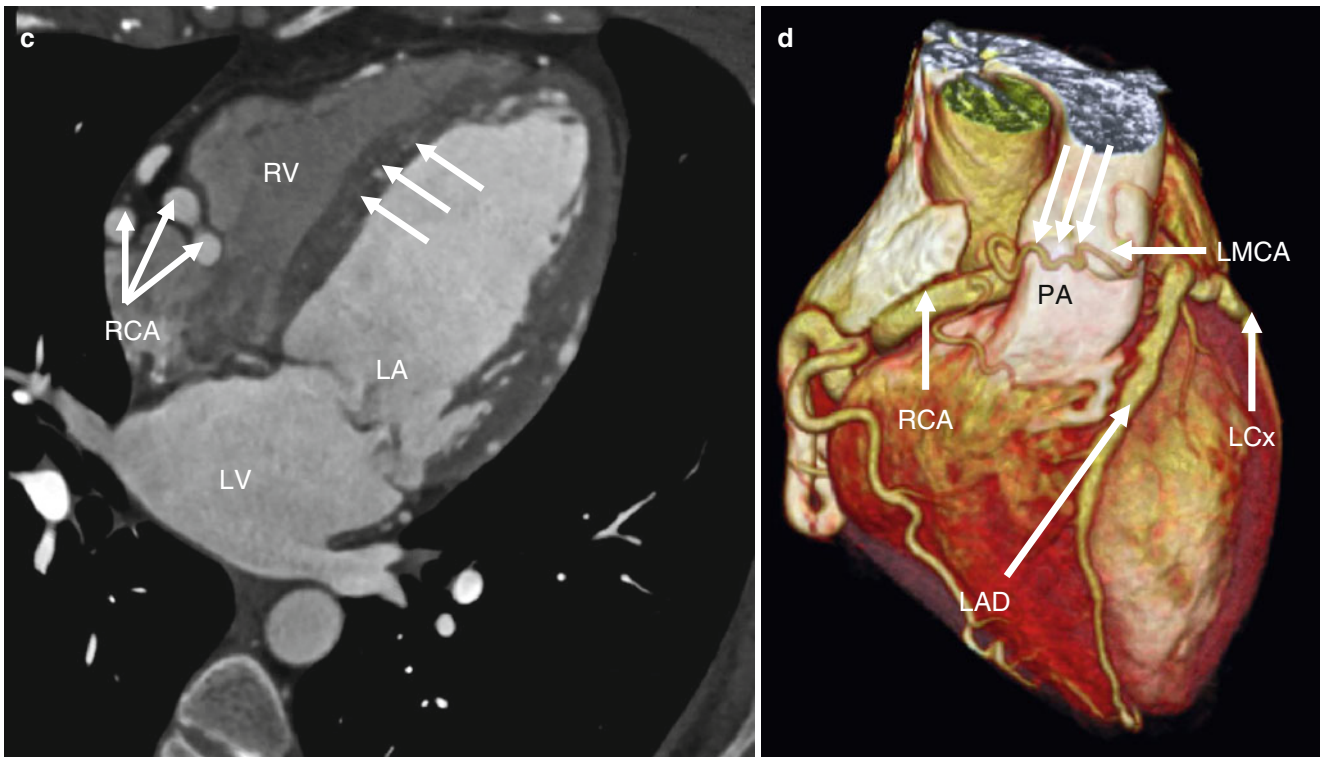


**Fig. 16.10** (continued)

vein, is preferable [28]. If coronary reimplantation is not feasible due to an unfavorable coronary anatomy and or a short length of the coronary artery, the Takeuchi procedure may restore dual coronary artery supply [88].

Adults after surgical repair should be evaluated every 3–5 years to assess the adequacy of repair and to exclude ongoing or recurrent myocardial ischemia [14]. Potential post-repair complications may include coronary artery and graft stenosis as well as aortic and mitral valve insufficiency. After the Takeuchi procedure, supravalvular pulmonary stenosis and baffle leaks or baffle stenosis may develop [29–31].

In the anomalous non-pulmonary origin variant, the anomalous coronary artery may arise from the right or left ventricle, aortic arch, ascending or descending aorta, as well as from the carotid, subclavian, innominate, internal thoracic, or bronchial arteries [6]. These origins are extremely rare and the clinical findings as well as the age at diagnosis are variable.

### 16.2.5 Single Coronary Artery

The single artery system is a rare abnormality in which only one coronary artery arises from a solitary ostium [32]. The incidence of this anomaly in series of patients undergoing invasive coronary angiography ranges from 0.008 to 0.066 % and accounts for 1.1–8.8 % of all coronary anomalies [33]. A single coronary artery may be an isolated finding or it may be associated with other congenital heart diseases including transposition of the great arteries, tetralogy of Fallot, truncus arteriosus, and coronary artery fistulas [26, 32].

Three different types of single coronary artery have been described: (1) single coronary artery following the course of either a normal RCA or LCA, (2) single coronary artery giving rise to the left main and RCA, and (3) single coronary artery having an anomalous course that does not meet criteria for type 1 or type 2 [34].

## 16.3 Anomalies of Intrinsic Coronary Arterial Anatomy

Anomalies of intrinsic coronary arterial anatomy represent a heterogeneous group of abnormalities, including coronary ostial atresia and coronary ostial stenosis, coronary ectasia and coronary aneurysm, absent coronary artery, coronary artery hypoplasia, muscular bridging, coronary crossing, double coronaries, and anomalous origin of coronary artery branches.

### 16.3.1 Coronary Artery Ostial Atresia or Stenosis

Coronary ostial atresia refers to complete atresia of the coronary ostium. There are two morphologic variants: (1) atresia of the LMCA (commonest form) and (2) atresia of the RCA

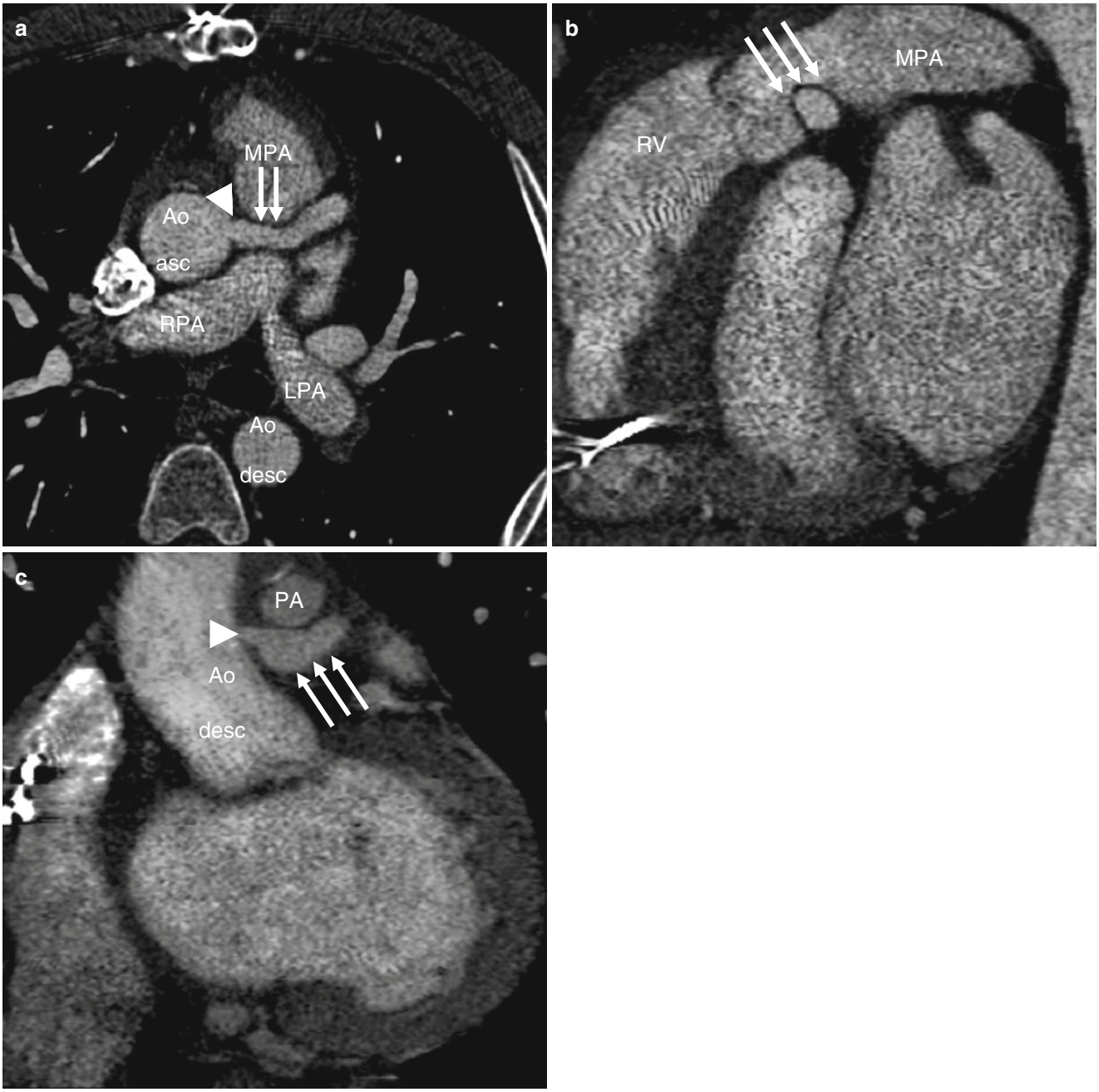


**Fig. 16.11** Takeuchi procedure in Bland–White–Garland syndrome (ALCAPA): Panels (**a**) and (**b**) are multiplanar reformats demonstrating the baffle from the main pulmonary artery (*MPA*) wall making an intrapulmonary tunnel (*arrows*) between the left coronary artery origin off of the MPA and the surgically created aortopulmonary window (creating a "pseudo left main coronary artery"). Panels (**a**) and (**c**) demonstrate the narrowed orifice of the surgically created intrapulmonary arterial baffle at aortic wall origin (*arrowhead*) with dilatation of the baffle after the stenosis (seen best in panel c). *Aoasc* ascending aorta, *Aodesc* descending aorta, *PA* pulmonary artery, *LPA* left pulmonary artery, *RPA* right pulmonary artery, *RV* right ventricle

[35]. In atresia of the left coronary ostium, the entire coronary arterial supply is from the RCA and its branches. The LAD and LCx artery are seen in their normal respective locations, but they join together and terminate at a proximal blind end, receiving blood only from RCA collaterals [36, 37]. The collateral circulation from the right to the left coronary system is usually inadequate, and thus, most affected patients develop early myocardial ischemia and die in infancy or childhood. However, asymptomatic survival until adulthood has been reported and cases may be discovered incidentally at angiography [38].

This anomaly can also be associated with findings of myocardial ischemia or infarction, heart failure, syncope, and sudden cardiac death [36]. Surgical reconstruction of a

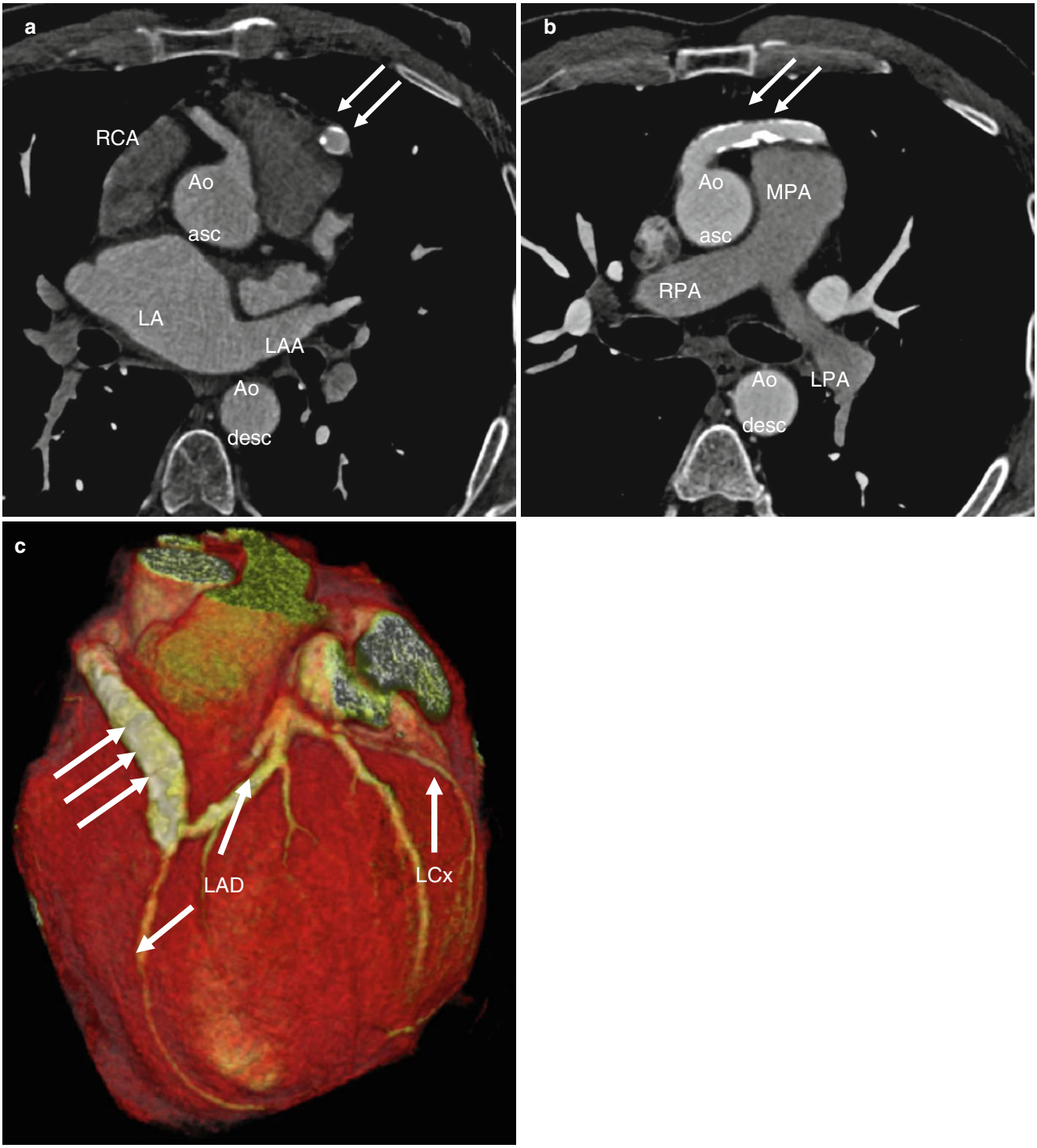


**Fig. 16.12** Coronary artery bypass grafting and ligation of the native left main coronary artery in a patient with ALCAPA (Bland–White–Garland syndrome): Panels (**a**), (**b**) are multiplanar reformats while panel (**c**) is a 3D volume-rendered image. Note the origin of the wide caliber of the right coronary artery (*RCA*) and the presence of the calcified venous graft (*arrows*) between the ascending aorta (*Aoasc*) and the left descending coronary artery (*LAD*). *Aodesc* descending aorta, *LA* left atrium, *LAA* left atrial appendage, *LCx* left circumflex artery, *LPA* left pulmonary artery, *RPA*, right pulmonary artery

two coronary artery system by a coronary artery bypass graft procedure is the preferred surgery [36].

In congenital right coronary ostial atresia, there is atresia of the right coronary ostium. In this rare condition, the RCA is supplied via collaterals from the LCA [39]. Surgical repair entails restoration of a dual coronary artery supply [39].

Congenital ostial stenosis is a multifactorial condition that may be caused by an acute angle takeoff of the coronary

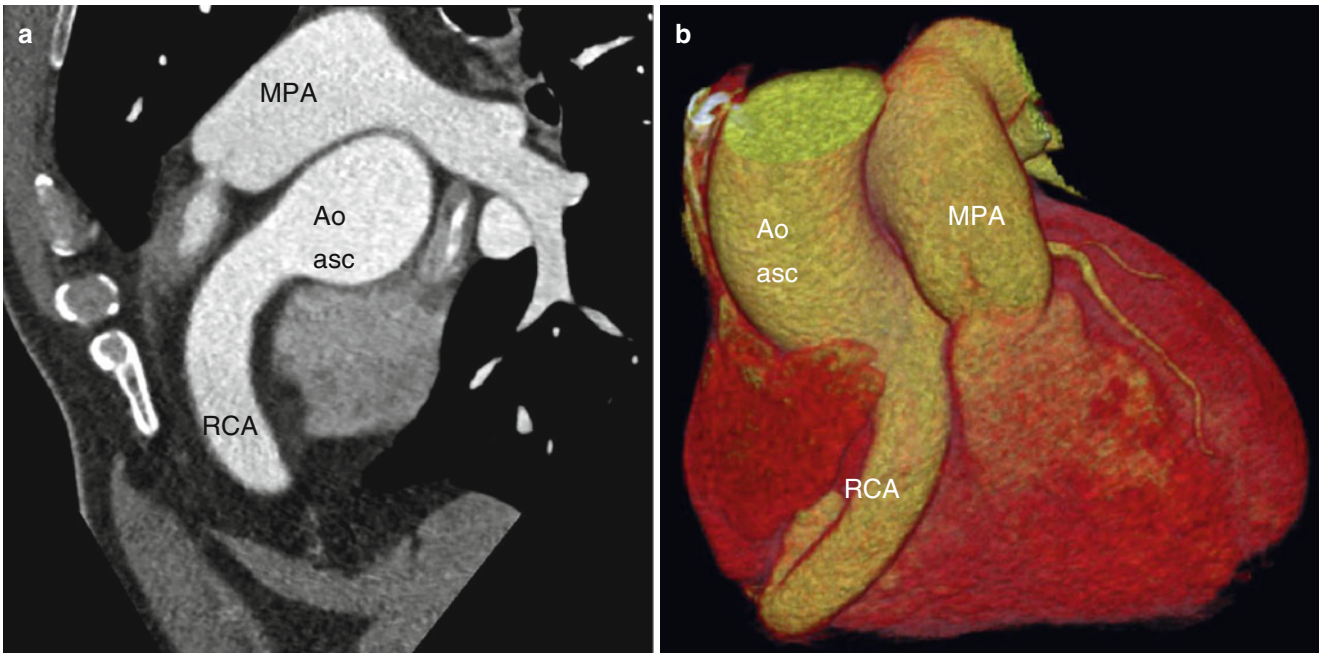


**Fig. 16.13** Right coronary artery (*RCA*) ectasia in a multiplanar reformat (panel **a**) and a volume-rendered image (panel **b**). *Aoasc* ascending aorta, *LPA* left pulmonary artery, *MPA* main pulmonary artery

artery, a slit-like orifice, intimal proliferation of an aortic valve leaflet, fusion of the aortic leaflets, and intramural course of the coronary artery [71, 77]. Coronary ostial stenosis has been associated with sudden cardiac death [77, 80].

### 16.3.2 Coronary Artery Ectasia or Aneurysm

Coronary artery ectasia or aneurysm is defined as a dilated coronary artery with a luminal diameter exceeding 1.5 times the diameter of the adjacent normal coronary segment or the largest diameter of the coronary artery (Fig. 16.13) [40–42]. The dilatation is commonly diffuse and can be either fusiform or saccular in shape [44]. A giant coronary aneurysm is usually defined as a coronary artery with a maximal diameter exceeding 20 mm, although other cutoff values (50–150 mm) have also been described [41, 43].

The two most common etiologies of coronary ectasia and aneurysm are atherosclerotic disease (acquired form) which occurs in >50 % and congenital coronary ectasia and aneurysm [44]. Congenital coronary aneurysms are most commonly described in the RCA and are frequently associated with fistulas, but other congenital abnormalities can coexist.

Complications include thrombosis, distal embolization, myocardial ischemia and infarction, heart failure, arrhythmias, dissection, vasospasm, calcification, fistula formation to the coronary sinus, cardiac rupture, and sudden cardiac death [44–48].

Management is not standardized, but surgery should be considered for large symptomatic aneurysms, while conservative approach may be justified for small, asymptomatic aneurysms [41].

### 16.3.3 Absent Coronary Artery

Absence of a coronary artery is a rare finding. It is usually partial, in contrast to total absence of the coronary artery (also known as single coronary artery, described above). Since the territory of the absent artery is supplied by a branch arising from another artery, this anomaly often has a good clinical outcome [49]. Absence of the LCx artery with a superdominant RCA is the most common form of absent coronary artery [49, 50]. In this scenario, the LMCA continues as the LAD and there is complete absence of the LCx and obtuse marginal arteries. The RCA is dominant with its distal branches supplying the LCx territory of the left ventricle.

### 16.3.4 Coronary Artery Hypoplasia

A hypoplastic coronary artery system is defined as the underdevelopment of one or more major coronary artery branches which have either significantly decreased luminal diameters and or length [51]. This abnormality may occur as an isolated finding or it may coexist with other coronary artery

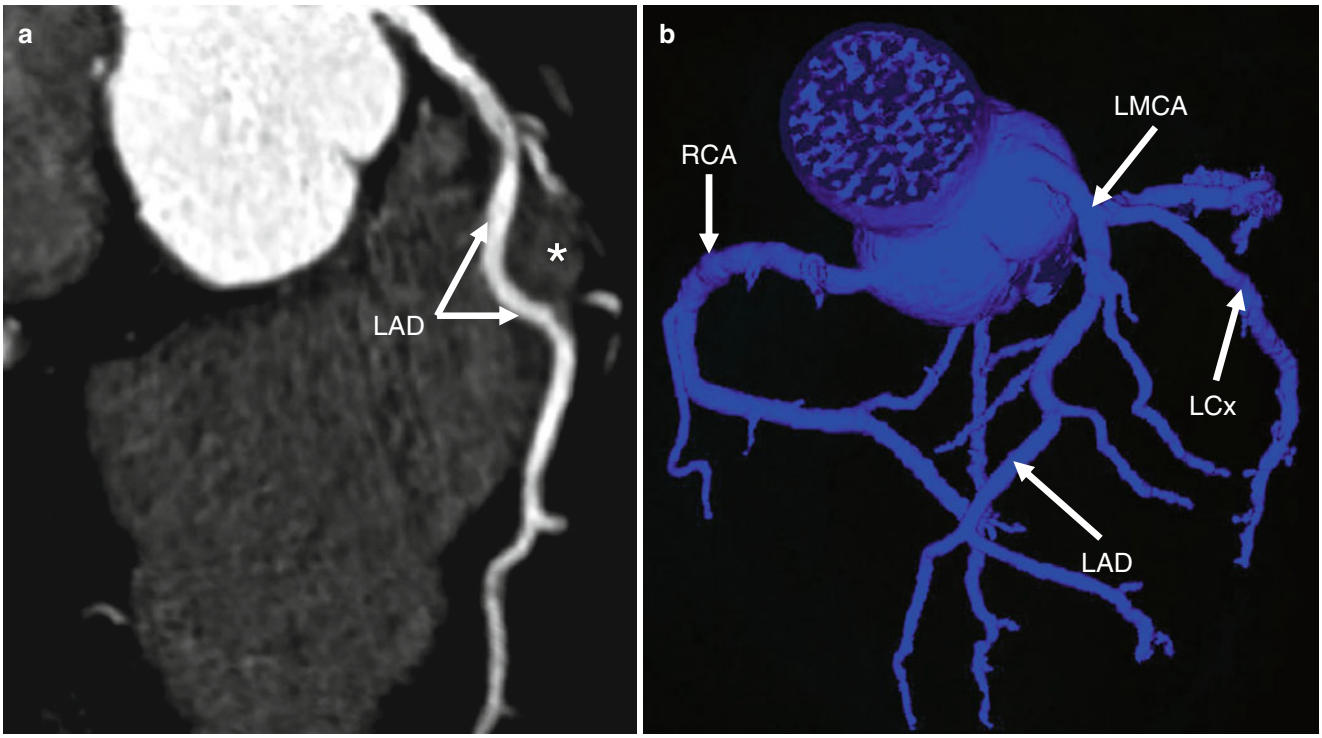


**Fig. 16.14** Myocardial bridge (*asterisk*) over the *midportion* of left anterior descending artery (*LAD*). Note the curved course of LAD in the multiplanar reconstruction (panel **a**) and coronary tree reformat (panel **b**). *LCx* left circumflex artery, *LMCA* left main coronary artery, *RCA* right coronary artery

anomalies. It has been reported in young individuals who die suddenly without antecedent symptoms [51, 52]. Its true incidence is unknown. Ogden [53] reported 5 cases of hypoplastic coronary arteries in an autopsy series of 224 congenital coronary anomalies. This anomaly is most frequently diagnosed at necropsy and rarely is it diagnosed antemortem. Affected individuals are at high risk of sudden cardiac death [54, 55].

### 16.3.5 Intramural Course (Muscular Bridging)

Myocardial bridging refers to a band of myocardial muscle overlying a segment of a coronary artery (Fig. 16.14). The abnormal artery traverses through the myocardium instead of having a normal epicardial location. The tissue overlying the artery is termed the myocardial bridge. Myocardial bridging is a common finding in cardiac computed tomographic angiography (CCTA) (4–39 %) [56–59] and at autopsy (5–86 %) [60–64]. It has a lower incidence in invasive coronary angiography (0.5–4.9 %) [65–69].

The characteristic finding on catheter angiography is systolic compression of the artery, termed "milking effect." Invasive angiography may be insensitive to minimal bridging that does not cause substantial systolic compression of the arterial lumen. CCTA may be more sensitive for diagnosis since it can directly delineate the coronary artery lumen and wall, in contrast to catheter angiography which only demonstrates the arterial lumen.

Myocardial bridging is usually an incidental finding, but it has been linked with symptoms of myocardial ischemia, myocardial infarction, arrhythmias, and sudden cardiac death. These symptoms have been attributed to the intramural course of the artery [70–73]. Myocardial bridging may also complicate coronary bypass surgery [74] by making it difficult to localize the tunneled coronary artery which may lead to ventricular wall perforation (most commonly the right ventricular wall) due to overly aggressive surgical dissection [75, 76]. Thus, the intramural course can be considered a relative contraindication to minimally invasive surgery [58, 75].

Myocardial bridging most commonly affects the middle or distal segment of the LAD artery. Myocardial bridging of the RCA and LCx arteries are less common [56–59]. Myocardial bridges have been further classified as superficial (≤1.0 mm), deep (>1.0 mm), and right ventricular type (when the intramuscular artery traverses through the right ventricular wall) [59]. The latter may correspond to the intracavitary coronary artery course, a variant that has been reported in the literature [74, 77].

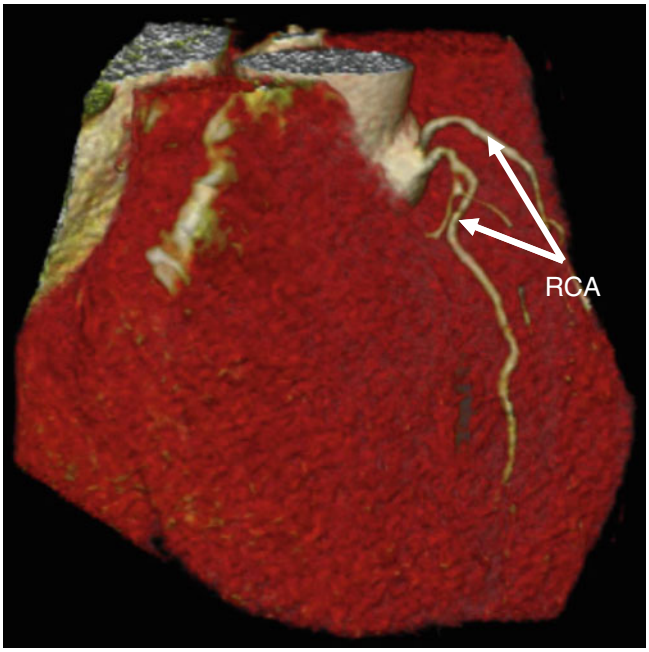


**Fig. 16.15** Duplication of the recessive right coronary artery (*RCA*) in a 3D volume-rendering reconstruction

### 16.3.6 Coronary Crossing

Coronary crossing is an extremely rare abnormality in which the epicardial course of one artery is crossed by another. This anomaly may be isolated [78] or accompanied by other abnormalities (i.e., double coronary artery, anomalous coronary artery origin) [79–81]. The potential risk of this anomaly is coronary artery compression [80].

### 16.3.7 Double Coronary Artery

Double coronary artery is a very uncommon congenital abnormality which usually has no clinical impact (Fig. 16.15). This anomaly may affect both coronary arteries and may be isolated or accompanied by other abnormalities [82–84]. If associated with coronary stenosis, it may have potential impact on revascularization procedures [83].

Based on the course of the coronary artery within the anterior interventricular sulcus and the number of branches, Spindola-Franko et al. [84] described four types of double LAD. The most common type is type 1 or duplication of the LAD. This type consists of both a short LAD which courses along the anterior interventricular sulcus without reaching the apex and a long artery that originates from the LAD or the RCA, enters the anterior interventricular sulcus, and descends over the left ventricle to reach the ventricular apex. In type 2 duplication, the artery descends over the right ventricle. In type 3 duplication, the artery demonstrates myocardial tunneling along the septum. With the type 4 variant, there are two separate LAD arteries, one originates from the LMCA and the other from the RCA.

Recently, Tuncer et al. [85] described a type 5 duplication where two LADs originate from the LMCA (either from the right or noncoronary sinus).

### 16.3.8 Anomalous Origination of Coronary Artery Branches

This anomaly is characterized by unusual origins of the coronary artery branches. The most common example is an anomalous origin of the posterior descending artery from the first septal branch. It usually has no clinical significance [86–88], although myocardial ischemia due to compression of the first septal branch has been reported [89]. Despite being asymptomatic, its presence can be important when a revascularization procedure is planned.

## 16.4 Anomalies of Termination

Abnormal coronary artery terminations include (1) decreased number of arteriole/capillary ramifications, (2) coronary arteriovenous fistulas, and (3) extracardiac connections [6]. The most common of these is the coronary artery fistula which represents the second most frequent congenital coronary artery anomaly after anomalous origin of the coronary arteries [3].

### 16.4.1 Coronary Artery Fistula

Coronary artery fistula is defined as an abnormal communication between the coronary system and a cardiac chamber or great vessel (Figs. 16.16 and 16.17). The incidence of this anomaly is approximately 0.18 % in patients who undergo selective coronary angiography [3].

Fistulas more commonly involve the RCA than the LCA. In less than 5 % of cases, fistulas originate from both the LCA and the RCA. The LCx artery is rarely affected [90]. There is usually a solitary communication, but multiple fistulas can occur. The involved coronary artery is dilated and often tortuous because of increased blood flow. The site of drainage is usually into a low-pressure venous circulation including right atrium, right ventricle, pulmonary artery, superior vena cava, and coronary sinus, thus resulting in a left-to-right shunt. Drainage into the left atrium or left ventricle is very rare [91]. When the connection is to a left-sided chamber, the hemodynamics can mimic those of aortic insufficiency.

Most adults with coronary artery fistulas are asymptomatic and the fistulas are found incidentally during coronary angiography. The clinical manifestations depend on the severity of the left-to-right shunt, which if severe can lead to a hemodynamic steal phenomenon. As symptoms develop,

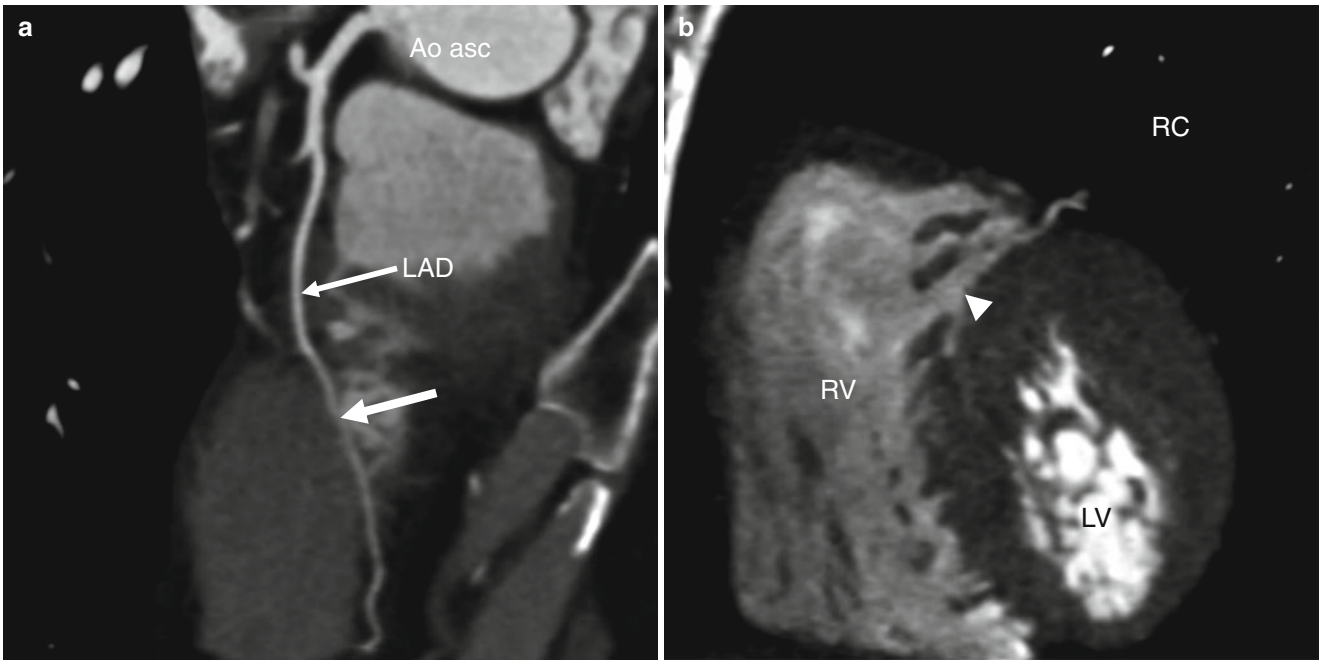


**Fig. 16.16** Coronary artery fistula. The fistula (*arrow* in panel **a** and *arrowhead* in panel **b**) between the *midportion* of left anterior descending artery (*LAD*) and the right ventricle (*RV*) seen in 2D multiplanar reformatting (panels **a** and **b**). *Aoasc* ascending aorta, *LV* left ventricle

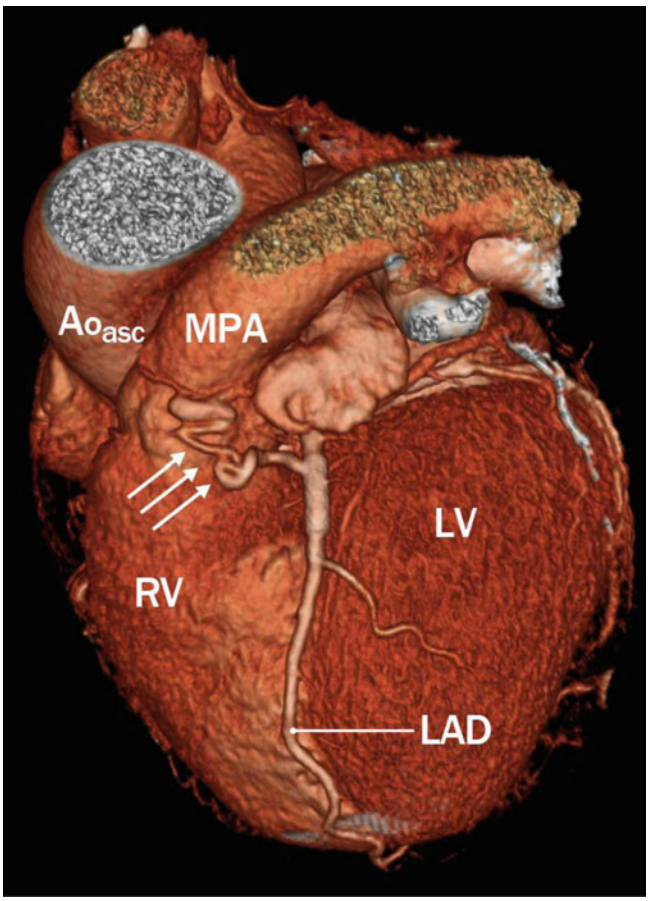


**Fig. 16.17** Coronary artery fistula: the fistula (*arrows*) is between the proximal portion of left anterior descending artery (*LAD*) and main pulmonary artery (*MPA*) is demonstrated in a volume-rendered reconstruction. *Aoasc* ascending aorta, *RV* right ventricle, *LV* left ventricle

patients may present with angina, myocardial infarction, arrhythmias, endocarditis, heart failure, pulmonary hypertension, pericardial effusion, and sudden cardiac death [92]. Potential complications include arterial aneurysm, fistula rupture, or fistula thrombosis. Treatment options include closing the fistula by coil embolization or by ligation without or without coronary artery bypass grafting. Intervention is indicated in large fistulas, regardless of symptomatology, and in small- to moderate-size symptomatic fistulas [14].

### 16.4.2 Extracardiac Connections

Coronary arteries may connect to extracardiac vessels, such as the bronchial, internal mammary, pericardial, mediastinal, phrenic and intercostal arteries, and esophageal branches of the aorta. These pathways can be hemodynamically significant if a pressure gradient exists between the two arterial systems, which most often occurs with development of atherosclerotic coronary artery disease.

## 16.5 Cardiac Computed Tomography (CT) in Assessing Coronary Anomalies

ECG-gated cardiac CT has emerged as a noninvasive imaging modality for detection and assessment of coronary artery anomalies [93]. In contrast to invasive coronary angiography, this technique allows definition of not only the coronary lumen but the coronary wall and neighboring structures, including myocardium, great arteries, and cardiac chambers.

CT enables precise assessment of the anomalous origin, course, and termination of the coronary arteries. Axial CT images provide an overview of the data, but three-dimensional volume-rendered images are required for comprehensive pathology depiction [94, 95]. While CT can show the ostial origin, proximal course, and termination of the coronary arteries, it cannot reliably assess the hemodynamic significance of congenital coronary anomalies, and additional clinical tests are needed to detect ischemia associated with these anomalies [58].

For anomalies of origin and course, cardiac CT provides a thorough, detailed depiction of the course and origin of the anomalous artery while demonstrating the spatial relation of the anomalous coronary artery to adjacent structures, which is crucial for management strategy. CT can clearly reveal the malignant interarterial course of the anomalous artery [94–96]. In patients with Bland–White–Garland syndrome, it is particularly useful to depict the intercoronary and other collateral arteries providing blood supply to the LCA circulation. In addition cardiac CT may be used to assess postoperative complications that require reintervention.

Cardiac CT is an accurate technique to depict and assess anomalies of intrinsic coronary arterial anatomy as well. In particular, it provides insight into the morphology of coronary artery ostial atresia or stenosis, ectasia or aneurysm, hypoplasia, and anomalous origin of coronary artery branches. In addition, it is recognized as a sensitive and reliable technique for detecting myocardial bridges and determining their depth, length, and course [56–59].

Cardiac CT is also an accurate technique for assessing anomalies of termination. Unlike invasive coronary angiography, CT not only allows diagnosis of a coronary fistulas and extracardiac connections but enables the accurate evaluation of the anomalous course, site of origin, and termination as well as the relationship to other structures.

CT is recognized as an accurate, noninvasive technique for the clinical work-up of patients with a continuous murmur, which may be produced by fistulous connection [14]. Cardiac CT may be also useful in planning fistula closure procedures and in planning for the reimplantation of extracardiac connections.

## References


1. Angelini P, Velasco JA, Flamm S. Coronary anomalies: incidence, pathophysiology, and clinical relevance. Circulation. 2002;105:2449–54.
2. Angelini P. Coronary artery anomalies: an entity in search of an identity. Circulation. 2007;115:1296–305. doi:10.1161/CIRCULATIONAHA.106.618082.
3. Yamanaka O, Hobbs RE. Coronary artery anomalies in 126,595 patients undergoing coronary arteriography. Cathet Cardiovasc Diagn. 1990;21:28–40.
4. Hill SF, Sheppard MN. Non-atherosclerotic coronary artery disease associated with sudden cardiac death. Heart. 2010;96:1119–25. doi:10.1136/hrt.2009.185157.
5. Eckart RE, Scoville SL, Campbell CL, Shry EA, Stajduhar KC, Potter RN, et al. Sudden death in young adults: a 25-year review of autopsies in military recruits. Ann Intern Med. 2004;141:829–34.
6. Angelini P. Normal and anomalous coronary arteries: definitions and classification. Am Heart J. 1989;117:418–34.
7. Kim SY, Seo JB, Do KH, Heo JN, Lee JS, Song JW, et al. Coronary artery anomalies: classification and ECG-gated multi-detector row CT findings with angiographic correlation. Radiographics. 2006;26:317–33. doi:10.1148/rg.262055068; discussion 333–4.
8. Tarhan A, Kehlibar T, Yilmaz M, Arslan Y, Pancaroglu C, Yigit S, et al. Right coronary artery with high takeoff. Ann Thorac Surg. 2007;83:1867–9. doi:10.1016/j.athoracsur.2006.11.032.
9. Land RN, Hamilton AY, Fuchs PC. Sudden death in a young athlete due to an anomalous commissural origin of the left coronary artery, and focal intimal proliferation of aortic valve leaflet at the adjacent commissure. Arch Pathol Lab Med. 1994;118:931–3.
10. Maron BJ, Shirani J, Poliac LC, Mathenge R, Roberts WC, Mueller FO. Sudden death in young competitive athletes. Clinical, demographic, and pathological profiles. JAMA. 1996;276:199–204.
11. Pelliccia A. Congenital coronary artery anomalies in young patients: new perspectives for timely identification. J Am Coll Cardiol. 2001;37:598–600.
12. Basso C, Maron BJ, Corrado D, Thiene G. Clinical profile of congenital coronary artery anomalies with origin from the wrong aortic sinus leading to sudden death in young competitive athletes. J Am Coll Cardiol. 2000;35:1493–501. doi:10.1016/S0735-1097(00)00566-0.
13. Maron BJ, Thompson PD, Puffer JC, McGrew CA, Strong WB, Douglas PS, et al. Cardiovascular preparticipation screening of competitive athletes. A statement for health professionals from the sudden death committee (clinical cardiology) and congenital cardiac defects committee (cardiovascular disease in the young), American Heart Association. Circulation. 1996;94:850–6.
14. Warnes CA, Williams RG, Bashore TM, Child JS, Connolly HM, Dearani JA, et al. ACC/AHA 2008 guidelines for the management of adults with congenital heart disease: a report of the American College of Cardiology/American Heart Association task force on practice guidelines (writing committee to develop guidelines on the management of adults with congenital heart disease). Circulation. 2008;118:e714–833. doi:10.1161/circulationahA.108.190690.
15. Taylor AJ, Rogan KM, Virmani R. Sudden cardiac death associated with isolated congenital coronary artery anomalies. J Am Coll Cardiol. 1992;20:640–7. doi:10.1016/0735-1097(92)90019-J.
16. Taylor AJ, Byers JP, Cheitlin MD, Virmani R. Anomalous right or left coronary artery from the contralateral coronary sinus: "high-risk" abnormalities in the initial coronary artery course and heterogeneous clinical outcomes. Am Heart J. 1997;133:428–35.
17. Kimbiris D, Iskandrian AS, Segal BL, Bemis CE. Anomalous aortic origin of coronary arteries. Circulation. 1978;58:606–15.
18. Frescura C, Basso C, Thiene G, Corrado D, Pennelli T, Angelini A, et al. Anomalous origin of coronary arteries and risk of sudden death: a study based on an autopsy population of congenital heart disease. Hum Pathol. 1998;29:689–95.
19. Fujimoto S, Kondo T, Orihara T, Sugiyama J, Kondo M, Kodama T, et al. Prevalence of anomalous origin of coronary artery detected by multi-detector computed tomography at one center. J Cardiol. 2011;57:69–76. doi:10.1016/j.jjcc.2010.10.006.
20. Page Jr HL, Engel HJ, Campbell WB, Thomas Jr CS. Anomalous origin of the left circumflex coronary artery. Recognition, antiographic demonstration and clinical significance. Circulation. 1974;50:768–73.
21. Kaku B, Shimizu M, Kita Y, Yoshio H, Ino H, Takeda R. Detection of anomalous origin of the left coronary artery by transesophageal echocardiography and magnetic resonance imaging. Jpn Heart J. 1994;35:383–8.

22. Catanzaro JN, Makaryus AN, Catanese C. Sudden cardiac death associated with an extremely rare coronary anomaly of the left and right coronary arteries arising exclusively from the posterior (non-coronary) sinus of valsalva. Clin Cardiol. 2005;28:542–4.
23. Agustsson MH, Gasul BM, Fell EH, Graettinger JS, Bicoff JP, Waterman DF. Anomalous origin of left coronary artery from pulmonary artery. JAMA. 1962;180:15–21.
24. Wesselhoeft H, Fawcett JS, Johnson AL. Anomalous origin of the left coronary artery from the pulmonary trunk. Its clinical spectrum, pathology, and pathophysiology, based on a review of 140 cases with seven further cases. Circulation. 1968;38:403–25.
25. Dodge-Khatami A, Mavroudis C, Backer CL. Anomalous origin of the left coronary artery from the pulmonary artery: collective review of surgical therapy. Ann Thorac Surg. 2002;74:946–55.
26. Dodge-Khatami A, Mavroudis C, Backer CL. Congenital heart surgery nomenclature and database project: anomalies of the coronary arteries. Ann Thorac Surg. 2000;69:S270–97.
27. Smith A, Arnold R, Anderson RH, Wilkinson JL, Qureshi SA, Gerlis LM, et al. Anomalous origin of the left coronary artery from the pulmonary trunk. Anatomic findings in relation to pathophysiology and surgical repair. J Thorac Cardiovasc Surg. 1989;98:16–24.
28. Kitamura S, Kawachi K, Nishii T, Taniguchi S, Inoue K, Mizuguchi K, et al. Internal thoracic artery grafting for congenital coronary malformations. Ann Thorac Surg. 1992;53:513–6.
29. Cochrane AD, Coleman DM, Davis AM, Brizard CP, Wolfe R, Karl TR. Excellent long-term functional outcome after an operation for anomalous left coronary artery from the pulmonary artery. J Thorac Cardiovasc Surg. 1999;117:332–42.
30. Isomatsu Y, Imai Y, Shin'oka T, Aoki M, Iwata Y. Surgical intervention for anomalous origin of the left coronary artery from the pulmonary artery: the Tokyo experience. J Thorac Cardiovasc Surg. 2001;121:792–7. doi:10.1067/mtc.2001.112834.
31. Schwartz ML, Jonas RA, Colan SD. Anomalous origin of left coronary artery from pulmonary artery: recovery of left ventricular function after dual coronary repair. J Am Coll Cardiol. 1997;30:547–53.
32. Sharbaugh AH, White RS. Single coronary artery. Analysis of the anatomic variation, clinical importance, and report of five cases. JAMA. 1974;230:243–6.
33. Wilson J, Reda H, Gurley JC. Anomalous right coronary artery originating from the left anterior descending artery: case report and review of the literature. Int J Cardiol. 2009;137:195–8. doi:10.1016/j.ijcard.2009.03.140.
34. Smith JC. Review of single coronary artery with report of 2 cases. Circulation. 1950;1:1168–75.
35. Koh E, Nakagawa M, Hamaoka K, Sawada T, Oga K. Congenital atresia of the left coronary ostium: diagnosis and surgical treatment. Pediatr Cardiol. 1989;10:159–62.
36. Musiani A, Cernigliaro C, Sansa M, Maselli D, De Gasperis C. Left main coronary artery atresia: literature review and therapeutical considerations. Eur J Cardiothorac Surg. 1997;11:505–14.
37. Nishida N, Chiba T, Ohtani M, Yoshioka N. Two adult cases of congenital atresia of the left coronary ostium-comparison of a sudden death case with a long-term survival case. Virchows Arch. 2005;447:742–6. doi:10.1007/s00428-005-0017-0.
38. Leivo IV, Laurila PK. Atresia of left coronary ostium and left main coronary artery. Arch Pathol Lab Med. 1987;111:1173–5.
39. McMahon CJ, El Said HG, Clapp SK. Atresia of the proximal right coronary artery in association with coronary artery fistula. Catheter Cardiovasc Interv. 2000;50:337–9.
40. Swaye PS, Fisher LD, Litwin P, Vignola PA, Judkins MP, Kemp HG, et al. Aneurysmal coronary artery disease. Circulation. 1983;67:134–8.
41. Li D, Wu Q, Sun L, Song Y, Wang W, Pan S, et al. Surgical treatment of giant coronary artery aneurysm. J Thorac Cardiovasc Surg. 2005;130:817–21. doi:10.1016/j.jtcvs.2005.04.004.
42. Diaz-Zamudio M, Bacilio-Perez U, Herrera-Zarza MC, Meave-Gonzalez A, Alexanderson-Rosas E, Zambrana-Balta GF, et al. Coronary artery aneurysms and ectasia: role of coronary CT angiography. Radiographics. 2009;29:1939–54. doi:10.1148/rg.297095048.
43. Pinheiro BB, Fagundes WV, Gusmao CA, Lima AM, Santos LH, Vieira GB. Surgical management of a giant left main coronary artery aneurysm. J Thorac Cardiovasc Surg. 2004;128:751–2. doi:10.1016/j.jtcvs.2004.03.027.
44. Daoud AS, Pankin D, TulganH FRA. Aneurysms of the coronary artery. Report of ten cases and review of literature. Am J Cardiol. 1963;11:228–37.
45. Sokmen G, Tuncer C, Sokmen A, Suner A. Clinical and angiographic features of large left main coronary artery aneurysms. Int J Cardiol. 2008;123:79–83. doi:10.1016/j.ijcard.2007.01.054.
46. von Rotz F, Niederhauser U, Straumann E, Kurz D, Bertel O, Turina MI. Myocardial infarction caused by a large coronary artery aneurysm. Ann Thorac Surg. 2000;69:1568–9.
47. Chamberlain MH, Henry R, Brann S, Angelini GD. Surgical management of a gigantic circumflex coronary artery aneurysm with fistulous connection to the coronary sinus. Eur J Cardiothorac Surg. 2001;20:1255–7.
48. Beach L, Burke A, Radentz S, Virmani R. Spontaneous fatal rupture of a coronary arterial aneurysm into the right ventricle*. Am J Cardiol. 2001;88:A8, 99–100.
49. Baskurt M, Okcun B, Caglar IM, Ozkan AA, Ersanli M, Gurmen T. Congenital absence of the left circumflex coronary artery and an unusually dominant course of the right coronary artery. Cardiovasc J Afr. 2010;21:286–8.
50. Vijayvergiya R, Kumar Jaswal R. Anomalous left anterior descending, absent circumflex and unusual dominant course of right coronary artery: a case report – R1. Int J Cardiol. 2005;102:147–8. doi:10.1016/j.ijcard.2004.03.075.
51. De Giorgio F, Abbate A, Stigliano E, Capelli A, Arena V. Hypoplastic coronary artery disease causing sudden death. Report of two cases and review of the literature. Cardiovasc Pathol. 2010;19:e107–11. doi:10.1016/j.carpath.2009.05.002.
52. Ho J, Jevon G, Sanatani S. Anomalous origin of the left coronary artery with diffuse coronary hypoplasia resulting in sudden death. Can J Cardiol. 2005;21:529–31.
53. Ogden JA. Congenital anomalies of the coronary arteries. Am J Cardiol. 1970;25:474–9.
54. Sim DS, Jeong MH, Choi S, Yoon NS, Yoon HJ, Moon JY, et al. Myocardial infarction in a young man due to a hypoplastic coronary artery. Korean Circ J. 2009;39:163–7. doi:10.4070/kcj.2009.39.4.163.
55. Zugibe FT, Zugibe Jr FT, Costello JT, Breithaupt MK. Hypoplastic coronary artery disease within the spectrum of sudden unexpected death in young and middle age adults. Am J Forensic Med Pathol. 1993;14:276–83.
56. Canyigit M, Hazirolan T, Karcaaltincaba M, Dagoglu MG, Akata D, Aytemir K, et al. Myocardial bridging as evaluated by 16 row MDCT. Eur J Radiol. 2009;69:156–64. doi:10.1016/j.ejrad.2007.09.038.
57. Kantarci M, Duran C, Durur I, Alper F, Onbas O, Gulbaran M, et al. Detection of myocardial bridging with ECG-gated MDCT and multiplanar reconstruction. AJR Am J Roentgenol. 2006;186:S391–4. doi:10.2214/AJR.05.0307.
58. Konen E, Goitein O, Sternik L, Eshet Y, Shemesh J, Di Segni E. The prevalence and anatomical patterns of intramuscular coronary arteries: a coronary computed tomography angiographic study. J Am Coll Cardiol. 2007;49:587–93. doi:10.1016/j.jacc.2006.09.039.
59. Zeina AR, Odeh M, Blinder J, Rosenschein U, Barmeir E. Myocardial bridge: evaluation on MDCT. AJR Am J Roentgenol. 2007;188:1069–73. doi:10.2214/AJR.06.0714.
60. Burnsides C, Edwards JC, Lansing AI, Swarm RL. Arteriosclerosis in the intramural and extramural portions of coronary arteries in the human heart. Circulation. 1956;13:235–41.
61. Polacek P, Kralove H. Relation of myocardial bridges and loops on the coronary arteries to coronary occlusions. Am Heart J. 1961;61:44–52.

62. Ferreira Jr AG, Trotter SE, Konig Jr B, Decourt LV, Fox K, Olsen EG. Myocardial bridges: morphological and functional aspects. Br Heart J. 1991;66:364–7.
63. Kosinski A, Grzybiak M. Myocardial bridges in the human heart: morphological aspects. Folia Morphol (Warsz). 2001;60:65–8.
64. Risse M, Weiler G. Coronary muscle bridge and its relations to local coronary sclerosis, regional myocardial ischemia and coronary spasm. A morphometric study. Z Kardiol. 1985;74:700–5.
65. Angelini P, Trivellato M, Donis J, Leachman RD. Myocardial bridges: a review. Prog Cardiovasc Dis. 1983;26:75–88.
66. Diefenbach C, Erbel R, Treese N, Bollenbach E, Meyer J. Incidence of myocardial bridges after adrenergic stimulation and decreasing afterload in patients with angina pectoris, but normal coronary arteries. Z Kardiol. 1994;83:809–15.
67. Frade Garcia J, Maldonado Villalon A, Paras Chavero E. Clinical significance of the muscular bands in the coronary arteries. Arch Inst Cardiol Mex. 1983;53:413–20.
68. Greenspan M, Iskandrian AS, Catherwood E, Kimbiris D, Bemis CE, Segal BL. Myocardial bridging of the left anterior descending artery: evaluation using exercise thallium-201 myocardial scintigraphy. Cathet Cardiovasc Diagn. 1980;6:173–80.
69. Noble J, Bourassa MG, Petitclerc R, Dyrda I. Myocardial bridging and milking effect of the left anterior descending coronary artery: normal variant or obstruction? Am J Cardiol. 1976;37:993–9.
70. Mohlenkamp S, Hort W, Ge J, Erbel R. Update on myocardial bridging. Circulation. 2002;106:2616–22.
71. Yetman AT, McCrindle BW, MacDonald C, Freedom RM, Gow R. Myocardial bridging in children with hypertrophic cardiomyopathy – a risk factor for sudden death. N Engl J Med. 1998;339:1201–9. doi:10.1056/NEJM199810223391704.
72. Juilliere Y, Berder V, Suty-Selton C, Buffet P, Danchin N, Cherrier F. Isolated myocardial bridges with angiographic milking of the left anterior descending coronary artery: a long-term follow-up study. Am Heart J. 1995;129:663–5.
73. Konen E, Goitein O, Di Segni E. Myocardial bridging, a common anatomical variant rather than a congenital anomaly. Semin Ultrasound CT MR. 2008;29:195–203.
74. Ochsner JL, Mills NL. Surgical management of diseased intracavitary coronary arteries. Ann Thorac Surg. 1984;38:356–62.
75. Hiratzka LF, McPherson DD, Brandt 3rd B, Lamberth Jr WC, Marcus ML, Kerber RE. Intraoperative high-frequency epicardial echocardiography in coronary revascularization: locating deeply embedded coronary arteries. Ann Thorac Surg. 1986;42:S9–11.
76. Iversen S, Hake U, Mayer E, Erbel R, Diefenbach C, Oelert H. Surgical treatment of myocardial bridging causing coronary artery obstruction. Scand J Thorac Cardiovasc Surg. 1992;26:107–11.
77. Tovar EA, Borsari A, Landa DW, Weinstein PB, Gazzaniga AB. Ventriculotomy repair during revascularization of intracavitary anterior descending coronary arteries. Ann Thorac Surg. 1997;64:1194–6.
78. Bilazarian SD, Jacobs AK, Fonger JD, Faxon DP. Case report of a coronary anomaly: crossing obtuse marginal arteries. Cathet Cardiovasc Diagn. 1991;23:130–2.
79. Czekajska-Chehab E, Staskiewicz GJ, Mazur-Stazka E, Drop A, Maciejewski R. An unusual crossed course of separately originating left circumflex and left anterior descending arteries with concomitant anomalies found in multi-slice computed tomography. Folia Morphol (Warsz). 2005;64:334–7.
80. Shepard TF, Srichai MB, Kim D, Lim R, Jacobs JE. Aberrant crossed left circumflex and left anterior descending arteries: diagnosis with multidetector cardiac CT angiography. J Comput Assist Tomogr. 2009;33:211–4. doi:10.1097/RCT.0b013e318173f081.
81. Yilmaz H, Demir I. Images in cardiology: crossing epicardial coronary arteries. Heart. 2005;91:1523. doi:10.1136/hrt.2005.066480.
82. Erbagci H, Davutoglu V, Turkmen S, Kizilkan N, Gumusburun E. Double right coronary artery: review of literature. Int J Cardiovasc Imaging. 2006;22:9–11. doi:10.1007/s10554-005-5139-6.
83. Stougiannos P, Tousoulis D, Trikas A, Stefanadis C. Anomalous origin and course of a dual left anterior descending coronary artery. Int J Cardiol. 2011;146:e53–5. doi:10.1016/j.ijcard.2008.12.185.
84. Spindola-Franco H, Grose R, Solomon N. Dual left anterior descending coronary artery: angiographic description of important variants and surgical implications. Am Heart J. 1983;105:445–55.
85. Tuncer C, Gumusalan Y, Sokmen A, Sokmen G, Koroglu S, Suner A. A previously undescribed anomaly of left anterior descending artery: type V dual left anterior descending artery. Int J Cardiol. 2009;134:e141–3. doi:10.1016/j.ijcard.2008.03.017.
86. Christiaens L, Ardilouze P, Allal J. Anomalous septal artery originating from the right coronary sinus and detection of the interarterial course using multislice computed tomography (MSCT). Int J Cardiol. 2007;116:410–2. doi:10.1016/j.ijcard.2006.03.083.
87. Errichetti A, Mills Jr RM, Mercadante NM, Lingley JF. Anomalous origin of the posterior descending artery from the first septal perforator. Cathet Cardiovasc Diagn. 1986;12:402–4.
88. Ilia R, Gilutz H, Gussarsky Y, Gueron M. Anomalous origin of the posterior descending artery from the obtuse marginal. Cathet Cardiovasc Diagn. 1990;20:200–1.
89. Yilmaz R, Demirbag R. Systolic compression of anomalous large septal branch: an unusual cause of myocardial ischemia. Int J Cardiovasc Imaging. 2005;21:487–90. doi:10.1007/s10554-005-0192-8.
90. Gowda RM, Vasavada BC, Khan IA. Coronary artery fistulas: clinical and therapeutic considerations. Int J Cardiol. 2006;107:7–10. doi:10.1016/j.ijcard.2005.01.067.
91. Levin DC, Fellows KE, Abrams HL. Hemodynamically significant primary anomalies of the coronary arteries. Angiographic aspects. Circulation. 1978;58:25–34.
92. Balanescu S, Sangiorgi G, Castelvecchio S, Medda M, Inglese L. Coronary artery fistulas: clinical consequences and methods of closure. A literature review. Ital Heart J. 2001;2:669–76.
93. Kang JW, Seo JB, Chae EJ, Jang YM, Do KH, Lee JS, et al. Coronary artery anomalies: classification and electrocardiogram-gated multidetector computed tomographic findings. Semin Ultrasound CT MR. 2008;29:182–94.
94. Manghat NE, Morgan-Hughes GJ, Marshall AJ, Roobottom CA. Multidetector row computed tomography: imaging congenital coronary artery anomalies in adults. Heart. 2005;91:1515–22. doi:10.1136/hrt.2005.065979.
95. Shriki JE, Shinbane JS, Rashid MA, et al. Identifying, characterizing and classifying congenital anomalies of the coronary arteries. Radiographics. 2012;32:453–68.
96. Dodd JD, Ferencik M, Leberthson RR, et al. Congenital anomalies of coronary artery origin in adults: 64-MDCT appearance. AJR Am J Roentgenol. 2007;188:W138–46.

# Congenital Venous Anomalies

# 17

## 17.1 Pulmonary Venous Anomalies

Pulmonary venous anomalies comprise a spectrum of abnormalities characterized by the abnormal number, connection, or drainage of pulmonary veins.

The spectrum of pulmonary venous anomalies includes (a) partial anomalous pulmonary venous return (PAPVR), (b) total anomalous pulmonary venous return (TAPVR), (c) common pulmonary vein atresia, (d) pulmonary venous stenosis, and (e) pulmonary varix. See Table 17.1.

### 17.1.1 Partial (Incomplete) Anomalous Pulmonary Venous Return

In partial anomalous pulmonary venous return (PAPVR), one or more pulmonary veins connect with the right atrium or one of its tributaries (venae cavae, azygos vein, coronary sinus, right atrium, portal vein, and hepatic veins) [1]. This anomaly results from persistence of fetal pulmonary venous drainage into the right atrium or systemic veins. The anomalous connection causes a left-to-right shunt that can lead to clinically significant hemodynamic changes. PAPVR may occur in isolation, but more often it is associated with a sinus venosus type of atrial septal defect (ASD). As an isolated anomaly, PAPVR is often asymptomatic. When both PAPVR and a septal defect are present, the shunt is more likely to lead to cardiovascular symptoms and pulmonary arterial hypertension.

The anomalous right upper lobe (RUL) pulmonary vein usually drains into the superior vena cava (SVC) or the SVC right atrial junction. In up to 90 % of cases, a sinus venosus ASD is also present [1, 2]. See Figs. 17.1 and 17.2.

An anomalous right lower lobe pulmonary vein usually drains into the inferior vena cava (IVC) or occasionally into the portal or hepatic veins (Fig. 17.3). When the anomalous drainage is associated with right lung and pulmonary artery hypoplasia, ipsilateral mediastinal shift, and cardiac dextroposition and/or dextrorotation, it is termed "scimitar, venolobar, or hypogenetic lung syndrome" [3, 4]. See Fig. 17.4. The term "scimitar" refers to the curved appearance of the anomalous pulmonary vein, which resembles a Turkish scimitar (a curved saber). Other anomalies in the spectrum of "scimitar" syndrome include arterial subdiaphragmatic supply to the right lower lobe and horseshoe lung. In the latter anomaly, the posterobasal segments of both lungs are fused behind the pericardial sac.

The anomalous left upper lobe pulmonary vein drains into the brachiocephalic or innominate vein via a vertical vein, which is the remnant of the left cardinal system (Fig. 17.5). PAPVR from the left upper lobe needs to be distinguished from a persistent left superior vena cava. The left pulmonary vein will be seen anterior to the left main bronchus in patients with left superior vena cava, whereas in PAPVR there is no pulmonary vein superior to the bronchus. In addition, the persistent left superior vena cava drains into a dilated coronary sinus.

The corrective surgical strategy involves redirection of the anomalous pulmonary veins to the left atrium or atrial appendage and closure of the intracardiac communication, if

**Table 17.1** Types of pulmonary venous anomalies

| |
|---|
| Partial anomalous pulmonary venous connections (PAPVC) |
| Total anomalous pulmonary venous connections (TAPVC) |
| Common pulmonary vein atresia |
| Pulmonary venous stenosis |
| Pulmonary varix |

W. Mazur et al., *CT Atlas of Adult Congenital Heart Disease*,
DOI 10.1007/978-1-4471-5088-6_17, © Springer-Verlag London 2013

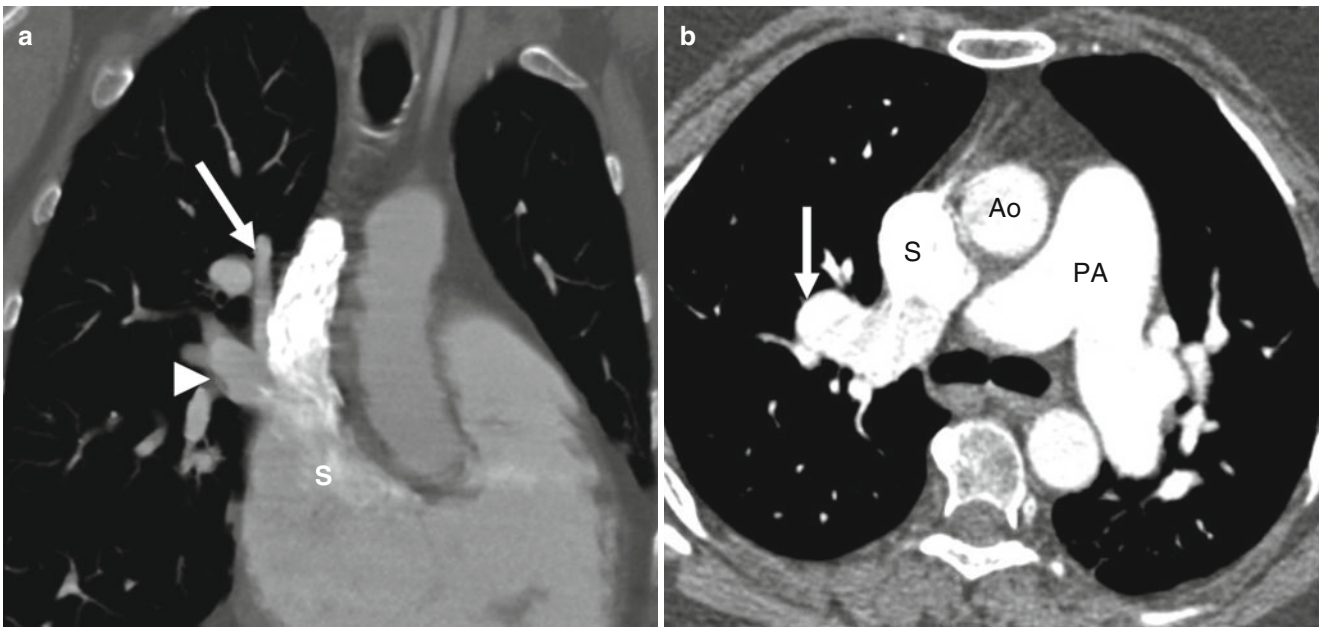


**Fig. 17.1** Panel (**a**) shows an anomalous right upper lobe and right middle lobe venous return. This maximum intensity projection shows the right upper lobe pulmonary vein (*arrow*) and right middle lobe pulmonary vein (*arrowhead*) draining into the superior vena cava (*S*). Panel (**b**) illustrates an anomalous right upper lobe and right middle lobe pulmonary venous return. The axial image in panel (b) shows the right upper lobe pulmonary vein (*arrow*) draining into the superior vena cava (*S*). The pulmonary arteries are dilated due to the left-to-right shunt. *PA* pulmonary artery, *Ao* aorta

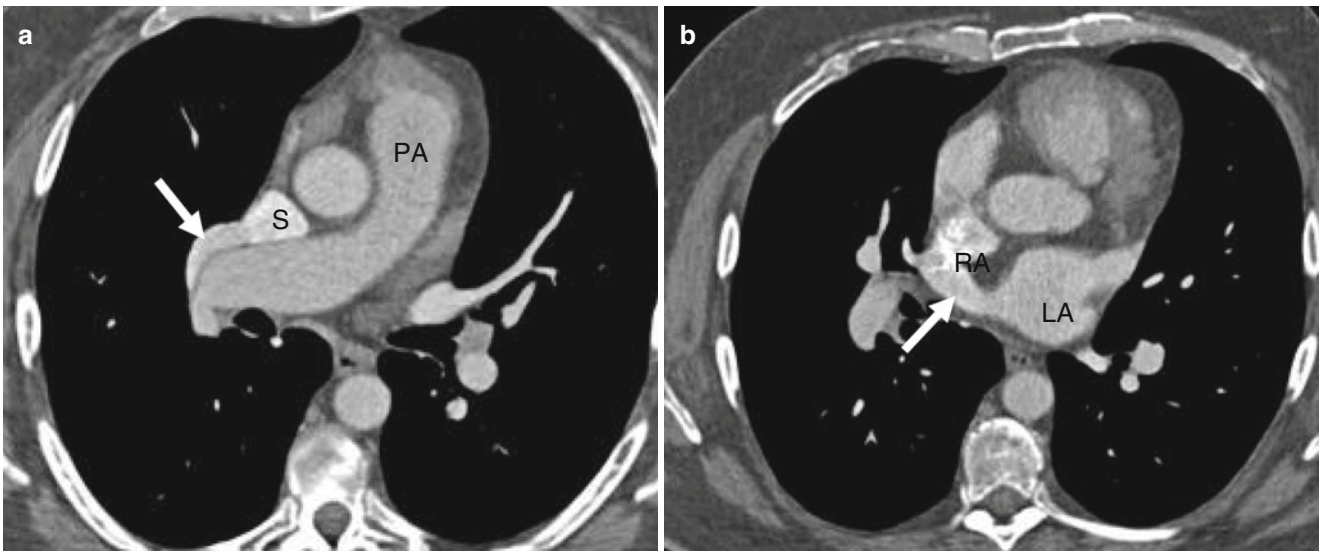


**Fig. 17.2** Anomalous right upper lobe venous return and sinus venosus atrial septal defect. Panel (**a**) is an axial image showing the right upper lobe pulmonary vein (*arrow*) draining into the superior vena cava (*S*). Panel (**b**) is a scan reconstructed at a lower level showing the contrast-filled sinus venosus atrial septal defect (*arrow*) between the right atrium (*RA*) and left atrium (*LA*). *PA* pulmonary artery

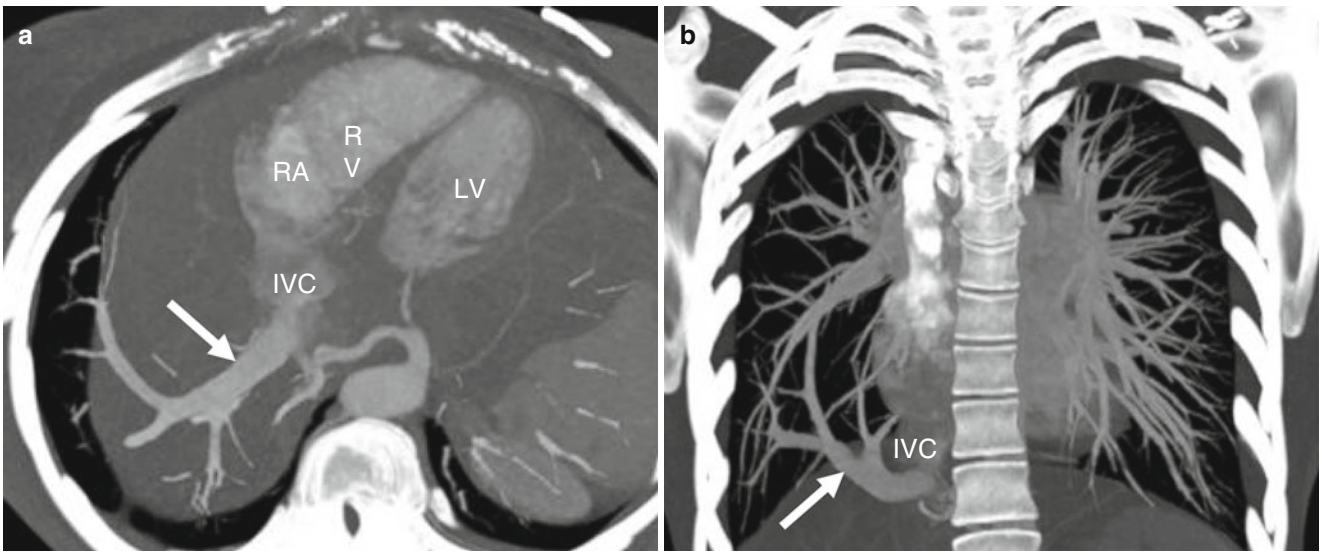


**Fig. 17.3** Anomalous right lower lobe venous return. Panel (**a**) is an axial image, while panel (**b**) is a coronal section. Both show the anomalous right lower lobe pulmonary vein (*arrows*) draining into the inferior vena cava (*IVC*). *RA* right atrium, *RV* right ventricle, *LV* left ventricle

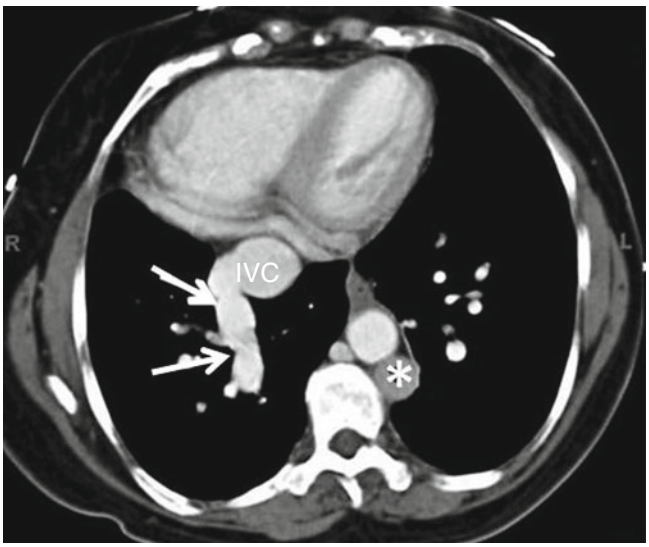


**Fig. 17.4** Scimitar syndrome. An axial CT image shows the anomalous right lower lobe pulmonary vein (*arrows*) draining into the inferior vena cava (*IVC*), a small right lung, and cardiac dextroposition. This patient also has hemiazygos continuation of the inferior vena cava (*asterisk*)

present (Fig. 17.6). Other options for repair of left upper lobe PAPVR include systemic vein translocation (referred to as a Warden procedure, which involves relocation of the superior vena cava to the right atrial appendage), creation of an ASD, and coronary sinus unroofing with baffle connection to the left atrium.

### 17.1.2 Total (Complete) Anomalous Pulmonary Venous Return

In total anomalous pulmonary venous return (TAPVR), all pulmonary veins fail to connect to the left atrium. Pulmonary venous drainage is to the right atrium or its tributaries via primitive connections [5]. An atrial septal defect is virtually always present and allows blood to reach the left heart. This anomaly occurs when the embryologic common pulmonary vein does not join the left atrium.

There are two classifications of TAPVR: (1) embryologic and (2) anatomic. Embryologically, TAPVR is divided into four groups based on connection sites of the embryologic common vein, which include (a) right atrium, (b) right common cardinal system (vena cava or azygos vein), (c) left common cardinal system (left innominate vein, coronary sinus), and (d) umbilicovitelline system (portal vein, ductus venosus) [1, 6]. The anatomic classification scheme is based on the anatomic route of venous drainage, which is classified as (a) type I, supracardiac level (connecting to the right or left superior vena cavae or their tributaries); (b) type II, cardiac level (connecting to the coronary sinus or right atrium); (c) type III, infracardiac level (connecting to the inferior vena cava or its tributaries); and (d) type IV, mixed level (combination of a–c) [7]. See Fig. 17.7.

The clinical findings of TAPVR are determined by the size of the atrial septal defect and the pulmonary vascular resistance. Pulmonary venous obstruction is usually present in the infracardiac form and may also be present in the

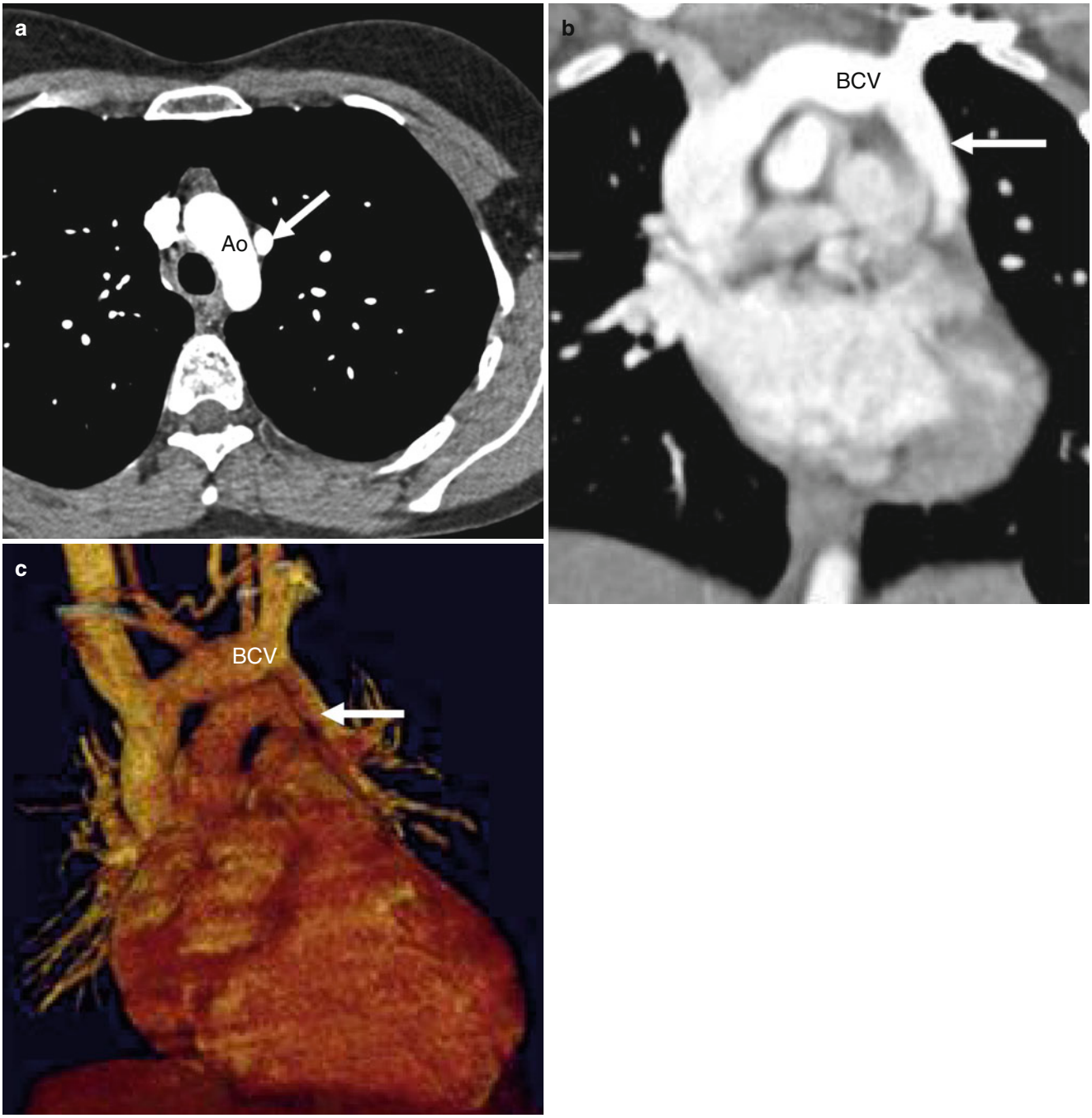


**Fig. 17.5** Anomalous left upper lobe venous return. Panel (**a**) a transverse image shows an abnormal vessel to the *left* of the aortic arch which is the vertical vein (*arrow*). Panel (**b**), an oblique axial scan, and panel (**c**), a 3D image, both show the vertical vein (*arrow*) draining into the left brachiocephalic vein (BCV). *Ao* aorta

supracardiac form, causing pulmonary venous hypertension and congestive heart failure [5]. Obstruction is rare in the cardiac subtype. Virtually all patients with TAPVR present in the neonatal period with cyanosis and congestive heart failure and require surgery.

The surgical options are tailored to the anatomy and intracardiac communication. In the supracardiac and infracardiac types of TAPVR, the redirection of pulmonary venous flow to the left atrium can be achieved via creation of a direct anastomosis of the common pulmonary venous

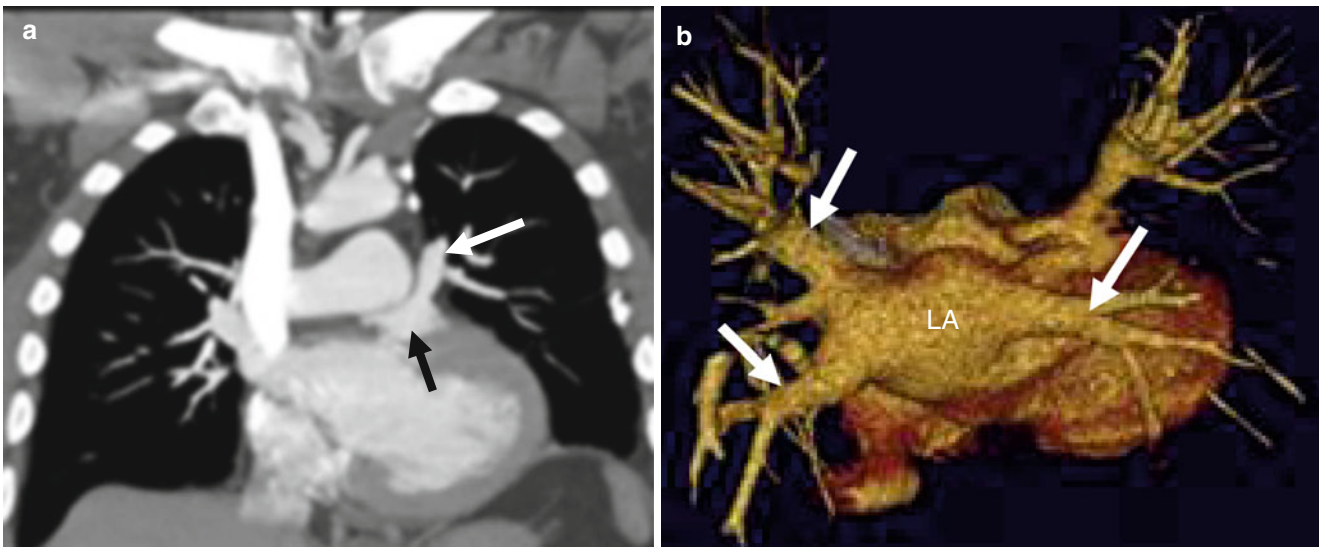


**Fig. 17.6** Repair of anomalous left upper lobe venous return. Panel (**a**) a coronal image, shows reimplantation of the anomalous superior right pulmonary vein (*white arrow*) into the left atrial appendage (*black arrow*). Panel (**b**) an axial 3D scan shows that the inferior left and superior and inferior right pulmonary veins (*arrows*) are in normal locations draining into the posterior aspect of the left atrium (*LA*). The superior right pulmonary vein is not seen draining into left atrium proper in this image as it normally should

sinus to the left atrium or atrial appendage. In the intracardiac type of TAPVR which drains into the right atrium, flow is redirected via an unrestricted interatrial communication to the left atrium. In the intracardiac type of TAPVR which drains into the coronary sinus, the roof of the coronary sinus may be incised to create an unrestricted connection between the anomalous vein and left atrium (coronary sinus unroofing procedure) [5]. Postsurgical complications include pulmonary vein stenosis and shunt at the site of intracardiac repair.

### 17.1.3 Common Pulmonary Vein Atresia

Common pulmonary vein atresia is a rare anomaly in which all of the pulmonary veins drain into a common pulmonary venous confluence that has no connection to the left atrium.

### 17.1.4 Pulmonary Venous Stenosis

Pulmonary venous stenosis is an uncommon anomaly due to congenital obstruction of the pulmonary veins. It is postulated to result from abnormal incorporation of the common pulmonary vein into the left atrium [8]. Venous obstruction may be diffuse, long segmental, short segmental, or ostial [1, 8]. Patients with diffuse pulmonary vein hypoplasia have poor prognoses, while those with short segmental or ostial stenosis have the best outcome [5]. The repair includes stent or patch augmentation of the stenotic vein. Postoperative complications include stenosis and leak.

### 17.1.5 Pulmonary Varix

A varicosity of the pulmonary vein, referred to as a varix, can be congenital or result from chronic pulmonary hypertension. Patients may be asymptomatic or present with hemoptysis. The contrast-enhanced computed tomography (CT) diagnosis is based on enhancement of the varix concurrent with the normal pulmonary venous anatomy and continuity between the varix and the left atrium.

#### 17.1.5.1 Cardiac Computed Tomography (CT) Assessment in Congenital Pulmonary Venous Anomalies

CT allows clear assessment of pulmonary venous anatomy. CT diagnosis of PAPVR is based on recognition of the abnormal course of the intraparenchymal pulmonary vein, which is especially well seen on 3D reconstructions [2, 9–12].

CT assessment should include delineation of (a) the morphology of the pulmonary veins, including size, course, location, presence/absence of stenosis, and connection site of the veins to the cardiac chambers; (b) size and course of any surgical connections between the pulmonary veins and atria;

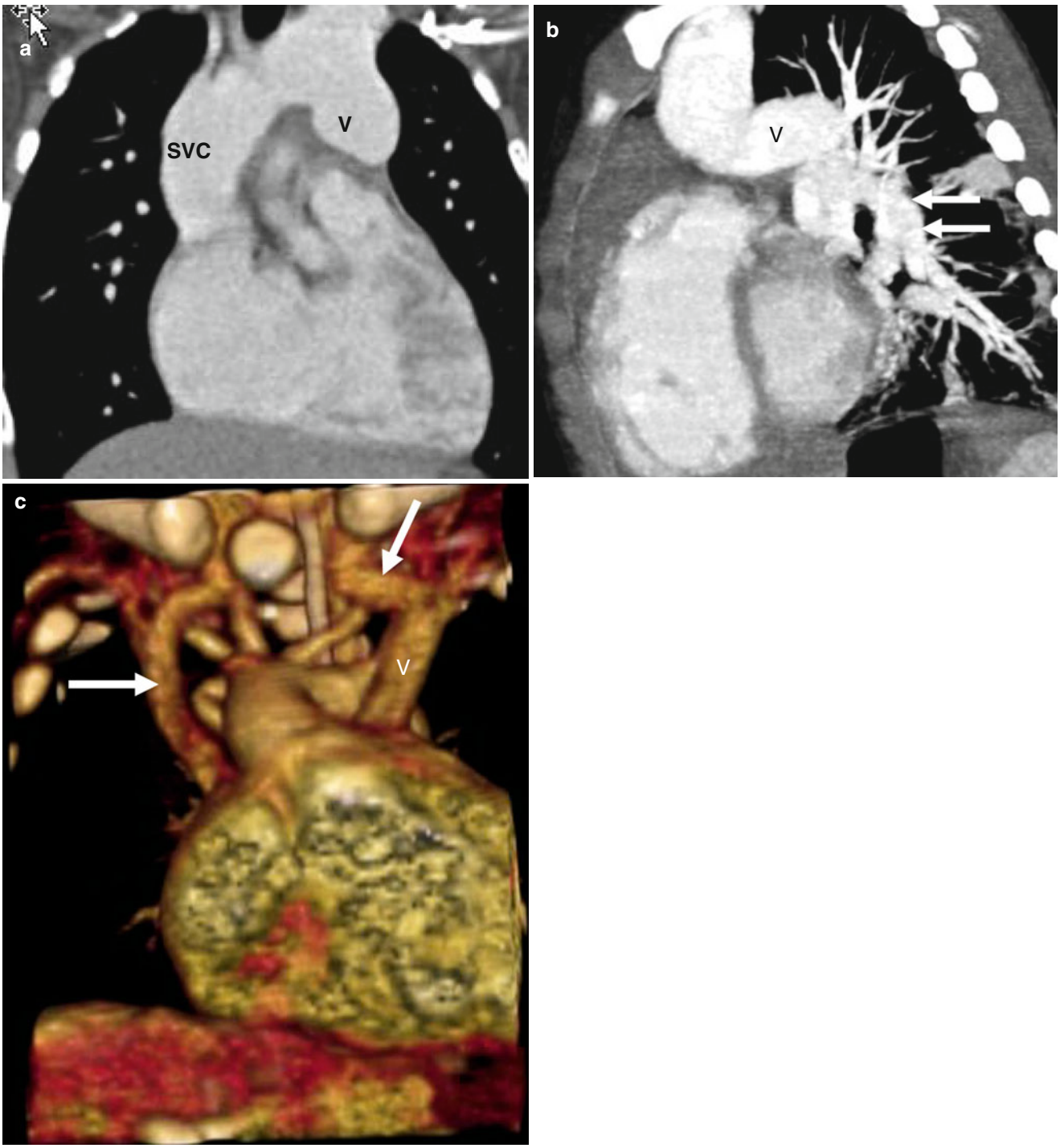


**Fig. 17.7** Supracardiac total anomalous venous return in a 2-year-old boy with worsening dyspnea. The congenital heart disease was undiagnosed at the time of this scan. Panel (**a**) a coronal image shows the large common supracardiac vein (*V*) draining into a dilated superior vena cava. Panel (**b**) a sagittal projection shows the pulmonary venous confluence (*arrows*) draining cephalad into the supracardiac vein (*V*) that ultimately returns blood to the superior vena cava (*SVC*). Panel (**c**) a coronal 3D reformat in an infant (separate patient) shows the vertical vein (*V*) draining into the superior vena cava (*arrows*)

**Table 17.2** Critical CT assessment in pulmonary venous anomalies

| |
|---|
| Size, location, course, patency, and connection sites of all pulmonary veins |
| Size, course, and anastomotic sites of surgical connections between the veins and atria |
| Integrity of surgical baffles or conduits, including obstruction and/or leakage |
| Location, size, and shunt direction in ASD defects, including leak at surgical repair site |
| Size and contractility of the cardiac chambers |
| Presence of coexisting anomalies |

(c) morphology of surgically created interatrial baffles or conduits, including obstruction and/or leak; (d) presence/absence of an ASD, including location, size, shunt direction, and leakage at surgical repair sites; (e) cardiac chamber size and contractility; and (f) presence of other anomalies. See Table 17.2. In the scimitar syndrome, CT assessment also should include the extent of hypoplasia of the right lung and pulmonary artery.

## 17.2 Systemic Venous Anomalies

Systemic venous anomalies comprise abnormalities characterized by abnormal connection or drainage of systemic veins [13–15]. The two major anomalies are persistent left superior vena cava (LSVC) and azygos interruption of the inferior vena cava.

### 17.2.1 Persistent Left Superior Vena Cava

The LSVC results from persistence of the embryologic left anterior cardinal vein. It occurs in up to 0.5 % of the general population and in 4.4 % of patients with congenital heart disease [16–18]. In most cases, the persistent LSVC is an isolated finding. However, about 40 % of patients have associated cardiac anomalies, including atrial septal defects, bicuspid aortic valve, aortic coarctation, cor triatriatum, and coronary sinus atresia [19].

In over 90 % of cases, the LSVC arises from the left brachiocephalic vein and travels inferiorly and lateral to the aortic arch, pulmonary artery, left hilum, and left atrium to drain into the coronary sinus through the vein of Marshal (Fig. 17.8) [16–18, 20]. In the remaining cases, the LSVC drains into the left atrium or an unroofed coronary sinus resulting in a right-to-left shunt. In the majority of cases of LSVC (90 %), a right superior vena cava (SVC) is also present. An anastomosis between the right and left superior venae cavae (bridging vein) occurs in about 35 % of cases. A right sided SVC draining into the left atrium in the presence of persistent LSVC has been reported as well [21].

### 17.2.2 Interrupted Inferior Vena Cava with Azygos Continuation

Azygos continuation of the inferior vena cava (IVC), also termed absence of the hepatic segment of the IVC with azygos continuation, results from in utero interruption of the intrahepatic IVC with atrophy of the right subcardinal vein. It has a prevalence of approximately 0.6 %. Blood flows cranially through the retrocrural azygos and hemiazygos veins in the paraspinal and retrocrural areas to drain into the SVC (Fig. 17.9). The suprarenal and intrahepatic portions of the IVC are absent. Although azygos continuation may be associated with congenital heart disease and asplenia or polysplenia, it is often an isolated finding.

Another variant of this anomaly is hemiazygos continuation of a left-sided IVC that is less frequent than azygos continuation. Blood returns to the heart by one of three routes. The hemiazygos vein can drain into (a) the azygos vein, (b) a persistent left SVC, or (c) the accessory hemiazygos vein, left superior intercostal vein, left brachiocephalic vein, and then into a right-sided SVC [16, 22].

### 17.2.3 Clinical Findings

The LSVC and interrupted IVC are usually not hemodynamically significant. However, patients with persistent LSVC draining to the left atrium or to an unroofed coronary sinus may present with cyanosis related to a right-to-left shunt.

Although most vena caval anomalies are not clinically significant, they need to be recognized because they can have an impact on heart surgery planned for other associated cardiac anomalies. An LSVC can affect the strategy for cardiopulmonary bypass (e.g., position and number of venous cannulae and choice of continuous perfusion or circulatory arrest). Identification of azygos continuation can affect the surgical strategy in patients with single-ventricle physiology. In this setting, the preferred surgical approach is usually palliation with a Kawashima procedure or superior cavopulmonary connection, rather than a total cavopulmonary connection which connects the IVC to the pulmonary artery.

### 17.2.4 Interventions for Persistent Left Superior Vena Cava and Azygos Continuation of the Inferior Vena Cava

Surgical intervention is reserved for LSVCs associated with left-to-right shunting. The procedures include (a) ligation of the LSVC, (b) creation of an atrial baffle directing the LSVC to the right atrium, (c) closure of an unroofed coronary sinus if present, (d) reimplantation of the LSVC to the right atrium


**Fig. 17.8** Persistent left superior vena cava (LSVC). Here, multiple axial CT images show the course of the LSVC as it travels to the coronary sinus. In panel (**a**) note the vessel lateral to the aortic arch (*Ao*) as the persistent LSVC (*arrow*). In panel (**b**) the LSVC (*arrow*) courses lateral toward the pulmonary artery (*PA*). In panel (**c**) the LSVC (*arrow*) is seen adjacent to the left atrium. In panel (**d**) the LSVC (*arrow*) drains into a dilated coronary sinus (*CS*). In panel (**e**) demonstrates an oblique coronal volume-rendered image depicting the course of the LSVC (*arrows*) as it drains into the coronary sinus (*CS*)

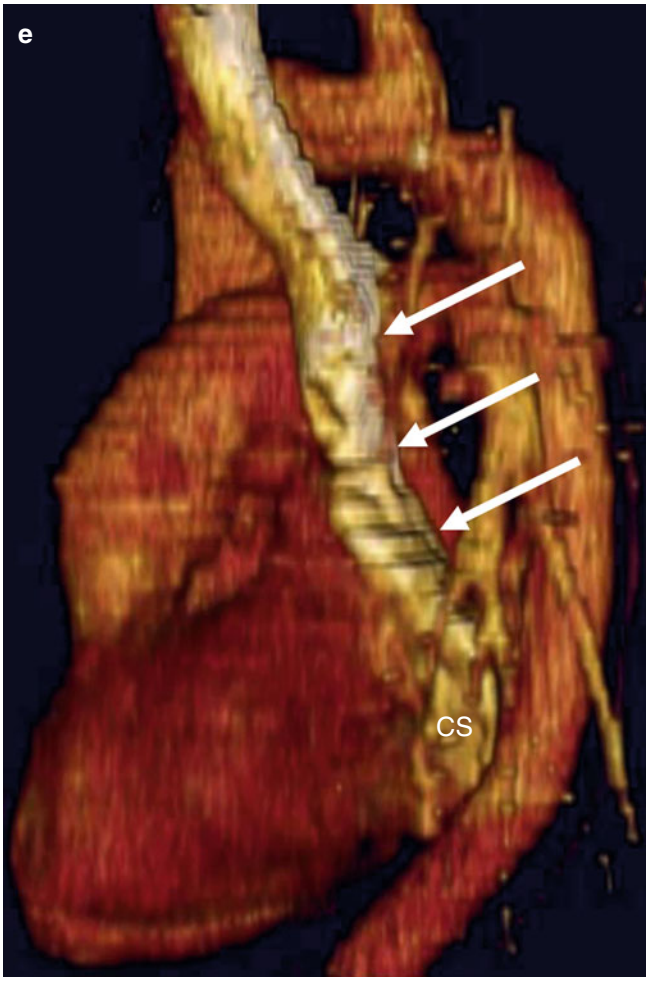


**Fig. 17.8** (continued)

or right SVC, and (e) bidirectional Glenn shunt [13]. Interrupted IVC with azygos continuation usually does not require interventions.

### 17.2.5 Other Systemic Venous Anomalies

The retroaortic innominate vein can take an anomalous course, passing below and posterior to the transverse aortic arch (Fig. 17.10). Its prevalence is about 0.1 % and it is not commonly associated with other anomalies [23].

The levoatrial cardiac vein is an anomalous pulmonary vein to systemic vein connection, which arises from the left atrium or the pulmonary vein and drains into the SVC or innominate vein. It is associated with left atrial outlet obstructive lesions and cor triatriatum [24].

### 17.2.6 Cardiac Computed Tomography (CT) in the Assessment of Anomalous Systemic Veins

Cardiac CT enables comprehensive assessment of the systemic veins. CT evaluation should include evaluation of (a) the morphology, course, size, and connections of the systemic veins and (b) presence of associated anomalies. In the postoperative patient, CT can be useful to identify obstruction or occlusion of reimplantation sites and patency of atrial baffles.


**Fig. 17.9** Azygos continuation of the inferior vena cava. Panel (**a**) is an axial image showing a dilated azygos arch (*Az*). Panel (**b**) is another axial image and panel (**c**) is a coronal cut. Both panels (b) and (c) show an enlarged azygos vein (*Az*) crossing anterior to the spine to connect with a dilated hemiazygos vein (*H*). *Ao* aorta

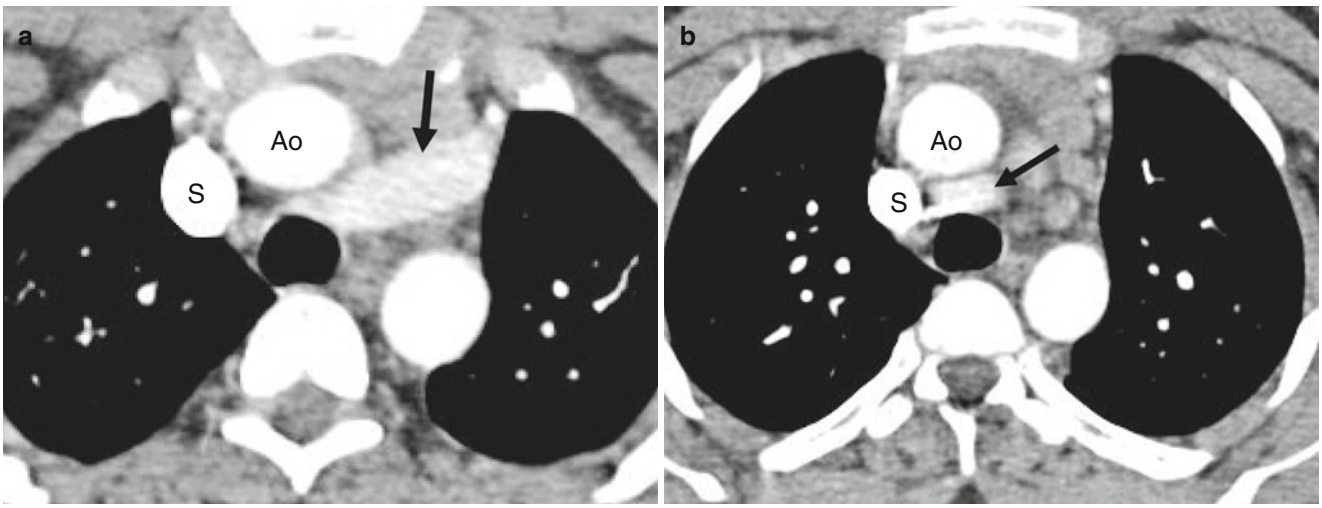


**Fig. 17.10** Retroaortic innominate vein. Panels (**a**) and (**b**) are two axial images showing the innominate vein coursing posterior to the aorta (*Ao*)

## References


1. Krabill K, Lucas R. Abnormal pulmonary venous connection. In: Emmanouilides GC, Moss AJ, Adams FH, editors. Moss and Adams' Heart disease in infants, children, and adolescents: including the fetus and young adult. 5th ed. Baltimore: Williams & Wilkins; 1995. p. 838–74.
2. Siegel MJ, Earls J, Chan F. Thoracic vascular anomalies. In: Rubin G, Rofsky N, editors. CT and MR angiography. Philadelphia: Lippincott Williams & Wilkins; 2009. p. 543–95.
3. Jue KL, Amplatz K, Adams Jr P, Anderson RC. Anomalies of great vessels associated with lung hypoplasia. The scimitar syndrome. Am J Dis Child. 1966;111:35–44.
4. Gao YA, Burrows PE, Benson LN, Rabinovitch M, Freedom RM. Scimitar syndrome in infancy. J Am Coll Cardiol. 1993;22:873–82.
5. Herlong JR, Jaggers JJ, Ungerleider RM. Congenital heart surgery nomenclature and database project: pulmonary venous anomalies. Ann Thorac Surg. 2000;69:S56–69.
6. Neill CA. Development of the pulmonary veins; with reference to the embryology of anomalies of pulmonary venous return. Pediatrics. 1956;18:880–7.
7. Craig JM, Darling RC, Rothney WB. Total pulmonary venous drainage into the right side of the heart; report of 17 autopsied cases not associated with other major cardiovascular anomalies. Lab Invest. 1957;6:44–64.
8. Latson LA, Prieto LR. Congenital and acquired pulmonary vein stenosis. Circulation. 2007;115:103–8. doi:10.1161/CIRCULATIONAHA.106.646166.
9. Hughes D, Siegel MJ. Computed tomography of adult congenital heart disease. Radiol Clin N Am. 2010;48:817–35.
10. Ko K-H, Goo JM, Im J-G, Kim W, Chung JW, Park JH. Systemic arterial supply to the lungs in adults: spiral CT findings. Radiographics. 2001;21:387–402.
11. Konen E, Raviv-Zilka L, Cohen RA, et al. Congenital pulmonary venolobar syndrome: spectrum of helical CT findings with emphasis on computerized reformatting. RadioGraphics. 2003;23:1175–84.
12. Zwetsch B, Wicky S, Meuli R, et al. Three-dimensional image reconstruction of partial anomalous pulmonary venous return to the superior vena cava. Chest. 1995;108:1743–5.
13. Dodge-Khatami A, Mavroudis C, Backer CL. Congenital heart surgery nomenclature and database project: anomalies of the coronary arteries. Ann Thorac Surg. 2000;69:S270–97.
14. Siewers R. Anomalies of systemic venous drainage. In: Kaiser LR, Kron IL, Spray TL, editors. Mastery of cardiothoracic surgery. Philadelphia: Lippincott-Raven Publishers; 1998. p. 649–56.
15. Hammon J, Bender H. Major anomalies of pulmonary and thoracic systemic veins. In: Sabiston DC, Spencer FC, editors. Surgery of the chest, vol. 1. 6th ed. Philadelphia: Saunders; 1996. p. 1405–29.
16. Demos TC, Posniak HV, Pierce KL, Olson MC, Muscato M. Venous anomalies of the thorax. Am J Roentgenol. 2004;182:1139–50.
17. Goyal SK, Punnam SR, Verma G, Ruberg FL. Persistent left superior vena cava: a case report and review of literature. Cardiovasc Ultrasound. 2008;6:50.
18. Kellerman GM, Alpern MB, Sandler MA, Craig BM. Computed tomography of vena caval anomalies with embryologic correlation. Radiographics. 1988;8(3):533–56.
19. Raghib G, Ruttenberg HD, Anderson RC, Amplatz K, Adams P, Edwards JE. Termination of left superior vena cava in left atrium, atrial septal defect, and absence of coronary sinus: a developmental complex. Circulation. 1965;31:906–18.
20. Siegel MJ, Earls J, Chan F. Thoracic vascular anomalies. In: Rubin G, Rofsky N, editors. CT and MR angiography. Philadelphia: Lippincott Williams & Wilkins; 2009. p. 543–95.
21. Pretorius PM, Gleeson FV. Right-sided superior vena cava draining into left atrium in a patient with persistent left-sided superior vena cava. Radiology. 2004;232:730–4.
22. Bass JE, Redwine MD, Kramer LA, Huynh PT, Harris JH. Spectrum of congenital anomalies of the inferior vena cava: cross-sectional imaging findings. Radiographics. 2000;20:639–52.
23. Berko NS, Jain VR, Godelman A, et al. Computed tomographic angiography in adults. J Comput Assist Tomogr. 2009;33:523–8.
24. Gaynor JW, Weinberg PM, Spray TL. Congenital heart surgery nomenclature and database project: systemic venous anomalies. Ann Thorac Surg. 2000;69:S7–76.

# Part VI

# Anomalies with Abnormal Chamber Sequence or Relationship

# Abnormal Relationship Between the Atria and Ventricles

# 18

## 18.1 Univentricular Heart (Double-Inlet Ventricle)

Univentricular heart, also termed "functionally single ventricle" and "single ventricle," refers to the congenital heart defects in which the heart functionally has only one pumping chamber. The unifying criteria to identify a univentricular heart is a main (dominant) ventricle with a malformed atrioventricular connection and a rudimentary (incomplete) ventricle, which lacks an inlet component or less commonly an outlet component [1–4]. A true single ventricle is exceedingly rare.

The spectrum of univentricular heart anomalies includes absence of one atrioventricular valve (mitral or tricuspid atresia) (see Chap. 12), atresia or severe stenosis of a semilunar valve (aortic atresia, hypoplastic left heart syndrome, and pulmonary atresia with intact ventricular septum) (see Chap. 14), heterotaxy syndrome with only one well-developed ventricle (univentricular heterotaxy syndrome) (see Chap. 20), and double-inlet ventricle (left or right). Double-inlet ventricle is the focus of the discussion in this section.

The well-developed single (dominant) ventricle may demonstrate left, right, or indeterminate morphology. The characteristics of the morphologic left and right ventricles are discussed in Chap. 2. Briefly, the morphologic left ventricle has relatively smooth walls and fine trabeculations and lacks septal chordal attachments to the atrioventricular valve. The morphologic right ventricles is more trabeculated and has septal chordal attachments to its atrioventricular valve [3, 4]. The rare solitary chamber demonstrates coarse apical trabeculation [5]. The atrioventricular connection can be a single (either tricuspid or mitral valve), double, or common inlet (Figs. 18.1 and 18.2).

W. Mazur et al., *CT Atlas of Adult Congenital Heart Disease*,
DOI 10.1007/978-1-4471-5088-6_18, © Springer-Verlag London 2013

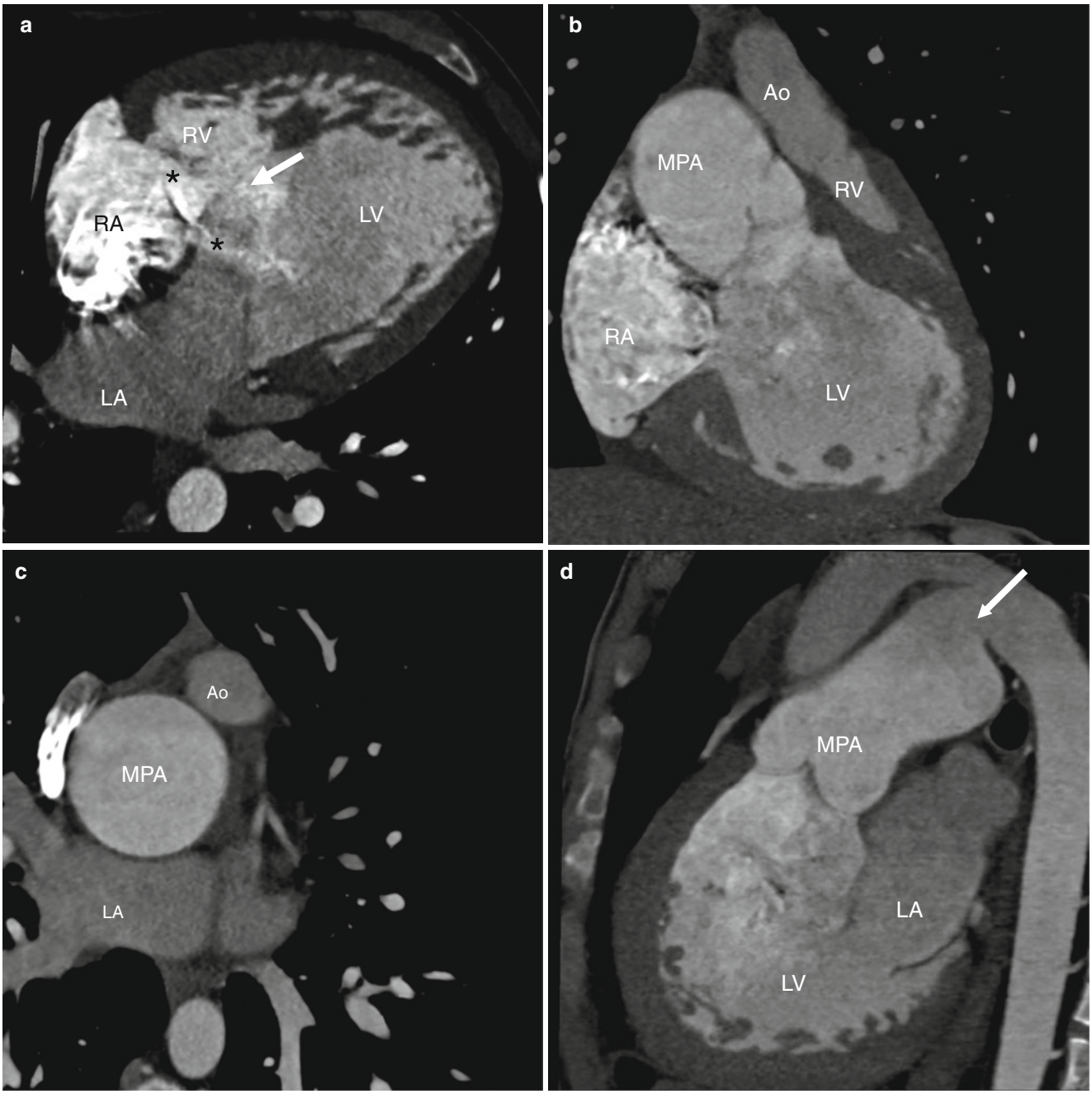


**Fig. 18.1** Double-inlet left ventricle with left ventricular morphology and two separate atrioventricular valves and L-transposition of the great arteries, hypoplastic ascending aorta, and persistent ductus arteriosus in a 21-year-old male. Panel (**a**) is an axial image showing the separate right and left atrioventricular junctions (*asterisks*) opening into the same dominant chamber with left ventricle (*LV*) morphology (smooth walls, fine trabeculations). The rudimentary right ventricle (*RV*) is positioned anteriorly and superiorly. The right atrium (*RA*) is located anteriorly and to the right, while the left atrium (*LA*) is positioned posteriorly and to the left, consistent with normal situs. Also note the ventricular septal defect (*arrow*). Panel (**b**) is an oblique coronal scan showing discordant ventriculoarterial connections. The dominant LV gives rise to the main pulmonary artery and the rudimentary right ventricle gives rise to a hypoplastic aorta. The aorta lies anteriorly and to the *left* of the main pulmonary artery (*MPA*) consistent with L-transposition. Panel (**c**) is an axial reconstruction again highlighting the hypoplastic aorta (*Ao*) which is positioned anteriorly and to the *left* of the pulmonary artery. Panel (**d**) is a sagittal cut demonstrating the persistent ductus arteriosus (PDA) (*arrow*) coursing between the main pulmonary artery and the aorta

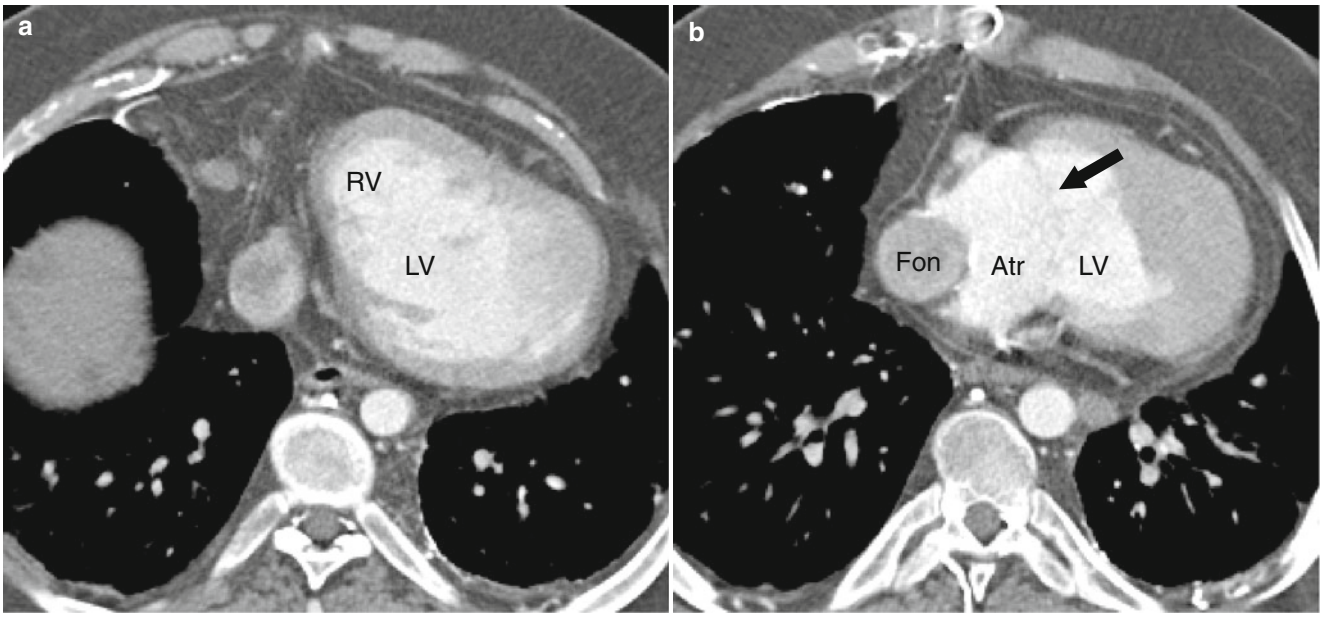


**Fig. 18.2** Double-inlet left ventricle with left ventricular morphology and common atrioventricular valve in an 18-year-old male status post Fontan operation. Panel (**a**), an axial reconstruction, demonstrates a dominant left ventricle (*LV*) and a hypoplastic right ventricle (*RV*) positioned anteriorly. Panel (**b**), another axial scan reconstructed at a lower plane, shows a common atrium (*Atr*) with a common atrioventricular valve (*arrow*) opening into the dominant left ventricular chamber (*LV*). *Fon* lateral Fontan tunnel

### 18.1.1 Double-Inlet Ventricle

This condition is characterized by abnormal atrioventricular connections, with both atria emptying into a single common ventricle (double inlet) that is morphologically predominantly left, predominantly right, or indeterminate (Figs. 18.1, 18.2, and 18.3) [5–9]. When there is a common valve and one well-developed ventricle, the anomaly is also called an unbalanced atrioventricular canal defect (see Chap. 11) [3, 6, 7].

Double-inlet ventricle is a rare cardiac malformation accounting for approximately 1.5 % of congenital heart diseases [8].

A comprehensive description of morphology should include (a) ventricle morphology (left, right, indeterminate), (b) atrioventricular valve connections (common, single, or two separate valves), (c) interventricular communication (unrestrictive or restrictive ventricular septal defect), (d) ventriculoarterial connections (concordant, discordant/transposition of great arteries, double-outlet configuration, and common arterial trunk), and (e) atriovisceral situs (solitus, inversus, isomerism) [3–5, 7, 8].

A double-inlet left ventricle has dominant left ventricular morphology and a rudimentary right ventricle located anterosuperiorly (Figs. 18.1, 18.2, and 18.3). A double-inlet right ventricle has dominant right ventricular morphology and a rudimentary left ventricle positioned posteroinferiorly (Fig. 18.4). Double-inlet left ventricle is the more common arrangement [5, 6]. A single ventricular chamber, which is rare, has indeterminate morphology.

The term double-inlet single ventricle indicates that more than 50 % of the time, both atrioventricular valves or a single common atrioventricular valve opens into one ventricular chamber. There may be a common, single, or double connection. With double-inlet connections, morphological features of the atrioventricular valve may not be distinct enough to distinguish between mitral and tricuspid configurations and the valves are better described as right- or left-sided valves.

The main and rudimentary chambers are separated by a septum, which does not extend to the crux of the heart and is connected to the dominant chamber via a ventricular septal defect (VSD). The VSD is often the muscular-type.

The VSD may be unrestrictive or restrictive initially or become restrictive over time [5]. A restrictive ventricular septal defect leads effectively to subaortic stenosis, which can increase pulmonary blood flow. Ventricular septal defect in a double-inlet ventricle should be differentiated from a true ventricular septal defect. In the latter setting, the septal defect is associated with normally developed right and left ventricular cavities [5].

The great arteries may be normally related (also called "Holmes heart") or the aorta may be anterior and rightward (D-transposition) or leftward (L-transposition) or "inverted" with a posterior and leftward orientation. In double-inlet left ventricle, the ventriculoarterial connections are generally discordant with the aorta arising from the hypoplastic right ventricle and lying anterior and to the left of the left ventricle (L-transposition). Concordant connections or common arterial trunk configuration

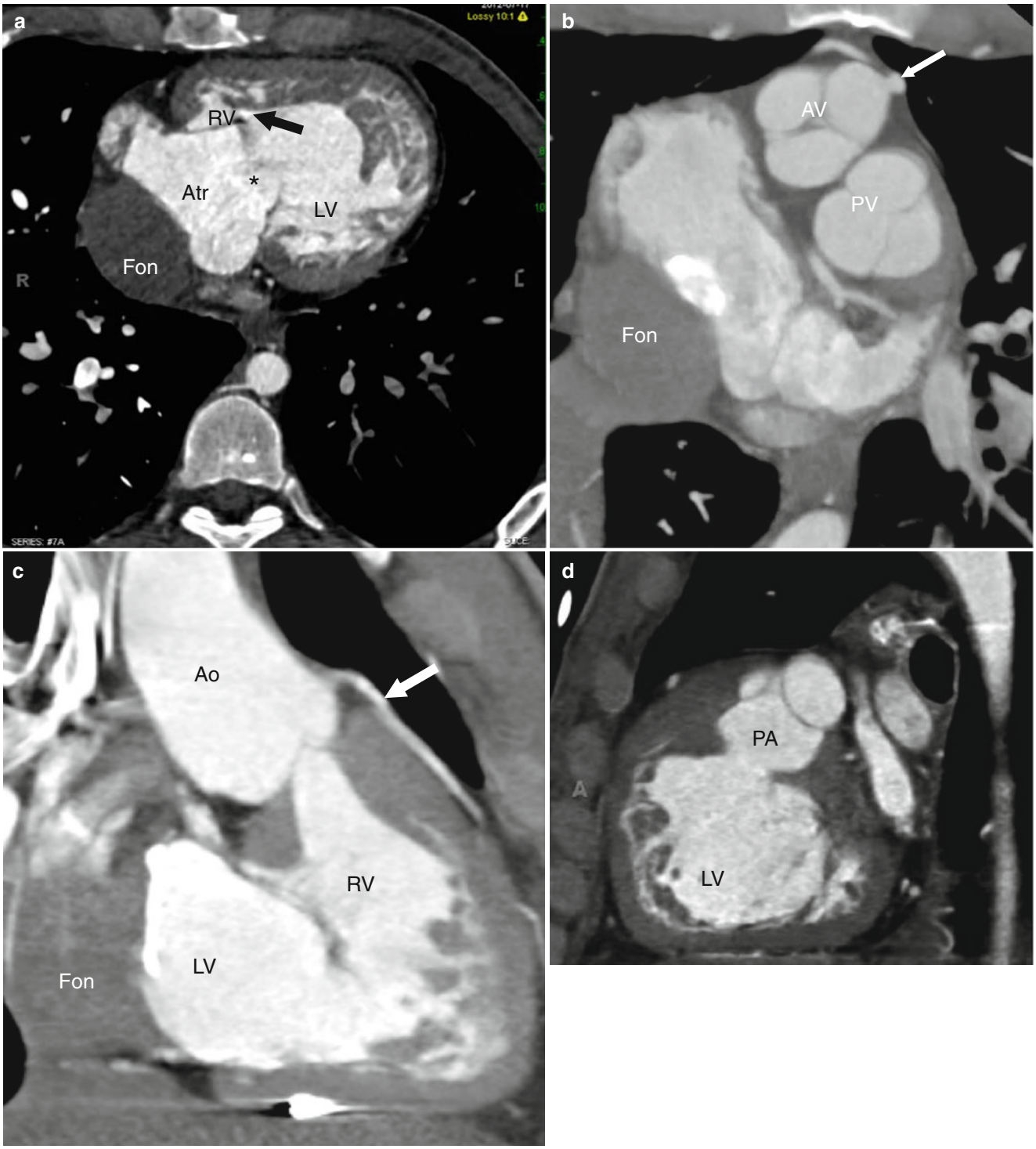


**Fig. 18.3** Double-inlet left ventricle with left ventricular morphology, single atrioventricular valve (tricuspid valve atresia), and D-transposition of the great arteries in a 28-year-old male status post Fontan operation. Panel (**a**) an axial image depicting a rudimentary right ventricle (*RV*) connected via a small ventricular septal defect (*arrow*) to the dominant left ventricle (*LV*). Connection to the common atrium (*Atr*) is through a single mitral valve (*asterisk*) since this patient has tricuspid valve atresia. There is no atrioventricular connection to the right ventricular chamber. Note the lateral Fontan circulation (*Fon*). Panel (**b**) an axial view showing the aortic valve (*AV*) with its coronary artery (*arrow*) anterior and to the *right* of the pulmonary valve (*PV*) consistent with D-transposition. The Fontan circulation is also visible. Panel (**c**) an oblique coronal view illustrating the hypoplastic right ventricle/conus (*RV*), which gives rise to the aorta (*Ao*). The Fontan conduit is seen next to the LV. Panel (**d**) an oblique sagittal image demonstrating the dominant left ventricle (*LV*) giving rise to the pulmonary artery (*PA*). *White Arrows*: coronary artery

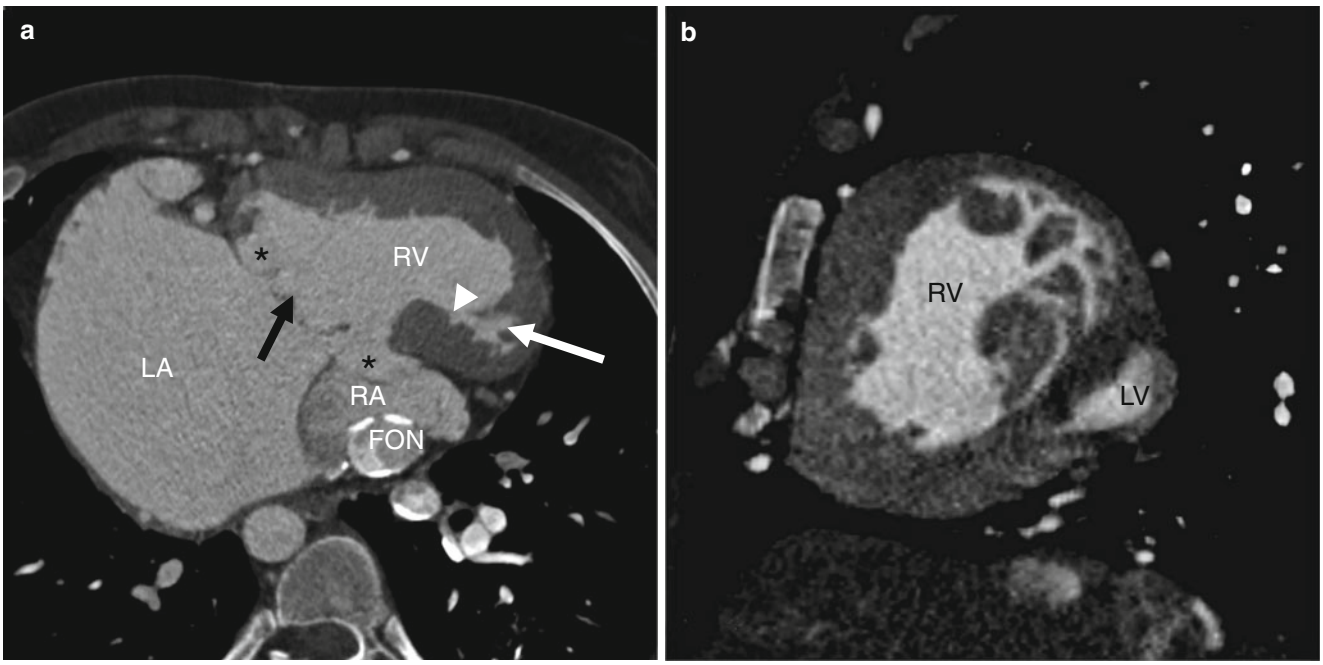


**Fig. 18.4** Double-inlet right ventricle with situs inversus in a 21-year-old male after Fontan procedure. Panel (**a**) an axial image showing that both atrioventricular junctions (*asterisks*) are supported by the same dominant ventricular chamber of right ventricle (*RV*) morphology. The rudimentary left ventricle (*white arrow*) is positioned posteriorly. Note the ventricular septal defect (*white arrowhead*). The morphological right atrium (*RA*) is located *posteriorly* and to the *left*, while the morphological left atrium (*LA*) is positioned *anteriorly* and to the *right* consistent with situs inversus. Panel (**b**) a sagittal view showing the dominant ventricle with coarse trabeculations typical of right ventricular morphology (*RV*) and hypoplastic left ventricle (*LV*). *Black arrow* in panel (**a**): common atrioventricular valve. *Fon* Fontan circulation

is less common [3–5, 10]. In double-inlet right ventricle morphology, both great arteries usually arise from the right ventricle (double-outlet arrangement) or they may have a concordant arrangement. Discordant connections and common arterial trunk are extremely rare in right ventricular morphology [3, 4]. In the solitary ventricle, the ventriculoarterial junction may be a double-outlet connection or common arterial trunk [3, 4].

Pulmonary outflow tract obstruction (stenosis or atresia) is common and is an important determinant of the clinical course. The obstruction may be subvalvular, valvular, or supravalvular or there may be complete pulmonary atresia. Severe pulmonary outflow obstruction will reduce pulmonary blood flow, which then becomes dependent on left-to-right shunting across a patent ductus arteriosus.

Systemic outflow obstruction (stenosis or atresia) can occur at the subvalvular level and/or the level of the aortic arch and/or isthmus or at multiple levels. In hearts with discordant ventriculoarterial connections, it can occur at the level of the ventricular septal defect and may coexist with aortic coarctation or interruption of aortic arch [8, 9].

Atrial situs possibilities include solitus, inversus, and right or left isomerism. Situs solitus arrangement is common in left and right double-inlet ventricular morphology. Right atrial isomerism is commonly associated with the solitary ventricle. Situs solitus is rare with a single ventricle.

Patients with unrepaired univentricular hearts have a poor prognosis with high mortality rates exceeding 70 % [4]. Actuarial survival following Fontan procedure is about 90 % at 10 years in patients with double-inlet left ventricles. Potential complications of the Fontan operation include arrhythmias, thromboemboli, hepatic dysfunction, protein-losing enteropathy, and worsening cyanosis from systemic venous collateralization or pulmonary arteriovenous malformations.

Clinical manifestations primarily depend on the presence or absence of pulmonary outflow obstruction. Double-inlet ventricle is usually diagnosed and surgically treated in infancy. In the absence of pulmonary stenosis or atresia, infants present with clinical findings of congestive heart failure due to pulmonary overcirculation. Thus, a mild degree of pulmonary stenosis is physiologically desirable to prevent pulmonary overcirculation. However, severe pulmonary outflow tract obstruction may result in hypoxemia and cyanosis. Aortic outflow obstruction can further increase the already excessive pulmonary blood flow and worsen congestive heart failure.

Adult patients with univentricular heart defects usually have had a Fontan operation. Very rarely, patients who have unobstructed systemic blood flow and mildly obstructed pulmonary flow reach adulthood without treatment [3, 8]. However, most adults who have not had the Fontan procedure will

begin to show symptoms of cyanosis, fatigue, and/or exercise intolerance, generally because of poor pulmonary blood flow.

Initial surgical palliation is performed to control pulmonary blood flow and ensure unobstructed systemic outflow. In patients with unrestrictive pulmonary blood flow, initial palliation includes pulmonary artery banding or pulmonary artery division with creation of an aortopulmonary shunt to limit pulmonary blood flow. In patients with severe pulmonary obstruction or atresia, palliative procedures include systemic to pulmonary shunts, such as the modified Blalock–Taussig shunt or bidirectional cavopulmonary anastomosis (Glenn shunt). A palliative shunt is usually performed about 6 months of age.

The Fontan procedure, performed between 18 months and 4 years of age, is the definitive repair (Fig. 18.2). [11] The goal of this operation is to separate the pulmonary and systemic circulations. In patients with univentricular heart and aortic outflow obstruction, surgical procedures include enlargement of a restrictive VSD and creation of an aortopulmonary window with ligation of the distal main pulmonary artery (Damus–Kaye–Stansel operation, see Chap. 27) [3, 8]. Biventricular repair is rarely performed in double-inlet hearts.

### 18.1.2 Cardiac Computed Tomography (CT) Assessment in Double-Inlet Ventricle

A comprehensive CT examination should consider assessment of (a) atrial and ventricular number, size, function, and morphology (left, right, indeterminate ventricle); (b) atrioventricular junction connections including number, size, function, and morphology of the atrioventricular valves (stenosis, regurgitation, ring, leaflets, overriding, straddling); (c) ventriculoarterial connections (discordant, concordant, double outlet, or common arterial trunk); (d) aorta and pulmonary artery including size, morphology, and potential obstruction; (e) atriovisceral situs; and (f) systemic and pulmonary venous return (presence of obstruction) [12]. See Table 18.1.

**Table 18.1** Cardiac CT assessment in double-inlet ventricle

| |
|---|
| Number, morphology, size, hypertrophy, geometry, and systolic function of ventricle and size and morphology of atria |
| Morphology, size, and function of atrioventricular valve(s) (stenosis, regurgitation, overriding, straddling) |
| Morphology of ventriculoarterial connections (valves, arterial commitment to ventricle(s)) |
| Anatomy, size, and presence/magnitude of aortic and/or pulmonary outflow track obstruction including the restrictiveness of interventricular communication, if present |
| Anatomy, size, spatial relationship, and potential obstruction of aorta and pulmonary artery |
| Atriovisceral situs and position of heart |
| Morphology and potential obstructions of systemic and pulmonary venous return |

## 18.2 Atrioventricular Discordance (Congenitally Corrected Transposition of the Great Arteries)

Levo-transposition of the great arteries (L-TGA), also known as double discordance or congenitally corrected transposition, is characterized by atrioventricular and ventriculoarterial discordant connections. It results from malrotation of the bulboventricular loop, which twists to the left (opposite of normal). The incidence of corrected transposition in patients with congenital heart disease is approximately 0.5 % [13].

Van Praagh et al. [14]. has reported three main anatomic variants of corrected transposition of the great arteries (TGA) with two ventricles: (1) TGA with solitus atria (S), L-loop ventricles (L), and L-TGA (L) (termed TGA-S,L,L) occurring in 94 % of cases; (2) TGA with solitus atria (S), L-loop ventricles (L), and D-TGA (D), (TGA-S,L,D), occurring in 3 % of cases; and (3) TGA with inverted atria (I), D-loop ventricles (D), and D-TGA (D) (TGA-I,D,D) in 3 % of cases [14]. Anomalies of the left-sided systemic tricuspid valve are present in 97 % of patients with the TGA-S,L,L with malformations of the left-sided systemic right ventricle reported in 91 % of these patients.

In classic L-TGA (TGA-S,L,L), the morphologic right ventricle, which gives rise to the aorta, lies on the left and the morphologic left ventricle, which gives rise to the pulmonary artery, lies on the right side (Figs. 18.5, 18.6, and 18.7). Systemic venous return from the venae cavae flows into a normally

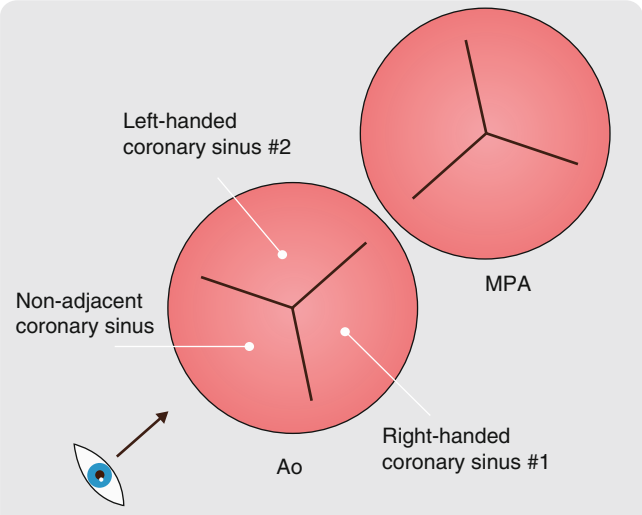


**Fig. 18.5** Corrected transposition of the great arteries. The Leiden convention for coronary sinus nomenclature. According to this classification system, the sinuses of the aorta (*Ao*) are defined by an observer who is positioned in the nonadjacent coronary sinus with the feet toward the heart and the face toward the main pulmonary artery (*MPA*). The facing sinus on the *right-hand side* is defined as sinus #1, while the sinus facing toward the left hand is termed sinus #2. In corrected transposition, sinus #1 (*right-handed sinus*), which is anatomically to the left and posteriorly, gives rise to the right coronary artery, and sinus #2 (*left-handed sinus*) which is to the right and anterior gives origin to the main stem of the left coronary artery

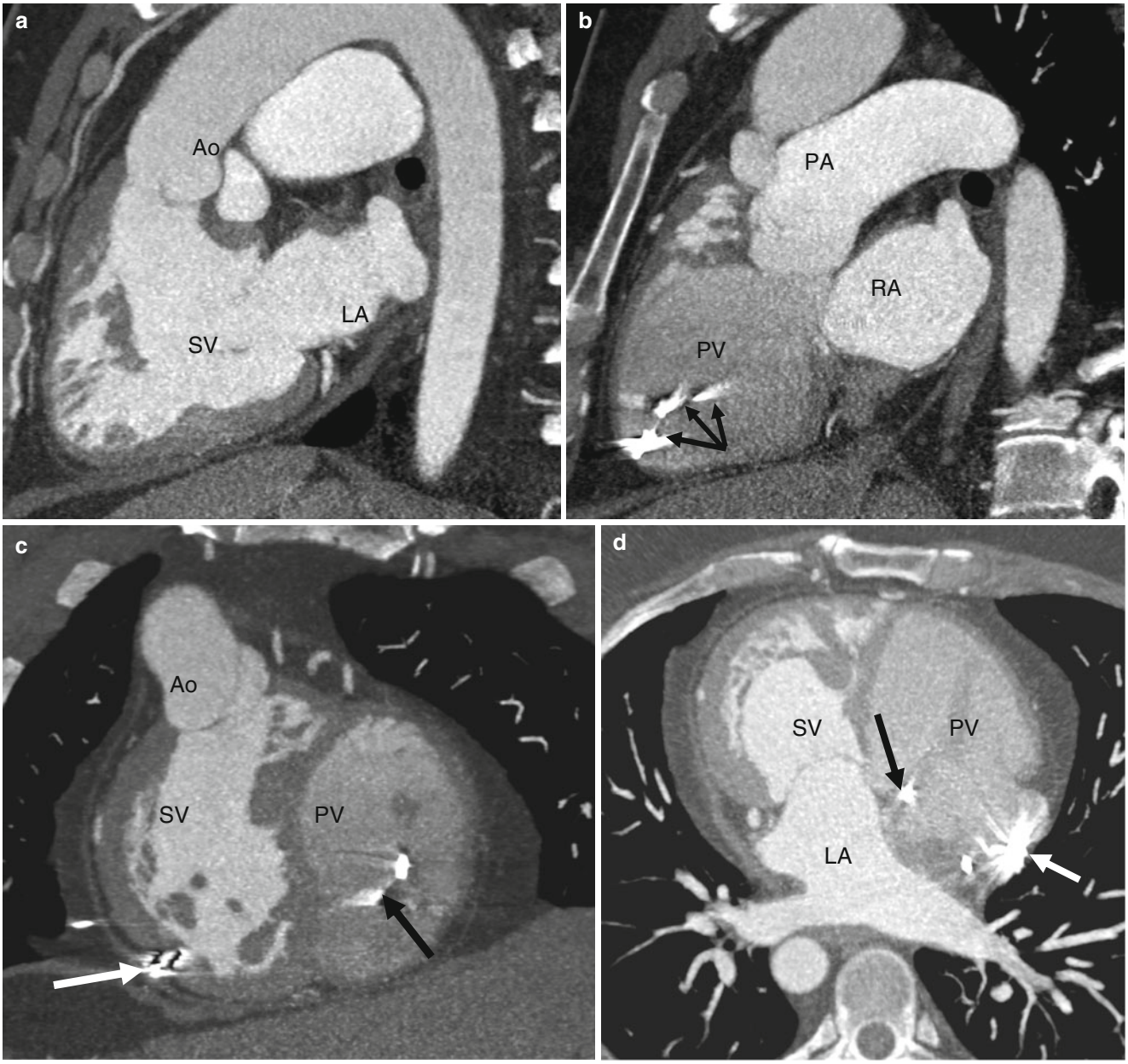


**Fig. 18.6** Corrected transposition of the great arteries with dextrocardia. Panel (**a**) is a sagittal view demonstrating double discordance. The left atrium (*LA*) connects to the systemic ventricle (*SV*, morphological right ventricle) and then to the aorta (*Ao*). Panel (**b**) a sagittal plane demonstrating double discordance, right atrium (*RA*) connecting to pulmonic ventricle (*PV*, morphological left ventricle) and subsequently to the pulmonary artery (*PA*). Note the endocardial pacemaker leads (*black arrows*). Panels (**c**) and (**d**) are coronal and axial images, respectively, again showing the endocavitary pacemaker lead (*black arrow*) in the pulmonic ventricle (*PV*, morphologically left ventricle). An epicardial lead (no longer functioning) is noted as well (*white arrow*). *SV* systemic ventricle, morphological right ventricle. *Ao* aorta

positioned right atrium, crosses the mitral valve, and enters the morphologic left ventricle which then leads to the pulmonary artery. Pulmonary venous return enters a normally positioned left atrium, crosses a tricuspid valve, and enters the morphologic right ventricle and exits to the aorta. The circulatory pattern is in series and therefore L-TGA is said to be congenitally corrected. That is, situs inversus with great artery transposition leads to a normal circuit (two wrongs make it right).

Associated cardiac anomalies are present in the vast majority of patients with L-TGA. Common lesions include ventricular septal defect (usually perimembranous and outlet types, incidence of approximately 70 %) of patients, pulmonary artery stenosis (valvular, subvalvular, 40 % incidence), ventricular septal aneurysm, Ebstein-like tricuspid valve abnormalities (displacement of the valve toward the apex, 32 % incidence), and conduction abnormalities.

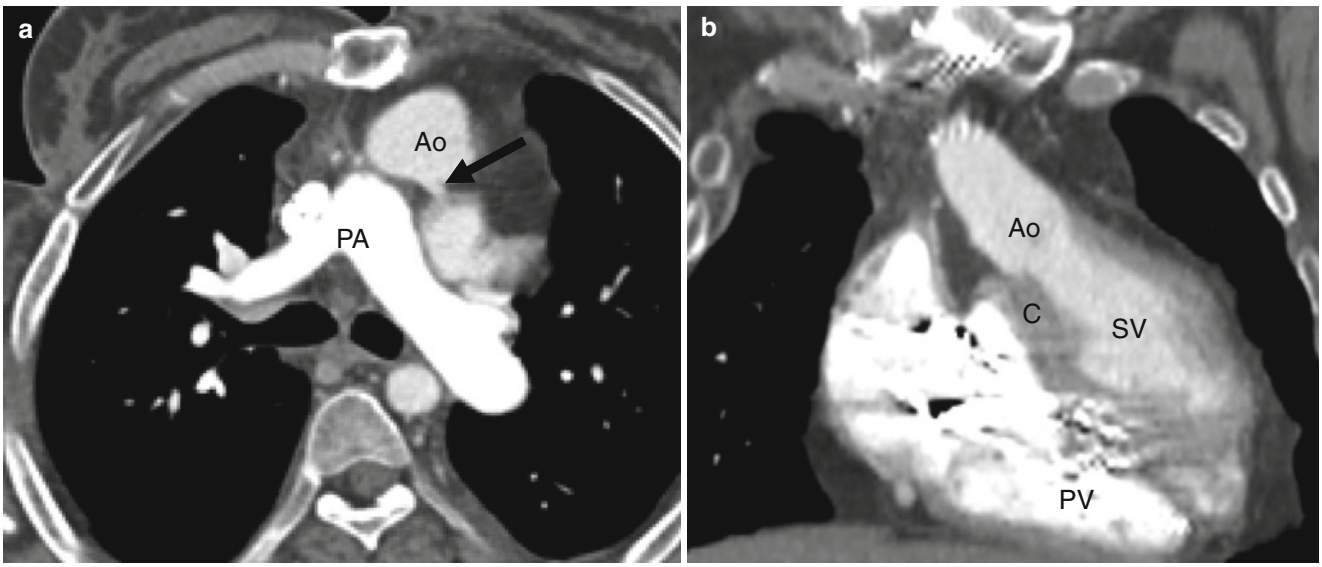


**Fig. 18.7** Corrected transposition of the great arteries in a 34-year-old man status post closure of atrial and septal defects. Panel (**a**) is an axial view illustrating the aorta (*Ao*) lying anterior and to the *left* of the main pulmonary artery (*PA*). The aorta gives rise to the coronary arteries (*arrow*). Panel (**b**) is a coronal view depicting the aorta (*Ao*) in continuity with the systemic, morphologic right ventricle (*SV*). Note the muscular conus (*C*), which is a morphologic feature of the right ventricle. *PV* pulmonic ventricle

**Table 18.2** Coexisting anomalies in congenitally corrected transposition of great arteries

| |
|---|
| Ventricular septal defect |
| Tricuspid (systemic) valve regurgitation |
| Pulmonary atresia |
| Ebstein-like tricuspid valve anomalies |
| Atrial septal defect |
| Coronary anomalies |
| Conduction anomalies |

See Table 18.2 for a list of coexisting anomalies.

Normal coronary anatomy is observed in the majority of patients, but coronary anomalies have been reported [15]. Coronary artery anomalies may affect the surgical approach and the presence of coronary anomalies not detected prior to surgical intervention is associated with poorer outcomes. Abnormal course of the AV node and bundle of His results in anomalies of the conduction system, which not uncommonly lead to complete heart block (incidence of 2 % per year) [16]. Dextrocardia is present in approximately one-fourth of patients with L-TGA. There is male predominance in patients with hemodynamically significant associated congenital defects.

### 18.2.1 Clinical Features

Since the pulmonary and systemic circulations in L-TGA are in series, affected patients are usually asymptomatic in infancy unless other cardiac anomalies are present. In the exceptional patient who has no associated anomalies, L-TGA can be asymptomatic until adulthood and thus escape early detection. Presenting findings in patients who do not undergo surgical correction include complete heart block, hemodynamically significant tricuspid regurgitation, and heart failure since the morphologic right ventricle (systemic ventricle) eventually fails since it was required to pump against the systemic vascular resistance. Approximately 25 % of uncorrected patients will develop congestive heart failure by age 45 years [16].

### 18.2.2 Interventions

Historically, surgical correction was directed at repair of the associated anomalies, not the underlying L-TGA anomaly. Because complications of uncorrected L-TGA have become more widely recognized (tricuspid regurgitation and heart failure), early surgical correction is now commonly recommended. Surgical treatment includes tricuspid valve replacement (before the systemic ventricle ejection fraction drops ≤40 % and pulmonary artery pressure exceeds 50 mmHg) and the double-switch procedure (Mustard or Senning operation, followed by either a Rastelli-type procedure or Jatene switch). The early operative morbidity is low, but the double-switch procedure is predisposed to the complications of its component surgeries (see Chaps. 23 and 24).

**Table 18.3** CT assessment in congenitally corrected transposition of the great arteries

| |
|---|
| Morphology, size, geometry, and systolic function of both ventricles |
| Morphology and size of atria |
| Morphology, course, and size of aorta and pulmonary arteries |
| Presence of coronary anomalies as well as coronary artery disease |
| Anatomy of cardiac valves |
| Coexisting anomalies |

### 18.2.3 Cardiac Computed Tomography (CT) in the Assessment of Congenitally Corrected Transposition of the Great Arteries

CT allows direct visualization of the anomalous great vessel anatomy [12, 17–20]. Gated cine CT can additionally assess ventricular function. CT examination should include a comprehensive assessment of the major anatomic abnormalities: (a) ventricular morphology (left or right), size, and systolic function; (b) atrial size and morphology; (c) aorta and pulmonary artery size, morphology, and relationship to each other; (d) coronary artery anatomy and associated coronary artery disease; (e) cardiac valvular anatomy; and (f) associated anomalies. In TGA, the trabeculated morphologic "right" ventricle lies on the left side and the smoother morphologic left ventricle is on the right side. The aorta arises from the morphologic right ventricle and lies anterior and to the left of the pulmonary artery. Sagittal reconstruction can clearly show the anterior lying aorta. See Table 18.3.

## References


1. Anderson RH, Macartney FJ, Tynan M, Becker AE, Freedom RM, Godman MJ, et al. Univentricular atrioventricular connection: the single ventricle trap unsprung. Pediatr Cardiol. 1983;4:273–80.
2. Anderson RH, Becker AE, Tynan M, Macartney FJ, Rigby ML, Wilkinson JL. The univentricular atrioventricular connection: getting to the root of a thorny problem. Am J Cardiol. 1984;54:822–8.
3. Jacobs ML, Mayer Jr JE. Congenital heart surgery nomenclature and database project: single ventricle. Ann Thorac Surg. 2000; 69:S197–204.
4. Khairy P, Poirier N, Mercier L-A. Congenital heart disease for the adult cardiologist. Circulation. 2007;115:800–12.
5. Cook AC, Anderson RH. The anatomy of hearts with double inlet ventricle. Cardiol Young. 2006;16 Suppl 1:22–6. doi:10.1017/S1047951105002283.
6. Cook AC, Anderson RH. The functionally univentricular circulation: anatomic substrates as related to function. Cardiol Young. 2005;15 Suppl 3:7–16. doi:10.1017/S1047951105001563.
7. Doherty A, Ho SY, Anderson RH, Rigby ML. Morphological nature of the atrioventricular valves in hearts with double inlet left ventricle. Pediatr Pathol. 1989;9:521–9.
8. Poirier NC, Gatzoulis MA. Double-inlet ventricle. In: Gatzoulis MA, Webb GD, Daubeney PEF, editors. Diagnosis and management of adult congenital heart disease. 1st ed. Edinburgh: Churchill Livingstone; 2003.
9. Vyas H, Hagler DJ. Double inlet left ventricle. Curr Treat Options Cardiovasc Med. 2007;9:391–8.
10. Dobell AR, Van Praagh R. The Holmes heart: Historic associations and pathologic anatomy. Am Heart J. 1996;132:437–45.
11. Ghanayem NS, Berger S, Tweddell JS. Medical management of the failing Fontan. Pediatr Cardiol. 2007;28:465–71. doi:10.1007/s00246-007-9007-0.
12. Leschka S, Oechslin E, Husmann L, Desbiolles L, Marincek B, Genoni M, et al. Pre- and postoperative evaluation of congenital heart disease in children and adults with 64-section CT. Radiographics. 2007;27:829–46. doi:10.1148/rg.273065713.
13. Connelly MS, Liu PP, Williams WG, Webb GD, Robertson P, McLaughlin PR. Congenitally corrected transposition of the great arteries in the adult: functional status and complications. J Am Coll Cardiol. 1996;27:1238–43. doi:10.1016/0735-1097(95)00567-6.
14. Van Praagh R, Papagiannis J, Grunenfelder J, Bartram U, Martanovic P. Pathologic anatomy of corrected transposition of the great arteries: medical and surgical implications. Am Heart J. 1998;135:772–85.
15. Dabizzi RP, Barletta GA, Caprioli G, Baldrighi G, Baldrighi V. Coronary artery anatomy in corrected transposition of the great arteries. J Am Coll Cardiol. 1988;12:486–91.
16. Graham Jr TP, Bernard YD, Mellen BG, Celermajer D, Baumgartner H, Cetta F, et al. Long-term outcome in congenitally corrected transposition of the great arteries: a multi-institutional study. J Am Coll Cardiol. 2000;36:255–61.
17. Reddy GP, Caputo GR. Diagnosis please. Case 15: Congenitally corrected transposition of the great arteries. Radiology. 1999;213:102–6.
18. Chang DS, Barack BM, Lee MH, Lee HY. Congenitally corrected transposition of the great arteries: imaging with 16-MDCT. AJR Am J Roentgenol. 2007;188:W428–30. doi:10.2214/AJR.05.0636.
19. Hughes Jr D, Siegel MJ. Computed tomography of adult congenital heart disease. Radiol Clin North Am. 2010;48:817–35. doi:10.1016/j.rcl.2010.04.005.
20. Siegel MJ. CT evaluation of congenital heart disease in adults. Appl Radiol. 2005;34:61–8.

# Abnormal Relationship Between Ventricles and Great Vessels

# 19

## 19.1 Tetralogy of Fallot

Tetralogy of Fallot (TOF) is characterized by four constant features: right ventricular outflow tract (RVOT) obstruction, malalignment (perimembranous) ventricular septal defect (VSD), biventricular origin of the aorta (overriding aorta), and right ventricular hypertrophy [1].

TOF is the most common cyanotic congenital heart defect, accounting for approximately 10 % of all congenital heart disease [2].

TOF is a conotruncal abnormality in which there is anterior deviation and underdevelopment of the outlet (infundibular) portion of the septum, resulting in narrowing and obstruction of the right ventricular outflow tract, an aortic root that overlies the right and left ventricles, and a large perimembranous VSD with the secondary development of right ventricular hypertrophy (Figs. 19.1 and 19.2) [3]. The RVOT obstruction is typically subvalvular (pulmonic infundibulum) stenosis, but it can be valvular or supravalvular and can occur at multiple levels (Figs. 19.1 and 19.3).

Infundibular pulmonic stenosis is mostly caused by overgrowth or hypertrophy of the septoparietal trabeculae. Hypoplasia of the pulmonary valve annulus, main pulmonary artery, and branch pulmonary arteries is common, and there may be branch pulmonary artery stenosis and peripheral pulmonary artery stenosis [1, 2]. Absence of the main pulmonary artery (left more often than right) may also coexist (Fig. 19.4). Other obstructions include a hypertrophied moderator band and apical trabeculation resulting in a two-chambered right ventricle [4] and infundibular or pulmonary valve atresia [5]. In the latter setting, the pulmonary arteries distal to the atresia are perfused via major aortopulmonary collateral vessels (MAPCAs) and/or the ductus arteriosus. In rare instances, the pulmonary arteries are supplied by a persistent fifth arch, an aortopulmonary window, or coronary artery fistulas [6–9]. Pulmonary atresia with VSD is discussed in Chap. 14; it is believed to result from right heart hypoplasia rather than maldevelopment of the outlet septum.

The overriding aorta, which lies above the ventricular septal defect, connects to both the right and the left ventricle. The aortic root can be displaced anteriorly or directly above the septal defect, but it is almost always abnormally located to the right of the pulmonary artery root. The aortic valve may originate predominantly from the left or right ventricle. The latter represents the coexistence of TOF with double-outlet right ventricle [3]. Aortic dilatation may occur due to aortic insufficiency (Fig. 19.5).

The malalignment VSD (also termed conal septal malalignment defect) is usually single, large, and nonrestrictive [3, 10]. Typically, it is located in the membranous septum in a subaortic position and is overridden by the aorta superiorly. Its superior margin is made up of the outlet septum, while its anterior margin is created by the fusion of the outlet

W. Mazur et al., *CT Atlas of Adult Congenital Heart Disease*,
DOI 10.1007/978-1-4471-5088-6_19, © Springer-Verlag London 2013

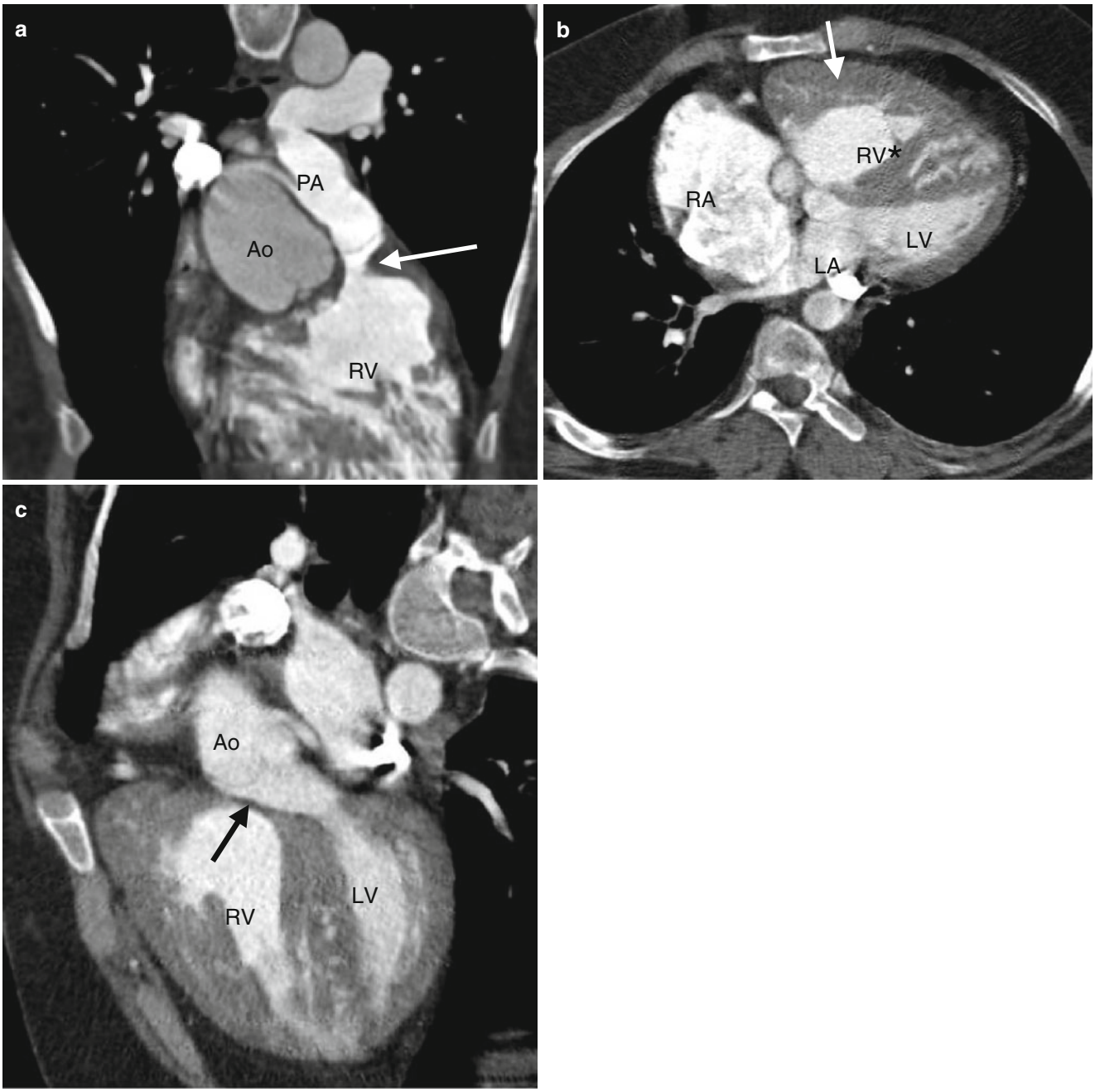


**Fig. 19.1** Tetralogy of Fallot. A 34-year-old woman who underwent repair at age 6 years with a right ventricular outflow tract patch (patch across the pulmonary valve annulus) and VSD closure. Panel (**a**) is a coronal image showing residual subvalvular stenosis (*arrow*). Notice the dilated aortic root (*Ao*). Panel (**b**) is an axial scan showing right ventricular (*RV*) hypertrophy (*arrow* in panel **b**) secondary to the right ventricular outflow tract (RVOT) obstruction. Note the hypertrophied moderator band (*asterisk*). The VSD defect is closed. Panel (**c**) an oblique multiplanar reformatted image showing malalignment of the perimembranous septum (*arrow*), which has been repaired, and an overriding aorta (*Ao*). Again note the RV hypertrophy. *LV* left ventricle, *PA* pulmonary artery

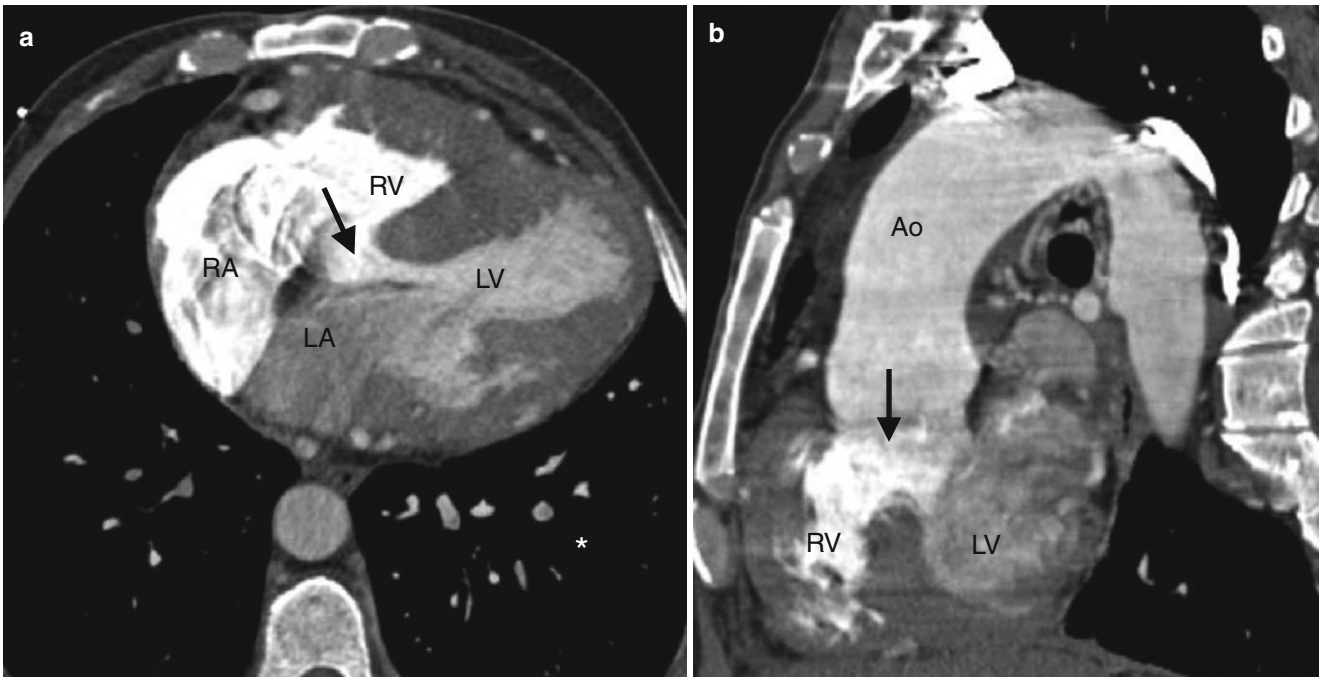


**Fig. 19.2** Tetralogy of Fallot. A 45-year-old man who has an unrepaired tetralogy of Fallot. Panel (**a**) is an axial image showing a large, nonrestrictive VSD (*arrow*) and right ventricular (*RV*) hypertrophy. Panel (**b**) is an oblique multiplanar reformat showing the malalignment of the unrepaired perimembranous VSD (*arrow*) and an overriding aorta (*Ao*). RV hypertrophy is again prominent. *LV* left ventricle, *RA* right atrium, *LA* left atrium

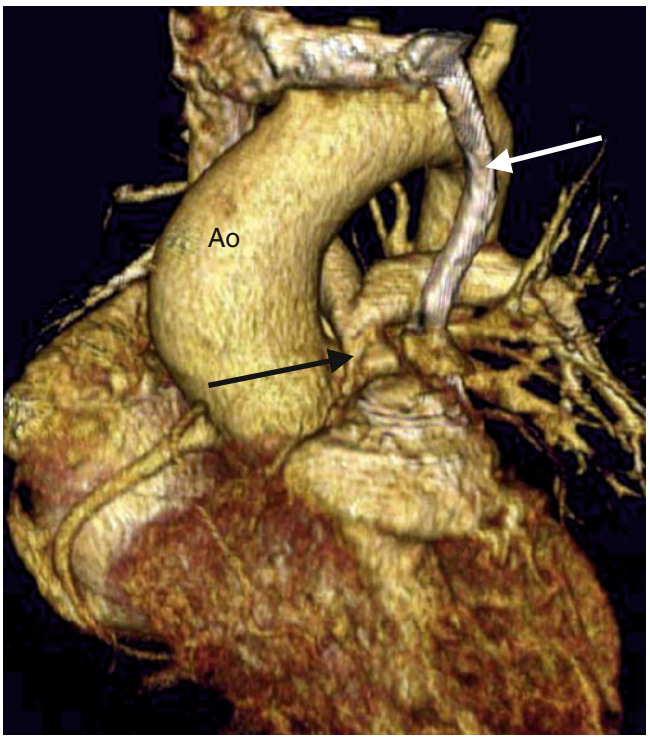


**Fig. 19.3** Tetralogy of Fallot. A 32-year-old man who had a VSD closure and patch enlargement of the RVOT at age 5 years and returned with residual pulmonary valve stenosis. This image is a volume-rendered reformat and shows the severe narrowing at the level of the pulmonary valve (*black arrow*). *White arrow*: left superior vena cava

septum with the anterior limb of septomarginal trabeculation. The posteroinferior part is formed by fibrous continuity between the leaflets of aortic, mitral, and tricuspid valves (80 % of cases) or by a muscular rim (20 % of cases) created by fusion of ventriculo-infundibular fold and the posterior limb of septomarginal trabeculation [11]. Rarely and most frequently in Asian and South American populations, the muscular outlet septum is completely absent and the interventricular communication represents a doubly committed, juxta-arterial VSD, which is also termed conal septal malalignment defect. The conal septal malalignment defect is also associated with conal septal hypertrophy [3, 12].

In 40 % of cases, TOF is associated with other associated abnormalities including right-sided aortic arch (Fig. 19.5), atrial septal defect (ASD), atrioventricular septal defect, anomalous coronary arteries (most frequently left anterior descending artery originating from right coronary artery) (Fig. 19.6), and persistent ductus arteriosus [1]. MAPCAs are also common and correlate with the degree of pulmonary stenosis or atresia.

The predominant clinical feature of most patients with TOF is cyanosis, and thus, most are diagnosed in infancy. Central cyanosis results from right-to-left shunting through a nonrestrictive VSD. The magnitude of shunting depends on the severity of obstruction at the RVOT, pulmonary valve, and/or pulmonary artery [10]. Surgical interventions are now performed in almost all neonates/infants with TOF, and the majority (>85 %) of adults have undergone primary repairs [13].

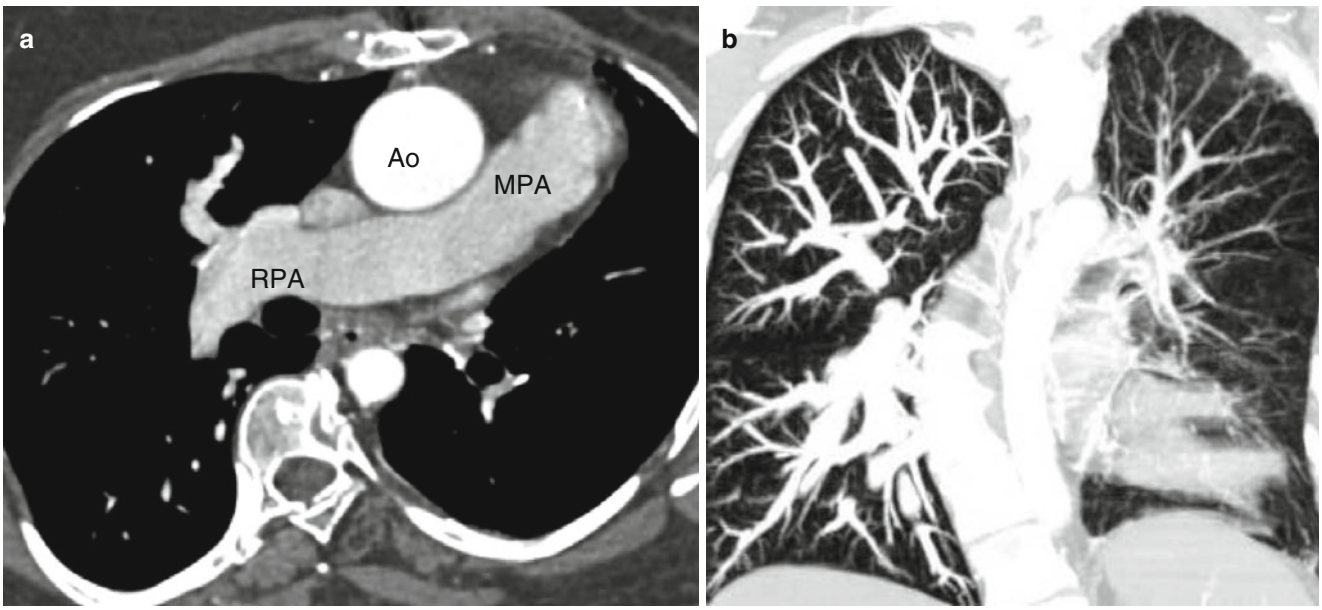


**Fig. 19.4** Tetralogy of Fallot with absence of the pulmonary artery. A 32-year-old woman who had resection of infundibular muscle bundles, VSD closure, and augmentation of the right ventricular outflow tract and pulmonary artery with a transannular patch at age 7 years. Panel (**a**) is an axial scan showing the absence of the left pulmonary artery. The main (*MPA*) and right pulmonary arteries (*RPA*) are mildly dilated. Also note the dilated ascending aorta (*Ao*) caused by aortic insufficiency. Panel (**b**) is a coronal image using a lung window and shows that the left lung is smaller than the right lung and has less vascularity as well. Flow to the left lung was via multiple aortopulmonary collateral vessels

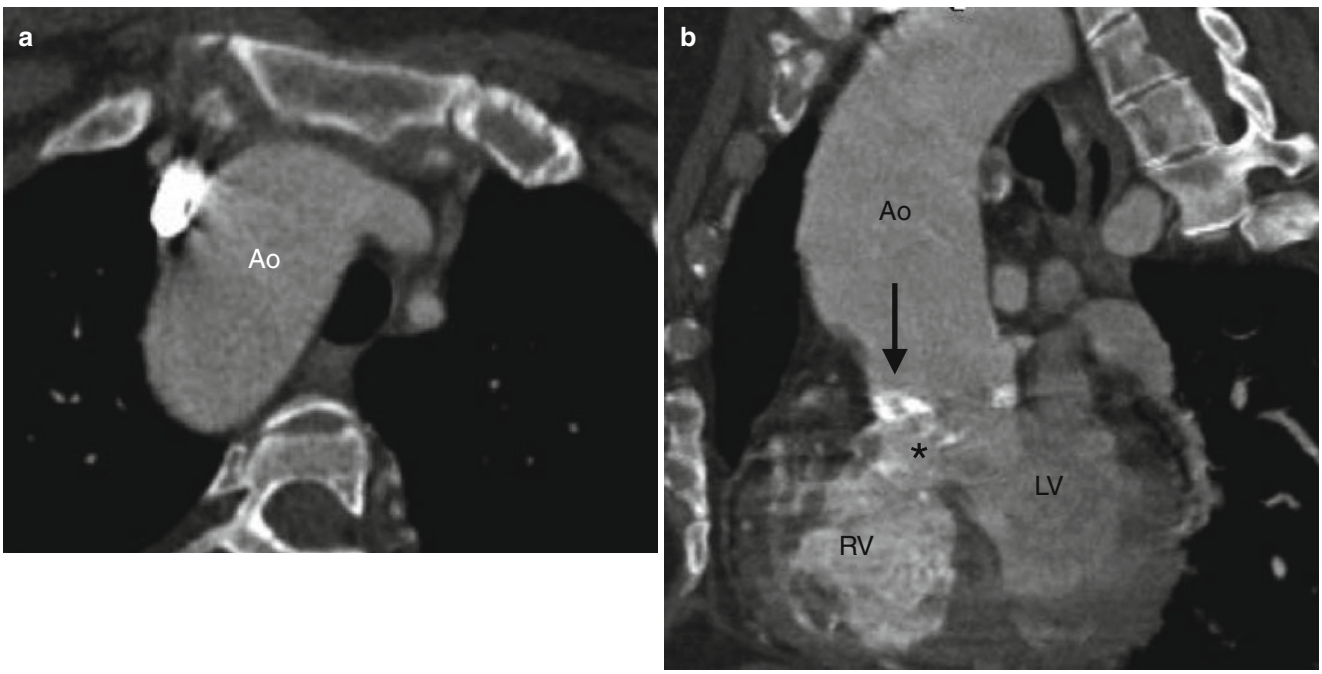


**Fig. 19.5** Tetralogy of Fallot with right aortic arch and aortic root dilatation. A 44-year-old woman who underwent placement of a Waterston shunt at age 7 years and no additional surgical procedures. Panel (**a**) is an axial image showing the right aortic arch (*Ao*). The aorta is dilated due to aortic insufficiency. Panel (**b**) is a sagittal image showing dilatation of the aortic root (*Ao*) which overrides an unrepaired perimembranous VSD (*asterisk*). Also noted a calcified aortic valve (*arrow*), related to atherosclerotic disease

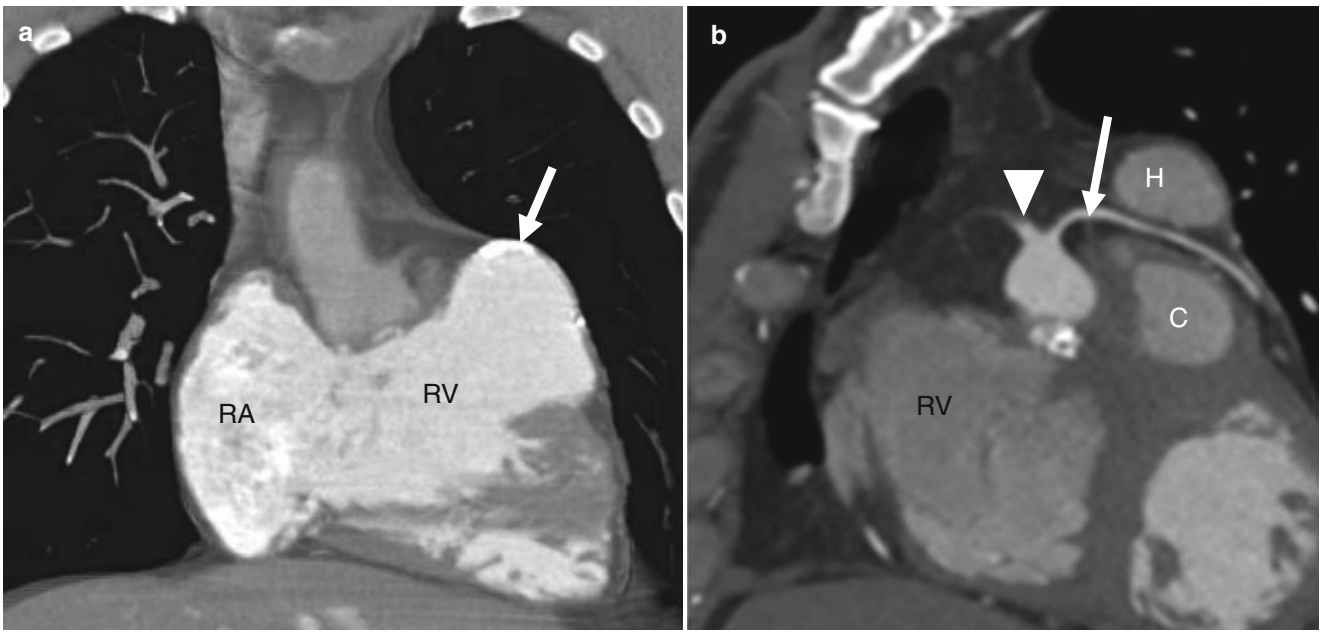


**Fig. 19.6** Tetralogy of Fallot with a coronary artery anomaly. A 33-year-old man who had homograft repair of RVOT obstruction and a conduit placed from the homograft to the main pulmonary artery at age 2 years. Resection of the infundibular muscle was limited by a coronary artery coursing over the upper part of the right ventricular outflow tract just beneath the pulmonary valve annulus. Panel (**a**) is a depiction of the aneurysmal, partially calcified right ventricular outflow repair (*white arrow*). Panel (**b**) a sagittal oblique view demonstrating the right coronary artery (*arrowhead*) giving rise to the left anterior descending coronary artery (*arrow*), which courses between the homograft (*H*) and conduit (*C*) with no evidence of compression

When the RVOT obstruction is mild, the degree of right-to-left shunting through the VSD will be less severe and physiology will be more similar to an isolated VSD. In this setting, patients may be acyanotic (so-called pink tetralogy) and the diagnosis will be made later in life. The clinical presentation in unrepaired adults may include cardiac murmur, right heart failure, or decreased exercise tolerance [2]. If the overriding aorta dilates, aortic regurgitation may develop and be a presenting symptom (Fig. 19.6).

Before advances in open heart surgery, palliative surgery in the form of a systemic-to-pulmonary artery shunt (Blalock–Taussig, Waterston, or Potts shunts) was performed prior to definitive repair (Chap. 22) [2]. With advances in surgical techniques, the current treatment is definitive repair in the first year of life. Most adults with TOF have undergone definitive repair, but occasionally patients reach adulthood having had only a palliative procedure. Definitive repair requires closure of the VSD and enlargement of the RVOT, relieving the outlet stenosis (Chap. 29) [2].

Postoperative complications (Chap. 29) of palliation include pulmonary artery distortion, pulmonary hypertension, left and right ventricular dysfunction, and congestive heart failure. Complications of definitive repair include aneurysmal dilatation of the RVOT and subsequent pulmonary regurgitation; stenosis at the anastomotic site of the pulmonary homograft, pulmonary valve, and/or main/branch pulmonary arteries; progressive aortic root dilatation and subsequent aortic regurgitation; biventricular failure; and residual VSD.

### 19.1.1 Cardiac Computed Tomography (CT) in the Assessment of Tetralogy of Fallot

In patients with unoperated TOF, CT can demonstrate the following morphologic findings needed to plan patient management: (a) the ventricular (right and left ) morphology including the wall thickness, size, and systolic function (contraction, volume); (b) the morphology and size of both atria; (c) the anatomy, size, and presence/magnitude of obstruction(s) of the RVOT, pulmonary valve, main pulmonary artery, and branch arteries; (d) morphology of the overriding aorta (size and degree); (e) the size and location of VSD(s); (f) the anatomy of the cardiac valves; (g) aortic arch sidedness; and (h) the presence of coexisting anomalies including ASD, patent ductus arteriosus, aortopulmonary

**Table 19.1** CT assessment in unrepaired tetralogy of Fallot

| |
|---|
| Morphology, wall thickness, size, and systolic dysfunction of both ventricles |
| Morphology and size of atria |
| Anatomy, size, and presence/magnitude of obstruction(s) of RVOT, pulmonary valve, main pulmonary artery, and branches |
| Anatomy and size of ascending aorta, including assessment of aortic root dilatation |
| Presence, size, and morphology of VSD |
| Anatomy of the cardiac valves |
| Side of the aortic arch |
| Coexisting anomalies, including atrial septal defect, patent ductus arteriosus, aortopulmonary collaterals, and coronary artery anomalies |

collaterals, and coronary artery anomalies [14–17]. Of high importance is the presence of a coronary artery branches crossing the RVOT, which can have an impact on the surgical strategy (Fig. 19.6). In addition, the presence of coexisting atherosclerotic coronary artery disease should be evaluated. See Table 19.1.

Of note, cardiac CT provides only limited information regarding valvular function. The assessment of pulmonary valve stenosis/regurgitation and aortic and tricuspid valve regurgitation is especially important and requires performance of echocardiography and cardiac magnetic resonance imaging.

The postsurgical assessment of these patients is discussed in Chap. 29.

## 19.2 Double-Outlet Ventricles

When both great arteries arise from one ventricular chamber, the ventriculoarterial connection is termed "double outlet." In double-outlet ventricles, the aorta and pulmonary artery may arise from the right ventricle (double-outlet right ventricle) or from the left ventricle (double-outlet left ventricle). Rarely, both arterial trunks arise from both ventricles. This arrangement is termed double-outlet both ventricles.

### 19.2.1 Double-Outlet Right Ventricle

Double-outlet right ventricle (DORV) is a heterogeneous group of congenital heart defects in which both the aorta and main pulmonary artery arise entirely or predominately from the morphologic right ventricle [18]. DORV is present when more than 50 % of the both arterial trunks arise from the morphologic right ventricle.

DORV accounts for 1–5 % of all congenital heart diseases with incidence of 1 per 10,000 births [19].

The basic morphology of DORV is malposition of the great arteries with a ventricular septal defect (VSD)

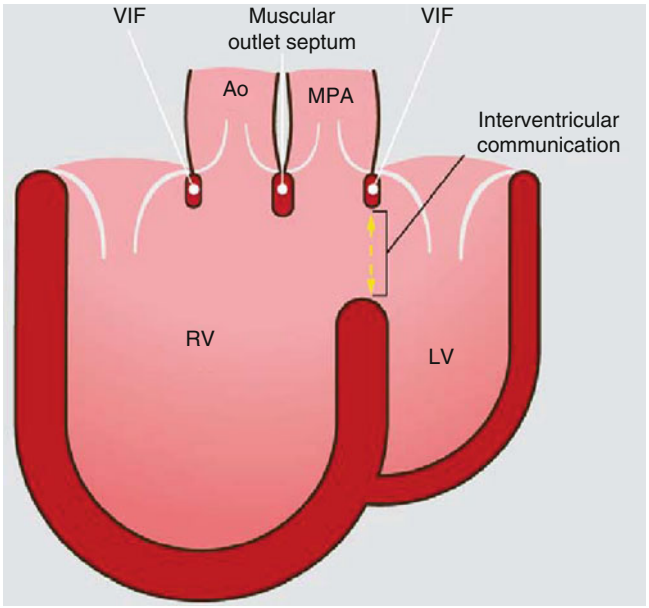


**Fig. 19.7** Diagram shows both the aorta (*Ao*) and main pulmonary artery (*MPA*) arising from the right ventricle (*RV*). *LV* left ventricle, *VIF* ventriculo-infundibular fold

(Fig. 19.7). There is great variability in the anatomy of the DORV. DORV represents the part of arterial override continua, when

(a) Overriding aorta transits from tetralogy of Fallot (ToF) or simple ventricular septal defect with overriding aorta to DORV configuration
(b) Overriding pulmonary artery transits from discordant ventriculo-arterial connection with ventricular septal defect to DORV configuration with subpulmonary interventricular communication
(c) Overriding aorta and pulmonary artery transit from double outflow left ventricle to DORV configuration [3, 20, 21]

The pathophysiologic classification of DORV is based on defining the position of the VSD relative to the arrangement of the great arteries. The VSD can be subaortic, subpulmonic, doubly committed (immediately beneath the semilunar valves), or noncommitted (remote from both semilunar valves) (Fig. 19.8). Most commonly, the VSD is single and nonrestrictive, but restrictive and multiple connections may occur [18]. Pulmonary and systemic blood flow and saturations are determined by the ratio of pulmonary to systemic resistance, which is related to the relative positions of the VSD and great arteries, the presence of pulmonary stenosis, and the amount of right ventricular mixing.

Subaortic VSD-type (tetralogy of Fallot-type) DORV accounts for more than 50 % of DORV cases (Fig. 19.9). The great arteries are normally related with the aortic origin posterior and to the right of the pulmonary origin [22, 23]. Because the normal spatial relationship is maintained, left ventricular outflow is directed toward the aorta, resulting in aortic oxygen saturations that are greater than those of the

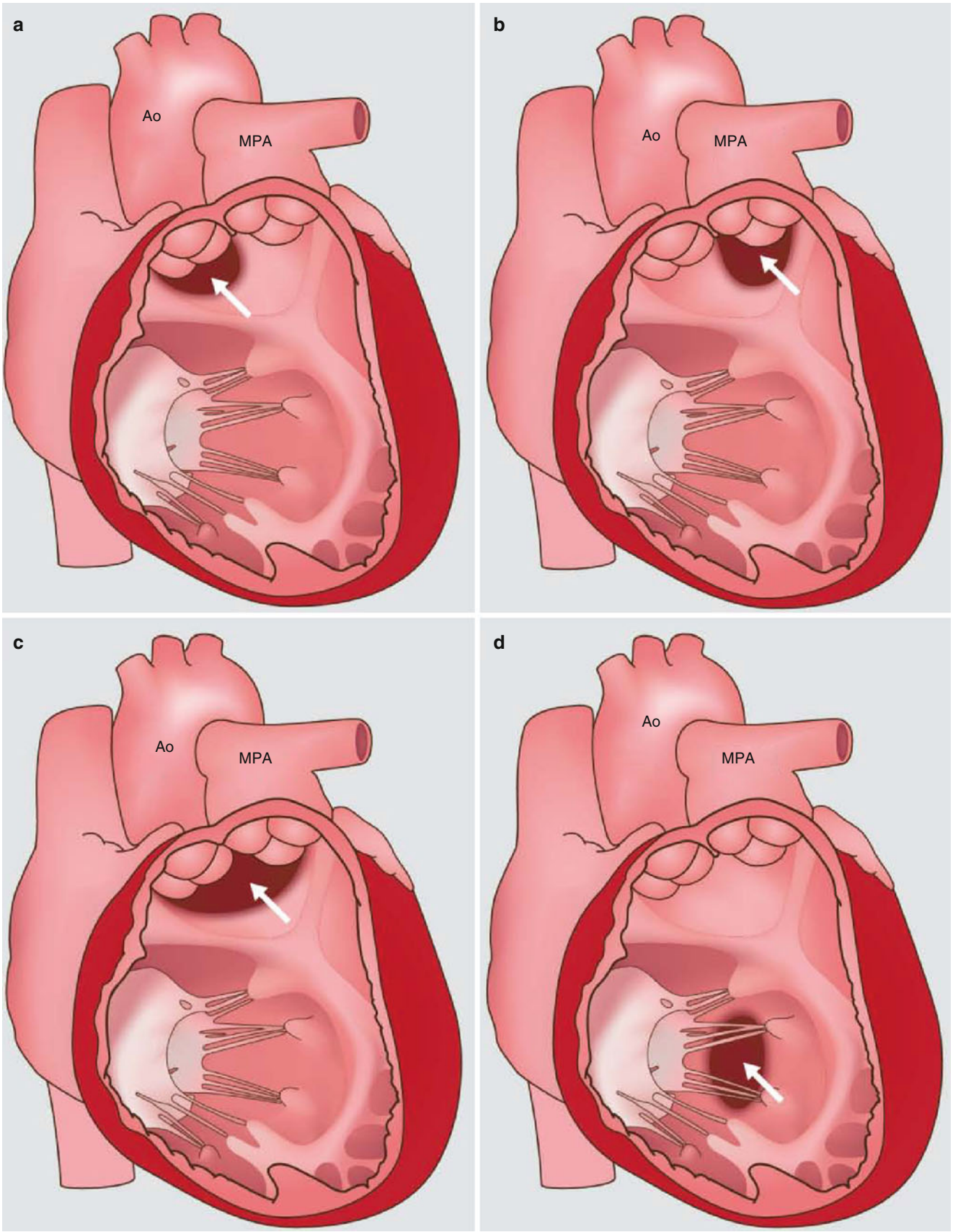


**Fig. 19.8** The variants of interventricular communication in double-outlet right ventricle. See text for a detailed description. (**a**) subaortic, (**b**) subpulmonary, (**c**) doubly committed, and (**d**) noncommitted (remote). *Ao* aorta, *MPA* main pulmonary artery. See text for description. *White arrows* point to the ventricular septal defect

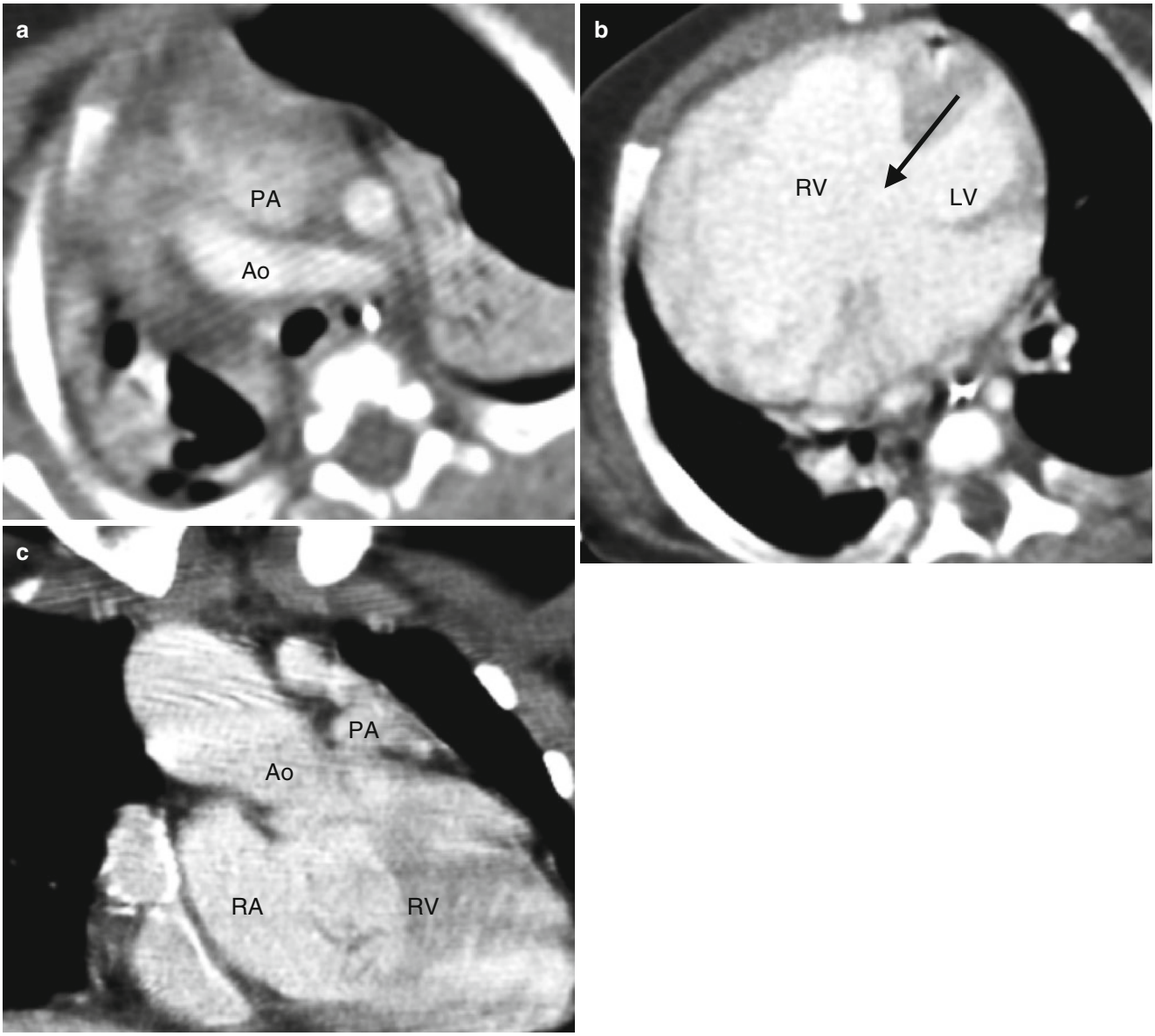


**Fig. 19.9** Subaortic VSD-type double-outlet right ventricle. The great arteries are normally related. Panel (**a**) is an axial scan showing the aorta posterior and to the *right* of the pulmonary artery. Panel (**b**) is an image showing the large ventricular septal defect (*arrow*). Panel (**c**) is a coronal view showing the aorta and the pulmonary artery arising from the right ventricle (*RV*). Most of the ventricular outflow is directed toward the aorta, which is larger than the pulmonary artery. *Ao* aorta, *PA* pulmonary artery, *LV* left ventricle, *RV* right ventricle

pulmonary artery. Pulmonary stenosis is present in up to 50 % of patients. In these patients, the physiology resembles that of tetralogy of Fallot, where the aorta completely overrides the right ventricle. In the absence of pulmonary stenosis, the physiology resembles that of a large isolated VSD [20]. This anatomy may result in congestive heart failure. Subaortic VSD is associated with L-transposition of the great arteries and an anomalous course of the right coronary artery, which crosses the pulmonary outflow tract [18].

Subpulmonary VSD-type DORV (so-called Taussig–Bing anomaly) is encountered in 30 % of patients with DORV [22–25]. The left ventricular outflow is directed toward the pulmonary artery, resulting in pulmonary artery saturations greater than aortic saturations. The great artery relationship is transposed [18]. The aortic and pulmonary origins have either a parallel arrangement (positioned side by side) or the aorta is to the right and slightly anterior to the pulmonary artery (Figs. 19.10 and 19.11). In the absence of pulmonary stenosis, the physiology is similar to that of transposition of the great arteries. If there is associated pulmonary stenosis, the physiology is similar to that of tetralogy of Fallot. The subpulmonary form of DORV is associated with subaortic stenosis and aortic arch obstruction (aortic coarctation and interrupted aortic arch). It is also associated with straddling and cleft mitral valves [18, 22, 23, 26, 27].

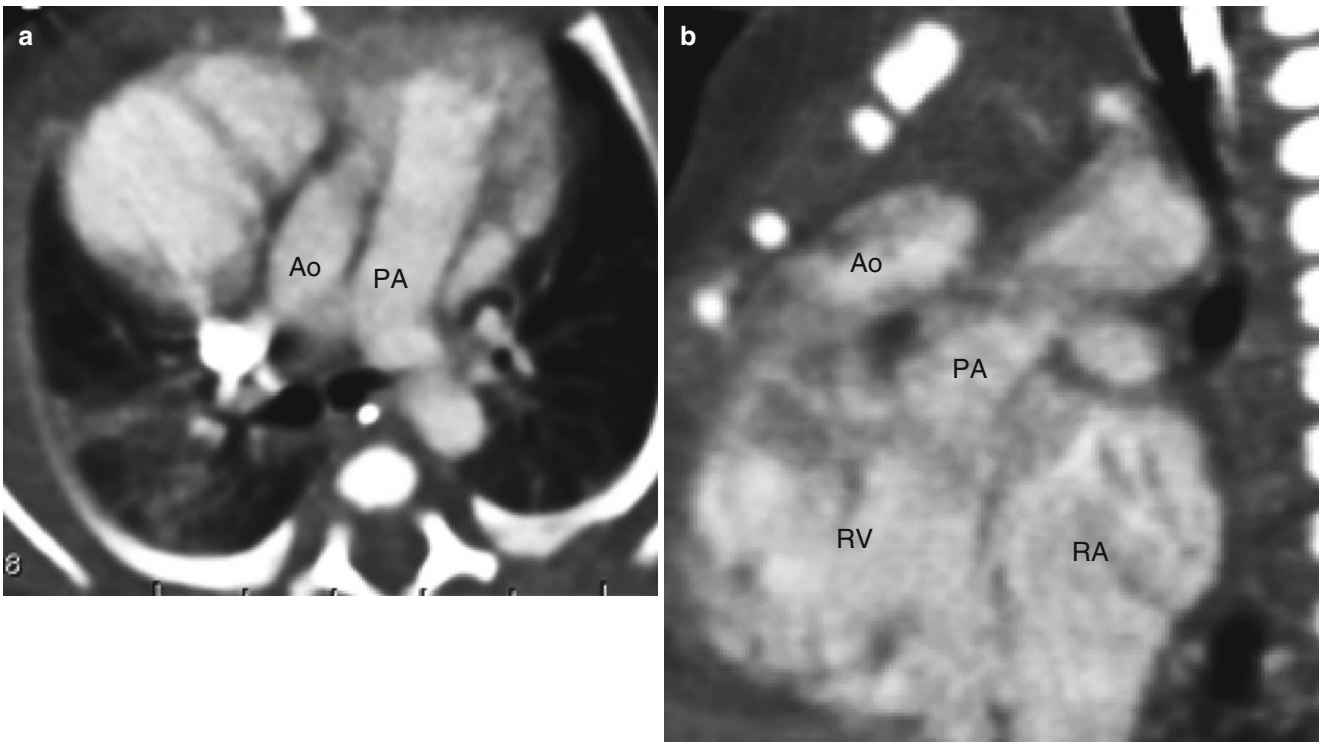


**Fig. 19.10** Subpulmonic VSD-type double-outlet right ventricle. Panel (**a**) is an axial scan showing the aorta and pulmonary artery in a parallel arrangement (positioned side by side). Panel (**b**) is a sagittal scan showing the aorta and the pulmonary artery arising from the right ventricle (*RV*). Most of the ventricular outflow is directed toward the pulmonary artery. *Ao* aorta, *PA* pulmonary artery, *RV* right ventricle, *RA* right atrium

Doubly committed VSD-type DORV occurs in 10 % of cases of DORV [25]. The left ventricular outflow is equally directed to the aorta and pulmonary artery. The great arteries are normally related [18]. Since the left ventricular outflow is equally shared by the aorta and pulmonary artery, the pathophysiology resembles that of a VSD.

Noncommitted or remote VSD-type DORV occurs in 10 % of DORV cases. The anatomy and physiology is similar to that of an isolated VSD or atrioventricular canal defect. Most commonly, the great arteries are normally related [24, 25].

Rarely, the interventricular connection will be absent, and DORV is then accompanied by a small atrial septal defect and hypoplasia of the mitral valve and left ventricle [28]. Due to commitment of both arteries to the right ventricle outlet (i.e., infundibular), the septum becomes a right ventricular structure.

Associated anomalies include situs abnormalities (dextrocardia, situs inversus, atrial isomerism), atrioventricular valve abnormalities (mitral stenosis, cleft mitral valve, straddling mitral and/or tricuspid valve, common atrioventricular valve), ventriculoarterial connection and outflow tract abnormalities (subaortic stenosis, atrioventricular discordance, atrioventricular valve atresia), atrial septal defects, and single ventricle [29–31]. Extracardiac anomalies include anomalous venous return, aortic coarctation, interrupted aortic arch, and persistent ductus arteriosus [18]. Coronary artery abnormalities are also common, including anomalous origin of the right coronary artery (RCA) from the left main coronary artery (LMCA), duplication of left anterior descending coronary artery (LAD), anomalous origin of LAD or left circumflex artery from the RCA, and single right or left coronary artery. The presence of pulmonary and aortic outflow tract obstructions can influence the pathophysiology of the heart malformation.

The clinical findings vary with the anatomy and include cyanosis, heart failure, and pulmonary hypertension. Most patients with DORV are diagnosed in the first month of life and undergo palliative repair (pulmonary artery banding or Blalock–Taussig shunt) or surgical repair. The surgical interventions depend on the location of the VSD, the size of the left ventricle, the type of ventriculoarterial connection, and the type of pulmonary blood flow (restricted on unrestricted) [18].

Definitive repairs vary and include intraventricular repair using a tunnel (baffle) to direct left ventricular flow to the aorta, arterial switch operation to connect the left ventricle to the neoaorta in combination with VSD closure, and univentricular-type repair, using a bidirectional Glenn shunt (superior vena cava to pulmonary artery) [32–36]. Rarely, unoperated patients survive to adulthood. The subaortic and doubly committed VSDs are often suitable for an intraventricular repair. The subpulmonic or "Taussig–Bing" anomaly with physiology similar to transposition may be treated with

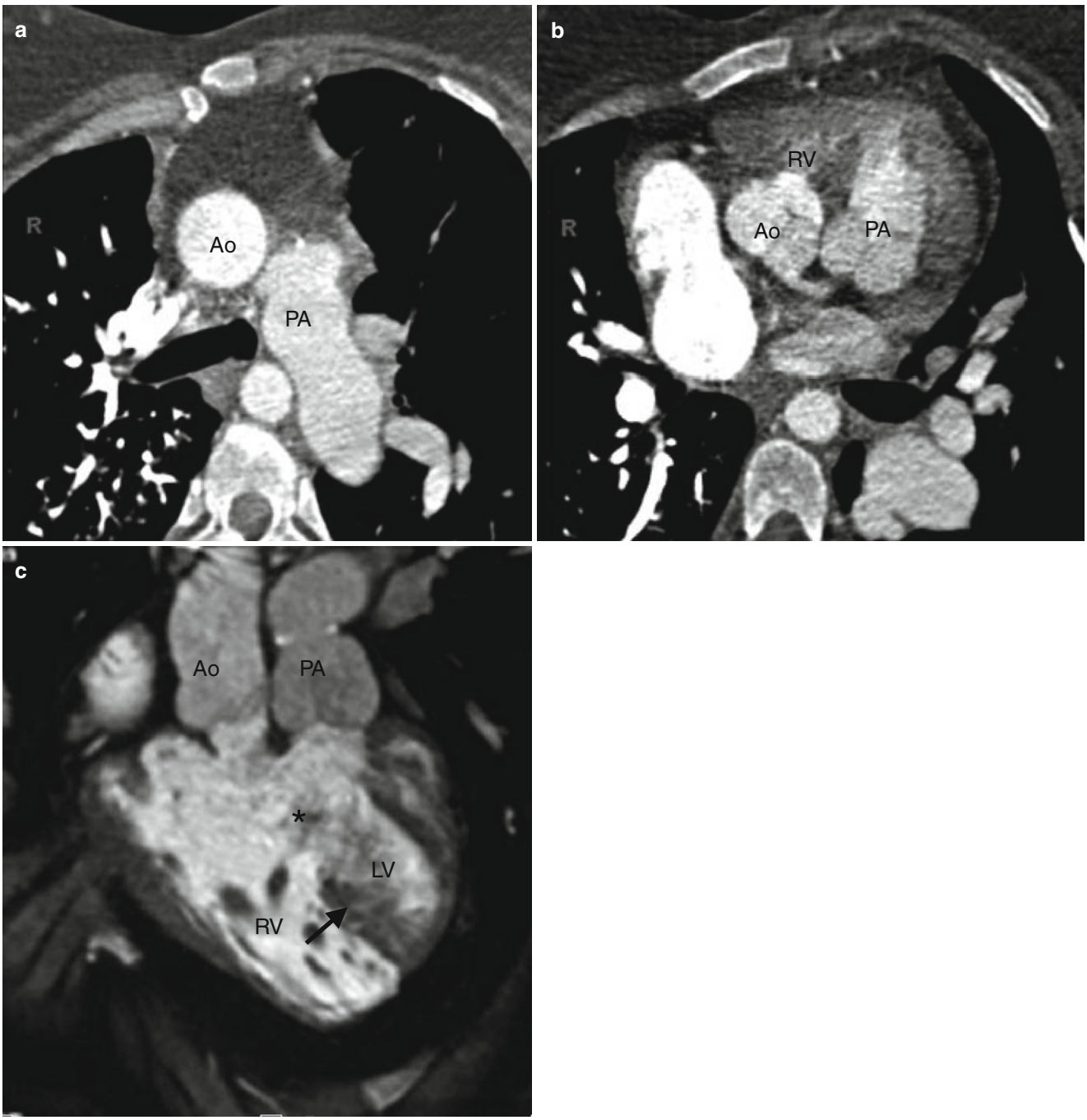


**Fig. 19.11** Subpulmonic VSD-type double-outlet right ventricle in a 31-year-old woman with a prior Fontan operation. Panel (**a**) is an axial view showing the aorta anterior and to the right of the pulmonary artery (D-transposition). Panel (**b**) is an axial scan and panel (**c**) is a coronal oblique cut. Both images demonstrate the two great arteries arising from the hypertrophied and dilated right ventricle (RV), medial and to the right of the interventricular septum (*arrow* in panel c), consistent with double-outlet right ventricle. Panel (c) demonstrates the very large VSD (*asterisk*)

an arterial switch operation. The noncommitted VSD may require a Fontan procedure.

Potential complications after surgical repair include residual or recurrent VSD, residual or recurrent outflow tract obstructions, and atrioventricular valve regurgitation. Complications of univentricular repair include stenosis/narrowing of the Glenn shunt and Fontan procedure.

### 19.2.2 Double-Outlet Left Ventricle

Double-outlet left ventricle (DOLV) is a congenital anomaly in which both the aorta and main pulmonary artery arise entirely or predominately from the morphologic left ventricle [37].

DOLV is a very rare anomaly. It accounts for approximately 5 % of patients with double-outlet ventricle and its incidence is estimated to be less than 1 in 200,000 live births [38].

Similar to DORV, DOLV is characterized by heterogeneous morphology and clinical presentations. The VSD's location may be subaortic, subpulmonary, doubly committed, or noncommitted (remote) [37, 39–41]. Subaortic and subpulmonic conal figurations are most common. DOLV occurs most often with atrial situs solitus and with atrioventricular concordance.

Subaortic VSD-type DOLV is present in 75 % of all DOLV patients. Pulmonary outflow tract obstruction is common, occurring in 90 % of cases. The great arteries are usually abnormally related and the aorta is usually anterior to the pulmonary artery [39, 41]. A right anterior aorta is more frequent than a left anterior aorta. DOLV with subaortic VSD with normally related great arteries is very rare [39]. The clinical presentation can resemble that of tetralogy of Fallot or complete transposition depending on the degree of pulmonary stenosis.

Subpulmonary VSD-type DOLV occurs in 15 % of cases [41]. Aortic outflow tract obstruction (aortic hypoplasia, aortic coarctation, or interrupted aortic arch) is common, occurring in about 80 % of cases [41]. The clinical manifestation is that of pulmonary overcirculation, similar to that of a large VSD.

Doubly committed VSD-type DOLV is present in 10 % of cases [41]. The VSD is overridden by both the main pulmonary artery and aorta. Of note, due to the varying degree of aortic and pulmonary artery override, the distinction between DOLV and DORV may be problematic, and thus, this anomaly has been referred to as double-outlet both ventricles [42]. In most cases, the great arterial relationship is side by side. Aortic or pulmonic outflow tract obstruction is rare.

Noncommitted (remote) VSD-type DOLV is extremely rare [43]. Pacifico et al. described one patient with DOLV with a posterior inlet VSD and a left-sided, anterior aorta.

Most patients with DOLV present in the neonatal period with cyanosis due to pulmonary outflow obstruction or with heart failure due to aortic outflow obstruction or a large VSD. Palliation or surgical repair is done early in life. Rare unoperated patients survive to adulthood.

Surgical repairs include a left ventricle-to-pulmonary outflow tract closure, rerouting of blood from the right ventricle to pulmonary artery using patch reconstruction, pulmonary root or pulmonary artery translocation onto the right ventricle with or without Lecompte maneuver, Rastelli-type procedure, or Fontan procedure and VSD closure [37]. In general, DOLV with two relatively well-developed ventricles is often repaired by left ventricle-to-pulmonary outflow tract closure, a Rastelli conduit from the right ventricle to pulmonary artery, or pulmonary root translocation and VSD closure. DOLV with a functionally single-ventricle or with tricuspid valve atresia usually requires a Fontan procedure.

### 19.2.3 Cardiac Computed Tomography (CT) in the Assessment of Both DORV and DOLV

CT allows a comprehensive heart evaluation including (a) the morphology, size, geometry, and systolic function of both ventricles; (b) location of the interventricular connections and relationships to the atrioventricular junction; (c) morphology and anatomic relationships of the ventriculoarterial connections, including the conal configuration as well as the degree of great vessel override/commitment to the ventricles; (d) presence, morphology, size, and extent of obstruction of the pulmonary and aortic outflow tracts; (e) the spatial relationship of the great arteries; (f) atrial size and morphology; (g) the anatomy of the cardiac valves; (h) evaluation of aortic arch anatomy; and (i) the presence of coronary artery and other coexisting abnormalities. See Table 19.2.

**Table 19.2** Cardiac CT assessment in double-outlet right and left ventricles

| |
|---|
| Morphology, size, wall thickness, geometry, and systolic function of both ventricles |
| Morphology and anatomic relation of atrioventricular junction connections to VSD |
| Morphology and anatomic relation of ventriculoarterial junction (conotruncal abnormalities and arterial override/commitment to ventricles) |
| Presence, anatomy, size, and magnitude of aortic and/or pulmonary outflow tract obstructions |
| Anatomy, size, and spatial relationship of aorta and pulmonary artery |
| Morphology and size of atria |
| Anatomy and function of cardiac valves |
| Evaluation of coronary artery and aortic arch anatomy |
| Other anomalies |

**Table 19.3** CT assessment of post-interventional complications in double-outlet ventricles

| |
|---|
| Left and right ventricular dilatation and dysfunction |
| Aortic and/or pulmonary outflow tract obstruction |
| Conduit obstructions/leaks |
| Residual interventricular connections |
| Great artery spatial relationship and evidence of obstruction |
| Atrioventricular regurgitation and atrial size |
| Compression of coronary arteries |
| Other anomalies |

Post-interventional imaging assessment should include evaluation of (a) ventricular morphology, size, and systolic function; (b) the anatomy, size, and presence/magnitude of residual aortic and pulmonary outflow tract obstruction(s) and extracardiac conduits (obstruction/leak); (c) the presence of residual interventricular communication; (d) the anatomy, size, course, and spatial arrangement of the aorta and pulmonary artery, with attention to aortic root dilatation and residual obstructions in the aortic arch; (e) the anatomy of the atrioventricular valves; (f) atrial morphology and size; (g) coronary artery anatomy with attention to compression/stenosis; and (h) coexisting anomalies [14, 15]. See Table 19.3.

## 19.3 Truncus Arteriosus

Truncus arteriosus, also known as common arterial trunk, is characterized by a single arterial trunk with a single truncal valve that arises from the base of the heart and gives rise to the coronary, pulmonary, and systemic circulation [44]. This rare anomaly accounts for 1–4 % of congenital heart defects [45–48].

Truncus arteriosus results from a developmental error in septation of the embryonic truncus arteriosus (i.e., the ventricular outlets and the proximal arterial segment of the heart tube). It is associated with a ventricular septal defect (VSD) and common truncal (semilunar) valve with biventricular origin that overrides the interventricular septal defect. Rarely, there is an intact ventricular septum or conjoined aortic and pulmonary valve [44]. A common arterial trunk originating almost entirely from the right or left ventricle can also be encountered. The VSD is usually large and nonrestrictive and is positioned between the anterior and posterior limbs of the septomarginal trabeculations.

The single truncal valve is typically dysplastic with thickened cusps and supernumerary leaflets (usually three but up to six), resulting in regurgitation and/or stenosis. The valve frequently remains in fibrous continuity with the mitral valve, but rarely with the tricuspid valve. The coronary arteries arise from poorly developed sinuses of Valsalva. The left and right coronary arteries often originate from the left posterolateral and right anterolateral truncal walls, respectively [49]. Coronary artery anomalies, in particular a single coronary artery and an intramural course, can be present.

Truncus arteriosus is generally an isolated finding, but it can be associated with hemodynamically significant anomalies, in particular interrupted aortic arch and aortic coarctation [44, 49]. Other associated malformations include right aortic arch, atrial septal defect, aberrant subclavian artery, persistent superior vena cava, and tricuspid stenosis [49]. A ductus arteriosus, if present, is usually absent or diminutive in patients with normal caliber aortic arches. Because the pulmonary arteries and both ventricles arise directly from the common trunk, a ductus is not required in most cases to support the circulation.

There are several classification systems for truncus arteriosus. The earliest classification by Collet and Edwards subdivided truncus arteriosus into four anatomic types based on the origin of the pulmonary arteries (Fig. 19.12) [50]. Type I is a common arterial trunk that divides into an aorta and short

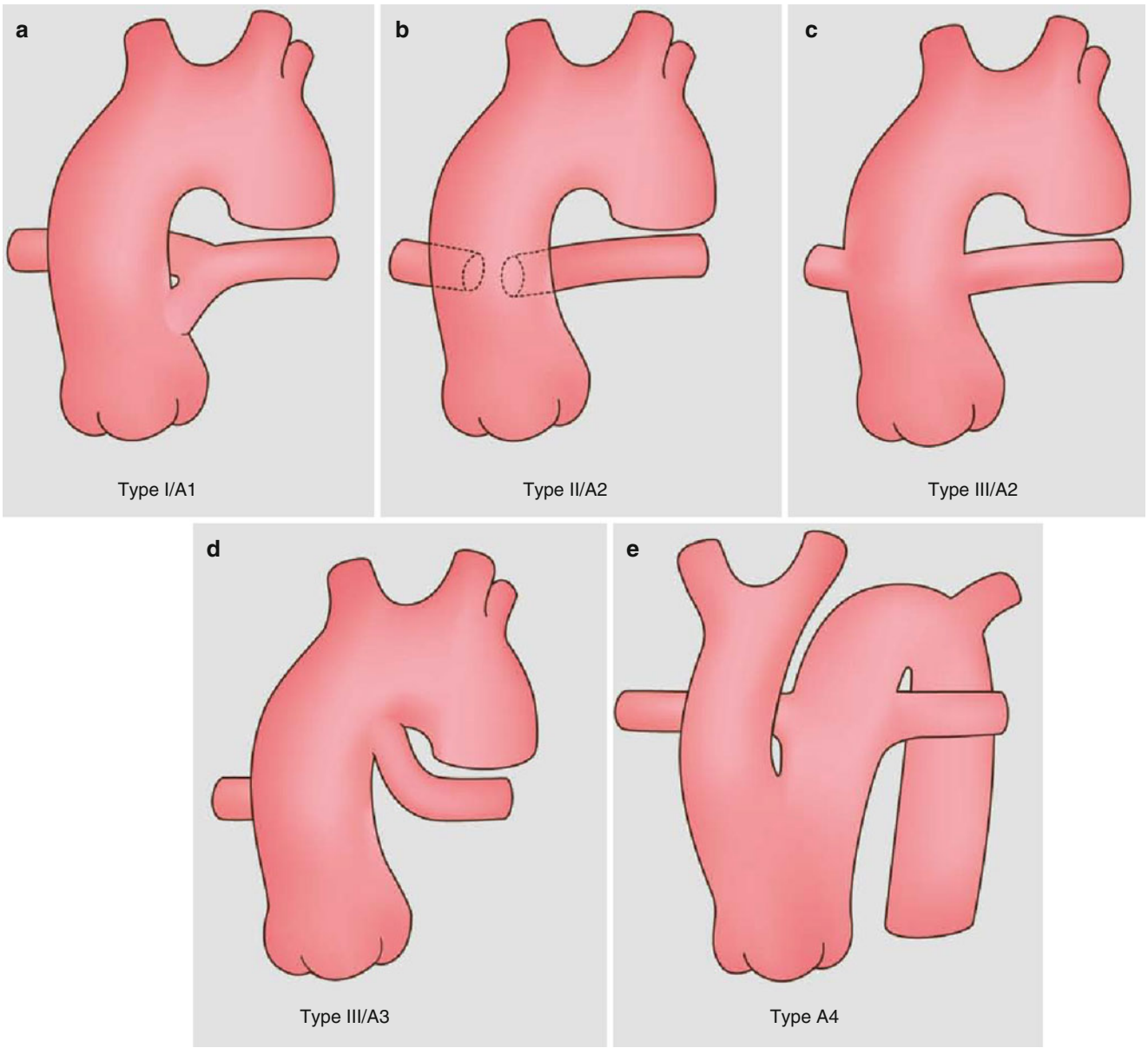


**Fig. 19.12** Combination of Collett and Edwards types (*types I*, *II*, *III*) with the Van Praagh classification scheme (*A1*, *A2*, *A3*, *A4*). See text for more detail

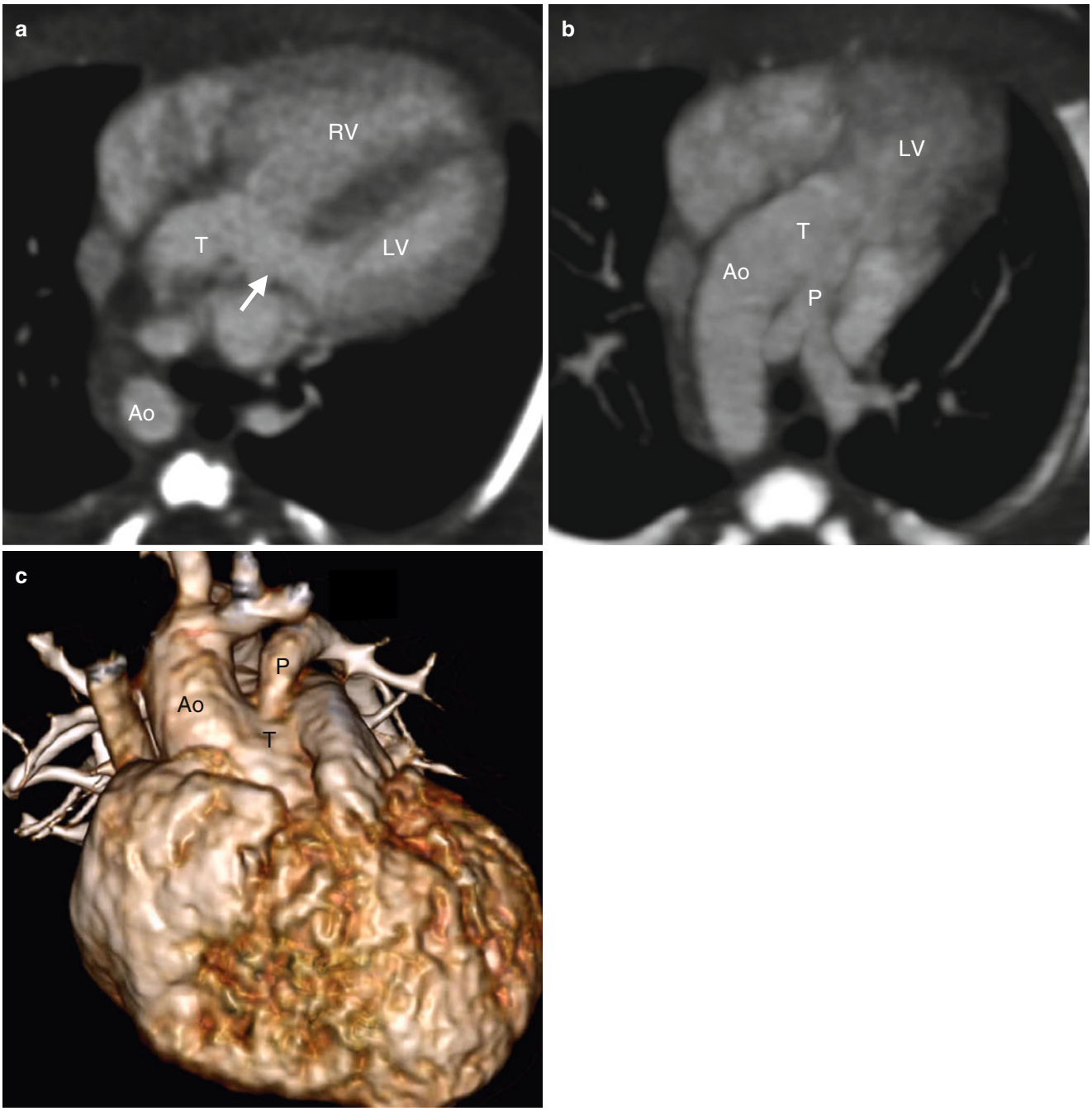


**Fig. 19.13** Truncus arteriosus, Collett and Edwards type I or Van Praagh type A1 (Van Praagh), in a neonate. Panel (**a**) is an oblique axial image showing a solitary arterial trunk (*T*) or truncus overriding a large subtruncal ventricular septal defect (*arrow*). Also note the right-sided descending aorta (*Ao*). Panel (**b**) is an oblique axial image demonstrating the solitary trunk branching into a right-sided ascending aorta (*Ao*) and short pulmonary trunk (*P*), which then divides into left and right pulmonary arteries. Panel (**c**) is a volume-rendered image confirming the origins of the aorta (*Ao*) and the main pulmonary artery (*P*) from the single trunk (*T*). *RV* right ventricle, *LV* left ventricle

pulmonary trunk, which then divides into left and right pulmonary arteries (Figs. 19.13, 19.14, and 19.15). Type II is when each pulmonary artery arises separately from the posterior aspect of the truncus but in close proximity to each other (Fig. 19.16).

Type III is when each pulmonary artery arises separately from the posterolateral aspect of the truncus, at a distance from each other. Type IV describes the case when neither of the pulmonary arteries arises from the common trunk and the lungs are supplied by major aortopulmonary collateral

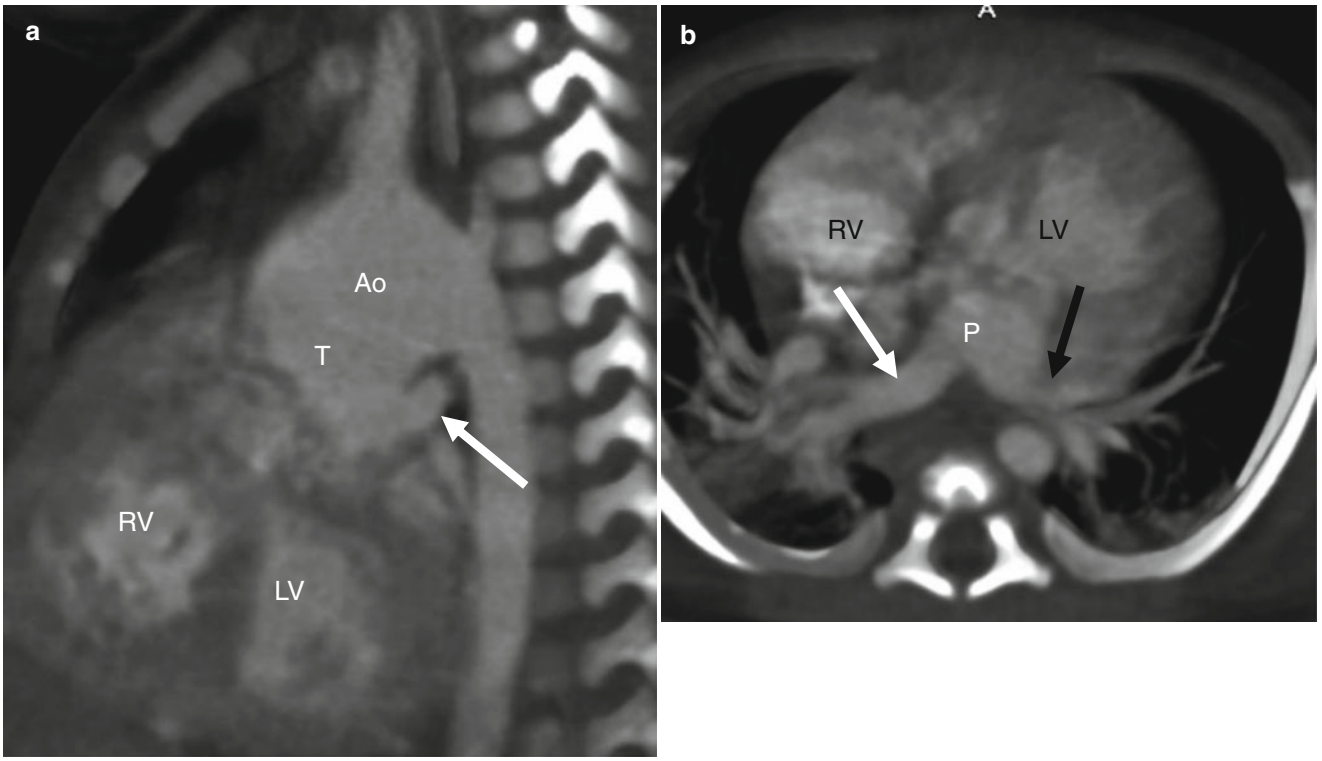


**Fig. 19.14** Truncus arteriosus, Collett and Edwards type I or Van Praagh type 1, in a neonate. Panel (**a**) is an oblique sagittal view illustrating the aorta (*Ao*) and main pulmonary artery trunk (*arrow*) arising from a truncus arteriosus (*T*). Panel (**b**) is an oblique axial image demonstrating that the left pulmonary artery (*black arrow*) and right pulmonary artery (*white arrow*) each arising from the short main pulmonary artery (*P*). *RV* right ventricle, *LV* left ventricle

arteries (MAPCAS). This type (also termed "pseudotruncus") is now considered to represent a form of pulmonary atresia with ventricular septal defect (i.e., severe form of tetralogy of Fallot) rather than a true truncus arteriosus.

A subsequent classification system by Van Praagh and Van Praagh takes into account the presence of a patent ductus arteriosus and interrupted aortic arch, associated anomalies that have important surgical implications (Fig. 19.12). In this classification system, type 1 parallels the Collette and Edwards' type I classification (Figs. 19.13 and 19.14).

Type 2 is a combination of Collette and Edwards' types II and III cases. Each pulmonary artery arises separately from the common trunk and the proximity of the origin of the pulmonary arteries not specified (Fig. 19.16). Type 3 describes cases which have the origin of one branch pulmonary artery from the common arterial trunk, with the other pulmonary artery arising from the ductus arteriosus or from the aortic arch (a variant of Collette and Edwards' type II cases). Type 4 is characterized by the presence of a hypoplastic or interrupted aortic arch and a large persistent ductus arteriosus.

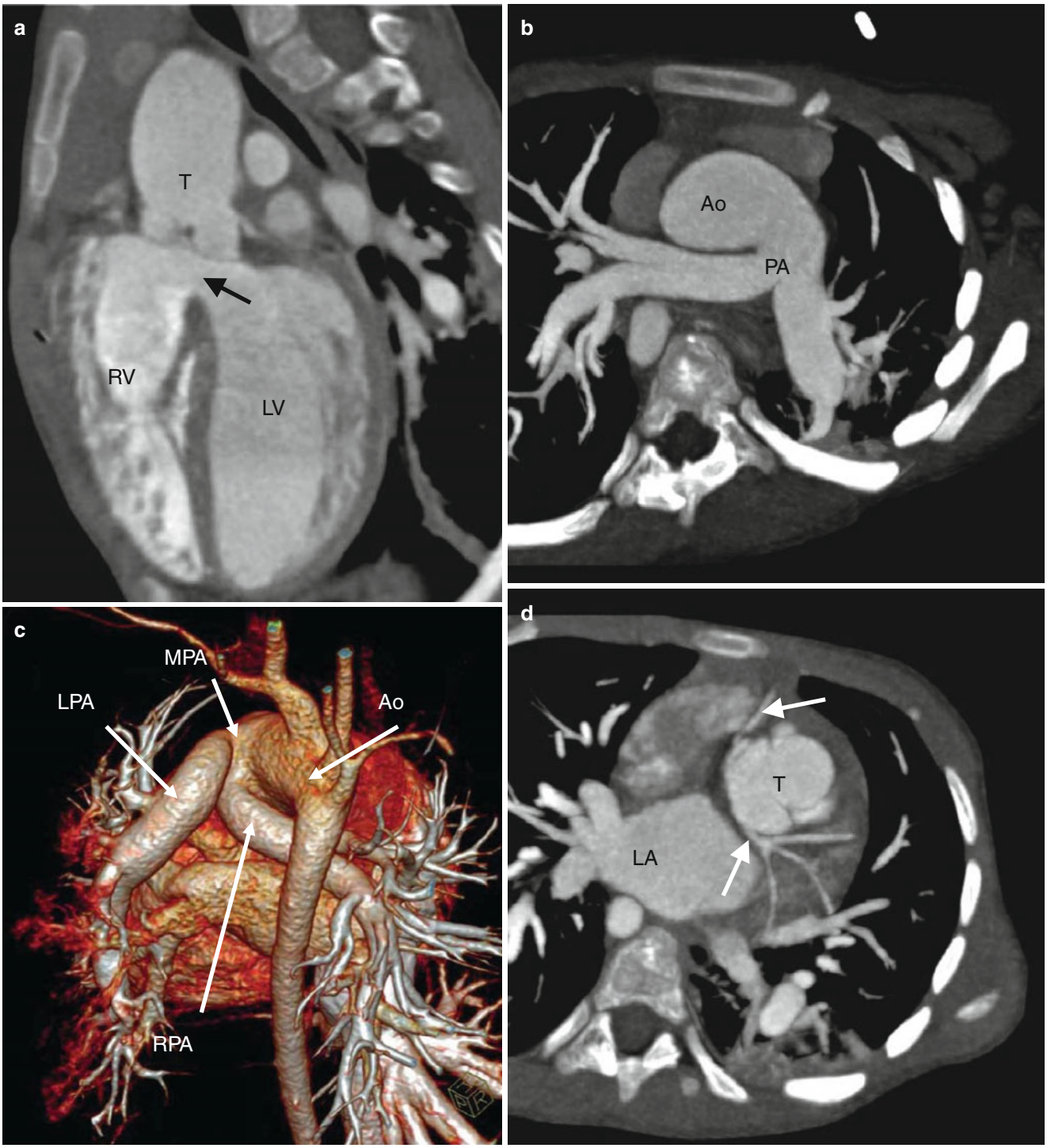


**Fig. 19.15** Truncus arteriosus (Collett and Edwards type I, Van Praagh type A1). Panel (**a**) is a maximum intensity projection demonstrating the truncus arteriosus (*T*). The *arrow* points to a large perimembranous ventricular septal defect. *LV* left ventricle, *RV* right ventricle. Panel (**b**) is an oblique image depicting the origin of both the aorta (*Ao*) and pulmonary artery (*PA*) from the truncus (not visualized). Panel (**c**) is a volume-rendered image also demonstrating the origins of the Ao and PA from the truncus (not visualized). Panel (**d**) depicts the coronary arteries (*arrows*) originating from the common truncus arteriosus (Images kindly provided by Vasco Silva, MD, Radiology Department, Clinica Girassol, Luanda, Angola). *LA* left atrium, *RPA* right pulmonary artery, *LPA* left pulmonary artery, *MPA* main pulmonary artery, *T* truncus

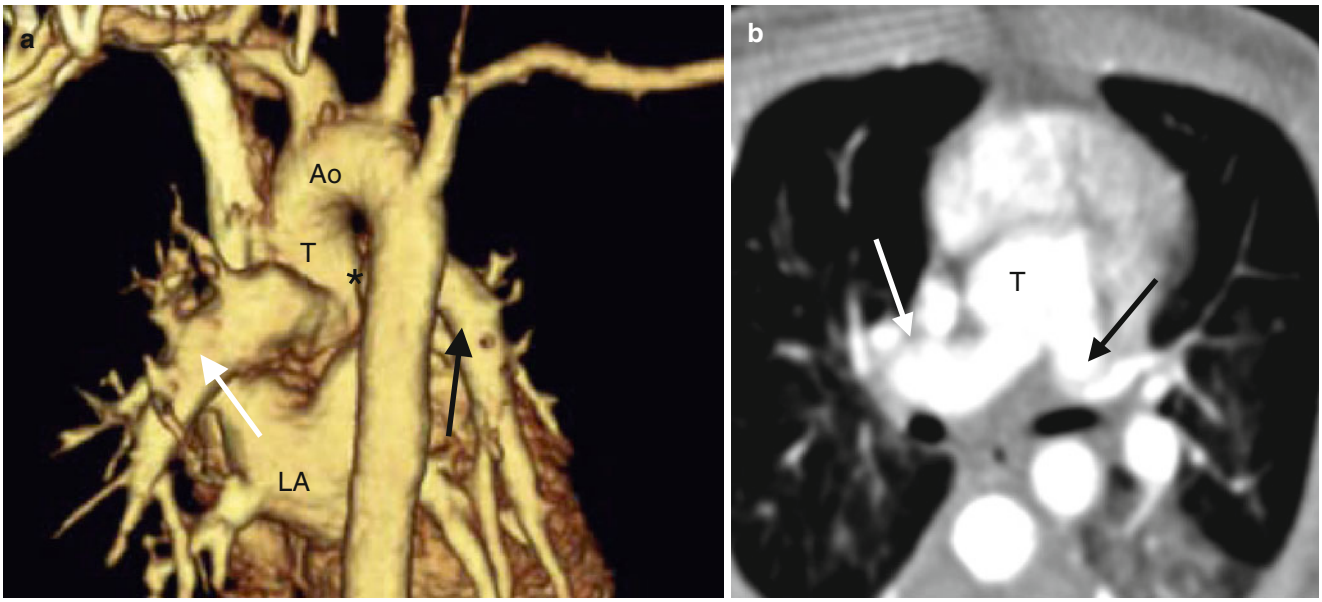


**Fig. 19.16** Truncus arteriosus, Collett and Edwards type II or Van Praagh type 2, in a neonate. Panel (**a**) is a volume-rendered coronal view showing the aorta (*Ao*) and each pulmonary artery emerging from the common truncus (*T*) in close proximity to each other. The *white arrow* is the right pulmonary artery and the *black arrow* is the left pulmonary artery. Panel (**b**) is an axial cut confirming the separate origins of the right pulmonary artery (*white arrow*) and left pulmonary artery (*black arrow*) from the truncus (*T*). In panel (a), the *asterisk* marks the ostium of the left pulmonary artery

The pulmonary arteries arise as a single branch from the common trunk (Collette and Edwards' type I cases).

The Van Praagh classification also specifies the presence of a VSD (type A) or the absence of a VSD (type B). Thus, each case has a nomenclature that includes a number and a letter.

To provide a uniformed classification, the Society of Thoracic Surgeons proposed a nomenclature system that takes into account both the origin of the pulmonary arteries and the presence of aortic arch anomalies [44]. Type A is a common arterial trunk with confluent or near confluent pulmonary arteries, type B describes a common arterial trunk with absence of one pulmonary artery, and type C is a common arterial trunk with interrupted aortic arch or severe aortic coarctation.

The presentation of patients with truncus arteriosus is virtually always cyanosis and cardiac failure in infancy, and these patients always undergo prompt operative repair. Unrepaired adults with this anomaly are rare. Both palliative and primary repair procedures have been performed. Since palliative pulmonary artery banding often results in complications (band migration, failure of pulmonary artery growth), surgical repair is preferred [49, 51]. Surgical management consists of patch closure of the VSD, connection of the truncus arteriosus and valve to the left ventricle, and detachment of the pulmonary arteries from the truncus with anastomosis to a prosthetic or aortic valved homograft from the right ventricle to the pulmonary artery (Rastelli procedure). In effect, the common trunk becomes the ascending aorta and the truncal valve becomes the aortic valve (Figs. 19.17 and 19.18).

Potential surgical complications include (a) right ventricle-to-pulmonary artery homograft anastomosis stenosis and/or regurgitation, (b) ventricular–truncal anastomosis and truncal/neoaortic valve stenosis and/or regurgitation, (c) myocardial ischemia, (d) ventricular dysfunction, (e) residual VSD, (f) aortic root dilatation, (g) branch pulmonary artery stenosis, (h) arrhythmias, (i) progressive pulmonary vascular disease, and (j) endocarditis [49]. Many of these require reintervention and can be detected using imaging modalities.

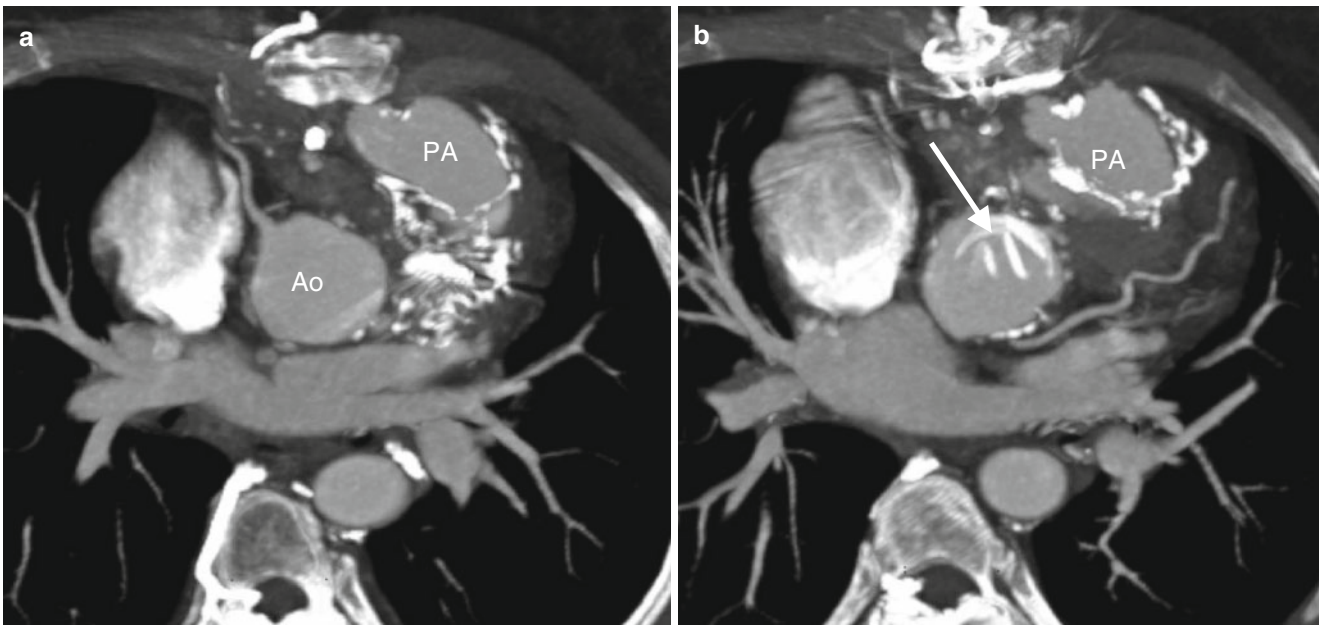


**Fig. 19.17** Truncus arteriosus repair. An example of a 42-year-old man with a diagnosis of Collett and Edwards type II or Van Praagh type 2 truncus at birth who underwent multiple-staged corrective procedures. At 3 months of age, he underwent pulmonary artery banding with VSD closure. At 10 years of age, a truncus-to-left ventricle anastomosis and a pulmonary arteries-to-pulmonary homograft connection was then performed. The truncal valve was replaced with a prosthetic valve at age 27 years for treatment of endocarditis. Panels (**a**) and (**b**) are two axial images showing a separate aorta (*Ao*) and pulmonary artery (*PA*). The prosthetic valve (*arrow*) is partially visualized in panel (b)

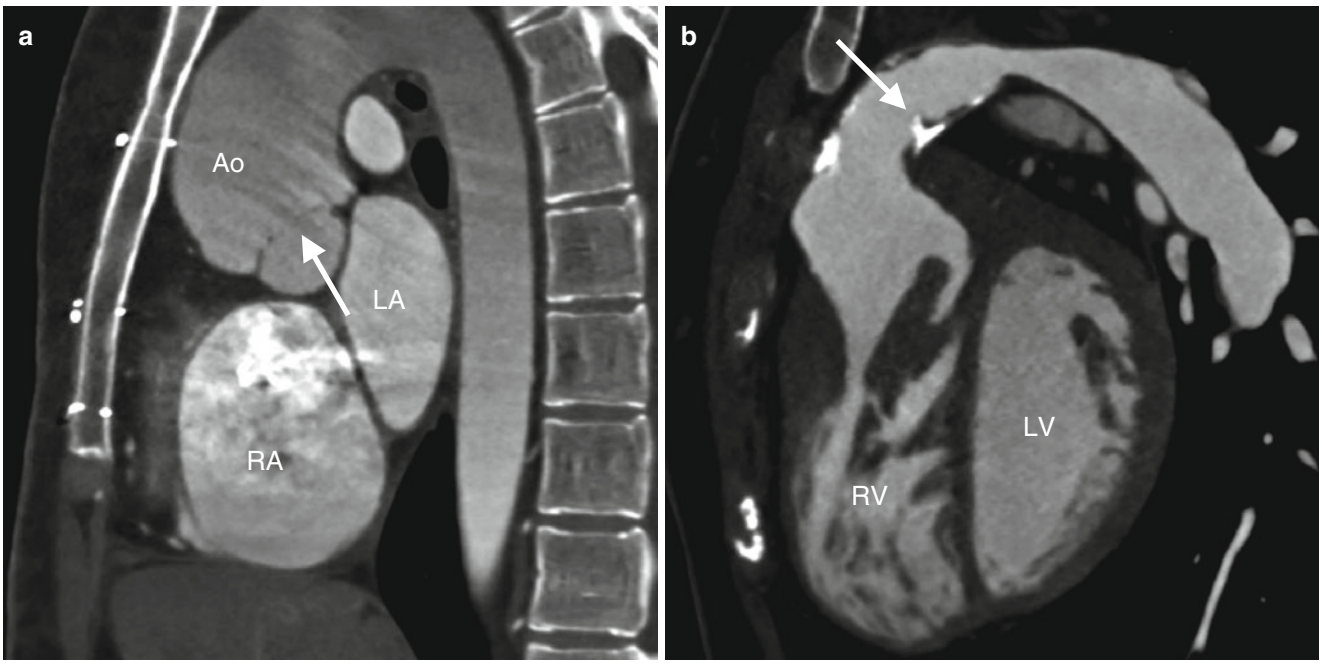


**Fig. 19.18** Truncus repair with right ventricle to main pulmonary artery conduit in a 23-year-old woman. Panel (**a**) is a sagittal scan showing the truncal semilunar valve (*arrow*) supporting the dilated ascending aorta (*Ao*). Panel (**b**) is a sagittal view showing the connection of the right ventricle (*RV*) to the pulmonary homograft (*arrow*). The distal portion of the conduit is narrowed and the proximal portion demonstrates calcifications. *LA* left atrium, *RA* right atrium, *LV* left ventricle

### 19.3.1 Cardiac Computed Tomography (CT) in Patients with Truncus Arteriosus

CT can clearly show the truncus arteriosus and its associated anomalies in untreated patients and can also be used to assess the post operative morphology [15, 52–54]. See Table 19.4. Important imaging information for patient management includes (a) the morphology, wall thickness, size, and systolic function of both ventricles; (b) the anatomy and size of the ventriculoarterial connections at the subvalvular, valvular, and supravalvular levels; (c) morphology and function of the cardiac valves including evaluation of truncal/neoaortic valve; (d) anatomy and patency of right ventricle-to-pulmonary artery conduit, including the presence and magnitude of obstruction and dilatation; (e) the presence of a residual VSD; (f) the anatomy, size, course, and spatial arrangement of the aorta and pulmonary arteries, with special attention to the presence of obstruction; (g) the morphology and size of the atria; and (h) the assessment of coexisting anomalies. Although CT can reliably show anatomic abnormalities, magnetic resonance imaging may be required for evaluation of valve/conduit insufficiency and the presence of endocarditis. However, CT is the imaging procedure of choice for visualizing the origin and course of the coronary arteries and can be useful for the diagnosis of coronary artery lesions in adults with suspected myocardial ischemia.

**Table 19.4** CT assessment in subjects postsurgical patients with truncus arteriosus

| |
|---|
| Morphology, size, wall thickness, geometry, and systolic function of both ventricles |
| Anatomy and size of ventriculoarterial connections at subvalvular, valvular, and supravalvular levels |
| Anatomy and function of cardiac valves including truncal/neoaortic/prosthetic valves |
| Presence and magnitude of right ventricle-to-pulmonary artery conduit obstruction/dilatation |
| Presence of residual VSD |
| Anatomy, size, and spatial relationship of aorta and pulmonary artery including the presence and magnitude of obstruction |
| Morphology and size of atria |
| Presence of other anomalies |

## 19.4 Hemitruncus Arteriosus

Hemitruncus arteriosus is a rare anomaly (about 0.1 % of all congenital heart disease) in which one pulmonary artery (more commonly the right) arises anomalously from the ascending aorta and the opposite pulmonary artery originates from the main pulmonary artery or the right ventricle (Fig. 19.19). Associated anomalies include patent ductus arteriosus and ventricular septal defect. Affected patients present in the neonatal period or infancy with congestive heart failure secondary to a large left-to-right shunt. Most patients do not survive infancy without surgical treatment which includes either direct implantation of the anomalous pulmonary artery into the main pulmonary artery or interposition of an aortic/pulmonary arterial flap. A combination of hemitruncus and tetralogy of Fallot has rarely been seen in adults [55, 56]. In unrepaired patients, CT can clearly show the origin and course of the anomalous pulmonary artery, and in surgically corrected patients, CT can be used to assess the postoperative anatomy and any complications.

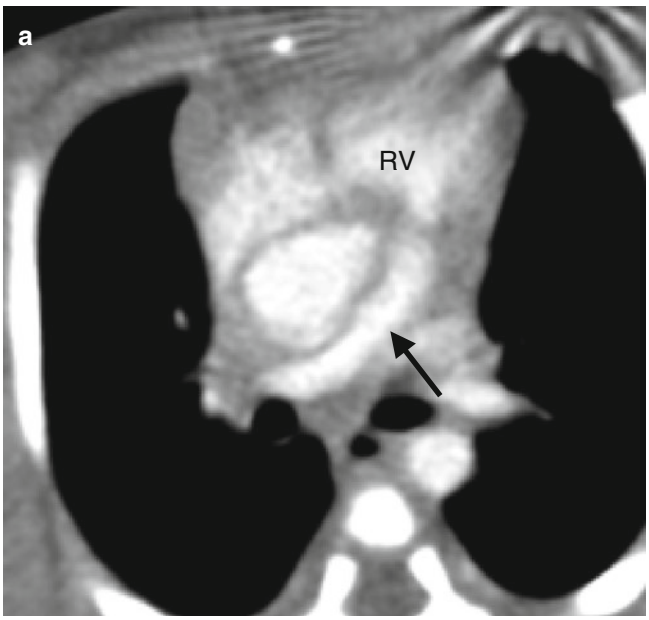


**Fig. 19.19** Right hemitruncus. Panel (**a**) an axial view showing the right pulmonary artery (*arrow*) arising from the right ventricle (*RV*). Panel (**b**) an axial view at a higher level demonstrating the left pulmonary artery (*arrow*) arising from the aorta (*Ao*). Panel (**c**) an axial image in another patient shows the right pulmonary artery (*white arrow*) arising from aorta (*Ao*). The left pulmonary artery (*black arrow*) arose from the main pulmonary artery (not seen in this image)

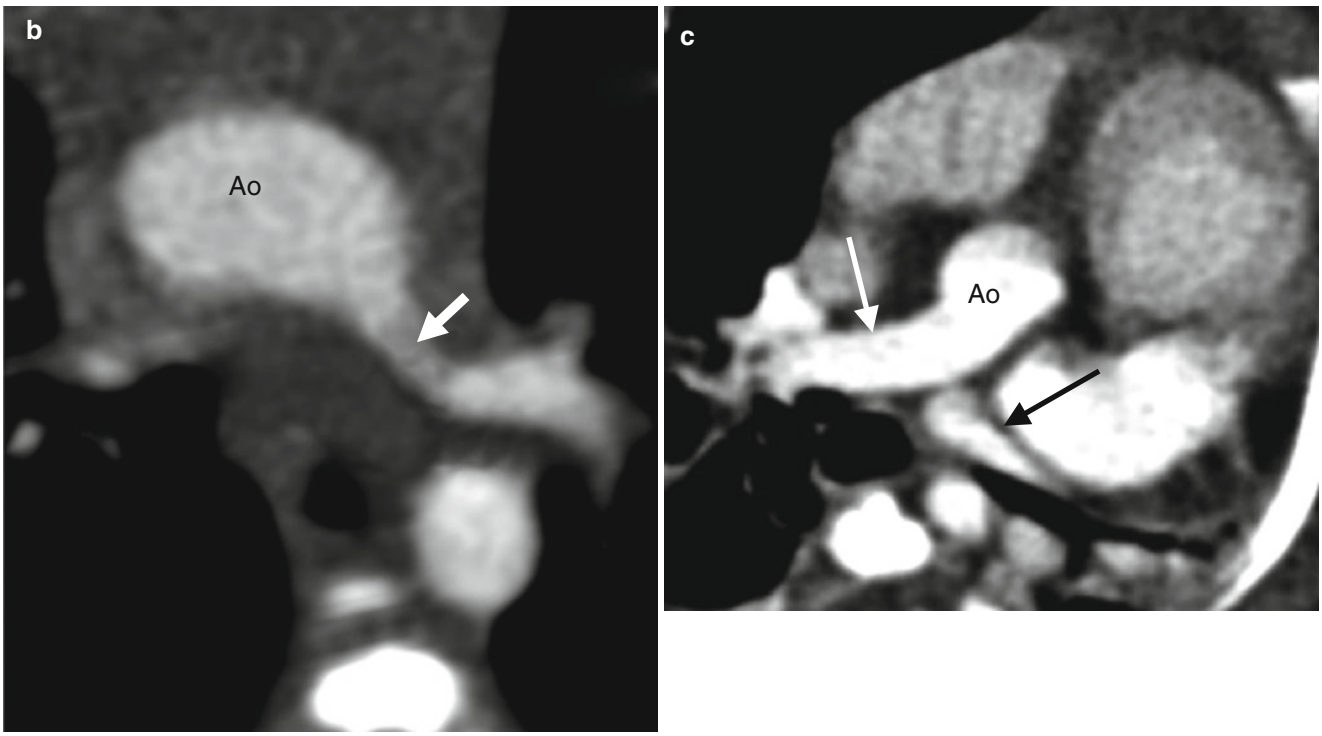


**Fig. 19.19** (continued)

## 19.5 Complete Transposition of the Great Vessels (Ventriculoarterial Discordance)

Transposition of the great arteries (TGA), also termed ventriculoarterial discordance, is an abnormality of ventriculoarterial connection in which the aorta originates from the morphologic right ventricle and the pulmonary artery originates from the morphologic left ventricle [57–59]. The frequently encountered term dextro (D)-TGA has been used interchangeably with TGA, but this is imprecise because TGA refers only to those hearts in which the aortic valve is positioned to the right of the pulmonary valve [60]. The term TGA is broader and includes both physiologically uncorrected transposition (D-TGA) and physiologically corrected transposition (also termed double discordance of the great arteries) and levo- or L-TGA because in both cases the great arteries arise from the wrong ventricle and thus are transposed. For the purposes of the discussion in this section, we define TGA as those heart defects which have physiologically uncorrected transposition of the great arteries.

TGA is the second most common cyanotic congenital cardiac defect, after tetralogy of Fallot, accounting for approximately 5–7 % of congenital heart diseases. The overall annual incidence is 20–30 in 100,000 live births [61].

The Van Praagh description of TGA includes hearts in which there is atrial situs solitus, concordant atrioventricular alignment, and discordant ventriculoarterial alignment and also hearts in which there is situs inversus, levo-looped ventricles, and either dextro (D)- or levo (L)-transposition. The segmental anatomy is designated {S,D,D}, {S,D,A}, and {S,D,L}, as well as {I,L,L} and {I,L,D}. Those with situs ambiguous technically cannot be classified as TGA by the Van Praagh nomenclature but may be physiologically uncorrected and appropriately treated by existing standard therapies for TGA [57, 59].

The most common variant of TGA (over 80 % of cases) reported by Van Praagh was D-TGA (aortic valve to right of the pulmonary valve). The remaining variants are usually L-TGA (aorta to left of pulmonary artery). Occasionally, the aorta is directly anterior to the pulmonary artery (A-TGA).

TGA is the result of abnormal conotruncal rotation with the aortic root positioned to the right and anterior to the pulmonary trunk [61]. It always has discordant ventriculoarterial alignment such that the aorta arises entirely or in large part from the right ventricle via a muscular subaortic infundibulum and the pulmonary artery arises entirely or in large part from the left ventricle without a subpulmonary infundibulum (Figs. 19.20 and 19.21) [58]. The muscular subaortic conus separates the transposed aortic valve from both atrioventricular valves, while the absence of a subpulmonary conus allows direct pulmonary–mitral fibrous continuity. Concordant atrioventricular alignment (normal situs) is nearly always present [58, 59]. The pulmonary and systemic circulations function in parallel, rather than in series (Fig. 19.22). Thus, blood flow is from the cavae to right atrium to right ventricle to aorta and pulmonary veins to left

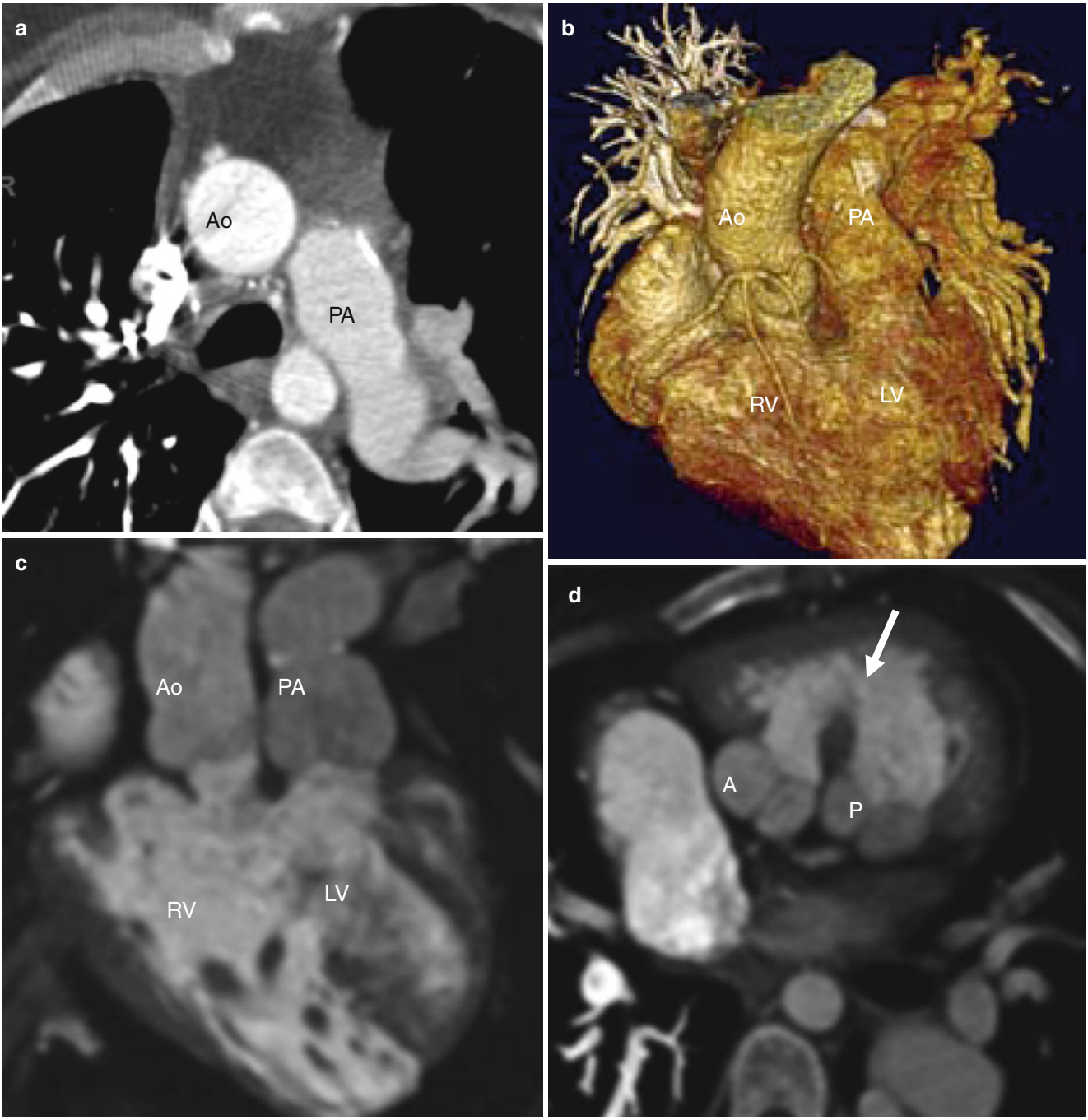


**Fig. 19.20** Uncorrected transposition of the great arteries. A 31-year-old woman with acute chest pain who had a Mustard procedure in infancy. A computed tomographic angiogram was performed to evaluate for pulmonary embolus. Panel (**a**) is an axial cut and panel (**b**) is an oblique coronal image. Both panels (**a**) and (**b**) illustrate the aorta (*Ao*) anterior and to the *right* of the pulmonary artery (*PA*). Panel (**c**) is an oblique coronal image demonstrating that the pulmonary artery (*PA*) arises from the smooth left ventricle (*LV*) and aorta (*Ao*) arises from the trabeculated right ventricle (*RV*), typical of physiologically uncorrected transposition. Panel (**d**) is an oblique axial view showing a large ventricular septal defect (*arrow*). *RV* right ventricle, *LV* left ventricle, *A* aortic valve, *P* pulmonic valve

atrium to left ventricle to pulmonary artery. Mixing of oxygenated and deoxygenated blood occurs via an obligatory atrial or ventricular septal defect or patent ductus arteriosus.

The clinical features and surgical management of patients with TGA are dependent on the presence or absence of a VSD and/or left ventricular outflow tract obstruction [59]. Based on these parameters, there are four anatomic subgroups of TGA: (1) transposition of the great arteries with intact ventricular septum, (2) transposition of the great arteries with ventricular septal defect, (3) transposition of the

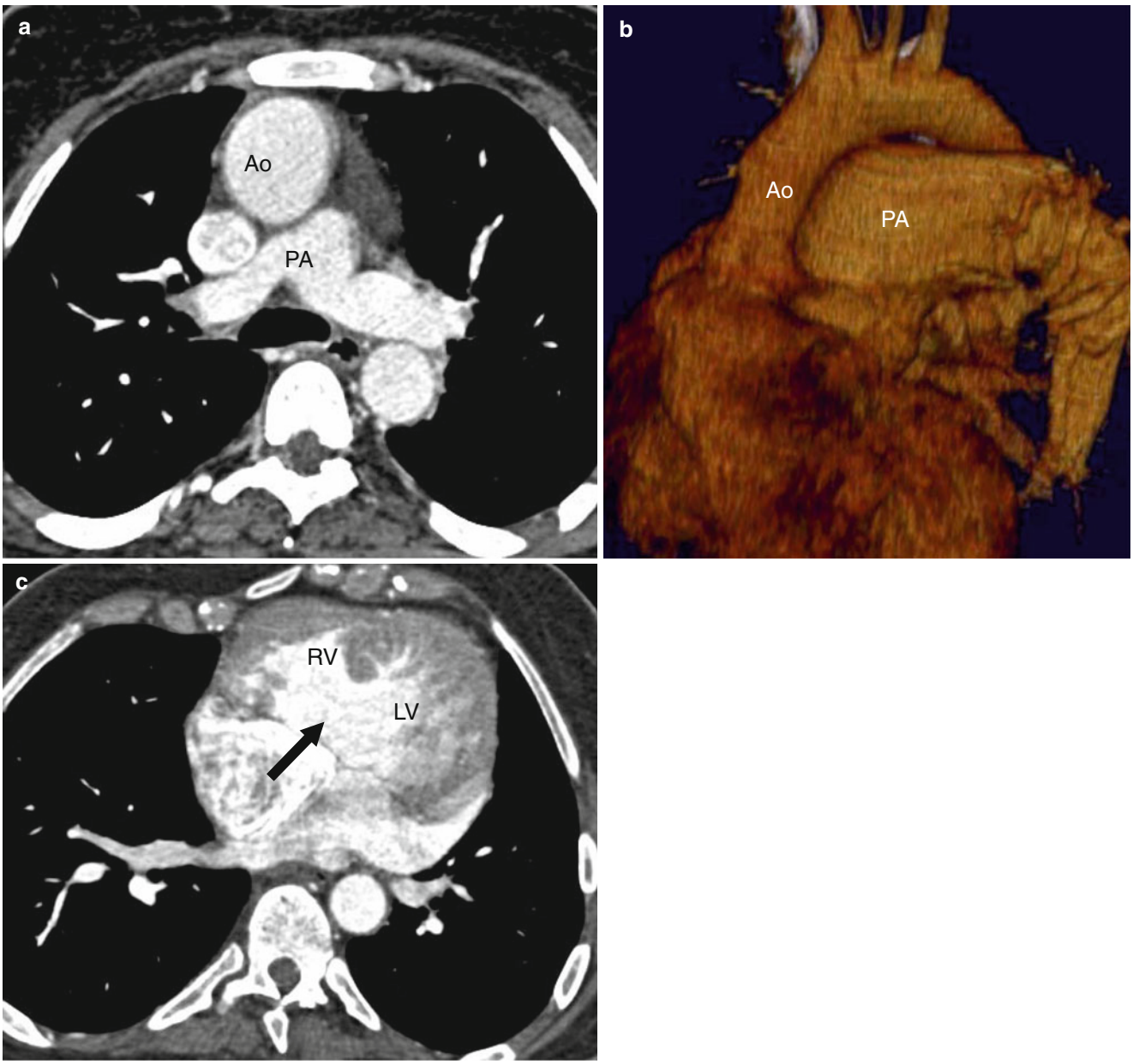


**Fig. 19.21** Uncorrected transposition of the great arteries. A 54-year-old woman with a right sided Blalock–Taussig and no further surgery. A computed tomogram was performed to evaluate for possible Eisenmenger physiology. Panel (**a**) is an axial cut and panel (**b**) is an oblique sagittal image, and both show the aorta (*Ao*) anterior and to the right of the pulmonary artery (*PA*). Panel (**c**) is an axial view illustrating a well-formed right ventricle (*RV*) and left ventricle (*LV*) with a large ventricular septal defect (*arrow*)

great arteries with ventricular septal defect and left ventricular outflow tract obstruction, and (4) transposition of the great arteries with ventricular septal defect and pulmonary vascular obstructive disease.

The VSDs are usually of perimembranous and muscular type. Left ventricular outflow tract obstruction can occur at both the valvular and subvalvular levels. The causes of obstruction include septal hypertrophy, posterior malalignment of the outlet septum, fibrous ridges, tissue tags, membranous septum aneurysm, and anomalous chordal attachment of the mitral valve [58].

Table 19.5 lists the common associated anomalies with uncorrected TGA.

Coronary artery anomalies in patients with TGA are often described on the basis of the Leiden convention [59, 63]. In this classification, the coronary arteries are termed "right" and "left" according to the predominant aortic sinus from which they arise and the aortic sinuses are designated as fac-

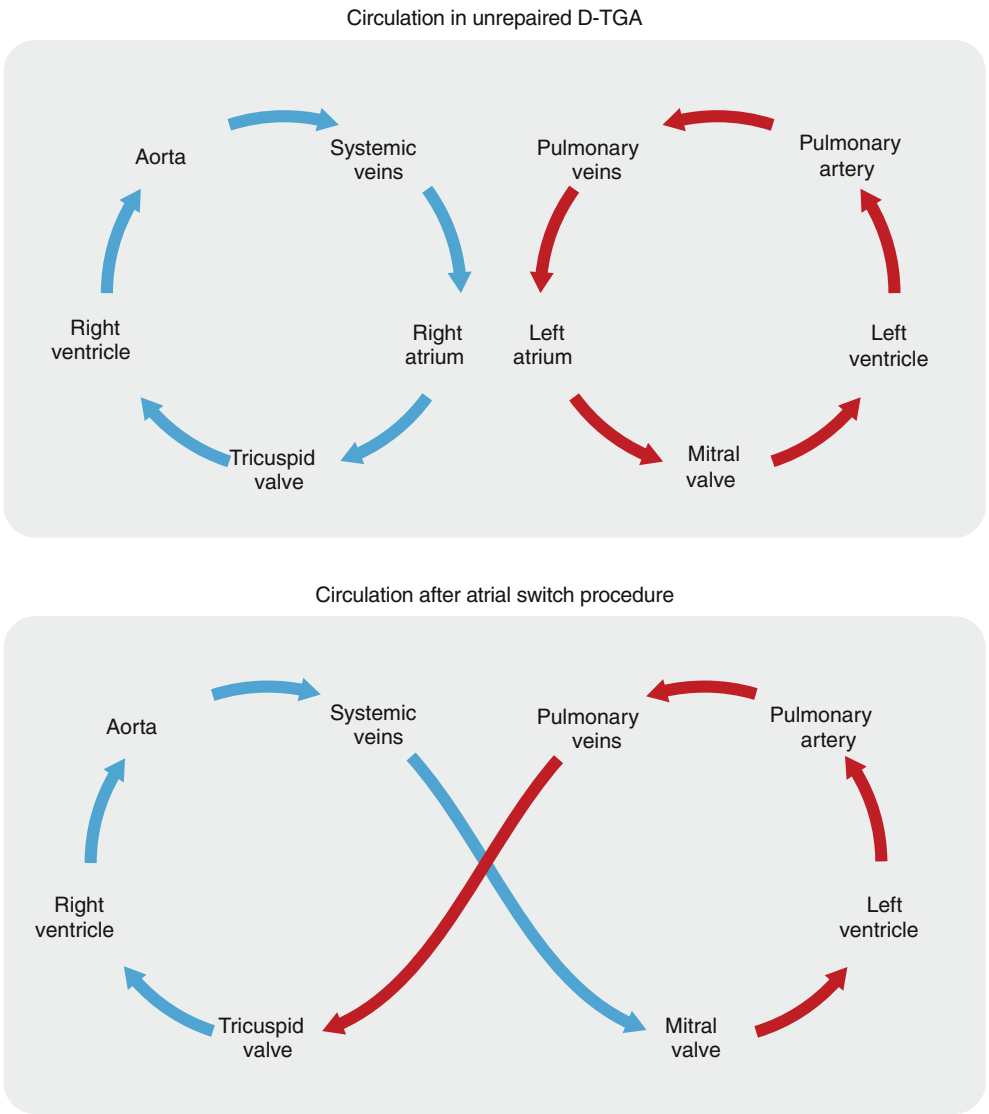


**Fig. 19.22** Diagram of the normal physiologic circulation (*in series*) and the abnormal parallel circulation in uncorrected transposition of the great arteries (*TGA*) (Radiological Society of North America, Oak Brook, IL from Lu et al. [62])

**Table 19.5** Coexisting anomalies in transposition of great arteries

| |
|---|
| Coronary artery anomalies |
| Patent ductus arteriosus |
| Ventricular septal defect |
| Left ventricular outflow tract obstruction |
| Atrial septal defect |
| Coarctation of aorta or interrupted aortic arch |
| Tricuspid valve abnormalities |
| Right aortic arch |

ing or nonfacing sinuses. This method of description is detailed in Chap. 18 and illustrated in Fig. 18.5. Briefly in review, this method of description positions a hypothetical observer in the aorta, with his head directed toward the pulmonary trunk and his feet toward the heart, and the sinuses are named sinus 1 (sinus facing toward the right hand), sinus 2 (sinus facing toward the left hand), and sinus 3 (nonfacing sinus). This means that the left coronary artery and the circumflex artery arise from sinus 1 and the right coronary artery arises from the sinus 2. These sinuses have a constant identity regardless of the spatial relationships of the great arteries. Conversely, if the observer is positioned in the pulmonary trunk looking toward the aorta, the left-facing sinus is called sinus 1, while the right-facing sinus is called sinus 2 [64]. The Leiden convention has been widely used by the surgical community, but it is limited by the inability to define epicardial or intramural course of the coronary arteries, origin of additional arteries like sinus node arteries, and the rare cases of coronary origin from the nonfacing sinus [59, 65].

Thus, a revised classification scheme has been suggested to capture all possible patterns of coronary anatomy with TGA. This includes the sinus from which the coronary artery arises (based on standard Leiden classification) as well as the position of the coronary artery within the sinus (central, right pericommissural, left pericommissural), the presence or an intramural course of the coronary artery, and the relationship

of the intramural coronary to the sinus and commissure (within sinus, above sinus, across commissure) [59].

Different coronary artery anatomy arrangements are present in subjects with TGA. The most common coronary artery pattern is the left coronary artery arising from sinus 1 (right-hand sinus) and the right coronary artery from sinus 2 (left-hand sinus) (62.5 %). The second most common type of coronary artery pattern is the right coronary artery and circumflex artery arising from (left-hand sinus) and the left anterior descending artery from sinus 1 (right-hand sinus) the coronary artery branches arise from the nonfacing sinus.

The coexisting anomalies include patent ductus arteriosus (75 % of cases), ventricular septal defect (VSD) (40–45 %), left ventricular outflow tract obstruction (25 %), atrial septal defect (ASD) (10–20 %), coarctation of the aorta or interrupted aortic arch (5 %), tricuspid valve abnormalities (4 %) (often Ebstein anomaly), and right aortic arch (4 %) [59, 66].

The clinical presentation in patients with complete transposition of the great vessels (ventriculoarterial discordance) depends on the presence or absence and size of the VSD. Patients with intact ventricular septum or with VSDs and left ventricular outflow tract obstruction usually have extreme cyanosis at birth. Patients with large VSDs may have mild cyanosis at birth and signs of heart failure. Patients with a VSD and pulmonary vascular obstructive disease may present later in life with right (systemic) ventricular failure due to high-pressure afterload.

In the neonate, initial treatment consists of maintaining ductal patency with prostaglandin $E_1$ to promote left-to-right mixing at the arterial level. This is particularly important in patients with left ventricular outflow tract obstruction. A balloon atrial septostomy also may be required to allow mixing of systemic and pulmonary venous return at the atrial level [67, 68]. Definitive repair has been accomplished by atrial switch repair, arterial switch operations, and Rastelli operations [69–72].

The atrial switch operation (creation of a baffle to redirect systemic and pulmonary venous return to the contralateral ventricle) was the initial operation for repair of TGA [66, 70, 71]. Because of significant complications, this was replaced by the arterial switch (Jatene) operation, which provides anatomical correction by re-anastomosing the great arteries to their respective ventricles. The arterial switch procedure is the ideal operation in patients with TGA with intact ventricular septum and in those with small or moderate nonrestrictive VSDs. The atrial switch repair, however, is still an option in patients with large nonrestrictive VSDs, left ventricular outflow obstruction, or pulmonary vascular obstruction. The Rastelli operation (VSD closure and creation of left ventricle-to-aortic tunnel and right ventricle-to-pulmonary artery conduit) also has been performed in patients with VSDs and left outflow tract obstruction [72].

See Chaps. 23, 24, and 26 for a further discussion of these procedures.

The prognosis in surgically uncorrected TGA is poor with a 6-month mortality rate of 90 %. Most infants die in the first few months of life. Occasionally, those with balanced circulation may reach adulthood without interventions. Reparative surgery has dramatically changed this outcome and operated patients survive frequently into adulthood. Nevertheless, they may develop a variety of complications, which should be thoroughly evaluated during regular follow-up.

The surgical complications are briefly reviewed herein but are discussed in more detail in their respective Chaps. (23, 24, and 26). The frequent complications of the atrial switch are stenosis or leak of the surgical caval or pulmonary venous baffle connections, tricuspid valve regurgitation, right (systemic) ventricular dysfunction, and heart failure. The major complications of the arterial switch (Jatene operation) are coronary artery stenosis related to reimplantation, obstruction of the right or left ventricular outflow tracts at the anastomotic sites, and aortic regurgitation. Complications of the Rastelli operation are residual or recurrent VSD and obstruction of the left or right ventricular outflow tracts.

### 19.5.1 Cardiac Computed Tomography (CT) in Complete Transposition of the Great Vessels (Ventriculoarterial Discordance)

CT is an important noninvasive imaging modality for detection and assessment of hemodynamically significant complications in patients with corrected TGA [14–17, 53]. CT is often preferred over magnetic resonance imaging due to the frequent presence of pacemakers in patients with arrhythmias.

CT evaluation of patients with surgically corrected TGA should include the following assessments: (a) morphology, size, and patency of surgical repairs (most commonly atrial, arterial, and Rastelli); (b) morphology, size, and function of both ventricles; (c) morphology, size, and function of both atria; (d) morphology of systemic and pulmonary veins to rule out obstruction; (e) morphology and size of left and right ventricular outflow tracts (aorta and pulmonary arteries) to exclude dilatation or stenosis; (f) morphology and size of septal defects; (g) cardiac valves for regurgitation; and (h) associated coronary or other anomalies.

Refer to the relevant Chaps. (23, 24, and 26) for more details on the CT evaluations.

## References

1. Huehnergarth KV, Gurvitz M, Stout KK, Otto CM. Repaired tetralogy of Fallot in the adult: monitoring and management. Heart. 2008;94:1663–9. doi:10.1136/hrt.2008.147249.
2. Gatzoulis MA. Tetralogy of Fallot. In: Gatzoulis MA, Webb GD, Daubeney PEF, editors. Diagnosis and management of adult

congenital heart disease. 1st ed. Edinburgh: Churchill Livingstone; 2003. p. 315.
3. Anderson RH, Weinberg PM. The clinical anatomy of tetralogy of Fallot. Cardiol Young. 2005;15 Suppl 1:38–47.
4. Alva C, Ho SY, Lincoln CR, Rigby ML, Wright A, Anderson RH. The nature of the obstructive muscular bundles in double-chambered right ventricle. J Thorac Cardiovasc Surg. 1999;117:1180–9.
5. Alfieri O, Blackstone EH, Kirklin JW, Pacifico AD, Bargeron Jr LM. Surgical treatment of tetralogy of Fallot with pulmonary atresia. J Thorac Cardiovasc Surg. 1978;76:321–35.
6. Wilcox BR. Lesions with normal segment connections. In: Wilcox BR, Cook AC, Anderson RH, editors. Surgical anatomy of the heart. 1st ed. Cambridge/New York: Cambridge University Press; 2004. p. 205.
7. Macartney FJ, Scott O, Deverall PB. Haemodynamic and anatomical characteristics of pulmonary blood supply in pulmonary atresia with ventricular septal defect – including a case of persistent fifth aortic arch. Br Heart J. 1974;36:1049–60.
8. Pahl E, Fong L, Anderson RH, Park SC, Zuberbuhler JR. Fistulous communications between a solitary coronary artery and the pulmonary arteries as the primary source of pulmonary blood supply in tetralogy of Fallot with pulmonary valve atresia. Am J Cardiol. 1989;63:140–3.
9. Rossi RN, Hislop A, Anderson RH, Martins FM, Cook AC. Systemic-to-pulmonary blood supply in tetralogy of Fallot with pulmonary atresia. Cardiol Young. 2002;12:373–88.
10. Apitz C, Webb GD, Redington AN. Tetralogy of Fallot. Lancet. 2009;374:1462–71. doi:10.1016/S0140-6736(09)60657-7.
11. Anderson RH, Allwork SP, Ho SY, Lenox CC, Zuberbuhler JR. Surgical anatomy of tetralogy of Fallot. J Thorac Cardiovasc Surg. 1981;81:887–96.
12. Neirotti R, Galindez E, Kreutzer G, Rodriguez Coronel A, Pedrini M, Becu L. Tetralogy of Fallot with subpulmonary ventricular septal defect. Ann Thorac Surg. 1978;25:51–6.
13. van Straten A, Vliegen HW, Lamb HJ, Roes SD, van der Wall EE, Hazekamp MG, et al. Time course of diastolic and systolic function improvement after pulmonary valve replacement in adult patients with tetralogy of Fallot. J Am Coll Cardiol. 2005;46:1559–64. doi:10.1016/j.jacc.2005.07.030.
14. Hughes D, Siegel MJ. Computed tomography of adult congenital heart disease. Radiol Clin N Am. 2010;48:817–35.
15. Leschka S, Oechslin E, Husmann L, et al. Pre- and postoperative evaluation of congenital heart disease in children and adults with 64-section CT. Radiographics. 2007;27:829–46.
16. Siegel MJ, Bhalla S, Gutierrez FR, Billadello JB. MDCT of postoperative anatomy and complications in adults with cyanotic heart disease. AJR Am J Roentgenol. 2005;184:241–7.
17. Wiant A, Nyberg E, Gilkeson RC. CT evaluation of congenital heart disease in adults. AJR Am J Roentgenol. 2009;19:388–96.
18. Walters 3rd HL, Mavroudis C, Tchervenkov CI, Jacobs JP, Lacour-Gayet F, Jacobs ML. Congenital heart surgery nomenclature and database project: double outlet right ventricle. Ann Thorac Surg. 2000;69:S249–63.
19. Mitchell SC, Korones SB, Berendes HW. Congenital heart disease in 56,109 births. Incidence and natural history. Circulation. 1971; 43:323–32.
20. Anderson RH, McCarthy K, Cook AC. Continuing medical education. Double outlet right ventricle. Cardiol Young. 2001;11: 329–44.
21. Brandt PW, Calder AL, Barratt-Boyes BG, Neutze JM. Double outlet left ventricle. Morphology, cineangiocardiographic diagnosis and surgical treatment. Am J Cardiol. 1976;38:897–909.
22. Van Arsdell GS. Double-outlet right ventricle. In: Gatzoulis MA, Webb GD, Daubeney PEF, editors. Diagnosis and management of adult congenital heart disease. 1st ed. Edinburgh: Churchill Livingstone; 2003. p. 389.
23. Mahle WT, Martinez R, Silverman N, Cohen MS, Anderson RH. Anatomy, echocardiography, and surgical approach to double outlet right ventricle. Cardiol Young. 2008;18 Suppl 3:39–51. doi:10.1017/S1047951108003284.
24. Kirklin JW, Pacifico AD, Blackstone EH, Kirklin JK, Bargeron Jr LM. Current risks and protocols for operations for double-outlet right ventricle. Derivation from an 18 year experience. J Thorac Cardiovasc Surg. 1986;92:913–30.
25. Musumeci F, Shumway S, Lincoln C, Anderson RH. Surgical treatment for double-outlet right ventricle at the Brompton Hospital, 1973 to 1986. J Thorac Cardiovasc Surg. 1988;96:278–87.
26. Sondheimer H, Freedom R, Olley P. Double outlet right ventricle: clinical spectrum and prognosis. Am J Cardiol. 1977;39:709–14. doi:10.1016/S0002-9149(77)80133-1.
27. Goor DA, Ebert PA. Left ventricular outflow obstruction in taussig-bing malformation. J Thorac Cardiovasc Surg. 1975;70:69–75.
28. Pandit SP, Shah VK, Daruwala DF. Double outlet right ventricle with intact interventricular septum – a case report. Indian Heart J. 1987;39:56–7.
29. Tabry IF, McGoon DC, Danielson GK, Wallace RB, Davis Z, Maloney JD. Surgical management of double-outlet right ventricle associated with atrioventricular discordance. J Thorac Cardiovasc Surg. 1978;76:336–44.
30. Alfieri O, Crupi G, Vanini V, Parenzan L. Successful surgical repair of double outlet right ventricle with situs inversus, l-loop, l-malposition and subaortic VSD in a 16-month-old patient. Eur J Cardiol. 1978;7:41–7.
31. Danielson GK, Tabry IF, Ritter DG, Maloney JD. Successful repair of double-outlet right ventricle, complete atrioventricular canal, and atrioventricular discordance associated with dextrocardia and pulmonary stenosis. J Thorac Cardiovasc Surg. 1978;76:710–7.
32. Piccoli G, Pacifico AD, Kirklin JW, Blackstone EH, Kirklin JK, Bargeron Jr LM. Changing results and concepts in the surgical treatment of double-outlet right ventricle: analysis of 137 operations in 126 patients. Am J Cardiol. 1983;52:549–54.
33. Ceithaml EL, Puga FJ, Danielson GK, McGoon DC, Ritter DG. Results of the damus-stansel-kaye procedure for transposition of the great arteries and for double-outlet right ventricle with subpulmonary ventricular septal defect. Ann Thorac Surg. 1984;38: 433–7.
34. Kanter K, Anderson R, Lincoln C, Firmin R, Rigby M. Anatomic correction of double-outlet right ventricle with subpulmonary ventricular septal defect (the "Taussig-Bing" anomaly). Ann Thorac Surg. 1986;41:287–92.
35. Rubay J, Lecompte Y, Batisse A, Durandy Y, Dibie A, Lemoine G, et al. Anatomic repair of anomalies of ventriculo-arterial connection (REV). Results of a new technique in cases associated with pulmonary outflow tract obstruction. Eur J Cardiothorac Surg. 1988;2:305–11.
36. Vouhe PR, Tamisier D, Leca F, Ouaknine R, Vernant F, Neveux JY. Transposition of the great arteries, ventricular septal defect, and pulmonary outflow tract obstruction. Rastelli or Lecompte procedure? J Thorac Cardiovasc Surg. 1992;103:428–36.
37. Tchervenkov CI, Walters 3rd HL, Chu VF. Congenital heart surgery nomenclature and database project: double outlet left ventricle. Ann Thorac Surg. 2000;69:S264–9.
38. Hagler DJ. Double-outlet right ventricle and double-outlet left ventricle. In: Moss AJ, Allen HD, editors. Moss and Adams' heart disease in infants, children, and adolescents: including the fetus and young adult. 7th ed. Philadelphia: Wolters Kluwer/Lippincott Williams & Wilkins; 2008.
39. Menon SC, Hagler DJ. Double-outlet left ventricle: diagnosis and management. Curr Treat Options Cardiovasc Med. 2008;10:448–52.
40. Bharati S, Lev M, Stewart R, McAllister Jr HA, Kirklin JW. The morphologic spectrum of double outlet left ventricle and its surgical significance. Circulation. 1978;58:558–65.

41. Van Praagh R, Weinberg PM, Srebro JP. Double-outlet left ventricle. In: Van Praagh R, Van Praagh S, editors. Diagnostic and surgical pathology of congenital heart diseases, vol. 2. Washington, DC: Health Video Dynamics, Inc.; 1991. p. 1106–30.
42. Kirklin JW. Double outlet left ventricle. In: Kirklin JW, Barratt-Boyes BG, editors. Cardiac surgery: morphology, diagnostic criteria, natural history, techniques, results, and indications. 2nd ed. New York: Churchill Livingstone; 1992.
43. Pacifico AD, Kirklin JW, Bargeron Jr LM, Soto B. Surgical treatment of double-outlet left ventricle. Report of four cases. Circulation. 1973;48:III19–23.
44. Jacobs ML. Congenital heart surgery nomenclature and database project: truncus arteriosus. Ann Thorac Surg. 2000;69:S50–5.
45. Van Praagh R, Van Praagh S. The anatomy of common aorticopulmonary trunk (truncus arteriosus communis) and its embryologic implications. A study of 57 necropsy cases. Am J Cardiol. 1965; 16:406–25.
46. Ebert PA, Turley K, Stanger P, Hoffman JI, Heymann MA, Rudolph AM. Surgical treatment of truncus arteriosus in the first 6 months of life. Ann Surg. 1984;200:451–6.
47. Di Donato RM, Fyfe DA, Puga FJ, Danielson GK, Ritter DG, Edwards WD, et al. Fifteen-year experience with surgical repair of truncus arteriosus. J Thorac Cardiovasc Surg. 1985;89: 414–22.
48. Marcelletti C, McGoon DC, Mair DD. The natural history of truncus arteriosus. Circulation. 1976;54:108–11.
49. Connelly M. Common arterial trunk. In: Gatzoulis MA, Webb GD, Daubeney PEF, editors. Diagnosis and management of adult congenital heart disease. 1st ed. Edinburgh: Churchill Livingstone; 2003. p. 265–72.
50. Collett RW, Edwards JE. Persistent truncus arteriosus; a classification according to anatomic types. Surg Clin North Am. 1949;29: 1245–70.
51. McGoon DC, Rastelli GC, Ongley PA. An operation for the correction of truncus arteriosus. JAMA. 1968;205:69–73.
52. Kimura-Hayama ET, Melendez G, Mendizabal AL, et al. Uncommon congenital and acquired aortic diseases: role of multidetector CT angiography. Radiographics. 2010;30:79–98.
53. Siegel MJ, Earls J, Chan F. Thoracic vascular anomalies. In: Rubin G, Rofsky N, editors. CT and MR angiography. Philadelphia: Lippincott Williams & Wilkins; 2009. p. 543–95.
54. Henry TS, Bhalla S, Siegel MJ. Pediatric congenital heart disease. Appl Radiol. 2011.
55. Patel RJ, Zakir RM, Sethi V, et al. A rare case of unrepaired tetralogy of Fallot with right hemitruncus in an adult. Texas Heart Inst J. 2007;34:250–1.
56. Rosa U, Wade KC. CT findings in hemitruncus. J Comput Assist Tomogr. 1987;11(4):698–700.
57. Van Praagh R, Perez-Trevino C, Lopez-Cuellar M, Baker FW, Zuberbuhler JR, Quero M, et al. Transposition of the great arteries with posterior aorta, anterior pulmonary artery, subpulmonary conus and fibrous continuity between aortic and atrioventricular valves. Am J Cardiol. 1971;28:621–31.
58. Anderson RH, Weinberg PM. The clinical anatomy of transposition. Cardiol Young. 2005;15 Suppl 1:76–87.
59. Jaggers JJ, Cameron DE, Herlong JR, Ungerleider RM. Congenital heart surgery nomenclature and database project: transposition of the great arteries. Ann Thorac Surg. 2000;69:S205–35.
60. Wilcox BR, Cook AC, Anderson RH. Lesions in hearts with abnormal segmental connections. In: Wilcox BR, Cook AC, Anderson RH, editors. Surgical anatomy of the heart. 1st ed. Cambridge/New York: Cambridge University Press; 2004. p. 215–74.
61. Hornung T. Transposition of the great arteries. In: Gatzoulis MA, Webb GD, Daubeney PEF, editors. Diagnosis and management of adult congenital heart disease. 1st ed. Edinburgh: Churchill Livingstone; 2003. p. 349–62.
62. Lu JC, Dorfman AL, Attili AK, Ghadimi Mahani M, Dillman JR, Agarwal PP. Evaluation with cardiovascular MR imaging of baffles and conduits used in palliation or repair of congenital heart disease. Radiographics. 2012;32:E107–27.
63. Gittenberger-de-Groot AC, Sauer U, Opeenheimer-Dekker A, Quaegebeur JM. Coronary artery anatomy in transposition of the great arteries: a morphologic study. Pediatr Cardiol. 1983;4(Suppl l):l-15–24.
64. Amato JJ, Zelen J, Bushong J. Coronary arterial patterns in complete transposition – classification in relation to the arterial switch procedure. Cardiol Young. 1994;4:329–39. doi:10.1017/S1047951100002304.
65. Skinner J, Hornung T, Rumball E. Transposition of the great arteries: from fetus to adult. Heart. 2008;94:1227–35. doi:10.1136/hrt.2006.104737.
66. Warnes CA, Williams RG, Bashore TM, Child JS, Connolly HM, Dearani JA, et al. ACC/AHA 2008 guidelines for the management of adults with congenital heart disease: a report of the American College of Cardiology/American Heart Association task force on practice guidelines (writing committee to develop guidelines on the management of adults with congenital heart disease). Circulation. 2008;118:e714–833. doi:10.1161/CIRCULATIONAHA.108.190690.
67. Rashkind WJ, Miller WW. Creation of an atrial septal defect without thoracotomy. A palliative approach to complete transposition of the great arteries. JAMA. 1966;196:991–2.
68. Blalock A, Hanlon CR. The surgical treatment of complete transposition of the aorta and the pulmonary artery. Surg Gynecol Obstet. 1950;90:1–15, illust.
69. Jatene AD, Fontes VF, Paulista PP, Souza LC, Neger F, Galantier M, et al. Anatomic correction of transposition of the great vessels. J Thorac Cardiovasc Surg. 1976;72:364–70.
70. Senning A. Surgical correction of transposition of the great vessels. Surgery. 1959;45:966–80.
71. Mustard WT. Successful two-stage correction of transposition of the great vessels. Surgery. 1964;55:469–72.
72. Rastelli GC, McGoon DC, Wallace RB. Anatomic correction of transposition of the great arteries with ventricular septal defect and subpulmonary stenosis. J Thorac Cardiovasc Surg. 1969;58: 545–52.

# Heterotaxy Syndrome

# 20

"Heterotaxy" is simply defined as an abnormality of situs where the internal thoracic and abdominal organs show an arrangement other than situs solitus or inversus [1]. The term is synonymous with "situs ambiguous."

The incidence of heterotaxy is estimated to be 1 in 10,000 live births [2]. It is associated with a spectrum of cardiac malformations varying from relatively simple anomalies to very complex defects [3].

Heterotaxy is not one specific finding but rather it is a constellation of atrial, visceral, and cardiovascular abnormalities. The morphologic spectrum of the heterotaxy syndrome includes atrial isomerism, abnormal thoracic and abdominal visceral situs (in particular the presence or absence of the spleen), anomalous systemic or pulmonary venous return, and associated cardiac defects [4–6].

## 20.1 Atrial Isomerism

The atria maintain their laterality throughout development; hence, they define the cardiac situs. In normal individuals, the morphologic right atrium is on the same side as the morphologic right-sided thoracic and visceral structures. Likewise, the morphologic left atrium is on the same side as the morphologic left-sided thoracic and abdominal structures.

At imaging, the atria can be recognized by their different anatomy (described in detail in Sect. 1.2). Briefly, the right atrium is the more trabeculated atrium with the broad-based appendage and receives blood from the vena cava. The left atrium has a smaller, narrower appendage and receives blood from the pulmonary veins (Fig. 20.1).

Atrial isomerism refers to hearts with bilaterally right or bilaterally left atrial appendages [4–6]. *Right atrial isomerism* is characterized by the presence of a morphologic right atrium on both the right and left sides of the midline (Fig. 20.2). Likewise, *left atrial isomerism* is characterized by morphologically bilateral left atria (Fig. 20.3). Although atrial isomerism is often present in heterotaxy syndrome, it is not a reliable term to describe the syndrome because it inaccurately reflects the full constellation of abnormalities.

If the atria are not distinguishable based on morphology, then determination of atrial situs can be made based on localization of noncardiac structures, namely, the tracheobronchial tree morphology (i.e., tracheobronchial situs). The right superior branch of the right main bronchus is eparterial, meaning that it is located above the segmental pulmonary artery that supplies the superior lobe of the right lung. The left superior bronchus is hyparterial and passes below the pulmonary arteries. The right, middle, and inferior lobar bronchi and left inferior lobar bronchus are also hyparterial, passing below the arteries. In right isomerism both bronchi are eparterial (Fig. 20.4), and in left isomerism, both bronchi are hyparterial (Fig. 20.5).

Of note, neither atrial nor tracheobronchial tree morphology is a reliable marker of the position of the ventricles, the cardiac apex, or the great arteries which must be identified and reported separately. A systematic approach to the diagnosis of visceroatrial situs, which is helpful in predicting the likelihood of associated heart disease, is discussed in more detail in Chap. 5.

W. Mazur et al., *CT Atlas of Adult Congenital Heart Disease*,
DOI 10.1007/978-1-4471-5088-6_20, © Springer-Verlag London 2013

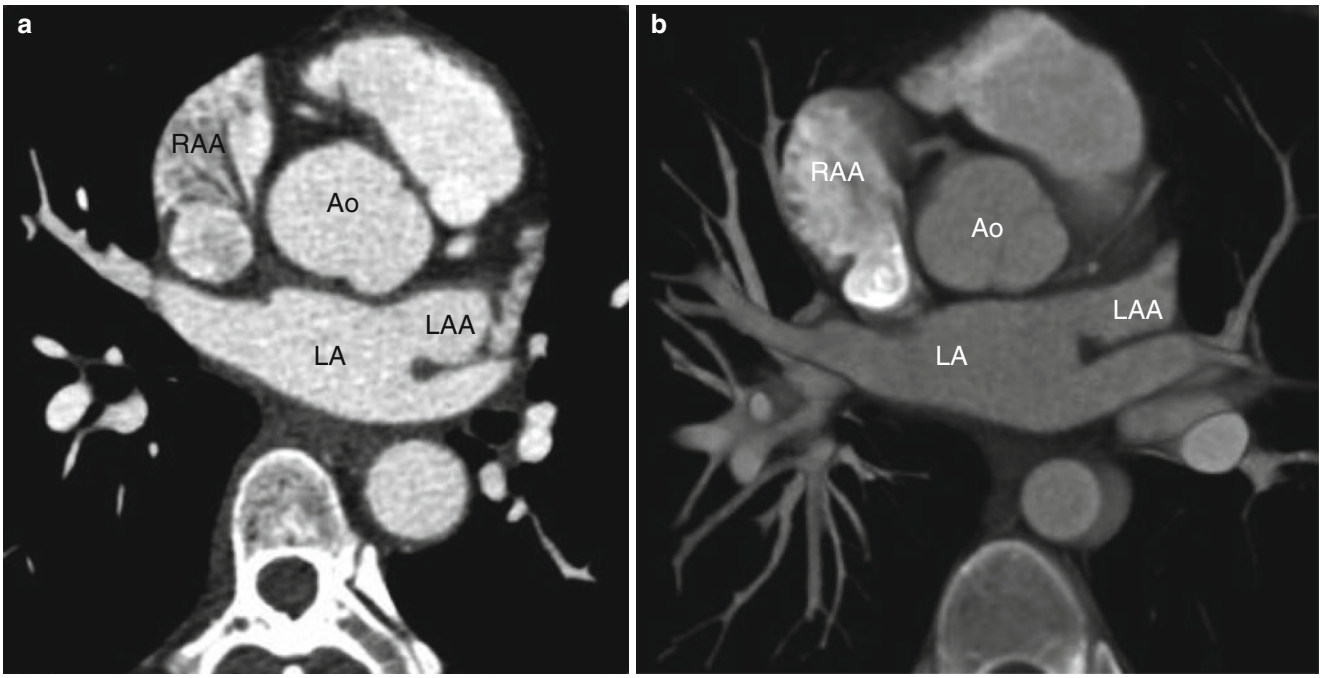


**Fig. 20.1** Atrial appendage morphology. Panels (**a**) and (**b**) are two axial computed tomography images. The right atrial appendage (*RAA*) is a blunt, broad-based structure lined with pectinate muscles that form a trabeculated surface. The left atrial appendage (*LAA*) is smaller and narrower and has a more restricted junction with the left atrium (*LA*). *Ao* aorta

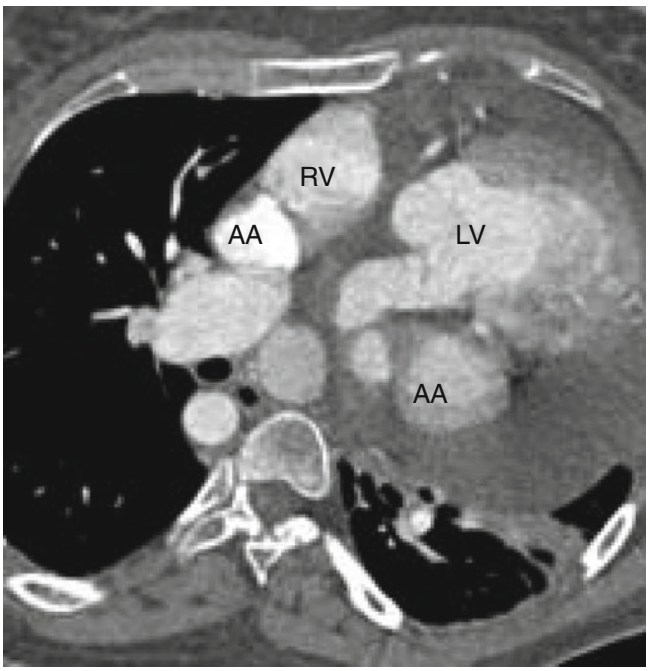


**Fig. 20.2** Right atrial isomerism. The atrial appendages (*AA*) bilaterally are broad-based structures, consistent with right atrial morphology. *RV* right ventricle, *LV* left ventricle

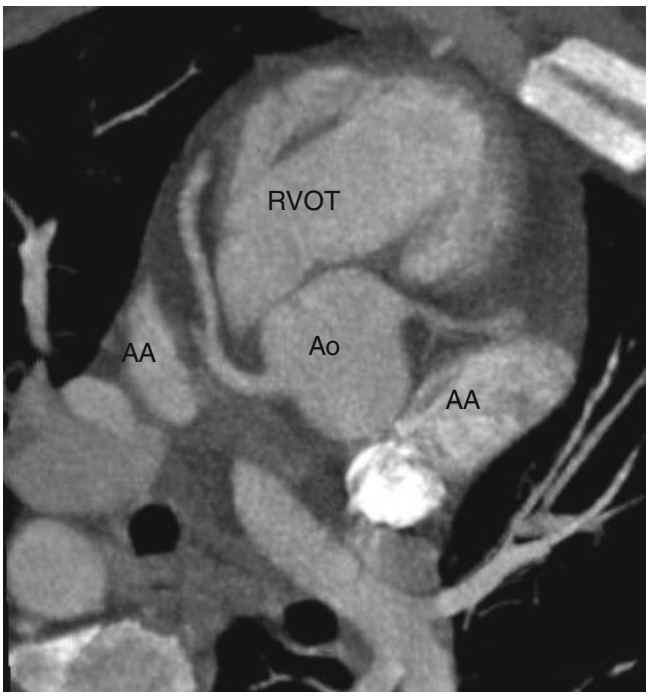


**Fig. 20.3** Left atrial isomerism. The atrial appendages (*AA*) bilaterally are elongated and fingerlike, consistent with left atrial morphology. *RVOT* right ventricular outflow tract

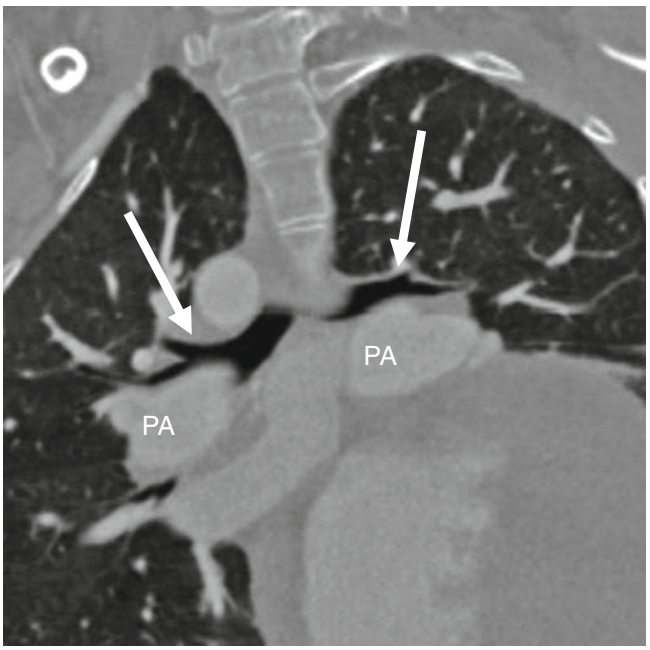


**Fig. 20.4** Right isomerism. Both bronchi (*arrows*) are eparterial and course above the pulmonary arteries (*PA*)

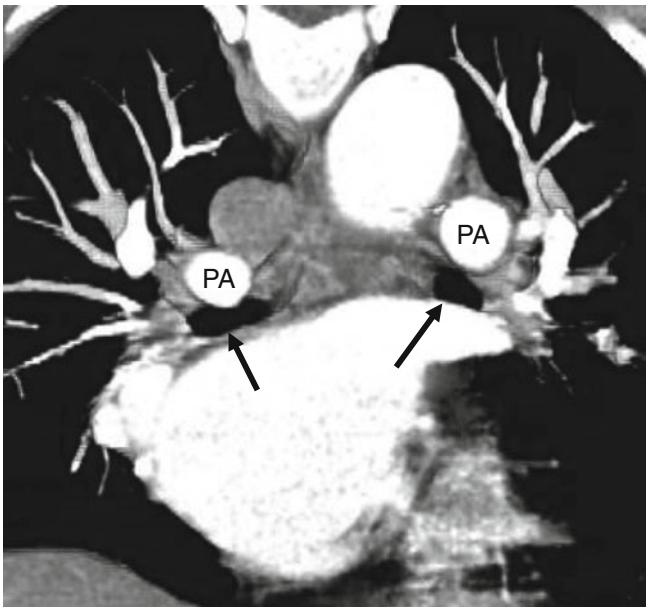


**Fig. 20.5** Left isomerism. Both bronchi (*arrows*) are hyparterial and course below the pulmonary arteries (*PA*)

## 20.2 Thoracic and Abdominal Situs

There are three types of situs: situs solitus (S), inversus (I), and ambiguous (A). As noted above, heterotaxy is synonymous with situs ambiguous.

Situs solitus is the usual arrangement of the atria and viscera. Situs solitus is characterized by a morphologic right atrium on the right side of the spine, a trilobed right lung with eparterial bronchus, and bilobed left lung with hyparterial bronchus, right-sided liver, left-sided spleen, and right-sided inferior vena cava. The normal ventricular relationship is a D-ventricular loop, with the anatomic right ventricle positioned to the right of the left ventricle. The cardiac apex and stomach are on the left side of the spine (Fig. 20.6).

Situs inversus (also called situs inversus totalis) is the "mirror image" of situs solitus. Situs inversus is characterized by a two-lobed right lung with a hyparterial bronchus and three-lobed left lung with eparterial bronchus (i.e., the morphologic left lung is right sided and the morphologic right lung is left sided), left-sided liver, and

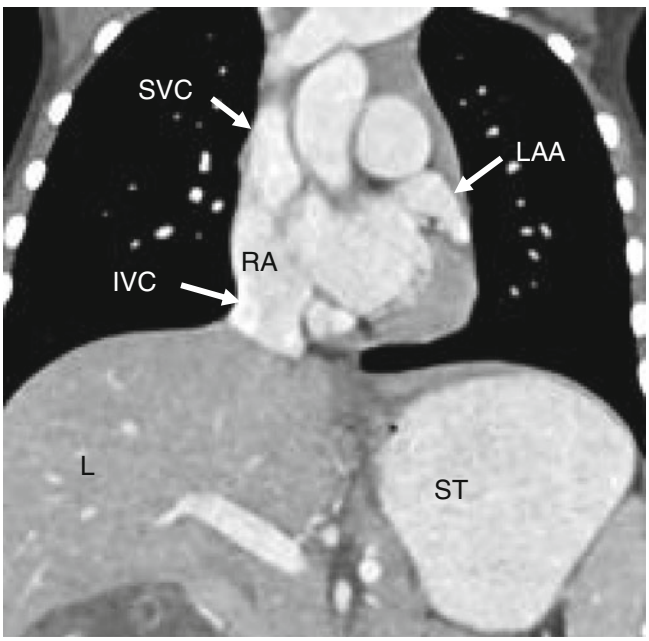


**Fig. 20.6** Situs solitus. This is the usual arrangement of organs and vessels. The morphologic right atrium (*RA*), superior vena cava (*SVC*) and inferior vena cava (*IVC*), and liver (*L*) are on the right side of the thorax. The left atrial appendage (*LAA*), cardiac apex, and stomach (*ST*) are on the left

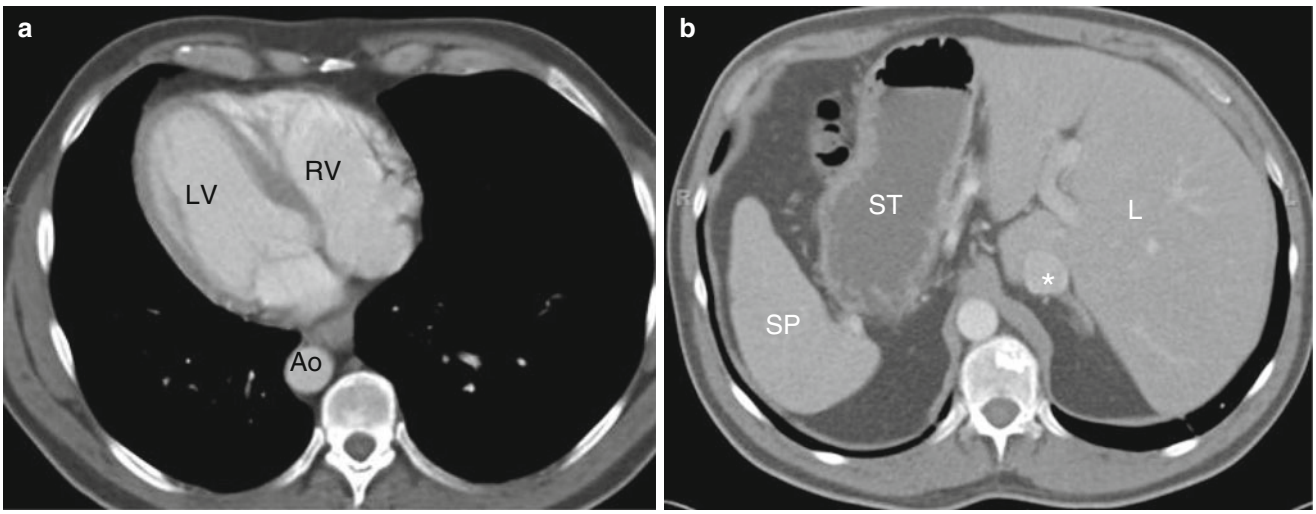


**Fig. 20.7** Situs inversus. The anatomic arrangement is the mirror image of situs solitus. Panel (**a**) illustrates that the cardiac apex and aorta (*Ao*) are on the right. The more trabeculated right ventricle (*RV*) is positioned to the left of the morphologic smoother left ventricle (*LV*). Panel (**b**) is an axial scan at a lower level showing a right-sided spleen (*SP*) and a right-sided stomach (*ST*) with a left-sided liver (*L*). Note also the left-sided inferior vena cava (*asterisk*)

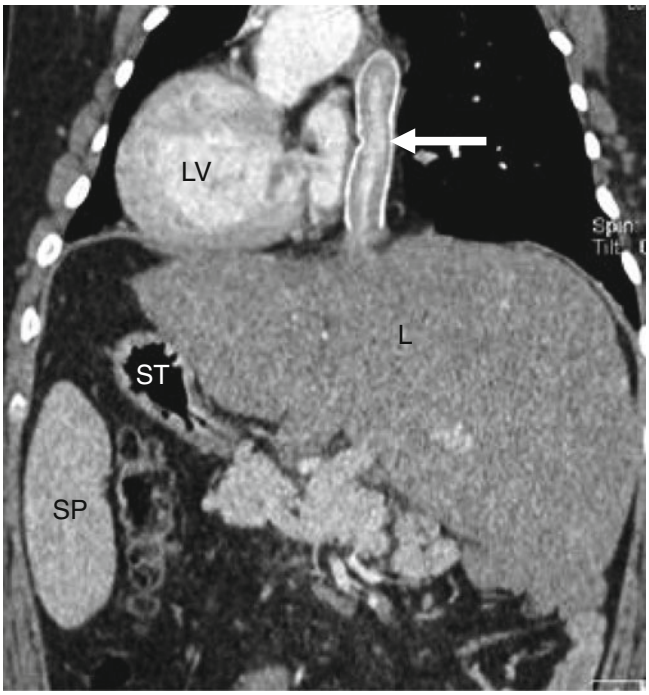


**Fig. 20.8** Situs inversus in a 30-year-old man who underwent cavopulmonary shunt for pulmonary atresia. This coronal image shows the cardiac apex, spleen (*SP*), and stomach (*ST*) on the right side of the body and the liver (*L*) on the left. *Arrow*: left-sided cavopulmonary shunt. *LV* left ventricle

right-sided spleen. There is usually an L-ventricular loop with the anatomic right ventricle positioned to the left of the left ventricle. The cardiac apex and stomach are right sided (Figs. 20.7 and 20.8).

**Table 20.1** Cardiac and extracardiac anomalies in asplenia (Ivemark syndrome)

| |
|---|
| Bilateral right sidedness |
| Cardiac anomalies: pulmonic stenosis and atresia, transposition of the great arteries or double-outlet ventricle, atrioventricular septal defect, and absent coronary sinus |
| Vascular anomalies including total anomalous venous return (frequently supracardiac type) and bilateral superior venae cavae |
| Airway morphology: trilobed lungs/eparterial bronchi |
| Abdominal findings: asplenia, horizontal liver, midline stomach, and malrotation |

Situs ambiguous refers to the abnormal arrangement of organs different from the arrangement in either situs solitus or situs inversus. There is abnormal bilateral symmetry of normally asymmetric viscera and duplication of either right- or left-sided structures. There is not one specific finding that is pathognomonic for situs ambiguous (heterotaxy) but rather there is a combination of findings seen in situs solitus and situs inversus. Heterotaxy syndromes are usually associated with congenital heart disease and splenic abnormalities and have been grouped into two major forms: (1) asplenia or Ivemark syndrome and (2) polysplenia syndrome.

Asplenia (Ivemark syndrome) (see Table 20.1) is characterized by duplication of right-sided structures (bilateral right sidedness) which includes bilateral trilobed lungs with bilateral eparterial bronchi (in other words bilateral morphologic right lungs) and bilateral right atria. Cardiac anomalies usually result in pulmonary undercirculation and cyanosis and include pulmonic stenosis or atresia (most common), discordant ventriculoarterial connection with transposition of the

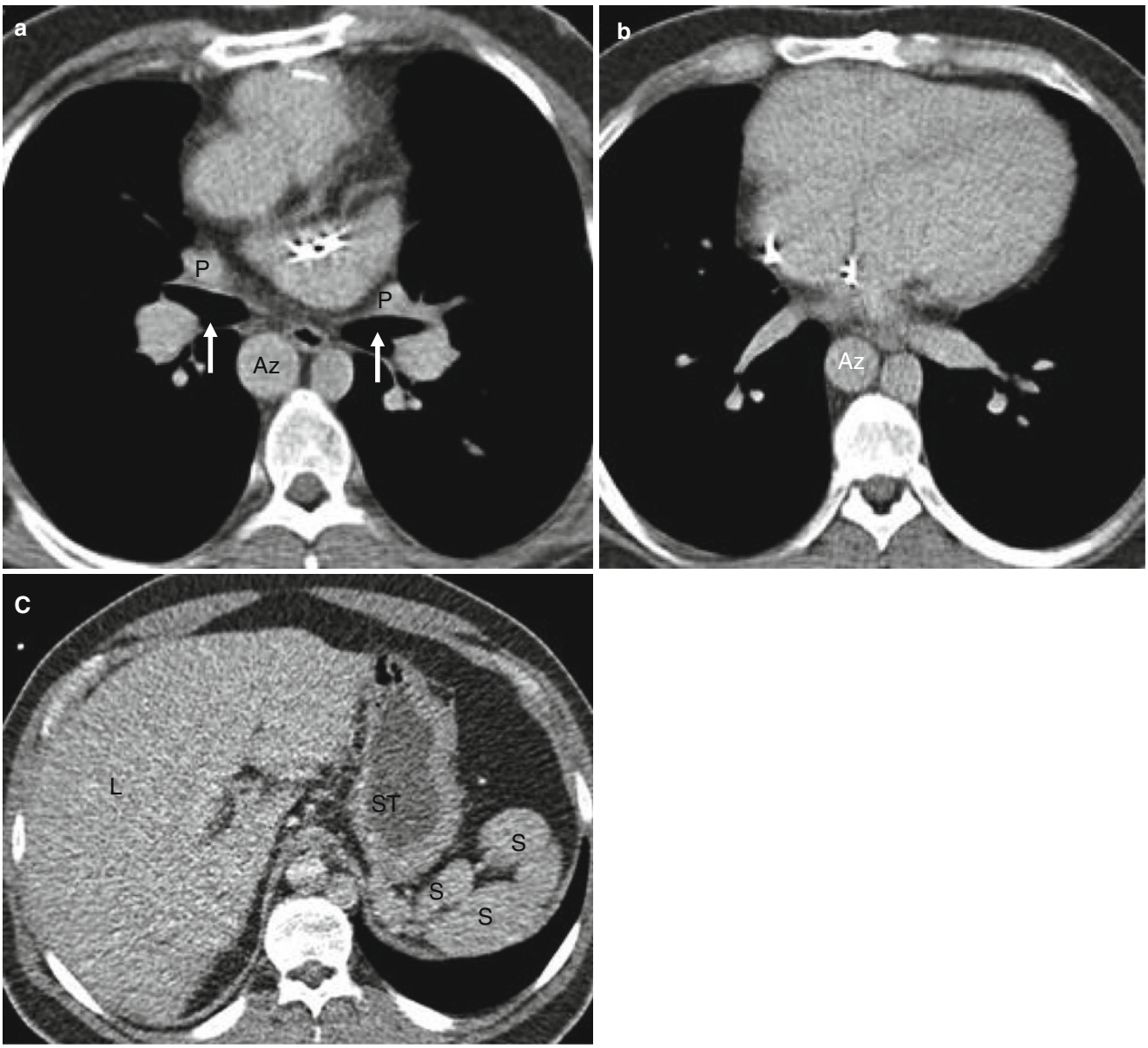


**Fig. 20.9** Polysplenia syndrome (situs ambiguous). This 27-year-old man had a history of repair of partial anomalous pulmonary venous return. Panel (**a**) demonstrates that both pulmonary arteries (*P*) are above the bronchi (*arrows*) in keeping with bilateral left sidedness. The vessels below the bronchi are pulmonary veins. Also note the dilated azygous vein (*Az*) associated with an interrupted inferior vena cava. Panel (**b**) is an image at a lower plane showing mesocardia and the dilated azygous vein (*Az*). Panel (**c**) is an axial scan through the upper abdomen showing several small, left-sided spleens (*S*) and absence of the intrahepatic segment of the inferior vena cava associated with caval interruption. Note that the liver (*L*) and stomach (*St*) are in their expected positions

great arteries or double-outlet ventricle with transposed great vessels, atrioventricular septal defect with a common atrioventricular valve, and absent coronary sinus [1, 7]. Associated vascular anomalies include total anomalous venous return (frequently supracardiac type) and bilateral superior venae cavae. Abdominal findings include an absent spleen, horizontal liver, small midline stomach, small bowel malrotation, and gallbladder agenesis (Figs. 20.9 and 20.10).

Polysplenia syndrome (see Table 20.2) is characterized by duplication of left-sided structures (bilateral left sidedness),

**Table 20.2** Cardiac and extracardiac anomalies in polysplenia

| |
|---|
| Bilateral left sidedness |
| Cardiac anomalies: atrial defect (primum or secundum), ventricular septal defect, common atrium, cor triatriatum, and double-outlet right ventricle |
| Vascular anomalies: interrupted inferior vena cava, partial anomalous pulmonary venous return, and duplicated superior vena cava |
| Airway morphology: bilobed lungs/hyparterial bronchi |
| Abdominal findings: multiple spleens, horizontal liver, intestinal malrotation, and biliary atresia |

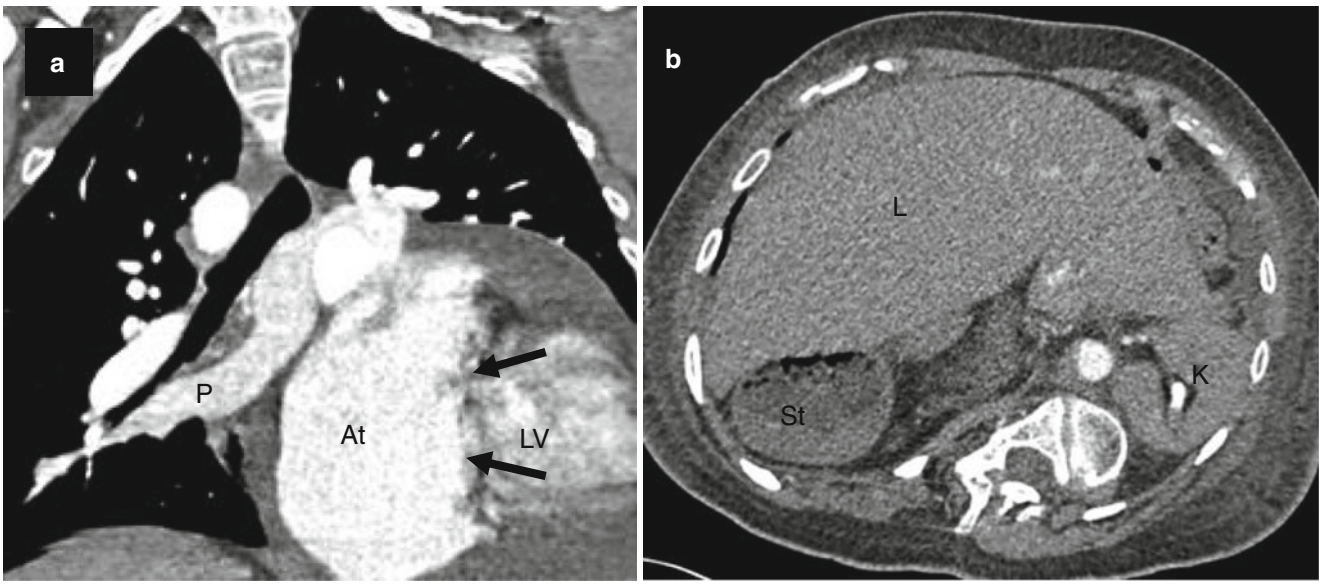


**Fig. 20.10** Asplenia syndrome (situs ambiguous) in a 31-year-old woman who has not undergone any surgical interventions. Panel (**a**) a coronal tomogram demonstrating the hyparterial right bronchus above the pulmonary artery (*P*) and a large ostium primum atrial septal defect with a common atrium (*At*) and common atrioventricular valve (*arrows*) between the common atrium and left ventricle (*LV*). Panel (**b**) an axial image showing a transverse liver (*L*), right-sided stomach (*St*), and absent spleen. *K* kidney

with bilateral bilobed lungs with bilateral hyparterial bronchi (i.e., bilateral morphologic left lungs) and bilateral left atria. Cardiac lesions associated with polysplenia are often acyanotic and include atrial septal defect (primum or secundum), ventricular septal defect, common atrium, cor triatriatum, and double-outlet right ventricle [8]. Associated vascular anomalies include interrupted inferior vena cava with azygous continuation, partial anomalous pulmonary venous return, and duplicated superior vena cava. Common concurrent abdominal anomalies are multiple small spleens, horizontal liver, small bowel malrotation, and biliary atresia.

Situs solitus, the normal pattern of organ arrangement, has less than a 1 % incidence of associated congenital heart disease. In situs inversus totalis, the incidence of associated congenital heart disease is 3–5 %. In heterotaxy, the incidence of associated congenital heart disease is also markedly increased.

Asplenia and polysplenia are clues to the presence of congenital heart disease. Asplenia is associated with congenital heart disease in 99–100 % of cases and polysplenia is associated with congenital heart malformations in approximately 75 % of cases.

Of note, about 20 % of patients with situs inversus totalis have Kartagener syndrome characterized by ciliary dyskinesia and the triad of situs inversus, chronic sinusitis, and bronchiectasis and a low incidence of associated congenital heart disease (Fig. 20.11) [8].

Palliative surgery for heterotaxy syndromes may be performed in neonates and includes systemic-to-pulmonary shunts used in the setting of decreased pulmonary blood

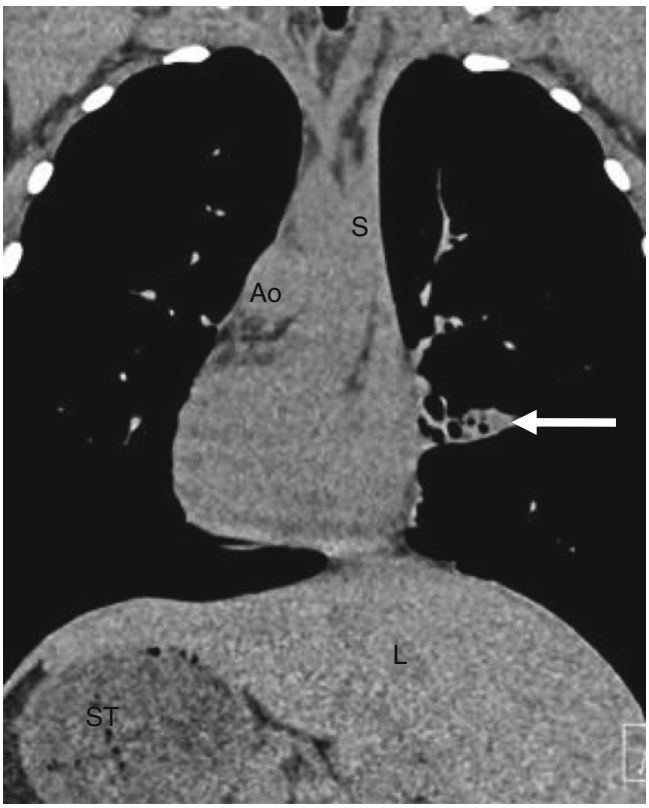


**Fig. 20.11** Kartagener syndrome in a 32-year-old man. This coronal view shows an inverted arrangement of the viscera with dextrocardia (cardiac apex to the right), right-sided aorta (*Ao*) and stomach (*St*), and left-sided superior vena cava (*S*) and liver (*L*). Note bronchiectasis (*arrow*) in the left-sided middle lobe

flow or pulmonary trunk banding in the presence of increased pulmonary blood flow. Biventricular repair is usually performed in patients with atrioventricular or ventricular septal defects with anomalies of systemic and pulmonary venous return, but with concordant ventriculoarterial connections (usually those with left atrial isomerism). Univentricular repairs are more often associated with complex malformations (usually right atrial isomerism) and include a Fontan-type procedure (bidirectional Glenn or total cavopulmonary shunt) and Kawashima operation (inferior caval vein, bidirectional cavopulmonary anastomosis in the setting of interrupted inferior caval vein with azygous continuation).

The prognosis for infants with heterotaxy and surgically uncorrected congenital heart disease is poor. Patients with left atrial isomerism tend to have a better prognosis than those with right atrial isomerism, attributed to the fact that left isomerism has less severe cardiac malformations and, hence, patients are more likely to undergo successful biventricular repairs. Patients with defects not suitable for biventricular repairs are likely to undergo univentricular procedures associated with poorer long-term prognosis [4]. Despite surgery, the percent of subjects with heterotaxy syndrome who reach adulthood is low. In right arterial isomerism, Hashimi et al. [7] reported a survival rate of 25 % at the age of 20 years and survival was associated with a high incidence of pulmonary venous obstruction. In left atrial isomerism, the survival rate at the age of 20 was 45 %; this better outcome was attributed to biventricular repairs [9, 10].

## 20.3 Cardiac Computed Tomography (CT) in Heterotaxy Syndromes

In heterotaxy syndrome, CT can provide comprehensive assessment of pre- and postoperative cardiac anatomy (Table 20.3). CT assessments should include evaluation of (a) the atriovisceral situs including atrial, airway, vascular, and abdominal organ arrangements; (b) the systemic and pulmonary venous connections with attention to the presence of obstruction; (c) the atrioventricular junction including the size, function, and morphology of the atrioventricular valve(s); (d) the atria and ventricle(s) in terms of their number, size, function, and morphology (left, right, indeterminate); (e) the ventriculoarterial connection (concordance, double outlet, obstruction); (g) the aorta and pulmonary artery with regard to their size, spatial relation, and abnormalities; and (h) the presence of other cardiac defects. In addition, the presence, absence, and number of spleens and the position of the liver and small bowel should be assessed [11–13].

**Table 20.3** CT assessment in the heterotaxy syndromes

| |
|---|
| Atriovisceral situs including atrial appendages, lungs and bronchi, and splenic status |
| Size, morphology, and potential obstructions of systemic and pulmonary venous return |
| Morphology and size of atria |
| Morphology, size, hypertrophy, geometry, and systolic function of ventricle(s) |
| Morphology and anatomy of atrioventricular junction (atrial commitment to ventricle(s)) |
| Anatomy, size, and presence/magnitude of aortic and/or pulmonary outflow track obstructions |
| Size, function, and morphology of valves |
| Anatomy, size, and spatial relationship of aorta and pulmonary artery |
| Presence of coexisting anomalies |

## References


1. Jacobs JP, Anderson RH, Weinberg PM, Walters 3rd HL, Tchervenkov CI, Del Duca D, et al. The nomenclature, definition and classification of cardiac structures in the setting of heterotaxy. Cardiol Young. 2007;17 Suppl 2:1–28. doi:10.1017/S1047951107001138.
2. Goldmuntz E, Lin AL. Genetics of congenital heart diseases. In: Allen HD, Driscoll DJ, Shaddy RE, Feltes TF, editors. Moss and Adams' heart disease in infants, children, and adolescents: including the fetus and young adult. 7th ed. Philadelphia: Wolters Kluwer/Lippincott Williams & Wilkins; 2008. p. 545–72.
3. Rose V, Izukawa T, Moes CA. Syndromes of asplenia and polysplenia. A review of cardiac and non-cardiac malformations in 60 cases with special reference to diagnosis and prognosis. Br Heart J. 1975;37:840–52.
4. Norgard G, Berg A. Isomerism (heterotaxia). In: Gatzoulis MA, Webb GD, Daubeney PEF, editors. Diagnosis and management of adult congenital heart disease. 1st ed. Edinburgh: Churchill Livingstone; 2003. p. 413–21.
5. Van Praagh R, Van Praagh S. Atrial isomerism in the heterotaxy syndromes with asplenia, or polysplenia, or normally formed spleen: an erroneous concept. Am J Cardiol. 1990;66:1504–6.
6. Uemura H, Ho SY, Devine WA, Kilpatrick LL, Anderson RH. Atrial appendages and venoatrial connections in hearts from patients with visceral heterotaxy. Ann Thorac Surg. 1995;60:561–9. doi:10.1016/0003-4975(95)00538-V.
7. Hashmi A, Abu-Sulaiman R, McCrindle BW, Smallhorn JF, Williams WG, Freedom RM. Management and outcomes of right atrial isomerism: a 26-year experience. J Am Coll Cardiol. 1998;31:1120–26.
8. Ghosh S, Harmish G, Godelman A, Haramati LB, Spindola-Franco H. Anomalies of visceroatrial situs. AJR Am J Roentgenol. 2009;193:1107–17.
9. Cohen MS, Anderson RH, Cohen MI, Atz AM, Fogel M, Gruber PJ, et al. Controversies, genetics, diagnostic assessment, and outcomes relating to the heterotaxy syndrome. Cardiol Young. 2007;17 Suppl 2:29–43. doi:10.1017/S104795110700114X.
10. Gilljam T, McCrindle BW, Smallhorn JF, Williams WG, Freedom RM. Outcomes of left atrial isomerism over a 28-year period at a single institution. J Am Coll Cardiol. 2000;36:908–16.
11. Applegate KE, Goske MJ, Pierce G, Murphy D. Situs revisited: imaging of the heterotaxy syndrome. Radiographics. 1999;19:837–52.
12. Goo HW, Park I-S, Ko JK, et al. CT of congenital heart disease: normal anatomy and typical pathologic conditions. Radiographics. 2003;23:S147–65.
13. Leschka S, Oechslin E, Husmann L, et al. Pre- and postoperative evaluation of congenital heart disease in children and adults with 64-section CT. Radiographics. 2007;27:829–46.

# Part VII

# Palliative and Corrective Procedures in Adult Congenital Heart Disease

# Percutaneous Closures

# 21

The most common indications for percutaneous closure of intracardiac communications in adults include atrial septal defect (ASD) and patent foramen ovale (PFO). Other indications for percutaneous closure include ventricular septal defects (VSD), patent ductus arteriosus (PDA), and surgical intracardiac connections, such as shunts (Blalock–Taussig, Glenn, and Fontan) and atrial switch baffles. Transcatheter closures are less invasive than surgical procedures, subject the patient to decreased risk of myocardial ischemia, provide increase patient comfort, and shorten hospitalization.

The various percutaneous closure methods discussed in this section include coils, AMPLATZER occlusion devices (including the duct occluder, septal occluder, muscular VSD occluder, and vascular plug occluder, AGA Medical Corp., Golden Valley, MN), and the CardioSEAL STARFlex septal occluder. The AMPLATZER devices are the most commonly used.

## 21.1 Percutaneous Closures of Atrial Septal Defect and Patent Foramen Ovale

Transcatheter closure of secundum ASD with an AMPLATZER septal occluder is a common alternative to surgical closure [1–3]. This AMPLATZER device is a self-expanding, self-centering, and recapturable. It has a central waist for defect closure and two disks for device fixation. One disk is positioned in each atrium and the disks are joined by the waist that is positioned across the defect. The size of the device is determined by the diameter of the waist and ranges from 4 to 40 mm (38 mm upper limit in the USA) in diameter (Fig. 21.1). To optimize success, AMPLATZER closure of secundum ASDs requires a sufficient rim of tissue around the septal defect (>4 mm) so that the closure device does not impinge upon the venae cavae or the atrioventricular valves. The CardioSEAL STARFlex septal occluder device (a double umbrella-shaped implant made of a metal framework along with polyester fabric) can be used for smaller defects (Fig. 21.2).

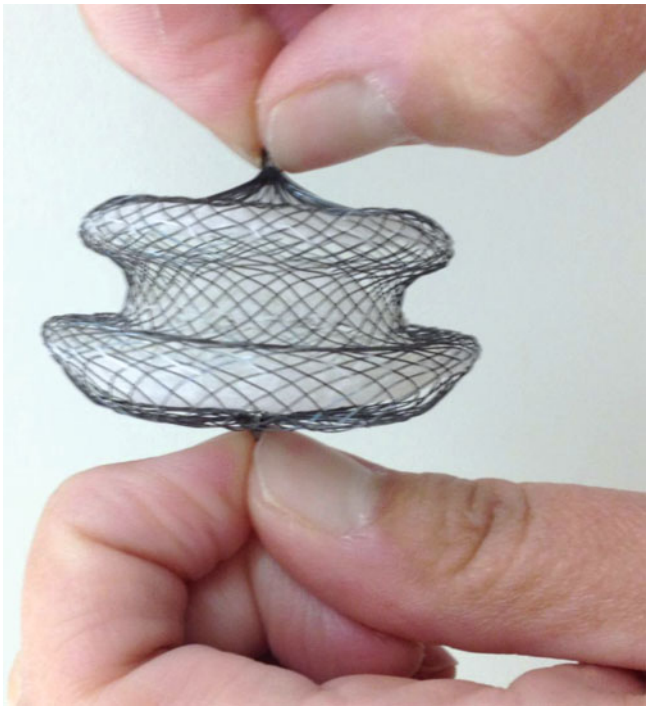

**Fig. 21.1** An image of a 38 mm diameter St. Jude Medical™ AMPLATZER™ septal occluder. The two disks are linked together by a short connecting waist. In order to increase its closing ability, the disks are covered with thin layer of polyester fabric. AMPLATZER and ST. Jude Medical are trademarks of St. Jude Medical, Inc (Photograph reprinted with the kind permission St. Jude Medical™. Copyright: 2012. All rights reserved)

Contraindications to device closure include sinus venosus and atrioventricular septal defects, secundum ASDs with rim deficiency [4], hypermobile (floppy) interatrial septum (may cause prolapse of the occluder), and a balloon-stretched ASD

W. Mazur et al., *CT Atlas of Adult Congenital Heart Disease*,
DOI 10.1007/978-1-4471-5088-6_21, © Springer-Verlag London 2013

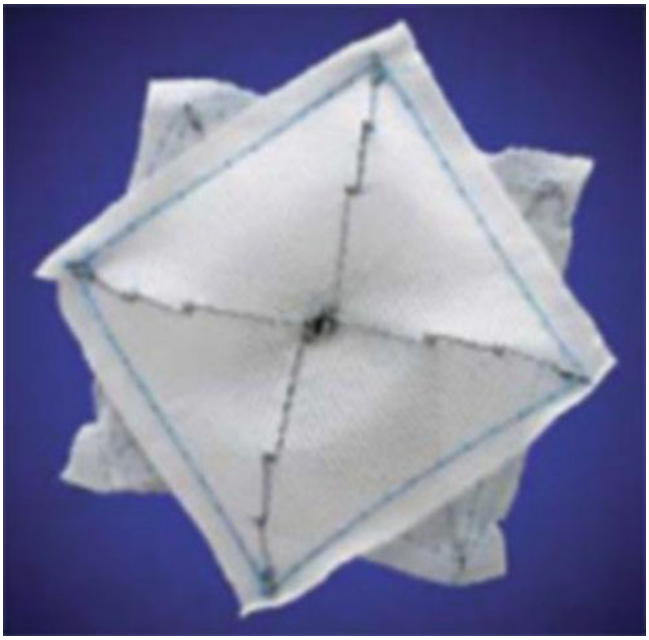

**Fig. 21.2** A picture of a CardioSEAL device (Nitinol Medical Technologies, Inc., Boston, MA). This device is constructed of a metal framework to which polyester fabric is attached

with a diameter >40 mm (higher risk of device dislodgment) [5]. Since the likelihood of device dislodgment increases if the size of the defect greatly exceeds the waist diameter of the device, the device diameter should be selected according to the balloon-stretched diameter of the ASD to ensure tight stenting of the defect with the prosthesis waist. Computed tomographic (CT) examples of percutaneous closure of secundum ASDs are presented in Figs. 21.3, 21.4, 21.5, 21.6, and 21.7.

Patent foramen ovale have been implicated in cryptogenic strokes and transient ischemia attacks presumably due to paradoxical embolization of clot that has developed either in the systemic veins or in the patent foramen itself. In the usual situation, left atrial pressure usually exceeds that of the right atrium, thereby closing the flap of the foramen ovale. If the pressure in the right atrium exceeds that in the left atrium, such as during Valsalva maneuvers or pulmonary hypertension with right ventricular failure, the foramen can open and allow flow from the right atrium to the left atrium with subsequent risk of embolic stroke. Both AMPLATZER and CardioSEAL septal occluder devices have been used for patent foramen ovale closure.

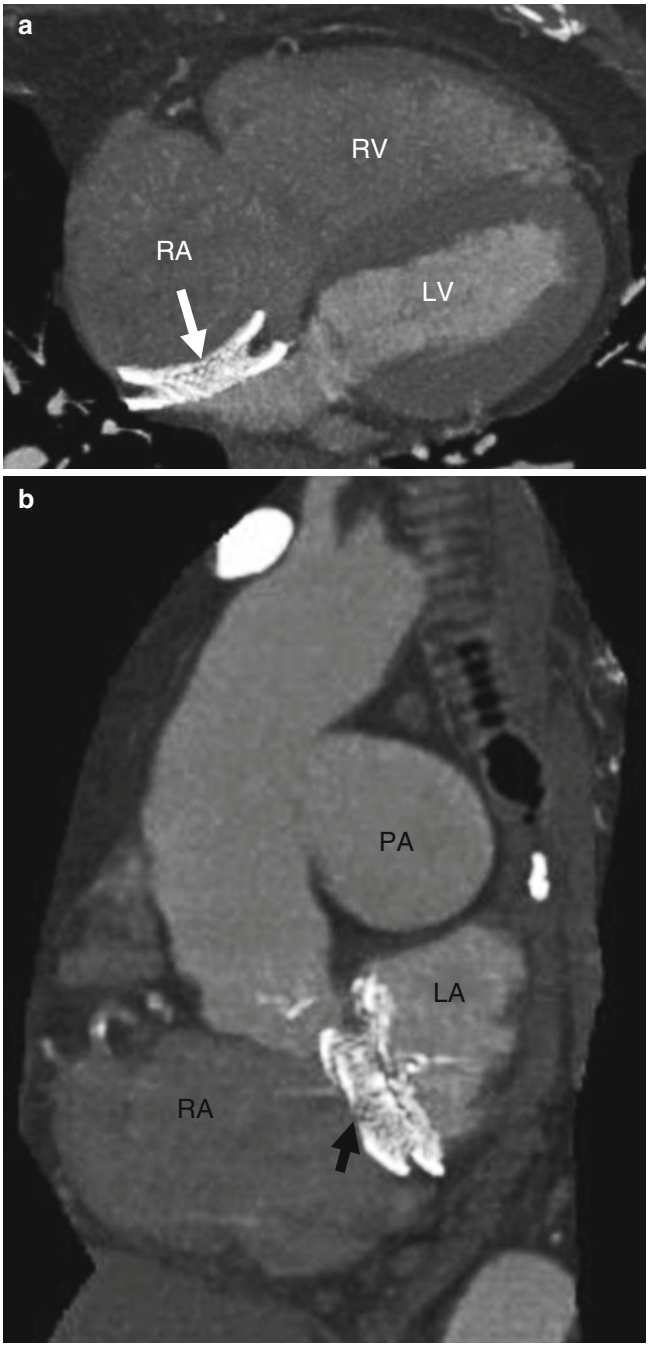


**Fig. 21.3** Panels (**a**) and (**b**) are axial and sagittal views respectively of an AMPLATZER atrial septal occluder (*arrow*) demonstrating proper positioning of the device. *PA* pulmonary artery, *RA* right atrium, *RV* right ventricle, *LV* left ventricle

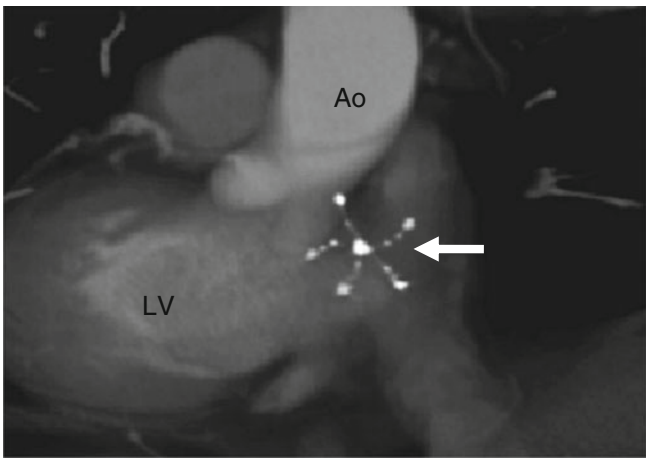


**Fig. 21.4** A CardioSEAL occluder. An oblique, sagittal scan showing the septal occluder device (*arrow*) in its expected position. *Ao* aorta, *LV* left ventricle (Reproduced from Johri et al. [6] with permission from BMJ Publishing Group Ltd.)

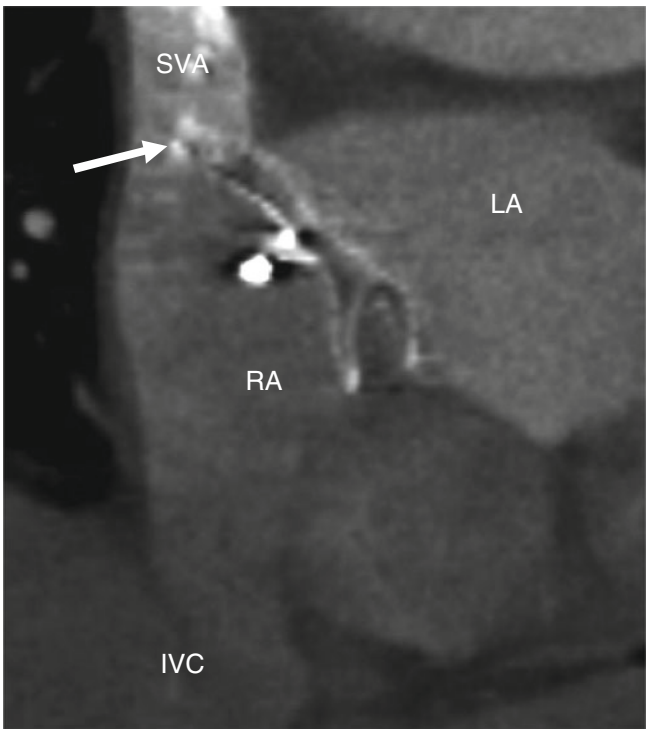


**Fig. 21.5** Malpositioned occluder. Minimal device protrusion is noted due to rim deficiency but no residual shunt is present. This oblique, sagittal image shows the upper portion of the AMPLATZER septal occluder device protruding into the right atrium (*RA*). Both left and right atrial disks (*arrow*) are in the right atrium. *IVC* inferior vena cava, *LA* left atrium, *SVC* superior vena cava (Reproduced with kind permission of the American Roentgen Ray Society, Leesburg, VA from Lee et al. [7])

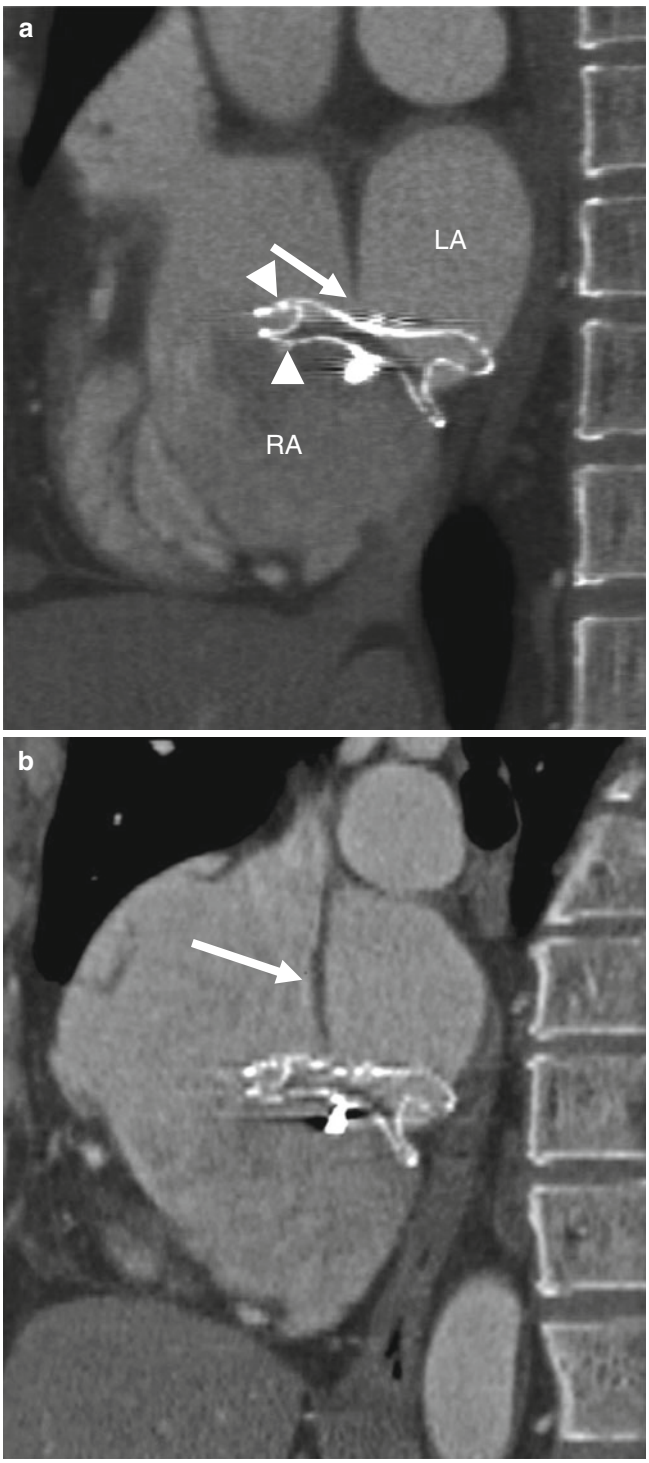


**Fig. 21.6** Malpositioned septal occluder. Panels (**a**) and (**b**) demonstrate marked protrusion of the AMPLATZER septal occluder. These oblique sagittal images show marked protrusion of the upper portion of both the left and right atrial disks (*arrowheads*) in the right atrium. A residual septal defect (*arrow*) also is evident. *LA* left atrium, *RA* right atrium (Reproduced with kind permission of the American Roentgen Ray Society, Leesburg, VA from Lee et al. [7])

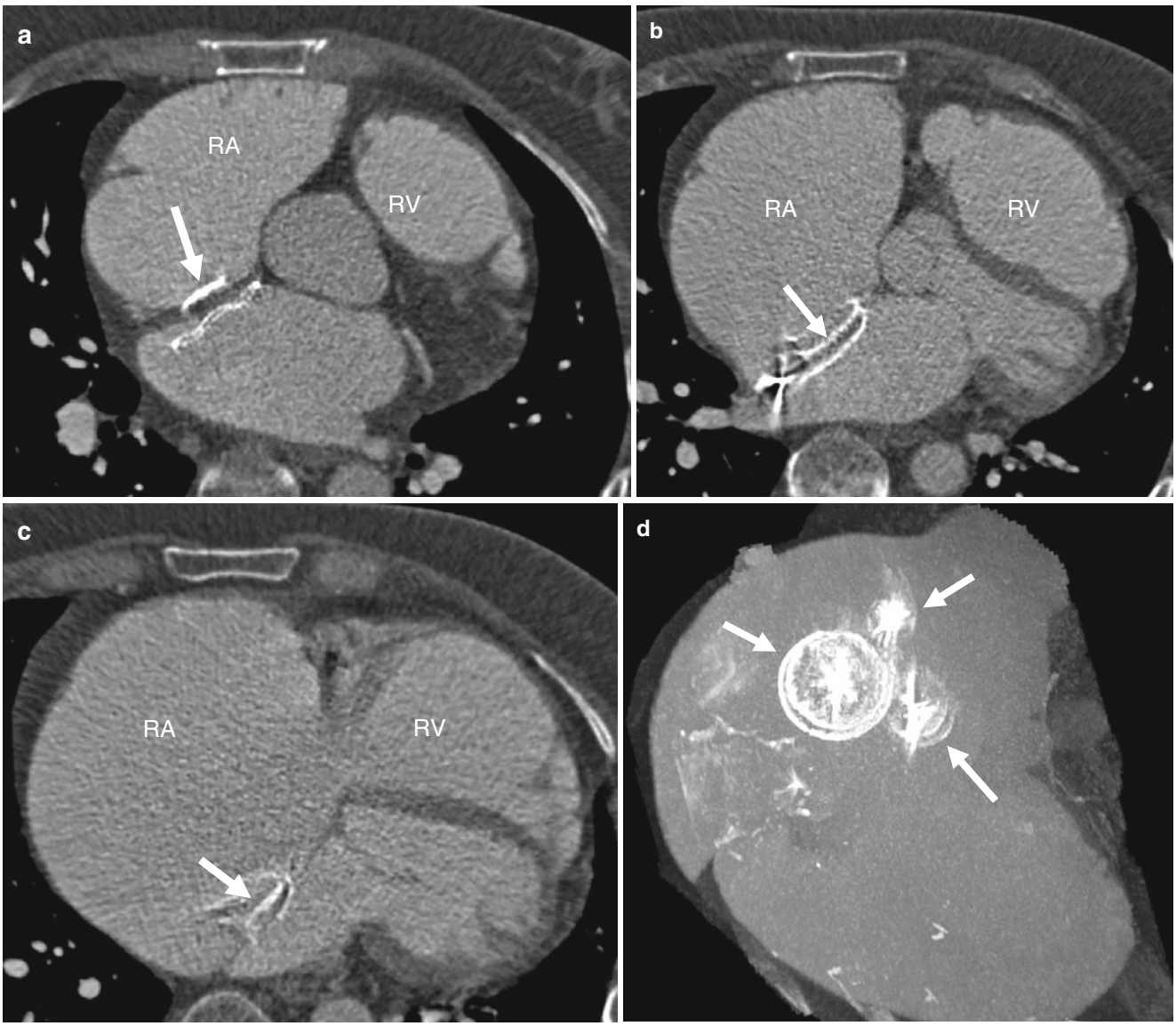


**Fig. 21.7** Three AMPLATZER closure devices in a patient who refused surgical intervention. Panels (**a**), (**b**), and (**c**) are three axial scans showing the three devices (*arrows*) at different cardiac planes. Note marked dilatation of the right atrium (*RA*). The right ventricle (*RV*) is mildly dilated. Panel (**d**) is an oblique coronal reconstruction showing the three occluder devices (*arrows*) once again

## 21.2 Percutaneous Closure of Ventricular Septal Defect

Percutaneous closure of a VSD is technically much more challenging than ASD closure. Early results with the AMPLATZER septal device closure of muscular VSDs, although encouraging, lack long-term outcome data [8]. Percutaneous closure of perimembranous VSD is even more technically challenging due to the proximity of the defect to the conduction system, aortic valve and tricuspic valve. Complications associated with percutaneous VSD closure include valve dysfunction and complete heart block. Newer design modifications have the potential to improve safety and efficacy [9].

## 21.3 Percutaneous Closure of Patent Ductus Arteriosus

Traditionally, transcatheter occlusion was the treatment of choice for most PDAs in adults. In patients with a calcified PDA and increased pulmonary vascular resistance, transcatheter closure offers advantages over more invasive surgical closure procedures. Currently, the AMPLATZER ductal occluder device is the most commonly used device for PDA closure in adults [10]. It is especially suitable for large PDAs >3 mm in diameter. Coil embolization or a vascular plug occluder device is usually used for smaller PDAs and for occluded PDAs with small residual leaks. Complete closure has been reported in more than 95 % of patients at 6-month follow-up with both occluder devices and embolization techniques [11]. Device embolization is rarely encountered [11].

## 21.4 Percutaneous Closure of Blalock–Taussig and Glenn Shunts

Palliative Blalock–Taussig and Glenn shunts are usually clamped during corrective surgical procedures carried out to treat underlying congenital heart disease. However, a bidirectional Glenn shunt may be left intact in patients with very small caliber pulmonary arteries since it has been shown that this type of shunt can induce pulmonary artery growth by introducing an element of pulsatile blood flow to the pulmonary arteries [12]. Subsequently, if closure is indicated, the method of choice is percutaneous embolization using embolization coils or devices such as the AMPLATZER duct occluder or AMPLATZER vascular plug devices [13].

The AMPLATZER vascular plug occluder is a device designed to close abnormal extracardiac vascular structures. This is a self-expandable cylindrical device made from 144 braided nitinol wires. The wire mesh is so closely knit that occlusive fabric is unnecessary, allowing the device to be delivered through smaller delivery catheters. Typically, the other occlusion devices have polyester fabric layers that provide a nidus for clot formation. The plugs range in diameter from 4 to 16 mm. Vascular plug devices are also applicable to other vascular communications, such as pulmonary arteriovenous malformations or collateral vessel formation associated with severe cyanotic heart diseases or surgical shunt operations.

**Fig. 21.8** An image of a St. Jude Medical™ AMPLATZER™ Vascular Plug II. This device is designed to occlude blood vessels in the peripheral vasculature. It is made of self-expanding nitinol wire mesh. Like the other occluder devices, vascular plugs have the ability to be recaptured and repositioned, if necessary. Note the absence of a polyester covering. AMPLATZER and St. Jude Medical are trademarks of St. Jude Medical, Inc (Photograph reprinted with the kind permission St. Jude Medical™. Copyright: 2012. All rights reserved)

Figure 21.8 is a picture of the AMPLATZER vascular plug occluder.

## 21.5 Fontan Fenestrations and Atrial Switch Baffle Leaks Closure

After a Fontan operation, patients may have spontaneous or surgically created fenestrations that can lead to right-to-left shunting and consequently to systemic oxygen desaturation, systemic emboli, and exercise incapacity. These fenestrations can be closed with the use of the CardioSEAL occluder device.

Many patients undergoing Mustard or Senning operations will demonstrate late baffle leaks due to suture dehiscence. Most of these shunts are of no hemodynamic significance

and do not require treatment. However, closure is indicated for large defects resulting in hemodynamically significant intracardiac shunting. Closure can be accomplished with either the AMPLATZER or CardioSEAL devices.

## 21.6 Cardiac Computed Tomographic Angiography (CT) in the Evaluation of Percutaneous Closure Procedures

After percutaneous closure of septal defects, CT is helpful after deployment of the closure device to determine device position, residual shunting, and compression of the venae cavae and tricuspid and mitral valves. In the evaluation of surgical shunts, CT is especially valuable for delineating the position of the valve, integrity of the shunt (patent, stenotic, closed), baffle leaks in atrial switch operations, and the size of central and branch pulmonary arteries.

## References


1. Du ZD, Hijazi ZM, Kleinman CS, Silverman NH, Larntz K, Amplatzer Investigators. Comparison between transcatheter and surgical closure of secundum atrial septal defect in children and adults: results of a multicenter nonrandomized trial. J Am Coll Cardiol. 2002;39:1836–44.
2. Masura J, Gavora P, Podnar T. Long-term outcome of transcatheter secundum-type atrial septal defect closure using amplatzer septal occluders. J Am Coll Cardiol. 2005;45:505–7. doi:10.1016/j.jacc.2004.10.066.
3. Yew G, Wilson NJ. Transcatheter atrial septal defect closure with the amplatzer septal occluder: five-year follow-up. Catheter Cardiovasc Interv. 2005;64:193–6. doi:10.1002/ccd.20268.
4. Mathewson JW, Bichell D, Rothman A, Ing FF. Absent posteroinferior and anterosuperior atrial septal defect rims: factors affecting nonsurgical closure of large secundum defects using the amplatzer occluder. J Am Soc Echocardiogr. 2004;17:62–9. doi:10.1016/j.echo.2003.09.018.
5. Ko SF, Liang CD, Yip HK, Huang CC, Ng SH, Huang CF, et al. Amplatzer septal occluder closure of atrial septal defect: evaluation of transthoracic echocardiography, cardiac CT, and transesophageal echocardiography. AJR Am J Roentgenol. 2009;193:1522–9. doi:10.2214/AJR.09.2854.
6. Johri AM et al. Non-invasive imaging: imaging of atrial septal defects: echocardiography and CT correlation. Heart. 2011;97:1441–53.
7. Lee T et al. MDCT evaluation after closure of atrial septal defect with an Amplatzer septal occluder. AJR Am J Roentgenol. 2007;188:W431–9.
8. Holzer R, Balzer D, Cao QL, Lock K, Hijazi ZM, Amplatzer Muscular Ventricular Septal Defect Investigators. Device closure of muscular ventricular septal defects using the Amplatzer muscular ventricular septal defect occluder: immediate and mid-term results of a U.S. registry. J Am Coll Cardiol. 2004;43:1257–63. doi:10.1016/j.jacc.2003.10.047.
9. Fu YC, Bass J, Amin Z, Radtke W, Cheatham JP, Hellenbrand WE, et al. Transcatheter closure of perimembranous ventricular septal defects using the new Amplatzer membranous VSD occluder: results of the U.S. phase I trial. J Am Coll Cardiol. 2006;47:319–25. doi:10.1016/j.jacc.2005.09.028.
10. Inglessis I, Landzberg MJ. Interventional catheterization in adult congenital heart disease. Circulation. 2007;115:1622–33. doi:10.1161/CIRCULATIONAHA.105.592428.
11. Pass RH, Hijazi Z, Hsu DT, Lewis V, Hellenbrand WE. Multicenter USA amplatzer patent ductus arteriosus occlusion device trial: initial and one-year results. J Am Coll Cardiol. 2004;44:513–9. doi:10.1016/j.jacc.2004.03.074.
12. Miyaji K, Shimada M, Sekiguchi A, Ishizawa A, Isoda T. Usefulness of pulsatile bidirectional cavopulmonary shunt in high-risk Fontan patients. Ann Thorac Surg. 1996;61:845–50. doi:10.1016/0003-4975(95)01121-8.
13. Rios-Mendez RE, Gamboa R, Mollon FP. Percutaneous closure of a modified Blalock-Taussig shunt using an amplatzer vascular plug. Rev Esp Cardiol. 2009;62:1180–3.

# Aortopulmonary Shunts: Blalock–Taussig, Potts, Waterston

# 22

## 22.1 Indications

Systemic artery-to-pulmonary artery shunts are palliative surgical procedures performed to increase the blood flow to the lungs for the relief of cyanosis and to enlarge the pulmonary arteries. Palliative procedures improve oxygen saturation, but they also can result in volume loading of the systemic ventricle and possible pulmonary hypertension.

## 22.2 Blalock–Taussig Shunts

The original (classic) Blalock–Taussig (BT) shunt (described in 1945) involved ligation and division of the left subclavian artery and an end-to-side anastomosis of the proximal left subclavian artery to the pulmonary artery. Restitution of flow in the ipsilateral upper limb was dependent on collateral vessel formation. Disadvantages of the classic BT shunt included possible distortion or kinking of the subclavian or pulmonary arteries at the anastomotic sites and the potential for abnormal growth of the arm ipsilateral to the shunt (due to a steal phenomenon). The classic BT shunt is now rarely used for palliative surgery.

The subsequent, modified Blalock–Taussig (MBT) shunt uses a synthetic graft of polytetrafluoroethylene to create a side-to-side shunt between the subclavian artery and ipsilateral right or left pulmonary artery (Figs. 22.1 and 22.2). Advantages of the MBT include less distortion of the pulmonary arteries (although it can still occur), better growth of the pulmonary tree, and preserved blood flow to the ipsilateral arm. Distortion of the ipsilateral pulmonary artery has been reported in 24–33 % of patients, hemodynamically significant pulmonary artery stenosis in 14 % of patients, and shunt narrowing at the anastomosis in 50 % of patients [1, 2]. Rarely, there is complete occlusion of the pulmonary artery or the shunt [1, 2]. Another not uncommon complication of the MBT shunt is shunt thrombosis (Fig. 22.3). This is usually a late complication but can occur in the early postoperative period.

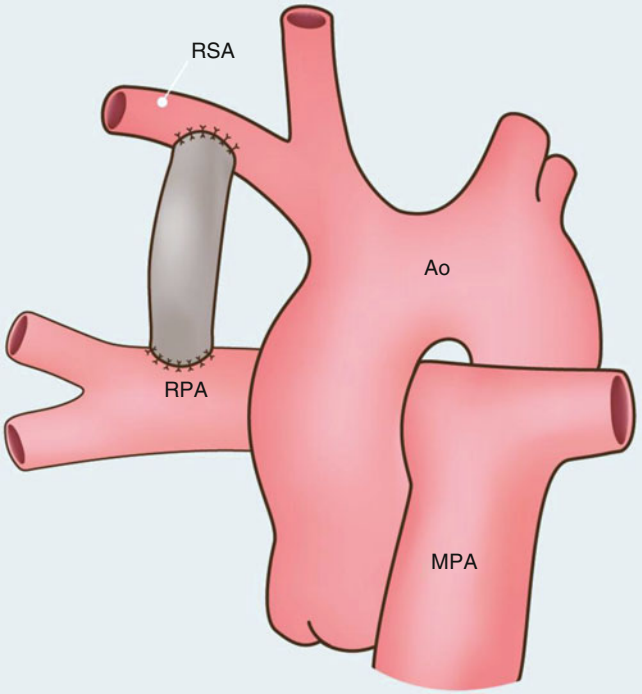


**Fig. 22.1** Modified Blalock–Taussig shunt. This procedure involves interposition of a prosthetic graft of polytetrafluoroethylene between the subclavian artery and ipsilateral right or left pulmonary artery. *Ao* aorta, *MPA* main pulmonary artery, *RPA* right pulmonary artery, *RSA* right subclavian artery

Pulmonary hypertension is a rare complication in both the BT and MBT shunts. The MBT shunt is currently used for palliation prior to complete surgical repair of a cyanotic congenital lesions, as an adjunct to repair of single-ventricle procedures, and in patients with diminished pulmonary blood flow who are not candidates for complete primary repairs (i.e., tricuspid atresia and pulmonary atresia).

W. Mazur et al., *CT Atlas of Adult Congenital Heart Disease*,
DOI 10.1007/978-1-4471-5088-6_22, © Springer-Verlag London 2013

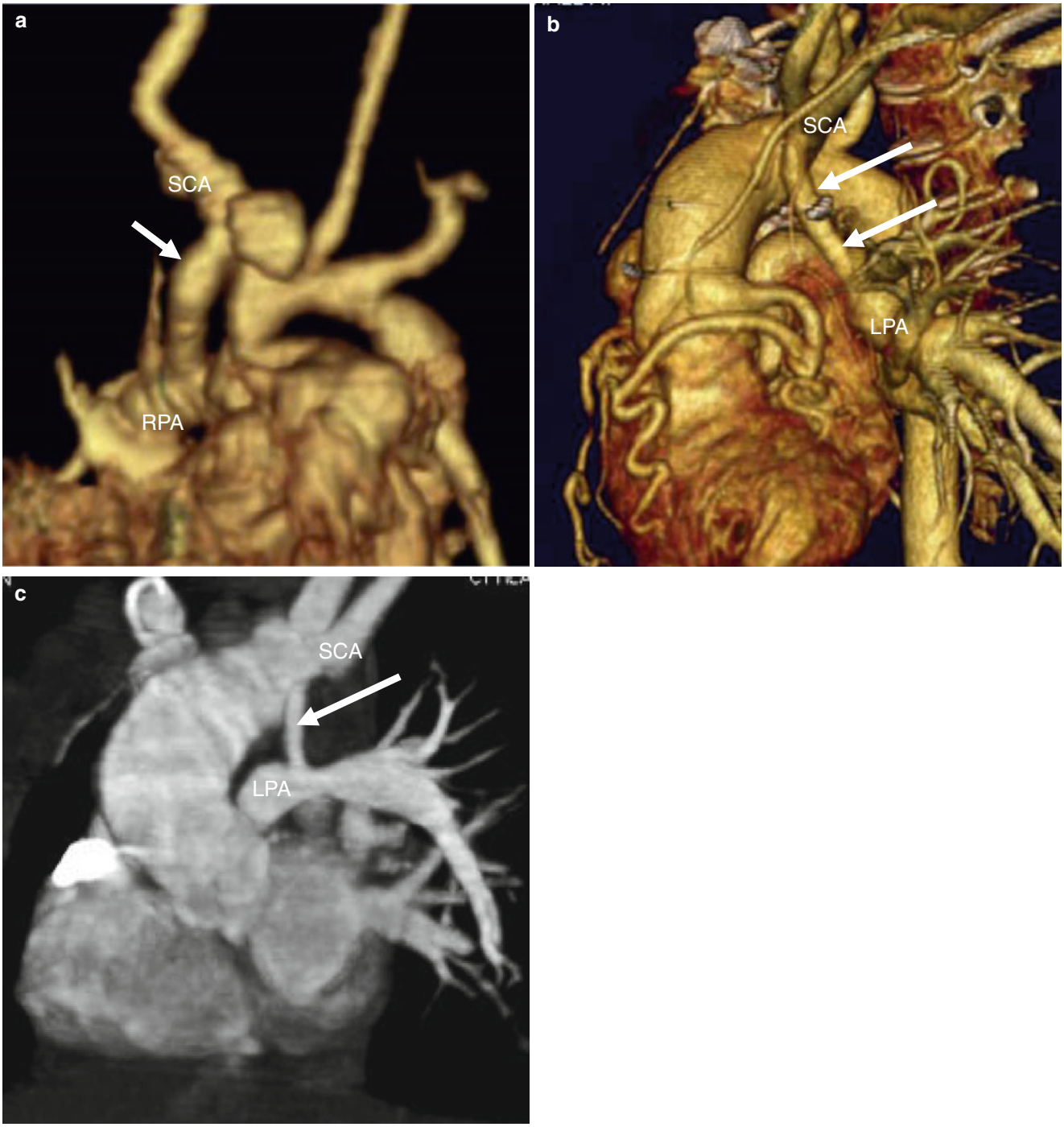


**Fig. 22.2** Modified Blalock–Taussig shunt. Panel (**a**) is a 3D reconstruction illustrating the shunt between the right subclavian artery and right pulmonary artery. Panels (**b**) and (**c**) are 3D views in two separate patients showing a shunt between the left subclavian artery and the left pulmonary artery. *Arrow* Blalock–Taussig shunt, *RPA* right pulmonary artery, *LPA* left pulmonary artery, *SCA* right subclavian artery

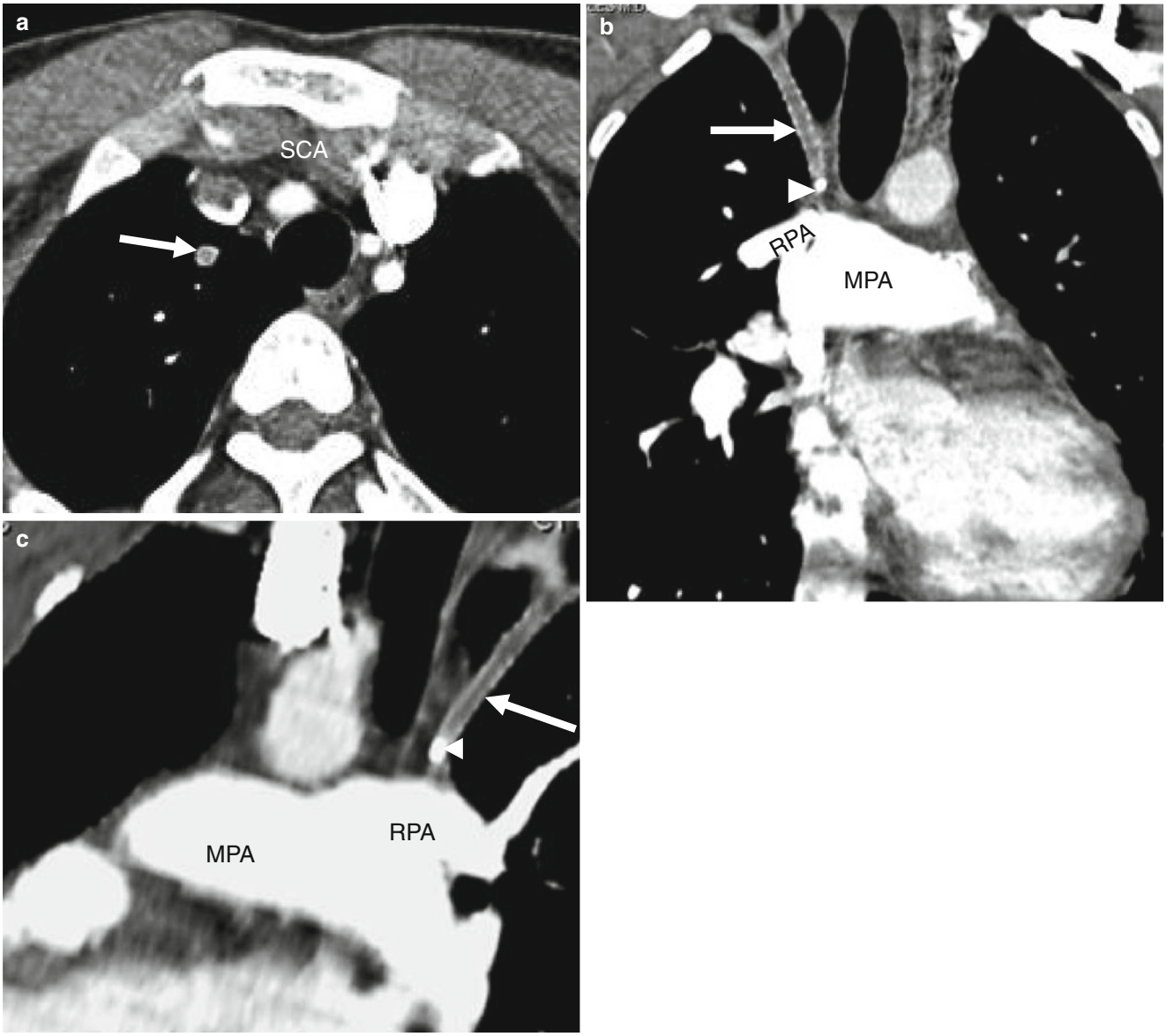


**Fig. 22.3** Shunt thrombosis in a patient with single-ventricle physiology. Panel (**a**) is an axial view showing no flow in the Blalock–Taussig shunt (*arrow*). Panel (**b**) is a coronal cut and panel (**c**) is an oblique sagittal view. In panels (b) and (c), the Blalock–Taussig shunt (*arrow*) extends from the right subclavian artery to the right pulmonary artery (*RPA*) with a metallic clip (*arrowhead*) noted near its entrance to the right pulmonary artery. Flow is absent in the shunt consistent with thrombosis. *MPA* main pulmonary artery, *SCA* subclavian artery

## 22.3 Waterston–Cooley and Potts Shunts

The Waterston–Cooley shunt is a side-to-side anastomosis between the ascending aorta and right pulmonary artery (Fig. 22.4). This procedure was often complicated by excessive pulmonary blood flow leading to pulmonary hypertension and distortion of the right pulmonary artery at the anastomotic site resulting in an acquired stenosis. For these reasons, it is no longer used for the treatment of congenital heart disease.

The Potts shunt is a side-to-side anastomosis between the left pulmonary artery and the descending aorta (Fig. 22.5). Like the Waterston shunt, this procedure is obsolete because of the high incidence of pulmonary hypertension and distortion of the pulmonary arteries.

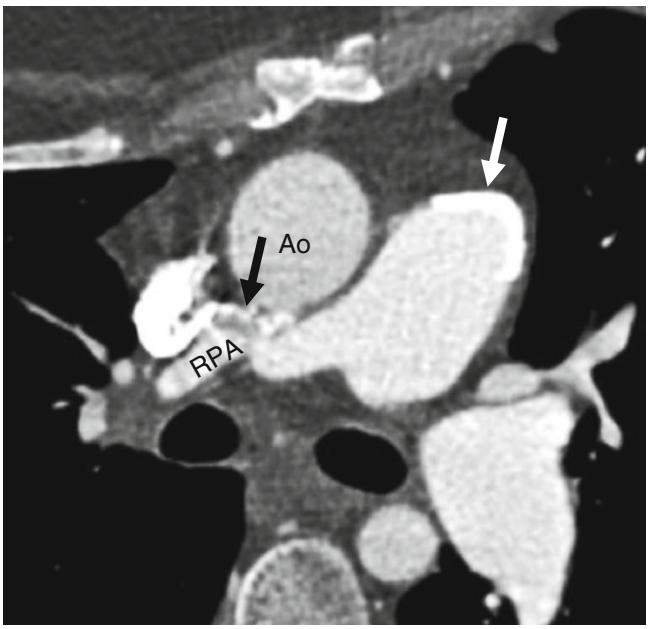


**Fig. 22.4** A Waterston–Cooley shunt. This example is an axial image in a 24-year-old man with a history of tetralogy of Fallot and pulmonary atresia and demonstrates a Waterston–Cooley shunt (*black arrow*) extending from the posterior wall of the ascending aorta (*Ao*) to the anterior wall of the right pulmonary artery (*RPA*). Note the calcification (*white arrow*) in the repaired pulmonary outflow tract

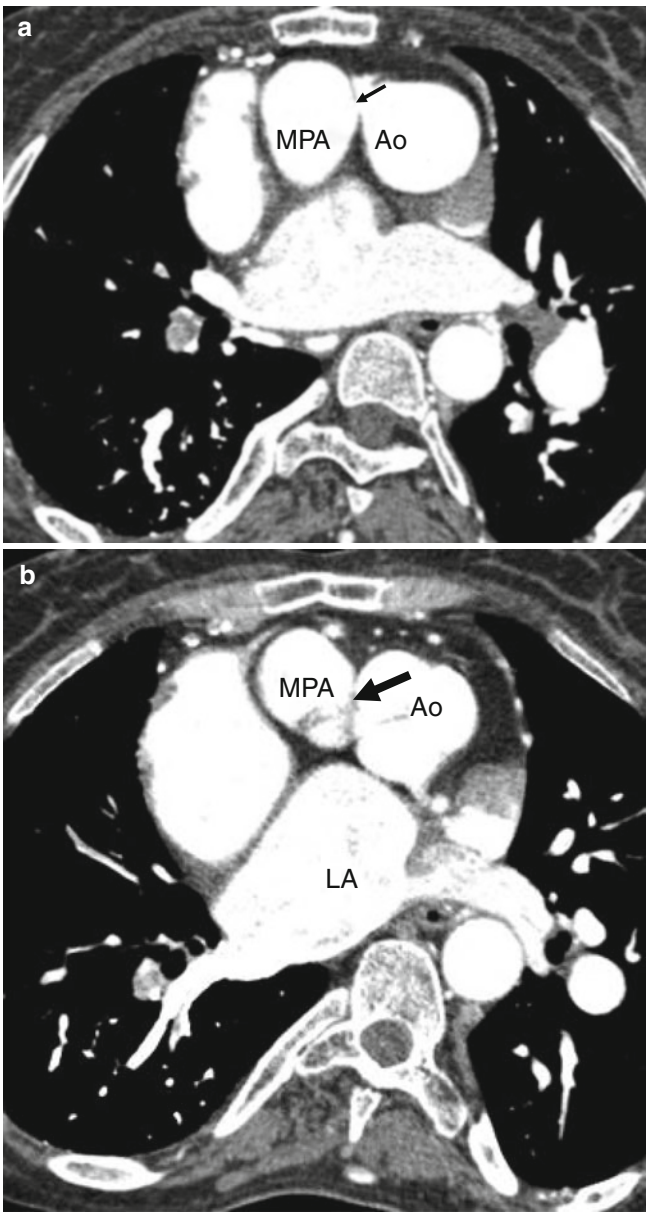


**Fig. 22.5** An example of a Potts shunt in a 23-year-old woman with a hypoplastic right ventricle. Panels (**a**) and (**b**) are two sequential axial views showing the anastomosis of the aorta (*Ao*) with the main pulmonary artery (*MPA*). The *arrow* indicates the anastomotic site (Potts shunt). *LA* left atrium

## 22.4 Pulmonary Artery Banding

Currently, pulmonary artery (PA) banding is performed by wrapping a ring of prosthetic material around the main pulmonary artery (Fig. 22.6) which diminishes pulmonary blood flow, thus protecting the pulmonary arterial bed from the potential changes of pulmonary hypertension. PA banding is usually a palliative procedure until definitive repair or palliation of the underlying heart defect can be performed. It is also used to "prepare" the left ventricle when a corrective procedure for transposition of the great arteries (TGA) (arterial switch) is planned (not undertaken until the second or third week of life). In unrepaired TGA, the left ventricle pumps only against the normally very low pulmonary vascular resistance. If TGA repair is delayed, the left ventricle will not be prepared to pump against the high systemic pressure that it will encounter after the procedure leading to left ventricular failure. PA banding prior to the arterial switch operation forces the left ventricle to pump against higher resistance leading to compensatory increases in left ventricular wall thickness and contractile ability thus preparing the ventricle to handle the higher systemic vascular resistance it will experience after the arterial switch procedure [3]. The major complication of PA banding is dilatation of the PA proximal to the banding site with possible resulting pulmonary valve insufficiency.

## 22.5 Cardiac Computed Tomographic Angiography (CT) in the Evaluation of Aortopulmonary Shunts

Echocardiography is the initial imaging technique used to evaluate the branch aortic arch arteries. However, the central and branch pulmonary arteries are not well imaged by ultrasound. Moreover, echocardiography is limited by acoustic window parameters such as thoracic deformities, air-filled lungs, sternal wires, and obesity. MRI is an alternative imaging modality but often in the postoperative patient, surgical clips or percutaneously placed coils create imaging artifacts impairing visualization of the branch pulmonary arteries. Computed tomography (CT) is not hampered by postoperative metal artifacts, and it is an ideal technique for evaluating postsurgical morphology. It is especially valuable for delineating the integrity of the surgical shunt (patency, stenosis,

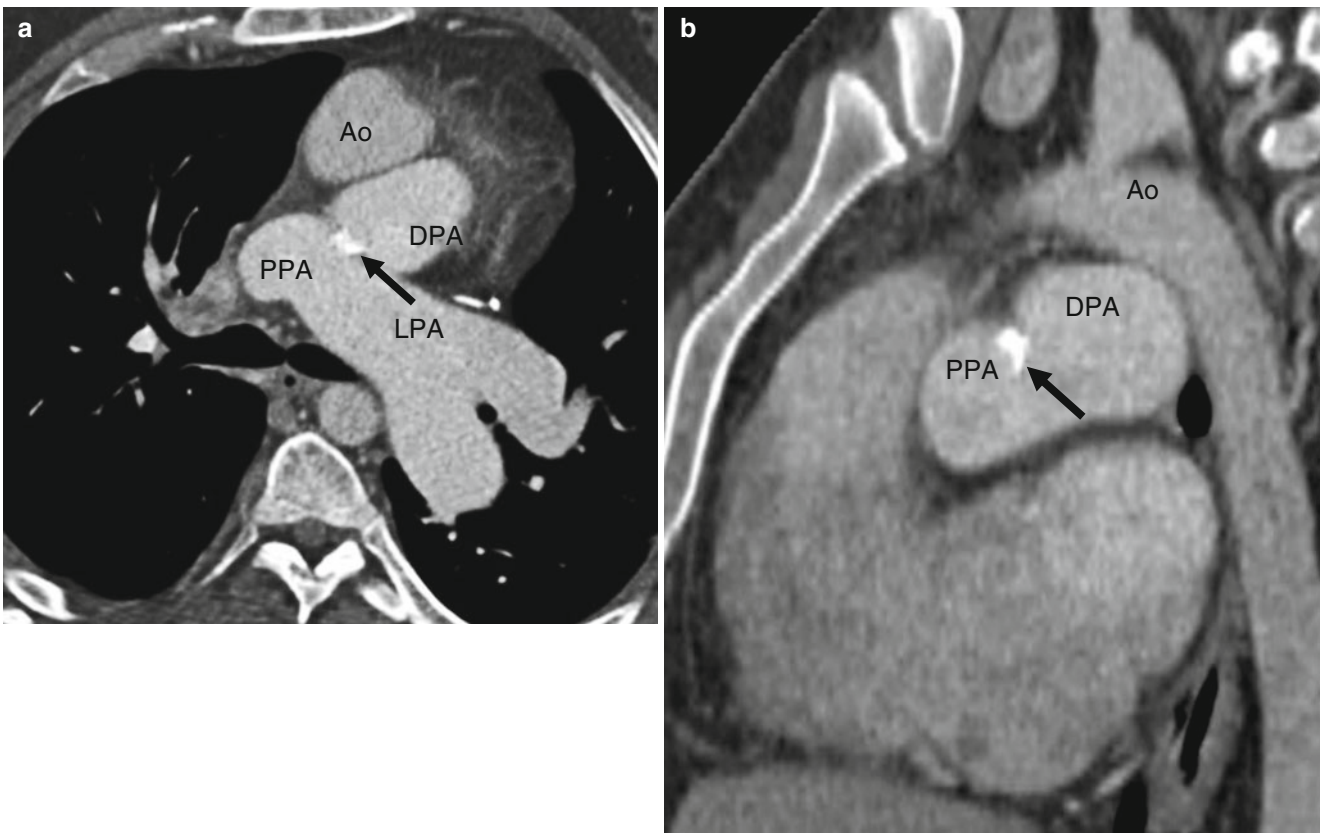


**Fig. 22.6** Pulmonary artery banding. A 27-year-old man with D-transposition of the great arteries, multiple ventricular septal defects, and a functional univentricular heart who is status post an atrial septostomy, a modified left Blalock–Taussig shunt, and pulmonary artery (*PA*) banding (performed to decrease excessive blood flow). Panel (**a**), an axial cut and panel (**b**), a sagittal view show the PA band (*arrows*). The banding divides the main pulmonary artery into a distal pulmonary artery (*DPA*) and a proximal pulmonary artery (*PPA*). *LPA* left pulmonary artery, *Ao* aorta

and occlusion), distortion or kinking of the pulmonary artery at the anastomotic sites, and for assessing perfusion of the central and branch pulmonary arteries [4–9].

## References


1. Godart F, Qureshi SA, Simha A, Deverall PB, Anderson DR, Baker EJ, et al. Effects of modified and classic blalock-taussig shunts on the pulmonary arterial tree. Ann Thorac Surg. 1998;66:512–7; discussion 518.
2. Gladman G, McCrindle BW, Williams WG, Freedom RM, Benson LN. The modified blalock-taussig shunt: clinical impact and morbidity in fallot's tetralogy in the current era. J Thorac Cardiovasc Surg. 1997;114:25–30.
3. Corno AE, Hurni M, Payot M, Sekarski N, Tozzi P, von Segesser LK. Adequate left ventricular preparation allows for arterial switch despite late referral. Cardiol Young. 2003;13:49–52.
4. Gaca AM, Jaggers JJ, Dudley LT, Bisset 3rd GS. Repair of congenital heart disease: a primer-part 1. Radiology. 2008;247:617–31. doi:10.1148/radiol.2473061909.
5. Hughes Jr D, Siegel MJ. Computed tomography of adult congenital heart disease. Radiol Clin North Am. 2010;48:817–35. doi:10.1016/j.rcl.2010.04.005.
6. Siegel MJ, Bhalla S, Gutierrez FR, Billadello JB. MDCT of postoperative anatomy and complications in adults with cyanotic heart disease. AJR Am J Roentgenol. 2005;184:241–7.
7. Siegel MJ. Thoracic vascular anomalies. In: Rubin GD, Rofsky NM, editors. CT and MR angiography: comprehensive vascular assessment. Philadelphia: Wolters Kluwer Health/Lippincott Williams & Wilkins; 2009. p. 543–95.
8. Soler R, Rodriguez E, Alvarez M, Raposo I. Postoperative imaging in cyanotic congenital heart diseases: part 2, complications. AJR Am J Roentgenol. 2007;189:1361–9. doi:10.2214/AJR.07.2105.
9. Spevak PJ, Johnson PT, Fishman EK. Surgically corrected congenital heart disease: utility of 64-MDCT. AJR Am J Roentgenol. 2008;191:854–61. doi:10.2214/AJR.07.2889.

# Atrial Baffles for the Treatment of Transposition of the Great Arteries (Mustard, Senning)

# 23

The first attempt to repair a patient with transposition of the great arteries (TGA) was performed by Senning who successfully constructed an atrial baffle in 1958 [1]. The procedure employed an atrial baffle created from autologous tissue to redirect caval blood to the left atrium which emptied into the left ventricle which then pumped the deoxygenated blood to the lungs. Pulmonary venous blood was redirected to the morphologic right atrium and through the tricuspid valve into the right ventricle which then filled the aorta with oxygenated blood. Subsequently, in 1964, Mustard introduced an atrial switch procedure utilizing prosthetic patch material to create an intra-atrial baffle (Figs. 23.1 and 23.2) [2, 3]. See Fig. 19.22 for a diagram of the uncorrected circulation and the circulation after the atrial switch procedure which normalizes the blood flow circuit.

Both the Senning and Mustard procedures involve the redirection of blood flow at the atrial level. The morphologic left ventricle is the pulmonary ventricle and the morphologic right ventricle is the systemic ventricle which is subject to systemic loading pressures and subsequent compensatory hypertrophy. Although the atrial switch provides physiologic correction of the circulation, normal anatomic relationships of the aorta and pulmonary artery are not restored (Fig. 23.3). Examples of CT images of patients after the Mustard procedure are presented in Figs. 23.4 and 23.5.

W. Mazur et al., *CT Atlas of Adult Congenital Heart Disease*,
DOI 10.1007/978-1-4471-5088-6_23, © Springer-Verlag London 2013

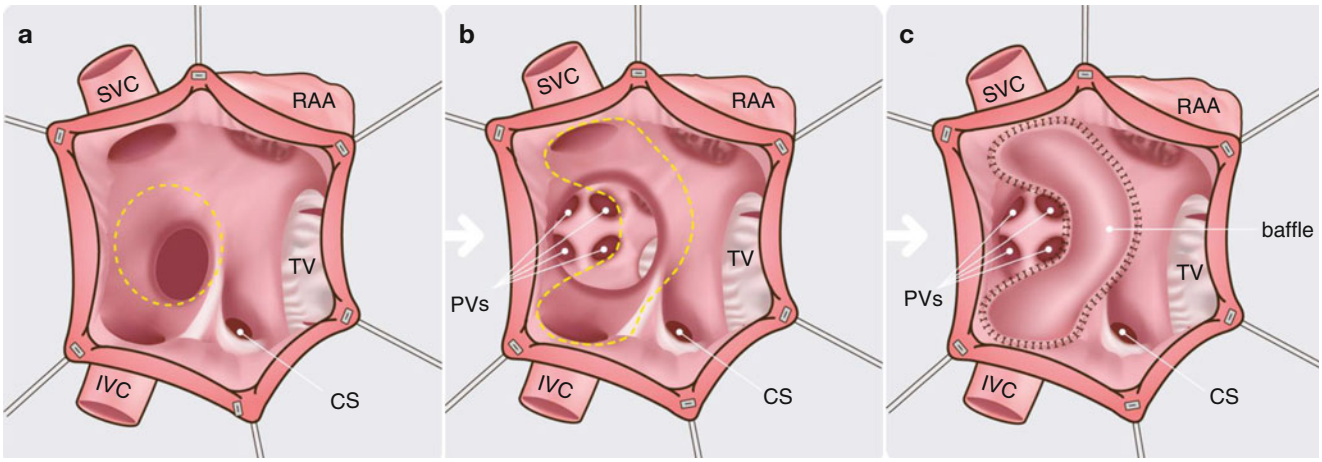


**Fig. 23.1** An artist's rendition of the Mustard operation. Panel (**a**) the right atrium is opened and the atrial septum is excised (*dashed line*). Panels (**b**) and (**c**) the interatrial baffle is sutured along the right atrium (*dashed line*) to redirect the systemic venous return to the left atrium, while the pulmonary venous return enters the right atrium. *CS* coronary sinus, *IVC*, inferior vena cava, *PVs* pulmonary veins, *RAA* right atrial appendage, *SVC* superior vena cava, *TV* tricuspid valve

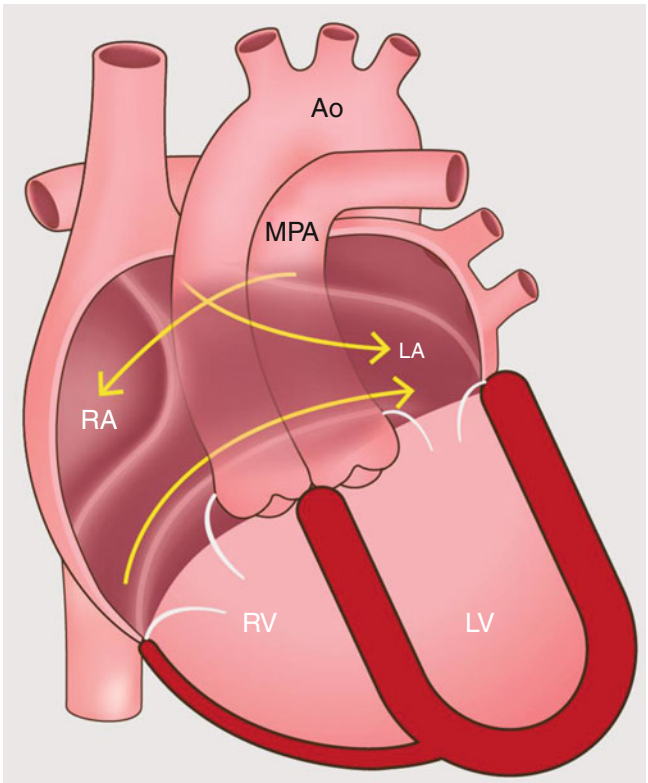


**Fig. 23.2** An artist's diagram of the atrial baffle surgery in the D-transposition of the great arteries. Note the presence of ventriculo-arterial discordance with the origin of the main pulmonary artery from the left ventricle and the aorta from the right ventricle. To restore physiologic circulation, systemic blood return is redirected by a baffle to the left atrium, and pulmonary venous return enters the right atrium. *Ao* aorta, *MPA* main pulmonary artery, *RA* right atrium, *RV* right ventricle, *LA* left atrium, *LV* left ventricle

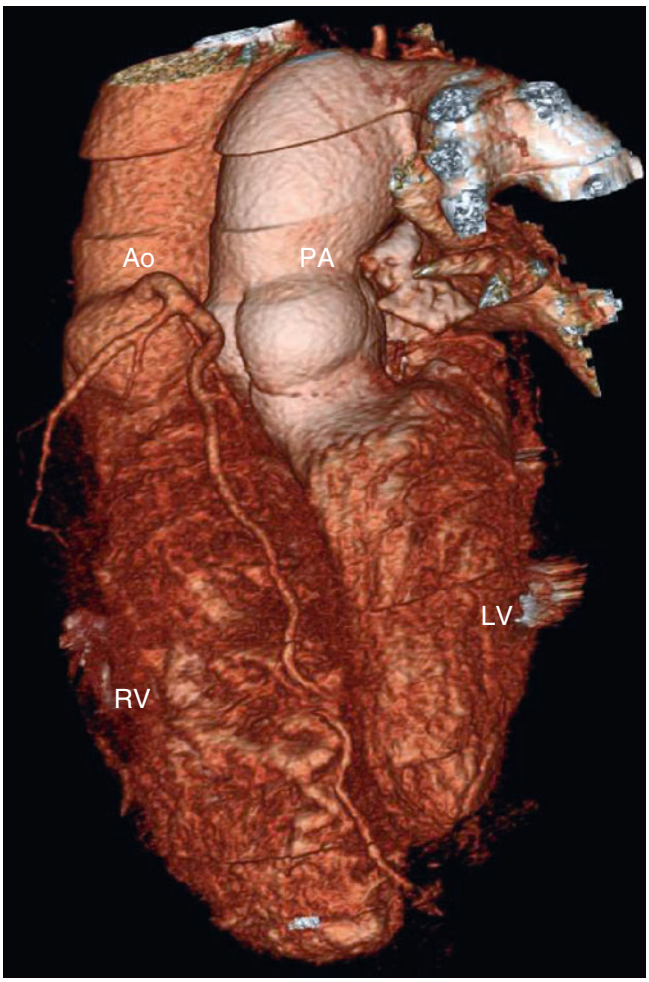


**Fig. 23.3** Adult with D-transposition of great arteries and acute chest pain who had a Mustard procedure in infancy. A computed tomography scan was performed to evaluate for pulmonary embolus. This coronal 3D image demonstrates the pulmonary artery (*PA*) arising from the morphologic left ventricle (*LV*) and aorta (*Ao*) arising from the morphologic right ventricle (*RV*), typical of D-transposition. In the atrial switch, the correction is at the atrial level

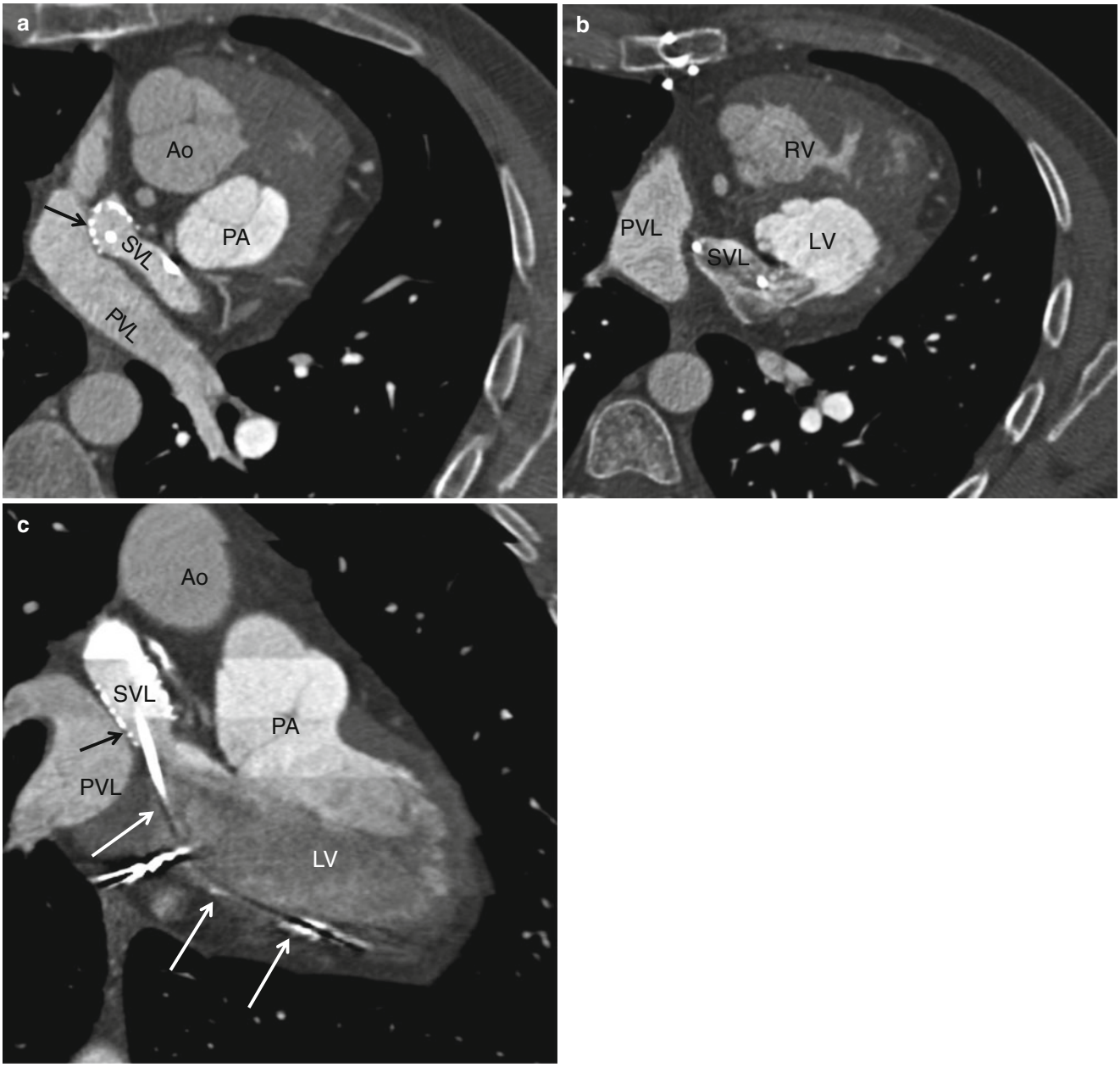


**Fig. 23.4** A Mustard procedure in an adult who subsequently developed stenosis of the superior vena cava, requiring percutaneous stenting. Panel (**a**) is an axial view shows the systemic vein limb (*SVL*) (superior vena cava to left atrium) and pulmonary vein limb (*PVL*) (pulmonary veins to the right atrium) of the baffle. Panel (**b**) is an axial cut in a different plane clearly showing the emptying of deoxygenated blood from the SVL to the left ventricle. Panel (**c**) is a sagittal cut also demonstrating the ultimate connection of the SVL to the morphologic left ventricle. Pacemaker wires (best noted in panel **c**, *arrows*) are present in the baffle extending into the morphologic left ventricle (pulmonic ventricle). Complete atrioventricular block is common in transpositions due to marked elongation of the AV node. Also note the stent patency with inflow of contrast-enhanced blood from the superior vena cava above and noncontrast-enhanced blood from the inferior vena cava below to the systemic baffle limb panel (**a** and **c**). *Ao* aorta, *PA* pulmonary artery, *LV* left ventricle. *Black arrows* in panels **a** and **c**: SVL stent

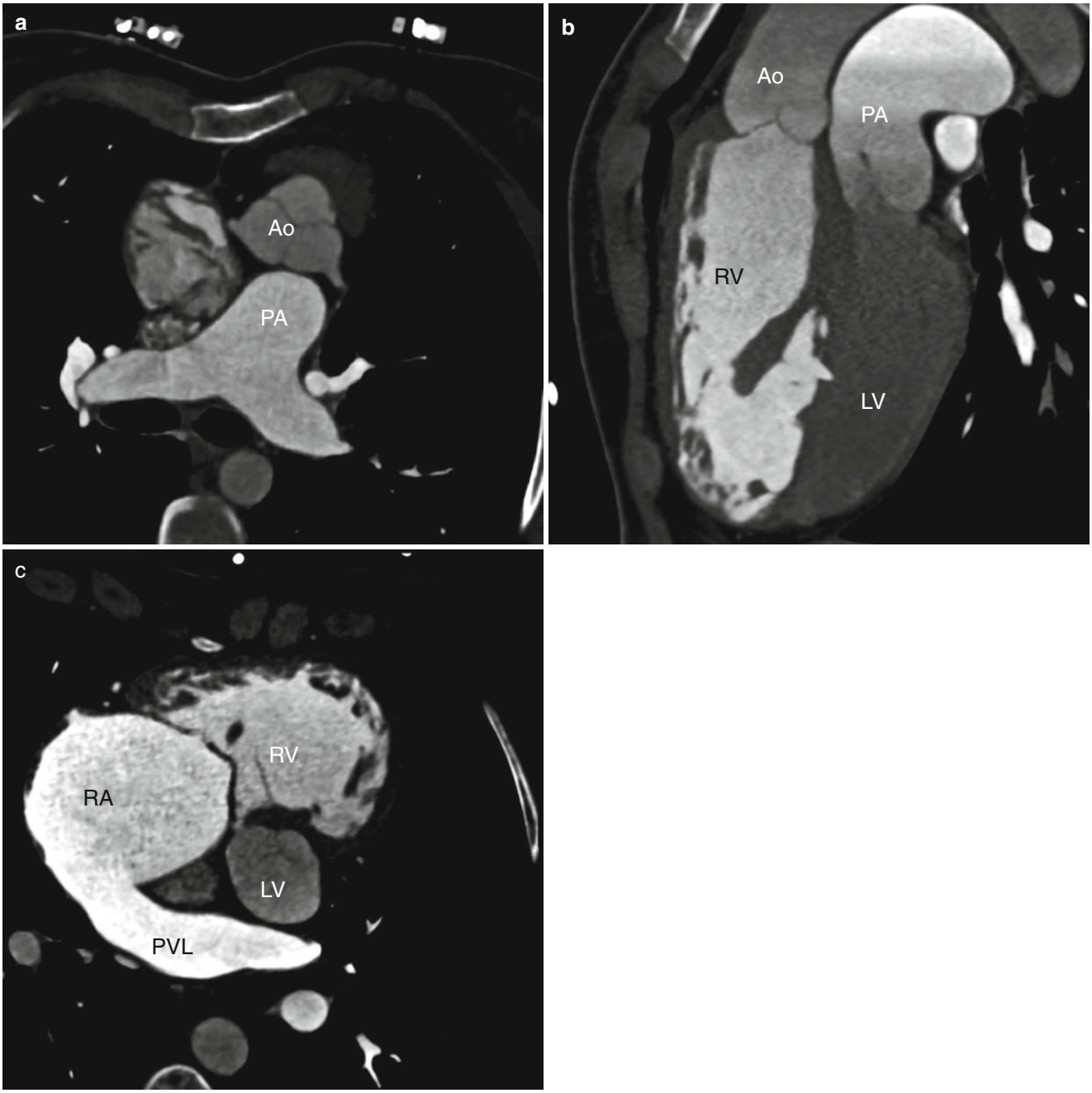


**Fig. 23.5** Mustard procedure. Panel (**a**) an axial view shows the aorta (*Ao*) anterior to the pulmonary artery (*PA*). Panel (**b**) is a sagittal reformation showing the aorta arising from the morphologic right ventricle and the pulmonary artery from the morphologic left ventricle. Panel (**c**) is a two-chamber reformation shows the pulmonary vein limb (*PVL*) entering the right atrium (*RA*). *RV* right ventricle

## 23.1 Cardiovascular Complications of the Atrial Baffling Procedure

Surgical complications of the Mustard and Senning procedures are related to the intra-atrial baffle and include baffle stenosis (Fig. 23.6), baffle leaks (Fig. 23.7), and vena cava obstruction [4]. Baffle leaks are more common than baffle stenosis or obstruction. Leaks usually have no significant hemodynamic impact but may result in paradoxical embolism. Large baffle leaks and significant baffle obstruction need to be repaired either percutaneously with placement of stents (Fig. 23.8) or via surgical procedures.

Obstruction of the systemic venous limb of the atrial baffle is substantially more common than obstruction of the pulmonary venous limb. Patients may develop superior vena cava syndrome, hepatic congestion, cirrhosis, and ascites. Hemodynamically significant stenosis can often be treated with percutaneous stenting. Pulmonary vein stenosis is much less common and it can result in pulmonary hypertension and pulmonary edema.

Other late cardiovascular complications include morphologic right ventricular (systemic ventricle) failure with secondary tricuspid valve regurgitation, occasionally requiring valve replacement (Fig. 23.9), arrhythmias (sinus node dysfunction, atrial flutter), and sudden death. These patients often develop end-stage heart failure and ultimately may require cardiac transplantation. Many patients now survive into the third and fourth decades of life and an 80 % survival at age 20 years has been reported [5, 6]. Because of the high incidence of cardiovascular complications, the atrial switch procedure was replaced by the arterial switch operation (see Chap. 24).

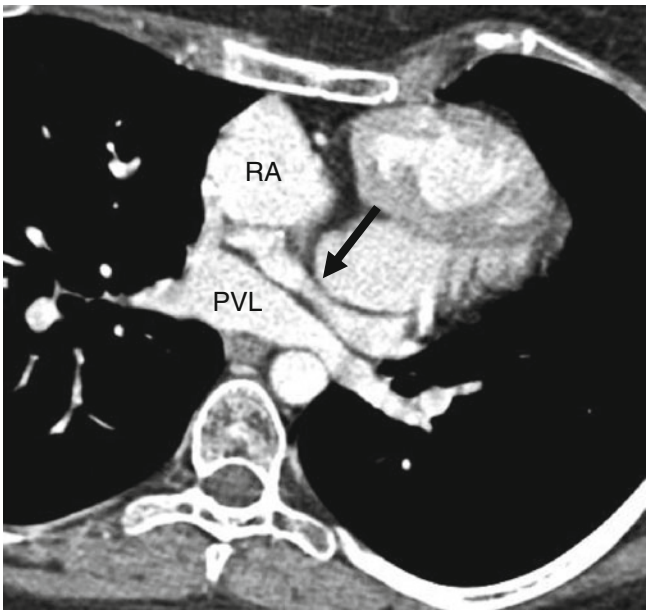


**Fig. 23.6** Baffle stenosis. Axial view shows a narrowed systemic venous limb (*arrow*). *RA* right atrium, *PVL* pulmonary venous limb

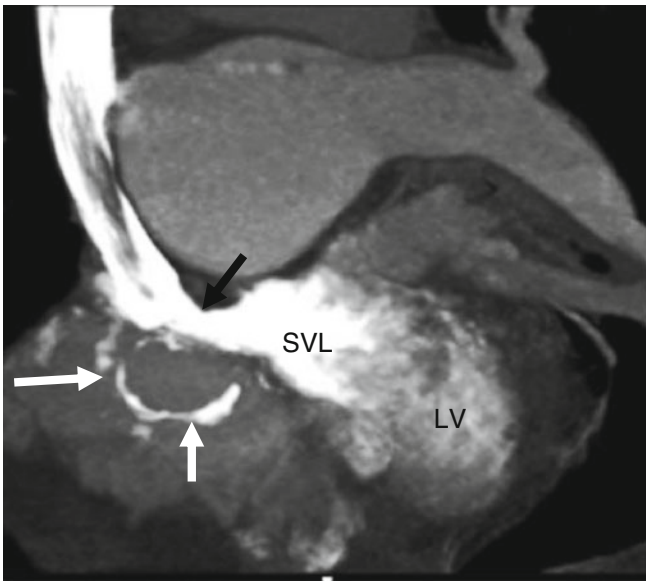


**Fig. 23.7** Baffle leak and stenosis. A reformatted view in a separate patient showing a small leak (*white arrows*) arising from the superior systemic venous limb (*SVL*) of the baffle. There is a small degree of stenosis (*black arrow*) in the superior limb. *LV* morphologic left ventricle

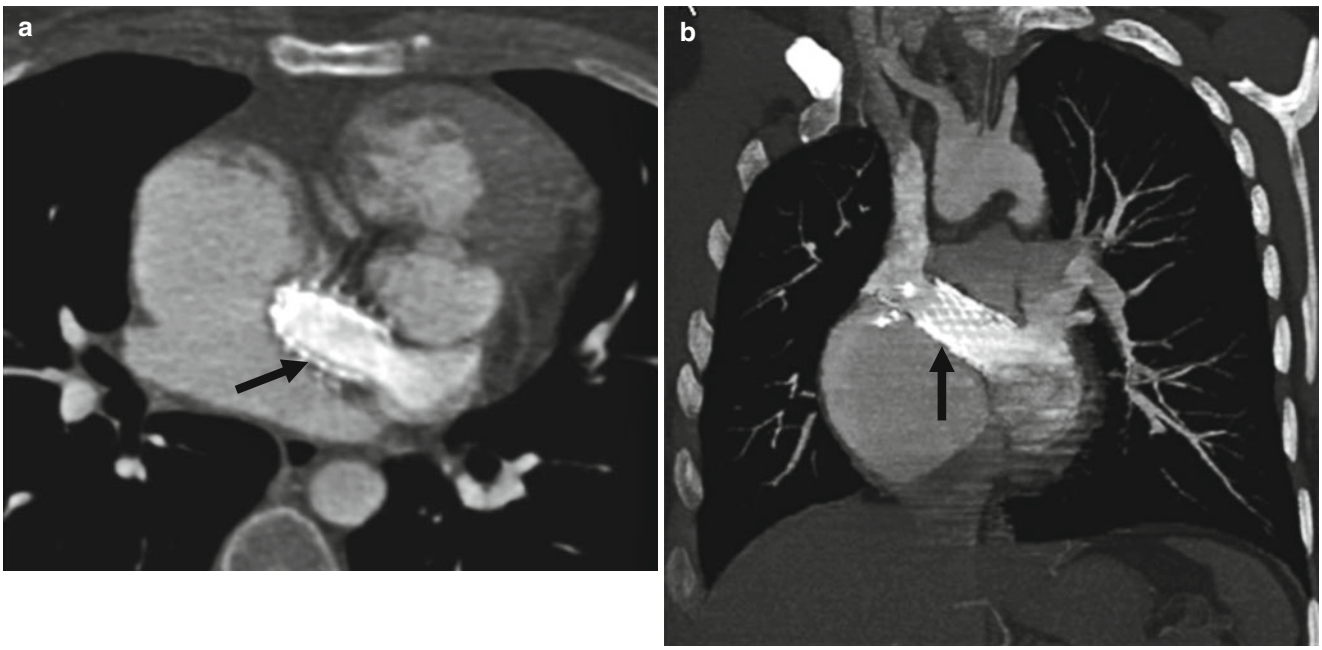


**Fig. 23.8** Baffle stent. Panel (**a**) axial and panel (**b**) coronal views show a stent (*black arrow*) in the systemic venous limb (caval, deoxygenated blood to the morphologic left heart)

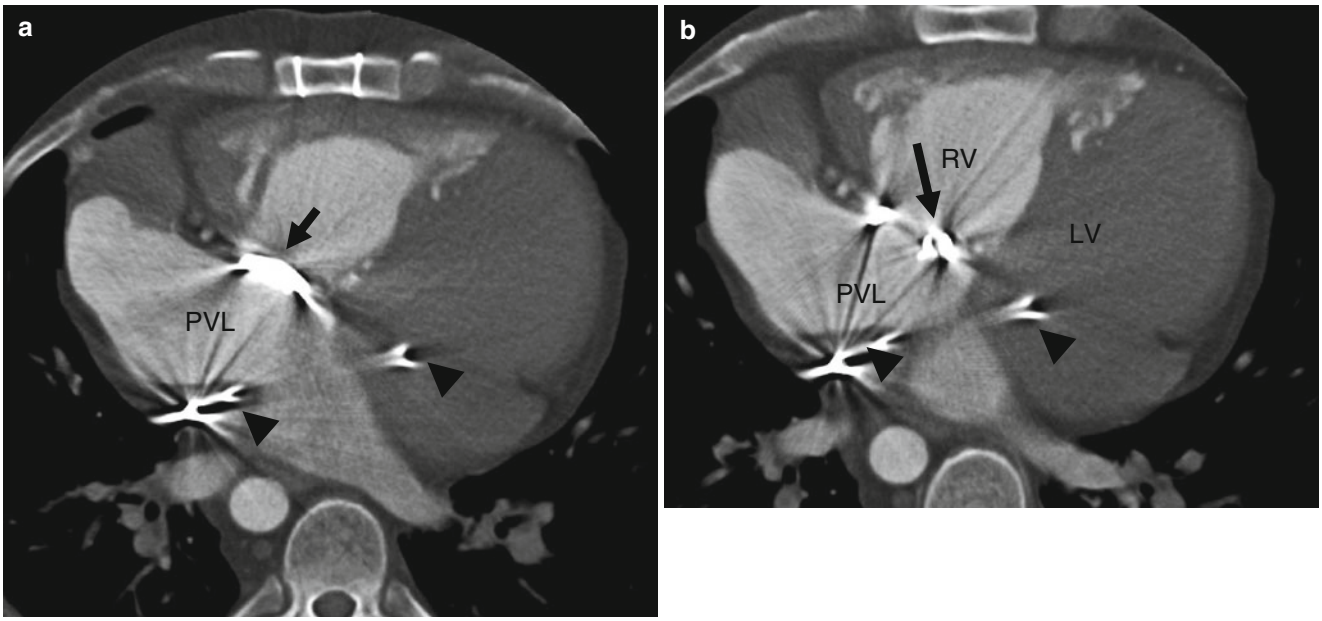


**Fig. 23.9** Mechanical tricuspid valve replacement in a patient status post a Mustard procedure in childhood complicated by severe morphologic tricuspid valve regurgitation (atrioventricular valve of the systemic ventricle). Panels (**a**) and (**b**) are axial views showing the prosthetic tricuspid valve (*arrow*) and the pulmonary venous limb (*PVL*) of the baffle. Note the pacemaker leads (*arrowheads*). *RV* morphologic right ventricle, *LV* morphologic left ventricle

## 23.2 Cardiac Computed Tomographic Angiography (CT) in the Evaluation of Atrial Switch Procedures

CT is an important noninvasive imaging modality for the detection and assessment of hemodynamically significant postoperative complications in patients with TGA [7–13]. CT is often preferred over magnetic resonance (MR) imaging due to the frequent presence of pacemakers in patients with arrhythmias (Fig. 23.10).

In patients who have undergone an atrial switch procedure, CT can be performed without gating. A noncontrast sequence can be performed to identify high density or calcified baffles and patches, followed by an arterial phase timed to the flow in the systemic ventricle (Fig. 23.11). Contrast (though less dense but diagnostic) will be seen in the pulmonary venous baffle during the arterial phase. However, a delayed phase may be acquired to assess the pulmonary venous baffle limb if this information is clinically important. Postoperative anatomy and surgical complications related to baffle obstruction and leaks and venae cavae obstruction can be effectively evaluated using CT.

In addition, CT may also be used to assess changes in ventricular size, wall thickness, and ventricular dysfunction caused by the systemic loading conditions.

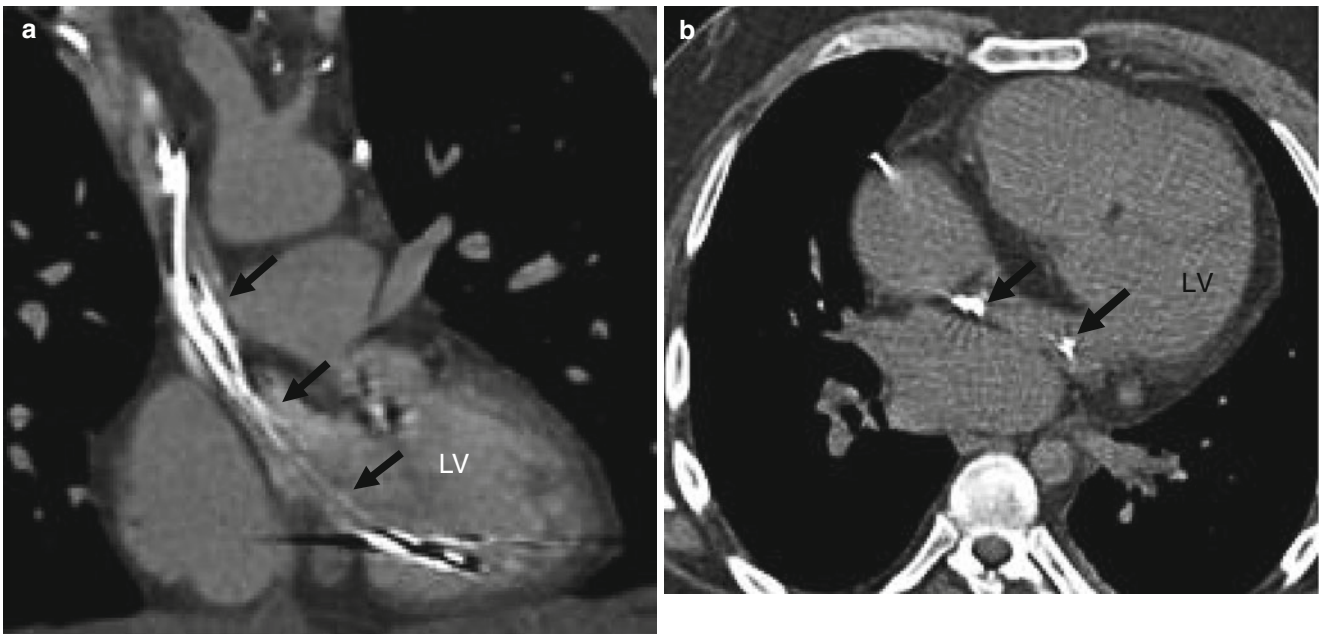


**Fig. 23.10** Senning baffle with pacemaker leads. The scout radiograph demonstrated an epicardial pacemaker. Panel (**a**) is a coronal view and panel (**b**) is an axial cut showing the pacemaker leads (*arrows*) extending from the superior vena cava through the systemic venous limb of the baffle to the morphologic left ventricle (*LV*) which is the pulmonary ventricle

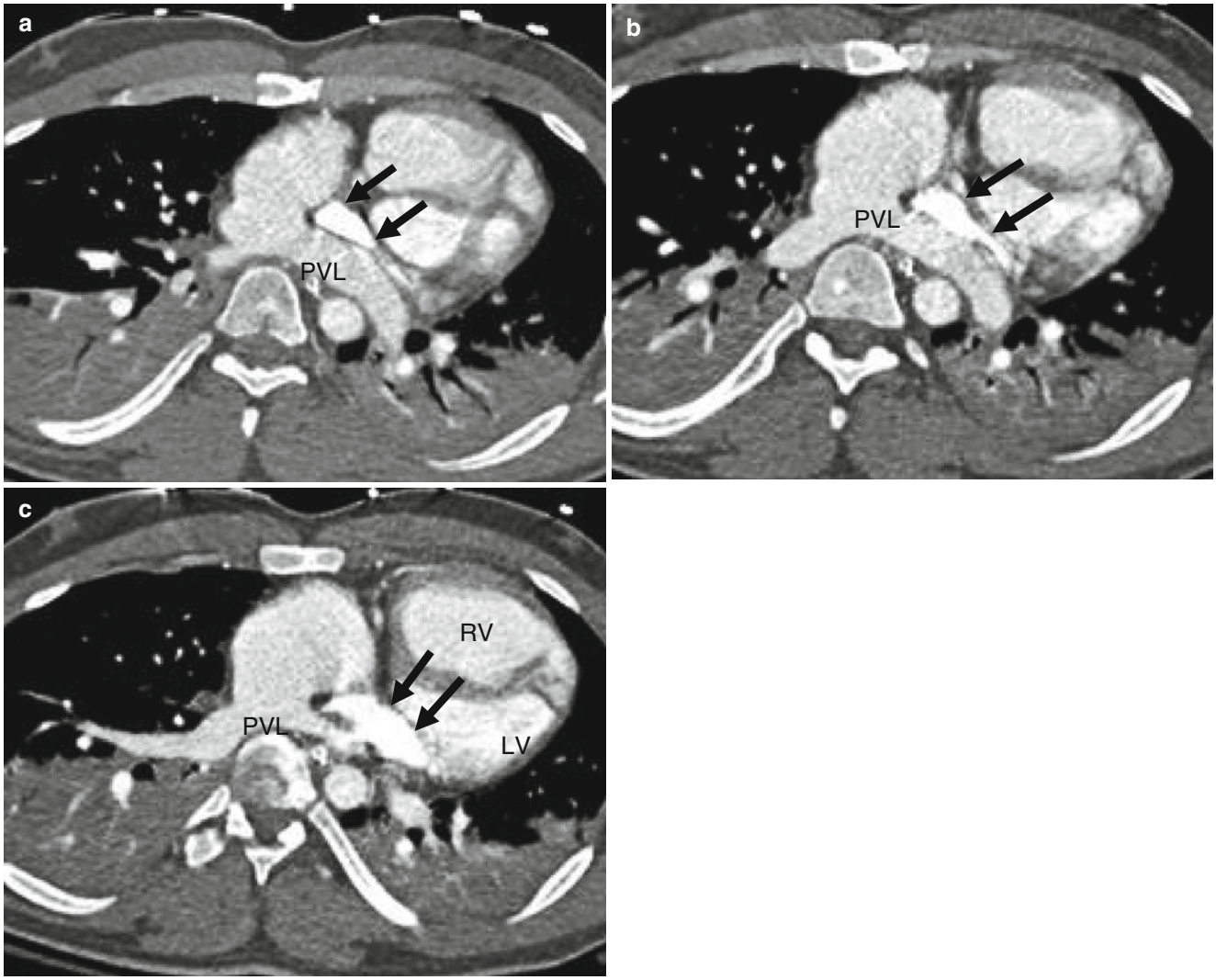


**Fig. 23.11** Atrial baffle enhancement. Panels (**a**), (**b**), and (**c**) demonstrate arterial phase images which illustrate a dense contrast-enhanced systemic venous baffle (*arrows*). The pulmonary venous baffle (*PVL*) is less dense but still adequately visualized. *RV* morphologic right ventricle, *LV* morphologic left ventricle

## References


1. Senning A. Surgical correction of transposition of the great vessels. Surgery. 1959;45:966–80.
2. Mustard WT. Successful two-stage correction of transposition of the great vessels. Surgery. 1964;55:469–72.
3. Wells WJ, Blackstone E. Intermediate outcome after mustard and senning procedures: a study by the congenital heart surgeons society. Semin Thorac Cardiovasc Surg Pediatr Card Surg Annu. 2000;3:186–97.
4. Dos L, Teruel L, Ferreira IJ, Rodriguez-Larrea J, Miro L, Girona J, et al. Late outcome of senning and mustard procedures for correction of transposition of the great arteries. Heart. 2005;91:652–6. doi:10.1136/hrt.2003.029769.
5. Wilson NJ, Clarkson PM, Barratt-Boyes BG, Calder AL, Whitlock RM, Easthope RN, et al. Long-term outcome after the mustard repair for simple transposition of the great arteries. 28-year follow-up. J Am Coll Cardiol. 1998;32:758–65.
6. Prieto LR, Hordof AJ, Secic M, Rosenbaum MS, Gersony WM. Progressive tricuspid valve disease in patients with congenitally corrected transposition of the great arteries. Circulation. 1998;98:997–1005.
7. Gaca AM, Jaggers JJ, Dudley LT, Bisset 3rd GS. Repair of congenital heart disease: a primer-part 1. Radiology. 2008;247:617–31. doi:10.1148/radiol.2473061909.
8. Hughes Jr D, Siegel MJ. Computed tomography of adult congenital heart disease. Radiol Clin North Am. 2010;48:817–35. doi:10.1016/j.rcl.2010.04.005.
9. Rodriguez E, Soler R, Fernandez R, Raposo I. Postoperative imaging in cyanotic congenital heart diseases: part 1, normal findings. AJR Am J Roentgenol. 2007;189:1353–60. doi:10.2214/07.2104.
10. Siegel MJ, Bhalla S, Gutierrez FR, Billadello JB. MDCT of postoperative anatomy and complications in adults with cyanotic heart disease. AJR Am J Roentgenol. 2005;184:241–7.
11. Siegel MJ. CT evaluation of congenital heart disease in adults. Appl Radiol. 2005;34:61–8.
12. Soler R, Rodriguez E, Alvarez M, Raposo I. Postoperative imaging in cyanotic congenital heart diseases: part 2, complications. AJR Am J Roentgenol. 2007;189:1361–9. doi:10.2214/AJR.07.2105.
13. Spevak PJ, Johnson PT, Fishman EK. Surgically corrected congenital heart disease: utility of 64-MDCT. AJR Am J Roentgenol. 2008;191:854–61. doi:10.2214/AJR.07.2889.

# Arterial Switch Operation for Transposition of the Great Arteries

# 24

Arterial switch (Jatene) procedure, which was developed in the late 1970s, is currently the method of choice for treatment of transposition of the great arteries (TGA). It reestablishes the left ventricle as a systemic pump, avoiding systemic ventricular failure associated with the atrial switch operation. This procedure is indicated for patients with TGA with an intact ventricular septum or with a small ventricular septal defect (VSD). Patients with large nonrestrictive VSDs, left ventricular outflow obstruction, or increased pulmonary vascular resistance may not be candidates for the arterial switch procedure.

The Jatene procedure is typically performed in the first 2 weeks of life. Following aortic cross-clamping, the left and right coronary artery ostia and a cuff of the adjacent aortic wall attached as "buttons" are excised from the aorta, and the proximal sections of the coronary arteries are separated from the surface of the heart. This technique prevents distortion after anastomosis to the neoaorta. Usually, the coronary implantation sites are located at the left and right anterior positions at the base of the neoaorta. Next the aorta is transected above the coronary artery ostia and the pulmonary artery is transected above the pulmonic valve.

Subsequently, a Lecompte maneuver (added in the 1980s) is performed and involves positioning the distal pulmonary artery and its branches anterior to the aortic root. This maneuver maximizes the length of the aorta, thus further reducing the risk of coronary artery kinking and stenosis. The distal ascending aorta is now anastomosed to the "new" aortic root (neoaorta) and the pulmonary artery is anastomosed to the new pulmonic root (neo-pulmonary artery). The coronary arteries are then shifted posteriorly and reimplanted into the facing sinuses of the neoaorta just above its origin from the morphologic left ventricle (Figs. 24.1 and 24.2). Because of the potential complication of stenosis at the anastomotic site of the pulmonary artery to the morphologic right ventricle, reconstruction of the pulmonary artery is often undertaken utilizing a pericardial patch or cryopreserved pulmonary artery homograft patch. Any VSD is also repaired at the time of surgery.

In settings where patients present later in life (after the first or second week), it may be necessary to recondition the left ventricle to handle systemic pressures before the Jatene switch. This is accomplished by placing a band around the main pulmonary artery to increase ventricular afterload.

W. Mazur et al., *CT Atlas of Adult Congenital Heart Disease*,
DOI 10.1007/978-1-4471-5088-6_24, © Springer-Verlag London 2013

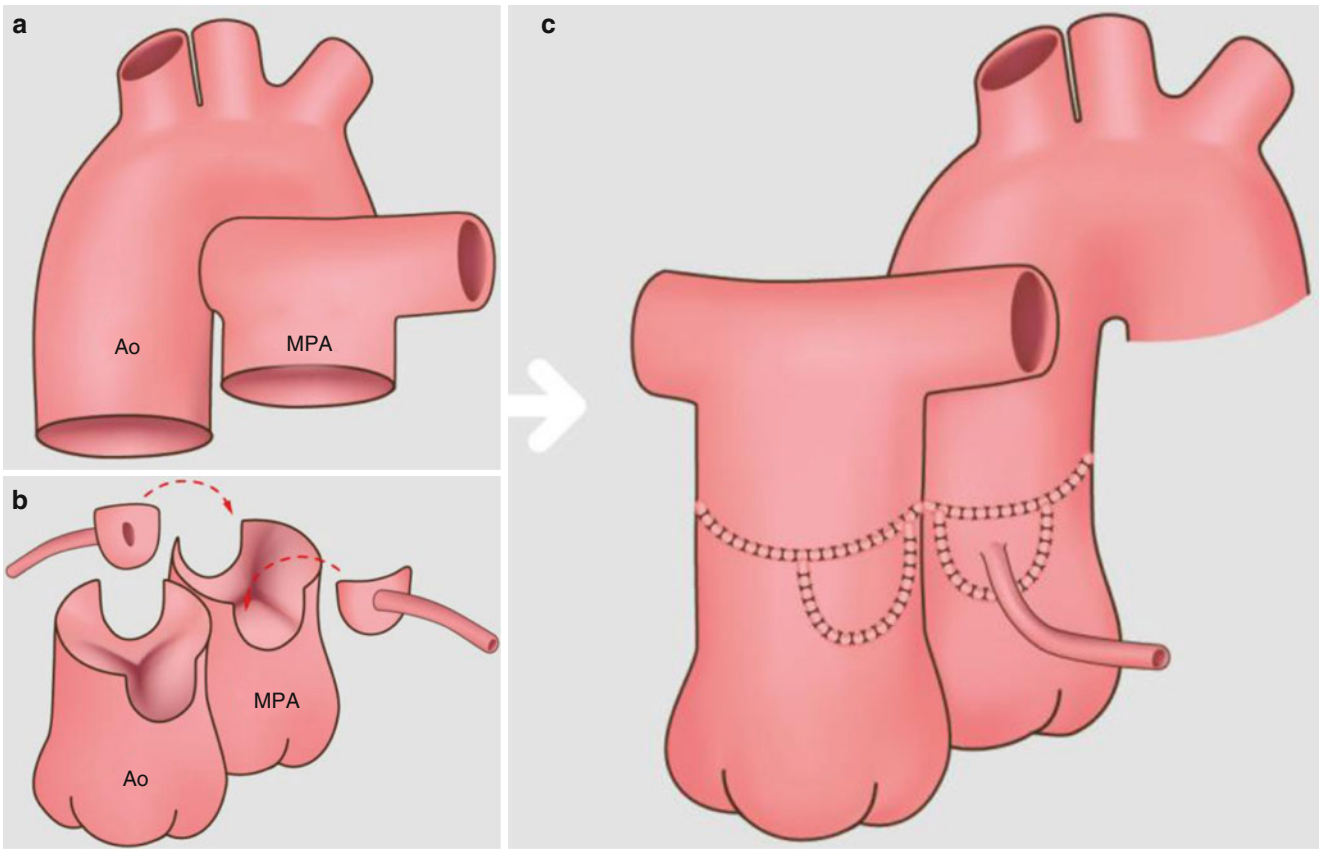


**Fig. 24.1** Arterial switch operation. Reattachment of the great arteries to the contralateral ventricles with reimplantation of the coronary artery ostia into the neoaorta. Panel (**a**) shows the unrepaired transposition morphology prior to surgery. The aorta is anterior and to the right of the pulmonary artery. Panel (**b**) depicts the Jatene procedure where the coronary ostia and a "button" of surrounding aortic wall are excised from the aorta and the proximal sections of the coronary arteries are separated from the heart, which prevents distortion after anastomosis to the neoaorta. Panel (**c**) shows the aorta transplanted onto the pulmonary root. The great arteries are arranged using the Lecompte maneuver, with the pulmonary artery positioned anterior to the ascending aorta. *Ao* aorta, *MPA* main pulmonary artery

**Fig. 24.2** Jatene arterial switch. A 22-year-old woman with transposition of the great arteries status post surgical repair and reimplantation of a single right coronary artery. Panel (**a**) axial and (**b**) sagittal images show the main pulmonary artery (*MPA*) anterior to the aorta (*Ao*). The right and left pulmonary arteries drape over the ascending aorta. There is no stenosis of the right or the left pulmonary artery. Note the parallel orientation of the aorta and pulmonary artery. Panel (**c**) is an axial view in a more caudal plane showing the pulmonic valve (*P*) anterior to the aortic valve (*A*). Panels (**d**) and (**e**) are reformatted scans showing a single, reimplanted coronary artery (*arrows*) originating above the sinotubular junction from the right coronary cusp of the aortic valve. The origin of the single coronary artery is immediately posterior to the main pulmonary artery (*MPA*) and anterior to the aorta (*Ao*). No definite stenosis is seen although the artery is flattened as it courses between the aorta and the pulmonary artery

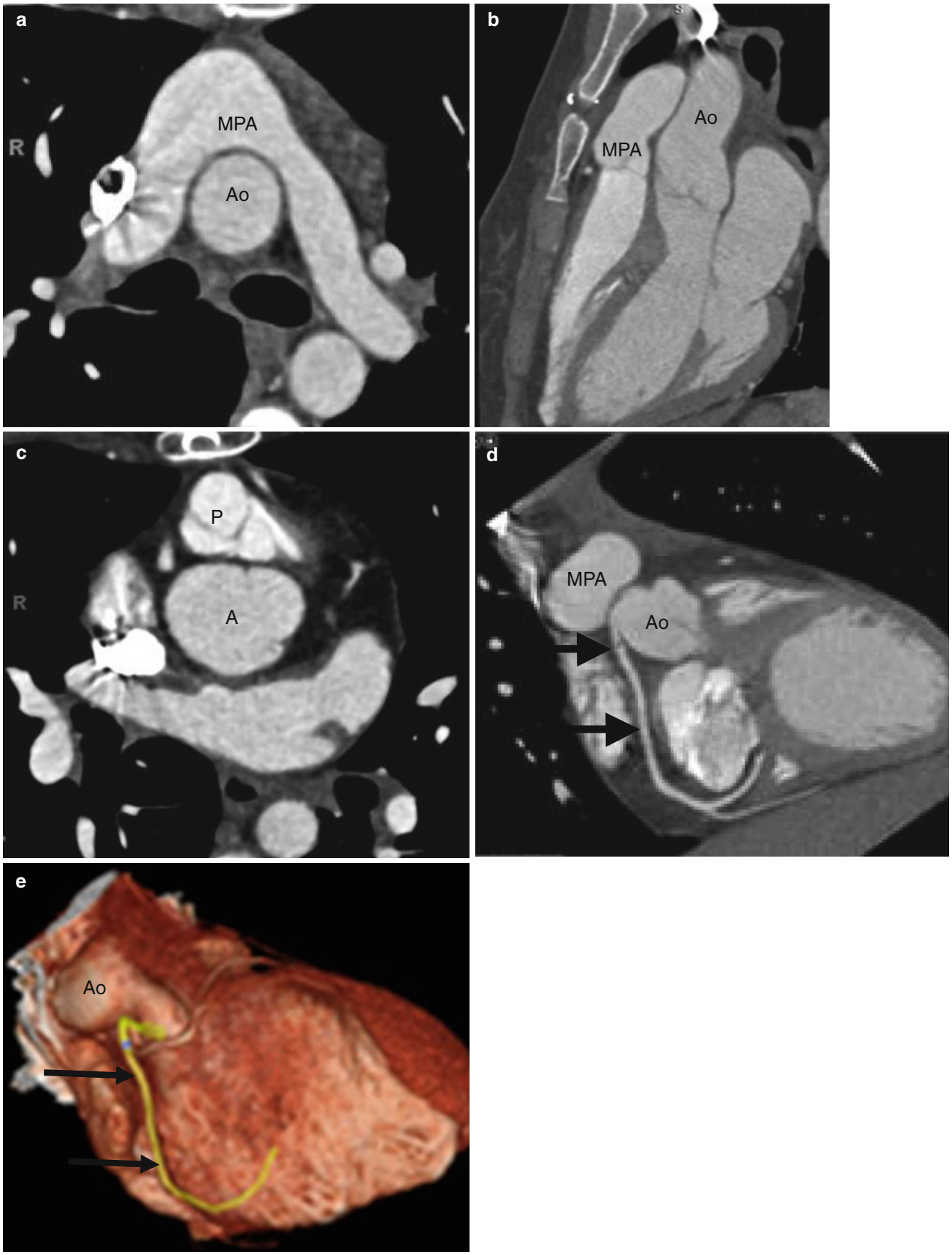
a
MPA
R
Ao
b
Ao
MPA
c
P
R
A
d
MPA
Ao
e
Ao

## 24.1 Complications of the Jatene Procedure

The arterial switch procedure has a more favorable outcome than the atrial switch operation because the morphologic ventricles are connected with their respective workloads. The most common complication of the arterial switch operation is stenosis at the anastomotic site of the pulmonary artery to the new pulmonic root, which usually occurs within the first postoperative year and is often correctable by balloon angioplasty. This complication, however, has been reduced with improvement in surgical techniques [1]. Narrowing of the pulmonary artery as it crosses the aorta also can occur (Fig. 24.3).

Later complications include left ventricular outflow obstruction and left ventricular dysfunction (rare), dilatation of the neoaortic root (50 % of cases) (Fig. 24.4) and neoaortic valve regurgitation, likely related to neoaortic dilatation [2–7]. Coronary artery complications (either kinking or stenosis at the reimplantation site) are also relatively common and may require percutaneous or surgical revascularization [2–7].

An additional important benefit of the arterial switch over the atrial switch procedure is a much lower incidence of arrhythmias.

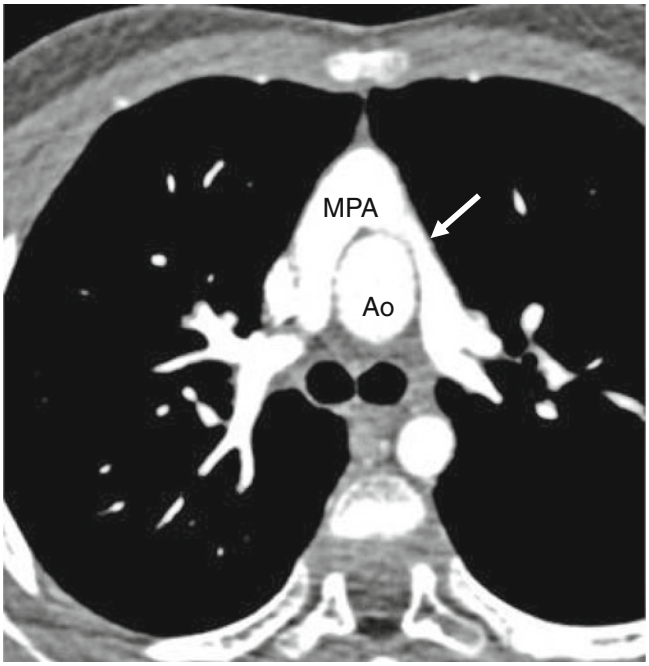


**Fig. 24.3** Jatene procedure with a narrowed left pulmonary artery. This axial image shows a mild narrowing of the left pulmonary artery (*white arrow*) as it crosses over the aorta which was of no hemodynamic significance. *MPA* main pulmonary artery, *Ao* aorta

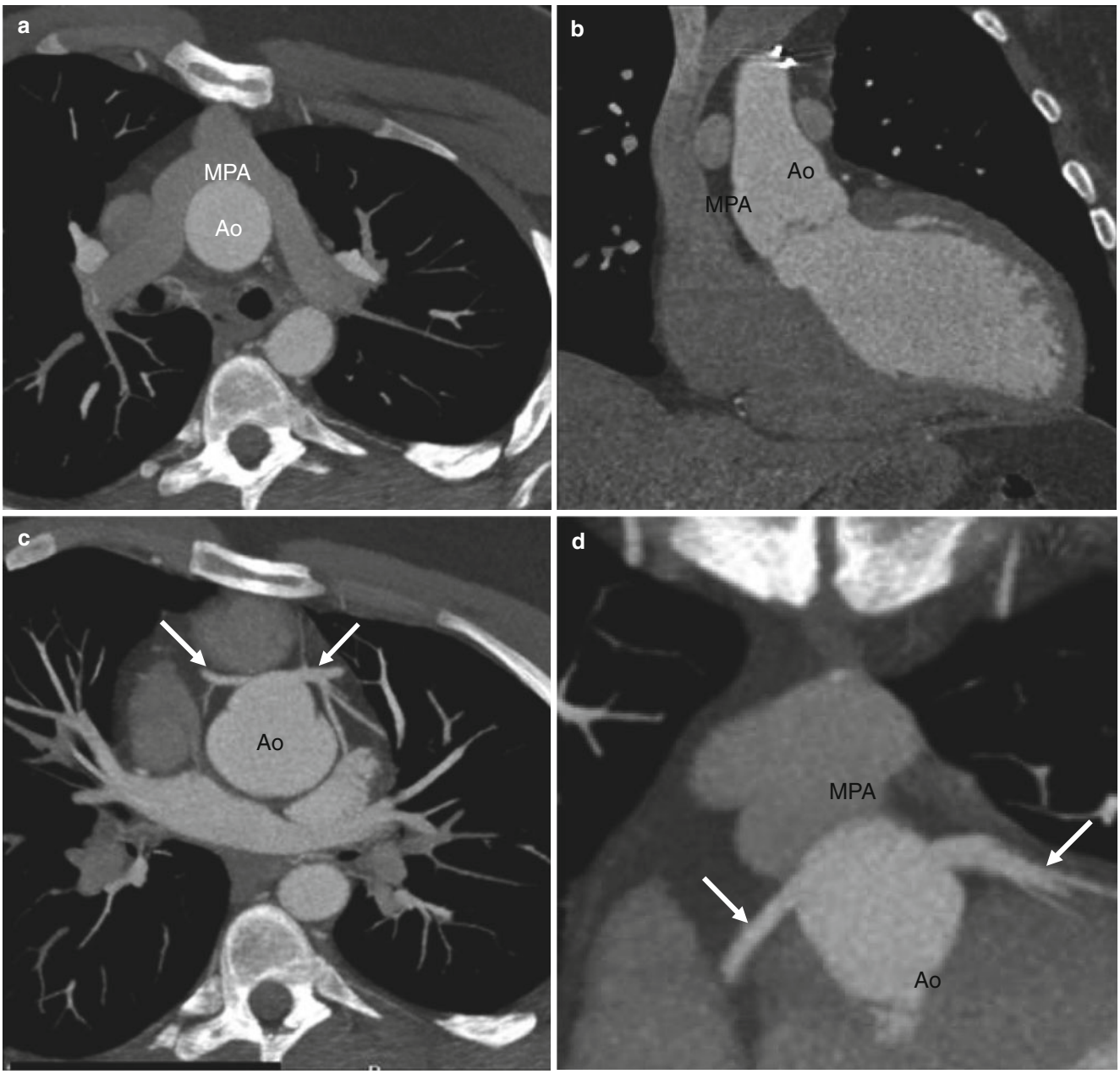


**Fig. 24.4** Jatene procedure with dilated aortic root in a 19-year-old male. Panel (**a**) is a axial image showing the main pulmonary artery (*MPA*) draping over the aorta (*Ao*). Panel (**b**) is a coronal slice showing dilatation of the root of the neoaorta (*Ao*). It measured 4.5 cm at the level of the sinus of Valsalva, 4.2 cm in diameter at the sinotubular junction, and 2.4 cm at the level of the pulmonary artery. Panels (**c**), (**d**), and (**e**) are reformatted views showing the reimplanted left main and right coronary arteries (*arrows*) arising from the anterior cusp of the neoaorta (*Ao*). In most cases, the coronary implantation sites will be at left and right anterior positions at the base of the neoaorta. *MPA* main pulmonary artery

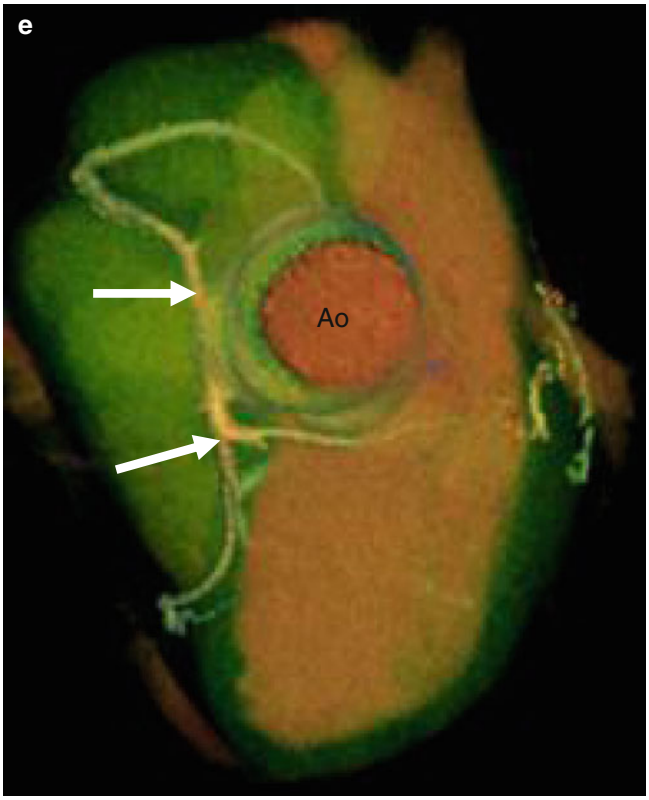


**Fig. 24.4** (continued)

## 24.2 Cardiac Computed Tomographic Angiography (CT) in the Evaluation of Arterial Switch Procedure

Imaging of the arterial switch operation can be reliably performed with computed tomography (CT) [8–14]. The arterial phase CT should be timed to flow in the aorta. Delayed phase imaging is not required. Coronary artery origins and course are usually seen without ECG gating, but if detailed coronary artery delineation is needed, CT with ECG gating should be performed. Morphology of the great vessels, pulmonic outflow tract stenosis, and neoaortic dilatation are well demonstrated on CT. Coronary artery kinking and stenosis can also be detected.

## References

1. Tobler D, Williams WG, Jegatheeswaran A, Van Arsdell GS, McCrindle BW, Greutmann M, et al. Cardiac outcomes in young adult survivors of the arterial switch operation for transposition of the great arteries. J Am Coll Cardiol. 2010;56:58–64. doi:10.1016/j.jacc.2010.03.031.
2. Bonnet D, Bonhoeffer P, Piechaud JF, Aggoun Y, Sidi D, Planche C, et al. Long-term fate of the coronary arteries after the arterial switch operation in newborns with transposition of the great arteries. Heart. 1996;76:274–9.
3. Legendre A, Losay J, Touchot-Kone A, Serraf A, Belli E, Piot JD, et al. Coronary events after arterial switch operation for transposition of the great arteries. Circulation. 2003;108 Suppl 1:II186–90. doi:10.1161/01.cir.0000087902.67220.2b.
4. Hausdorf G, Kampmann C, Schneider M. Coronary angioplasty for coronary stenosis after the arterial switch procedure. Am J Cardiol. 1995;76:621–3.
5. Prifti E, Bonacchi M, Luisi SV, Vanini V. Coronary revascularization after arterial switch operation. Eur J Cardiothorac Surg. 2002;21:111–3.
6. Pasquali SK, Hasselblad V, Li JS, Kong DF, Sanders SP. Coronary artery pattern and outcome of arterial switch operation for transposition of the great arteries: a meta-analysis. Circulation. 2002;106:2575–80.
7. Hutter PA, Kreb DL, Mantel SF, Hitchcock JF, Meijboom EJ, Bennink GB. Twenty-five years' experience with the arterial switch operation. J Thorac Cardiovasc Surg. 2002;124:790–7.
8. Gaca AM, Jaggers JJ, Dudley LT, Bisset 3rd GS. Repair of congenital heart disease: a primer-part 1. Radiology. 2008;247:617–31. doi:10.1148/radiol.2473061909.
9. Hughes Jr D, Siegel MJ. Computed tomography of adult congenital heart disease. Radiol Clin North Am. 2010;48:817–35. doi:10.1016/j.rcl.2010.04.005.
10. Rodriguez E, Soler R, Fernandez R, Raposo I. Postoperative imaging in cyanotic congenital heart diseases: part 1, normal findings. AJR Am J Roentgenol. 2007;189:1353–60. doi:10.2214/07.2104.
11. Siegel MJ, Bhalla S, Gutierrez FR, Billadello JB. MDCT of postoperative anatomy and complications in adults with cyanotic heart disease. AJR Am J Roentgenol. 2005;184:241–7.
12. Siegel MJ. CT evaluation of congenital heart disease in adults. Appl Radiol. 2005;34:61–8.
13. Soler R, Rodriguez E, Alvarez M, Raposo I. Postoperative imaging in cyanotic congenital heart diseases: part 2, complications. AJR Am J Roentgenol. 2007;189:1361–9. doi:10.2214/AJR.07.2105.
14. Spevak PJ, Johnson PT, Fishman EK. Surgically corrected congenital heart disease: utility of 64-MDCT. AJR Am J Roentgenol. 2008;191:854–61. doi:10.2214/AJR.07.2889.

# Systemic Vein to Pulmonary Artery Shunts: Glenn, Fontan, and Kawashima Procedures

25

In a normal biventricular heart, the systemic and pulmonary circulations are in series and each circulation is supported by its respective ventricle. In patients with single ventricular chamber morphology, the two circulations are in parallel and patients only survive by mixing of the systemic and pulmonary venous blood, usually via a septal defect. Systemic venous to pulmonary artery surgical connections have been created to provide venous flow to the pulmonary circulation to allow oxygenation of the blood.

## 25.1 Glenn Shunt

The original (classic) Glenn shunt is an end-to-end anastomosis of the superior vena cava to the right pulmonary artery, which is divided from the main pulmonary artery. All proximal superior vena cava blood flow is directed to the right pulmonary artery (Figs. 25.1 and 25.2). The azygous vein is also ligated. This shunt was used to palliate congenital heart defects with right-sided hypoplasia or atresia such as tricuspid atresia, Epstein anomaly, and pulmonary atresia with intact ventricular septum.

The modified Glenn shunt, also known as the bidirectional Glenn shunt, consists of an end-to-side anastomosis of the superior vena cava to the right pulmonary artery, which is not divided from the main pulmonary artery (Figs. 25.3 and 25.4). Because the right pulmonary artery maintains continuity with the main pulmonary artery, blood flows from the superior vena cava into both the right and left pulmonary arteries. The complication of both the original and modified Glenn shunts is the development of pulmonary arteriovenous malformations. Currently, the modified Glenn shunt is used as a staging procedure in children with single-ventricle physiology who will later undergo a Fontan procedure.

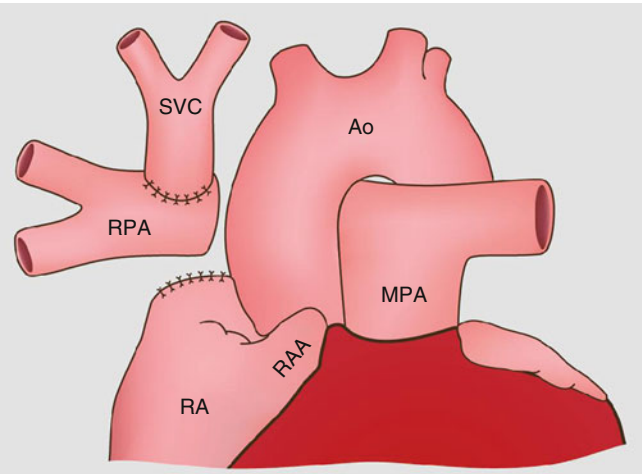


**Fig. 25.1** Glenn shunt. This shunt is an end-to-end anastomosis of the right pulmonary artery (*RPA*), which is divided from the main pulmonary artery to the superior vena cava (*SVC*), directing all proximal SVC blood flow to the RPA. The SVC is ligated at its entrance to the right atrium (*RA*). *Ao* aorta, *MPA* main pulmonary artery, *RAA* right atrial appendage, *RPA* right pulmonary artery


**Fig. 25.2** Glenn shunt for tricuspid atresia. This coronal image shows the shunt (*white arrows*), which extends from the superior vena cava to right pulmonary artery

W. Mazur et al., *CT Atlas of Adult Congenital Heart Disease*,
DOI 10.1007/978-1-4471-5088-6_25, © Springer-Verlag London 2013

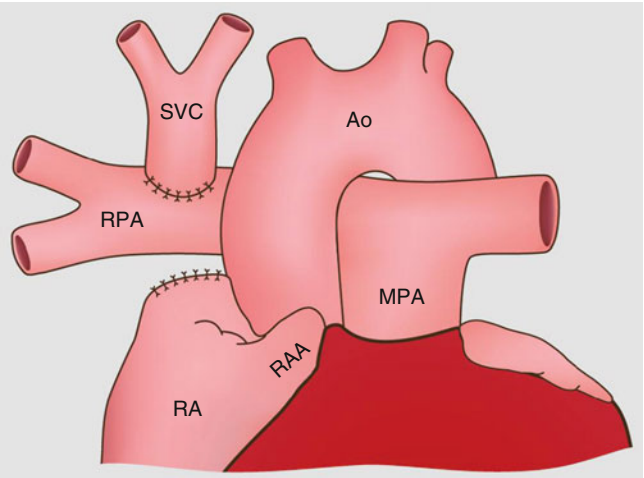


**Fig. 25.3** Modified or bidirectional Glenn shunt. This shunt is an end-to-side anastomosis between the superior vena cava (*SVC*) and the right pulmonary artery. The SVC is divided from the right atrium. The right pulmonary artery is not separated from the main pulmonary artery (*MPA*) so venous blood flows into both the right and left pulmonary arteries. *RAA* right atrial appendage, *RPA* right pulmonary artery, *Ao* aorta. This procedure is used in patients with single-ventricle physiology who eventually will undergo a Fontan procedure

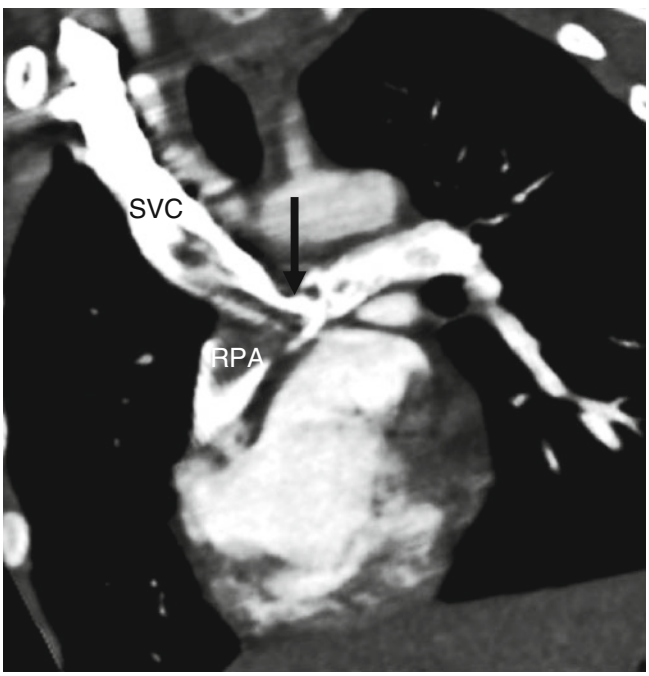


**Fig. 25.4** Bidirectional Glenn shunt. This coronal view shows the end-to-side anastomosis between the superior vena cava (*SVC*) and the right pulmonary artery (*RPA*) at the junction with the main pulmonary artery (*arrow*). Note that contrast-enhanced blood flows to both the right and left pulmonary arteries. The non-opacified blood from the superior vena cava is a flow artifact (not thrombus). Artifact can be differentiated from thrombus by reimaging at 2 min which allows enough time for optimal venous opacification

## 25.2 Fontan Operation

In 1971, Francis Fontan and Eugene Baudet described a procedure that diverted all systemic venous blood into the pulmonary arteries without the interposition of a ventricle as surgical palliation for tricuspid atresia. The Fontan procedure revolutionized the treatment of complex congenital heart defects and remains the palliative treatment of choice for patients born with one functional ventricle. The primary aim of the Fontan procedure is to establish a circulation in which the systemic venous return enters the pulmonary arteries directly.

Creation of the Fontan circulation is considered in all patients with complex congenital heart disease when a biventricular repair is not possible. These include patients with tricuspid atresia, pulmonary atresia with intact ventricular septum, double-inlet left ventricle, hypoplastic left heart syndrome, double-outlet right ventricle, and complete unbalanced atrioventricular septal defects. Candidates for Fontan procedure should be in sinus rhythm and have adequately developed central pulmonary arteries and good ventricular function. The absence of any one of these criteria is a strong predictor of an early poor outcome.

The classic Fontan operation consists of a valved conduit between the right atrium or right atrial appendage and main pulmonary artery (Figs. 25.5 panel a and 25.6). However, this procedure virtually always resulted in severe enlargement and dilatation of the atria which eventually loses contractility and then fails which ultimately further diminishes pulmonary blood flow. Subsequently, there have been many variations of the Fontan procedure, most recently the extracardiac conduit Fontan and lateral tunnel Fontan (Figs. 25.5 panels b, c, 25.7, and 25.8).

The Fontan is usually done early in life as a two-staged repair. Initially a bidirectional Glenn shunt is done to direct superior vena caval blood flow to the lungs, and a tunnel or conduit Fontan is performed with the aim of directing inferior vena cava blood flow to the lungs. In some neonates, a classic or modified Blalock–Taussig shunt may be performed prior to the Fontan procedure in order to establish pulmonary blood flow.

Stage 1 Fontan consists of a bidirectional Glenn shunt or a hemi-Fontan procedure and is usually undertaken as soon as the pulmonary arteries have grown sufficiently to allow a low pulmonary vascular resistance, usually between 2 and 6 months of age. The hemi-Fontan procedure involves formation an atriopulmonary anastomosis between the dome of the right atrium and the underside of the right pulmonary artery with patch in the superior portion of the right atrium to direct blood flow from the superior vena cava atriocaval junction into the atriopulmonary anastomosis (Fig. 25.9). The stage 1 operation provides low-pressure pulmonary blood flow to the lungs and decreases

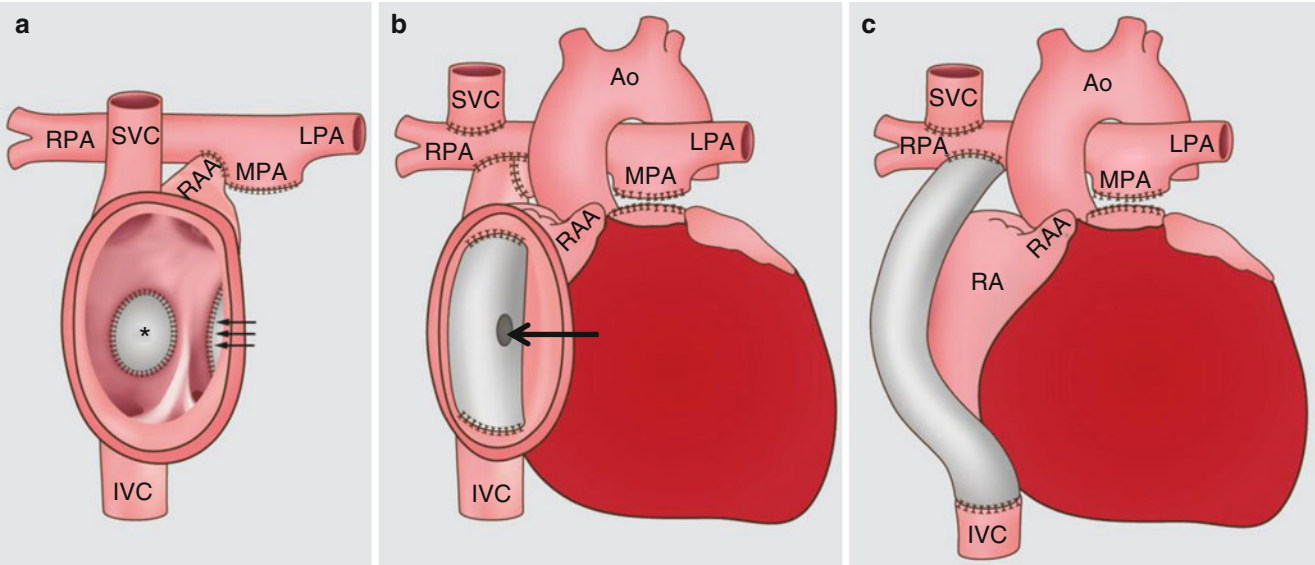


**Fig. 25.5** Fontan procedures. Panel (**a**) demonstrates the classic Fontan procedure. The right atrial appendage (*RAA*) is connected to the pulmonary artery. The asterisk (*) marks the closed atrial septal defect. The three *arrows* point to the over sewn tricuspid valve. Panel (**b**) shows the lateral tunnel procedure. Systemic blood from the inferior vena cava (*IVC*) is redirected via an intra-atrial tunnel to the pulmonary arteries. The main pulmonary artery is ligated. The superior vena cava (*SVC*) is connected to the right pulmonary artery as a bidirectional cavopulmonary anastomosis (bidirectional Glenn shunt). Note the presence of fenestration (*arrow*) in the interatrial tunnel. Panel (**c**) illustrates an extracardiac conduit procedure. Systemic blood flow from the IVC is redirected via an extracardiac conduit to the pulmonary arteries. Similar to the intra-atrial tunnel, the SVC is connected to the right pulmonary artery as a bidirectional cavopulmonary anastomosis. Currently, the Fontan circulation is achieved by using a bidirectional Glenn shunt and a lateral tunnel or extracardiac conduit Fontan. *Ao* aorta, *MPA* main pulmonary artery, *LPA* left pulmonary artery, *RPA* right pulmonary artery

the volume load on the single ventricle. The atria continue to receive venous blood directly from the inferior vena cava and oxygenated blood returning via the pulmonary veins. There is mixing of oxygenated and deoxygenated blood via an atrial septal defect, resulting in peripheral oxygen saturation in the range of 80–85 %. Because patients have residual mixing of oxygenated and deoxygenated blood and hypoxia, a second-stage operation (described below) is required after the pulmonary arteries grow adequately and are less fragile.

Stage 2 Fontan, also called Fontan completion, is usually performed at 2–5 years of age when pulmonary arteries are of sufficient size to allow high pulmonary flow. It involves redirecting blood from the inferior vena cava or hepatic veins into the pulmonary circuit either via a lateral tunnel (Figs. 25.5 panel b and 25.7) or an extracardiac conduit Fontan (Figs. 25.5 panel c and 25.8). With the lateral tunnel Fontan, a tunnel is created in the right atrium using prosthetic material. The tunnel is anastomosed inferiorly to the inferior vena cava and superiorly to the right or main pulmonary artery. With an extracardiac conduit Fontan, the inferior vena cava is separated from the right atrium and a synthetic (polytetrafluoroethylene) tube graft is created adjacent to the right atrium (rather than within it) to connect the inferior vena cava with the right or main pulmonary arteries. A small fenestration or opening may be created between the venous conduit or tunnel and the atrium to prevent volume overload to the pulmonary circulation. The fenestration limits caval pressure and venous congestion. It also results in increased systemic ventricular preload and cardiac output at the expense of mild desaturation. The stage 2 Fontan corrects the hypoxia and leaves the single ventricle responsible only for supplying blood to the body.

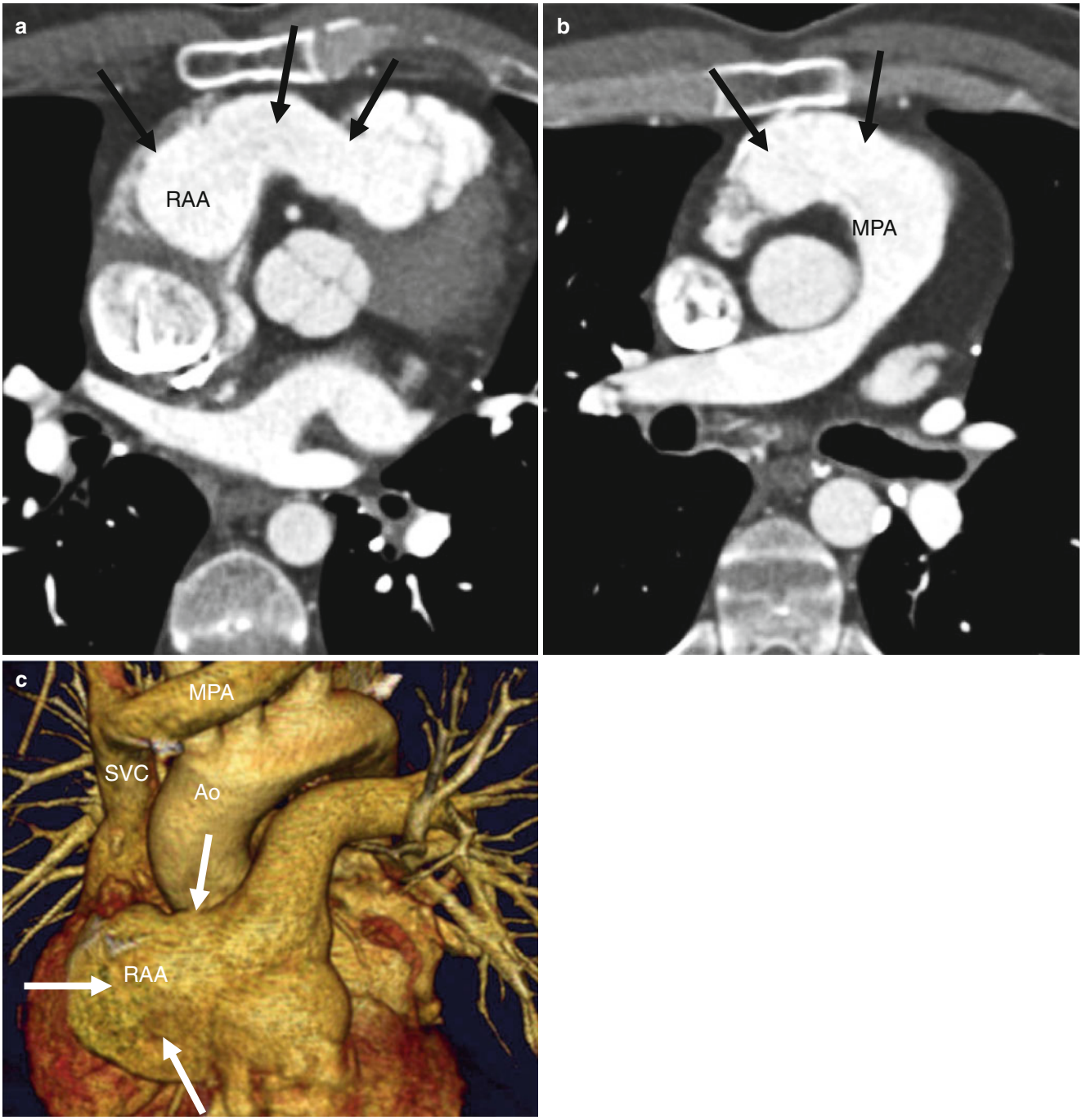


**Fig. 25.6** Classic Fontan shunt for tricuspid atresia. Panels (**a**) and (**b**) are transaxial views. Panel (**c**) is a 3D image. The classic Fontan (*arrows*) from the right atrial appendage (*RAA*) to the main pulmonary artery (*MPA*) is depicted. In panel (c), note the superior vena cava (*SVC*) which is surgically connected to the right pulmonary artery (the anastomosis is posterior and thus not visualized in this image)

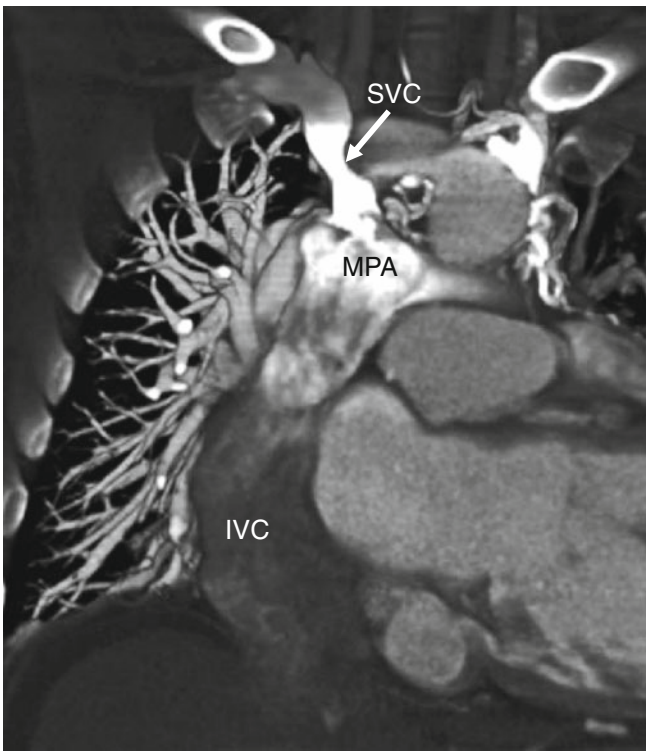


**Fig. 25.7** Lateral tunnel Fontan for tricuspid atresia. A coronal 3D image shows the opacified superior vena cava (*SVC*) and unopacified inferior vena cava (*IVC*), both of which are connected to the main pulmonary artery (*MPA*). The tunnel is created within the right atrium using prosthetic material. *RA* right atrium

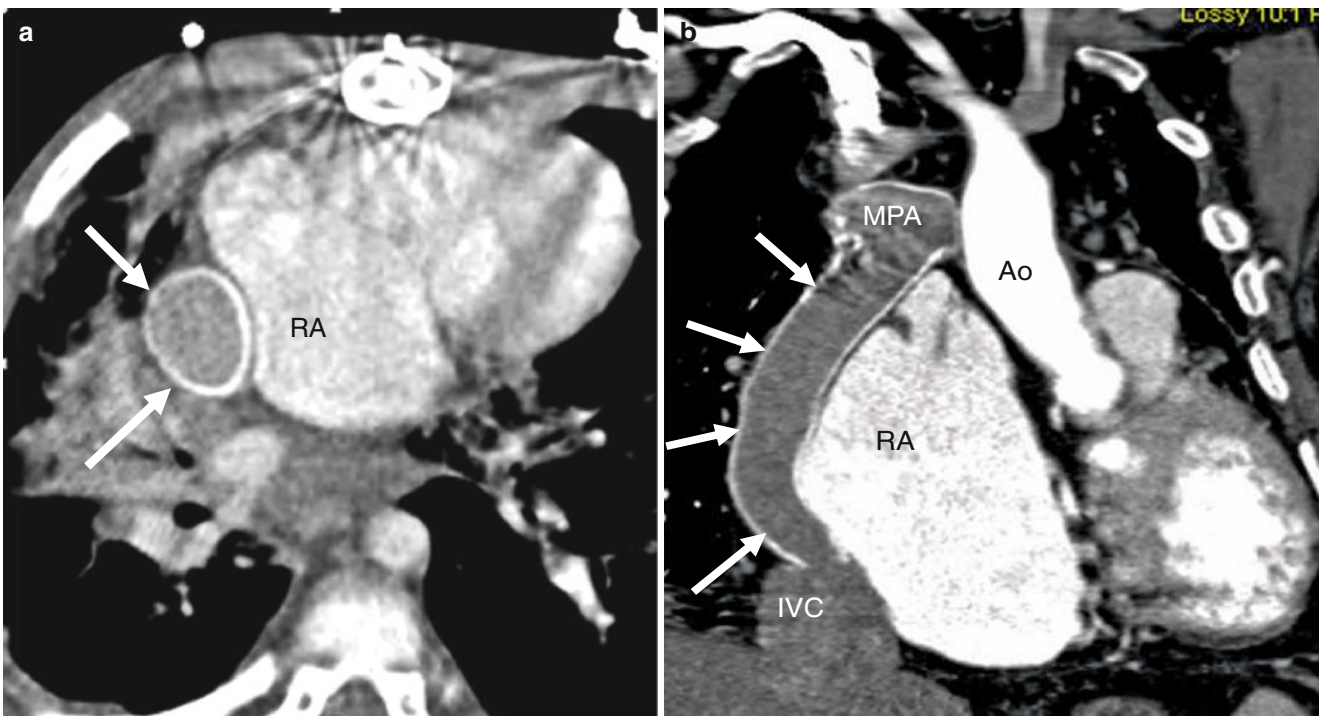


**Fig. 25.8** Extracardiac conduit Fontan. Panel (**a**) is an axial image and panel (**b**) is a coronal reformatted image, showing a synthetic tube graft (*arrows*) adjacent to the enlarged right atrium (*RA*). The shunt connects the inferior vena cava with the main pulmonary artery (*MPA*). *Ao* aorta, *IVC* inferior vena cava

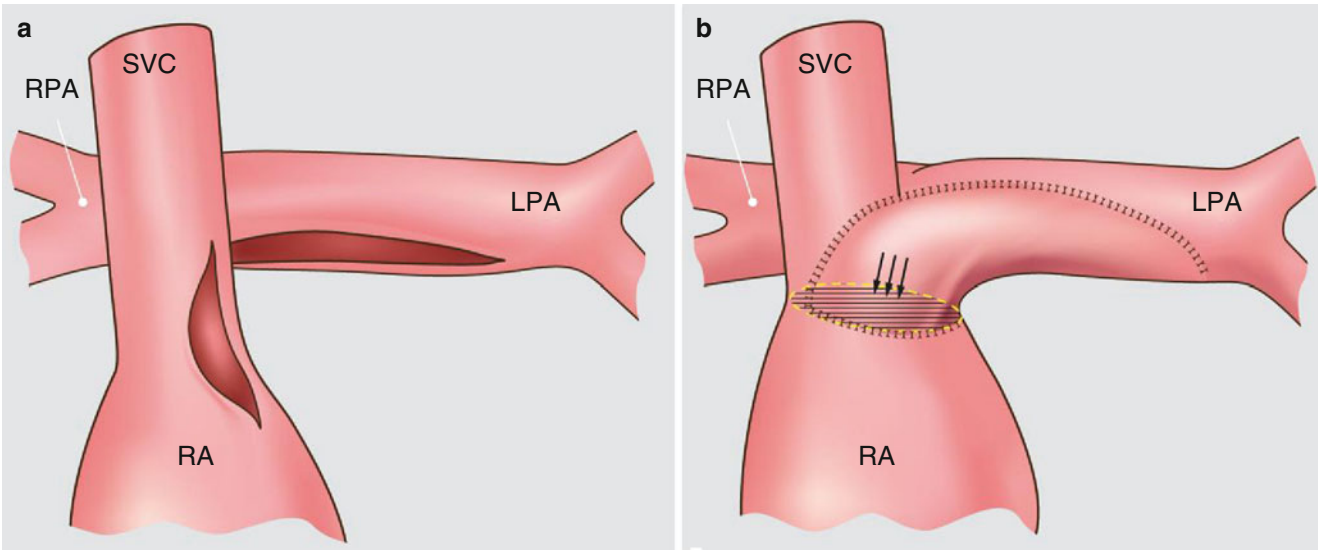


**Fig. 25.9** The hemi-Fontan procedure. This is an alternative first stage procedure to the Glenn shunt in the Fontan operation. Panel **a**. The procedure involves an atriopulmonary anastomosis between the dome of the right atrium (*RA*) and the underside of the right pulmonary artery (*RPA*). A patch is placed in the superior aspect of the *RA* (shown in Panel **b**, *arrows*) to direct blood flow from the superior vena cava (*SVC*) atriocaval junction into the atriopulmonary anastomosis. The patch typically extends into the left pulmonary artery (*LPA*) augmenting the pulmonary artery area

## 25.3 Cardiovascular Complications of Fontan Circulation

Despite the advances in surgical procedures, there are several complications associated with the Fontan procedure. A well-known complication of both the Glenn and original Fontan circulation (right atrial appendage to pulmonary artery) is the development of pulmonary arteriovenous malformations (Fig. 25.10). It is thought that lack of admixture with hepatic venous blood and the absence of pulsatile flow in the pulmonary bed resulting from the absence of a pumping ventricle between the systemic venous return and the pulmonary bed play a role the development of arteriovenous malformations. These have been reported to resolve with reestablishment of exposure to inferior vena cava blood flow. Arteriovenous malformations can result in ventricular volume overload and may lead to irreversible pulmonary hypertension and ultimately failure of the Fontan circulation.

Venovenous connections may also develop between the deoxygenated venous drainage of the upper extremities and the oxygenated pulmonary veins or left atrium. They likely develop secondary to elevated central venous pressures and can result in right-to-left shunting and exacerbation of cyanosis.

Thrombus can develop within conduits or cardiac chambers due to low-velocity pulmonary flow, atrial fibrillation, hypercoagulability, or exposure to thrombogenic suture material (Fig. 25.11) and can result in systemic or pulmonary thromboembolic events. Thromboembolic complications have been reported rarely of in patients within 10 years of the procedure. These include cerebrovascular accidents, pulmonary embolism, and systemic venous clots. Varma et al. reported

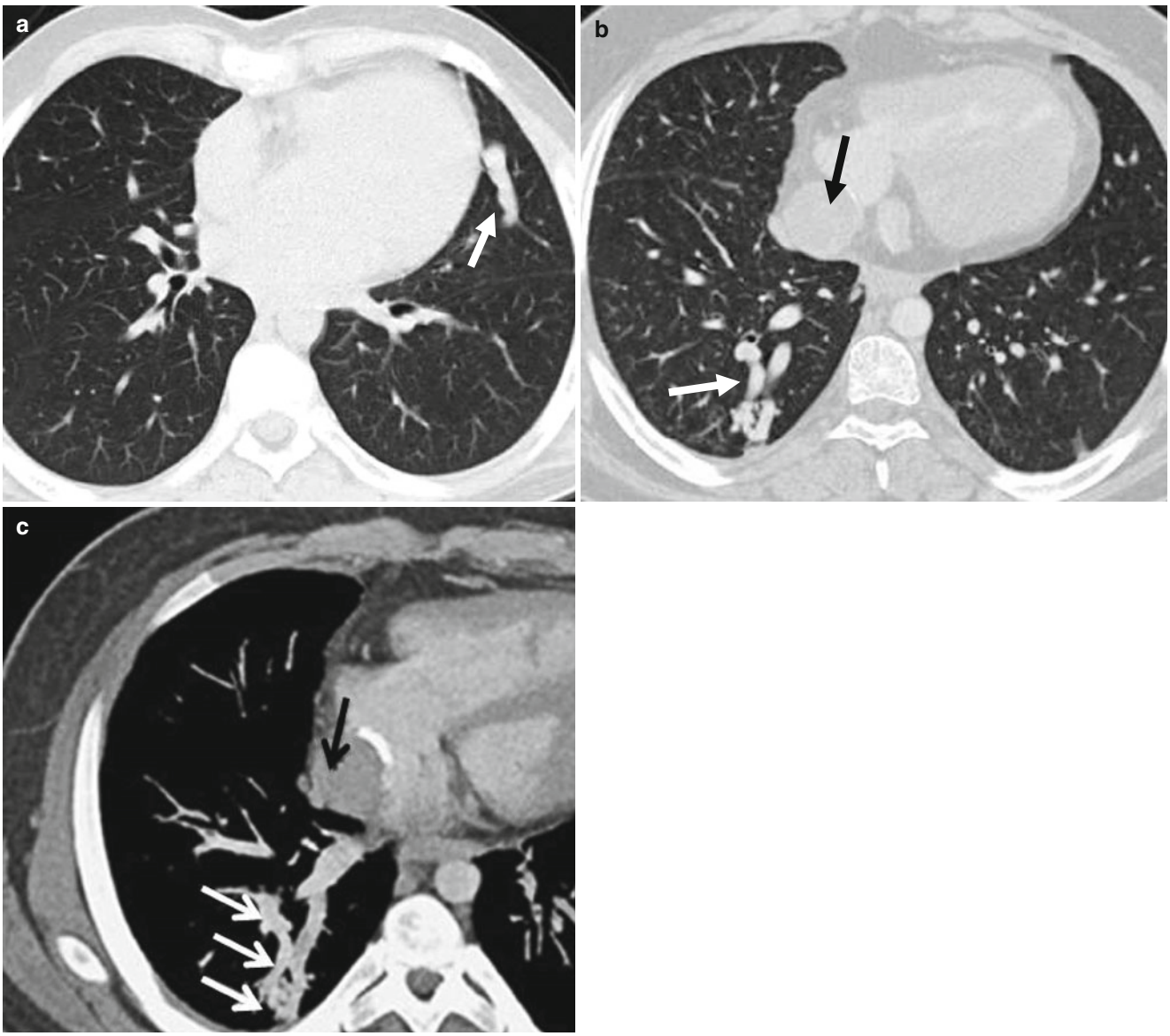


**Fig. 25.10** Arteriovenous malformation (AVM) with a Glenn shunt. Panel (**a**) is an axial image showing a pulmonary AVM (*arrow*) in the lingula. Panel (**b**) is an axial slice and panel (**c**) is a maximum intensity projection (MIP). Both panels (**b**) and (**c**) show an AVM in the right lower lobe (*white arrows*) as well as the extracardiac Fontan (*black arrow*). Note that the use of thick-slab MIPs improves delineation of the feeding arteries and draining veins of the AVM

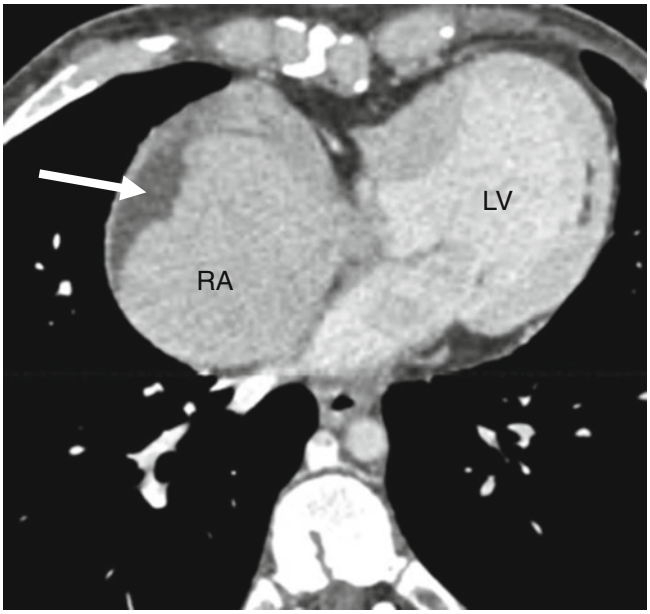


**Fig. 25.11** Fontan shunt with thrombus. Axial image showing thrombus formation (*arrow*) in the enlarged right atrium (*RA*) in a patient with tricuspid atresia. *LV* morphologic left ventricle

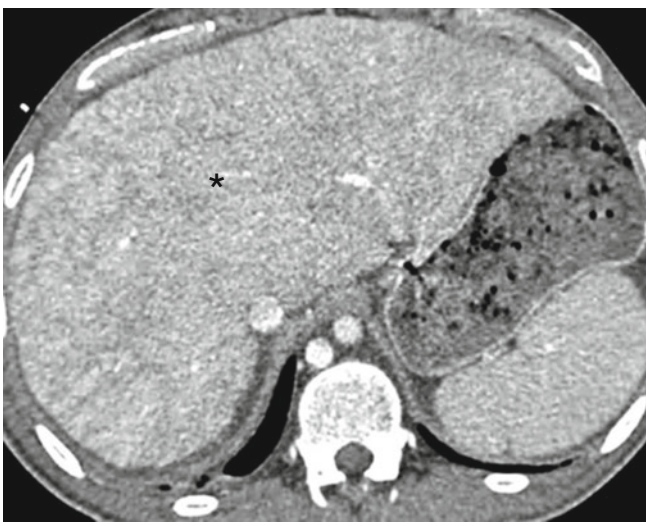


**Fig. 25.12** Hepatic congestion secondary to Fontan circulation. This axial computed tomogram shows a heterogeneous enhancement pattern of the liver (*asterisk*), most prominent in the periphery

clinically silent pulmonary emboli in 17 % of patients with Fontan circulation [1]. The univentricular heart after the Fontan operation occasionally exhibits a blind pouch formed by the pulmonary stump or rudimentary ventricle. Almost 2 % of patents have thrombosis in the blind pouch [2].

Systemic ventricular dysfunction can develop as a result of complications mentioned above. Systolic dysfunction of the single ventricle is seen frequently in patients 10 years after the procedure. Ventricular dilatation, global hypokinesis, hypertrophy, and atrioventricular valve regurgitation can occur. Mild desaturation is common secondary to right-to-left shunting via surgical fenestrations and pulmonary arteriovenous malformations. Additionally, anastomotic stenosis can occur resulting in increased venous pressure and decreased cardiac output. Long-term extracardiac complications include hepatic dysfunction (congestion, fibrosis, and cirrhosis) (Fig. 25.12) and protein-losing enteropathy which often lead to the patient's demise [3].

## 25.4 Cardiac Computed Tomographic Angiography (CT) in the Evaluation of Glenn Shunts and Fontan Circulation

Computed tomography (CT) has a role in evaluating the patency of Glenn shunts and the Fontan circulation as well as the potential complications of these procedures. A noncontrast sequence should be performed in order to identify calcified conduits followed by an arterial phase timed to the aorta. Care must be taken in imaging patients with Fontan anatomy so as not to confuse an unenhanced conduit with thrombus. Hence, a delayed venous-phase CT scan may be useful to allow for contrast enhancement of the conduit or inferior vena cava since more time is required for contrast to opacify these structures (Fig. 25.13) [4]. CT is also helpful in defining complications of shunting at the atrial-conduit level, arteriovenous malformations (Fig. 25.10), and pulmonary embolus/thrombus [5–11]. Arteriovenous malformations are best seen on thick-slab (4–20 mm) maximum intensity projections. CT can also be used to evaluate the percutaneous coil embolizations performed to treat these malformations.

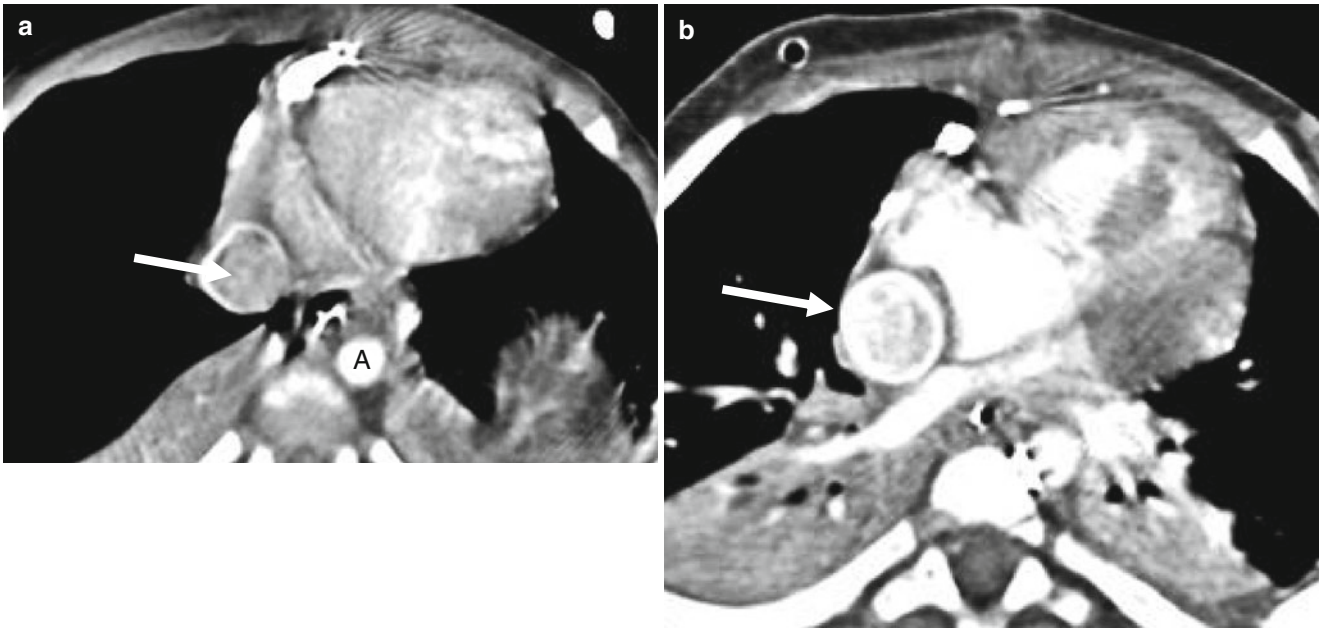


**Fig. 25.13** Fontan shunt enhancement techniques. Panel (**a**) an arterial phase image 15 s after injection of contrast medium. The Fontan conduit (*arrow*) is not opacified, while the aorta (*A*) shows intense enhancement. Panel (**b**) a delayed image at 30 s shows enhancement of the conduit (*arrow*)

## 25.5 Kawashima Procedure

The Kawashima procedure is performed in patients with heterotaxy syndrome and refers to creation of a bidirectional Glenn shunt in the setting of interruption of the inferior vena cava with azygous continuation to the superior vena cava. The azygous continuation of the inferior vena is then anastomosed to the pulmonary artery (Fig. 25.14). This results in redirection of systemic venous blood to the lungs with the exception of the hepatic and coronary venous return. Mild cyanosis is present postoperatively because desaturated hepatic venous blood mixes with pulmonary venous blood. Hepatic venous blood flow is often not redirected because of the complexity of the surgery. However, the complication of not redirecting hepatic venous flow is a high prevalence of the development of pulmonary arteriovenous malformations [12]. If arteriovenous malformations develop, a conduit may be created between the hepatic veins and the innominate vein to redirect hepatic blood flow into the pulmonary circuit, reducing the hemodynamic impact of the malformations [13]. Complications of hepatic conduits include thrombosis or stenosis which also may be evaluated reliably with CT.

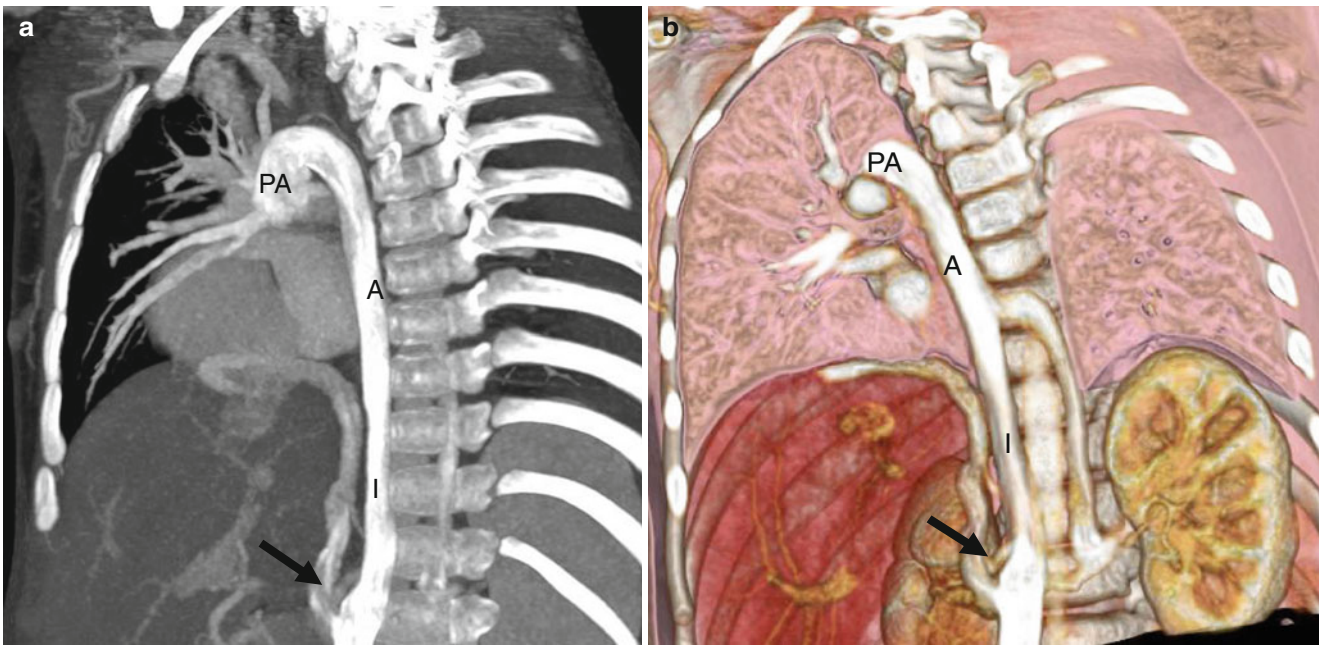


**Fig. 25.14** A Kawashima procedure in a patient with interrupted inferior vena cava with azygous continuation, atrioventricular canal defect, and hypoplastic left heart. Panels (**a**) (sagittal image) and (**b**) (3D reconstructions) show the interruption of the inferior vena cava (*I* and *black arrow*) with azygous (*A*) continuation to the pulmonary artery (*PA*) (Images provided kindly by Frandics Chan, MD. Stanford University)

## References


1. Varma C, Warr MR, Hendler AL, Paul NS, Webb GD, Therrien J. Prevalence of "silent" pulmonary emboli in adults after the Fontan operation. J Am Coll Cardiol. 2003;41:2252–8.
2. Lee SY, Baek JS, Kim GB, Kwon BS, Bae EJ, Noh CI, et al. Clinical significance of thrombosis in an intracardiac blind pouch after a Fontan operation. Pediatr Cardiol. 2012;33:42–8. doi:10.1007/s00246-011-0074-x.
3. Kiesewetter CH, Sheron N, Vettukattill JJ, Hacking N, Stedman B, Millward-Sadler H, et al. Hepatic changes in the failing Fontan circulation. Heart. 2007;93:579–84. doi:10.1136/hrt.2006.094516.
4. Park EA, Lee W, Chung SY, Yin YH, Chung JW, Park JH. Optimal scan timing and intravenous route for contrast-enhanced computed tomography in patients after Fontan operation. J Comput Assist Tomogr. 2010;34:75–81. doi:10.1097/RCT.0b013e3181ae292c.
5. Gaca AM, Jaggers JJ, Dudley LT, Bisset 3rd GS. Repair of congenital heart disease: a primer-part 1. Radiology. 2008;247:617–31. doi:10.1148/radiol.2473061909.
6. Hughes Jr D, Siegel MJ. Computed tomography of adult congenital heart disease. Radiol Clin North Am. 2010;48:817–35. doi:10.1016/j.rcl.2010.04.005.
7. Rodriguez E, Soler R, Fernandez R, Raposo I. Postoperative imaging in cyanotic congenital heart diseases: part 1, normal findings. AJR Am J Roentgenol. 2007;189:1353–60. doi:10.2214/07.2104.
8. Siegel MJ, Bhalla S, Gutierrez FR, Billadello JB. MDCT of postoperative anatomy and complications in adults with cyanotic heart disease. AJR Am J Roentgenol. 2005;184:241–7.
9. Siegel MJ. CT evaluation of congenital heart disease in adults. Appl Radiol. 2005;34:61–8.
10. Soler R, Rodriguez E, Alvarez M, Raposo I. Postoperative imaging in cyanotic congenital heart diseases: part 2, complications. AJR Am J Roentgenol. 2007;189:1361–9. doi:10.2214/AJR.07.2105.
11. Spevak PJ, Johnson PT, Fishman EK. Surgically corrected congenital heart disease: utility of 64-MDCT. AJR Am J Roentgenol. 2008;191:854–61. doi:10.2214/AJR.07.2889.
12. Srivastava D, Preminger T, Lock JE, Mandell V, Keane JF, Mayer Jr JE, et al. Hepatic venous blood and the development of pulmonary arteriovenous malformations in congenital heart disease. Circulation. 1995;92:1217–22.
13. McElhinney DB, Kreutzer J, Lang P, Mayer Jr JE, del Nido PJ, Lock JE. Incorporation of the hepatic veins into the cavopulmonary circulation in patients with heterotaxy and pulmonary arteriovenous malformations after a Kawashima procedure. Ann Thorac Surg. 2005;80:1597–603. doi:10.1016/j.athoracsur.2005.05.101.

# Rastelli Procedure

# 26

In 1969, Rastelli and colleagues introduced a procedure that bypasses left ventricular outflow tract obstructions (LVOT) in complex congenital heart disease patients [1, 2]. In the first step of the Rastelli procedure, the pulmonary artery is separated from the morphologic left ventricle just above the valve, and the cardiac end of the left ventricular outflow tract is closed. Next, an intraventricular tunnel is created using a patch to redirect blood from the left ventricle across the ventricular septal defect (VSD) into the right ventricle and out into the ascending aorta. Then, the right ventricle is anastomosed to the pulmonary artery with an extracardiac conduit, usually using a pulmonary allograft. In the setting of transposition of the great vessels, this procedure corrects the abnormal blood flow pattern at the ventricular level and allows the left ventricle to function as the systemic ventricle [3].

Figures 26.1 and 26.2 illustrate the Rastelli procedure.

The most frequent indication for the Rastelli procedure is transposition of the great vessels associated with VSD and left ventricular outflow tract (LVOT) obstruction. Because of the LVOT obstruction, the Jatene arterial switch is not a feasible procedure. The atrial switch procedure along with closure of the VSD and repair of the LVOT obstruction also has limitations and it is often associated with recurrent LVOT obstruction. In addition to management of transposition of the great arteries, the Rastelli procedure is also used for management of pulmonary atresia with a VSD and double-outlet right ventricle with pulmonary atresia or stenosis.

W. Mazur et al., *CT Atlas of Adult Congenital Heart Disease*,
DOI 10.1007/978-1-4471-5088-6_26, © Springer-Verlag London 2013

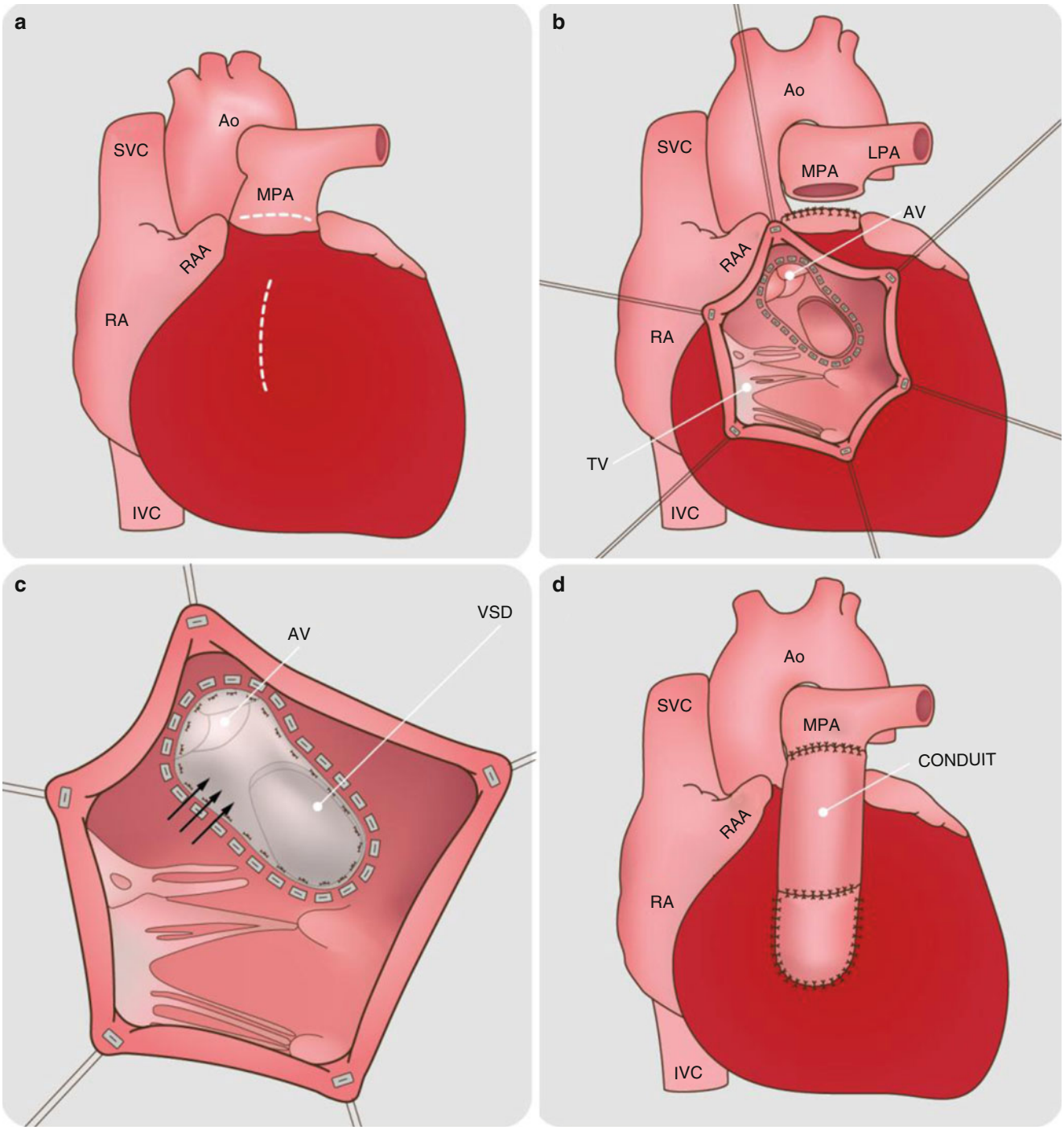


**Fig. 26.1** An artist's rendition of the Rastelli procedure. In panel (**a**) the right ventricle free wall and main pulmonary artery (*MPA*) are incised (*dashed lines*). In panel (**b**) the left ventricle to MPA connection is transected and sutured. Panel (**c**) shows the creation of an intraventricular tunnel or baffle (*arrows*) is created to establish a communication between left ventricle and aorta. The VSD and aortic annulus are incorporated within the right ventricle. This step redirects blood from the left ventricle into the right ventricle and out the ascending aorta. Finally, in panel (**d**), the right ventricle is connected to MPA via a valved conduit. *Ao* aorta, *AV* aortic valve, *LPA* left pulmonary artery, *IVC* inferior vena cava, *RA* right atrium, *RAA* right atrial appendage, *TV* tricuspid valve

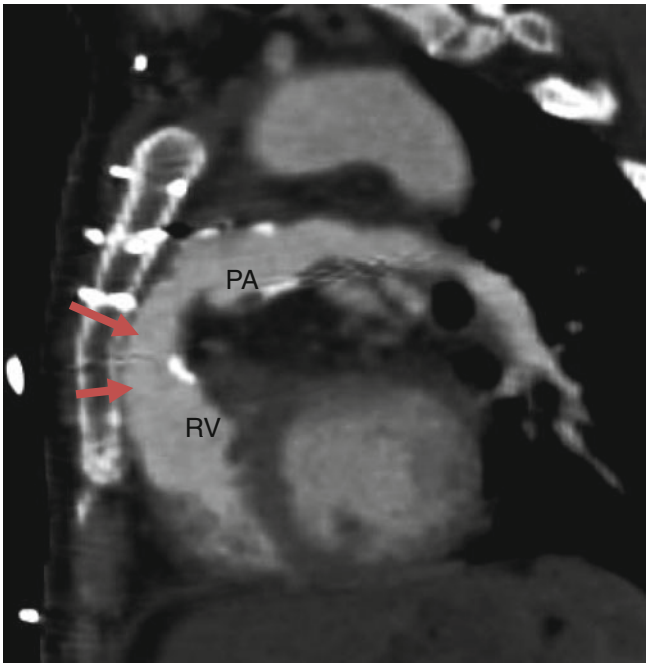


**Fig. 26.2** Rastelli procedure. Sagittal image demonstrates the connection of the pulmonary artery (*PA*) to the right ventricle (*RV*) with an extracardiac, peripherally calcified conduit (*arrows*)

## 26.1 Complications of the Rastelli Procedure

Long-term survival after the Rastelli operation is disappointing, and approximately 50 % of patients either die or need cardiac transplantation 20 years after the procedure. Complications include stenosis (with or without regurgitation), calcification, kinking and aneurysm of the extracardiac conduit, as well as recurrent LVOT obstruction. These complications may require percutaneous intervention with stent placement or surgical repairs, including aortic root translocation with right ventricular outflow tract (RVOT) reconstruction (Nikaidoh procedure), pulmonary translocation (Lecompte), or Réparation à l'Etage Ventriculaire (the REV procedure) [4]. For further information about these complex repairs, see ref. [4]. The tunnel patch from the left ventricle to the aortic valve can be complicated by leakage, obstruction, stenosis, or aneurysm. Other complications are biventricular dysfunction, branch pulmonary artery stenosis, and arrhythmias [4].

## 26.2 Cardiac Computed Tomographic Angiography (CT) in the Evaluation of the Rastelli Procedure

Arterial phase CT timed to the aortic blood flow can be used to show postoperative anatomy and any complications [5–9]. CT can show right ventricle-to-pulmonary artery conduit patency, stenosis, calcification and aneurysm formation, and LVOT obstruction. Ventricular dysfunction and branch pulmonary artery stenosis can also be detected.

## References

1. Konstantinov IE, Rosapepe F, Dearani JA, Alexi-Meskishvili VV, Li J. A tribute to giancarlo rastelli. Ann Thorac Surg. 2005;79:1819–23. doi:10.1016/j.athoracsur.2004.11.037.
2. Rastelli GC. A new approach to "anatomic" repair of transposition of the great arteries. Mayo Clin Proc. 1969;44:1–12.
3. Morell VO, Jacobs JP, Quintessenza JA. Surgical management of transposition with ventricular septal defect and obstruction to the left ventricular outflow tract. Cardiol Young. 2005;15 Suppl 1:102–5.
4. Kreutzer C, De Vive J, Oppido G, Kreutzer J, Gauvreau K, Freed M, et al. Twenty-five-year experience with rastelli repair for transposition of the great arteries. J Thorac Cardiovasc Surg. 2000;120:211–23. doi:10.1067/mtc.2000.108163.
5. Gaca AM, Jaggers JJ, Dudley LT, Bisset 3rd GS. Repair of congenital heart disease: a primer-part 1. Radiology. 2008;247:617–31. doi:10.1148/radiol.2473061909.
6. Hughes Jr D, Siegel MJ. Computed tomography of adult congenital heart disease. Radiol Clin North Am. 2010;48:817–35. doi:10.1016/j.rcl.2010.04.005.
7. Rodriguez E, Soler R, Fernandez R, Raposo I. Postoperative imaging in cyanotic congenital heart diseases: part 1, normal findings. AJR Am J Roentgenol. 2007;189:1353–60. doi:10.2214/07.2104.
8. Soler R, Rodriguez E, Alvarez M, Raposo I. Postoperative imaging in cyanotic congenital heart diseases: part 2, complications. AJR Am J Roentgenol. 2007;189:1361–9. doi:10.2214/AJR.07.2105.
9. Spevak PJ, Johnson PT, Fishman EK. Surgically corrected congenital heart disease: utility of 64-MDCT. AJR Am J Roentgenol. 2008;191:854–61. doi:10.2214/AJR.07.2889.

# Damus–Kaye–Stansel Procedure

# 27

The Damus–Kaye–Stansel (DKS) operation is a palliative procedure for patients with a single functioning ventricle with an obstructed rudimentary outflow chamber. It is not used for treatment of hypoplastic left heart syndrome which is treated using the Norwood procedure. This operation is used for in double-inlet left ventricle, tricuspid atresia with transposition of the great arteries (TGA), and a common atrioventricular canal with small left ventricular cavity.

In the DKS operation, the proximal pulmonary artery is divided near its bifurcation and anastomosed to the side of the ascending aorta, thus bypassing any systemic outflow obstruction. Blood flow to the distal pulmonary arteries is reestablished by a modified Blalock–Taussig (preferred in neonates), bidirectional Glenn shunt, or an extracardiac cavopulmonary Fontan procedure (preferred in adults) [1, 2]. Later modifications of the DKS procedure include surgical closure of the aortic valve to prevent development of aortic valve insufficiency [2, 3] and patch augmentation of the aortic arch if the arch is hypoplastic.

Figures 27.1, 27.2, 27.3, and 27.4 demonstrate the DKS procedure.

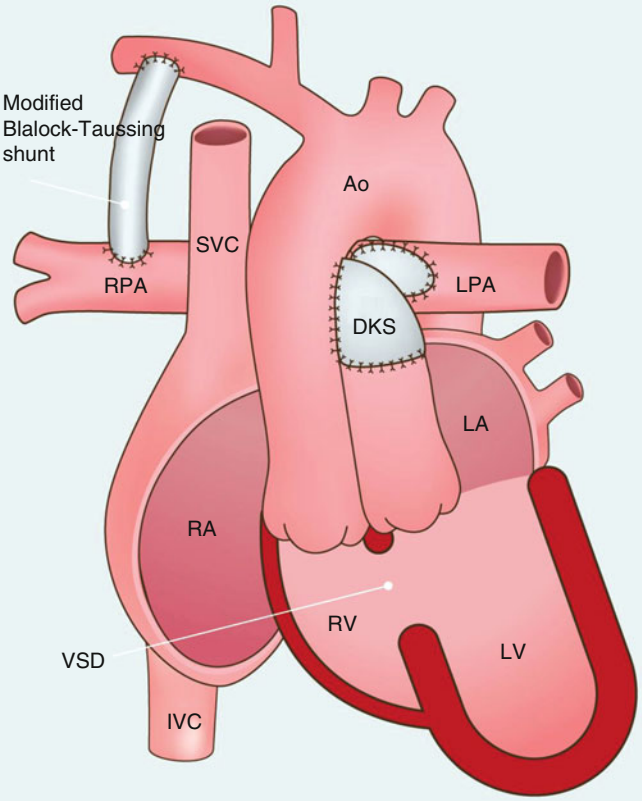


**Fig. 27.1** Damus–Kaye–Stansel operation. This diagram shows a surgical connection between the ascending aorta (*Ao*) and pulmonary artery (PA). The pulmonary artery is ligated just below the anastomotic site. The right and left pulmonary arteries attach to an extracardiac Fontan (FC) conduit (preferred connection in adults, not shown here). The Blalock–Taussig shunt (*arrows*) is also shown and preferred in infants. The aorta arises from a rudimentary right ventricle. *RPA* right pulmonary artery, *SVC* superior vena cava, *DKS* damus-kaye-stansel anastomosis, *LPA* left pulmonary artery, *LA* left atrium, *RA* right atrium, *RV* right ventricle, *LV* left ventricle, *VSD* ventricular septal defect, *IVC* inferior vena cava

W. Mazur et al., *CT Atlas of Adult Congenital Heart Disease*,
DOI 10.1007/978-1-4471-5088-6_27, © Springer-Verlag London 2013

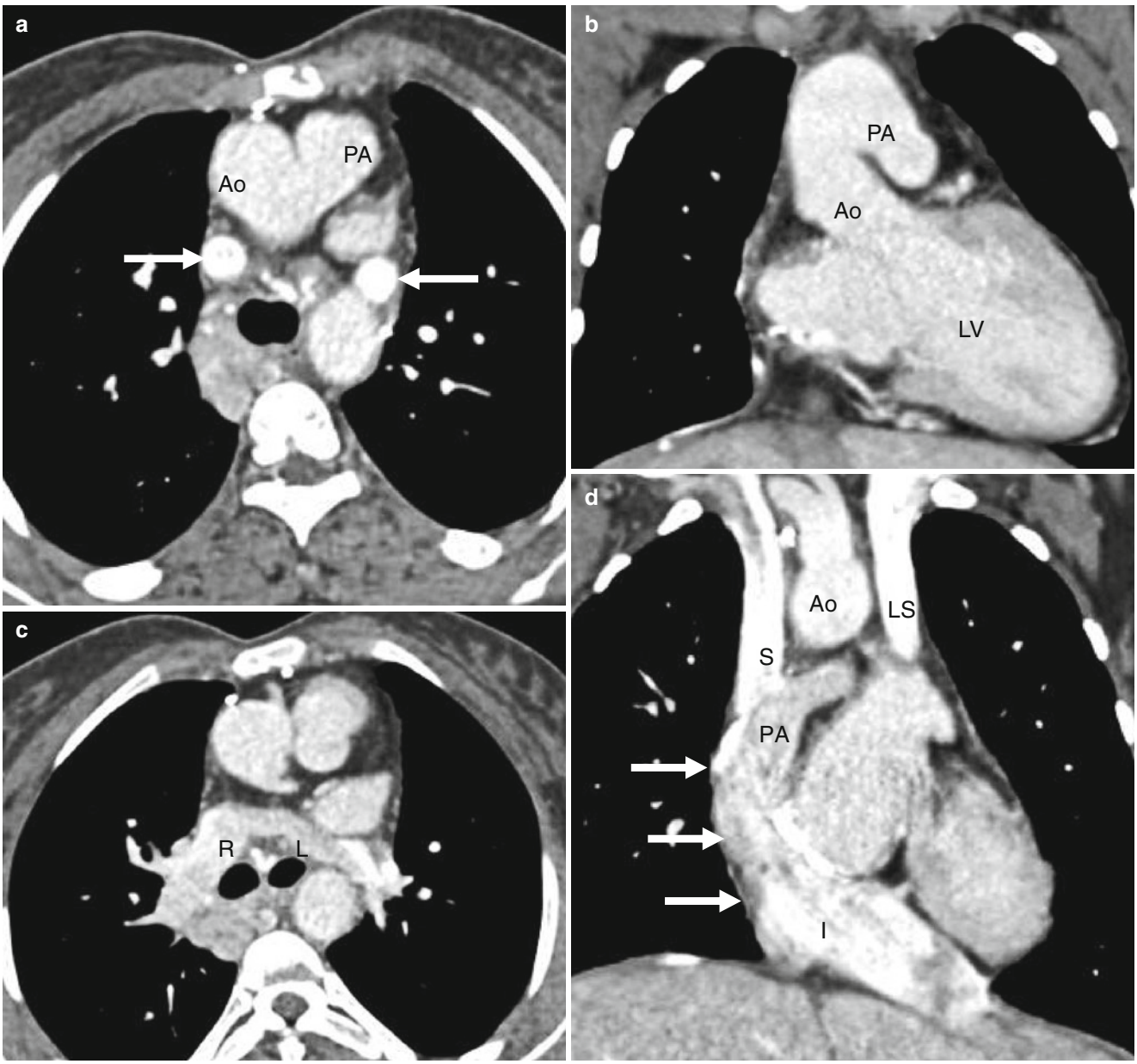


**Fig. 27.2** Damus–Kaye–Stansel operation in a 21-year-old female with complicated congenital heart disease consisting of an atrioventricular canal with predominance of the right ventricle and hypoplastic left ventricle (functionally single ventricular heart), severe subaortic stenosis, and bilateral superior venae cavae. Her initial surgery at birth was a Damus–Kaye–Stansel procedure and Blalock–Taussig shunt. A Fontan operation was performed at age 3 years. Computed tomography (CT) was performed to assess anatomy prior to possible transplant. Panels (**a**) (axial), (**b**) (coronal) CT scans show the aorta (*Ao*) connected to the side of the main pulmonary artery (*PA*). The aorta and the anastomosed pulmonary artery arise from the left ventricle (*LV*). Note bilateral superior venae cavae (panel a *arrows*). Panel (**c**) an axial view below the level of the outflow tracts shows the confluence of the right (*R*) and left (*L*) pulmonary arteries which are separated from the main pulmonary artery. Panel (**d**) a coronal CT scan shows the superior (*S*) and inferior vena cava (*I*) connected to the tunneled Fontan (*arrows*) created in the right atrium which in turn connects to the confluence of the right and left pulmonary arteries (*PA*). The left superior vena cava was also connected to the Fontan. *LS* persistent left superior vena cava, *Ao* aorta

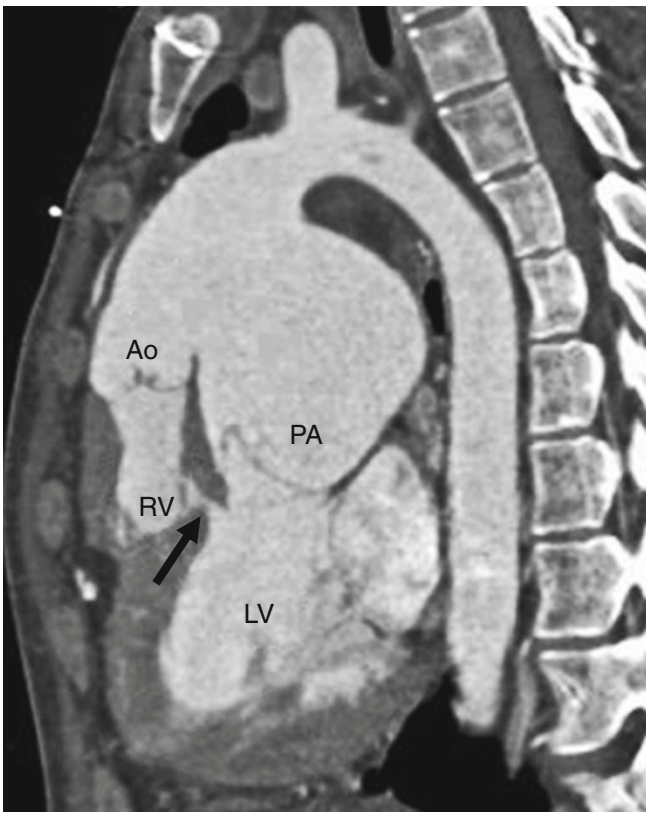


**Fig. 27.3** Damus–Kaye–Stansel operation. An oblique sagittal CT image in a patient with tricuspid atresia and L-transposition of the great vessels. The aorta (*Ao*) which arises from the hypoplastic right ventricle (*RV*) has been connected to the pulmonary artery (*PA*) arising from the left ventricle (*LV*). A septal defect (*arrow*) provides communication between the two ventricles

## 27.1 Complications of the DKS Procedure

Early mortality in the Damus–Kaye–Stansel operation procedure is approximately 20 % [2, 3]. Complications include pulmonary valvular regurgitation, usually mild [4], and stenosis at the site of aorta to pulmonary artery anastomosis [5].

## 27.2 Cardiac Computed Tomographic Angiography (CT) in the Evaluation of the DKS Procedure

Arterial phase CT timed to flow in the aorta can be used to show the postoperative anatomy and complications, such as stenosis at the anastomotic site and valvular regurgitation [6–8].

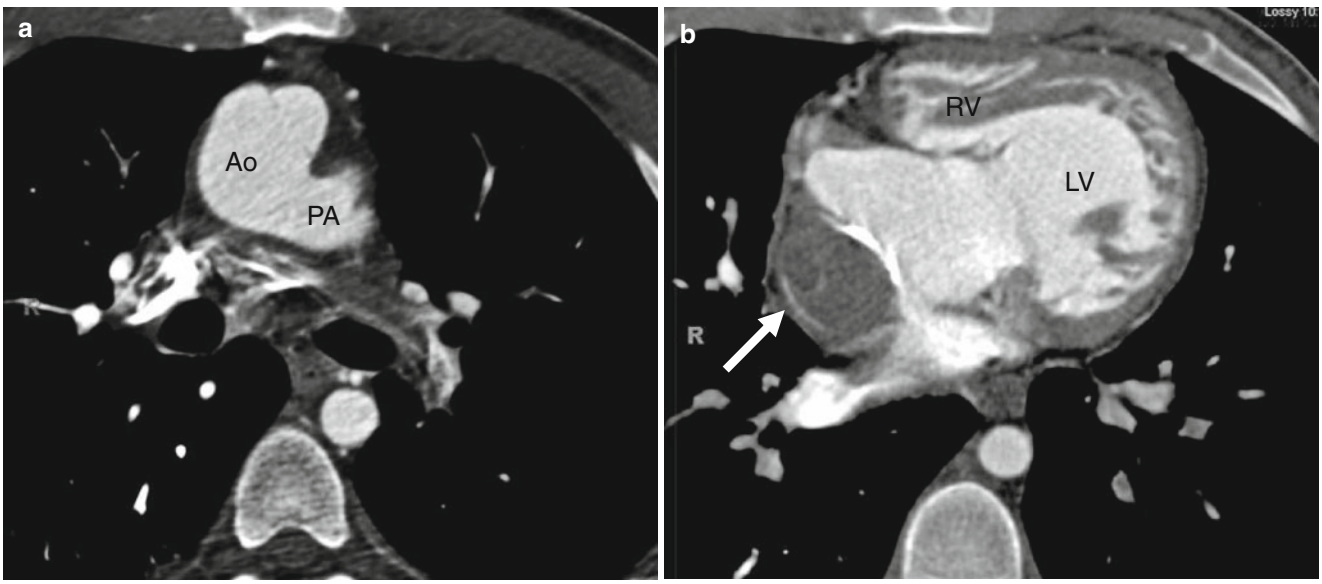


**Fig. 27.4** Damus–Kaye–Stansel operation in a patient with univentricular heart, double-inlet left ventricle with mitral atresia, and D-transposition of the great arteries. Panel (**a**), an axial image, shows the Damus–Kaye–Stansel end-to-side anastomosis of the pulmonary artery (*PA*) and aorta (*Ao*). Panel (**b**) is also an axial image and shows the lateral tunnel Fontan (*arrow*) and the single ventricle with a dominant left ventricular configuration (*LV*). As noted previously, a delayed scan would be necessary to adequately enhance the Fontan circulation. There is a hypoplastic right ventricle (*RV*) which gives rise to the aorta

## References


1. Laks H, Gates RN, Elami A, Pearl JM. Damus-Stansel-Kaye procedure: technical modifications. Ann Thorac Surg. 1992;54:169–72.
2. McElhinney DB, Reddy VM, Silverman NH, Hanley FL. Modified Damus-Laye-Stansel procedure for single ventricle, subaortic stenosis, and arch obstruction in neonates and infants: midterm results and techniques for avoiding circulatory arrest. J Thorac Cardiovasc Surg. 1997;114:718–25.
3. Brawn WJ, Sethia B, Jagtap R, et al. Univentricular heart with systemic outflow obstruction: palliation by primary Damus procedure. Ann Thorac Surg. 1995;59:1441–7.
4. Chin AJ, Barber G, Helton JG, et al. Fate of the pulmonic valve after proximal pulmonary artery-to-ascending aorta anastomosis for aortic outflow obstruction. Am J Cardiol. 1988;62:435–8.
5. Gates RN, Laks H, Elami A, et al. Damus-Stansel-Kaye procedure:current indications and results. Ann Thorac Surg. 1993; 56:111–9.
6. Gaca A, Jaggers JJ, Dudley T, Bisset GS. Repair of congenital heart disease: a primer-part 1. Radiology. 2008;247:617–31.
7. Hughes D, Siegel MJ. Computed tomography of adult congenital heart disease. Radiol Clin North Am. 2010;48:817–35.
8. Spevak PJ, Johnson PT, Fishman EK. Surgically corrected congenital heart disease: utility of 64-MDCT. AJR Am J Roentgenol. 2008;191:854–61.

# Double-Switch Procedure

# 28

Until the mid-1990s, the standard surgical approach to repair congenitally corrected transposition of the great arteries was repair of the associated lesions (ventricular septal defect and pulmonary stenosis or atresia), allowing the right ventricle to remain as the systemic pump. Since this approach has a high prevalence of complications, surgical correction is now advocated in early childhood (several months to a few years of age). Correction is achieved with the double-switch procedure which uses a combination of the atrial switch and arterial switch surgeries previously described in Chaps. 23 and 24 [1–3]. Either a Mustard or Senning procedure is performed followed by either a Jatene switch or Rastelli-type procedure. The result of this operation is anatomically correct anatomy and removal of the systemic pressure load from the right ventricle. See Figs. 28.1 and 28.2.

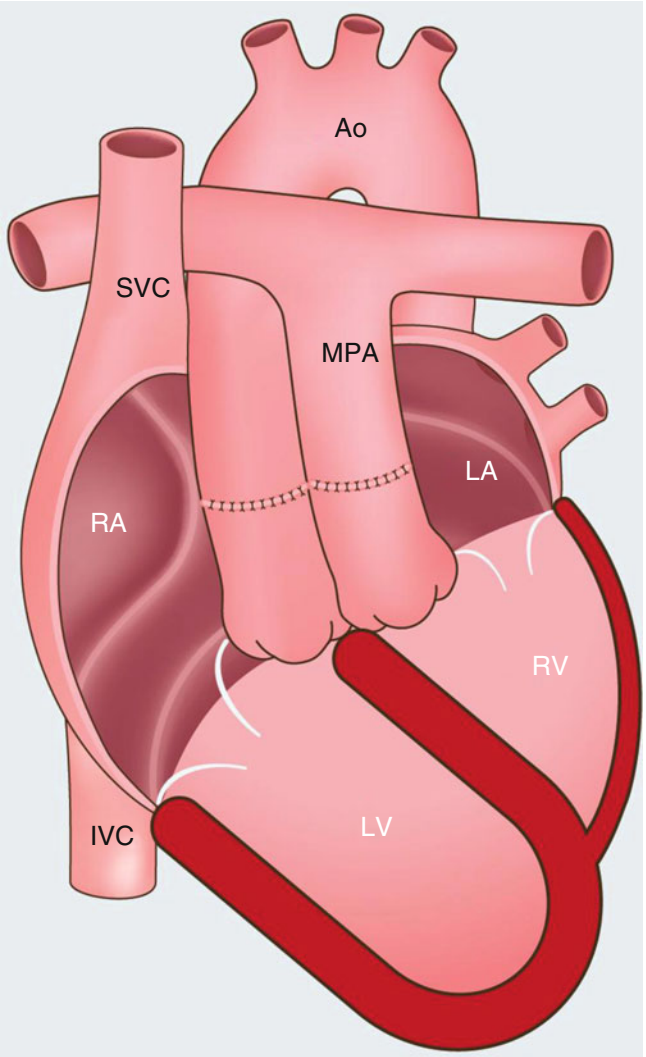


**Fig. 28.1** Double-switch operation for corrected transposition of the great arteries using the Mustard atrial baffle technique combined with the arterial switch procedure. The ventricular septal defect is closed with a patch. Venous blood from the superior and inferior vena cava (*SVC*, *IVC*) is directed to the right ventricle (*RV*) and then to the pulmonary trunk, and pulmonary venous blood is directed to the left ventricle (*LV*) and then to the aorta. *Ao* aorta, *MPA* main pulmonary artery, *LA* left atrium, *RA* right atrium

W. Mazur et al., *CT Atlas of Adult Congenital Heart Disease*,
DOI 10.1007/978-1-4471-5088-6_28, © Springer-Verlag London 2013

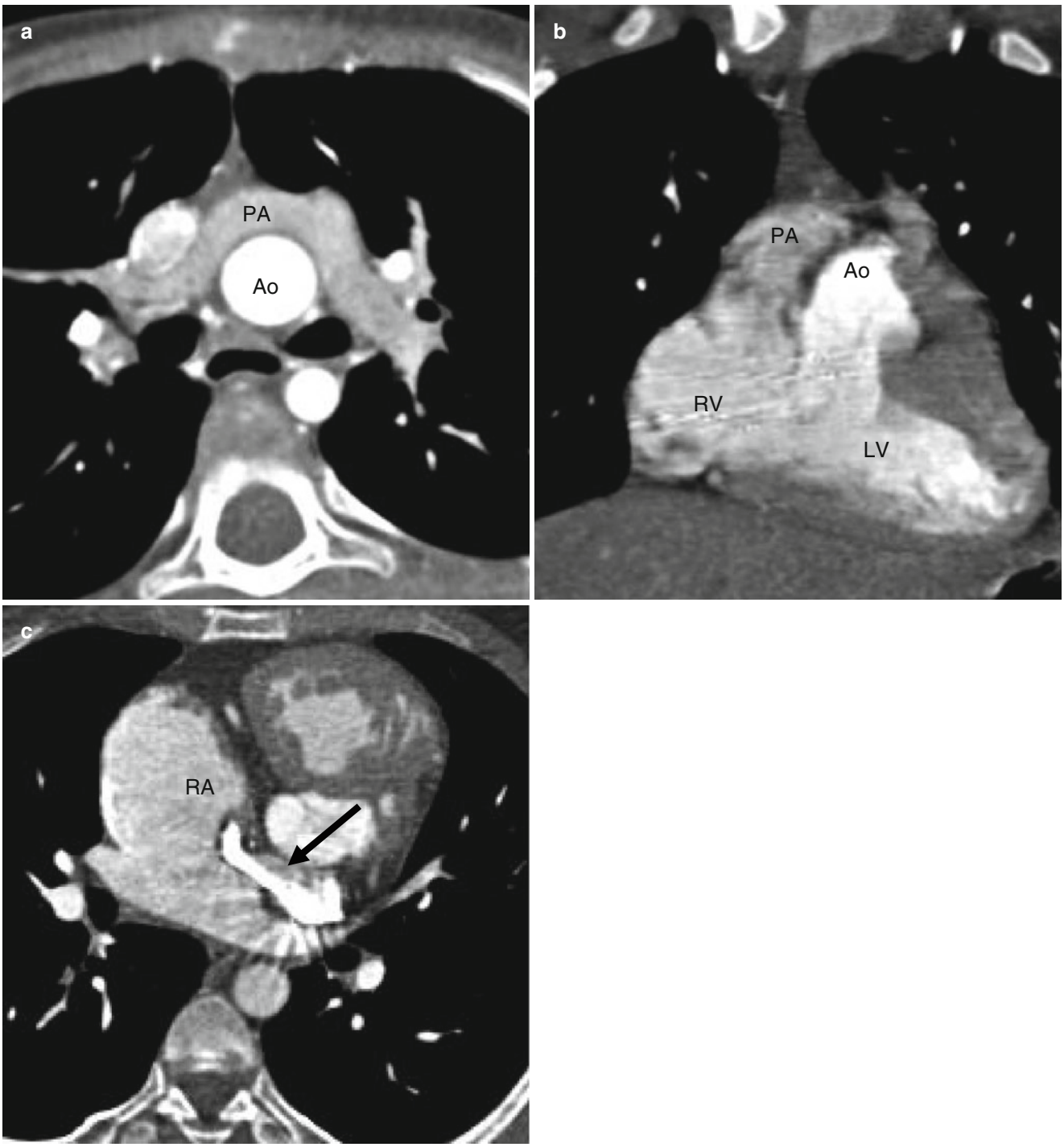


**Fig. 28.2** Double-switch operation for corrected transposition of the great arteries using the Mustard atrial baffle technique and the arterial switch procedure. Panel (**a**) is an axial scan showing the Jatene correction with the pulmonary artery (*PA*) draping over the aorta (*Ao*). Panel (**b**) is a coronal cut showing the aorta (*Ao*) connecting to the left ventricle (*LV*) and the pulmonary artery (*PA*) connecting to the right ventricle (*RV*). Note the parallel orientation of the great vessels which is characteristic of transposition of the great arteries. Panel (**c**) is an axial slice showing the changes of a Mustard procedure with the right atrium (*RA*) connected via a baffle (*arrow*) to the left ventricle

## 28.1 Complications of the Double-Switch Procedure

The double-switch operation is associated with a low risk of early- and intermediate-term outcome complications but long-term follow-up is lacking [4]. Left ventricular dysfunction is a rare complication [3]. Other complications are those associated with the individual atrial and arterial switch procedures, which have been described in prior sections.

## 28.2 Cardiac Computed Tomographic Angiography (CT) in the Evaluation of the Double Switch Procedure

Arterial phase CT is used to demonstrate postoperative anatomy and complications which are described in prior sections [5].

## References

1. Reddy VM, McElhinney DB, Silverman NH, Hanley FL. The double switch procedure for anatomical repair of congenitally corrected transposition of the great arteries in infants and children. Eur Heart J. 1997;18:1470–7.
2. Imai Y. Double-switch operation for congenitally corrected transposition. Adv Card Surg. 1997;9:65–86.
3. Duncan BW, Mee RB, Mesia CI, Qureshi A, Rosenthal GL, Seshadri SG, et al. Results of the double switch operation for congenitally corrected transposition of the great arteries. Eur J Cardiothorac Surg. 2003;24:11–9; discussion 19–20.
4. Pecoraro A, Sreeram N, Dodge-Khatami A, Hitchcock F, Bennink G. The double-switch procedure for atrioventricular and ventriculoarterial discordance. Neth Heart J. 2003;11:210–2.
5. Gaca AM, Jaggers JJ, Dudley LT, Bisset 3rd GS. Repair of congenital heart disease: a primer-part 1. Radiology. 2008;247:617–31. doi:10.1148/radiol.2473061909.

# Tetralogy of Fallot Repair

# 29

The classic lesions of tetralogy of Fallot (TOF) include pulmonary stenosis, ventricular septal defect (VSD), overriding aorta, and right ventricular hypertrophy. The hemodynamically significant lesions are the VSD and pulmonary stenosis that results in right ventricular outflow tract (RVOT) obstruction. Originally, a two-stage repair was performed for repair of TOF. First pulmonary blood flow was increased with systemic-to-pulmonary artery shunts (classic and modified Blalock–Taussig shunt, Waterston shunt, or Potts shunt) followed by a complete repair when the child was older. Complications associated with this strategy include pulmonary hypertension and congestive heart failure from the augmented pulmonary blood flow and stenosis of the pulmonary artery at the anastomotic site.

The current treatment for TOF with pulmonary stenosis is a primary single-stage repair in the first year of life, usually at 3–6 months of age. This obviates the need for multiple surgeries and prevents the associated complications. Definitive repair consists of closing the VSD and relieving the RVOT obstruction. The older surgical technique relieved the RVOT obstruction using a right ventricular free-wall incision with insertion of an infundibular patch graft or homograft to enlarge the outflow tract and also included a repair of the VSD with a GORE-TEX patch (Figs. 29.1 and 29.2). The pulmonary homograft replaced the pulmonary valve and proximal pulmonary artery. This repair is no longer performed due to the frequent complication of dilatation of the RVOT homograft leading to progressive pulmonary valve regurgitation requiring valve replacement and the development of right ventricular failure (Fig. 29.3).

Currently, surgical techniques are aimed at avoiding a ventriculotomy and sparing the pulmonary valve. The preferred surgical technique is closure of the VSD via the right atrium and repair of the RVOT obstruction using a simple pulmonary valvotomy with minimal or no transannular incision. This surgical strategy is referred to as a transatrial repair (Fig. 29.4).

In patients with TOF and pulmonary valvular atresia, surgical repair is performed in the neonatal period. The VSD is closed through a right ventriculotomy and a right ventricle-to-pulmonary artery conduit is placed using a valved aortic or pulmonary homograft (Fig. 29.5).

W. Mazur et al., *CT Atlas of Adult Congenital Heart Disease*,
DOI 10.1007/978-1-4471-5088-6_29, © Springer-Verlag London 2013

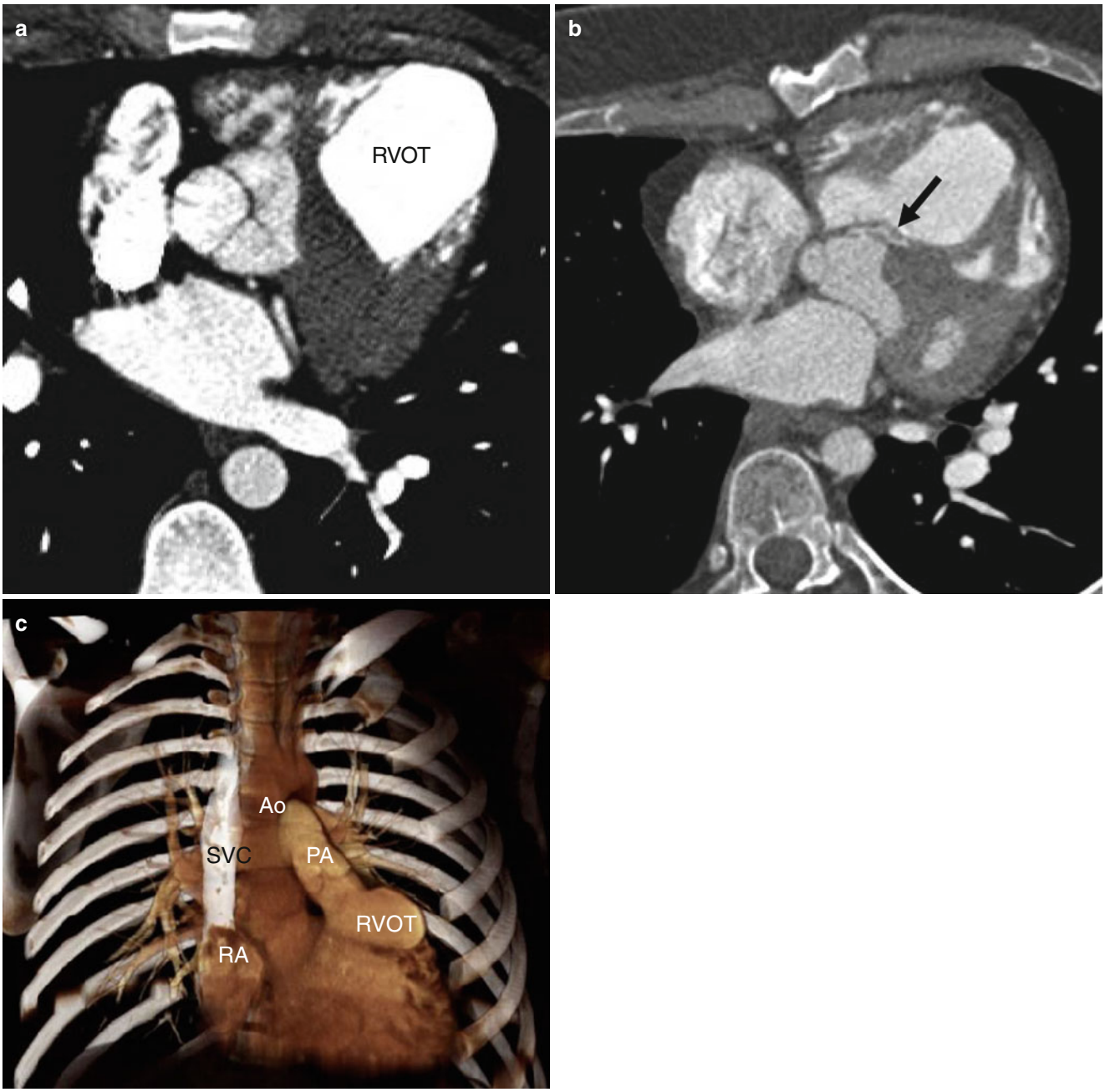


**Fig. 29.1** Repaired tetralogy of Fallot, using a patch to close the ventricular septal defect and a homograft to enlarge the right ventricular outflow tract. Panel (**a**) is an axial scan showing a right ventricular outflow tract (*RVOT*) homograft. Notice mild dilatation of the graft. Panel (**b**) is an axial cut showing a high-density ventricular septal defect patch (*arrow*). Panel (**c**) is a coronal image showing the mildly dilated RVOT and proximal pulmonary artery (*PA*). *SVC* superior vena cava, *PA* pulmonary artery, *Ao* aorta

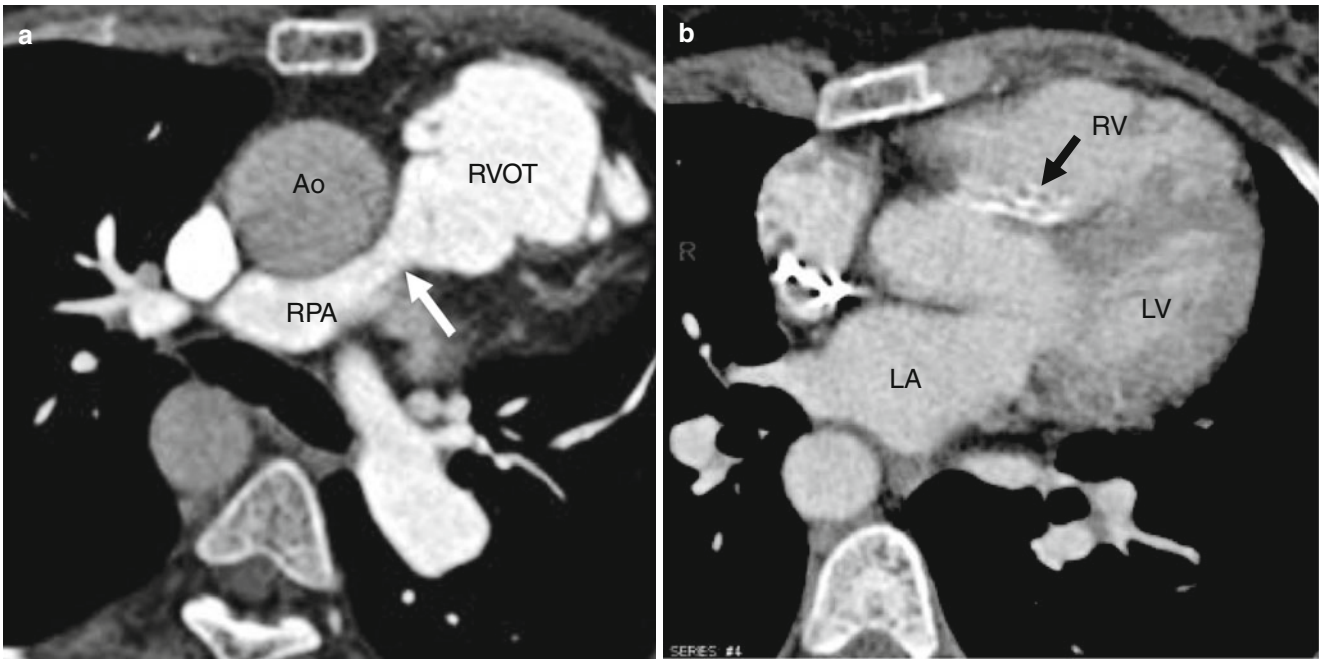


**Fig. 29.2** Repaired tetralogy of Fallot in a 54-year-old woman who has mild pulmonic regurgitation and normal right ventricular function. Panel (**a**) is an axial scan showing enlargement of the right ventricular outflow tract (*RVOT*) homograft. Also note the narrowing at the junction of the right pulmonary artery (*RPA*) with the homograft (*white arrow*). Panel (**b**) an axial image showing calcification in the ventricular septal defect patch (*arrow*)

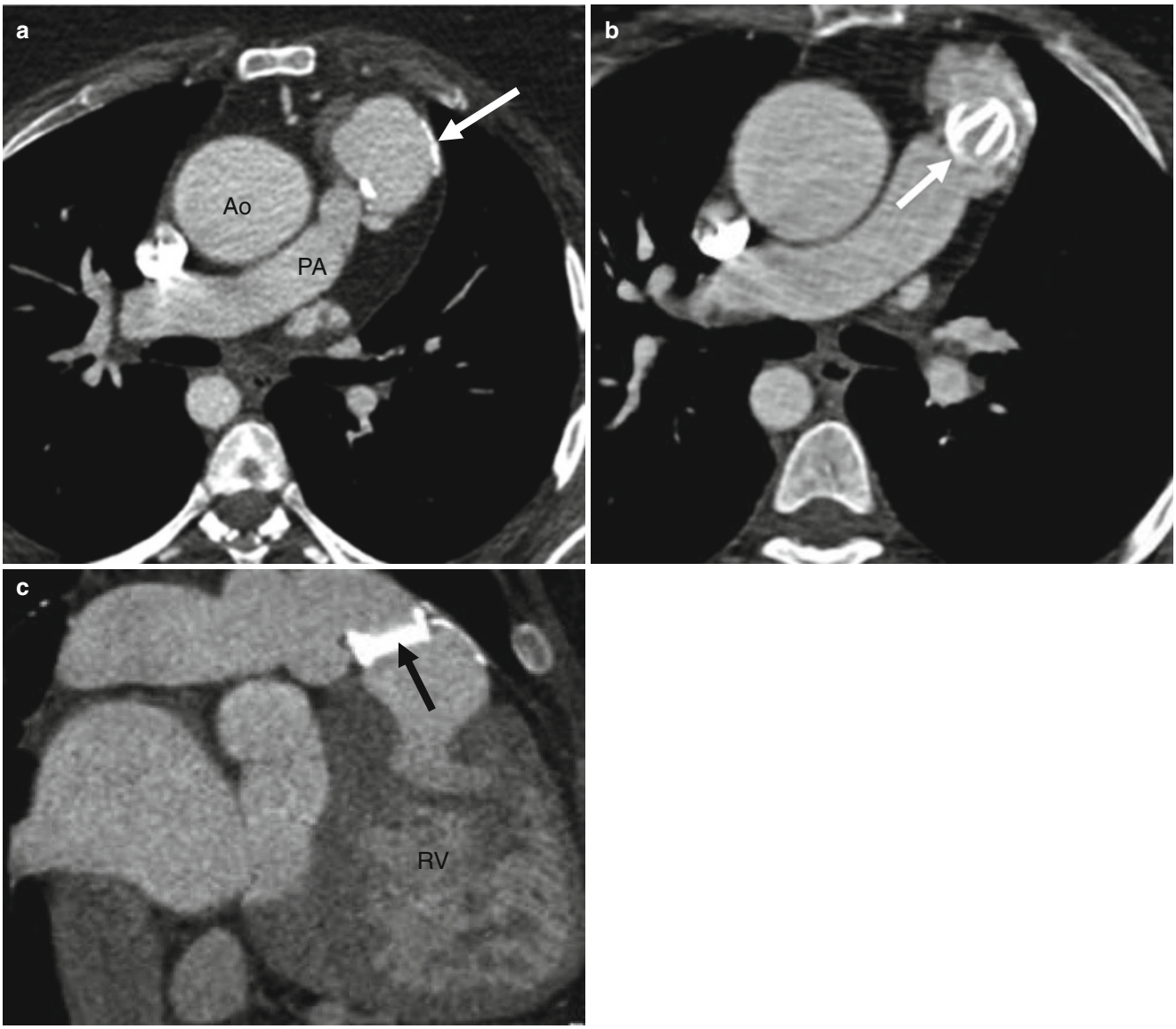


**Fig. 29.3** Repaired tetralogy of Fallot complication by dilatation of the right ventricular outflow tract patch graft leading to wide open pulmonary valve regurgitation and mechanical valve replacement. Panel (**a**) is an axial image showing a calcified, dilated right ventricular outflow tract (*arrow*). Also note the right-sided aortic arch and dilatation of the ascending aorta (*Ao*) leading to aortic regurgitation. Panel (**b**), an axial reformat, and panel (**c**), an oblique sagittal view, showing a mechanical St. Jude pulmonic valve (*arrows*). Note the right ventricular (*RV*) dilatation and hypertrophy (panel c). *RV* right ventricle, *PA* pulmonary artery

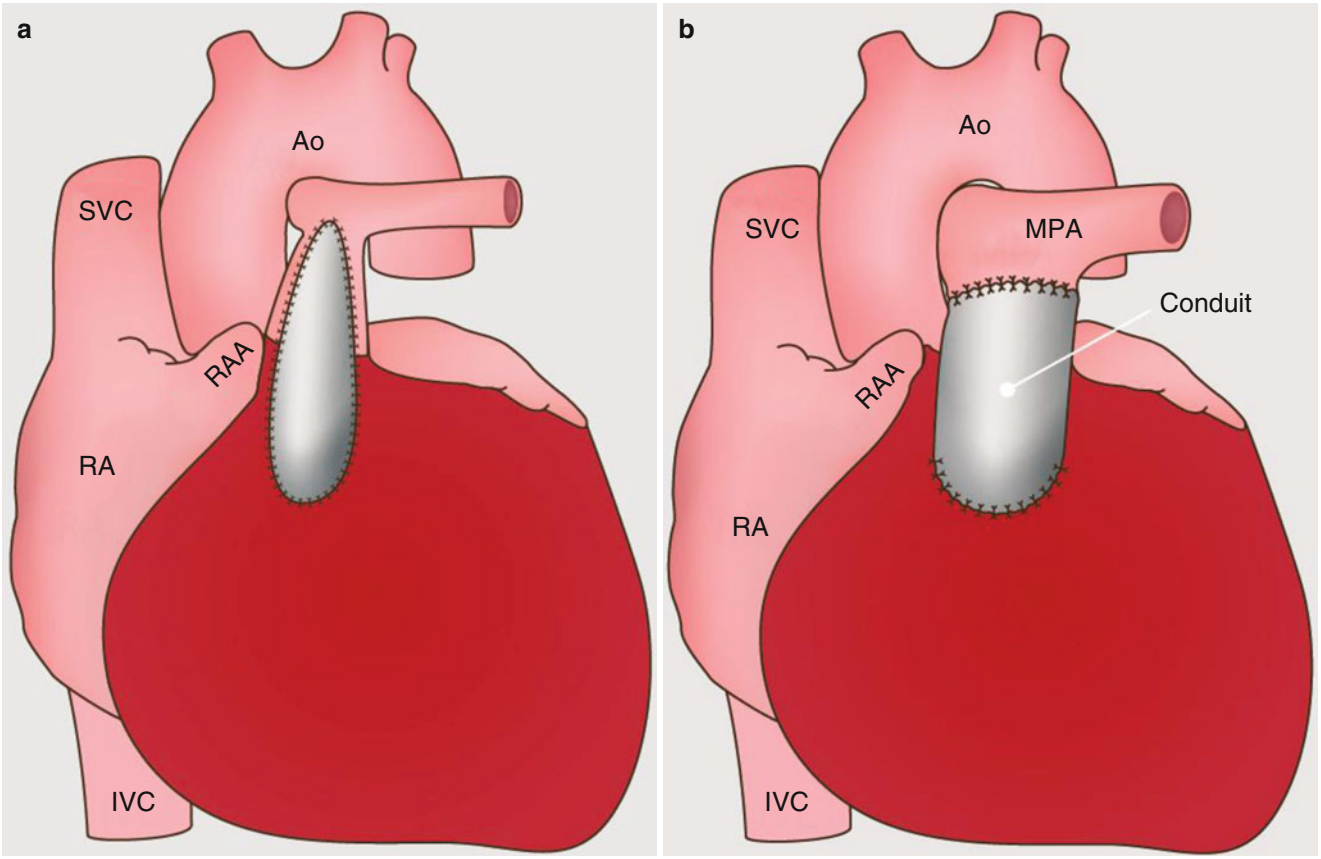


**Fig. 29.4** Panel (**a**) shows a tetralogy of fallot (TOF) transannular ventricular septal defect (VSD) patch repair in which the ventricular septal defect has been repaired through a right ventricular incision. Panel (**b**) shows the TOF repair after a transatrial repair in which the VSD has been repaired through a right atrial incision. In both examples, the right ventricular outflow tract has also been enhanced. *SVC* superior vena cava, *Ao* aorta, *RAA* right atrial appendage, *RA* right atrium, *IVC* inferior vena cava, *MPA* main pulmonary artery

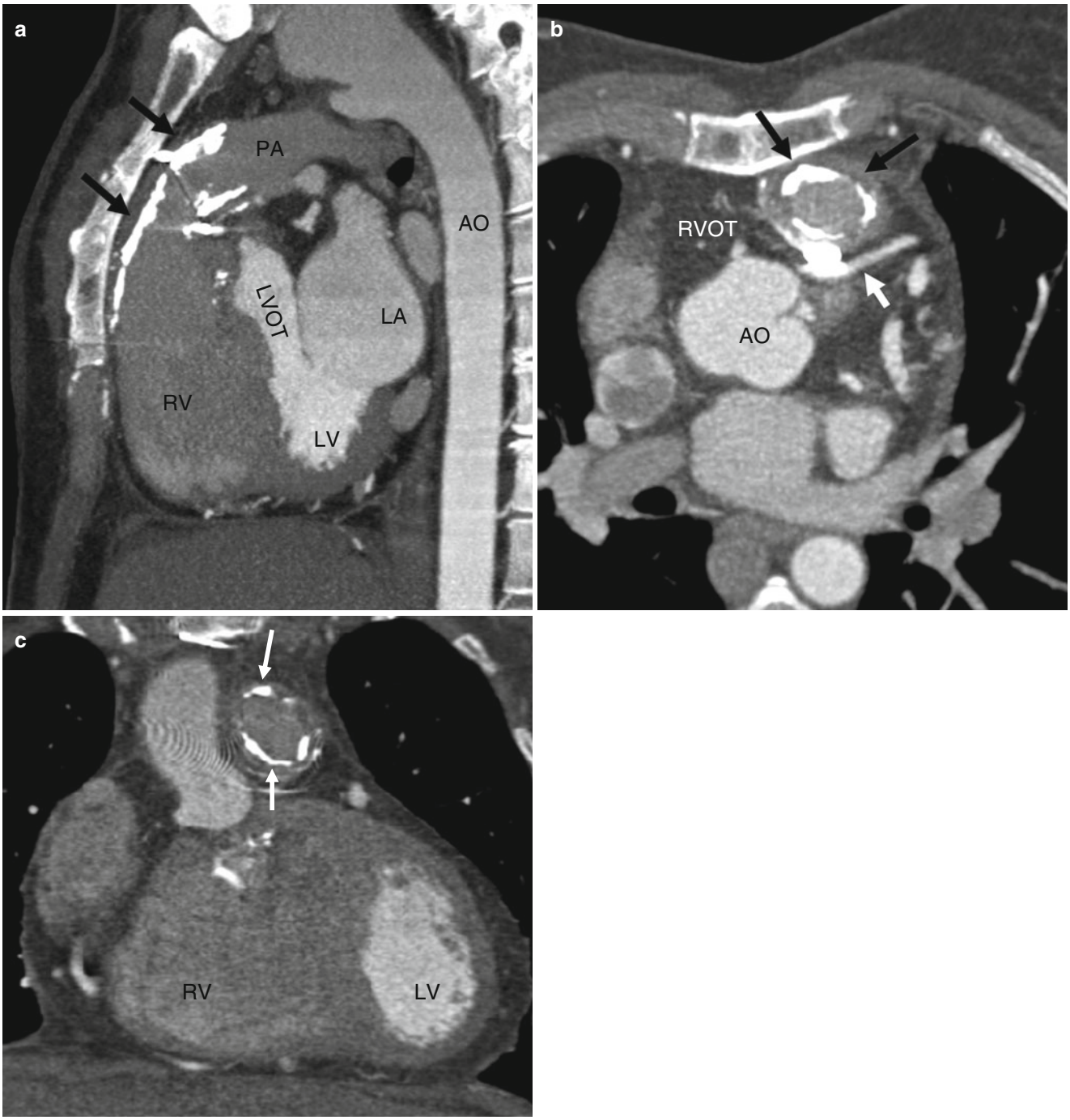


**Fig. 29.5** Tetralogy of Fallot in a patient with pulmonary valve atresia who underwent surgical repair in childhood with a valved pulmonary homograft from the right ventricle to the pulmonary artery. The patient now presented with worsening dyspnea and occasional angina. Panel (**a**) is a sagittal view and panels (**b**) and (**c**), are two axial images, all showing a calcified external conduit (*black arrows*) between the right ventricle (*RV*) and pulmonary artery (*PA*). Note an anomalous left anterior descending coronary artery (*white arrow*) originating from right coronary cusp with a malignant course between the aortic root and the conduit. There is obliteration of the native right ventricular outflow tract (*RVOT*). *Ao* aorta, *LVOT* left ventricular outflow tract, *LV* left ventricle, *LA* left atrium

## 29.1 Complications of TOF Repair Procedures

Long-term survival of TOF repair is excellent and approaches 90 % at 20 years following a complete repair [1]. The most common long-term complication of surgical repair is progressive pulmonary regurgitation which leads to right ventricular dilatation, right ventricular failure, and tricuspid regurgitation. In such cases, pulmonary valve replacement is often needed (see Fig. 29.3) [2]. Other postoperative complications are stenosis at the anastomotic site of the pulmonary homograft (see Fig. 29.2) and progressive aortic root dilatation with aortic regurgitation, which may lead to biventricular failure and arrhythmias. New techniques such as percutaneous valve replacement (Fig. 29.6), arrhythmia ablation surgery, and strategies that preserve the pulmonary valve even at the cost of leaving some degree of residual stenosis have been reported and are likely to change long-term outcomes in treated TOF patients [3].

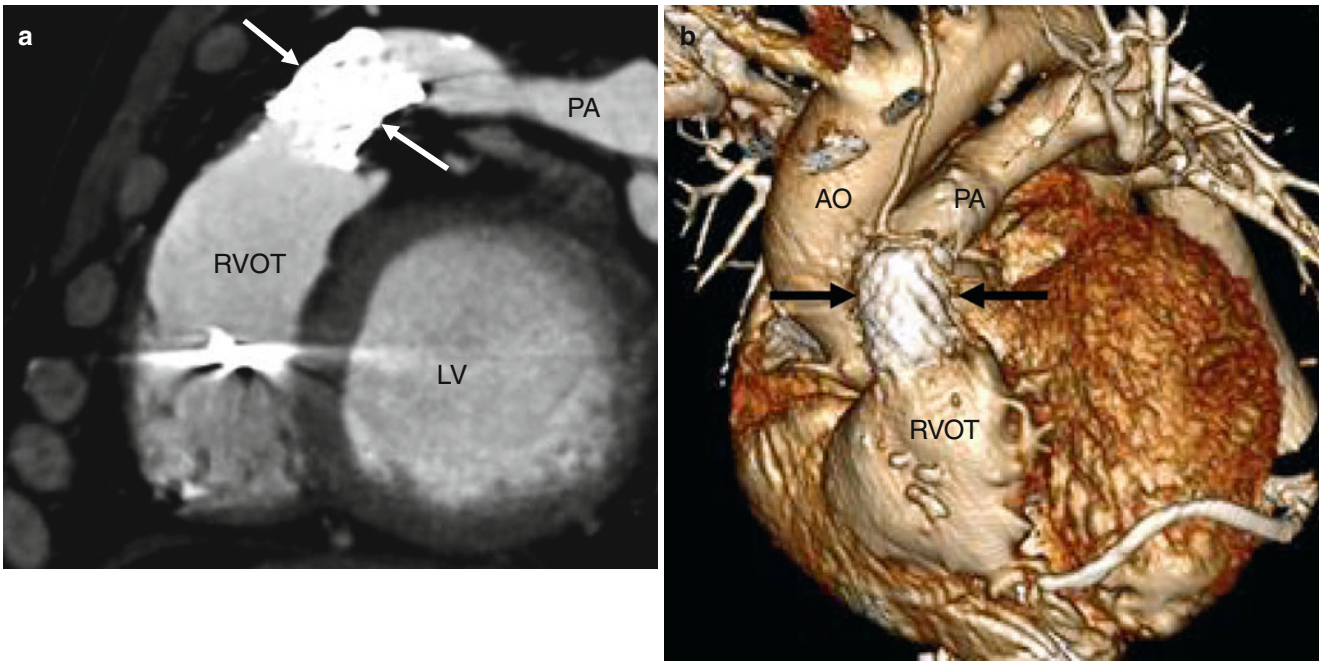


**Fig. 29.6** Melody valve in a 43 year-old man with marked pulmonary regurgitation following homograft placement as a child. A Melody valve is a transcatheter pulmonary valve used as replacement for a pulmonary heart valve that has already been previously repaired. The valve (*arrows*) is in the expected position between the right ventricular outflow tract (*RVOT*) and pulmonary artery. Panel (**a**) sagittal view, Panel (**b**) 3D reconstruction. *PA* pulmonary artery, *Ao* aorta, *LV* left ventricle

## 29.2 Cardiac Computed Tomographic Angiography (CT) in the Evaluation of TOF Repair

Phase contrast and cine magnetic resonance (MR) imaging is preferred over CT to quantify pulmonary regurgitation and right ventricular ejection fraction in order to determine the optimal timing for pulmonary valve replacement in order to prevent irreversible damage to the ventricle. CT, however, can be used for evaluation of the postoperative anatomy, including the pulmonary artery and pulmonary valve (stenosis and/or regurgitation), RVOT (aneurysmal dilatation), aortic root, and ascending aorta (dilatation and aortic regurgitation). In addition, ventricular scarring and fibrosis at the right ventricular surgical site can be diagnosed based on delayed contrast enhancement. Although residual VSDs are rare, they can be assessed by CT [4–10]. The central pulmonary arteries should be evaluated for peripheral stenoses which are not technically postoperative complications but are associated with TOF.

## References

1. Kirklin JK, Kirklin JW, Blackstone EH, Milano A, Pacifico AD. Effect of transannular patching on outcome after repair of tetralogy of fallot. Ann Thorac Surg. 1989;48:783–91.
2. Geva T. Repaired tetralogy of fallot: the roles of cardiovascular magnetic resonance in evaluating pathophysiology and for pulmonary valve replacement decision support. J Cardiovasc Magn Reson. 2011;13:9. doi:10.1186/1532-429X-13-9.
3. Karamlou T, McCrindle BW, Williams WG. Surgery insight: late complications following repair of tetralogy of fallot and related surgical strategies for management. Nat Clin Pract Cardiovasc Med. 2006;3:611–22. doi:10.1038/ncpcardio0682.
4. Gaca AM, Jaggers JJ, Dudley LT, Bisset 3rd GS. Repair of congenital heart disease: a primer-part 2. Radiology. 2008;248:44–60.
5. Hughes Jr D, Siegel MJ. Computed tomography of adult congenital heart disease. Radiol Clin North Am. 2010;48:817–35. doi:10.1016/j.rcl.2010.04.005.
6. Rodriguez E, Soler R, Fernandez R, Raposo I. Postoperative imaging in cyanotic congenital heart diseases: part 1, normal findings. AJR Am J Roentgenol. 2007;189:1353–60. doi:10.2214/07.2104.
7. Siegel MJ, Bhalla S, Gutierrez FR, Billadello JB. MDCT of postoperative anatomy and complications in adults with cyanotic heart disease. AJR Am J Roentgenol. 2005;184:241–7.
8. Siegel MJ. CT evaluation of congenital heart disease in adults. Appl Radiol. 2005;34:61–8.
9. Soler R, Rodriguez E, Alvarez M, Raposo I. Postoperative imaging in cyanotic congenital heart diseases: part 2, complications. AJR Am J Roentgenol. 2007;189:1361–9. doi:10.2214/AJR.07.2105.
10. Spevak PJ, Johnson PT, Fishman EK. Surgically corrected congenital heart disease: utility of 64-MDCT. AJR Am J Roentgenol. 2008;191:854–61. doi:10.2214/AJR.07.2889.

# Ross Procedure

# 30

In the Ross procedure, the normal pulmonary valve with part of the pulmonary artery is moved to the aortic position to replace a diseased aortic valve and the native pulmonary artery and valve are replaced with a pulmonary homograft. The coronary arteries are transplanted into the neoaorta (native pulmonary artery). This procedure is the operation of choice in infants and children, since it allows the valve replacement to grow as the patient matures thus eliminating the need for anticoagulation to prevent thromboembolism. Its use in adults remains controversial.

See Figs. 30.1 and 30.2 for an illustration of the Ross procedure.

W. Mazur et al., *CT Atlas of Adult Congenital Heart Disease*,
DOI 10.1007/978-1-4471-5088-6_30, © Springer-Verlag London 2013

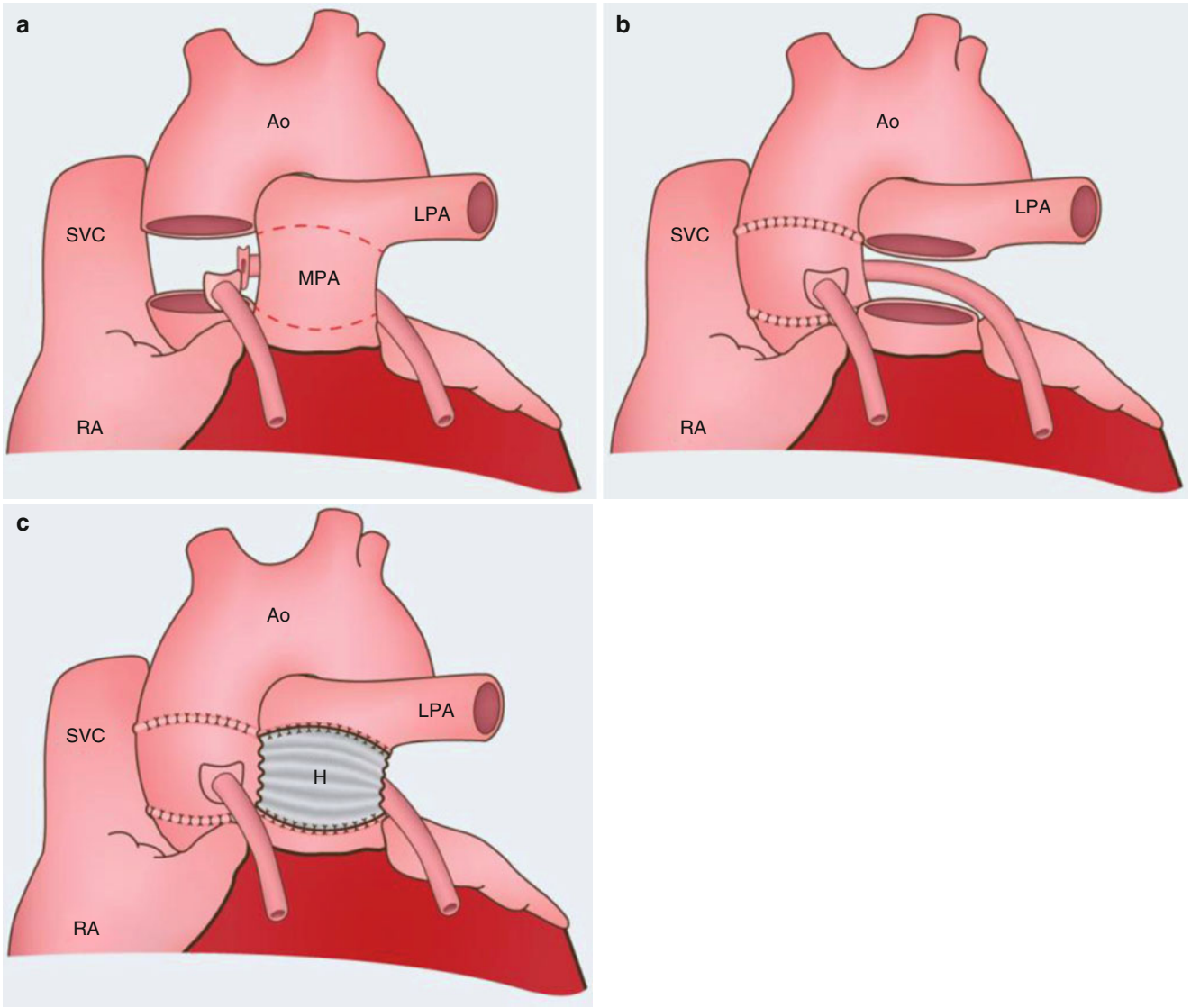


**Fig. 30.1** A diagram of the Ross procedure. Panel (**a**) shows aorta (*Ao*) and main pulmonary artery (*MPA*) roots with their respective valves are transected. In panel (**b**) the pulmonic root is anastomosed to the residual native aorta (*Ao*) and the coronary arteries are reanastomosed. In panel (**c**), the native pulmonary artery and valve are replaced with a pulmonary homograft (*H*). *LPA* left pulmonary artery, *SVC* superior vena cava, *PA* pulmonary artery, *RA* right atrium

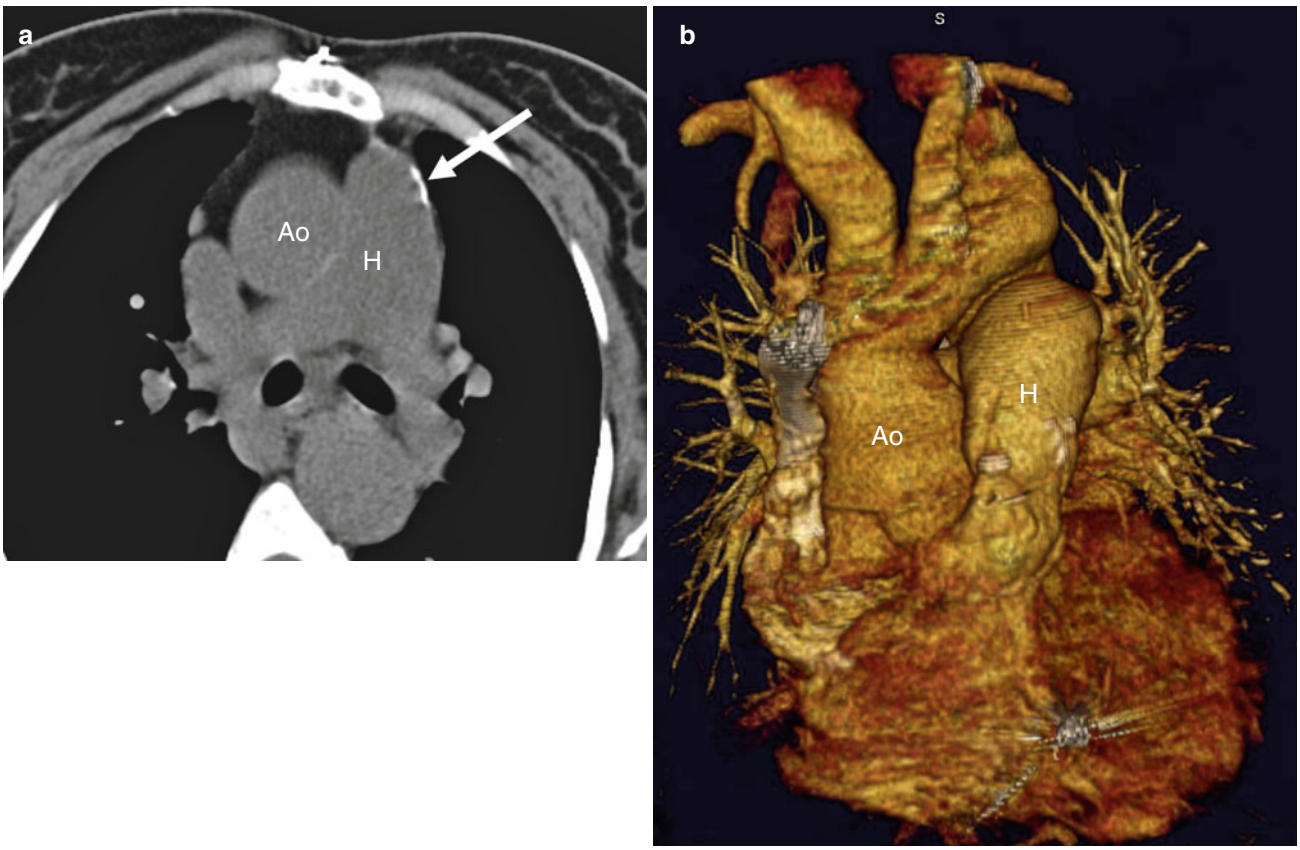


**Fig. 30.2** Ross procedure. A 25-year-old female who underwent a Ross procedure for subaortic stenosis and coarctation of the aorta. Panel (**a**) is a noncontrast scan showing calcification (*arrow*) in the pulmonary homograft (*H*). *Ao* neoaorta (relocated native pulmonary artery). Panel (**b**) is a 3D scan showing the mildly dilated neoaorta (*Ao*) and the pulmonary homograft (*H*)

## 30.1 Complications of the Ross Procedure

The cryopreserved homograft is an excellent means to reconstruct the right ventricular outflow tract, with a good long-term outcome. In recent series, overall patient survival was 97 % at 18 years following the Ross procedure [1]. Homograft stenosis occurred in 54 % of patients and regurgitation in 18 % [1]. Almost 85 % of patients did not require reoperation or percutaneous intervention 10 years after implantation [1]. The homograft long-term durability depends on both homograft-related and patient-related factors, such as homograft diameter, donor age, and cold ischemia time [1].

## 30.2 Cardiac Computed Tomographic Angiography (CT) in the Evaluation of the Ross Procedure

CT is an excellent procedure to assess the size of the aortic root, ascending aorta, and the pulmonic root and its branch vessels in order to diagnose stenosis or dilatation (associated with valvular regurgitation) [2].

## References

1. Fukuma A, Moritake K, Fukuda M, Kuwabara S. Experimental study on the difference of ischemic threshold between cerebral cortex and thalamus with middle latency auditory evoked potentials. No To Shinkei. 1990;42:481–8.
2. Gaca A, Jaggers JJ, Dudley T, Bisset GS. Repair of congenital heart disease: a primer-part 1. Radiology. 2008;247:617–31.

# Norwood Procedures and Sano Modification

# 31

## 31.1 Palliative Treatment of Hypoplastic Left Heart Syndrome

Hypoplastic left heart syndrome (HLHS) is characterized by hypoplasia of the left heart and varying degrees of hypoplasia or atresia of the aortic valve and ascending aorta. It is included in the spectrum of conditions that can result in a cardiac circulation with a functionally single ventricle. Left untreated, HLHS is invariably lethal. Advances in palliative surgical procedures (Norwood procedure, bidirectional cavopulmonary shunt, modified Fontan procedure) have increased the survival rate in children with HLHS.

In the 1980s, Norwood et al. described a two-stage palliative surgical procedure for the treatment of HLHS [1]. Later, this approach was modified to the currently used three-stage reconstruction [2]. The surgery is done in stages to protect the pulmonary circulation and to avoid right ventricular volume overload.

Stage I of the modified Norwood procedure is performed within the first few days of life. It isolates the hypoplastic left ventricle from the circulation and converts the right ventricle into the main ventricle pumping blood to the lungs and the body (univentricular physiology). The main pulmonary artery and the aorta with its associated coronary arteries are connected using a side-to-side anastomosis, creating a neoaorta (Figs. 31.1 and 31.2). The atrial septum is excised, creating a nonrestrictive ASD or common atrium to facilitate systemic circulation. Pulmonary flow is established via a modified Blalock–Taussig shunt or more recently a right ventricle-to-pulmonary artery conduit (Sano procedure) (Figs. 31.3 and 31.4) [3]. The disadvantage of the Blalock–Taussig shunt is that coronary artery blood flow which occurs during both diastole and systole causes a coronary "steal phenomenon" (coronary blood flow is diverted to the low-pressure pulmonary circulation) leading to myocardial ischemia and ventricular dysfunction [4–7]. The Sano procedure eliminated the diastolic runoff of coronary blood flow thus avoiding the coronary steal phenomenon [8–10]. The complications of the Sano procedure, however, are conduit stenosis and right ventricular aneurysm formation [11, 12].

Occasionally, a hybrid procedure may be performed before the Norwood operation is undertaken. This operation consists of bilateral pulmonary artery banding to limit pulmonary blood flow and stent implantation into the ductus arteriosus to maintain unrestrictive flow from the right ventricle to the systemic circulation (Figs. 31.5 and 31.6). This hybrid procedure is performed in neonates who are poor candidates for the Norwood procedure (severe heart failure,

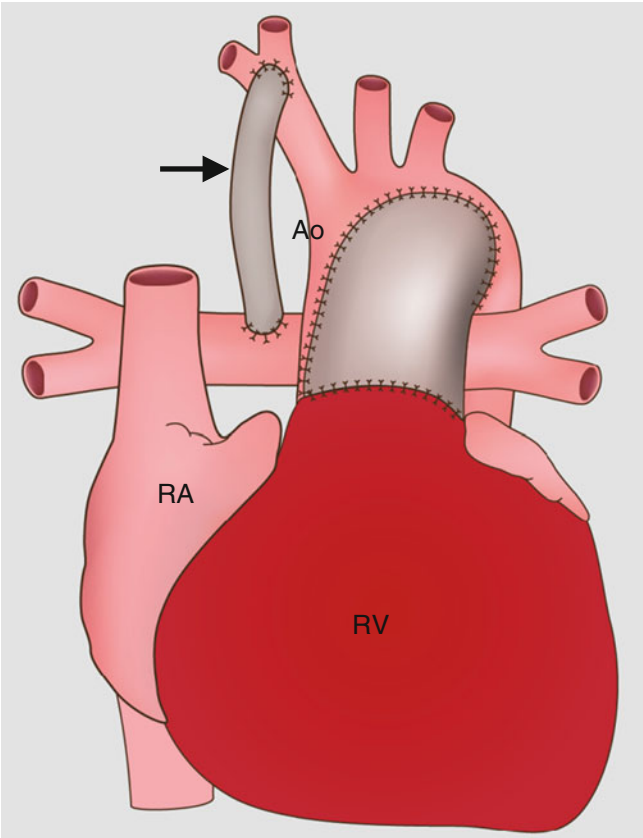


**Fig. 31.1** Stage 1 of the modified Norwood procedure comprises an aortic arch reconstruction via a side-to-side anastomosis of the main pulmonary artery (PA) to the ascending aorta (Ao), an atrial septectomy, and a modified Blalock–Taussig shunt (*arrow*). *Ao* aorta, *RV* right ventricle, *RA* right atrium

W. Mazur et al., *CT Atlas of Adult Congenital Heart Disease*,
DOI 10.1007/978-1-4471-5088-6_31, © Springer-Verlag London 2013

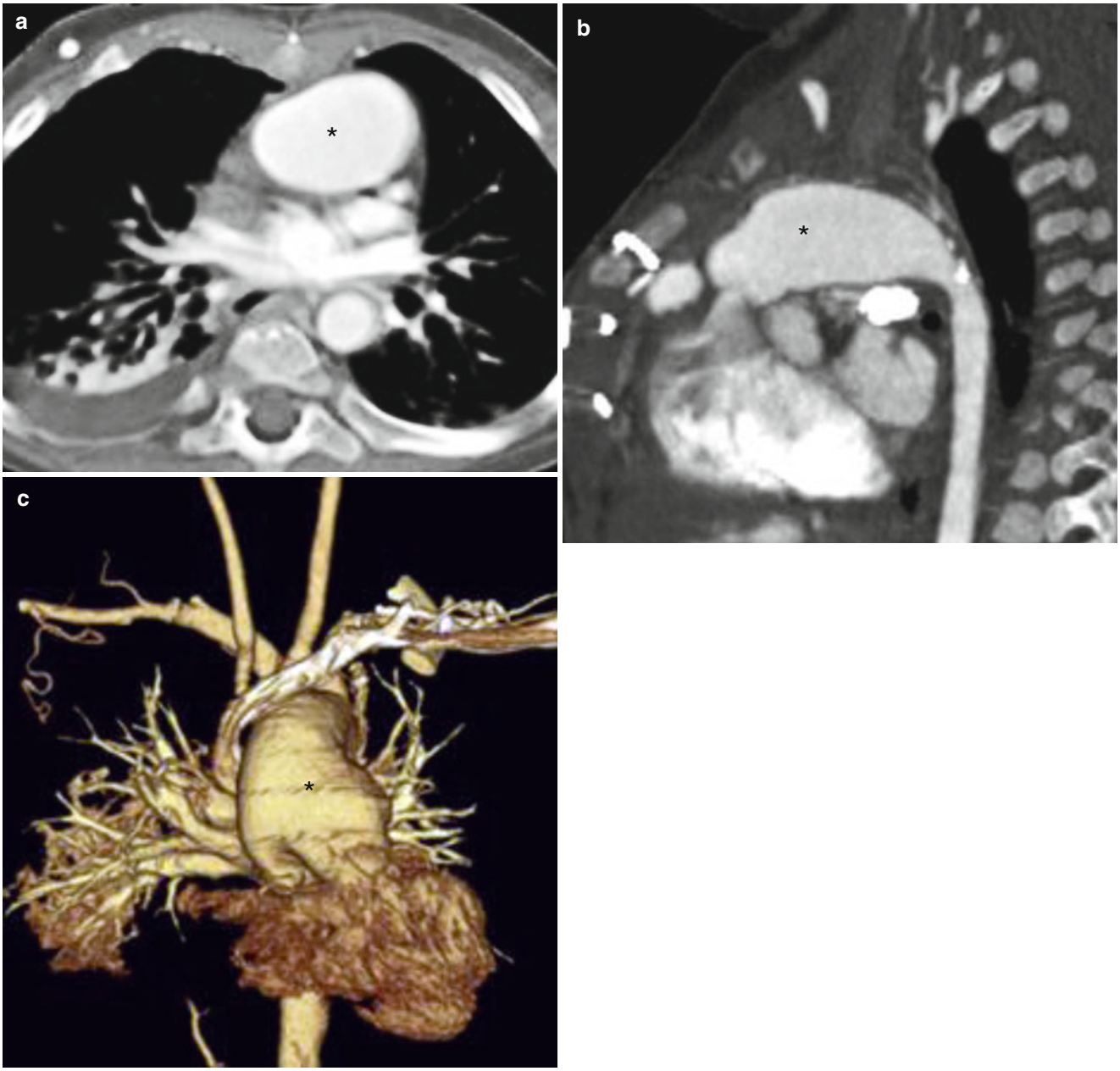


**Fig. 31.2** Modified Norwood procedure, stage I. Axial (**a**), sagittal (**b**), and coronal volume-rendered (**c**) images. Each panel shows the neoaorta (*asterisk*) created by the side-to-side anastomosis of the main pulmonary artery to the ascending aorta

poor end-organ perfusion). The banding is used as a short-term alternative to increase systemic blood flow and end-organ perfusion before the Norwood procedure.

Stage II of the modified Norwood procedure (cavopulmonary shunt) is usually performed at 4–6 months of age when pulmonary arterial resistance has decreased to normal levels. A bidirectional Glenn shunt is performed to establish flow from the superior vena cava to the pulmonary arteries (Fig. 31.7). The previously placed Blalock–Taussig and Sano shunts are disconnected. This allows deoxygenated blood to flow directly to the lungs without going through the ventricle and decreases the volume load on the right ventricle.

Stage III of the modified Norwood procedure (a modified Fontan-like procedure) is performed between 18 and 48 months of age. The inferior vena cava is connected to the undersurface of the main pulmonary artery using an intracardiac lateral tunnel Fontan or an extracardiac conduit (Fig. 31.8). This stage completes the isolation of the pulmonary and systemic circulations such that all deoxygenated blood flows passively through the lungs.

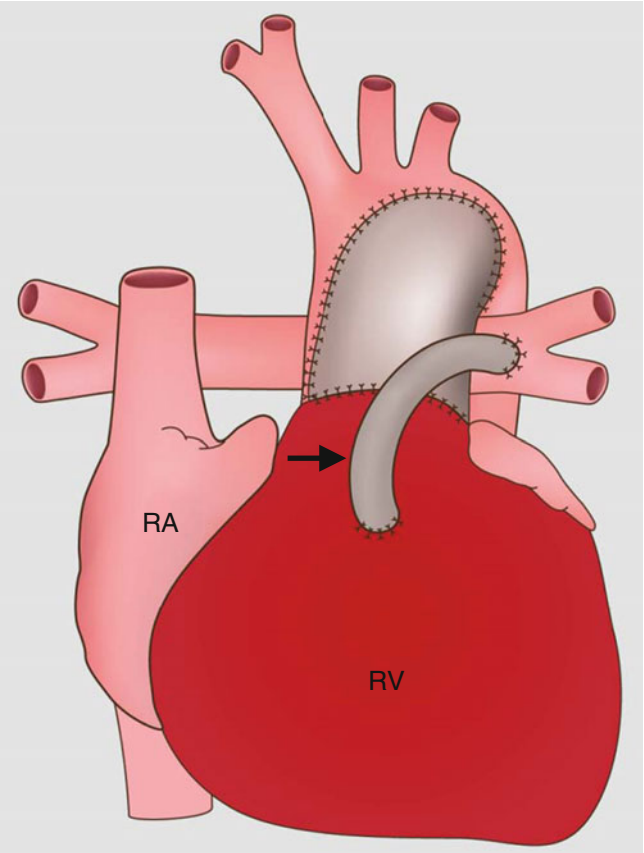


**Fig. 31.3** Sano modification in the modified Norwood procedure, stage I. This approach creates a right ventricle-to-pulmonary artery conduit (*arrow*). The Sano shunt modification avoids the problem of competitive flow between the lungs and coronary arteries. *RA* right atrium, *RV* right ventricle

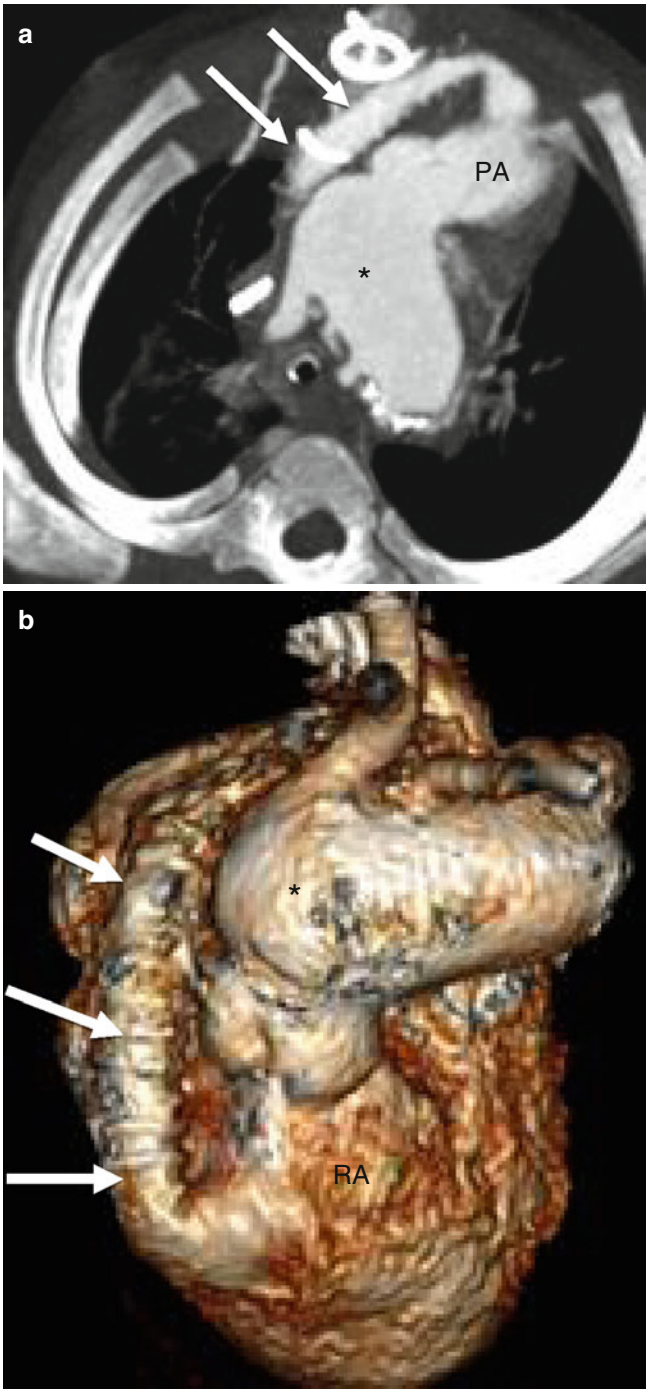


**Fig. 31.4** Sano modification in the modified Norwood procedure, stage I. Panel (**a**), an oblique axial, and panel (**b**), a volume-rendered scan showing the right ventricle (*RV*)-to-pulmonary artery (*PA*) conduit (*arrows*). *Asterisk* neoaorta

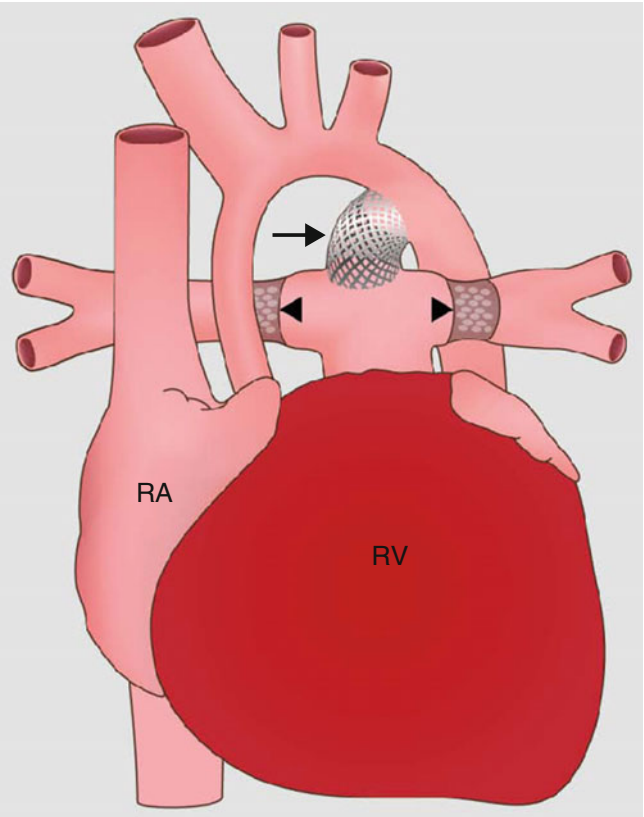


**Fig. 31.5** Hybrid procedure. Here, bilateral pulmonary artery banding (*arrowheads*) and ductus arteriosus stent implantation (*arrow*) is performed prior to the modified Norwood procedure. *RA* right atrium, *RV* right ventricle

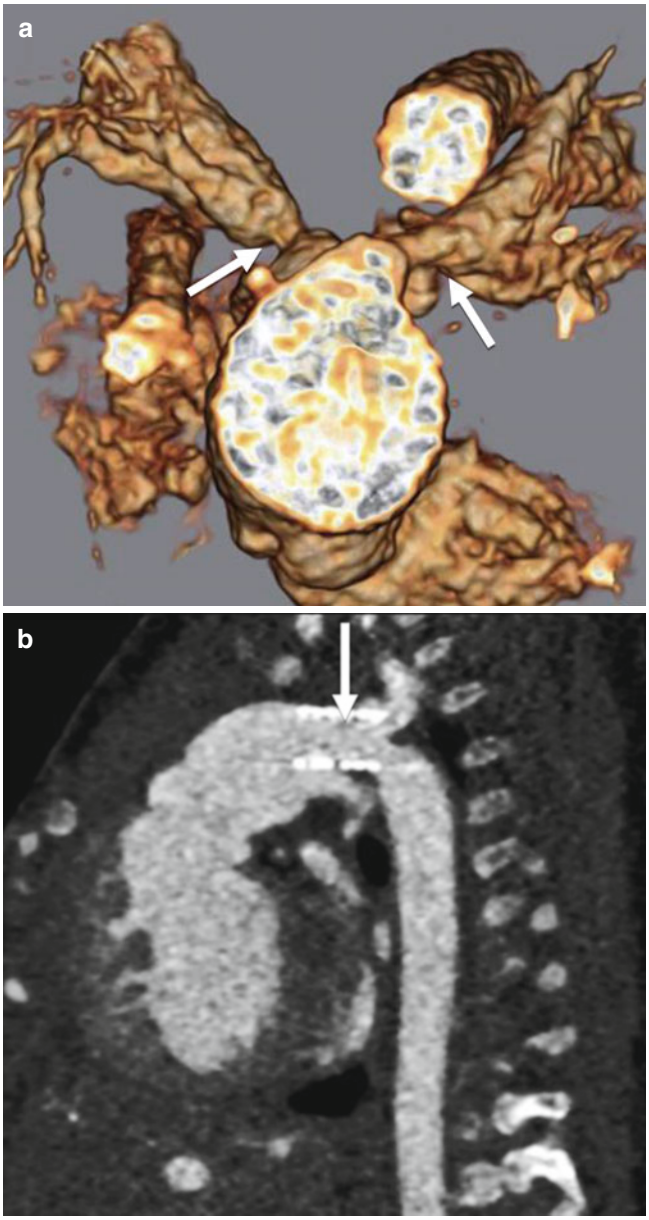


**Fig. 31.6** Hybrid procedure consisting of bilateral pulmonary artery banding and ductus arteriosus stenting. Panel (**a**) is a 3D image showing the narrowed pulmonary arteries (*arrows*) resulting from the surgical banding procedure. Panel (**b**) is an oblique sagittal reconstruction showing the ductal stent (*arrow*) (Images provided courtesy of Anthony M. Hlavacek, M.D., Medical University South Carolina)

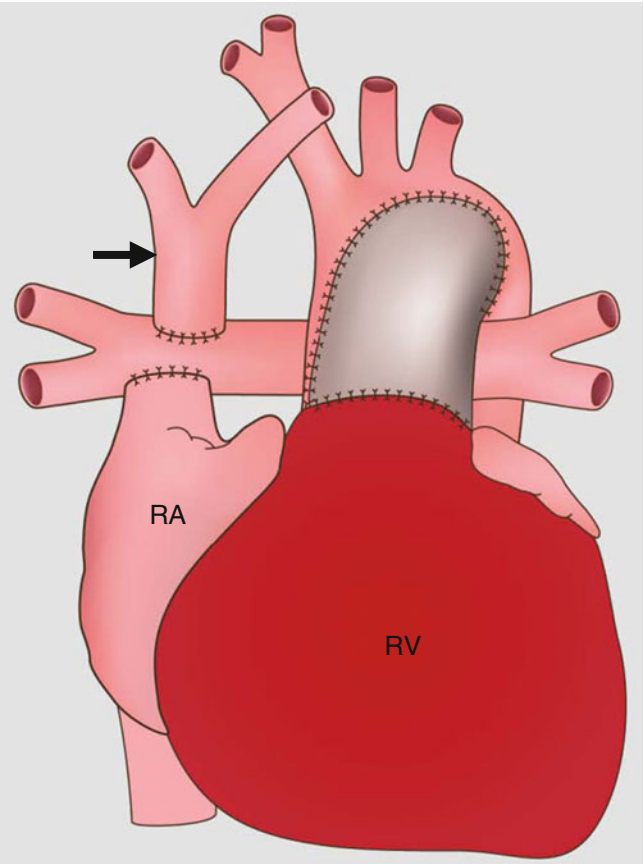


**Fig. 31.7** Stage II of the modified Norwood procedure. A bidirectional Glenn shunt (superior vena cava to pulmonary artery, *arrow*) is performed along with interruption of the Blalock–Taussig shunt or right ventricle-to-the pulmonary artery conduit. *RA* right atrium, *RV* right ventricle

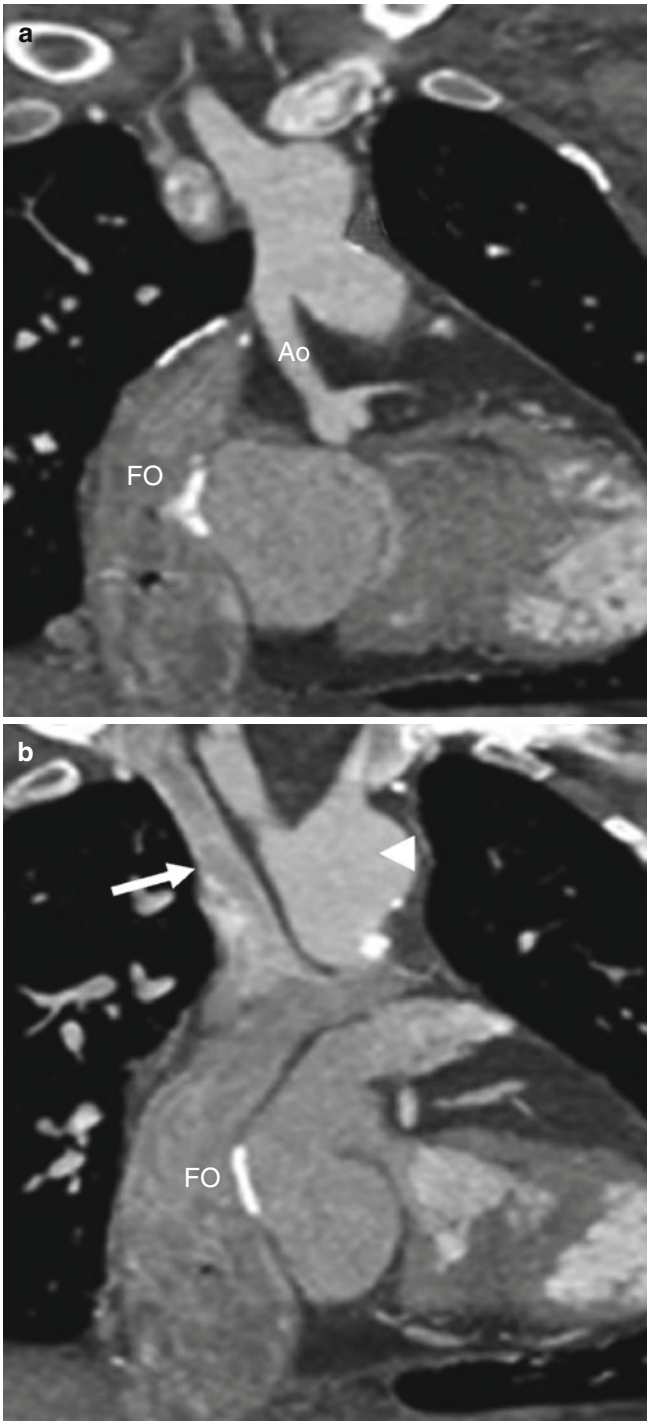


**Fig. 31.8** Stage III of the modified Norwood procedure. This example is from a 20-year-old man with mitral and aortic atresia who underwent a three-stage Norwood operation prior to age 3 years and was asymptomatic at the time. In stage III, a Fontan procedure is performed. This computed tomography (CT) was performed to evaluate right ventricular systolic function and to assess the Fontan pathway. Panels (**a**) and (**b**) are oblique coronal CT scans showing a severely hypoplastic ascending aorta (*Ao*), neoaorta (*arrowhead*), patent Glenn (superior vena cava to right pulmonary artery anastomosis, *arrow*), and inferior vena cava to right pulmonary artery Fontan (*Fo*) connection (Images courtesy of Kelly Han, M.D., Minneapolis Heart Institute, Minneapolis, MN)

## 31.2 Complications of the Norwood Procedure

The major complication of the Norwood operation is pulmonary overcirculation and pulmonary edema because the volume of blood flowing to the pulmonary arteries is increased. Other complications of the Fontan circulation as part of the completion of the Norwood operation are pleural and pericardial effusions and hepatomegaly, hepatic congestion, or superior vena cava syndrome caused by the increased right atrial pressure. Additionally, stenosis can occur at the anastomotic sites.

## 31.3 Cardiac Computed Tomographic Angiography (CT) in the Evaluation of the Norwood Procedure

After a Norwood procedure, CT is performed to visualize the ventricular or aortopulmonary artery anastomoses and to assess the presence and extent of complications [13, 14]. A noncontrast scan should be performed in order to identify calcified conduits followed by an arterial phase timed to the aorta to allow for contrast enhancement of the pulmonary and systemic arterial circulations. In patients with Fontan anatomy, a delayed venous-phase CT scan will often be required to allow contrast enhancement of the conduit and the inferior vena cava to occur. This is important lest an unenhanced conduit be mistaken for thrombus.

Aortic arch narrowing is an important complication to identify in order to avoid pressure overload on the systemic right ventricle. CT can also identify pleural and pericardial effusions and superior vena cava syndrome.

## References

1. Norwood WI. Hypoplastic left heart syndrome. Cardiol Clin. 1989;7:377–85.
2. Norwood Jr WI. Hypoplastic left heart syndrome. Ann Thorac Surg. 1991;52:688–95.
3. Ohye RG, Ludomirsky A, Devaney EJ, Bove EL. Comparison of right ventricle to pulmonary artery conduit and modified blalock-taussig shunt hemodynamics after the Norwood operation. Ann Thorac Surg. 2004;78:1090–3. doi:10.1016/S0003-4975(03)01386-9.
4. Azakie T, Merklinger SL, McCrindle BW, Van Arsdell GS, Lee KJ, Benson LN, et al. Evolving strategies and improving outcomes of the modified Norwood procedure: a 10-year single-institution experience. Ann Thorac Surg. 2001;72:1349–53.
5. Khouri EM, Gregg DE, Rayford CR. Effect of exercise on cardiac output, left coronary flow and myocardial metabolism in the unanesthetized dog. Circ Res. 1965;17:427–37.
6. Mahle WT, Spray TL, Gaynor JW, Clark 3rd BJ. Unexpected death after reconstructive surgery for hypoplastic left heart syndrome. Ann Thorac Surg. 2001;71:61–5.
7. Charpie JR, Dekeon MK, Goldberg CS, Mosca RS, Bove EL, Kulik TJ. Serial blood lactate measurements predict early outcome after neonatal repair or palliation for complex congenital heart disease. J Thorac Cardiovasc Surg. 2000;120:73–80. doi:10.1067/mtc.2000.106838.
8. Ohye RG, Sleeper LA, Mahony L, Newburger JW, Pearson GD, Lu M, et al. Comparison of shunt types in the Norwood procedure for single-ventricle lesions. N Engl J Med. 2010;362:1980–92. doi:10.1056/NEJMoa0912461.
9. Sano S, Ishino K, Kawada M, Arai S, Kasahara S, Asai T, et al. Right ventricle-pulmonary artery shunt in first-stage palliation of hypoplastic left heart syndrome. J Thorac Cardiovasc Surg. 2003;126:504–9; discussion 509–10.
10. Maher KO, Pizarro C, Gidding SS, Januszewska K, Malec E, Norwood Jr WI, et al. Hemodynamic profile after the Norwood procedure with right ventricle to pulmonary artery conduit. Circulation. 2003;108:782–4. doi:10.1161/01.CIR.0000087338.09589.21.
11. Muyskens S, Nicolas R, Foerster S, Balzer D. Endovascular stent placement for right ventricle to pulmonary artery conduit stenosis in the Norwood with Sano modification. Congenit Heart Dis. 2008;3:185–90. doi:10.1111/j.1747-0803.2008.00181.x.
12. Karimi M, Farouk A, Stork J, Hennein HA. Right ventricular aneurysm following modified norwood-sano operation for hypoplastic left heart syndrome. Interact Cardiovasc Thorac Surg. 2008;7:664–6. doi:10.1510/icvts.2007.171777.
13. Gaca AM, Jaggers JJ, Dudley LT, Bisset 3rd GS. Repair of congenital heart disease: a primer-part 1. Radiology. 2008;247:617–31. doi:10.1148/radiol.2473061909.
14. Spevak PJ, Johnson PT, Fishman EK. Surgically corrected congenital heart disease: utility of 64-MDCT. AJR Am J Roentgenol. 2008;191:854–61. doi:10.2214/AJR.07.2889.

# Aortic Coarctation Repairs

# 32

## 32.1 Repair Techniques of Coarctation of the Aorta and Interrupted Aortic Arch

### 32.1.1 Surgical Repairs

The first surgical repair of aortic coarctation was performed in 1944 [1]. Since then three basic surgical methods have evolved for repair of classic short-segment aortic coarctation (CoAo): resection of the coarcted segment with end-to-end anastomosis (Fig. 32.1), subclavian flap aortoplasty (distal left subclavian artery used to augment aortic lumen at the coarctation site), and prosthetic patch aortoplasty (prosthetic patch inserted to widen the aortic lumen) [2]. The choice of procedure depends on the age of the patient, the type of associated malformations, and the morphology of the coarctation itself. Surgical treatment is preferred in neonates and infants. The other procedure types have been used in adults. Subclavian flap aortoplasty is no longer commonly performed because it requires sacrifice of the left subclavian artery which leads to arm claudication with exercise and diminished growth of the left arm [3].

Less frequently used techniques include insertion of a graft in situ or in an extra-anatomic location (Fig. 32.2). Interposition grafts using aortic homografts have been used when the resected segment of coarctation is too long to allow an end-to-end anastomosis. Interposition graft insertion creates proximal and distal anastomoses.

### 32.1.2 Endovascular Repairs

#### 32.1.2.1 Balloon Angioplasty

Percutaneous balloon angioplasty is often used in the treatment of residual stenosis or recoarctation. Its use for treatment of native coarctation is more controversial, although it has been recommended as an alternative to surgery in adolescents and adults [4, 5]. Its use is limited in younger patients because restenosis is common [6].

#### 32.1.2.2 Stent Placement

Aortic stent placement has been used in patients with primary coarctation as well as in those with recurrent coarctation after surgical repair or balloon angioplasty (Fig. 32.3) [7]. Recurrence is a frequent problem after balloon dilatation, and endovascular stents have become an integral component for the treatment of recurrent lesions following balloon angioplasty.

**Fig. 32.1** A 25-year-old man after surgical repair in early childhood of aortic coarctation using the end-to-end anastomosis technique. This oblique sagittal scan shows the normal postoperative appearance of a repaired coarctation. The *arrow* points to the site of the anastomosis. The *arrowhead* points to the origin of left subclavian artery above the site of repair. There was no significant gradient at the anastomotic site

W. Mazur et al., *CT Atlas of Adult Congenital Heart Disease*,
DOI 10.1007/978-1-4471-5088-6_32, © Springer-Verlag London 2013

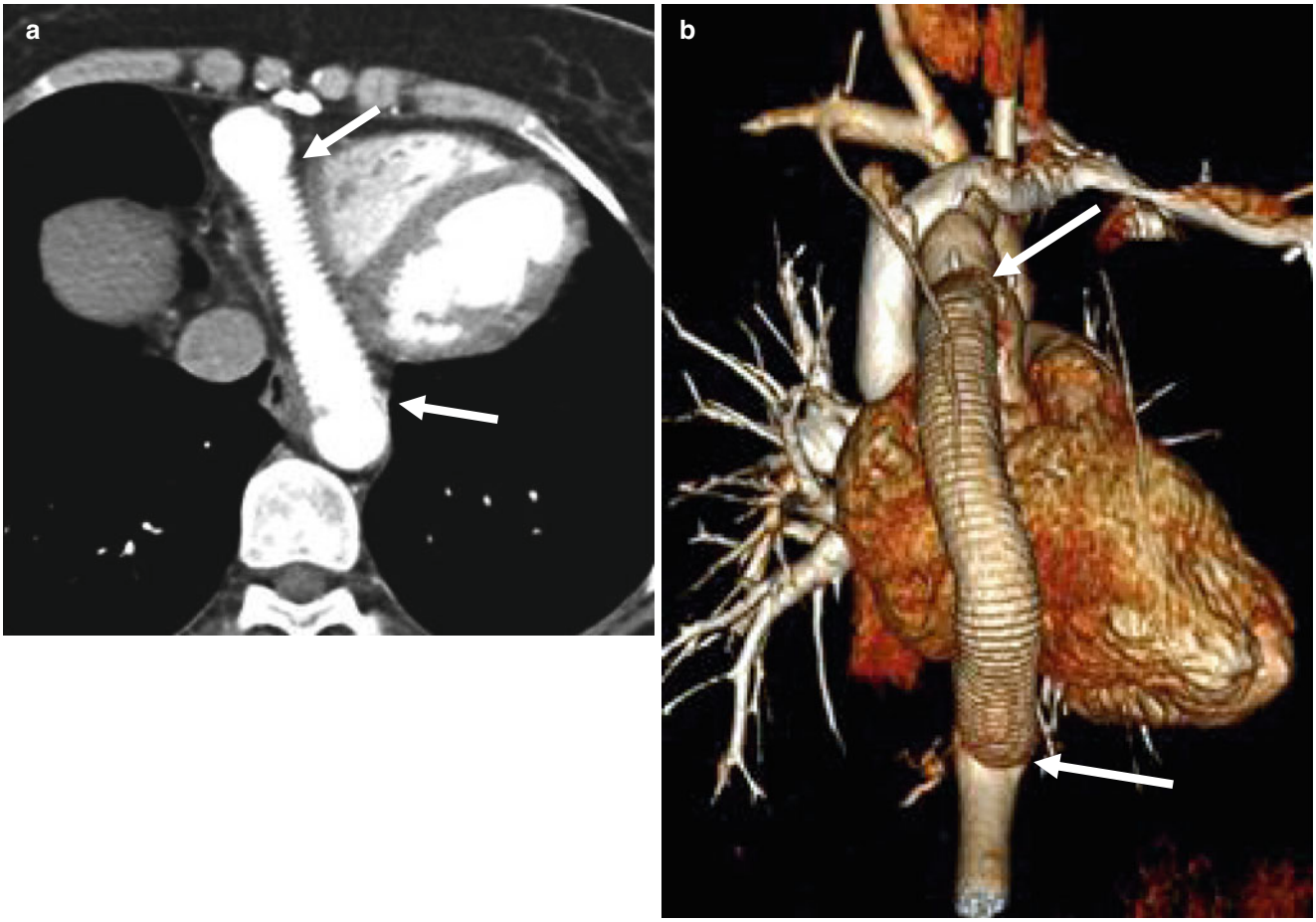


**Fig. 32.2** Graft interposition. A 38-year-old woman who had a patch repair of an aortic coarctation as a child and subsequent ascending to descending aortic bypass graft placed when she had a recurrent coarctation. Panel (**a**) is an axial scan and panel (**b**) is a volume-rendered reformat showing the normal appearance of a bypass graft from the ascending to descending aorta. This procedure is used in patients with long-segment aortic coarctation. The *arrows* point to the proximal and distal anastomoses of the graft


**Fig. 32.3** Stent placement. Two patients with history of coarctation who had a patch repair of the coarctation at young ages and developed recurrent aortic coarctation. Panels (**a**), (**b**) and (**c**) are oblique sagittal views showing complete resolution of stenosis after balloon dilatation and stent placement (*arrows*) in the region of coarctation. No pressure gradient was seen at the end of procedure in either patient

## 32.2 Post-Treatment Complications

Following the use of surgical or endovascular repairs, survival has improved dramatically, although life expectancy is not that of unaffected peers. Post-intervention, morbidity and mortality are often determined by associated major cardiovascular anomalies, degree of systemic hypertension, and complications of the repair [8, 9]. The most common complications associated with surgical and endovascular techniques are recurrent coarctation and aneurysm formation.

### 32.2.1 Recurrent Coarctation or Restenosis

Recurrent coarctation is considered to be present whenever the pressure gradient across the anastomotic stenosis is higher than 20 mmHg at rest and occurs after both surgical and endovascular treatment (Fig. 32.4). Residual coarctation is defined as the presence of a gradient in the early postoperative period.

The risk of recurrent coarctation increases if surgical repair is performed before 1 year of age, while the risk of hypertension increases when repair is performed after 1 year of age [8, 10, 11]. In subjects who have undergone patch aortoplasty, hemodynamically significant recurrent coarctation was reported in up to 50 % of survivors who had repair in the neonatal period with an overall recurrence rate of about 5 % [12].

### 32.2.2 Aneurysm Formation

Aneurysm formation is defined as an area of focal dilatation with a diameter that is 1.5 times that of the aorta at the level of the diaphragm (Figs. 32.5 and 32.6). Aneurysm formation occurs after both surgical and endovascular treatment, with

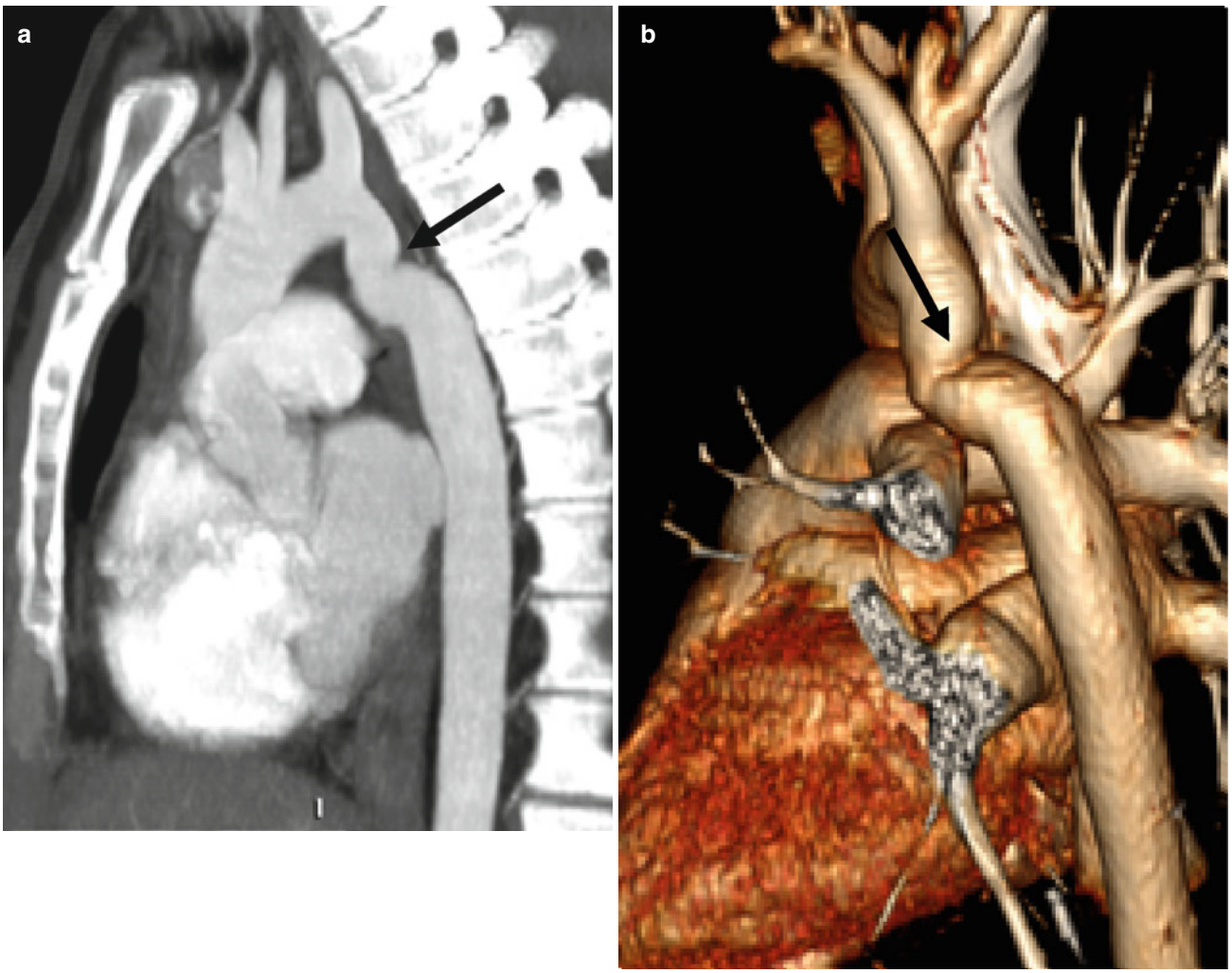


**Fig. 32.4** Recurrent coarctation. A 24-year-old female with a history of coarctation of the aorta status post-balloon angioplasty 6 months previously who presented again with increasing hypertension and a recurrent gradient of 25 mmHg. Panels (**a**) and (**b**) are two sagittal computed tomographic views showing a focal tortuosity and mild narrowing of the proximal descending aorta (*arrows*). She subsequently underwent stenting

an incidence of about 5 % [13]. Its occurrence is most common after patch aortoplasty [12]. Approximately 7 % of deaths after coarctation repair have been attributed to aneurysm formation [8]. Delayed aneurysm formation in the ascending aorta, proximal to the surgical repair site, has also been reported as a late complication (Fig. 32.7) [14, 15].

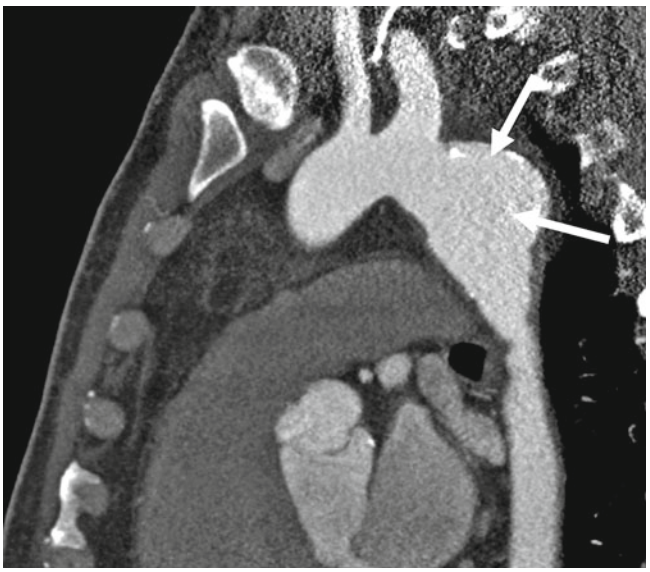

**Fig. 32.5** Pseudoaneurysm formation at site of a previous patch aortoplasty coarctation repair. This scan shows a focal dilatation of the aorta (*arrows*) in the region of the aortic isthmus which was site of initial coarctation repair

### 32.2.3 Other Post-intervention Complications

Aneurysm rupture, albeit rare, has been described after all types of repair [16, 17]. This condition is usually fatal. Both percutaneous angioplasty and stent placement can lead to aortic rupture. Dissection of the aorta is primarily a complication of percutaneous angioplasty (Fig. 32.8), and its treatment often entails stent placement to exclude the false lumen and provide patency of the true lumen. Aortic thrombosis has also been described after surgical and endovascular treatment and often requires additional surgery.

Other complications associated with stent placement include stent fracture (Fig. 32.9), stent malposition or migration (Fig. 32.10), and thromboembolic events [18, 19]. Malpositioning or stent migration may result in inadvertent coverage of an aortic branch vessel (often the left subclavian artery) (Fig. 32.10). Occlusion of the left subclavian artery origin by the stent can result in upper extremity ischemia or cerebral symptoms from vertebrobasilar insufficiency.

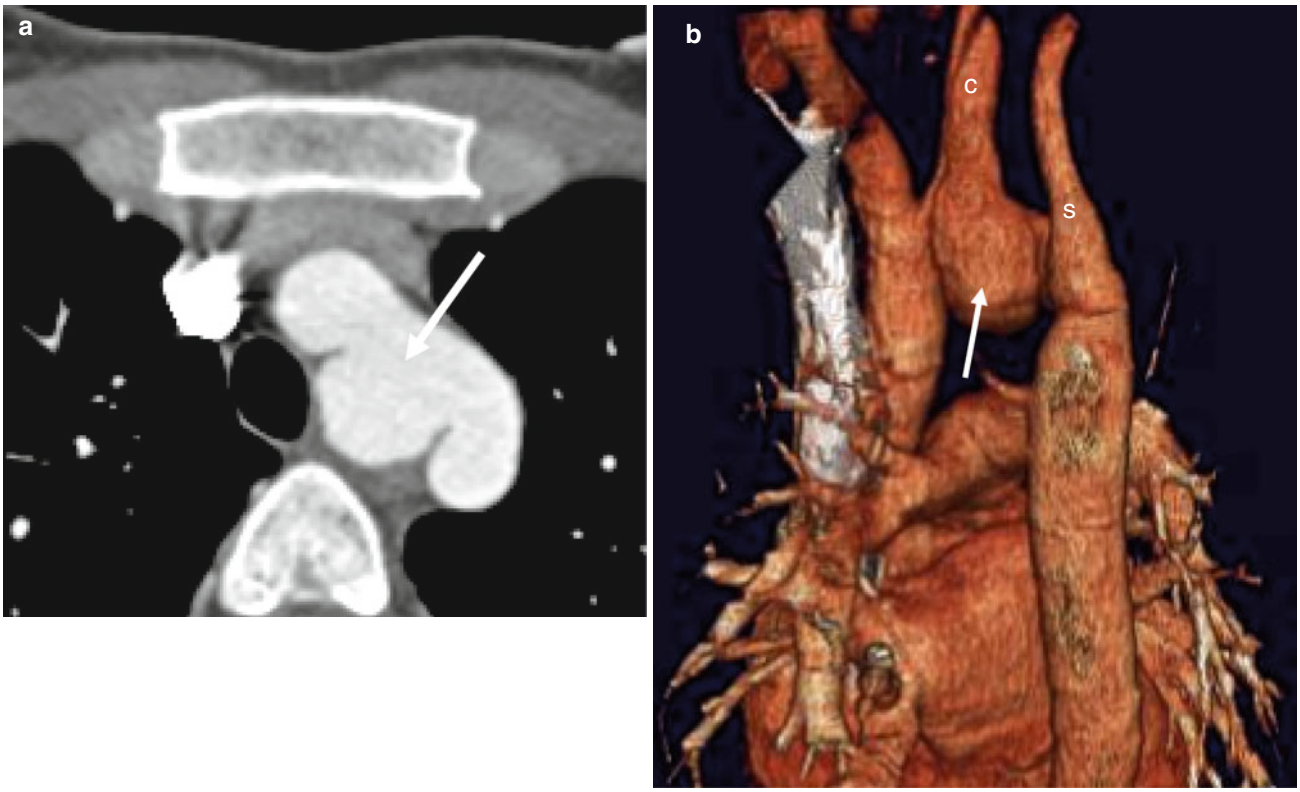


**Fig. 32.6** Pseudoaneurysm formation at site of a previous repair of a coarctation using balloon angioplasty. Panel (**a**), axial, and panel (**b**), volume-rendered images show a pseudoaneurysm (*arrow*) at the proximal descending aorta between the origins of the left subclavian (*S*) and left carotid (*C*) arteries

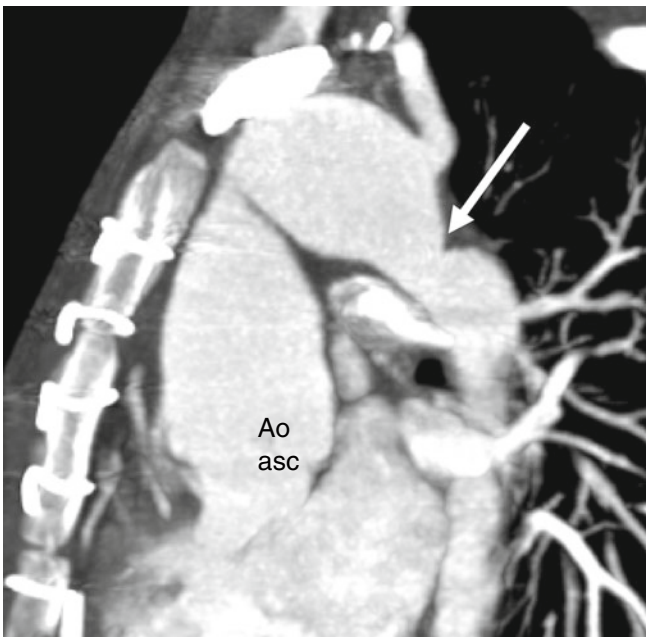


**Fig. 32.7** Delayed aneurysm formation in the ascending aorta. A 15-year-old male with a history of surgical repair of a coarctation as a child who presents with increasing hypertension. A computed tomogram shows recurrent coarctation (*arrow*) of the proximal descending aorta at the site of the surgical repair and marked dilatation of the proximal ascending aorta ($Ao_{asc}$)

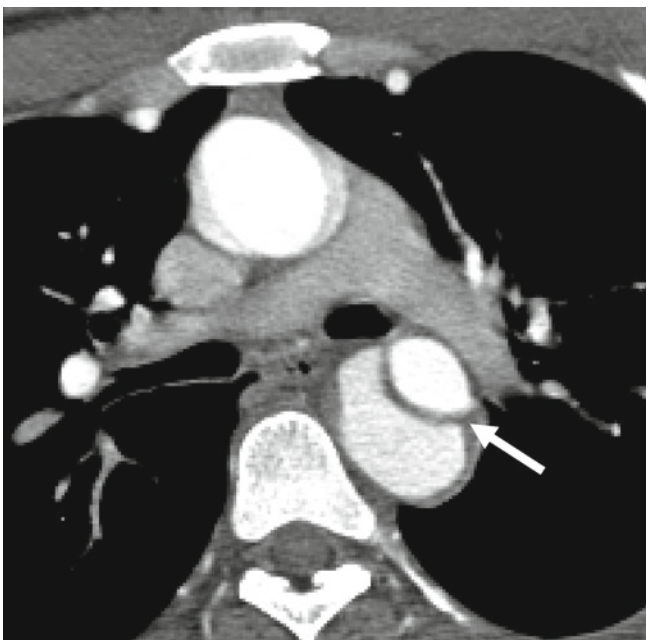

**Fig. 32.8** Aortic dissection after percutaneous angioplasty repair of a coarctation. This axial image shows an aortic dissection (*arrow*) just below the site of the aortoplasty. A dissection flap separates the true and false lumen

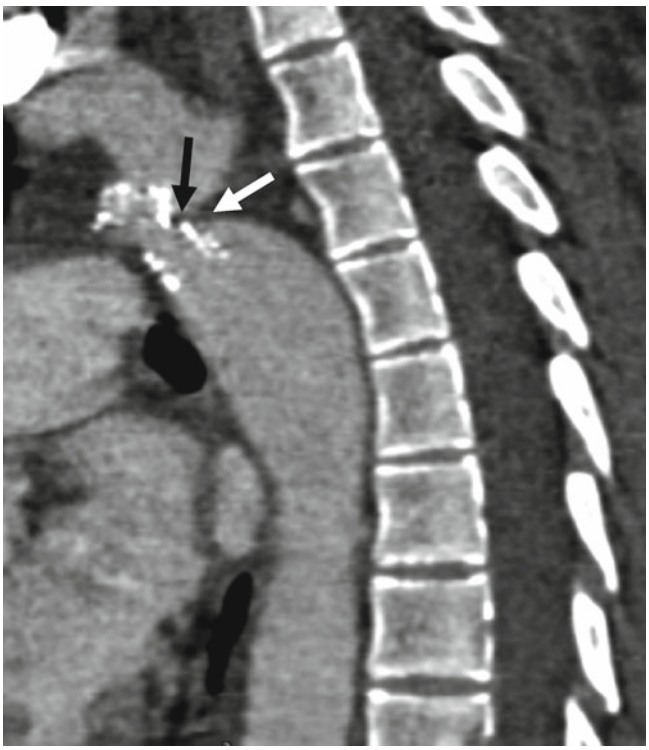

**Fig. 32.9** Stent fracture and restenosis. This oblique scan depicts a recurrent stenosis (*white arrow*) at the site of a fractured stent (*black arrow*) (Image courtesy of Catherine Owens, M.D. Great Ormond Street Hospital. London, England)

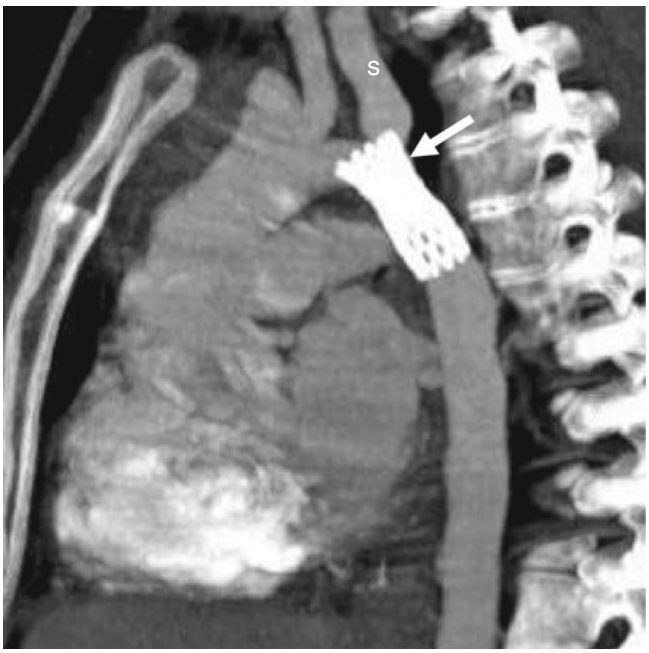


**Fig. 32.10** Stent malposition after endovascular repair of a coarctation. A sagittal image shows a stent in the proximal descending thoracic aorta. The malpositioned stent (*arrow*) occludes the origin of the left subclavian artery (*S*)

## 32.3 Complications Unrelated to Interventions

Complications unrelated to intervention procedures include early-onset coronary artery disease and myocardial infarction, renal failure, and cerebrovascular accidents, such as stroke and aneurysms of the circle of Willis from hypertension. Myocardial infarction accounts for one-third of late deaths [14, 15] and cerebrovascular accidents are responsible for approximately 7 % of late deaths, the latter related to long-standing hypertension or ruptured aneurysm of the circle of Willis [9].

## 32.4 Cardiac Computed Tomography (CT) in the Evaluation of Coarctation of the Aorta

CT is suited for the assessment of postoperative anatomy and posttreatment complications (recurrent coarctation, aneurysm, dissection) as well as for detection of coronary artery disease. It has an advantage over magnetic resonance (MR) imaging since it is not affected by the frequently present metallic artifacts related to stent placement. Reconstructed images in sagittal and parasagittal planes are best to show the location and extent of recurrent coarctation and of aneurysm formation [20–22].

## References


1. Shih MC, Tholpady A, Kramer CM, et al. Surgical and endovascular repair of aortic coarctation: normal findings and appearance of complications on CT angiography and MR angiography. Am J Roentgenol. 2006;187(3):w302–12.
2. Gibbs JL. Treatment options for coarctation of the aorta. Heart. 2000;84:11–3.
3. Diemont FF, Chemla ES, Julia PL, Sirieix D, Fabiani JN. Upper limb ischemia after subclavian flap aortoplasty: unusual long-term complication. Ann Thorac Surg. 2000;69:1576–8.
4. Hijazi ZM, Fahey JT, Kleinman CS, Hellenbrand WE. Balloon angioplasty for recurrent coarctation of aorta. Immediate and long-term results. Circulation. 1991;84:1150–6.
5. Fletcher SE, Nihill MR, Grifka RG, O'Laughlin MP, Mullins CE. Balloon angioplasty of native coarctation of the aorta: midterm follow-up and prognostic factors. J Am Coll Cardiol. 1995; 25:730–4. doi:10.1016/0735-1097(94)00437-U.
6. Mendelsohn AM, Lloyd TR, Crowley DC, Sandhu SK, Kocis KC, Beekman 3rd RH. Late follow-up of balloon angioplasty in children with a native coarctation of the aorta. Am J Cardiol. 1994;74: 696–700.
7. Thanopoulos BD, Hadjinikolaou L, Konstadopoulou GN, Tsaousis GS, Triposkiadis F, Spirou P. Stent treatment for coarctation of the aorta: intermediate term follow up and technical considerations. Heart. 2000;84:65–70.
8. Cohen M, Fuster V, Steele PM, Driscoll D, McGoon DC. Coarctation of the aorta. Long-term follow-up and prediction of outcome after surgical correction. Circulation. 1989;80:840–5.
9. Presbitero P, Demarie D, Villani M, Perinetto EA, Riva G, Orzan F, et al. Long term results (15–30 years) of surgical repair of aortic coarctation. Br Heart J. 1987;57:462–7.
10. Seirafi PA, Warner KG, Geggel RL, Payne DD, Cleveland RJ. Repair of coarctation of the aorta during infancy minimizes the risk of late hypertension. Ann Thorac Surg. 1998;66:1378–82.
11. Walhout RJ, Lekkerkerker JC, Oron GH, Hitchcock FJ, Meijboom EJ, Bennink GB. Comparison of polytetrafluoroethylene patch aortoplasty and end-to-end anastomosis for coarctation of the aorta. J Thorac Cardiovasc Surg. 2003;126:521–8.
12. Backer CL, Paape K, Zales VR, Weigel TJ, Mavroudis C. Coarctation of the aorta. Repair with polytetrafluoroethylene patch aortoplasty. Circulation. 1995;92:II132–6.
13. Lundqvist B, Almgren B, Bowald S, Lorelius LE, Eriksson I. Deterioration and dilatation of Dacron prosthetic grafts. Acta Chir Scand Suppl. 1985;529:81–5.
14. Heikkinen LO, Ala-Kulju KV, Salo JA. Dilatation of ascending aorta in patients with repaired coarctation. Scand J Thorac Cardiovasc Surg. 1991;25:25–8.
15. Maron BJ, Humphries JO, Rowe RD, Mellits ED. Prognosis of surgically corrected coarctation of the aorta. A 20-year postoperative appraisal. Circulation. 1973;47:119–26.
16. Mahadevan V, Mullen MJ. Endovascular management of aortic coarctation. Int J Cardiol. 2004;97 Suppl 1:75–8. doi:10.1016/j.ijcard.2004.08.011.
17. de Suarez Lezo J, Pan M, Romero M, Segura J, Pavlovic D, Ojeda S, et al. Percutaneous interventions on severe coarctation of the aorta: a 21-year experience. Pediatr Cardiol. 2005;26:176–89. doi:10.1007/s00246-004-0961-5.
18. de Suarez Lezo J, Pan M, Romero M, Medina A, Segura J, Lafuente M, et al. Immediate and follow-up findings after stent treatment for severe coarctation of aorta. Am J Cardiol. 1999;83:400–6.
19. Harrison DA, McLaughlin PR, Lazzam C, Connelly M, Benson LN. Endovascular stents in the management of coarctation of the aorta in the adolescent and adult: one year follow up. Heart. 2001;85:561–6.
20. Hughes Jr D, Siegel MJ. Computed tomography of adult congenital heart disease. Radiol Clin North Am. 2010;48:817–35. doi:10.1016/j.rcl.2010.04.005.
21. Shih MC, Tholpady A, Kramer CM, Sydnor MK, Hagspiel KD. Surgical and endovascular repair of aortic coarctation: normal findings and appearance of complications on CT angiography and MR angiography. AJR Am J Roentgenol. 2006;187:W302–12. doi:10.2214/AJR.05.0424.
22. Siegel MJ. CT evaluation of congenital heart disease in adults. Appl Radiol. 2005;34:61–8.

# Part VIII

# Congenital Pericardial Abnormalites

# Congenital Absence of the Pericardium

# 33

Congenital absence of the pericardium is an abnormality characterized by a spectrum of findings ranging from a small defect to complete absence of the pericardium.

Congenital absence of the pericardium is rare with an estimated incidence of 0.0001–0.044 % based on surgical/pathologic series [1, 2].

Associated abnormalities occur in 30–50 % of patients and include atrial septal defect, patent ductus arteriosus, mitral valve stenosis, and tetralogy of Fallot [1, 2]. Pericardial defects are typically discovered incidentally during surgery, imaging, or postmortem examinations, but patients can present with non-exertional stabbing chest pain, which often is induced or relieved by postural changes [3, 4].

In healthy individuals, the aortopulmonary window contains fat and is covered by pericardium. Most pericardial defects are partial and occur on the left and less frequently on the right side or diaphragmatic surface (Figs. 33.1, 33.2, and 33.3). Left-sided absence of the pericardium allows extension of the main pulmonary artery beyond the confines of the mediastinum and interposition of lung tissue between the pulmonary artery and aorta, which is a characteristic diagnostic feature [1, 5, 6]. Occasionally, the left atrial appendage or other chambers bulge through the defect. The heart rotates to the left, resulting in levocardia.

The complications associated with congenital pericardial absence depend on the extent of the pericardial defect. Complete absence of either the entire left or right pericardium or the whole pericardium usually has an excellent prognosis with no complications. Rarely, there may be ventricular dilatation due to increases in preload. Partial pericardial absence is associated with hemodynamically significant events, including herniation and entrapment of cardiac chambers, leading to strangulation of the atria, appendages, and parts of the ventricles and tricuspid insufficiency due to traction on the chordal structures [3, 4]. Pericardiectomy or pericardioplasty may be needed in patients with cardiac chamber entrapment. Complete absence usually requires no intervention.

W. Mazur et al., *CT Atlas of Adult Congenital Heart Disease*,
DOI 10.1007/978-1-4471-5088-6_33, © Springer-Verlag London 2013

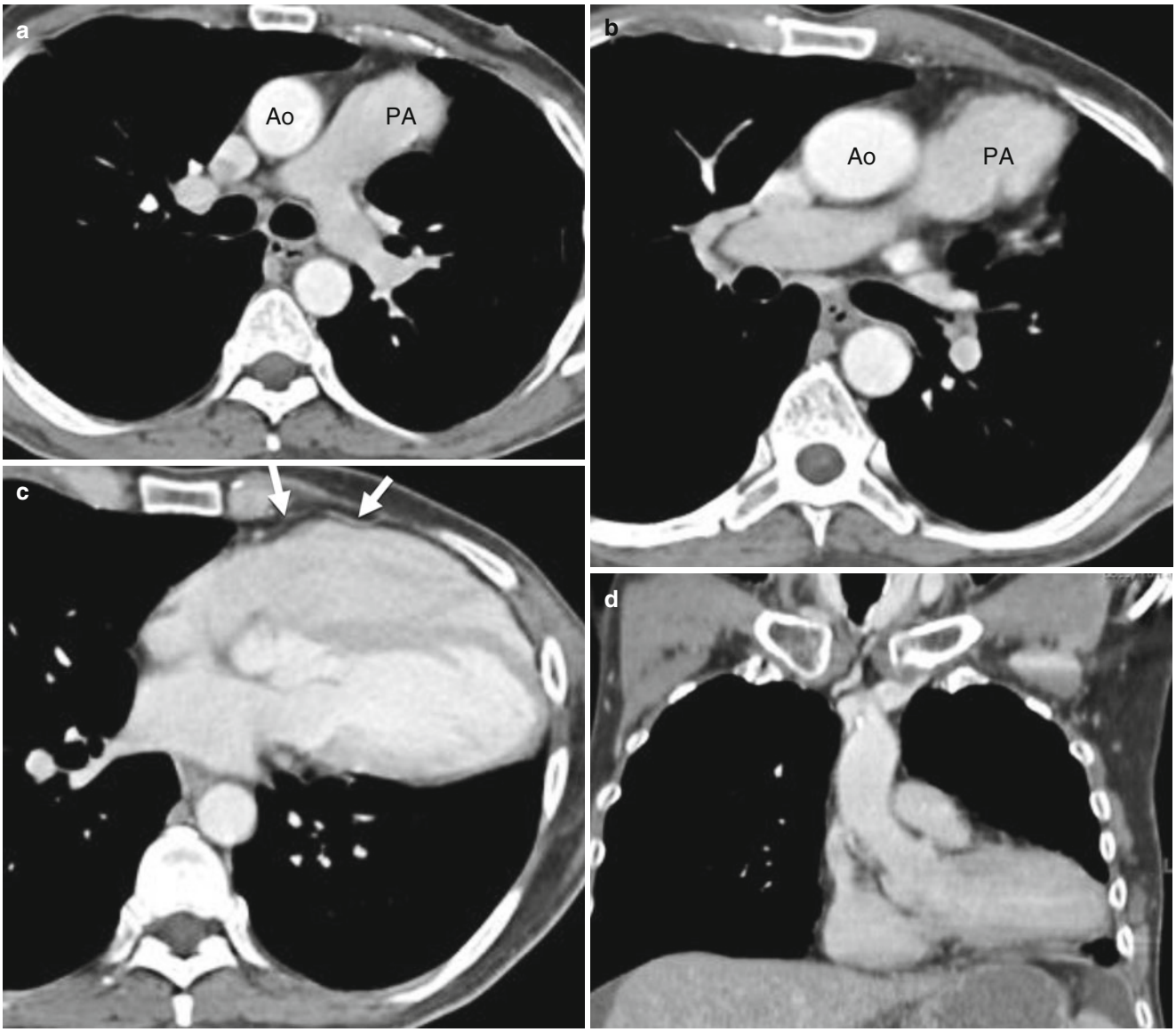


**Fig. 33.1** Partial absence of the pericardium. An example of a 54-year-old man with known tricuspid insufficiency and who underwent a computed tomography (CT) angiogram for evaluation of an abnormal chest radiograph. Panels (**a**) and (**b**) are axial CT images showing the main pulmonary artery (*PA*) extending far beyond the mediastinal margins into the left hemithorax. Panel (**c**) is an axial scan, while panel (**d**) is a coronal image. Both panels (c) and (d) demonstrate a leftward shift of the heart and cardiac axis, which is nearly horizontal. At this level, the pericardium is only partially visualized around the heart (panel c, *arrows*). *Ao* aorta

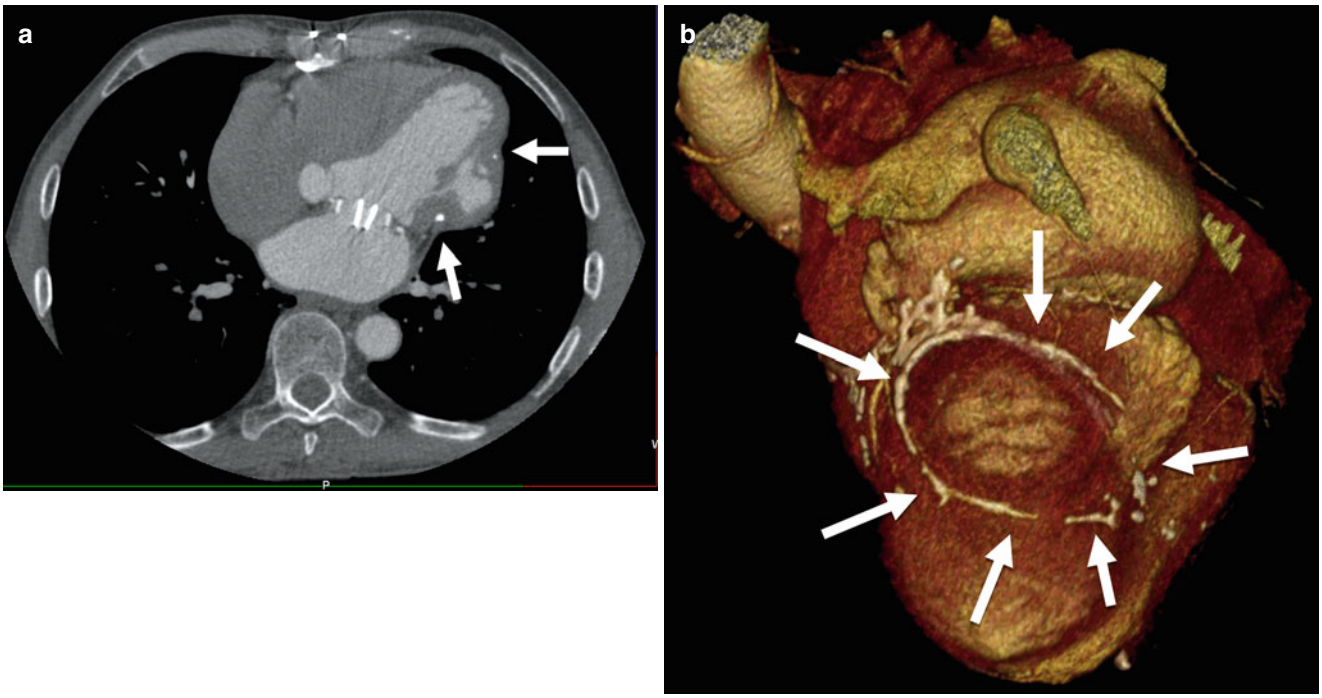


**Fig. 33.2** Partial absence of the pericardium. Panel (**a**) is an axial scan in a patient with a history of a mitral valve replacement shows a focal pericardial defect resulting in herniation of a relatively small segment of the left ventricular free wall (*arrows*). Panel (**b**) is a 3D volume-rendered image showing calcification at the edges of the pericardial tissue through which the herniation occurs (*arrows*)

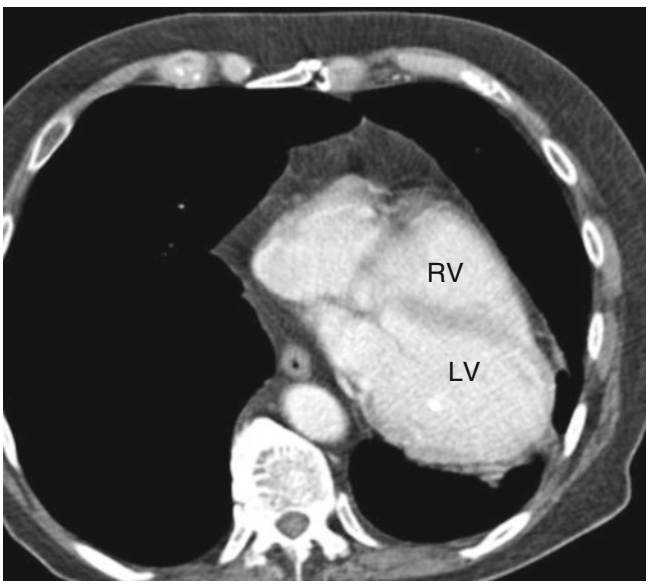


**Fig. 33.3** Complete absence of the pericardium. This is an axial contrast-enhanced computed tomogram demonstrating complete absence of the pericardium and marked displacement of the heart into the left hemithorax with the cardiac apex directed posteriorly. *RV* right ventricle, *LV* left ventricle

## 33.1 Congenital Pericardial Cysts and Diverticula

A pericardial cyst is an intrathoracic cyst that is typically found at the cardiophrenic angle in asymptomatic individuals. When there is a connection with the pericardial cavity, it is referred to as a pericardial diverticulum, but usually it is clinically indistinguishable from a general cyst. For this discussion, diverticula will be considered to be cysts.

The incidence of pericardial cysts is estimated to be 1 person per 100,000 [8].

Pericardial cysts are usually asymptomatic and discovered as an incidental finding on a chest radiography or echocardiography. When symptoms occur, they are due to compression of adjacent organs and include atypical chest pain, dyspnea, and cough. Albeit extremely rare, life-threatening complications, such as cardiac tamponade due to intrapericardial rupture of the cyst or spontaneous hemorrhage into the cyst and obstruction of the right main stem bronchus, have been reported [7]. Treatment is usually not indicated, except in symptomatic patients. Occasionally, pericardial cysts resolve spontaneously.

Congenital pericardial cysts are formed when a portion of the pericardium is sequestered from the parent pericardium during early embryonic development. Histologically they are lined with a single layer of mesothelial cells and surrounded by a smooth wall composed of connective tissue. They contain clear water-like fluid without internal septa. Approximately 75 % are located at the right cardiophrenic angle, with the remainder on the left side (Figs. 33.4 and 33.5). Rarely, they are located in the posterior or anterior superior mediastinum remote from the diaphragm. The size has been reported to vary from 2 to 28 $cm^2$ [7].

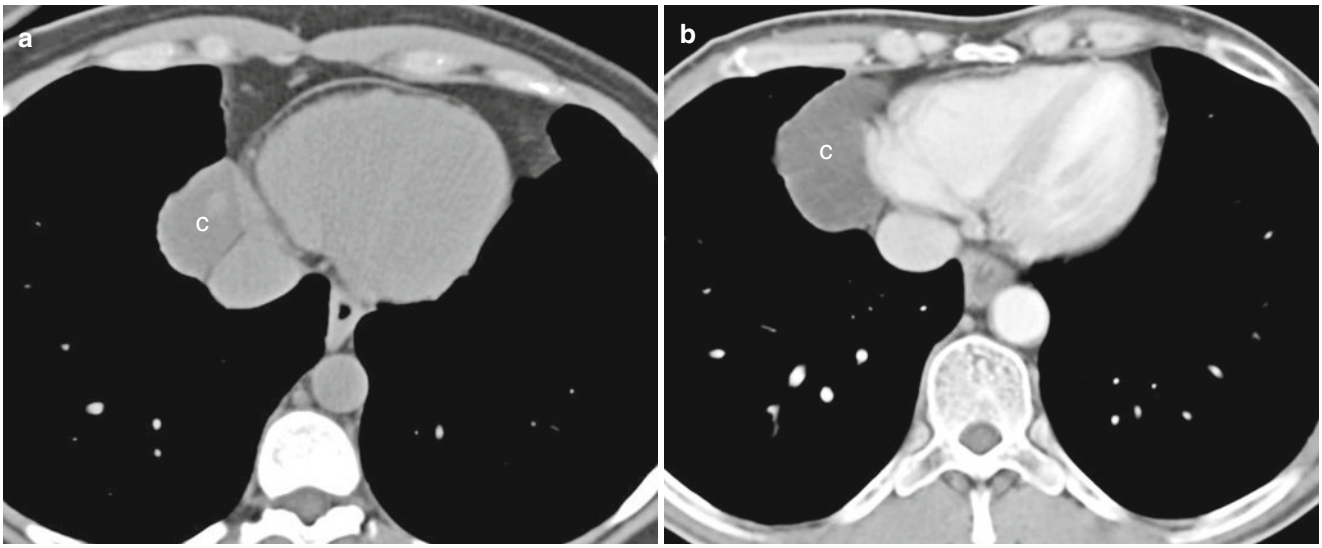


**Fig. 33.4** Pericardial cyst in a 32-year-old woman who underwent computed tomography (CT) for an abnormal cardiac contour on a chest radiograph. Panel (**a**) an axial noncontrast CT shows a right cardiophrenic angle cystic mass with a CT density consistent with fluid contents (*C*). Panel (**b**) an axial CT after contrast administration showing no enhancement of the contents of the mass which is pathognomonic of a cyst

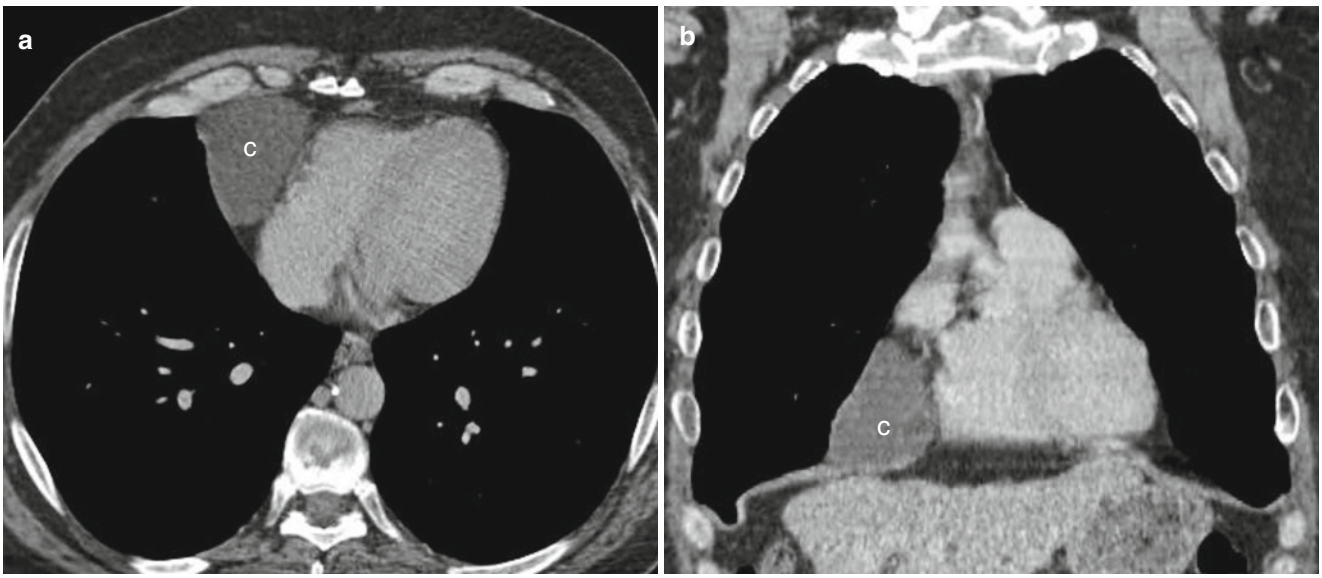


**Fig. 33.5** Pericardial cyst in a 56-year-old man with incidental discovery of a cardiophrenic mass on a chest radiograph. Panel (**a**), an axial scan, and panel (**b**), a coronal view, show a well-defined, right cardiophrenic angle cystic mass (*c*). The position, water attenuation of the fluid, thin wall, and unilocular, non-enhancing contents allow the diagnosis of a pericardial cyst to be established with confidence

## 33.2 Cardiac Computed Tomographic Angiography (CT) in the Evaluation of Congenital Pericardial Anomalies

Although chest radiographs can suggest the diagnosis of pericardial absence or cyst, a definitive diagnosis can be made easily with CT [6, 8]. CT findings of absence of the pericardium include lack of visualization of the pericardium and secondary signs, including posterior and leftward shift of the cardiac axis, extension of the main pulmonary artery and left atrial appendage or left ventricle beyond the mediastinal borders, and the presence of lung between the main pulmonary artery and the aorta (Figs. 33.1, 33.2, and 33.3). Thickening of soft tissues and calcification can occur around the site of the pericardial defect. Decubitus imaging may be of use in differentiation between partial and complete absence of pericardium [9].

At CT, pericardial cysts appear as thin-walled, unilocular, non-enhancing masses with fluid attenuation slightly higher than water density – 30 to 40 HU (Figs. 33.4 and 33.5). Occasionally, the attenuation is higher due to the presence of highly proteinaceous material. Cysts can also change their size and shape according to body position and respiration.

## References

1. Nasser WK. Congenital absence of the left pericardium. Am J Cardiol. 1970;26:466–70.
2. Gatzoulis MA, Munk MD, Merchant N, Van Arsdell GS, McCrindle BW, Webb GD. Isolated congenital absence of the pericardium: clinical presentation, diagnosis, and management. Ann Thorac Surg. 2000;69(4):1209–15.
3. Robin E, Ganguly SN, Fowler MS. Strangulation of the left atrial appendage through a congenital partial pericardial defect. Chest. 1975;67:354–5.
4. Van Son JA, Danielson GK, Schaff HV, Mullany CJ, Julsrud PR, Breen JF. Congenital partial and complete absence of the pericardium. Mayo Clin Proc. 1993;68:743–7.
5. Ilhan E, Unal S, Sinana T, et al. Congenital absence of the pericardium: a rare cause of right ventricular dilatation and levoposition of the heart. Cardiol J. 2012;19:1–4.
6. Wang ZJ, Reddy GP, Gotway MB, Yeh BM, Hetts SW, Higgins CB. CT and MR imaging of pericardial disease. Radiographics. 2003;23: S167–80.
7. Patel J, Park C, Michaels J, Rosen S, Kort S. Pericardial cyst: case reports and a literature review. Echocardiography. 2004;21:269–72.
8. Oyama N, Oyama N, Komuro K, Nambu T, et al. Computed tomography and magnetic resonance imaging of the pericardium: anatomy and pathology. Magn Reson Med Sci. 2004;3:145–52.
9. Hoey ET, Yap KS, Darby MJ, Mankad K, Puppala S, Sivananthan MU. Complete left pericardial defect: evaluation with supine and decubitus dual source CT. J Cardiovasc Comput Tomogr. 2009;3: 417–9.

# Index



W. Mazur et al., *CT Atlas of Adult Congenital Heart Disease*,
DOI 10.1007/978-1-4471-5088-6, © Springer-Verlag London 2013

**B**